DETERMINATION OF FATIGUE CHARACTERISTICS OF NBG18 GRAPHITE

by

Johan George Roberts

Thesis submitted for the degree of

Philosophiae Doctor

in

Mechanical Engineering

in the

School of Mechanical Engineering

of the

North-West University, Potchefstroom Campus

Promoter: Professor J. Markgraaff

November 2007

Potchefstroom

ABSTRACT

The topic of this research thesis is the determination of the fatigue characteristics of NBG18 graphite, which is the preferred material for the graphite structures of a high temperature gas-cooled nuclear reactor (HTR). This is a newly developed fine grained (maximum grain size of 1,6 mm) near-isotropic graphite grade, that was developed by SGL Carbon for Pebble Bed Modular Reactor company (PBMR), for the application mentioned. SGL Carbon is an overseas company who develops and manufactures graphite materials for nuclear and other applications. PBMR is a South African company who is pioneering the German invented, pebble bed type, high temperature gas-cooled nuclear reactor for power generation purposes.

A new test specimen geometry, complete with associated test machine grips, is designed for the determination of the uniaxial fatigue properties of this material across a wide spectrum of load ratios. The geometry of this specimen, called the S70 specimen, is based on the cylindrical ASTM E466 specimen. Tests are conducted for load ratios that range from the static tensile tests, R = +1/+1 to the static compression tests, R = -1/-1. The fatigue cycle ratios are R = +0.5, 0, -0.5, -1, -2, -∞ and +2. The stress-life curve (S-N diagram) is determined by testing eight specimens per load with four loads for each load ratio.

The Maximum Principal stress is the stress basis for these load ratios. Constant-life charts are compiled for NBG18 from the logarithmic regression equations of the S-N curves. The results of the static strengths compare well with the values quoted by the supplier for NBG18. The uniaxial fatigue characteristics of NBG18 are superior to those of V483T2 for all load ratios. The fatigue characteristics of V483T2 were determined before by Schmidt (2001a). The latter material, which is also a product of SGL Carbon, was the German industry standard material for this application.

A novel multiaxial fatigue test specimen, called the S60B specimen, complete with hydrostatic test equipment, is designed for the determination of the multiaxial fatigue characteristics of NBG18 for the same spectrum of load ratios as for the uniaxial fatigue tests. The geometry of the specimen approaches that of a hemisphere. The main features of the new test specimen are its low cost, low cost of associated test equipment and its relative insensitivity to orientation with regard to the grain direction of the graphite.

The Maximum Principal stress is the stress basis for the load ratios, similar to the uniaxial tests. Constant-life charts are compiled for NBG18 using the regression equations of the S-N diagrams. The static tensile strength compares reasonably well with the results of the

manufacturer. The static compressive strength subject to this multiaxial loading mode is much higher than expected. This may be attributed to internal friction that is created by the tangential principal stresses.

The modified Maximum Deformation Strain Energy stress (MDE) that is prescribed as the stress basis in the KTA 3232 design code, does not yield satisfactory predictions of the multiaxial static failure of the S60B specimen, manufactured from NBG18 graphite.

Possible damage due to low pressure (10 MPa), isostatic loading of the graphite, is too small to be conclusive. The measured reduction in strength is less than 3% for all static strengths and a fatigue life of 100 cycles.

This research establishes the capability to perform uniaxial and multiaxial fatigue tests in South Africa. The technology is established at the Nelson Mandela Metropolitan University in Port Elizabeth and the North-West University in Potchefstroom respectively.

UITTREKSEL

Die onderwerp van hierdie proefskrif is die bepaling van die vermoeidheidseienskappe van NBG18 grafiet, wat die voorkeur material is vir die struktuurelemente in 'n hoë temperatuur gasverkoelde kernreaktor. Hierdie grafiet is 'n nuwe graad materiaal wat deur SGL Carbon vir Pebble Bed Modular Reactor maatskappy (PBMR) ontwikkel is vir hierdie toepassing. Dit is byna isotroop en het 'n klein grein (maksimum greingrootte van 1,6 mm). SGL Carbon is 'n buitelandse maatskappy wat grafietmateriaal vir die kern- en ander industrieë ontwikkel en vervaardig. PBMR is 'n Suid-Afrikaanse maatskappy wat die Duitse uitvindsel van 'n korrelbed-tipe hoë temperatuur gasverkoelde kernreaktor verder ontwikkel.

'n Nuwe toetsmonster, genaamd S70, en gepaardgaande kloukoppe vir die toetsmasjien is ontwerp vir die bepaling van die enkelas-belasting vermoeidheidseienskappe van die materiaal oor 'n wye bereik van lasverhoudings. Die geometrie van die toetsmonster is gebaseer op dié van die ASTM E466 standaard silindriese toetsmonster. Die lasverhoudings strek vanaf statiese trektoetse, R = +1/+1 tot statiese druktoetse, R = -1/-1. Vermoeidheidsverhoudings van R = +0.5, 0, -0.5, -1, -2, -∞ en +2 is gebruik. Agt monsters per lastoestand en vier lastoestande per lasverhouding is getoets om die spanningsleeftydkurwe (S-N kurwe) vir elke lasverhouding te bepaal.

Die Maksimum Hoofspanning is gebruik as basis vir hierdie lasverhoudings. Konstante-leeftyd kaarte is opgestel vir NBG18 met behulp van die logaritmiese krommepassingsvergelykings van die S-N kurwes. Die resultate vir die statiese sterkte vergelyk goed met die statiese sterkte wat deur die vervaardiger vir NBG18 gemeet is. Die enkel-as vermoeidheidsterkte van NBG18 is vir alle lasverhoudings beter as dié van V483T2, wat voorheen deur 'n ander navorser bepaal is. V483T2, wat ook deur SGL Carbon vervaardig word, was die Duitse industrie standaard materiaal vir hierdie toepassing.

'n Nuwe toetsmonster, genaamd S60B, en gepaardgaande hidroustatiese toetstoerusting is ontwerp en vervaardig vir die bepaling van die multi-as-belasting vermoeidheidseienskappe van NBG18 oor dieselfde lasverhoudingsbestek as vir die enkelastoetse. Die geometrie van hierdie toetsmonster benader dié van 'n hemisfeer. Die kenmerkende eienskappe van die nuwe toetsmonster is sy lae koste, lae koste van toerusting wat benodig word vir die belasting en sy relatiewe onsensiwiteit vir oriëntasie van die monster t.o.v. die greinrigting van die grafiet.

Soos vir die enkelas-belasting monsters is die Maksimum Hoofspanning gebruik as basis vir hierdie lasverhoudings. Konstante-leeftyd kaarte is opgestel vir NBG18 met behulp van die

krommepassingsvergelykings van die S-N kurwes. Die statiese treksterkte vergelyk redelik met die vervaardiger se resultate. Die statiese druksterkte onder hierdie multi-as-belasting is egter baie hoër as verwag. Dit kan moontlik toegeskryf word aan interne wrywing wat deur die tangensiale hoofspannings opgestel word.

Daar is gevind dat die gemodifiseerde Maksimum Vervormingsenergie spanning wat deur die KTA 3232 ontwerpkode as spanningsbasis gebruik word, nie die multi-as statiese faling van die S60B toetsmonster, wat uit NBG18 grafiet vervaardig is, bevredigend voorspel nie.

Die moontlike skadelike effek van laedruk (10 MPa) isostatiese belasting op die grafiet is te klein om dit onteenseglik te bewys. 'n Afname van minder as 3% in statiese – sowel as vermoeidheidsterkte by 100 siklusse is gemeet.

Met hierdie navorsing is die vermoë geskep om enkel-as en multi-as vermoeidheidstoetse op grafiet in Suid-Afrika te doen. Die tegnologie is gevestig by die Nelson Mandela Metropolitan University in Port Elizabeth en die Noordwes-Universiteit in Potchefstroom respektiewelik.

ACKNOWLEDGEMENTS

This dissertation is dedicated to the memory of my parents, Marthinus Johannes Roberts and Hester Cecilia Roberts.

I would like to thank the following:

PBMR (Pty) Ltd with specific reference to Mark Mitchell and Shahed Fazluddin, for placing the Graphite Fatigue research contract on the North-West University, which enabled this effort.

Prof. Johan Markgraaff, my promoter, for his valuable inputs.

Prof. Danie Hattingh, Dr Annelize Els-Botes, William Rall and Gideon Gouws from the Automotive Components Test Centre at Nelson Mandela Metropolitan University, who performed the uniaxial fatigue tests for me.

Janik Bessinger, Leon Malan, Renier Markgraaff, Gustav, Martin and Carien Roberts. These are the students, who suffered with me, during university holidays, often through Potchefstroom's chilly winter nights, to do the experimental work on the multiaxial specimens.

Danie Vorster of the Centre for Advanced Manufacturing, Pieter Erasmus of the Instrument Makers and their teams of talented artisans, who manufactured or modified components on this project.

Dennis Naude, who wrote the Labview program for the control and main data acquisition of the multiaxial fatigue test rig.

Jorina le Roux, for all her administrative work on this project.

My wife, Oba and children for all their support, encouragement and love, through a very busy time in our lives.

God, for sparing my life and granting me health and intellect to unravel some minute details of his awesome creation.

TABLE OF CONTENTS

Abstract i
Uittreksel iii
Acknowledgements v
Table of Contents vi
List of Figures x
List of Tables xvii
Nomenclature xviii

Chapter 1
Introduction 1-1
1.1 Background 1-1
1.2 Problem Statement 1-3

Chapter 2
Literature Survey 2-1
2.1 Introduction 2-1
2.2 Test Standards 2-2
2.2.1 Metallic Fatigue Tests 2-2
2.2.2 Graphite Tensile Tests 2-4
2.3 Multiaxial Tests 2-5
2.3.1 Metallic Materials 2-5
2.3.2 Graphite 2-9
2.4 Mohr-Circle Stress Excursions 2-17
2.5 Aim of the Study 2-19
2.6 Research Constraints 2-20
2.7 Closing Remarks 2-21

Chapter 3
Specimen Sampling Plan 3-1
3.1 Introduction 3-1
3.2 Graphite Blocks 3-1
3.3 Sampling Lay-out 3-2
3.4 Specimen Serial Numbers 3-4

3.5 Summary and Conclusions 3-5

Chapter 4

Uniaxial Fatigue Tests 4-1

4.1 Introduction 4-1

4.2 Alignment 4-1

4.3 General Fatigue Design Requirements 4-4

4.4 KTA 3232 Design Rule and Developed MDE Stress 4-4

4.5 Uniaxial Fatigue Test Design 4-7

4.5.1 Selection of Geometry 4-7

4.5.2 Clamping Force 4-11

4.5.3 Risk Abatement Tests 4-12

4.5.4 Modification of Test Equipment 4-14

4.6 Experimental Work 4-16

4.6.1 Machining Requirements 4-16

4.6.2 Condition of Specimens 4-17

4.6.3 Fatigue Testing Machine 4-20

4.6.4 Strain Calibration and Test Procedure 4-20

4.6.4.1 Introduction 4-20

4.6.4.2 Strain Calibration 4-21

4.6.4.3 Test Procedure 4-22

4.7 Uniaxial Results 4-23

4.7.1 Mechanical Properties from Static Tests, R = 1 4-23

4.7.2 Tabular Presentation 4-23

4.7.3 Graphical Presentation – S-N Diagrams 4-23

4.7.4 Combined S-N Diagrams 4-28

4.7.5 Constant-Life Diagrams 4-30

4.7.6 Stress versus Strain (Hysteresis Loops) 4-32

4.7.7 Modulus of Elasticity 4-37

4.7.8 Run-Out Specimens 4-42

4.7.9 Fracture Position 4-42

4.8 Discussion 4-42

4.8.1 Fatigue Test Design 4-42

4.8.2 Absolute Values of Static Strength 4-43

4.8.3 S-N Diagrams 4-44

4.8.4 Relative Fatigue Strength 4-44

4.8.5 Hysteresis Loops 4-45
4.8.6 Run-Out Specimens 4-45
4.8.7 Modulus of Elasticity 4-46
4.8.8 Constant-Life Diagram 4-46
4.9 Summary and Conclusions 4-47

Chapter 5

Multiaxial Fatigue Tests 5-1
5.1 Introduction 5-1
5.2 Specimen Design 5-1
5.2.1 Existing Geometries 5-1
5.2.2 Specific Design Requirements 5-2
5.2.3 Analysis Methodology 5-4
5.2.3.1 Description of Methodology 5-4
5.2.3.2 Governing Equations for Basic Geometry 5-5
5.2.3.3 Stress Distribution in Gauge Section 5-7
5.2.4 Design for Stress Distribution 5-10
5.2.5 Failure Zone Verification 5-20
5.2.6 Summary 5-24
5.3 Developed MDE Stress 5-26
5.4 Fatigue Testing Equipment 5-27
5.5 Machining Requirements 5-30
5.6 Condition of Specimens 5-31
5.7 Calibration 5-34
5.7.1 Load Measurement System 5-34
5.7.2 Strain Measurement System 5-35
5.8 Test Procedure 5-37
5.8.1 Isostatic Loading 5-37
5.8.2 Fatigue Testing 5-38
5.9 Multiaxial Results 5-39
5.9.1 Mechanical Properties From Static Tests, R = 1 5-39
5.9.2 Tabular Presentation 5-40
5.9.3 Graphical Presentation – S-N Diagrams 5-40
5.9.4 Combined S-N Diagrams 5-45
5.9.5 Constant-Life Diagrams 5-47
5.9.6 Verification of Equality of Tangential Strains 5-50

5.9.7 Stress versus Strain (Hysteresis Loops) 5-51
5.9.8 Fracture Position 5-60
5.10 Discussion 5-62
5.10.1 Multiaxial Fatigue Test Design 5-62
5.10.2 Absolute Values of Static Strength 5-62
5.10.3 S-N Diagrams 5-64
5.10.4 Relative Fatigue Strength 5-65
5.10.5 Hysteresis Loops 5-66
5.11 Summary And Conclusions 5-67

Chapter 6

Comparison Of Uniaxial And Multiaxial Fatigue Characteristics 6-1
6.1 Introduction 6-1
6.2 Static Strength 6-1
6.3 Stress-Strain Characteristics 6-3
6.4 Constant-Life Charts 6-6
6.4.1 Maximum Principal Stress 6-7
6.4.2 Volume Weighted Maximum Principal Stress 6-7
6.4.3 Maximum MDE Stress 6-8
6.4.4 Volume Weighted MDE Stress 6-9
6.5 Fatigue Strength Factors 6-13
6.6 Conclusions 6-15
6.6.1 Static Strength 6-15
6.6.2 Stress-Strain Characteristics 6-16
6.6.3 S-N Diagrams 6-16
6.6.4 Constant-Life Charts 6-17
6.6.5 Fatigue Strength Factors 6-17

Chapter 7

Conclusions 7-1
7.1 Uniaxial Fatigue Tests 7-1
7.2 Multiaxial Fatigue Tests 7-1
7.3 Pretest Isostatic Exposed Specimen Exploration 7-2
7.4 Proposals for Further Research 7-2

References R1

LIST OF FIGURES

Figure 1-1: Proposed Layout of the PBMR High Temperature Gas Cooled Nuclear Reactor (Courtesy of PBMR) 1-1

Figure 1-2: Lower Part of Graphite Core Structures of PBMR Reactor (Courtesy of PBMR) 1-4

Figure 2-1: Scaled Comparison of Existing Test Specimens 2-7

Figure 2-2: Load Ranges of Graphite Fatigue Tests 2-20

Figure 3-1: Specimen Orientation In Block A 3-2

Figure 3-2: Specimen Orientation In Block B 3-3

Figure 4-1: Shear Forces and Bending Moments Induced in Uniform Column by Misalignment 4-3

Figure 4-2: Stress State in Uniaxial Specimen 4-6

Figure 4-3: (A) Maximum Principal Stress Excursion for R = -1, (B) Related MDE Stress Excursion, (C) Developed MDE Stress Excursion 4-7

Figure 4-4: Full Section Scaled Comparison of All Test Specimens 4-8

Figure 4-5: S70 Uniaxial Fatigue Specimens Machined from RFS Grade Graphite 4-11

Figure 4-6: Von Mises Stress Distribution in Collet Clamped Quarter Section of S70 Uniaxial Specimen under Full Tensile Load 4-12

Figure 4-7: Simple Compression Test Setup to Assess Gripping Force 4-13

Figure 4-8: Collet Clamping Footprint on Test Piece 4-14

Figure 4-9: Full Section of Uniaxial Fatigue Specimen Grip Assembly 4-15

Figure 4-10: Instron 8801 With Collet Grips, Anti-Rotation Bar and Strain Gauged S70 Specimen 4-16

Figure 4-11: Typical No Clamping Zone of S70 Specimen 4-17

Figure 4-12: Geometric Measurement of S70 Specimen 4-18

Figure 4-13: Weighing of S70 Specimen 4-18

Figure 4-14: Typical S70 Fatigue Specimen from NBG18 graphite 4-19

Figure 4-15: Definition of Parameters and Results of Bow Calculation 4-20

Figure 4-16: Example of Gauged Sample 4-21

Figure 4-17: Wheatstone Bridge Configuration 4-22

Figure 4-18: S-N Diagram for R = +0.5 Uniaxial Fatigue 4-24

Figure 4-19: S-N Diagram for R = 0 Uniaxial Fatigue 4-24

Figure 4-20: S-N Diagram for R = -0.5 Uniaxial Fatigue 4-25

Figure 4-21: S-N Diagram for R = -1 Uniaxial Fatigue 4-25

Figure 4-22: S-N Diagram for R = -2 Uniaxial Fatigue 4-26

Figure 4-23: S-N Diagram for R = -∞ Uniaxial Fatigue 4-26

Figure 4-24: S-N Diagram for R = +2 Uniaxial Fatigue 4-27

Figure 4-25: Combined S-N Diagram for Tension Dominant R-values, Uniaxial Fatigue ... 4-28

Figure 4-26: Combined S-N Diagram for Compression Dominant R-values, Uniaxial Fatigue 4-29

Figure 4-27: Combined S-N Diagram for All R-values, Uniaxial Fatigue 4-29

Figure 4-28: Constant-Life Chart Based on Maximum Principal Stress in Uniaxial Loading .. 4-30

Figure 4-29: Constant-life Chart - Maximum & Minimum Stress 4-31

Figure 4-30: Constant-Life Chart Based on MDE Stress in Uniaxial Loading 4-32

Figure 4-31: Stress Versus Strain for R = +1/+1 (Tensile Test) 4-33

Figure 4-32: Stress Versus Strain (Hysteresis Loop) as Function of Life for R = +0.5 4-33

Figure 4-33: Stress Versus Strain (Hysteresis Loop) as Function of Life for R = 0 4-34

Figure 4-34: Stress Versus Strain (Hysteresis Loop) as Function of Life for R = -0.5 4-34

Figure 4-35: Stress Versus Strain (Hysteresis Loop) as Function of Life for R = -1 4-35

Figure 4-36: Stress Versus Strain (Hysteresis Loop) as Function of Life for R = -2 4-35

Figure 4-37: Stress Versus Strain (Hysteresis Loop) as Function of Life for R = -∞ 4-36

Figure 4-38: Stress Versus Strain (Hysteresis Loop) as Function of Life for R = +2 4-36

Figure 4-39: Stress Versus Strain for R = -1/-1 (Compression Test) 4-37

Figure 4-40: Best Fit Quadratic Equation of Tensile Loading - First Cycle 4-38

Figure 4-41: Best Fit Quadratic Equation of Compressive Loading - First Cycle 4-39

Figure 4-42: Constant-Life Diagram Comparison Based on Maximum Principal Stress 4-47

Figure 5-1: Full Section Showing Alignment Axes of Spherical Specimen with Grain Direction to Yield Lowest Strength 5-3

Figure 5-2: Full Section Showing Alignment Axes of Specimen S9 with Grain Direction to Yield Lowest Strength 5-4

Figure 5-3: Logic Diagram Illustrating Design Methodology For Multiaxial Specimen 5-5

Figure 5-4: General Equations for Stresses in a Thick-walled Cylinder 5-5

Figure 5-5: General Equations for Stresses in a Thick-walled Sphere 5-6

Figure 5-6: Ideal Theoretical Stress Distribution through Gauge Section Wall - Tension 5-9

Figure 5-7: Ideal Theoretical Stress Distribution through Gauge Section Wall – Compression 5-10

Figure 5-8: Stress Distribution in Specimen S9 Subject to Internal Pressurization Only 5-11

Figure 5-9: Sequential Development of the Multiaxial Fatigue Specimen Geometry 5-12

Figure 5-10: Maximum Principal Stress Contours during Sequential Development of the Specimen - Tensile Loading (Internal Pressurization). 5-13

Figure 5-11: Von Mises Stress Distribution in Internally Pressurized Specimen S60A 5-14

Figure 5-12: Full Section Showing 90° Alignment Cone of Specimen S60B with Grain Direction to Yield Lowest Strength 5-15

Figure 5-13: Von Mises Stress Distribution in Internally Pressurized Specimen S60B (MDE and Von Mises Stresses Shown For Specific Nodes) 5-16

Figure 5-14: Von Mises Stress Distribution in Externally Pressurized Specimen S60B (MDE and Von Mises Stresses Shown For Specific Nodes) 5-16

Figure 5-15: Maximum Principal Stress Distribution for 10 MPa Internal Pressure..... 5-17

Figure 5-16: Minimum Principal Stress Distribution for 10 MPa Internal Pressure..... 5-17

Figure 5-17: Maximum Principal Stress Distribution for 35 MPa External Pressure 5-18

Figure 5-18: Minimum Principal Stress Distribution for 35 MPa External Pressure 5-18

Figure 5-19: MDE Stress Distribution for Internal Pressurization (Tension)..... 5-19

Figure 5-20: MDE Stress Distribution for External Pressurization (Compression) 5-19

Figure 5-21: Full Section Model of S60B Specimen in Hydraulic Test Chamber 5-20

Figure 5-22: Failure Probability of S60B in Tension 5-22

Figure 5-23: Failure Probability of S60B in Compression..... 5-22

Figure 5-24: Compression (Left) and Tensile (Right) Failure Zone of Specimen S60B in RFS Grade Graphite..... 5-23

Figure 5-25: Full Section of Graphite Part of S60B Specimen, Showing Nominal Geometry. 5-25

Figure 5-26: Tensile Stress State at Inner Wall of Multiaxial Specimen..... 5-26

Figure 5-27: Tensile Stress State at Outer Wall of Multiaxial Specimen..... 5-26

Figure 5-28: Compressive Stress State at Inner Wall of Multiaxial Specimen 5-26

Figure 5-29: Compressive Stress State at Outer Wall of Multiaxial Specimen..... 5-26

Figure 5-30: Maximum Principal Stress Excursion for R = -1, Related MDE Stress Excursion and Developed MDE Stress Excursion in Multiaxial Specimen 5-27

Figure 5-31: Subsystems and Relations of Multiaxial Fatigue Testing System 5-28

Figure 5-32: Multiaxial Fatigue Test System 5-29

Figure 5-33: Isostatic Test Chamber Being Pressurized 5-30

Figure 5-34: Typical No Clamping Zone of S60B Specimen 5-31

Figure 5-35: Wall Thickness Measurement of S60B Specimen 5-32

Figure 5-36: Sensitivity Analysis of Geometry of S60B Specimen 5-33

Figure 5-37: Drying of Graphite Specimens after Washing 5-34

Figure 5-38: Bonding of Graphite Specimen to Base Plate 5-34

Figure 5-39: Volumetric Dispensing of Two Parts of Epoxy 5-34

Figure 5-40: Example of Gauged Sample 5-36

Figure 5-41: Wheatstone Bridge Configuration 5-36

Figure 5-42: Pressure Profile of Isostatic Loading 5-38

Figure 5-43: S-N Diagram for R = +0.5, Multiaxial Fatigue 5-41

Figure 5-44: S-N Diagram for R = 0, Multiaxial Fatigue 5-41

Figure 5-45: S-N Diagram for R = 0.5, Multiaxial Fatigue 5-42

Figure 5-46: S-N Diagram for R = 1, Multiaxial Fatigue 5-42

Figure 5-47: S-N Diagram for PIE R = 1, Multiaxial Fatigue 5-43

Figure 5-48: S-N Diagram for R = -2, Multiaxial Fatigue 5-43

Figure 5-49: S-N Diagram for R = $-\infty$, Multiaxial Fatigue 5-44

Figure 5-50: S-N Diagram for R = +2, Multiaxial Fatigue 5-45

Figure 5-51: Combined S-N Diagram for Tension Dominant R-values, Multiaxial Fatigue. 5-46

Figure 5-52: Combined S-N Diagram for Compression Dominant R-values, Multiaxial Fatigue 5-46

Figure 5-53: Combined S-N Diagram for All R-values, Multiaxial Fatigue 5-47

Figure 5-54: Constant-Life Chart for Maximum Principal Stress 5-48

Figure 5-55: Constant-Life Chart for Volume Weighted Maximum Principal Stress 5-49

Figure 5-56: Constant-Life Chart for Maximum MDE Stress 5-49

Figure 5-57: Constant-Life Chart for Volume Weighted MDE Stress 5-50

Figure 5-58: Verification of Equality of Tangential Strains 5-51

Figure 5-59: Stress Versus Strain for R = +1/+1 (Tensile Test) 5-52

Figure 5-60: Stress Versus Strain (Hysteresis Loop) as Function of Life for R = +0.5 5-53

Figure 5-61: Stress Versus Strain (Hysteresis Loop) as Function of Life for R = 0 5-54

Figure 5-62: Stress Versus Strain (Hysteresis Loop) as Function of Life for R = -0.5 5-55

Figure 5-63: Stress Versus Strain (Hysteresis Loop) as Function of Life for R = -1 5-56

Figure 5-64: Stress Versus Strain (Hysteresis Loop) as Function of Life for R = -2 5-57

Figure 5-65: Stress Versus Strain (Hysteresis Loop) as Function of Life for R = -∞ 5-58

Figure 5-66: Stress Versus Strain (Hysteresis Loop) as Function of Life for R = +2 5-59

Figure 5-67: Stress Versus Strain for R = -1/-1 (Compression Test) 5-60

Figure 5-68: Typical O-Type Fracture of 37 A2-10 5-61

Figure 5-69: Typical H-Type Fracture of 79 I-1 5-61

Figure 5-70: Typical D-Type Fracture of 79 K-1 5-61

Figure 5-71: Typical E-Type Fracture of 79 I-9 5-61

Figure 5-72: Typical O-Type Fracture in Compression of 37 C-10 5-61

Figure 5-73: Comparison of Physical Stress Excursions of Load Ratios Near 85% Static Strength 5-66

Figure 6-1: Graphical Comparison of Static Test Results (R = 1) 6-2

Figure 6-2: Stress-Strain Comparison in Tension 6-3

Figure 6-3: Stress-Strain Comparison in Compression 6-4

Figure 6-4: Comparison of Constant Life Charts - Uniaxial and Multiaxial Stress Based on Maximum Principal Stress 6-7

Figure 6-5: Comparison of Constant-Life Charts - Uniaxial and Multiaxial Stress Based on Volume Weighted Maximum Principal Stress 6-8

Figure 6-6: Comparison of Constant Life Charts - Uniaxial and Multiaxial Stress Based on Maximum MDE Stress 6-9

Figure 6-7: Comparison of Constant Life Charts - Uniaxial and Multiaxial Stress Based on Volume Weighted MDE Stress 6-10

Figure 6-8: Comparison of Constant Life Charts - Uniaxial and Multiaxial Stress Based on Volume Weighted MDE Stress with Modified Poisson Ratios 6-11

Figure 6-9: Comparison of Constant Life Charts - Uniaxial and Multiaxial Stress Based on Volume Weighted MDE Stress with Arbitrary Shape Factor 6-13

Figure 6-10: Uniaxial Fatigue Strength Factors 6-14

Figure 6-11: Multiaxial Fatigue Strength Factors 6-14

Figure 6-12: Fully Reversed Maximum Principal Stress Fatigue Life Comparison 6-15

LIST OF TABLES

Table 3-1 : Allocation of Specimens to Load Ratios 3-4

Table 4-1: Summary of Relative Cost, Type of Test and Type of Test Equipment 4-10

Table 4-2: Fracture Loads and Strengths of Specimens that Ran Out 4-42

Table 4-3: Comparison of Median Strengths of Blocks 4-44

Table 5-1: Calculated Theoretical Stresses in a Sphere 5-7

Table 5-2: Summary of Static Strength of Multiaxial Specimens 5-40

NOMENCLATURE

A	Area
AISI	American Institute of Steel Industries
B	Bending Moment
CS	Core Structures
CUD	Core Unloading Device
d	Diameter
DSP	Digital Signal Processing
E	Modulus of Elasticity or Young's Modulus
EES	Engineering Equation Solver
EFFGD	Equivalent Fission Fluence of Graphite Damage
EMI	Electromagnetic Induced Interference
Eq.	Equation
Equiv.	Equivalent
F	Force
f	Stength Ratio Factor, (UTS/UCS)
FEA	Finite Element Analysis
G	Strain Gauge Factor
HIP	Hot Isostatic Pressing
HTR	High Temperature Gas Cooled Nuclear Reactor
KIC	Critical Stress Intensity in Mode I Fracture
ℓ	Length
Lc	Probability of Survival
LVDT	Linear Voltage Differential Transformer
m	Weibull Shape Factor
MDE	Modified Maximum Deformation Strain Energy
N	Number of Cycles
NWU	North-West University
P	Pressure
p	Pressure
P_A	Internal Pressure on S60B Specimen
P_B	External Pressure on S60B Specimen
PBMR	Pebble Bed Modular Reactor
PF	Probability of Failure

PIA	Principle of Independent Action
PIE	Pretest Isostatic Exposed
pt	Point
R	Load or Stress Ratio
r	Radius
RCS	Reactivity Control System
RH	Relative Humidity
RPV	Reactor Pressure Vessel
RSS	Reserve Shutdown System
RVDT	Rotary Variable Differential Transformer
S	Strength
SAE	Society of Automotive Engineers
Sc	Weibull Characteristic Strength
SF	Shape Factor
SMiRT	Structural Mechanics in Reactor Technology
T	Torque
TBDL	To Be Determined Later
UCS	Ultimate Compressive Strength
UTS	Ultimate Tensile Strength
VMDE	Volume Weighted MDE
α	Angular Misalignment Angle
γ	Torsion angle
ε	Strain
ε	Parallel Misalignment Distance
μ	Coefficient of Friction
μm	Micron
$\mu\varepsilon$	Microstrain
σ	Normal Stress
$\sigma 1$	Largest Principal Stress
$\sigma 2$	Intermediate Principal Stress
$\sigma 3$	Smallest Principal Stress
τ	Shear Stress
υ	Poisson ratio
Ω	Electrical Resistance Unit, Ohm

∞	Infinite
1σ	One Standard Deviation

Subscript

a	Amplitude
i	Inner / Inside
i	Index Number
ℓ	Longitudinal
m	Midrange
o	Outer / Outside
r	Radial
t	Tangential
uc	Ultimate Compressive
ut	Ultimate Tensile
x	Axial
υ	MDE

Chapter 1

INTRODUCTION

1.1 BACKGROUND

The Pebble Bed Modular Reactor (PBMR), a High Temperature Gas Cooled Reactor, makes use of spherical fuel elements that are randomly arranged within a cavity defined by the graphite core internal structures. The design of these structures and the parts these comprise are critical to the successful deployment of the reactor. Venter (2005) presented the design of the PBMR core structures at the 18th International Conference on Structural Mechanics in Reactor Technology (SMiRT).

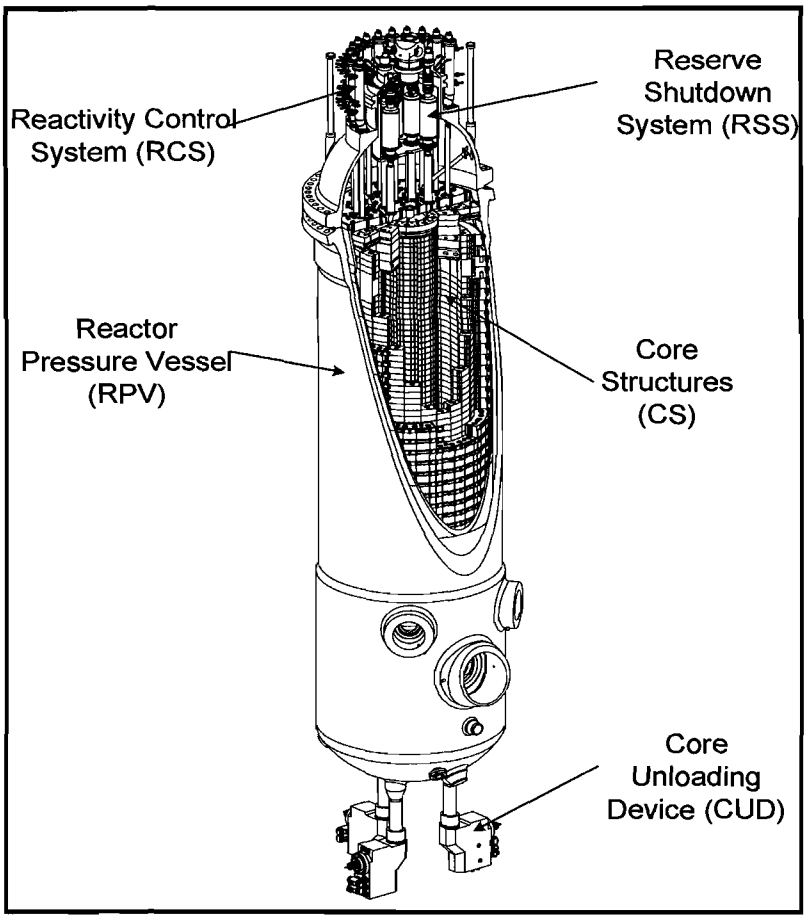


Figure 1-1: Proposed Layout of the PBMR High Temperature Gas Cooled Nuclear Reactor (Courtesy of PBMR)

Graphite is used for the core structures in high temperature gas cooled nuclear reactors (HTR) to perform a few critical functions. These include providing structural stability for the bores of the reactivity control systems inside the side reflectors, the riser channels of the

helium streams, the cold – and hot gas chambers and the bores of the reserve shut down systems in the central reflector. Furthermore, the reflectors define the cavity that houses the fuel.

A second set of functions is to act as a neutron reflector shield against radiation and to provide the steel pressure boundary with a shield against heating (Burchell *et al.*, 2006). The proposed layout of the PBMR is shown in Figure 1-1.

At the typical temperatures inside a HTR, irradiation causes the graphite to first shrink and then to swell over the lifetime of the reactor. The fast neutrons cause this damage to the graphite. Fast neutrons are slowed down from the core towards the non-generating regions. Mitchell, (2005) showed that the fast flux is reduced by a factor of 2,5 for every 10 centimeter in the graphite reflector. The geometric change of the graphite due to irradiation, combined with the differential thermal expansion through the thickness of the core barrel, induce a large portion of the stresses that need to be accommodated by the design. Failure from stresses of this origin falls under the domain of static strength analysis.

The large cyclic stress in a HTR is caused by the reactor shutdown outages. This stress cycle is driven by differential thermal expansion between the cold condition and hot condition of the reactor. The number or cycles associated with this stress range is of the order of 50 during a 40 year design lifetime of such reactors. Failure from stresses of this origin falls under the domain of dynamic or fatigue strength analysis.

HTR based power plants, which are designed for electrical load following (i.e. variable output power plants), have another small fatigue cycle. This cycle is caused by the daily change in power and thus pressure distribution inside the reactor. The number or cycles associated with this stress range is of the order of 15000 during a 40 year design lifetime of such reactors.

An important activity in the licensing process of nuclear reactors is the compilation of the Safety Case. This is the document that needs to convince the Nuclear Regulator of a country to grant a license for the construction and operation of a nuclear facility because it is safe enough to do so under all reasonable conditions. An important part of the Safety Case is the strength analyses (both static and fatigue) of all critical components.

The allowable stress in the graphite is derived from materials tests of irradiated and unirradiated material and internationally accepted failure criteria. As from the 1960's, a lot of research was conducted on graphite for nuclear applications. This work led to the design

and construction of a number of HTRs across the world. However, only the static tests reached the maturity of international standards.

1.2 PROBLEM STATEMENT

The NBG18 graphite, selected for the design of the core structures of the reactor of the PBMR, is a new grade developed by the SGL Carbon Group in conjunction with PBMR. As part of the qualification effort for this material, the physical and mechanical properties are determined through material testing. This includes testing to determine the fatigue strength of the material. The uniaxial test is the simplest fatigue tests but also the most important, because it establishes a base for comparison of the NBG18 to other graphite grades. Because a local technology base in testing of graphite is of strategic and economic importance for South Africa, the first problem is to determine the uniaxial fatigue characteristics of NBG18 graphite in South Africa.

The second problem is to determine the multiaxial fatigue characteristics of NBG18 graphite in South Africa. The multiaxial loading conditions are of particular interest, since this is the most common loading state of the graphite core structures of the reactor. Figure 1-2 shows the bottom end of the PBMR reactor, with the outer liner (Inner and Outer Side Reflector) stripped down to below the V-shaped pebble exit funnels, called De-fuel Cones. The fixed inner liner or column is called the Centre Reflector. The fuel pebbles (balls), not shown in any of these figures, occupy the annular volume between the Inner Side – and Outer Centre Reflector.

The majority of bricks are subject to a radial compressive load due to the quasi-hydrostatic loading by the nuclear fuel pebbles, and an axial compressive load due to the weight of the stack of graphite bricks on top of it. Other loads include, pressure loading due to differential pressures, thermal strains due to differential thermal expansions, and differential shrinkage stresses due to gradients in dose and or irradiation temperature, i.e. differential shrinkage strains. These types of loads also induce tensile stresses in the bricks.

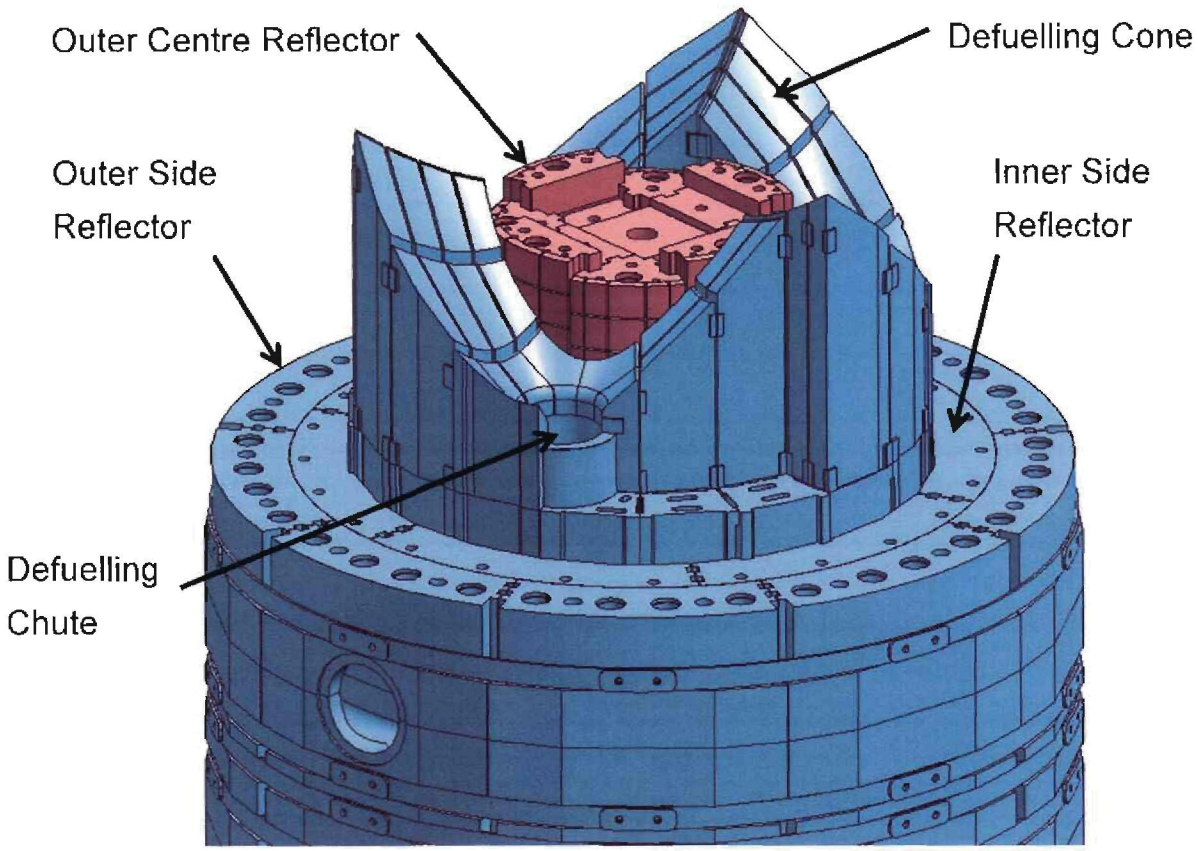


Figure 1-2: Lower Part of Graphite Core Structures of PBMR Reactor (Courtesy of PBMR)

The environmental state of the graphite, for which the fatigue characteristics are required, needs some attention at this stage. Ideally, it is required at the operating temperature of the reactor, which is around 900°C, and at different doses of fast neutron irradiation.

Chapter 2

LITERATURE SURVEY

2.1 INTRODUCTION

As a point of departure, a literature survey was conducted to find the various applicable materials testing standards and to find information on multiaxial fatigue test in general.

The aim of this survey was to establish the state-of-the-art in multiaxial testing in general, and then specifically in fatigue testing of graphite material. The focus was on experimental methodology, rather than the validation or generation of new failure criteria, which seemed to be topical of the majority of the publications.

Another objective was to point out any deficiencies in the published literature on experimental methodologies that need further research.

A number of publications revealed some experimental methodology. The geometry of the fatigue specimens and associated equipment to perform the tests, are critically evaluated in terms of accuracy of load measurement and Mohr-circle stress excursions.

The load ratio concept in fatigue loading, used throughout this research, is defined by Eq.(2.1) for convenience of the reader (Shigley *et al.*, 2004). The load ratio is per definition the ratio of minimum to maximum stress in the time domain stress waveform produced by the cyclic load.

$$R = \frac{\sigma_{min}}{\sigma_{max}} \qquad .....(2.1)$$

A common and important load ratio is R = -1. In this case, the minimum and maximum (valley and peak) value in the stress-time waveform has the same magnitude, but opposite sign. This is the well-known fully reversed stress cycle that has a stress amplitude equal to the maximum tensile and compressive stress and a midrange stress of zero.

2.2 TEST STANDARDS

Standards, applicable to graphite fatigue testing, were searched. None could be found. In this survey, three standards for static strength testing of graphite are discussed. All flexure tests were disregarded, since they could not assist in establishing a fatigue testing scheme for load ratios that were required. All compression tests were also disregarded since the most commonly used cylindrical specimen geometry is trivial.

This section is organized in relevant standards for metallic fatigue tests and graphite tensile tests.

2.2.1 Metallic Fatigue Tests

ASTM E466-96 (2002) specifies the methodology and requirements for fatigue testing of metallic materials. Two circular cross section specimen geometries and two rectangular cross section specimen geometries are supported by this specification. The geometry of a continuous radius section and a uniform gauge section is specified by this standard. This standard also establishes maximum allowable parasitic stress due to misalignment.

ASTM E1012-99 (2002) is used to verify the alignment of the grips during uniaxial static and fatigue testing. With this standard as baseline, the alignment verification checks are expanded to include checks in the compressive state as well. Alignment verification for a single test (Type T) or for the test apparatus (Type A) are prescribed with a choice between 3 methods. Method 2, employing 4 equally spaced strain gauges around the circumference of the gauge section, was selected for this research.

ASTM E468-90 (2002) specifies the requirements for presenting the tabulated results, S-N diagrams and constant-life diagrams. The main purpose of this specification is to minimize the possibility of misinterpretation or improper application of the fatigue results. The requirements of this specification are implemented except on comparisons of constant-life charts between uniaxial and multiaxial fatigue results. This is omitted intentionally to prevent swamping the figures with information that will distract the reader's focus off the main purpose of those comparisons.

ASTM E1823-96 (2002) defines the standard terminology relating to fatigue and fracture testing. All terms that are used in this research are defined in accordance with this specification.

ASTM E74-02 (2002) specifies the requirements for the calibration of load-measuring devices of testing machines. In the case of this research, it is used as guideline for the calibration of the pressure transducer channels (upper and lower chamber) of the hydrostatic loading device used in the multiaxial fatigue tests.

ASTM E1942-98 (2002) specifies the requirements for data acquisition systems used in fatigue testing. The data acquisition system of this research is designed to conform to this specification. Phase differences are completely eliminated by using a simultaneous sample-and-hold Digital Signal Processing (DSP) card for data capture. The data rates exceed the 400 x f requirement set for the capture of triangular waveforms, while in the case of most load ratios, the forcing function is sinusoidal, requiring only a 50 x f data rate. Although the noise level of the data acquisition system was not measured, all the necessary precautions are taken to avoid EMI induced noise in the data signals. All instrument cables are shielded and grounded according to best practice.

ASTM E1049-85 (2002) defines various standard practices for cycle counting in fatigue analysis. The basic source of these fatigue excursions are dynamic inputs from measurements on complex structures. Although the various counting methods were studied, none is deemed suitable for use in the fatigue testing of graphite. There are two reasons for this statement.

The first is that the measurement excursion is a function of the dynamic bandwidth of the measuring equipment. This means that if the measuring equipment has a low bandwidth, the high frequency excursions that may be superimposed on the low frequency signal is filtered out and vice versa. In the present research, no filtering is applied to the signals and high bandwidth (more than 1 kHz) measuring devices are used. The hydraulic system resonance, which is two orders of magnitude larger in frequency than the forcing frequency, can theoretically be filtered out, if low pass filters are employed.

The second reason is related to how fracture during the first excursion is counted. For the load ratios that are investigated in this research, it is generally agreed that 100 cycles without failure at R = 0 should have the same count base as 100 cycles at R = -1. The only counting method that will yield that is the Rainflow counting method. The problem comes in when the specimen fractures during the first excursion. For tensile (R = +0.5 and 0) or compressive load ratios (R = +2 and $-\infty$), the Rainflow counting method will yield a count of 1 per complete cycle and 1 where the specimen fractures at the peak value (which is always the case). However, for load ratios that are both tensile and compressive (R = -0.5, -1 and -2), it will yield a count of 1 during the first excursion with fracture if the load path is first to the non-

governing stress state but it will yield a count of 0 if the load path is first to the governing stress state.

In order to maintain the essence of the S-N diagram and to preserve a common count base for all load ratios, failure during the first excursion cycle (irrespective of the direction of the load path) is counted as 1 in this research.

2.2.2 Graphite Tensile Tests

Specimen S14 in Figure 2-1 represents the standard geometry of the static tensile strength testing of graphite according to ASTM C565-93 (2005). It is applicable to graphite with grain size smaller than 0,79 mm. This standard is used for quality control testing where the emphasis is on mean values rather than variances. It is cheaper to conduct than tensile tests according to ASTM C749. The specimen is a continuous radius specimen. The gripping devices are stainless steel split halve cavities that enclose the head of the specimen and is locked by a stainless steel ring. The grips are connected to the testing machine via eyebolts and chains. Large emphasis is placed on the alignment of the load train and non-transference of bending moments via the chains.

Specimen S15 in Figure 2-1 represents the standard geometry for the dumbbell (continuous radius) shaped specimen of the static tensile strength testing of graphite according to DIN 51914: 1985-04 (1985). This standard also provides for a cylindrical shape that is bonded to metal end-pieces. The latter is seldom used due to the complexity of aligning the 3 parts of the assembly, and the risk of bond failures. This standard is restricted to room temperature tests in air and prescribes five specimens unless stated otherwise. The maximum load rate is specified as no sooner than 30s after commencement of load.

Specimen S16 in Figure 2-1 represents the standard geometry of the static tensile strength testing of graphite according to ASTM C749-92 (2005). It is applicable to graphite with grain size from 0.0254 mm to larger than 6.4 mm. This standard is used for generating quality engineering data at room temperature or at elevated temperature, where the emphasis is on high quality mean values and variances. The specimen is a uniform section specimen. The gripping devices are split halve shouldered sleeves that enclose the head of the specimen and is locked by a grip sleeve. The grips are connected to the testing machine via pinned grip attachment yokes, split halve chain journals and a minimum of 4 links precision chains. As for ASTM C565, large emphasis is placed on the alignment of the load train and non-transference of bending moments via the chains. According to this standard, the gauge

diameter should be a minimum of 3 to 5 times the maximum grain size of the graphite under test. It also specifies how out-of-gauge fractures are treated.

The most important conclusion from a study of the test standards is that the alignment of the specimen to the applied load in the testing machine is of utmost importance for high quality test results.

2.3 MULTIAXIAL TESTS

The first seven specimens on the left-hand side in Figure 2-1 were tests of metallic materials. The applicable results of the published research articles pertaining to the metallic specimens are summarised in Section 2.3.1. The remaining specimens in this figure were tests of graphite materials. The applicable results of the published research articles pertaining to the graphite specimens are summarised in Section 2.3.2.

2.3.1 Metallic Materials

Socie *et al.* (1985) investigated the biaxial fatigue of Inconel 718 under high strain conditions. This research included the effect of mean stress on the fatigue characteristics of the material. The strains were calculated from Linear Voltage Differential Transformer (LVDT) and Rotary Variable Differential Transformer (RVDT) measurements of the axial and rotational deflections respectively. The reason for putting the extensometers inside the specimen was easy access of the outer surface to take acetyl cellulose firm replicas of the surface topography to determine the size of small cracks. The biaxial specimen that was used is shown as S1 in Figure 2-1. Two samples per load were tested on a modified MTS Model 809, under strain control. The specimen was loaded in the axial direction, in a torsional mode and in a combined torsion/axial mode to a maximum strain ratio, γ/ε = 1,732 with load ratios R = -1 and R = 0. The maximum torsional stress on the outer surface of the gauge section was determined by extrapolation of the stress-strain curve (hysteresis curve) that was measured on the inner surface, where the extensometers were attached. The crack directions along maximum shear planes were demonstrated beautifully. The test equipment comprised axial and torsional servo-hydraulic actuators.

McDiarmid (1985) investigated fatigue under out-of-phase biaxial stresses of different frequencies on EN24 steel, heat treated to the T-condition. A 250 kN Schenck fatigue testing machine was used in conjunction with a 35 MPa high pressure hydraulic pump. The

actuators of the testing equipment were thus axial and hydrostatic servo-hydraulic actuators. These were load controlled tests at a maximum frequency of 30 Hz. The biaxial specimen that was used is shown as S2 in Figure 2-1. A pressure test cell was used, using an O-ring seal to allow relative displacement between the drawbar of the specimen and the pressure cell. The magnitude of error that could be induced to the axial load measurement by the frictional force (which is proportional to the cell pressure) was not discussed. The tests comprised fully reversed cycles of hoop stress and axial stress in different ratios of frequencies and employing different phase angles. Failure was defined as a detectable leak from the pressure cell. This was caused by 3 mm long cracks that could barely be seen by the naked eye. Stress amplitudes were of the order of 300 to 400 MPa. In the theoretical analysis, a rainflow counting technique was used to count the various fatigue cycles and Miner's rule was used to assess the relative damage. No mention was made about the assumptions regarding hoop stress, but it is assumed that a uniform stress, as calculated from thin-walled theory, was used as the tangential stress component. No mention was made of how the axial and pressure measurements were uncoupled during the tests.

Fash *et al.* (1985) investigated high strain fatigue life estimates for a simple notched component under biaxial loading. The latter component was the SAE notched specimen, designated S3 in Figure 2-1. The simple test equipment comprised 2 linear servo-hydraulic actuators and the test was conducted under load control. The test material was AISI 1045, in its hot rolled (HR) state. Only one specimen was tested in the majority of the cases. The ratio of torque to bending moment in the notch radius of the specimen was varied during these tests. The ratios tested were 0, 0.7, 0.9, 1.4, 1.9, 2.8, 3.7 and ∞. The strains associated with the loads were determined using a FEA program, utilizing an elastic-plastic stress-strain model. The FEA resulted in shear and normal strains on all faces of the strain element. Fatigue life estimates were done for the notched tests and for data of earlier specimen S1 tests, as published by Socie *et al.* (1989). The Maximum Principal Strain, the Effective Strain, the Maximum Shear Strain, the Lohr-Ellison Parameter and the Kandil-Brown-Miller Parameter were used as failure criteria. Although it was not mentioned, it was assumed that the bending moment and torque loads were in phase for all tests.

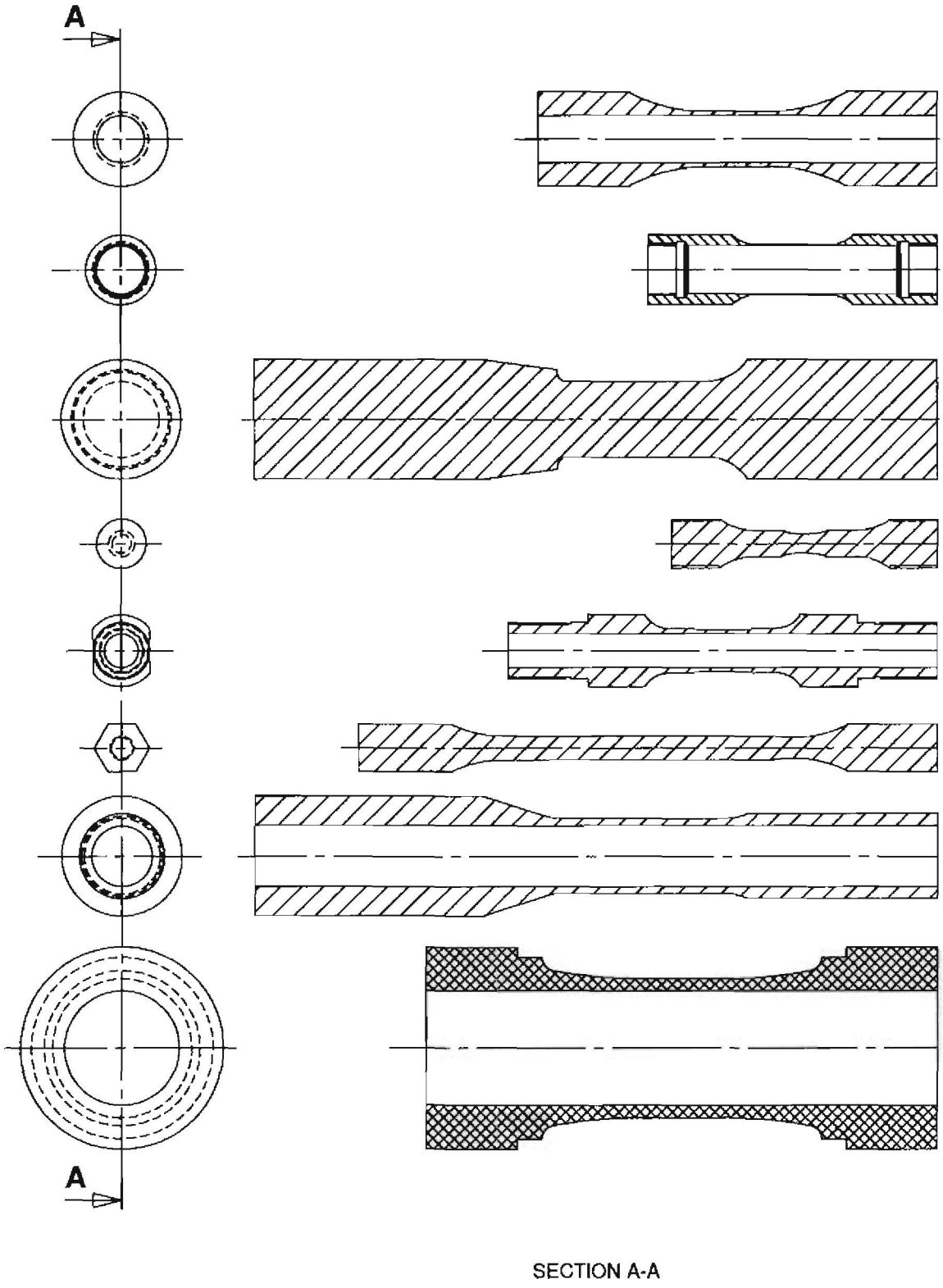
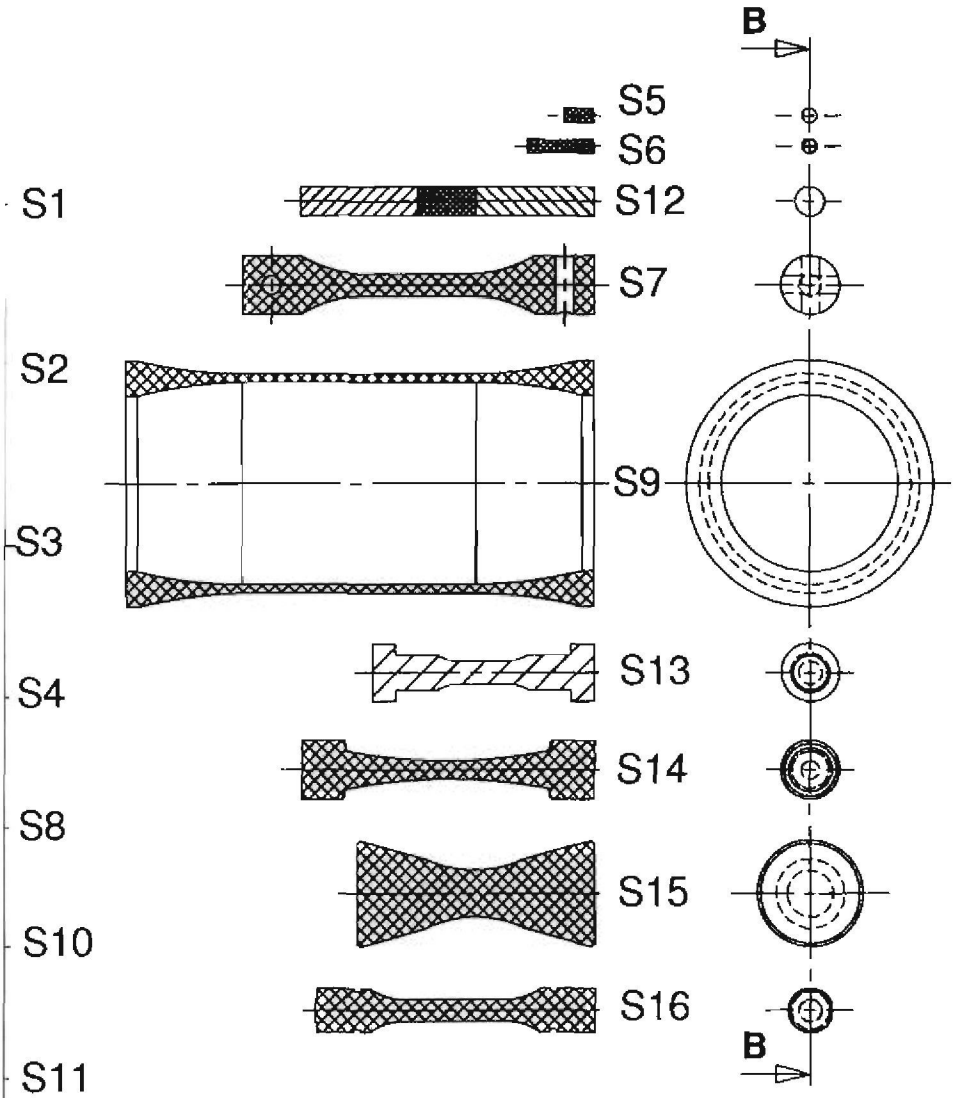


Figure 2-1: Scaled Comparison of Existing Test Specimens



SECTION B-B

Sonsino and Grubisic (1985) investigated the fatigue behaviour of cyclically softening - and hardening steels under multiaxial elastic-plastic deformation. Cyclically softening high-strength steel 30Cr-Ni-Mo 8 (equiv. AISI 4340) and cyclically hardening stainless steel X 10Cr-Ni-Ti 18 9 (equiv. AISI 321) were tested. A minimum of 3 specimens, designated S4 in Figure 2-1, per load setting were tested in axial, torsional and combined strain control at an amplitude ratio of γ/ε = 1,732 and a frequency of 1 Hz. Phase angles between 0° and 180° were used in fully reversed excursions (R = -1). The test equipment consisted of a 100 kN axial and a 25 kN torsional servo-hydraulic actuator. Strains measured by extensometers were calibrated to strain gauges that were bonded onto the specimen.

Found *et al.* (1985) investigated the requirements of a new multiaxial fatigue testing facility and presented a suitable specimen design. The new multiaxial fatigue testing facility comprises a Schenck 4 column tension-torsion testing machine with a load capability of ± 400 kN and ± 1 kNm combined with a hydraulic pressure system consisting of two servo-hydraulic actuators driving hydraulic intensifiers. The pressure capability of this equipment is 1700 bar. Cross-coupling between external pressure to specimen and axial load is handled by a pressure feedback loop in the axial load controller. The fatigue testing machine can load a thin-walled tubular specimen, designated S8 in Figure 2-1, independently in axial tension, torsion and tangential (hoop stress) modes. Two concerns with this machine are firstly, how is the Upper Sealing Rod restrained torsionally and secondly, what error is made in the axial load measurement due to the O-ring seal friction at the mentioned component.

Lee (1985) investigated fully reversed out-of-phase torsion and bending on specimen S10 in Figure 2-1, made of SM45C (equiv. SAE 1045 HR) steel, and proposed a new failure criterion called SLEE for application to this particular mode of loading. Fully reversed fatigue tests were done on a Schenck deflection controlled torsion and bending machine at a frequency of 20 Hz. This machine employs phase control between torsion and bending. Failure was defined as a load reduction of 10% due to cracking of the specimen. Phase angles of 0° and 90° were investigated.

As part of the Society of Automotive Engineers' biaxial fatigue research program, Leese *et al.* (1985) investigated the low cycle fatigue properties of AISI 1045 hot rolled and normalised steel in torsion. The equipment used was a SAE Biaxial Fatigue Testing Machine comprising two 45 kN, 150mm stroke hydraulic actuators. It is a servo-hydraulic system based on MTS fatigue test components and controllers. The control was modified to produce pure torsion at a maximum frequency of 3 Hz. The geometry of the specimen was that of specimen S11 in Figure 2-1. A RVDT was installed inside the specimen to measure the torsional deflection. High strain tests were conducted under strain control using 3 specimens

per strain setting. Five strain amplitudes at R = -1 (fully reversed load ratio) were tested at γ = 0.0250, 0.0150, 0.0080, 0.0050 and 0.0040. Fracture was defined as load drop-off which varied between 10 and 20% and was associated with through-thickness cracks in the wall of the gauge section of the specimen.

From above literature, the following was learnt:

- The state-of-the art test equipment comprises servo-hydraulic actuators with proven test equipment controllers.
- The most damaging multiaxial load combinations involve out-of-phase torsion and bending or torsion and axial force.
- The hydraulic seals required by hydrostatically loaded specimens in conjunction with axial and/or torsional loading, presents a risk that must be quantified.
- Failure of metallic specimens can be defined as a drop-off in load, a detectable leak or a visible crack.
- Typical test frequencies vary between 1 and 20 Hz.

2.3.2 Graphite

Brocklehurst (1977) presents a comprehensive review of the fracture behaviour of graphite with specific reference to fatigue experiments that were conducted by other researchers. All the experiments that are referenced were in uniaxial loading mode only. Although Brocklehurst did not perform any experimental fatigue tests, his review is a good source of knowledge on the overall fracture behaviour of graphite.

Burchell *et al.* (2006) investigated the modelling of the multiaxial strength of extruded, near-isotropic grade H-451 nuclear graphite, manufactured by Great Lakes Carbon. H-451 is a medium-grained graphite. Static tests with the specimen designated S17 in Figure 2-1 were conducted under load ratio control. The test equipment used was a 489 kN, 4 post MTS load frame plus a hydrostatic actuator controlled by a MTS 442 controller. This produced a hydrostatic and axial load that could be controlled independently. The purpose of these tests was to get additional multiaxial load data in order to verify the Burchell fracture model of graphite. Six specimens were tested per load ratio. Nine load ratios defined as axial stress : hoop stress were tested. Only tensile hoop stresses were induced by internal pressurization of the specimen. Tensile failure probabilities were predicted with the Stress

Induced Fracture in Graphite (SIFTING) code ver.3.0 (1994), which requires inputs of the physical condition of the graphite e.g. pore-size distribution, mean pore size, K_{Ic}, mean filler particle size, bulk density, specimen volume, specimen breadth. The principle of independent action (PIA) was assumed which states that the probability of failure under stress σ_1 and σ_2 are considered to be independent events. The stresses were not treated in a combined stress state. Good prediction of failure in the 1st and 4th quadrant of the axial versus hoop stress plot was found. The Burchell model produced a better fit than the Maximum Principal stress criterion in the 1st quadrant. The PIA assumption does not apply to the 4th quadrant but with an effective stress formulation, the SIFTING code predictions of failure, fit the experimental data much better than the Maximum Principal stress predictions in the 4th quadrant.

Taylor *et al.* (1967) investigated the mechanical properties of three undisclosed grades of reactor graphite. Specimen geometries S5 and S6 (Figure 2-1), in an unirradiated state as well as at various doses of irradiation, were used for uniaxial static compressive and tensile tests respectively. Shear tests were also conducted, but are not discussed here. Tests were conducted in a Hounsfield or Mand testing machine. Specimens were sampled parallel and perpendicular to the grain direction of the graphite and strengths determined for each direction by taking a minimum of 4 measurements per condition. Specimen S5 was also used in triaxial compression tests, which were conducted in a pressure vessel that was by design inherently compensated for hydrostatic pressure. This means that if no additional axial load is exerted on the specimen, the load cell would read the force due to the hydraulic pressure. The pressure capability of the system was 60 MPa. Triaxial compressive tests showed that the allowable maximum compressive stress increased as the lower equal stresses were increased by hydrostatic loading. Triaxial compressive tests were also conducted for irradiated specimens with dose rates of (0.75, 1.55, 2.75, 3.6, 7.5 and 11.5) x 10^{20} n.cm^{-2}. Irradiated graphite was stronger than unirradiated graphite. It was found that the Coulomb-Navier equation, Eq.(2.2), fitted the unirradiated triaxial tests well. This relation assumes that the maximum shear strength of the material in uniaxial loading is increased by μ times the normal stress σ (pressure) across the fracture plane:

$$\tau = S_0 - \mu.\sigma \qquad .....(2.2)$$

Where :

$\tau \equiv$ Shear stress on plane [MPa]

$S_0 \equiv$ Maximum shear strength of material [MPa]

$\mu \equiv$ Coefficient of internal friction [-]

$\sigma \equiv$ Normal pressure on shear plane [MPa]

Unfortunately, no shear angle measurements were presented for uniaxial compression that could serve as control to verify the observations made regarding the shear angles in triaxial compression.

Price (1978) investigated the uniaxial cyclic fatigue of near-isotropic graphite. The focus of this research was the influence of the stress cycle (load ratio between -1 and +1/+1) and neutron irradiation on the fatigue characteristics of the graphite. The graphite grades investigated were the extruded, near-isotropic H-451 (Great Lakes Carbon) and moulded PGX graphite, manufactured by Union Carbide (the latter was investigated to a lesser extent). Only H-451 specimens were irradiated. V-block jigs were used for alignment during cementing of the cylindrical steel ends with epoxy. *The problem with this type of setup is that the alignment is also a function of the diameter of the parts that are placed in the V-blocks. Variance in diameter of any of the 3 components of the assembly introduces parallel misalignment.* Eight unirradiated and eight irradiated specimens, designated S12 in Figure 2-1, were tested at each of four stress levels per load ratio. The equipment used was a Fatigue Dynamics Model VSP 150 crank & lever actuated machine that was modified to accept a test case that ran on co-axial linear ball bearings. Since this is a constant deflection type of machine, the minimum and maximum loads were checked occasionally during the tests. The testing frequency was 7 Hz. The following load ratios were tested for H-451 graphite: R = +1/+1, R = +0.5, R = 0, R = -0.5 and R = -1. Only R = 0 and R = -1 tests were conducted for PGA graphite. Fast neutron irradiation was performed at temperatures between 900°C and 990°C at energy levels greater than 29 fJ (0,18 MeV) and doses of 3.8, 7.1 and 10.6 x 10^{25} n/m^2 equivalent fission fluence for graphite damage (EFFGD). Stress results were normalized by the mean tensile strength determined first and plotted on a log-log scale. Least squares fits were used to fit the data points on the S-N diagrams according to the statistical model presented in Eq.(2.3).

$$\log_{10}\left(\frac{\sigma_{max}}{\overline{S}}\right) = \alpha + \beta.\log_{10}(N) + \varepsilon_1 \qquad \text{.....(2.3)}$$

Where:

σ_{max} ≡ peak tensile stress [MPa]

$\overline{S}$ ≡ mean tensile strength [MPa]

α ≡ constant (intercept of least squares line)

β ≡ constant (slope of least squares line)

N ≡ number of cycles [-]

ε_1 ≡ random variable distributed normally with mean value zero and standard variation s.

Tensile data was entered at N = 0.25 and runout (defined as 10^5 cycles) data was disregarded. The former also caused some problems in that the count base for R = -1 and R = 0 for example differs. According to Price, R = -1 is made up of 4 quarter cycles (first quarter is from 0 to tensile peak) which means by implication that R = 0 is made up of 2 half cycles (first half is from 0 to tensile peak). Since both these load ratios are driven by the tensile strength of the graphite, failure during the first excursion from 0 to whatever tensile load should have the same count base.

Bazaj and Cox (1969) investigated the stress-concentration factors and notch-sensitivity of H205, fine-grained graphite, manufactured by Great Lakes Carbon at room temperature as well as at elevated temperatures (1000 and 2000°C). The test equipment was an Instron 10000 lbf fatigue testing machine with special graphite grips in the high temperature load train. These tests were conducted under load control. The type of actuators of the machine was not stated, but one can assume that it was a servo-hydraulic actuator. The geometry of the unnotched specimen that was used is designated S7 in Figure 2-1. The geometry of specimen S7 was based on the geometry of a graphite tensile test specimen, as specified for item 113 (3/8" section diameter) in ASTM C749-92 (2005), except that it had a different grip attachment and employed a larger transition radius of 6 times the section diameter rather than 8/3 times as specified. As a consequence of the larger transition radius, specimen S7 was longer than the specified item 113. Tensile tests as well as uniaxial fatigue tests at 5 – 80%, 5 – 85%, 5 - 90% and 5 – 95% of tensile strength were conducted ($R \approx 0$), using 6 specimens per load case. It was found that for coarse-grained graphite (less than 8,89 mm) the experimental stress concentration factor for a groove was only 1,03 – 1,09, while for fine-grained graphite (less than 0,76 mm), it varied between 1,54 and 1,61 for diameter ratios of 1,25 and 1,50 respectively. The experimental stress concentration factors of fine-grained graphite were constant for temperatures between ambient and 2000°C.

Ho *et al.* (1983) investigated the biaxial failure of fine-grained 2020 graphite (grains less than 0,152 mm) from Stackpole Carbon Company and coarse-grained PGX graphite (grains less than 2,54 mm) from Union Carbide under static loading conditions. The geometry of the specimen that was used is designated S9 in Figure 2-1. Bonded to the ends of this specimen were two steel end plates that were not shown or discussed. Approximately 5 specimens were used per load case and the equipment, which was not described, was apparently able to exert hydrostatic and axial loads. The specimen was subjected to internal and external hydrostatic loads for tensile and compressive hoop stresses respectively. Axial loads were also tensile and compressive. The stress in the gauge section was calculated using thick-walled cylinder theory and the strains were measured by three sets of strain

gauges bonded to the inner surface of the specimen's gauge section. Judging from the lay-out of data points, ratio control must have been used with the two loading modes (hydrostatic and axial) in phase. The fracture patterns indicated typical Mode I (cleavage mode) failures (ASTM E1823-96, 2002), with the cracks perpendicular to the maximum tensile stress direction in the test section. The ratios of hoop-to-axial stress employed were ½, 1/1, 1/-4, -1/-1, -6/-1, -4/-1, -6.5/1, 1/0 and 2/1 for 2020 graphite and 2.2/1, 1/1, ½, 1/0, 1/-1, 1/-4, 1/-2 and 0/1 for PGX graphite. The biaxial stress chart of these tests were compiled and compared with the Maximum Normal Stress, Maximum Shear Stress, Maximum Distortion Energy and Tsai-Wu Strength Tensor theories. The Coulomb-Mohr modified according to Paul with tension-cutoffs fitted the test data best. Although the ratio between hoop stress and radial stress at the inner wall of the gauge section is high (11,9) the actual stress state is triaxial and not biaxial as assumed in this analysis.

Schmidt (2000) reported the low cycle, uniaxial fatigue of fine-grained, isostatically pressed V483T graphite. The geometry of the specimen that was tested is designated S13 in Figure 2-1. By implication, load control was exercised to test 26 specimens at different loads for the following load ratios: R = +1/+1, 0, -1, -2, $-\infty$ and -1/-1. Tests were conducted on a servo-hydraulic fatigue testing machine using a sinusoidal forcing function at a frequency of 1 Hz. The ramp rates for static testing were 400 and 800 N/s for tensile and compression tests respectively. Separate S-N curves were drawn for specimen axes parallel and perpendicular to the grain direction. By implication the grain direction of the isostatically pressed column is in the longitudinal direction of the column. Compression tests were also done on cylindrical shaped specimens that yielded the same compressive strength. The compressive strength was thus found to be independent of the shape of the test specimen. If a specimen failed during the first stress excursion, its count was taken as 0.25, regardless of its load ratio. Contrary to expectation, the tensile strength, measured perpendicular to the grain using 10 specimens, was higher than that measured parallel to the grain using 50 specimens. This discrepancy was waived because the number of specimens differed in these tests. However, the compressive strength, measured using 10 specimens perpendicular to grain, was lower than that measured parallel to grain using 48 specimens, as expected. The constant-life diagrams presented in this report are used in Section 4.6.7, Chapter 4 as an absolute comparison between NBG18 and V483T and V483T2 nuclear grade graphite.

The remaining specimens in Figure 2-1, S14, S15 and S16, are the geometries of standard graphite tensile test specimens. The applications of these tests are briefly described in Section 2.2.2

Boey and Bacon (1986a) investigated the bend strength of graphite under an isostatic nitrogen pressure of 4.14 MPa. Four point bend tests were conducted on 15 off 50 x 5 x 5 rectangular specimens per material per environmental pressure load in a pressure vessel. The materials tested were isotropic Gilsocarbon and 2 pitchcoke graphites. The specimens were unsealed. Tests were done at 0 and +4,2 MPa gauge pressure. It was found that the mean fracture stress and strain was reduced under pressure by approximately 3 and 13% respectively. Bend specimens were found to be stiffer under pressure. This was attributed to the closure of micropores under hydrostatic loading. The observation that the mean fracture stress was lowered by isostatic pressure was reported to be contradictory to the findings of Taylor *et al.* (1967). However, the results of the mentioned tests are not directly comparable because the tests differ both in type and in sealing state of the graphite.

Yoda *et al.* (1984) investigated the effects of prehydrostatic loading on the mechanical and physical properties of two isostatically moulded graphites. This terminology can be confusing, therefore the term pre-test isostatic exposed (PIE) specimens is used in this research for specimens that are subject to isostatic compressive loading prior to other testing. Toyo Tanso IG-11 (grain size of 20 μm) and Iso-20 (2 μm grain size) graphite specimens were hydrostatically loaded prior to 4 point bend testing. During isostatic loading, the specimens were encased in a rubber sheath. Changes in volume, resistivity, elasticity, porosity and flexural strength were measured as a function of hydrostatic loading pressure. Elasticity tests were also performed but not described. It was found that the resistivity increased under pressure, and this phenomenon was ascribed to a growth in microcracks. Plastic deformation occurs under hydrostatic loading due to changes in pore shape and deformation by slips. Flexural strength is reduced due to increase in microcracks. Elasticity is reduced in IG-11 and increased in Iso-20, which could not be explained properly.

Boey and Bacon (1986b) investigated the deformation of polycrystalline graphite under pressure. Isotropic Gilsocarbon and anisotropic pitchcoke and PGA graphites were tested. Pitchcoke graphite was irradiated at 400°C at 3 dose rates up to 17 x 10^{20} n/cm^2. Strain was measured with strain gauges in the longitudinal and circumferential directions. Hydrostatic testing up to 4,14 MPa was done in 0,69 MPa steps for unsealed, sealed and irradiated specimens. Uniaxial compression tests were done afterwards to determine E, ν and S_{uc}. Elevated temperature hydrostatic tests were conducted at 300°C and 4,14 MPa. It was found that the stress-strain curves are linear with a small amount of permanent set, which remained constant in subsequent loading cycles. Large variations were observed in maximum strain between graphite types and specimens. Maximum strains were larger for sealed than for unsealed specimens. Irradiation produced non-linear stress-strain curves

with an increase in bulk modulus and E. The irradiated properties returned to unirradiated characteristics after annealing for 1 h at 2350°C in an Argon atmosphere. The results were explained in terms of open and closed porosity volume fractions.

Zukas and Green (1971) investigated the creep behaviour of hot isostatically pressed graphite. ATJ (fine grained, moulded) and ZTA (fine grained moulded & hot-pressed) graphite from Union Carbide Corp. were vacuum canned in tantalum and hydrostatically pressed in He at 100 MPa and 2700°C for several hours. Creep tests were performed under tensile and compressive loads. It was found that hot isostatic pressing (HIP) had no effect on creep and recovery curves, overall strength and ductility. Pores in graphite are not sealed during HIP.

Yoda and Eto (1983) investigated the tensile deformation behaviour of nuclear-grade isotropic graphite after hydrostatic loading. Toyo Tanso IG-11 and Iso-20 graphite specimens were hydrostatically loaded at 100, 300, 500 and 700 MPa prior to tensile testing. Strains were measured with 2 strain gauges on opposite sides of the Ø10 x 40 gauge section. The surface roughness was measured before and after hydrostatic loading. It was found that graphite deforms plastically under hydrostatic loading due to closing/shrinking of pores or cracks and slips that are induced along the basal planes of the graphite crystals. Prehydrostatic loading weakens the graphite due to induced microcracks. The residual strain generated by an applied tensile stress increases with an increase in hydrostatic pressure according to $\varepsilon = A\sigma^n$ with an inflection point at 300 MPa, which corresponds to the pressure at which there is hardly any further deformation under increased hydrostatic loading. A linear relationship between log (σ/σ_0) and log P was observed. This relation is expressed by Eq.(2.4).

$$\frac{\sigma}{\sigma_0} = 48.1\left(P^{-0.218}\right) \qquad \text{.....(2.4)}$$

where:

$\sigma \equiv$ Tensile strength after isostatic pressure exposure [MPa]

$\sigma_0 \equiv$ Tensile strength without isostatic pressure exposure [MPa]

$P \equiv$ Isostatic pressure [Pa]

Extrapolation of the pressures according to Eq.(2.4) implies that for NBG18 graphite (should it apply) the isostatic pressure damage threshold is 52 MPa, which is about 62% of the Ultimate Compressive Strength (UCS) of the material. Since no work was done at low isostatic pressures, limited PIE fatigue tests are included in this research, because the HTR application is an isostatic environment.

Tucker *et al.* (1986) investigated the fracture of polygranular graphites. Six failure theories for graphite materials were implemented on the following test data: Strength distribution (3 point vs. 4 point bending), mean filler particle size, porosity fraction, acoustic emission count, knife edge spacing (3 point & 4 point), specimen volume, stress gradient, absolute gas pressure, biaxial stress effects, fast neutron irradiation, radiolytic oxidation. The six failure models were: Weibull theory, Rose/Tucker model, fracture mechanics model using a Griffith crack, Critical strain energy density criterion, Critical stress theory and Critical strain theory. It was found that the Rose/Tucker and fracture mechanics models predicted failure better than Weibull. The Critical strain energy, Maximum Principal stress and Maximum Principal strain criteria were least successful in predicting all test scenarios, because the microstructure of the graphite is not taken into account in the latter group.

The effect of elevated temperature on the elastic modulus and bend strength of graphite was researched by Maruyama *et al.* (1987). Little or no change in elastic modulus and 4 point bend strength was found up to 500°C. Above this temperature, the elastic modulus and bend strength increased almost linearly with temperature by 24% at 1400°C and 18% at 1200°C respectively.

From above literature, the following was learnt:

- Irradiated graphite is stronger than unirradiated graphite.
- Graphite exhibits an increase in stiffness and strength at high temperature.
- All graphite specimens subject to multiaxial loading involve a combination of hydrostatic and axial forces.
- Hydraulic fluid impregnation of the specimens is prevented by rubber sleeves or bladders or sealing of the specimen's surface with a synthetic rubber compound.
- The physical size of multiaxial loaded graphite specimens tend to be large.
- Irradiated graphite specimens are typically small sized cylindrical components.
- There is no international consensus on a suitable failure criterion for graphite subject to multiaxial loading.
- High isostatic pressure exposure of graphite (of the order of the uniaxial compressive strength and higher) causes damage to the material, and hot isostatic pressing (HIP)

does not improve the strength of the graphite. The graphite specimens must be prepared with care to prevent pre-test damage due to clamping stresses.

- A hydrostatic load generally influences the axial force in a multiaxial loaded specimen.

2.4 MOHR-CIRCLE STRESS EXCURSIONS

The stress state of the fatigue tests in the mentioned research papers were analyzed by plotting typical Mohr-circles of the combined stresses at 45° cycle intervals or $1/8^{th}$ stress intervals in the case of static tests. The absolute amplitudes are of no consequence in these plots, but the intent is to show the relative amplitudes with specific reference to the direction of Maximum Principal stress relative to the axis of the specimen. These plots are shown in **Appendix G**. Only the Mohr-circles with maximum diameter are shown in these plots. The other two Mohr-circles of the triaxial stress state are encircled by the circle shown.

Mohr-circle stress excursions of the combined (multiaxial) loading condition researched by Socie *et al.* (1985), using specimen S1 are presented. The combination of in-phase axial and torsional load causes a constant angle between the maximum principal stress and the specimen axis and the load reversal for R = -1 in contrast to no load reversal for R = 0 is illustrated graphically.

The effect of phase angle, investigated by McDiarmid (1985) is illustrated for specimen S2 in **Appendix G**. The hoop stress and axial stress have equal amplitudes in these plots. The 60° hoop stress phase lead creates two high stress states (circles of large radii) per axial stress frequency cycle for a frequency ratio of 2 : 1 versus only one for the 180° phase lead condition. (The two other peak states of the latter excursion have small amplitudes.) The specimen and maximum principal stress directions are co-linear.

Typical Mohr-circle excursions on specimen S3 for T/B = 0,581 and T/B = 1,378 investigated by Fash *et al.* (1985) are shown in **Appendix G**. The combination of in-phase torque and bending causes a constant angle between the maximum principal stress and the specimen axis. Changing the relative magnitude of torque to bending moment changes the magnitude of this angle.

The 50% decrease in fatigue life under strain controlled multiaxial tests with 90° phase shift using specimen S4, observed by Sonsino and Grubisic (1985), is not explained by the magnitude of the Mohr-circle excursions (constant load) showing lower peak amplitudes than for 0° or 180° phase shift. However, the 90° phase shift causes cyclic rotation of the

direction of the maximum principal stress relative to the specimen axis. This phenomenon could be responsible for the lower fatigue life observed.

No Mohr-circle excursions were compiled for the research by Found *et al.* (1985) with specimen S8 because no actual test data was presented, and there are so many load combinations possible with this equipment.

Mohr-circle excursions of the two load ratios yielding the same life of 1×10^5 cycles, as determined by Lee (1985) using specimen S10, are illustrated in **Appendix G**. Note that the state with the smaller maximum shear stress (circle diameter) but with a rotating Maximum Principal stress direction relative to the fixed specimen axis (phase offset) has the same fatigue life as the state with the larger maximum shear stress but a fixed Maximum Principal stress direction (in-phase). The same observation, mentioned above, was made by Sonsino and Grubisic (1985).

The Mohr-circle excursion of a fully reversed pure torsion test as conducted by Leese and Morrow (1985), using specimen S11, is illustrated in **Appendix G**. The constant principal stress directions at ±45° from the longitudinal axis that cause the typical 45° fracture plane of a torsion failure is indicated by the 90° angle between the specimen axis and the maximum principal stress axis in the Mohr-circle domain. Mohr-circle domain angles represent twice the value of angles in the physical domain.

Mohr-circle excursions of the static tests by Burchell *et al.* (2006) of hoop-to-axial stress ratios +1/+1 and +1/-1 are shown in **Appendix G**. The applicable specimen is S17. Although the internal pressure was not stated in the publication, it was reverse-engineered for the given geometry. The result was an internal pressure value of approximately 1/5 of the hoop stress value. The maximum diameter Mohr-circle of the +1/+1 stress ratio is defined by the internal pressure (radial stress) and the hoop stress. In this case, the hoop stress and axial stress coincides and defines a circle with diameter of zero.

Taylor *et al.* (1967) used specimen S5 for static tests in a triaxial loading state. A constant hydrostatic pressure was applied before the specimen was loaded in compression in the axial direction, as shown by the Mohr-circle excursion. The Mohr-circle excursion of specimen S6 is representative of a typical tensile test.

The typical uniaxial Mohr-circle excursions of R = 0 and R = -1 applied by Price (1978) on specimen S12 are illustrated in **Appendix G**. These are not much different from the 5 – 95% of tensile strength excursion applied by Bazaj and Cox (1969) on specimen S7.

The static multiaxial test by Ho *et al.* (1983), using specimen S9 is described by the Mohr-circle stress excursion for a hoop-to-axial stress ratio of +1/-4. The constant alignment of the maximum principal stress with the specimen axis (z-axis) is evident in **Appendix G**.

No Mohr-circle excursions were drawn for the tests by Schmidt (2000) (specimen S13) because it is similar to those drawn for S12.

The following conclusions can be made from the literature survey and this analysis:

- Most fatigue damage is done to a specimen when the direction of the maximum principal stress is not aligned at a fixed angle relative to the specimen axis.
- None of the existing multiaxial graphite fatigue test specimens was loaded in the most damaging way.

This leads to the hypothesis that an omni-directional principal stress, which exerts the maximum stress in all directions relative to the specimen axis, should yield the shortest fatigue life. Such condition could exist in a sphere subject to cyclic isostatic pressure. A positive isostatic pressure condition (triaxial compressive condition) is easily realised, but a negative isostatic pressure condition (triaxial tensile condition) is quite unpractical at present. A practical geometry closest to the solid sphere, mentioned above, is a hollow hemisphere. Such geometry can be loaded in biaxial tension and compression.

2.5 AIM OF THE STUDY

The aim of the study is three-fold:

- To perform a comprehensive range of uniaxial fatigue tests in South Africa. The "comprehensive range" is shown in Figure 2-2.
- To propose a "maximum damage" multiaxial fatigue specimen design and obtain a comparable set of results (comparable to the uniaxial test results) in South Africa for this specimen.
- To do a limited exploration of the probability of PIE damage due to isostatic loading at HTR system pressure.

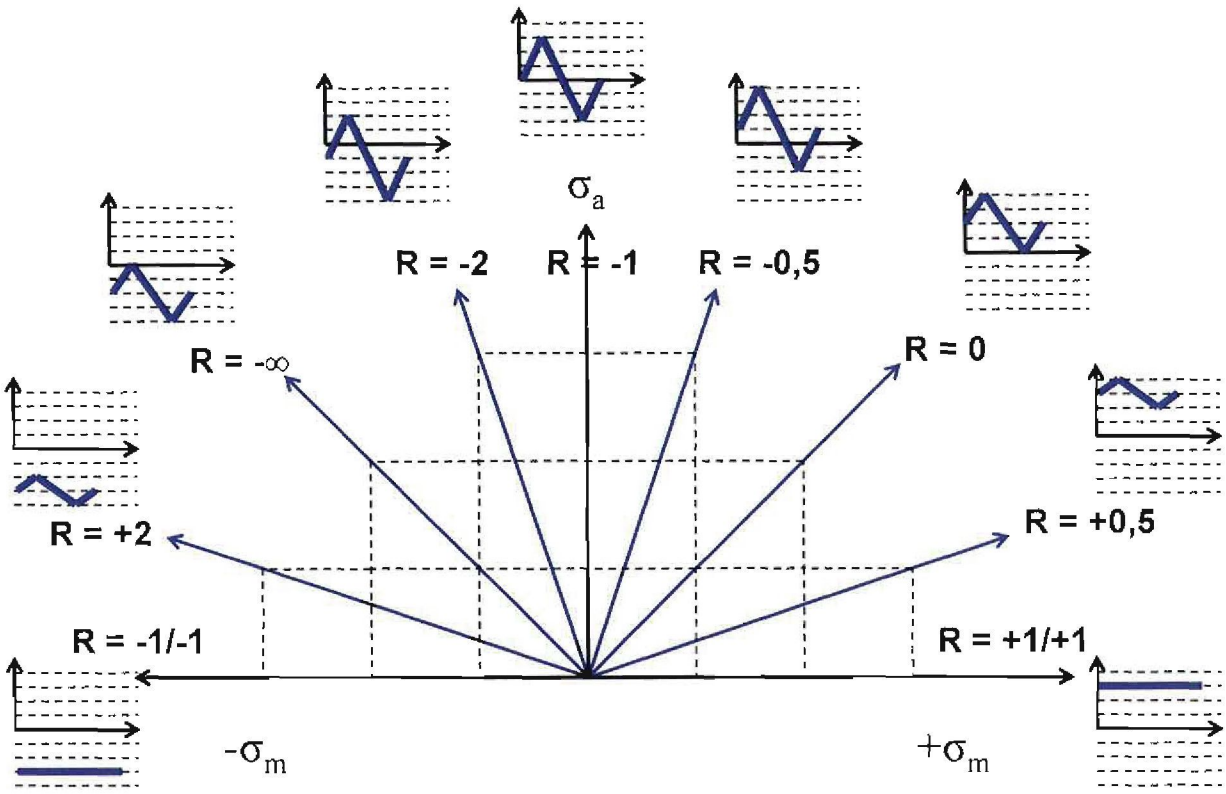


Figure 2-2: Load Ranges of Graphite Fatigue Tests

Above figure is a plot of stress amplitude as a function of midrange stress. It shows the seven radial lines of constant load ratio loci for cyclic stress waveforms and the two horizontal lines of constant load ratio loci for "static" stress waveforms. A small picture of the relative stress waveform containing a single cycle for each load ratio is added to relate the physical stress cycle to the load ratio value.

2.6 RESEARCH CONSTRAINTS

During the literature survey, it became clear that determining the fatigue characteristics of NBG18 under uniaxial and multiaxial loading conditions at 900°C is not trivial and that it is an expensive task. Because the strength of graphite increases from room temperature to the operating temperature of the reactor (Nightingale *et al.* (1962)), tests at room temperature yield most conservative results. Because conservative fatigue characteristics are required, this research is constrained to tests at room temperature only.

Losty (1962) reports that irradiation has a similar effect to temperature on the mechanical characteristics of graphite, at low fluence levels. At high fluence levels i.e. towards end-of-life, the breakdown of graphite is a known phenomenon, which needs to be quantified for

NBG18. However, this research is constrained to determining the characteristics of *unirradiated (virgin state) graphite.*

The literature survey revealed that the published fatigue research was limited to just a few peak stress combinations (load ratios). The present research is constrained to be more exploratory, but statistically less accurate. In other words, more load ratios are to be covered, with fewer specimens per load case.

As described earlier in this chapter, the multiaxial loading states are usually attained by combining hydrostatic loads and axial loads. Theoretically, the combinations of load directions in a multiaxial fatigue state can be numerous, which necessitates a new definition for the load ratio concept. In order to avoid this dilemma, the load ratio definition is based on the Maximum Principal stress, as for the uniaxial fatigue application.

The North-West University did not have a servo-hydraulic fatigue testing machine that could form the backbone of a multiaxial fatigue testing facility. The cost of the test equipment is therefore a major constraint.

Since the aim of the study (refer to Section 2.5) already includes novel work, the research is constrained to measuring only the fatigue characteristics. The problem of finding a suitable multiaxial stress design criterion, which fits the measured characteristics well, is not part of the scope of this research.

Very soon in the literature review, the strange phenomenon of damage to graphite from previous isostatic load exposure was discovered. This led to an urge to explore whether this phenomenon also occurred at lower pressures than covered by the literature, because in a HTR, all components in the reactor environment are also exposed to an isostatic load, due to the gas system pressure. This investigation is constrained to measuring only the static and fully reversed fatigue characteristics of Pretest Isostatic Exposed (PIE) specimens, for comparative purposes.

2.7 CLOSING REMARKS

The problem of measuring the fatigue characteristics of NBG18 in South Africa at the reactor operating conditions was simplified through a study of the available literature.

The load range of fatigue characteristics is expanded to the most comprehensive range to date, shown in Figure 2-2. Uniaxial tests are to be conducted using existing equipment with

least expensive modifications or accessories, whilst maintaining or improving the quality of the measurements. The uniaxial fatigue tests are presented in Chapter 4.

The same load range of fatigue characteristics is required for multiaxial loading. A new specimen design is required which incorporates stresses that cause most damage. Low cost test equipment is required to perform these tests. The multiaxial fatigue tests are presented in Chapter 5.

In the next chapter, the specimen sampling plan that was used in this research is presented.

Chapter 3

SPECIMEN SAMPLING PLAN

3.1 INTRODUCTION

Any material test requires a well designed specimen sampling plan that describes the location of the specimens relative to the manufactured shape of the material from which it was taken. The orientation of the specimens relative to the preferred orientation of the coke particles (hereafter referred to as grain orientation) is normally designed to measure the parallel-to-grain and perpendicular-to-grain properties of the material. NBG18 was designed to be as near-isotropic as practicable.

The cutting plan ensured that specimens were taken from comparable centre and edge locations inside the block and in similar ratios of near-edge specimens and near-centre specimens. The specimens, taken according to this cutting plan, represented the maximum variation that could be expected within a manufactured block.

3.2 GRAPHITE BLOCKS

The graphite blocks of nominal dimensions 2000 x 500 x 540 mm (X x Y x Z) are manufactured using a vibratory moulded process. This is the same process that is used for manufacturing of the reflector blocks of the PBMR reactor. The direction of vibration is the Z-direction in Figure 3-1, causing any preferred grain orientation to be in the XY-plane.

Only two axis orientations are used. Alignment of the uniaxial specimen axis with the Z-axis is expected to yield worse results since any needle shaped coke particles tend to align perpendicular to the direction of the compaction of the block during manufacturing. Alignment of the uniaxial specimen axis with the X-axis is expected to yield better results, since this is parallel to the grain direction of the material, if the graphite is anisotropic. This direction is also important from the reactor design point of view, since this will be the direction of the tangential and bending stresses in the core structures. Due to the limited number of tests, no specimens are aligned with the Y-direction.

From a material cost point of view, the obvious choice is to use the minimum number of blocks. Two blocks enable the formation of two subgroups of 4 specimens per test point.

Half the specimens per test point are taken from the one block and half from the other, to ensure the largest possible variation.

Although the intent was to select blocks with absolute characteristic values in the lower margin of acceptable manufactured material, the SGL Carbon Group could not guarantee that the selected blocks conformed to this intent, due to the statistical nature of the mechanical test results, and the limited number of specimens in the standard tests done per block. The block identification numbers are shown in Figure 3-1 and Figure 3-2.

3.3 SAMPLING LAY-OUT

The location of the specimens in the two NBG18 graphite blocks is shown in Figure 3-1 and Figure 3-2. The uniaxial and multiaxial specimens in each load group were selected from the centre group and edge group of each block and from both X and Z directions, as shown in Table 3-1. The rational thereof was to ensure that the tests yielded the most conservative results i.e. the weakest characteristics of the NBG18 graphite.

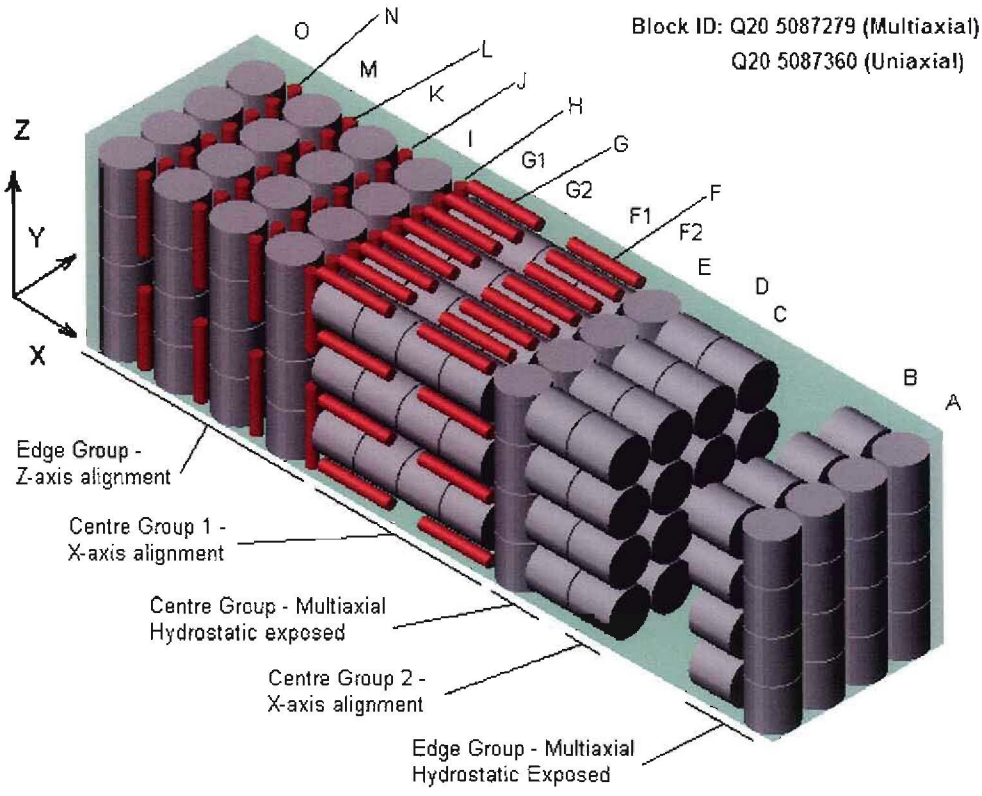


Figure 3-1: Specimen Orientation In Block A

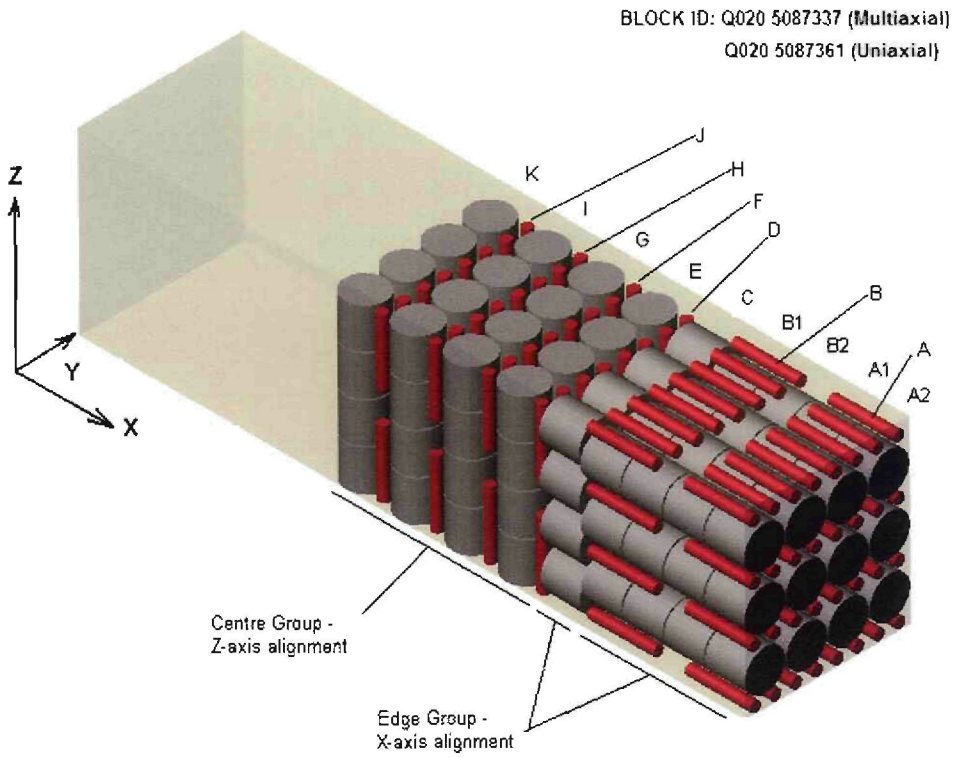


Figure 3-2: Specimen Orientation In Block B

The detailed allocation of specimen numbers to the load ratios, as summarised in Table 3-1, appears in **Appendix A.**

Table 3-1 : Allocation of Specimens to Load Ratios

No.	Load Combination	Load Amplitudes	Align	Location	Block	Qty.	# R-values	Total Qty.
1	R = +1/+1 or -1/-1	1	X	Edge	A	1	2	2
2	R = +1/+1 or -1/-1	1	X	Centre	A	1	2	2
3	R = +1/+1 or -1/-1	1	Z	Edge	A	1	2	2
4	R = +1/+1 or -1/-1	1	Z	Centre	A	1	2	2
5	R = +1/+1 or -1/-1	1	X	Edge	B	1	2	2
6	R = +1/+1 or -1/-1	1	X	Centre	B	1	2	2
7	R = +1/+1 or -1/-1	1	Z	Edge	B	1	2	2
8	R = +1/+1 or -1/-1	1	Z	Centre	B	1	2	2
					Total Static Samples			14
9	R = +0.5/0/-0.5/-1/-2/-∞/+2	4	X	Edge	A	4	7	28
10	R = +0.5/0/-0.5/-1/-2/-∞/+2	4	X	Centre	A	4	7	28
11	R = +0.5/0/-0.5/-1/-2/-∞/+2	4	Z	Edge	A	4	7	28
12	R = +0.5/0/-0.5/-1/-2/-∞/+2	4	Z	Centre	A	4	7	28
13	R = +0.5/0/-0.5/-1/-2/-∞/+2	4	X	Edge	B	4	7	28
14	R = +0.5/0/-0.5/-1/-2/-∞/+2	4	X	Centre	B	4	7	28
15	R = +0.5/0/-0.5/-1/-2/-∞/+2	4	Z	Edge	B	4	7	28
16	R = +0.5/0/-0.5/-1/-2/-∞/+2	4	Z	Centre	B	4	7	28
				Total Fatigue Samples (Virgin)				224
17	R = -1	4	X	Edge	A	4	1	4
18	R = -1	4	X	Centre	A	4	1	4
19	R = -1	4	Z	Edge	A	4	1	4
20	R = -1	4	Z	Centre	A	4	1	4
21	R = -1	4	X	Edge	A	4	1	4
22	R = -1	4	X	Centre	A	4	1	4
23	R = -1	4	Z	Edge	A	4	1	4
24	R = -1	4	Z	Centre	A	4	1	4
				Total Fatigue Samples (Isostati				32

3.4 SPECIMEN SERIAL NUMBERS

The specimen serial numbers were allocated by SGL Carbon according to their detailed drawings, shown in **Appendix A**.

The specimen serial numbers have the following structure:

XX Y-Z

Where:

XX	≡	Last two numbers of Block Identity Number
Y	≡	Section plane in Cut Layout drawings
Z	≡	Serial number within section plane as shown on drawings

3.5 SUMMARY AND CONCLUSIONS

The specimen sampling and allocation plan is discussed in Chapter 3. The specimens are allocated to load ratios in such a way that each load group has X and Z oriented specimens of Block A and B from near edge and near centre locations in the block. This applies to both the uniaxial and multiaxial test specimens. Therefore, the widest possible variance in test results is expected from this sampling scheme.

The design, execution and results of the uniaxial specimen tests are described in the next chapter.

Chapter 4

UNIAXIAL FATIGUE TESTS

4.1 INTRODUCTION

The reason for doing a set of uniaxial fatigue tests in South Africa is stated in Chapter 1. In Chapter 3, the specimen sampling plan, that applies to both the uniaxial fatigue tests (presented in this chapter) and the multiaxial fatigue tests, presented in Chapter 5, is discussed.

The outcome of the literature survey, discussed in Chapter 2, is that all three publications on uniaxial fatigue tests on graphite involved different specimen geometries namely S12 of Price (1978), S7 of Bazaj and Cox (1969) and S13 of Schmidt (2000). No internationally accepted standard for uniaxial fatigue testing of graphite exists.

The criticality of alignment is evident from a study of the ASTM specifications for static tensile testing of graphite. A suitable specimen, from both a geometry and test facility point of view, has to be selected from the list mentioned above. Alternatively, a new specimen design must be proposed and justified.

In this chapter, the design of the uniaxial fatigue tests, its execution as well as its results, are discussed.

4.2 ALIGNMENT

In Chapter 2, the importance of proper alignment for graphite tensile testing was pointed out. This requirement sets equally high standards for alignment during fatigue testing, which is even more difficult to attain when one realises that it must hold true for tensile and compressive excursions.

An estimate of the maximum allowable misalignment of a uniform diameter rod can be made with the assumption that the bending stress may not exceed 5% of the mean tensile stress as specified in ASTM C749-92 (2005). Figure 4-1 shows the loading diagram, shear force diagram and bending moment diagram of a uniform diameter rod subject to parallel and angular misalignment. The axial force increases the bending moment in the gauge section,

when it is compressive, and vice versa. This additional bending moment is shown in red in Figure 4-1. The additional moment at the test section due to the axial load is neglected in these simplistic calculations of the two individual cases of misalignment, because in reversed loading, it adds in one case and subtracts in the other case. So for fully reversed loading, its mean value is zero.

From this simple analysis, it is clear that angular misalignment is more detrimental than parallel misalignment, because in the former case, the bending moment remains constant along the gauge section, while it varies linearly from a positive to a negative value along the length of the gauge section in the latter case. In the centre, it is zero. In both cases, it is assumed that the load vectors are co-linear, as shown in the loading diagrams.

The governing equations, derived for the 5% allowable bending stress, are Eq.(4.1) and Eq.(4.2) for parallel and angular misalignment respectively.

The true state of misalignment of the specimen in the testing machine is a combination of the simplistic approach mentioned above.

Maximum parallel misalignment :

$$\frac{\varepsilon}{F} \leq \frac{0{,}25.\ell^2}{3.\pi.E.d^3} \qquad \text{.....(4.1)}$$

Maximum angular misalignment :

$$\frac{\alpha}{F} \leq \frac{0{,}4.\ell}{E.d^3} \qquad \text{.....(4.2)}$$

Where :

$\varepsilon \equiv$ Parallel misalignment [mm]

$F \equiv$ Axial force [N]

$\ell \equiv$ Length of rod [mm]

$E \equiv$ Modulus of elasticity [MPa]

$d \equiv$ Uniform section diameter [mm]

$\alpha \equiv$ Angular misalignment angle relative to force line [rad]

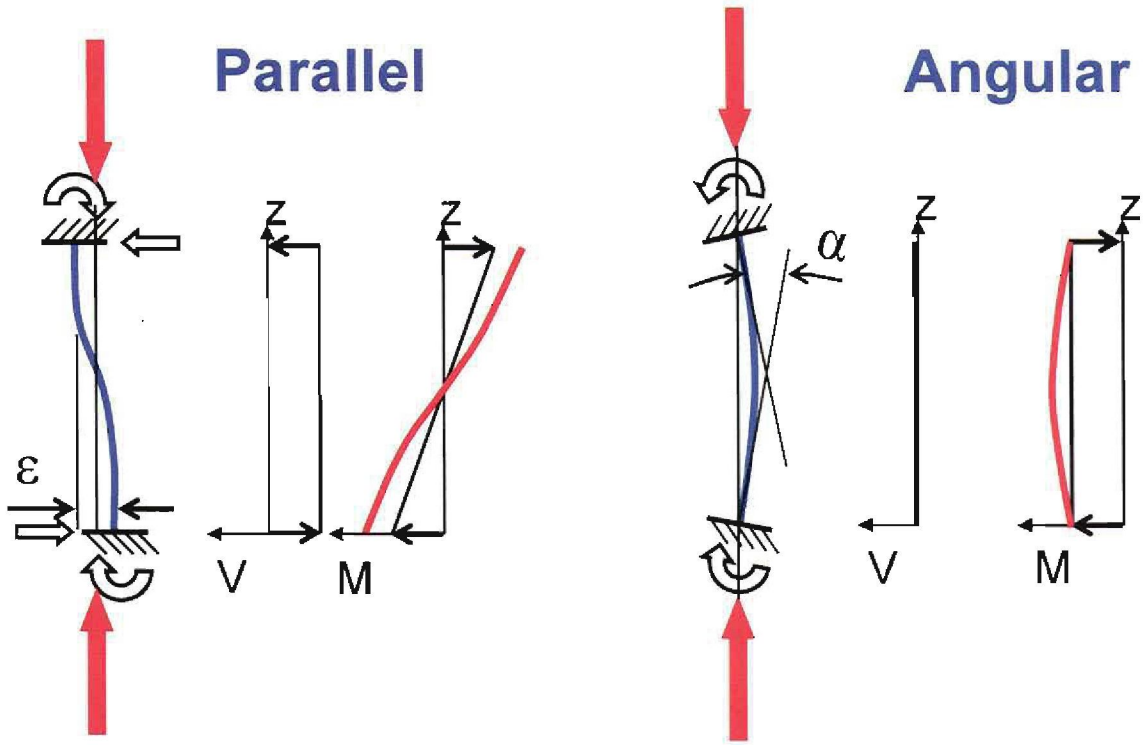


Figure 4-1: Shear Forces and Bending Moments Induced in Uniform Column by Misalignment

In order to quantify the alignment goal for the uniaxial specimens, the assumption is made that the effective length of the test specimen equals four times the gauge section diameter. (The typical gauge length of a uniaxial specimen is 2 to 4 times the gauge diameter.) A portion of the transition section from the gauge diameter to the grip diameter forms part of the effective length.

The maximum allowable parallel misalignment calculated with Eq.(4.1) is 3 µm and the maximum allowable angular misalignment calculated with Eq.(4.2) is 15,2 x 10^{-3} degrees of arc, for each 1000 N axial force. The maximum number of cycles, where the axial load is the smallest, therefore drives the allowable misalignment. These requirements are so stringent that it is probably impossible to meet it with existing equipment.

The primary requirement for the selection of suitable uniaxial test specimen geometry is that the alignment of the grips of the testing machine shall be easily verifiable.

Since alignment cannot be controlled properly in threaded interfaces (ASTM E466-96, 2002), Specimen S4 in Figure 4-4 was rejected as a contender for the uniaxial tests.

The bonding or neat-fitting of clamping fixtures to the specimen, as is done for the cylindrical specimen of DIN 51914 : 1985-04 (1985) and ASTM C749-92 (2005) respectively, not only

increase the misalignment risk, but also introduce a significant cost component to the total cost of the specimen. This eliminated S12 and S16 in Figure 4-4 as contenders.

4.3 General Fatigue Design Requirements

A number of generic requirements for the design of the fatigue tests of NBG18 graphite, are defined. These generic requirements are:

- Minimum thickness of gauge section: 10 x average grain size (approximately 5 x maximum grain size according to ASTM C749-92 (2005)).
- Low production cost for specimens
- Use of existing equipment or low development cost for new equipment
- Combinations of alternating and midrange stresses shall span the whole range from static tensile to static compressive loading as shown in Figure 2-2 of Chapter 2.

The average and maximum grain size of the vibration moulded NBG18 graphite is 0,7 and 1,6 mm respectively. In order to comply with the minimum thickness requirement, the dimension of the gauge section has to be equal to or greater than 7 mm. ASTM C749-92 requires the minimum thickness of the gauge section to fall between 3 and 5 times the maximum grain size.

4.4 KTA 3232 Design Rule and Developed MDE Stress

The design of the HTR of the PBMR is done according to the KTA 3232 design rule (Schmidt, 2003). According to this rule, the governing stress equation to design for strength of graphite is the modified Maximum Deformation Strain Energy (MDE) criterion (Schmidt, 2001b).

The MDE stress criterion is shown mathematically in Eq. (4.3) and Eq. (4.4).

$$\sigma_v^2 = \left\{\bar{\sigma}_1^2 + \bar{\sigma}_2^2 + \bar{\sigma}_3^2 - 2.\nu.\left(\bar{\sigma}_1.\bar{\sigma}_2 + \bar{\sigma}_2.\bar{\sigma}_3 + \bar{\sigma}_3.\bar{\sigma}_1\right)\right\} \le S_{ut}^2 \qquad \text{.....(4.3)}$$

Where :

$$\bar{\sigma}_i = \begin{cases} \sigma_1.1 & \text{if } \sigma_i \ge 0 \\ \sigma_1.f & \text{if } \sigma_i < 0 \end{cases}$$

and

$$f = \frac{S_{ut}}{S_{uc}} \qquad \text{.....(4.4)}$$

$\sigma_v \equiv$ MDE Stress [MPa]

$\nu \equiv$ Poisson's ratio with loss of physical interpretation [-]

$S_{ut} \equiv$ Ultimate Tensile Strength [MPa]

$S_{uc} \equiv$ Ultimate Compressive Strength [MPa]

$\sigma_1 \equiv$ Principal Stress, i [MPa]

The probability of survival is calculated according to a modified two-parameter Weibull distribution, given by Eq.(4.5). The probability of failure (PF) of the component is determined, using Eq.(4.6).

$$L_c = e^{-\left\{\sum_i \left(\frac{\sigma_i}{S_c}\right)^m \cdot \frac{V_i}{\sum V_i}\right\}} \qquad \text{.....(4.5)}$$

Further :

$$PF = 1 - L_c \qquad \text{.....(4.6)}$$

Where :

$L_c \equiv$ KTA 3232 Probability of survival [-]

$\sigma_i \equiv$ Local MDE Stress [MPa]

$S_c \equiv$ Weibull characteristic strength (all tensile data) [MPa]

$m \equiv$ Weibull distribution shape parameter (all tensile data) [-]

$PF \equiv$ Probability of failure [-]

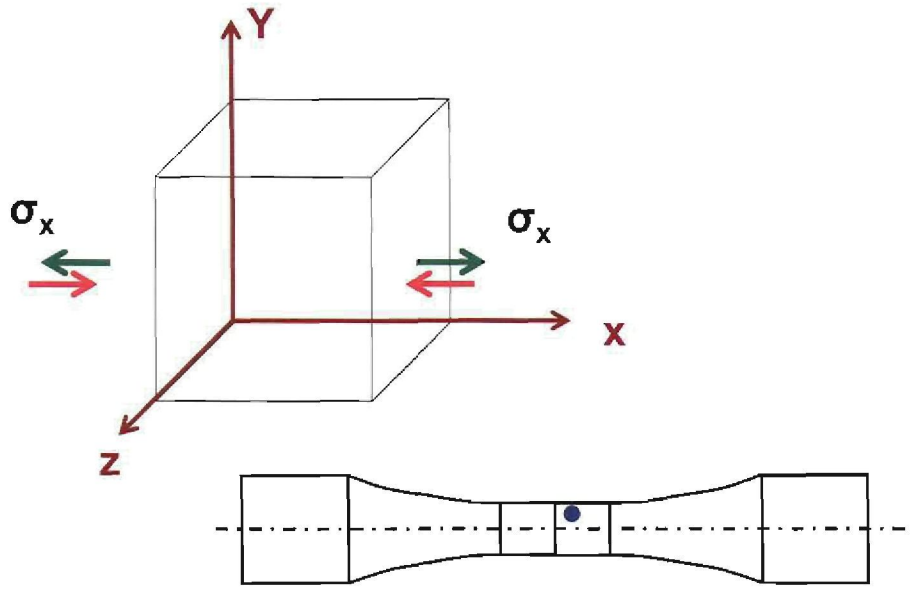


Figure 4-2: Stress State in Uniaxial Specimen

Since the MDE stress is a single scalar that expresses the equivalent stress state of the 3 principal stress state of the material, this stress is always positive (like the Von Mises stress).

The stress element of the uniaxial specimen is shown in Figure 4-2 for any location in the gauge section, indicated by the dot. It has only one principal stress, and when Eq.(4.3) is applied to calculate the MDE stress at fracture, it equals the Ultimate Tensile Strength (UTS) for static tensile loading. For static compressive loading, assuming the factor f in Eq.(4.4) was calculated from test results of this specific material, the calculated MDE stress at fracture equals the UTS.

For the uniaxial specimen, subject to R = -1 loading, the Maximum Principal stress excursion and MDE stress excursions are shown in view (A) and (B) in Figure 4-3. A developed MDE stress excursion is proposed here to prevent the clutter on the constant-life chart when MDE stress ratios are mapped to one quadrant only, if this is not done. The MDE stress excursion of view (B) is developed by changing the sign of the MDE stress of the dominant negative principal stress excursion, as shown in view (C) of this example. The definition of midrange stress, σ_m and stress amplitude, σ_a are the customary values, as shown graphically in this figure.

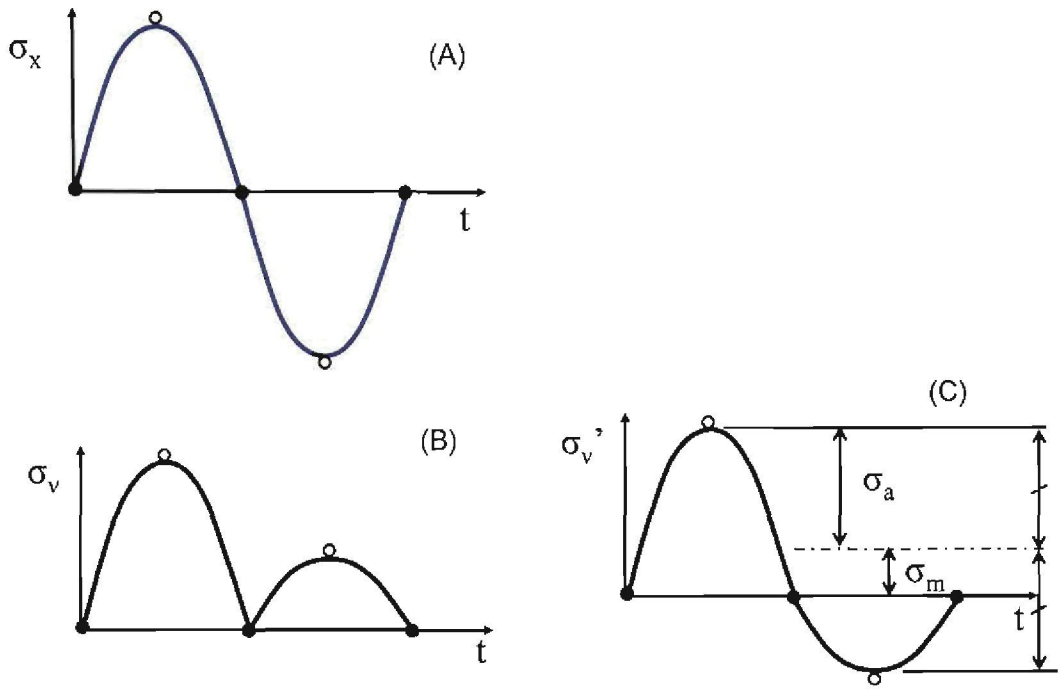


Figure 4-3: (A) Maximum Principal Stress Excursion for R = -1, (B) Related MDE Stress Excursion, (C) Developed MDE Stress Excursion

4.5 UNIAXIAL FATIGUE TEST DESIGN

4.5.1 Selection of Geometry

The research into existing geometries of multiaxial specimens in general and graphite specimens in particular yielded a fair number of geometries that were critically evaluated for the uniaxial and multiaxial tests of this investigation. These geometries are illustrated on the same scale for comparison in Figure 4-4.

Detailed drawings were made of the specimen geometries that were reported in the literature (refer to Chapter 2). Some assumptions were made where information was lacking. The machining cost of each specimen was estimated by the Centre for Advanced Manufacturing, North-west University. The relative machining cost of the specimens (relative to the cost of the cheapest specimen, S5) was calculated and tabulated in Table 4-1. This figure and table also contain the geometries, relative cost and equipment data of the uniaxial and multiaxial specimens that are proposed in this research, for the sake of completeness.

Specimen S9 has two additional undefined steel discs bonded to its ends to create an enclosure for hydrostatic loading, which makes it even more expensive. The relative machining cost shown in the table only applies to the graphite part of the specimen.



Figure 4-4: Full Section Scaled Comparison of All Test Specimens

The continuous radius type specimens were not considered suitable because of its infinitesimal small volume in the gauge section against the KTA-3232 failure criterion employed. This criterion, which is discussed in detail in Section 4.4, states that the

probability of failure of graphite is dependent on the volume weighted stress in the material. This ruled out Specimens S14 and S15 as contenders for the tests.

With this background, the new uniaxial specimen, S70 is proposed, based on the geometry of a metallic axial fatigue specimen with circular cross section and tangentially blended fillets according to ASTM E466-90 (2002). In order to remove all axial play in the load train and to retain precision alignment, it was decided in principle to use collet chucks for gripping the specimen. The availability of standard collet chucks constrains the gripping diameter to a maximum of 26 mm. In order to maximise the fracture load (matching the tests better with the load cells of existing fatigue test equipment that is normally used for testing of metals), the gauge section diameter was maximised within the prescribed geometry. The length of the gauge section was minimised to minimise the cost and fragility of the specimen.

These design considerations precipitated the following geometry of the S70 uniaxial fatigue test specimen:

- Diameter of gauge section: 13 mm (exceeds ASTM C749-92 requirement)
- Diameter of grip: 26 mm
- Length of gauge section: 26 mm
- Radius of tangent fillet: 105 mm
- Overall length: 150 mm

The machinability of this geometry is better than that of specimen S16 because of its smaller L/d ratio in the gauge section. Although this decision is in conflict with the alignment requirement of maximum L/d ratios for minimum sensitivity according to Eq. (4.1) and (4.2), the machining and fragility risk (specimens were machined in Germany and air freighted to South Africa) outweighs the misalignment risk.

The final selection of a geometry for the uniaxial tests was done by comparing the machining cost of the specimens with cognisance of the misalignment risk. If one evaluates the uniaxial fatigue specimens on the basis of cost, the following remaining specimens can comply with the load range requirement for uniaxial fatigue tests: S10, S5, S6, S7, S13, and S70. The relative machining cost of Specimen S5 and S6 is less than that of specimen S70, but it has much higher stresses in its gripping zones.

Specimen S7 has approximately the same machining cost as S70, but the pin-and-hole gripping method induces high stress concentrations and alignment is not guaranteed with the existing grips. Specimen S13 has also approximately the same machining cost as S70, but the shouldered grips are more difficult to align than the friction grips.

Specimen S10 is a factor 10 more expensive, and cannot offer the same precision of alignment.

Table 4-1: Summary of Relative Cost, Type of Test and Type of Test Equipment

Speci-men	Ref.	Relative Cost of Machining	Type of Test	Type of Test Equipment
S1	Socie *et al.*	66,7	Multiaxial fatigue of steel	Servo-hydraulic fatigue tester with axial and torsional actuators
S2	McDiarmid	200	Multiaxial fatigue of steel	Servo-hydraulic fatigue tester with axial and hydrostatic actuators
S3	Fash *et al.*	8	Multiaxial fatigue of steel	Servo-hydraulic fatigue tester with 2 linear actuators causing bending and torsion
S4	Sonsino & Grubisic	10,7	Multiaxial fatigue of steel	Servo-hydraulic fatigue tester with axial and torsional actuators
S5	Taylor *et al.*	1	Multiaxial static of graphite	Hydrostatic and Axial actuator
S6	Taylor *et al.*	1,3	Uniaxial static of graphite	Axial actuator
S7	Bazaj & Cox	3,3	Uniaxial static of graphite	Axial actuator
S8	Found *et al.*	80	None reported – only capabilities	Servo-hydraulic fatigue tester with axial, torsional and hydrostatic actuators
S9	Ho *et al.*	58,7	Multiaxial fatigue of graphite	Axial and hydrostatic actuators
S10	Lee	33,3	Multiaxial fatigue of steel	Torsion and bending actuators
S11	Leese & Morrow	80	Multiaxial fatigue of steel	Servo-hydraulic fatigue tester with 2 linear actuators causing bending and torsion
S12	Price	2	Uniaxial fatigue of graphite	Crank and lever actuator
S13	Schmidt	3,3	Uniaxial fatigue of graphite	Not stated
S17	Burchell *et al.*		Multiaxial static of graphite	Servo-hydraulic fatigue tester with axial and hydrostatic actuators
S60B		9,6	Multiaxial fatigue	Hydraulic chamber with pressure control
S70		3,3	Uniaxial fatigue	Servo-hydraulic fatigue tester with well aligned custom designed collet chucks

The machinability of the S70 specimen was assessed by machining six units from RFS grade graphite, which was available ex stock from SGL Carbon, South Africa. The machining trials were successful and the results are shown in Figure 4-5.



Figure 4-5: S70 Uniaxial Fatigue Specimens Machined from RFS Grade Graphite

4.5.2 Clamping Force

Gripping of the S70 specimen depends on the friction between the collet and the graphite. The static coefficient of friction was determined experimentally by measuring the slope of a steel rail at which a graphite part, placed on top of the rail, just started to slide down. A static coefficient of friction of 0,7 was calculated for RFS grade graphite on steel.

Since the compressive strength of graphite is approximately 4 times higher than its tensile strength, and the grip section is already highly loaded by the compression of the collet, the clamping pressure in the grip is designed to only withstand the tensile force. The grip is designed to counteract the compressive load via an end stop, as shown in Figure 4-9.

Eq.(4.7) is derived to quantify the required clamping pressure.

Clamping pressure to prevent slip in tension :

$$p = \frac{n.S_{ut}.d^2}{4.\mu.D.h} \qquad .....(4.7)$$

Where :

p ≡ Clamping pressure between collet and graphite [MPa]

n ≡ Factor of safety [-]

S_{ut} ≡ Ultimate tensile strength of graphite [MPa]

d ≡ Diameter of gauge section [mm]

μ ≡ Coefficient of friction between graphite and collet material [-]

D ≡ Grip diameter of specimen [mm]

h ≡ Grip height in collet [mm]

A conservative clamping pressure of 12 MPa on the full grip height is calculated for the S70 uniaxial specimen. The Von Mises stress distribution in a quarter section model of the S70 specimen, using this clamping pressure is shown in Figure 4-6. The finite element parameters for this analysis are shown in **Appendix L**.

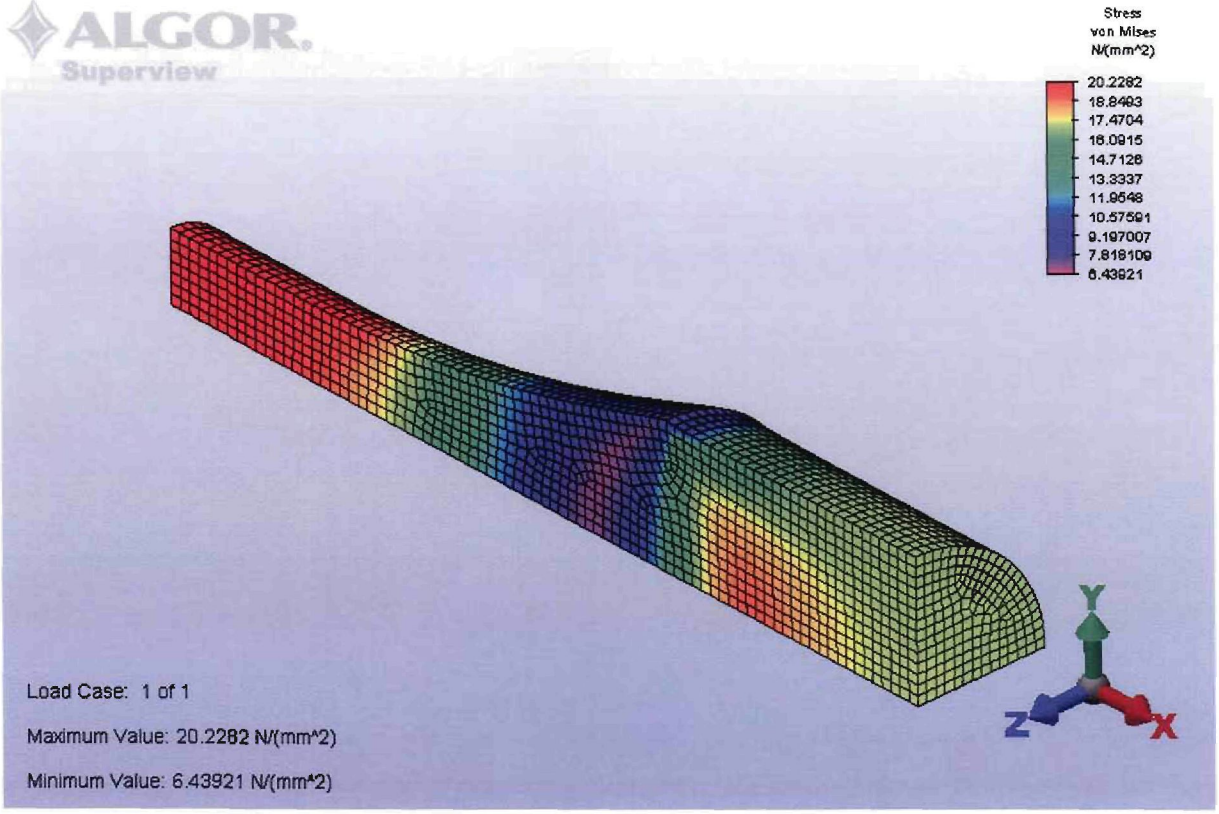


Figure 4-6: Von Mises Stress Distribution in Collet Clamped Quarter Section of S70 Uniaxial Specimen under Full Tensile Load

4.5.3 Risk Abatement Tests

The risk of insufficient collet pressure resulting in slipping of the specimen was assessed with a simple compression test as shown in Figure 4-7. A number of cylindrical graphite bars were machined to the dimensions of the grip diameter of the S70 specimen from RFS grade graphite. These bars were clamped in a collet at different clamping pressures (turn increments of the clamping nut from a "hand-tight" reference position) and loaded in compression with the hydraulic jack. The force at which the bar started to slip was measured with a 1000 kg loadcell.

It is found that a high contact pressure is required to prevent slippage. The footprint of the collet is clearly visible on the graphite in Figure 4-8 due to the high clamping pressure.

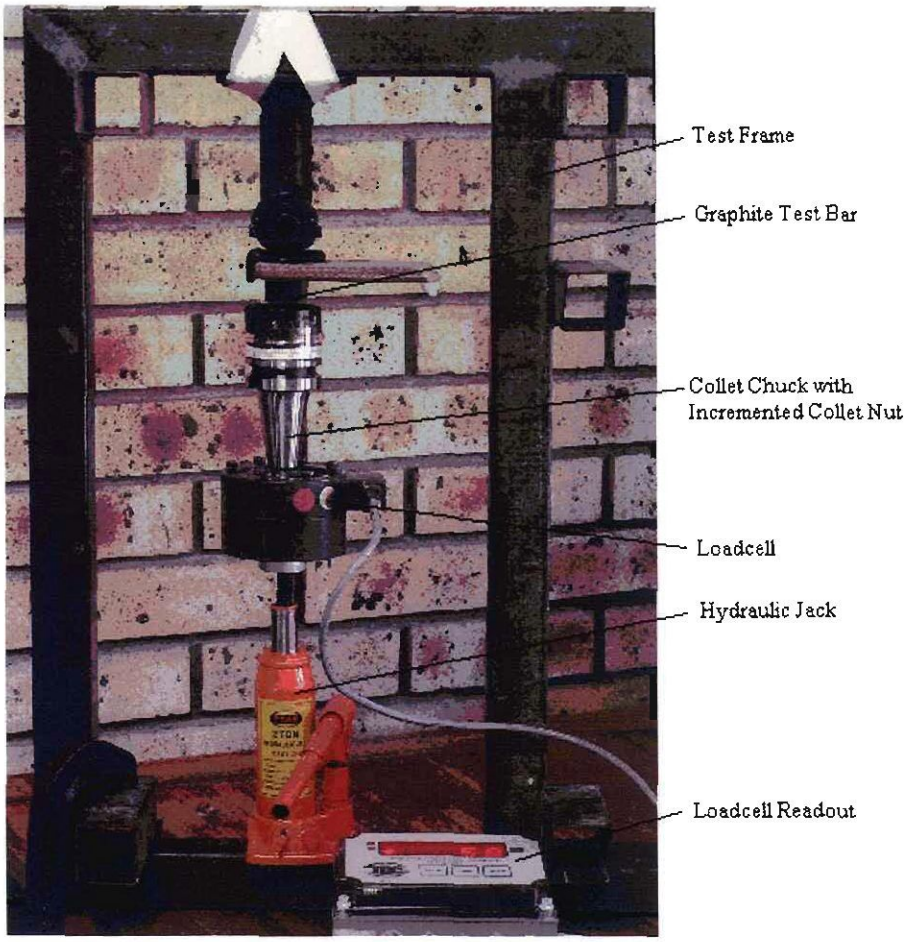


Figure 4-7: Simple Compression Test Setup to Assess Gripping Force

It is found that the moment the bar slips, the gripping force required to hold it thereafter is significantly more. This can be attributed to the local wear of the graphite which creates a thin layer of loose graphite powder on the interface (without significantly altering the dimensions). This loose powder then acts as a dry lubricant which makes it difficult to grip the component.

Due to the high risk of slippage, it was decided to also machine four shallow circumferential V-grooves in the collets at 5 mm axial intervals to enhance the clamping effect of the grips.

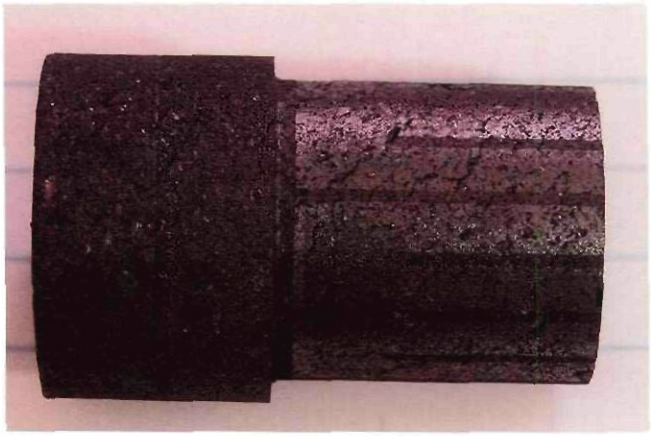


Figure 4-8: Collet Clamping Footprint on Test Piece

In addition to the grooves in the collets, a few sealants and surface treatments were applied to increase the coefficient of friction between the graphite rod and the collet. The best results are obtained with Quality Stone Chip Sealer (Luxor Paints). This product is diluted with water in a ratio of 1 : 1 (volumetric basis) to yield a low viscosity paint.

4.5.4 Modification of Test Equipment

The 1CC dead length collet chuck, manufactured by Kalamazoo Industries Inc, Kalamazoo, Michigan, USA, with accompanying C5 collets that are grooved as mentioned in section 4.5.3 form the basis of the custom designed friction grips. Aluminium end stops, held in place by waved washers, and adapter pieces to interface with an Instron 8801 were designed and manufactured.

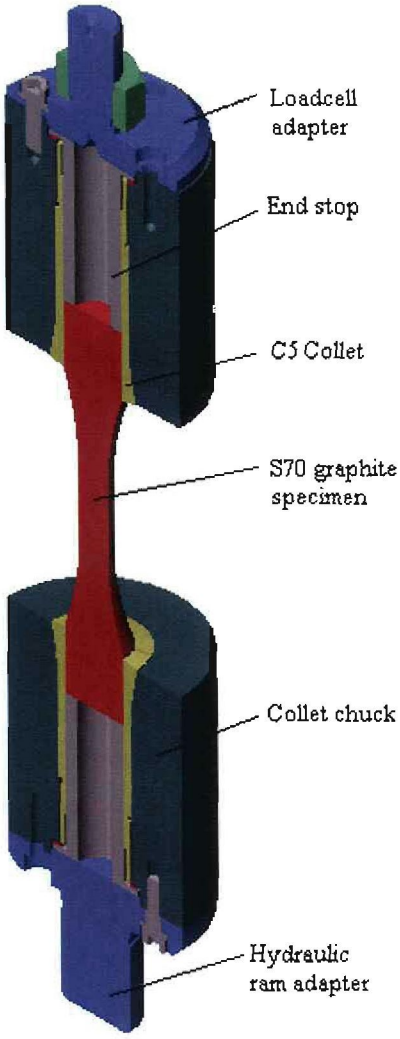


Figure 4-9: Full Section of Uniaxial Fatigue Specimen Grip Assembly

The only other modification that is required to prevent any unwanted torsional loads on the specimen, is the application of an anti-rotation bar to the hydraulic ram of the Instron. This mechanism is shown in Figure 4-10.

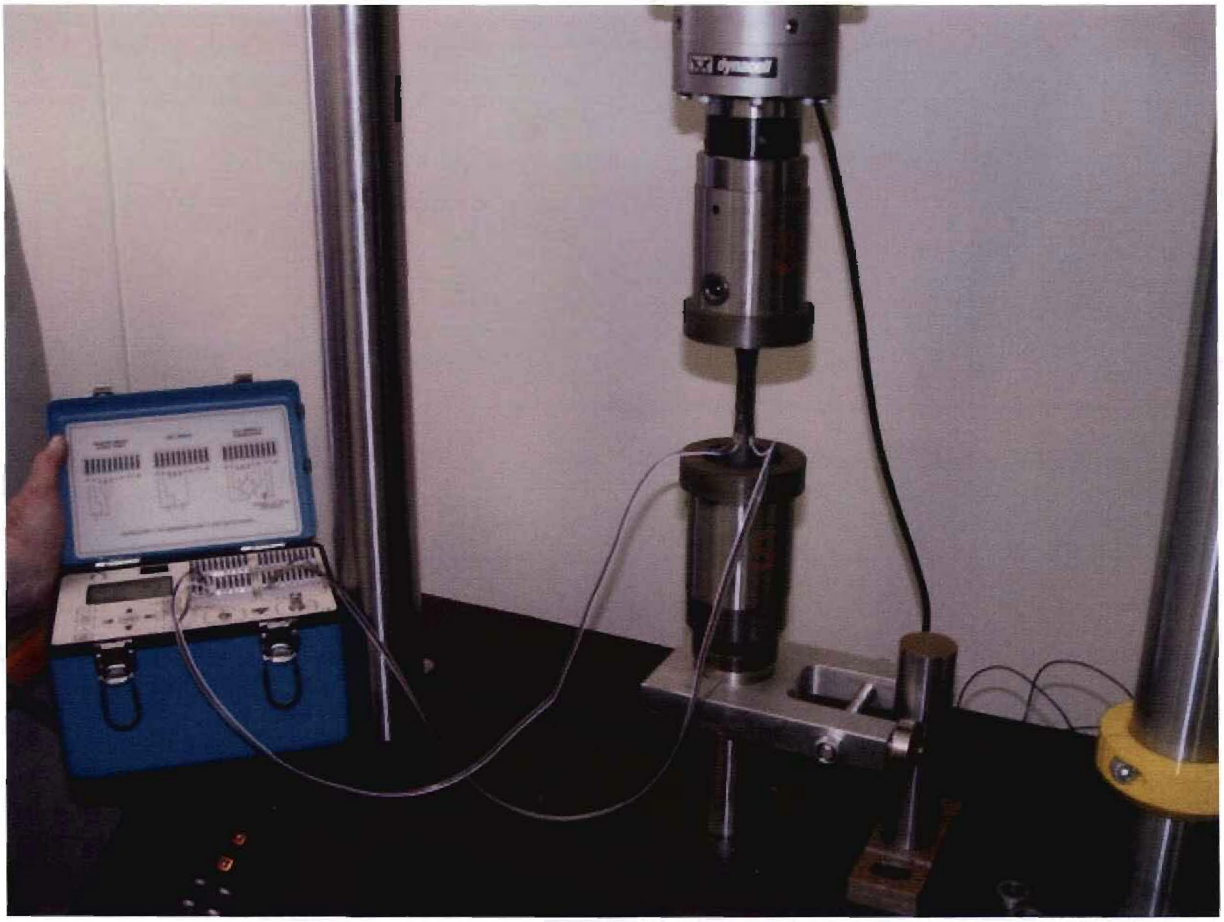


Figure 4-10: Instron 8801 With Collet Grips, Anti-Rotation Bar and Strain Gauged S70 Specimen

4.6 EXPERIMENTAL WORK

4.6.1 Machining Requirements

The first important requirement for machining is that the specimen has to be machined in one setup from the pre-machined round bar. This is specified to ensure that the specimens have no radial run-out (or none apart from that induced by the running accuracy of the machine spindle).

The second requirement is that the cutting methods, to obtain the shape of the raw material as well as the final specimens, have no clamping loads (compressive or tensile loads) producing stresses larger than 5 MPa to the test section volume of the material.

Clamping is typically required during sawing or core drilling operations, rough turning and parting of the cylindrical rods, and finally during CNC turning of the specimens. Limited clamping is allowed in the axial direction of the specimen, since the uniaxial specimen cannot be machined without a rotating centre, and any axial load will stress the specimen test section. Typical radial clamping and "no clamping" zones are shown in Figure 4-11.

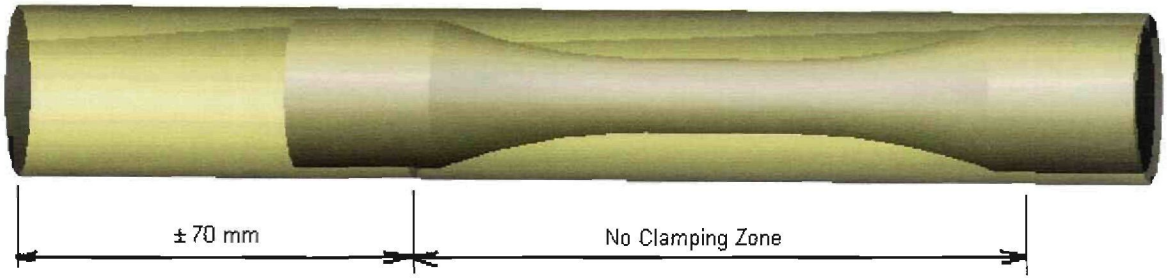


Figure 4-11: Typical No Clamping Zone of S70 Specimen

4.6.2 Condition of Specimens

PBMR was responsible for the supply of the specimens in its final machined condition. All material is manufactured and machined by SGL Carbon according to the specimen sampling plan, as discussed in Chapter 3.

The specimens are supplied in the as-machined condition. The test section diameter is measured, as shown in Figure 4-12, with a Tesa micrometer with an accuracy of ±2 μm. The test section diameter is calculated by averaging 4 measurements for each specimen. The mass of the specimens is measured on a Sartorius model L420P mass balance as shown in Figure 4-13, with an accuracy of ±1 mg.

The surface finish that is specified on the drawings serves as a guide to the machinist for setting cutting speeds, feed rates and depths. The surface finish is not measured, since such measurements will include the surface porosity effects of the graphite, which is a materials characteristic and not a machining characteristic.



Figure 4-12: Geometric Measurement of S70 Specimen

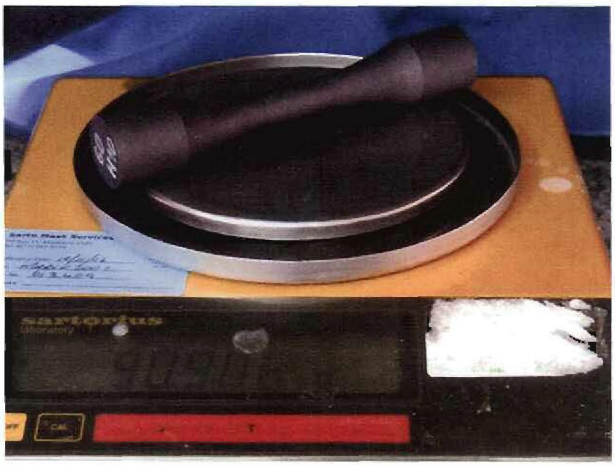


Figure 4-13: Weighing of S70 Specimen

The grip sections of the specimens, subject to loading in the tensile direction, are painted with Quality Stone Chip Sealer (Luxor Paints), to improve its coefficient of friction. This paint is applied in one thin layer to the two cylindrical grip sections of the specimen to prevent any significant dimensional changes. A painted specimen as can be seen on the photograph in Figure 4-14.

The specimens are all similar in shape, size and nominal dimensions. A typical S70 test specimen in NBG18 graphite is shown in Figure 4-14 with nominal dimensions as indicated. The tolerances and other dimensions are shown on the detailed drawing of the S70 specimen, Drawing No. GRA-S70-02, Revision B in **Appendix B**.

The Nominal dimensions of these specimens, machined to Revision B, were:

A = 25.60mm B = 13.00mm C = 26.00mm D = 26.00mm E = 105.00mm

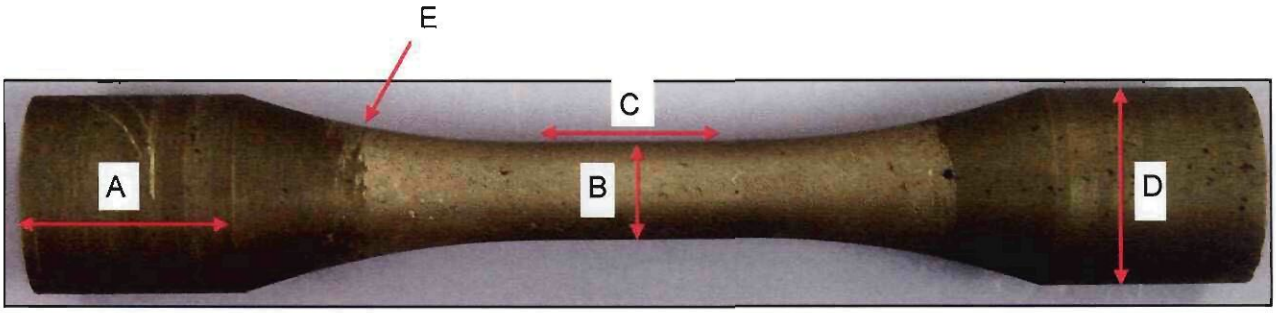
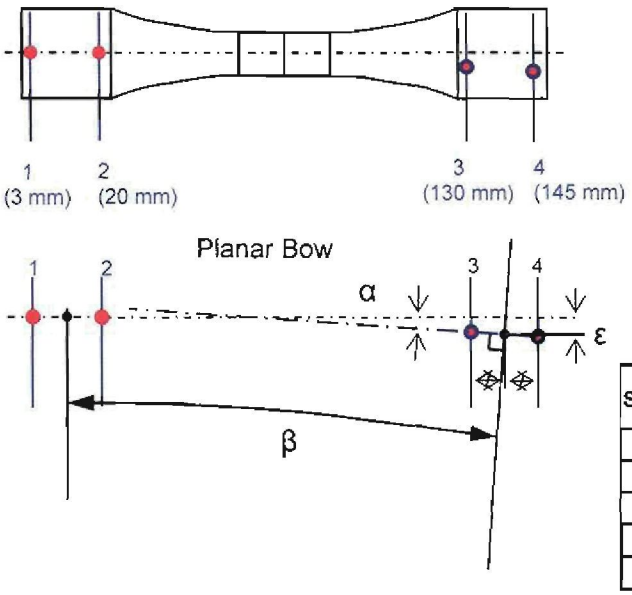


Figure 4-14: Typical S70 Fatigue Specimen from NBG18 graphite

The straightness or run-out of some machined specimens was not as specified. Because the bow of some specimens was only discovered at a late stage in the project, this deviation was not fully quantified. Only 5 severely bowed specimens were measured on a 3D measuring machine. All exhibited planar bow that was later confirmed to have been caused by stress inducing machining procedures.

The cylindricity of the measured specimens ranged between 0,35 and 0,79 mm where the expected cylindricity is of the order of 0,020 mm. The latter is not explicitly stated on the drawing because it is implicitly suggested in the Cutting Plan, as described in Chapter 3.

This inherent bow causes higher residual bending stresses in the gauge section of the specimen, which can adversely affect the test results.



Specimen	δ [mm]	ε[mm]	α [°]	β [°]
60 F-32	0.405	0.19075	0.090	0.087
60 G-46	0.354	0.15325	0.181	0.070
60 F-15	0.790	0.36225	0.250	0.165
60 N-14	0.551	0.25075	0.189	0.114
61 B-31	0.585	0.26725	0.193	0.122

Figure 4-15: Definition of Parameters and Results of Bow Calculation

4.6.3 Fatigue Testing Machine

The uniaxial fatigue tests are conducted on an Instron 8801, 100kN servo-hydraulic testing machine with a 25kN calibrated load cell (see **Appendix F** for calibration certificates). The shape of the forcing function is sinusoidal, and the frequency varies between 1 and 30 Hz. The frequency of force application for each test is indicated in **Appendix C**.

4.6.4 Strain Calibration and Test Procedure

4.6.4.1 Introduction

A major effort went into the alignment of the grips of the testing machine, as part of the machine set-up. The AlignPRO alignment fixture and software was purchased from Instron to enable this. The alignment of the machine is demonstrated according to ASTM E 1012-99 (2002), Type A, Method 2 at a load producing 50% of the typical Ultimate Tensile Strength of the material. The alignment according to this practice is further extended to include Type A, Method 2 at a load producing 50% of the typical Ultimate Compressive Strength of the material. The alignment results for the uniaxial fatigue tests are shown in **Appendix D**.

The uniaxial tests are conducted according to ASTM E466-96 (2002) as far as applicable, extended to include data recording of the stress-strain cycles of one specimen per load ratio (R-value).

4.6.4.2 Strain Calibration

HBM LY11-6/120 type gauges are applied to one graphite sample per load ratio, using HBM X280 epoxy glue. The gauges are connected in a full Wheatstone bridge in the manner shown in Figure 4-16 and Figure 4-17. The gauge factor (G) for the gauges is noted as 2.06 and the bridge factor due to the Wheatstone bridge connection is V.G.(1+ν)/2.

Strain calibration is done by means of a shunt resistor. Two resistors are used for the calibration depending on the strain difference to be measured. The measured resistance values of the two resistors are 119.7 kΩ and 11.88 kΩ. The 119.7 kΩ resistor is used to calibrate the bridge for samples subject to lower strain values (±4000 μm/m), whilst the 11.88 kΩ resistor is used to calibrate samples subject to large strain values (±12000 μm/m).

During the calibration process, the shunt resistor is connected across gauge 1 in order to simulate an output voltage. The simulated strain value is calculated using Eq.(4.8) and a Poisson's ratio (ν) of 0,21. The derivation of this equation is shown in **Appendix K**. (Dally and Riley, 1978).

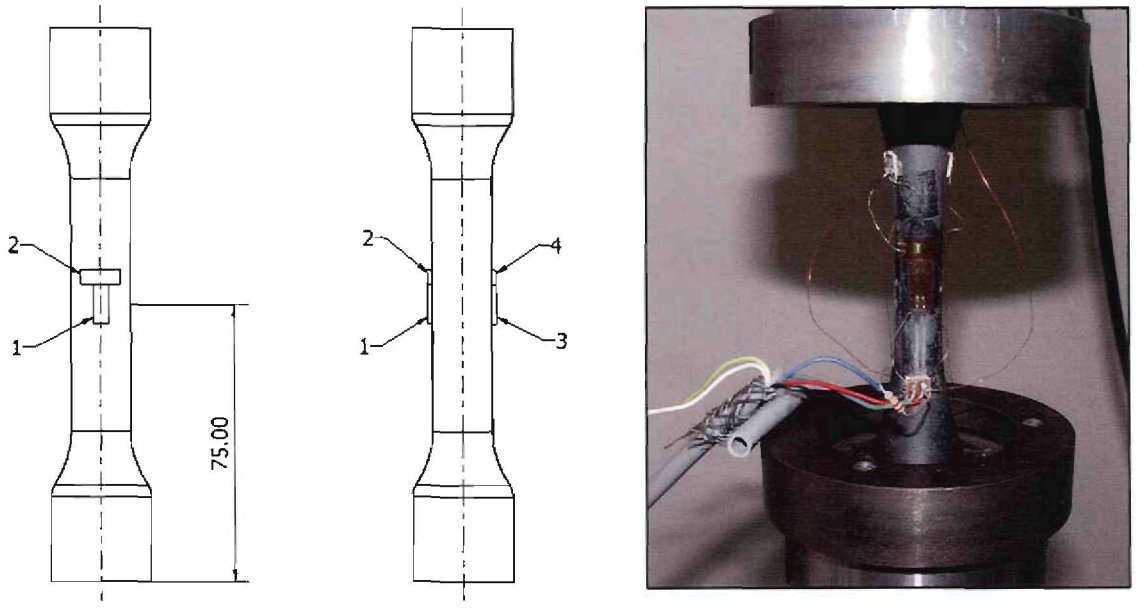


Figure 4-16: Example of Gauged Sample

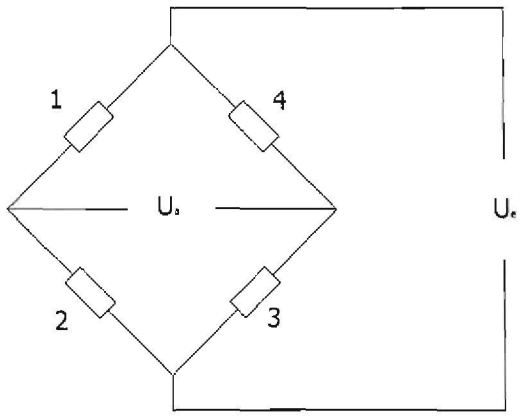


Figure 4-17: Wheatstone Bridge Configuration

$$\varepsilon_c = \frac{-R_1}{G.2.(1+\nu).(R_1 + R_c)} \qquad .....(4.8)$$

Where:

ε_c = simulated strain

G = strain gauge factor

R_1 = 120Ω (gauge 1 resistance)

R_c = shunt resistor value

ν = Poisson's ratio

The ε_c calculated for the 119.7 kΩ shunt resistor is -200.9 μm/m, whilst the ε_c value for the 11.88 kΩ resistor is -2005.9 μm/m.

4.6.4.3 Test Procedure

Eight specimens, from locations explained in Chapter 3, are tested for each load setting. One specimen per load ratio is strain gauged, to measure the stress-strain characteristic at that R-value. Four load settings are used for each dynamic load ratio, resulting in 32 specimens per R-value. Eight specimens are used for each of the two static R-values.

As a starting point, the first load for all tests is guessed at approximately 85% of the average ultimate force (tensile or compression). The subsequent loads are then predicted assuming a straight line approximation on a log-log scale, using the results of the static data and the

results obtained from the first load. Failure is defined as complete separation and run-out is defined as $2x10^5$ cycles.

4.7 UNIAXIAL RESULTS

4.7.1 Mechanical Properties from Static Tests, R = 1

Tensile testing is conducted using ASTM C749-92 (2005) as a guideline. The specimen shape and grip arrangement are different. The average data for the eight tension and compression tests are as follows:

Median ultimate tensile load:	**2641,2 N**
Median ultimate tensile strength:	**19,91 MPa (1σ = 6,4%)**
Median ultimate compressive load:	**11229,5 N**
Median ultimate compressive strength:	**84,67 MPa (1σ = 4,2%)**

Two strain gauged samples (1 tension and 1 compression) form part of above tests. The strain gauged samples are prepared according to the method as explained in Section 4.6.4.2.

4.7.2 Tabular Presentation

All results and test conditions are presented in **Appendix C**.

4.7.3 Graphical Presentation – S-N Diagrams

The following S-N diagrams are plotted according to the definition of the 50% probability S-N curve (Society of Automotive Engineers, 1997). This definition entails calculating the median of the number of cycles per load case, and doing a logarithmic regression through these points (best-fit straight line through 5 points, in this case, on a logarithmic N scale). All information on these diagrams is in accordance with ASTM E468-90 (2002). The broken line and associated equation in these diagrams, is a regression through all individual data points, for comparative purposes. The solid line and associated equation in these diagrams, is a regression through the 5 median values.

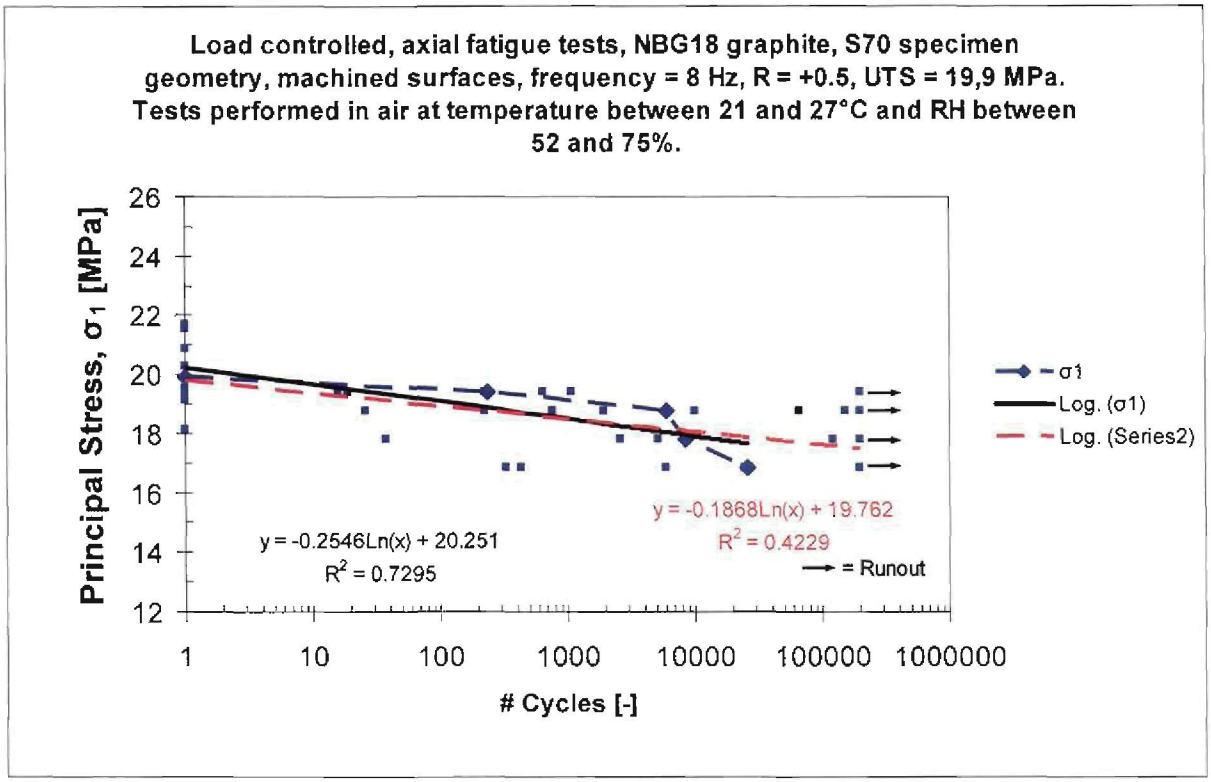


Figure 4-18: S-N Diagram for R = +0.5 Uniaxial Fatigue

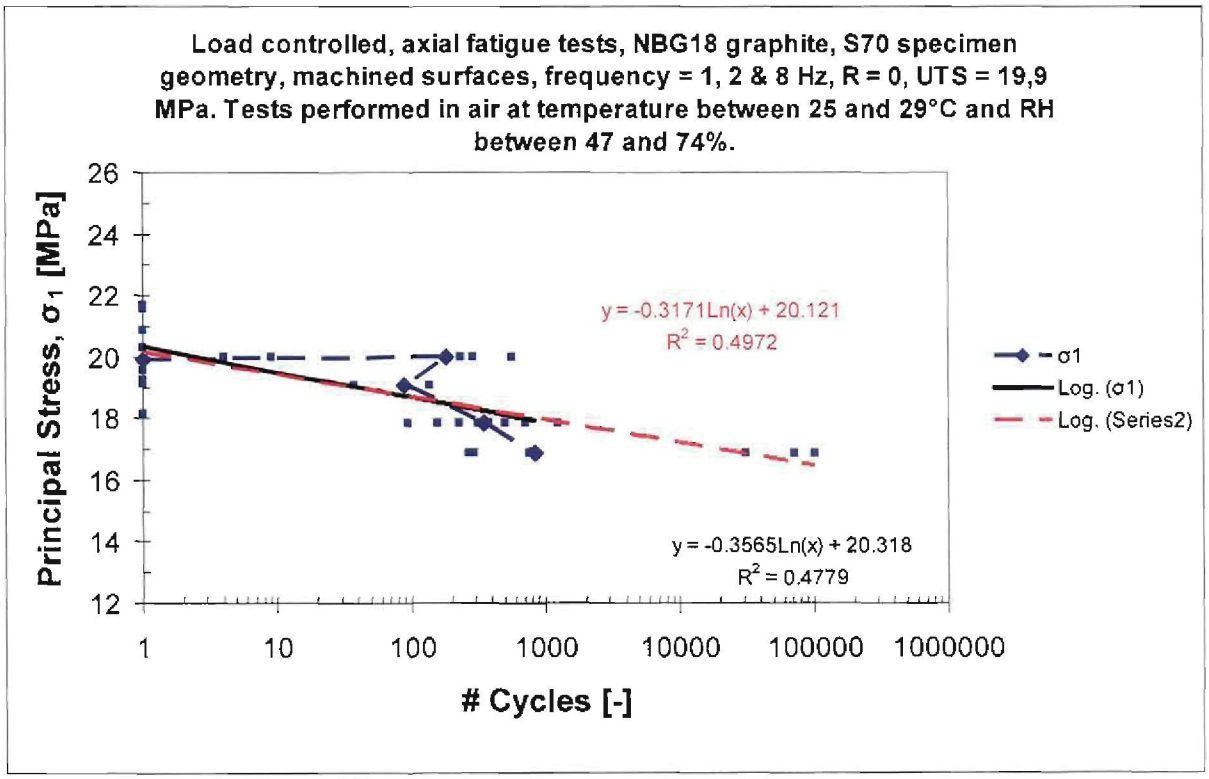


Figure 4-19: S-N Diagram for R = 0 Uniaxial Fatigue

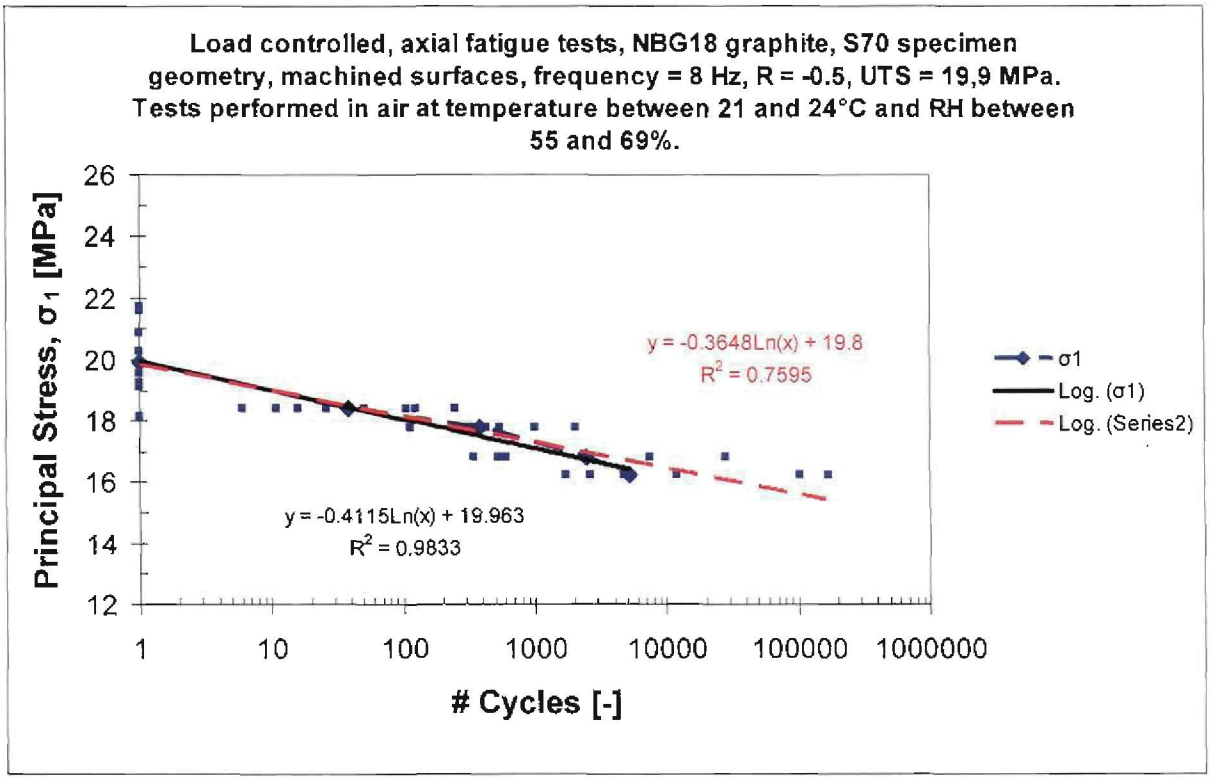


Figure 4-20: S-N Diagram for R = -0.5 Uniaxial Fatigue

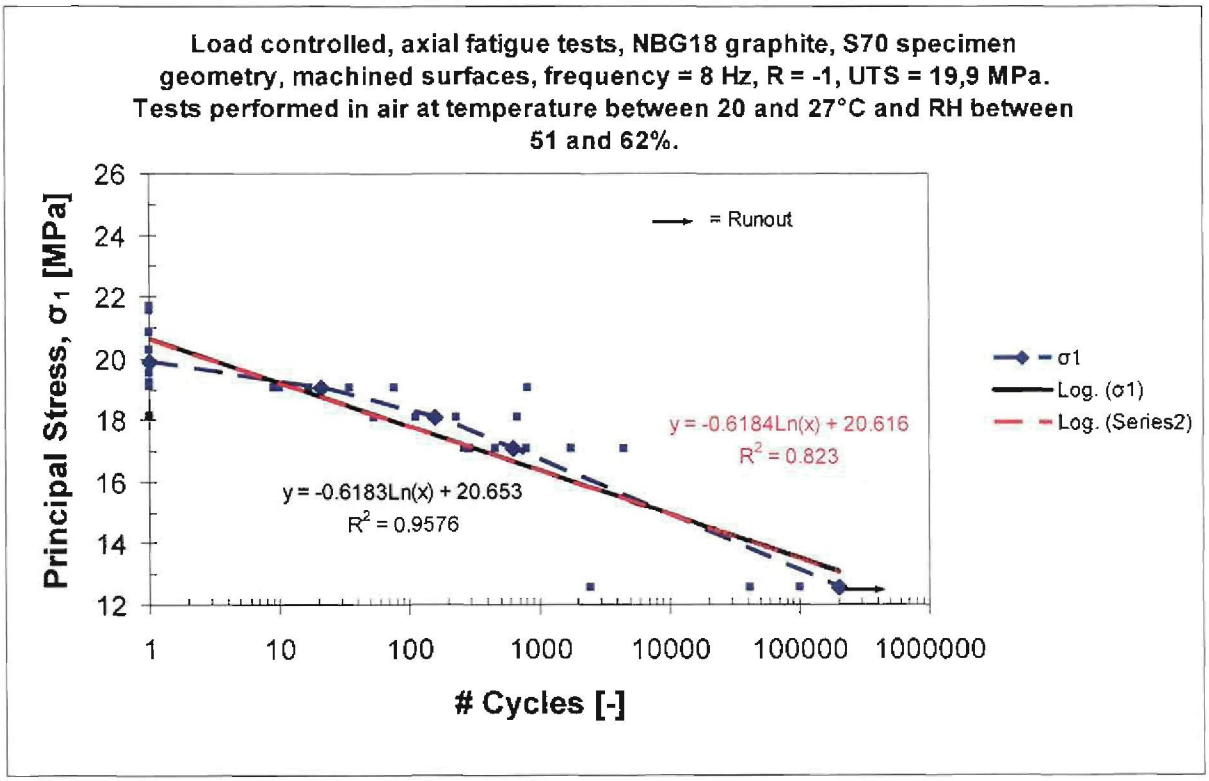


Figure 4-21: S-N Diagram for R = -1 Uniaxial Fatigue

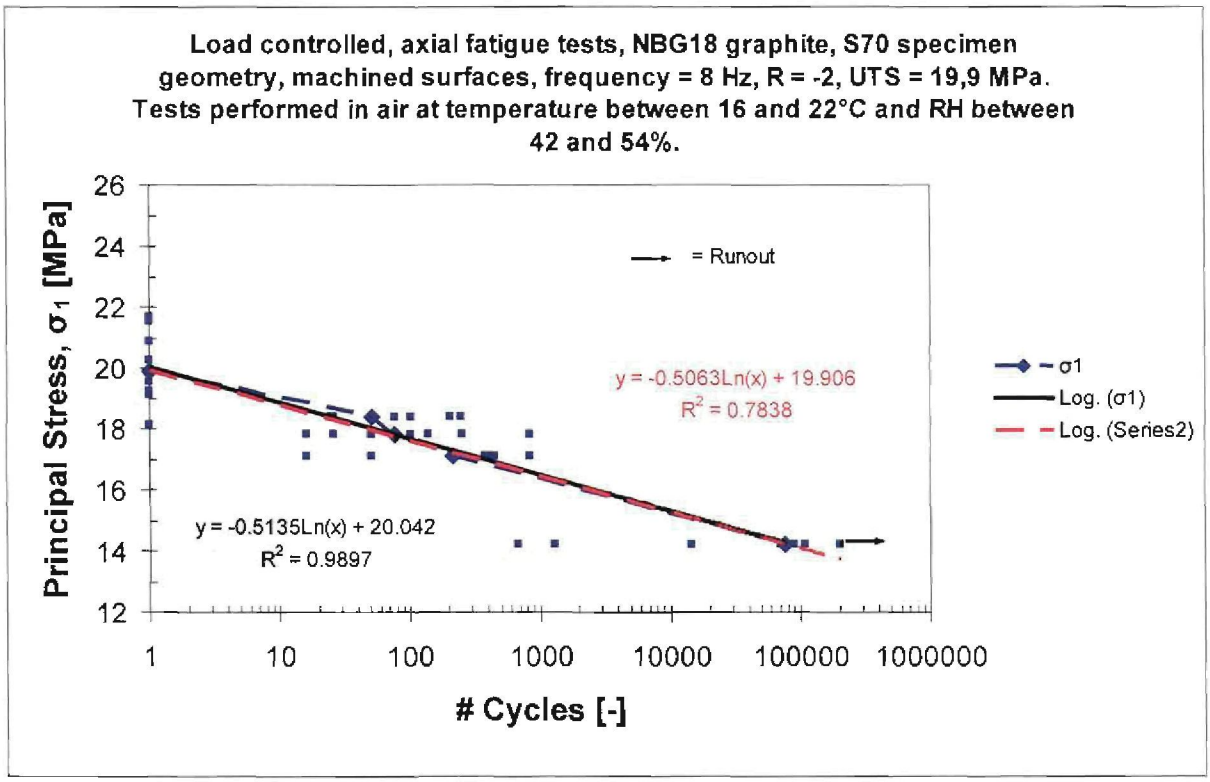


Figure 4-22: S-N Diagram for R = -2 Uniaxial Fatigue

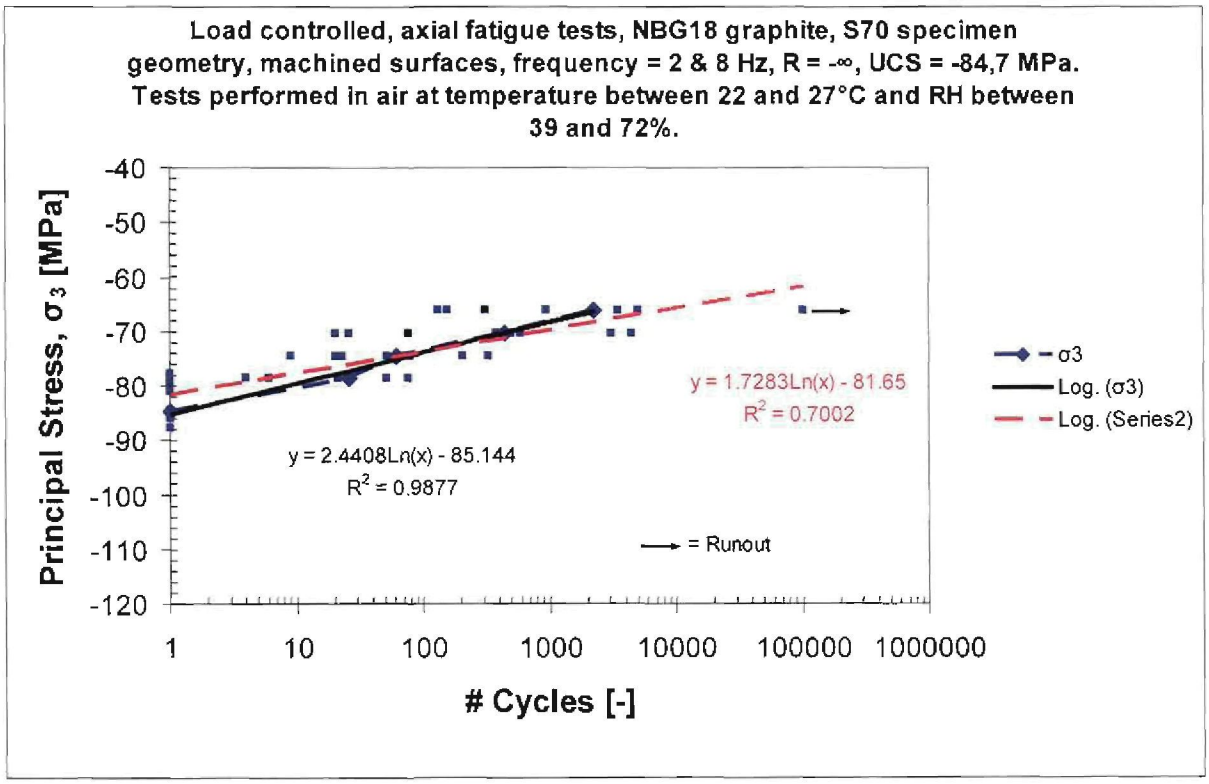


Figure 4-23: S-N Diagram for R = -∞ Uniaxial Fatigue

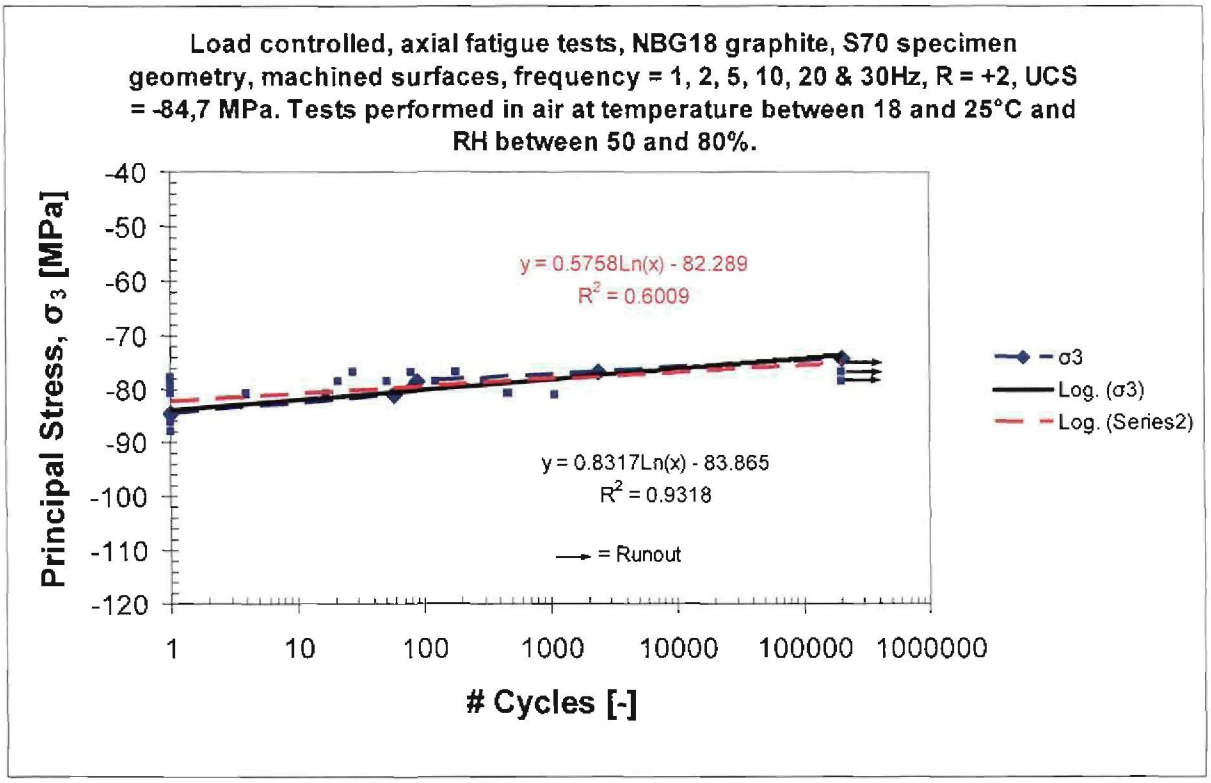


Figure 4-24: S-N Diagram for R = +2 Uniaxial Fatigue

4.7.4 Combined S-N Diagrams

The regression equations, determined from the S-N diagrams, are used to predict the maximum allowable principal stress as a function of life. These curves are combined in Figure 4-25 to Figure 4-27 to graphically show the effect of the load ratio on the slope of these lines.

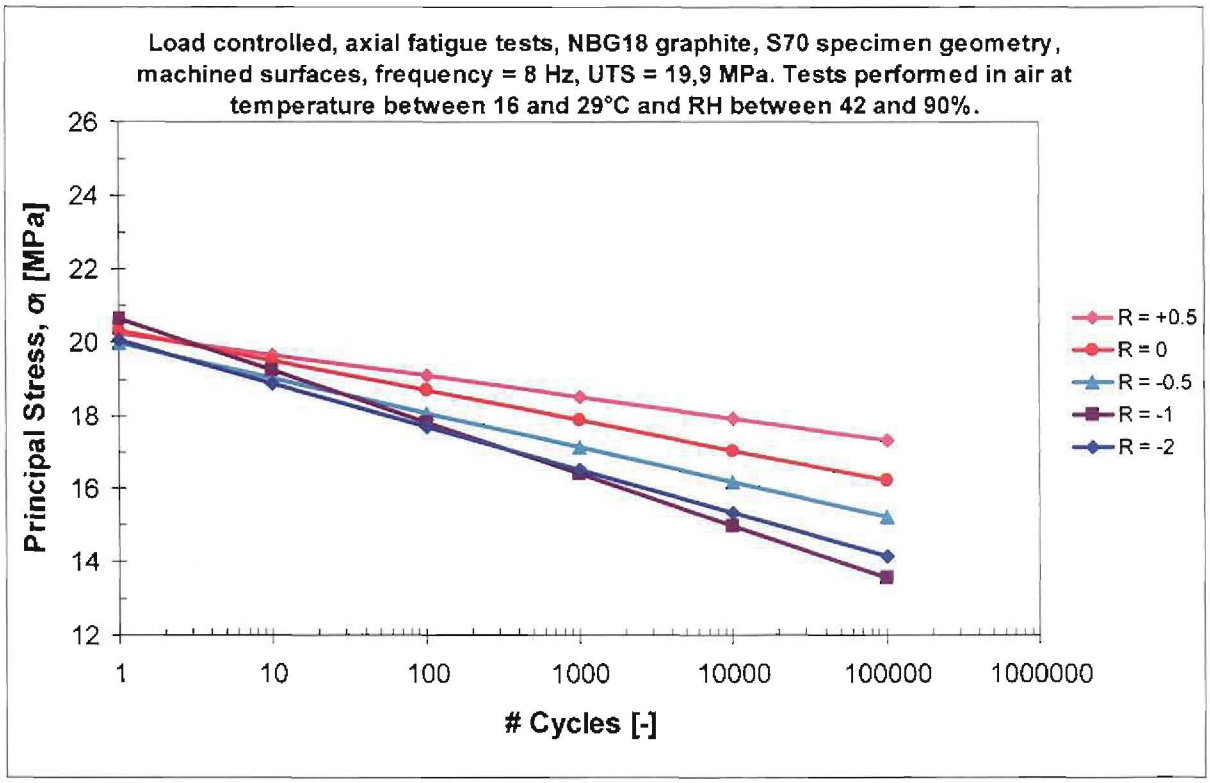


Figure 4-25: Combined S-N Diagram for Tension Dominant R-values, Uniaxial Fatigue

Although the relative humidity and temperature varied a lot during these tests, the effect of the water vapour on the mechanical strength of the graphite is considered negligible, because the graphite weight loss due to oxidation is negligible at these low temperatures. Even at high temperatures, Nomura *et al.* (1986) showed that the effect of water vapour on the compressive strength of graphite at 800°C is insignificant.

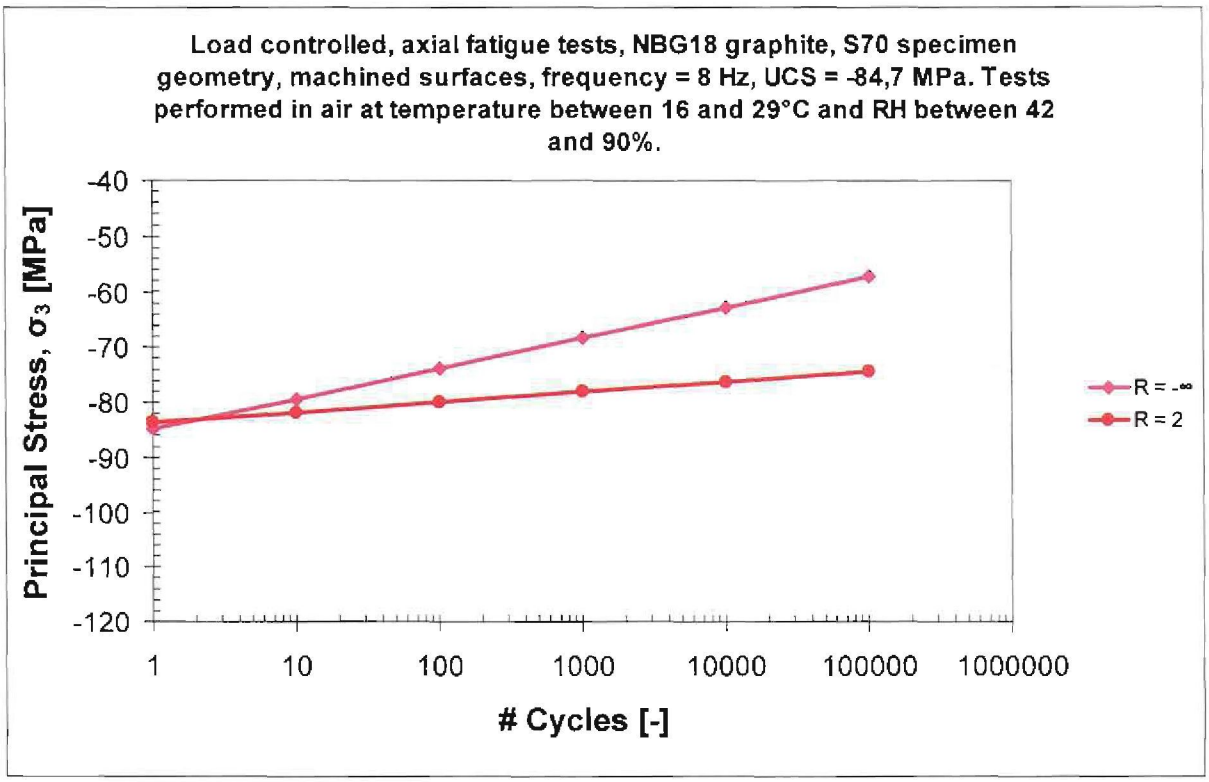


Figure 4-26: Combined S-N Diagram for Compression Dominant R-values, Uniaxial Fatigue

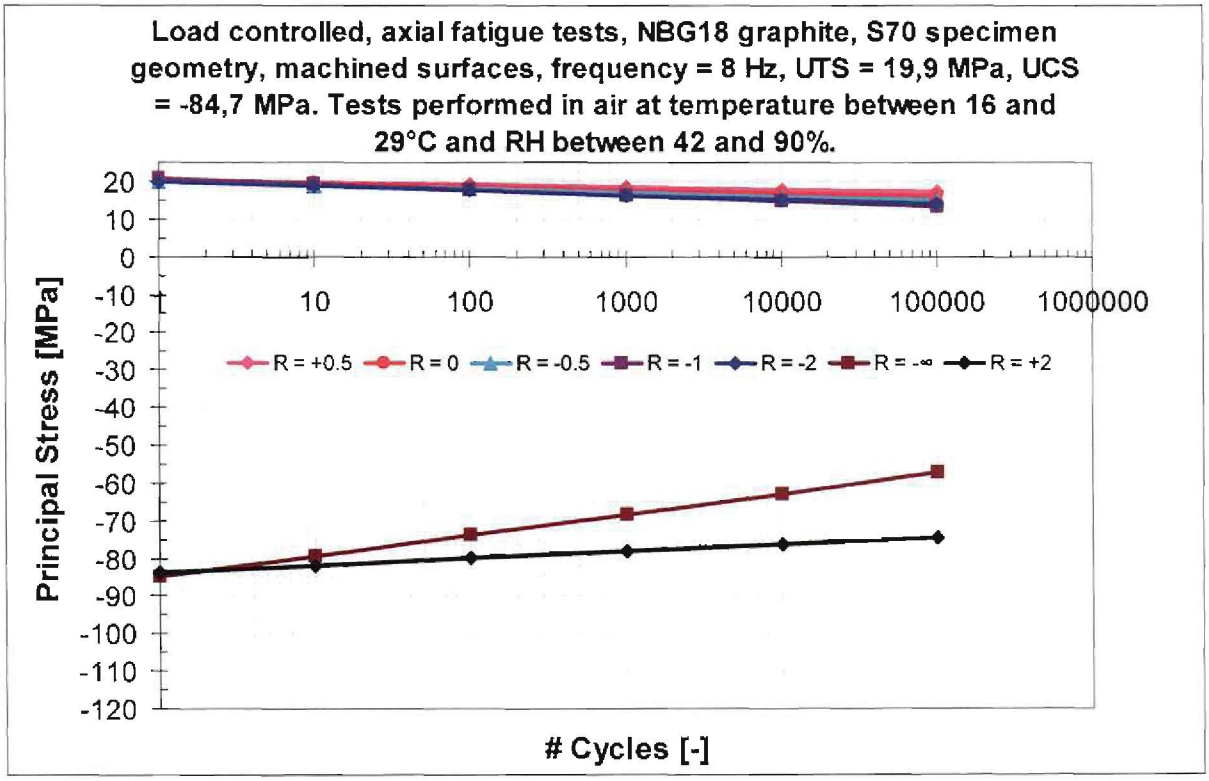


Figure 4-27: Combined S-N Diagram for All R-values, Uniaxial Fatigue

4.7.5 Constant-Life Diagrams

The constant-life chart for 50% failure probability based on Maximum Principal stress is shown in Figure 4-28, in terms of midrange stress and stress amplitude. Another format of the constant-life chart is shown in Figure 4-29, where maximum stress is plotted as a function of minimum stress. The fatigue life is calculated using the regression equations of the S-N curves of paragraph 4.7.3.

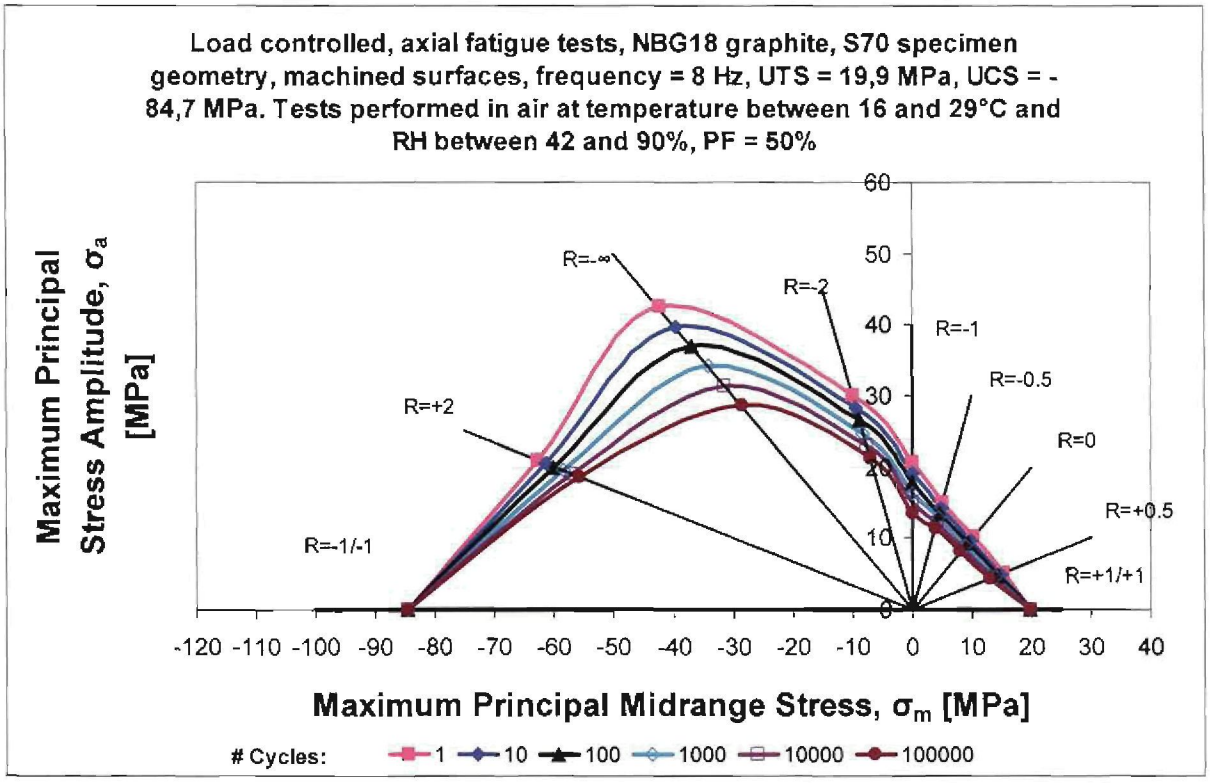


Figure 4-28: Constant-Life Chart Based on Maximum Principal Stress in Uniaxial Loading

The six load ranges R = +1/+1, R = +0,5, R = 0, R = -0,5, R = -1 and R = -2 are governed by the tensile strength of the graphite. Only the three load ranges R = -∞, R = +2 and R = -1/-1 are governed by the compressive strength of the graphite. This is due to the S_{ut}/S_{uc} ratio of this grade of graphite which is close to ¼ whereas R = -2 only have a ratio of ½ between the magnitude of tensile and compressive stress. The approximate transition load ratio would thus be R = -4.

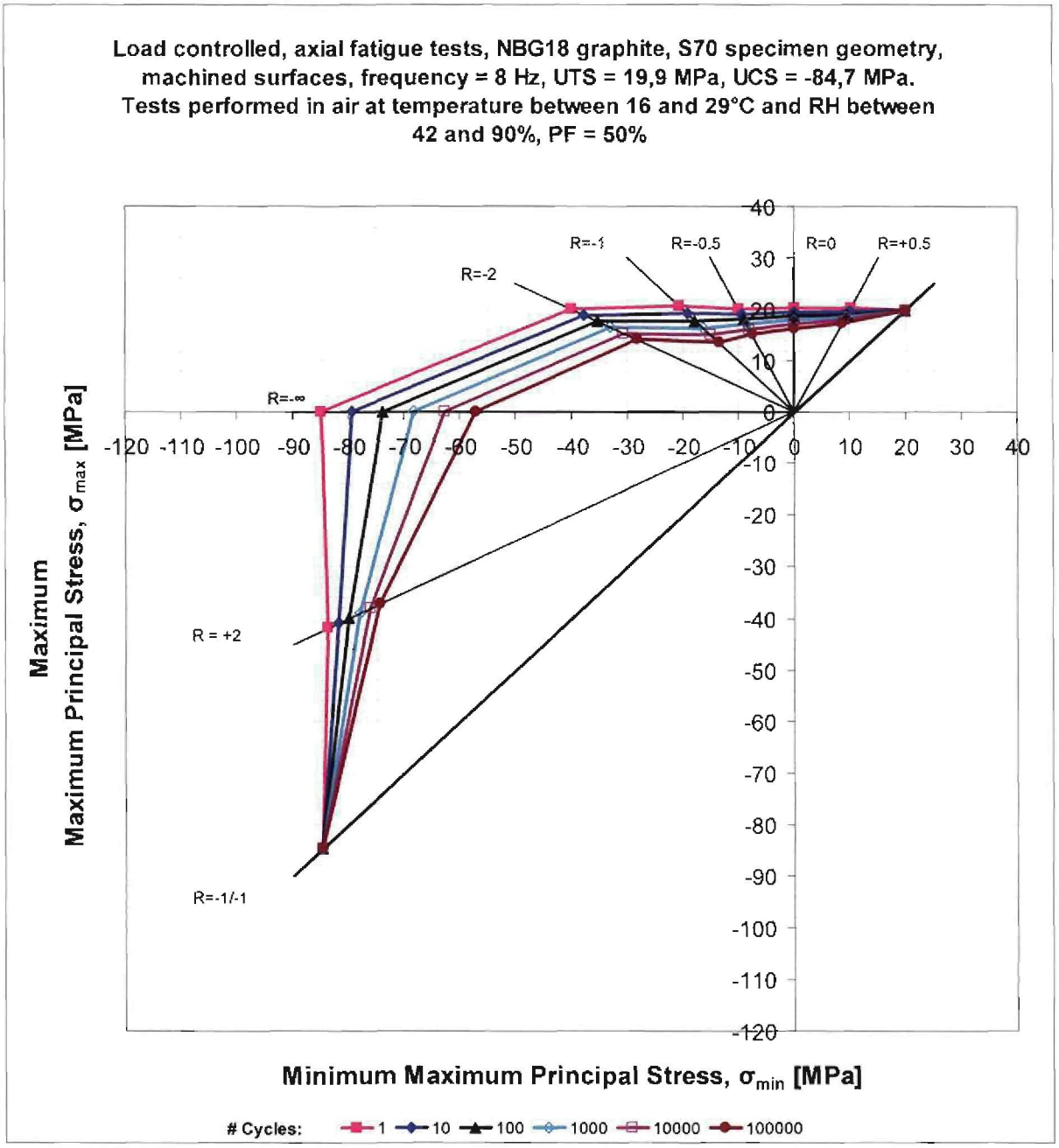


Figure 4-29: Constant-life Chart - Maximum & Minimum Stress

In order to compare the constant-life charts of the uniaxial and multiaxial fatigue tests, the MDE stress is used as the strength parameter. Refer to Section 4.4 for details about the calculation of the MDE stress. A constant Poisson ratio of 0,21, which is the value according to Fechter (2007) obtained through material tests, is used for all MDE stress calculations, unless stated otherwise. The strength ratio factor f, used in this research to calculate MDE stress is calculated using the UTS and Ultimate Compressive Strength (UCS) that is measured in these uniaxial tests for NBG18 (Refer to Section 4.7.1). The "developed MDE

stress waveform", as proposed in the section mentioned above, is implemented to enable MDE stresses to be plotted on a constant-life chart that has the same lay-out as Figure 4-28.

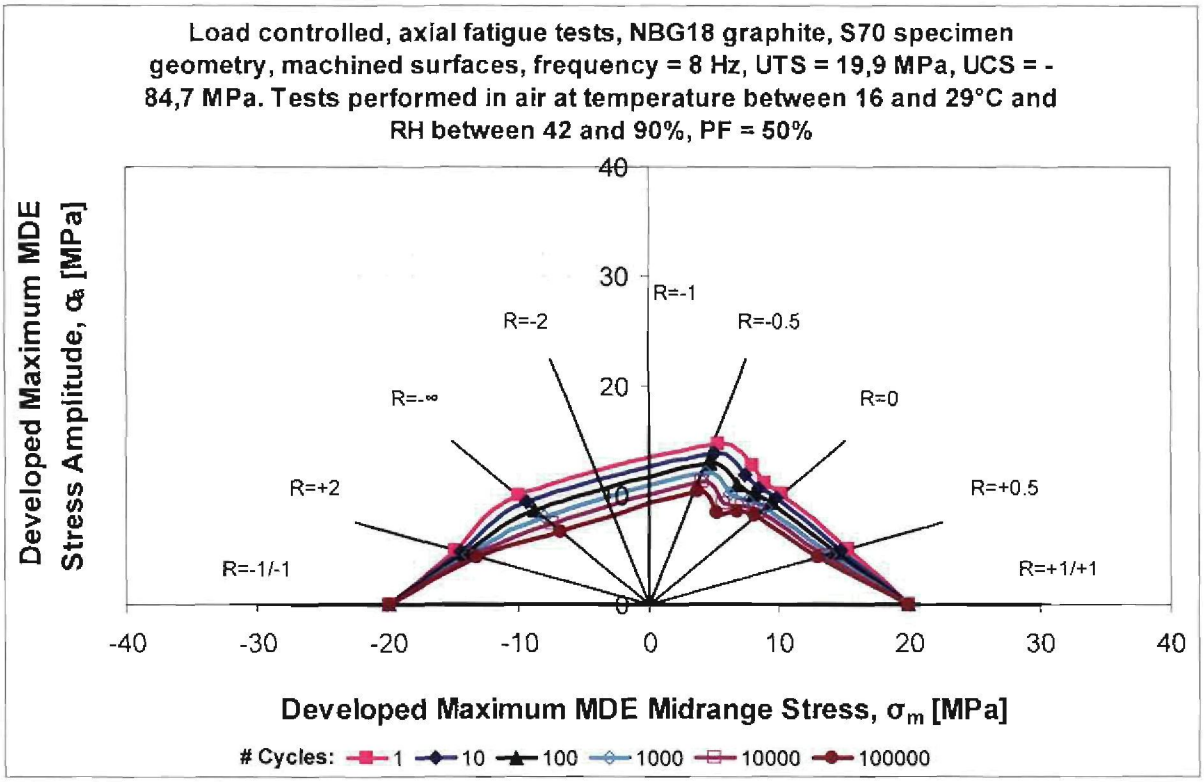


Figure 4-30: Constant-Life Chart Based on MDE Stress in Uniaxial Loading

The constant-life chart of NBG18, based on MDE stress in uniaxial loading, is shown in Figure 4-30. The data points near the abscissa are biased between R = 0 and R = -0.5 because the stress basis of these tests is the Maximum Principal stress and not the MDE stress. Additional tests to define the fatigue life based on MDE stress ratios of R = -0.5, R = -1 and R = -2 may make the chart more symmetrical about the abscissa. The static strength values are equal by the decision to use the results of these tests to define the strength ratio, f in Eq.(4.4). This value of f is used consistently throughout this research.

4.7.6 Stress versus Strain (Hysteresis Loops)

Graphical representations of the data for stress-strain cycles at different life cycles and for the various loading conditions are given below.

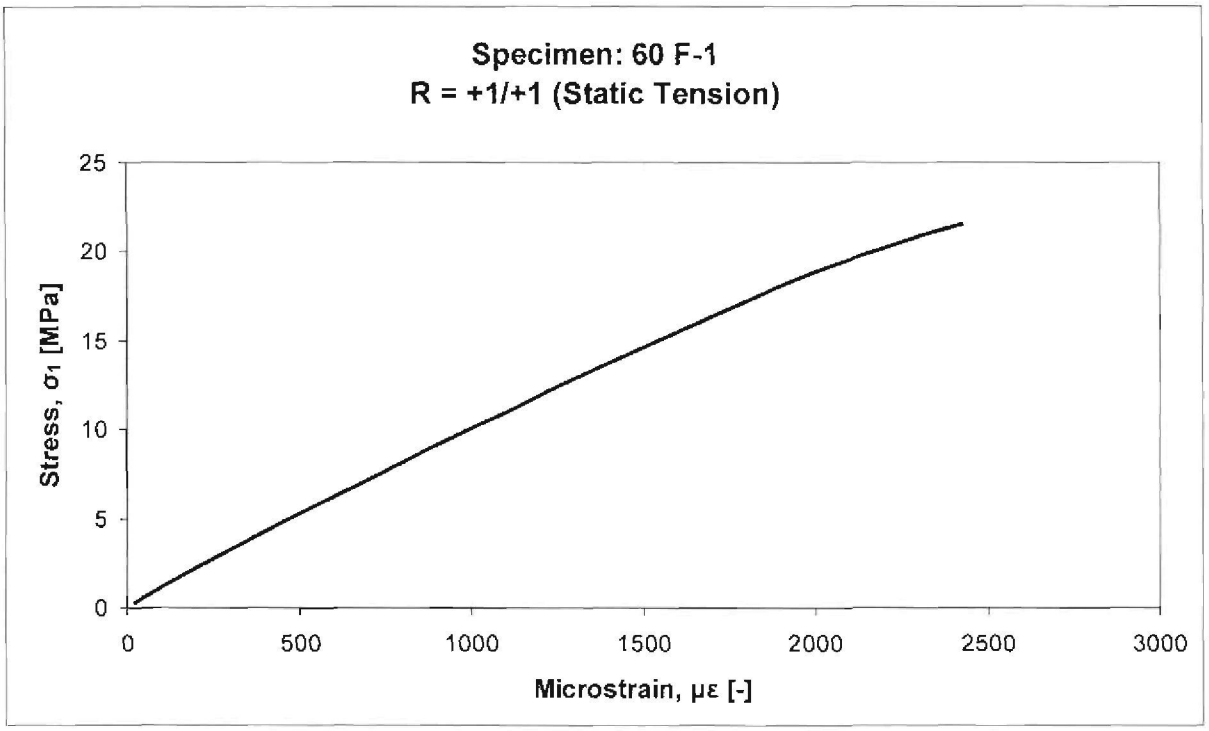


Figure 4-31: Stress Versus Strain for R = +1/+1 (Tensile Test)

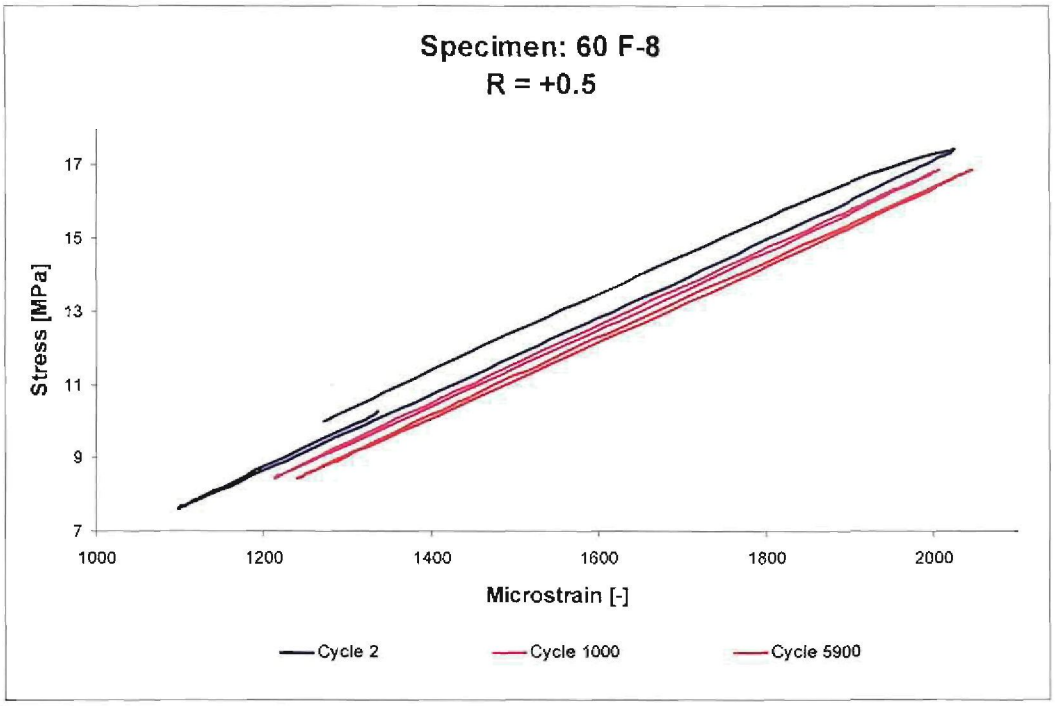


Figure 4-32: Stress Versus Strain (Hysteresis Loop) as Function of Life for R = +0.5

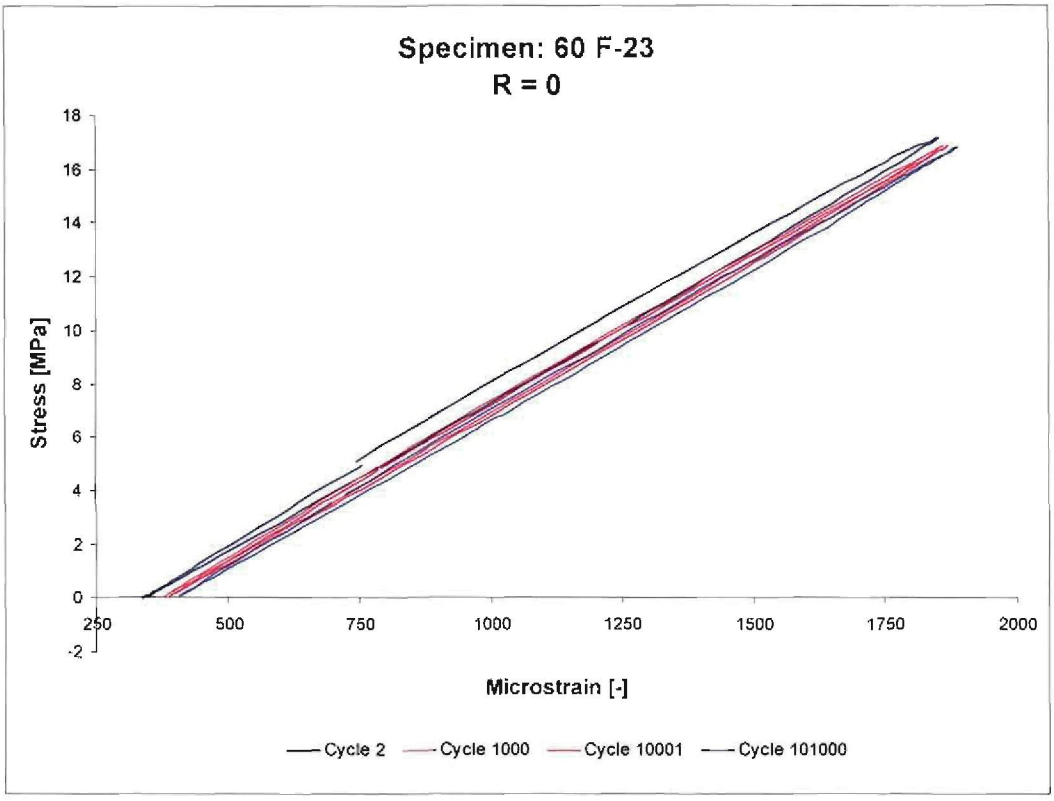


Figure 4-33: Stress Versus Strain (Hysteresis Loop) as Function of Life for R = 0

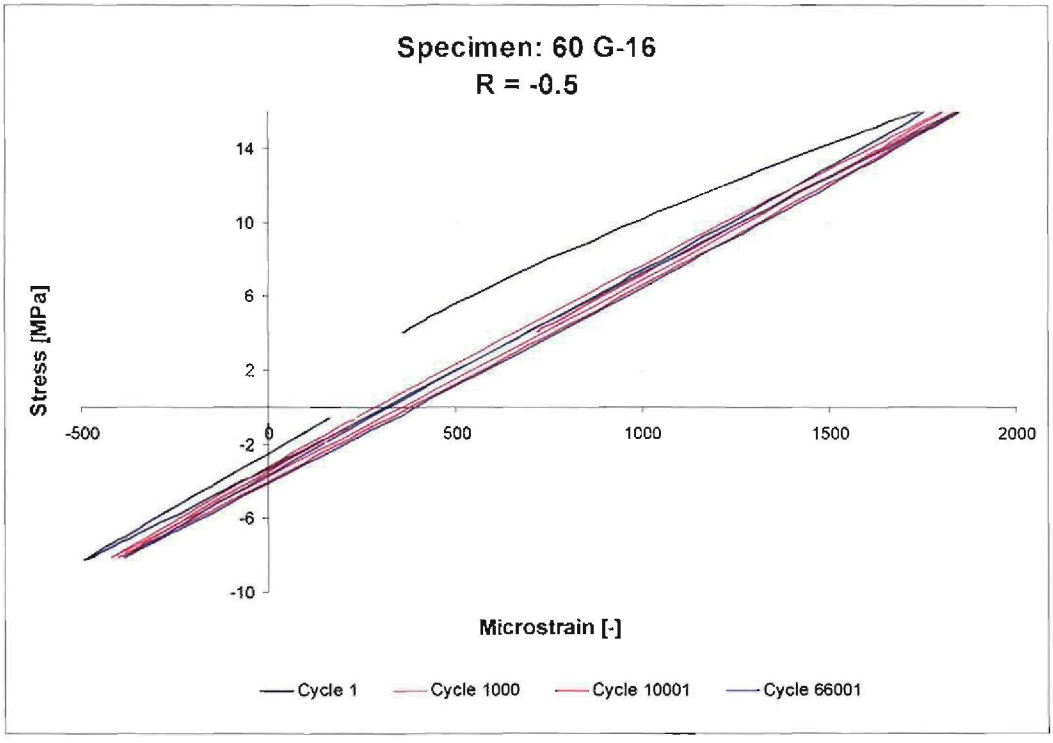


Figure 4-34: Stress Versus Strain (Hysteresis Loop) as Function of Life for R = -0.5

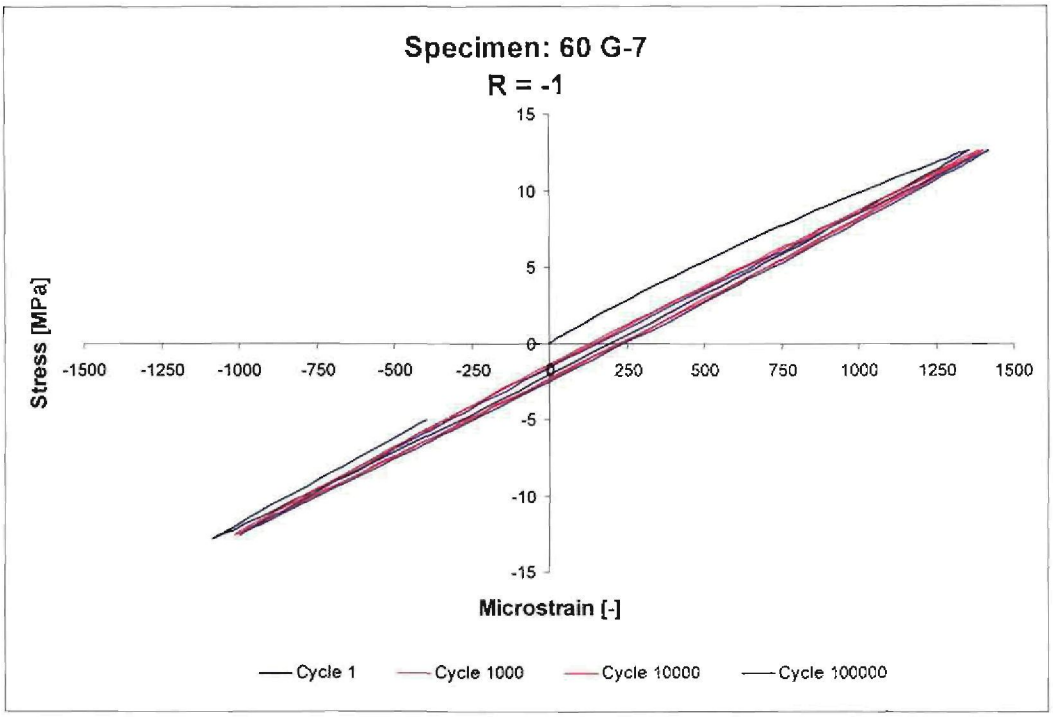


Figure 4-35: Stress Versus Strain (Hysteresis Loop) as Function of Life for R = -1

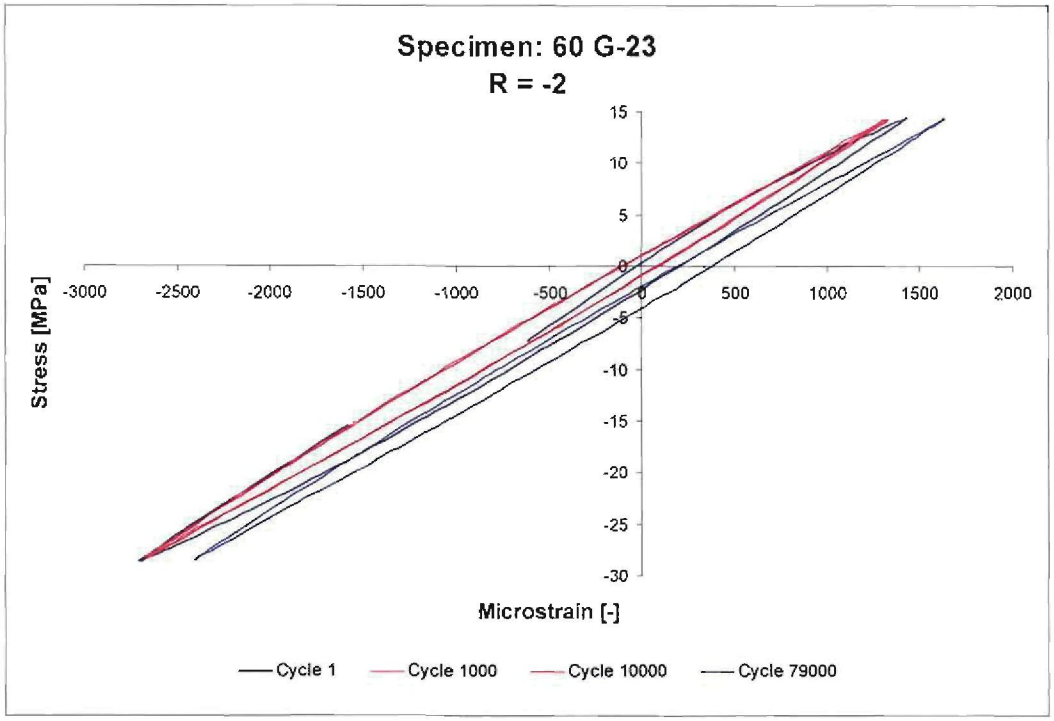


Figure 4-36: Stress Versus Strain (Hysteresis Loop) as Function of Life for R = -2

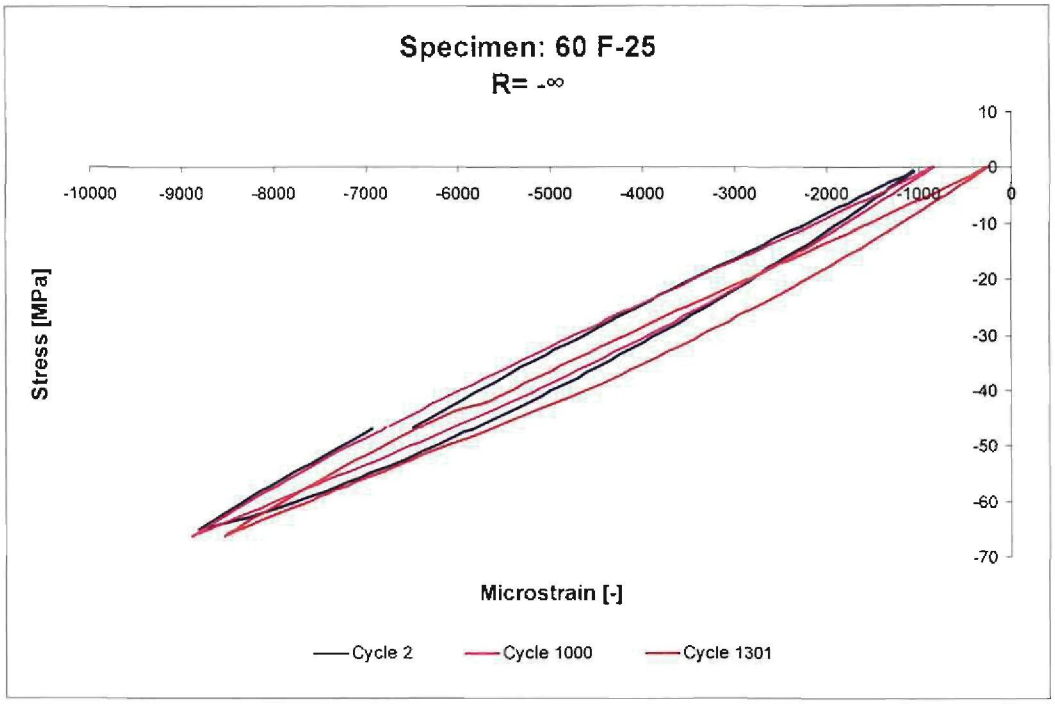


Figure 4-37: Stress Versus Strain (Hysteresis Loop) as Function of Life for R = -∞

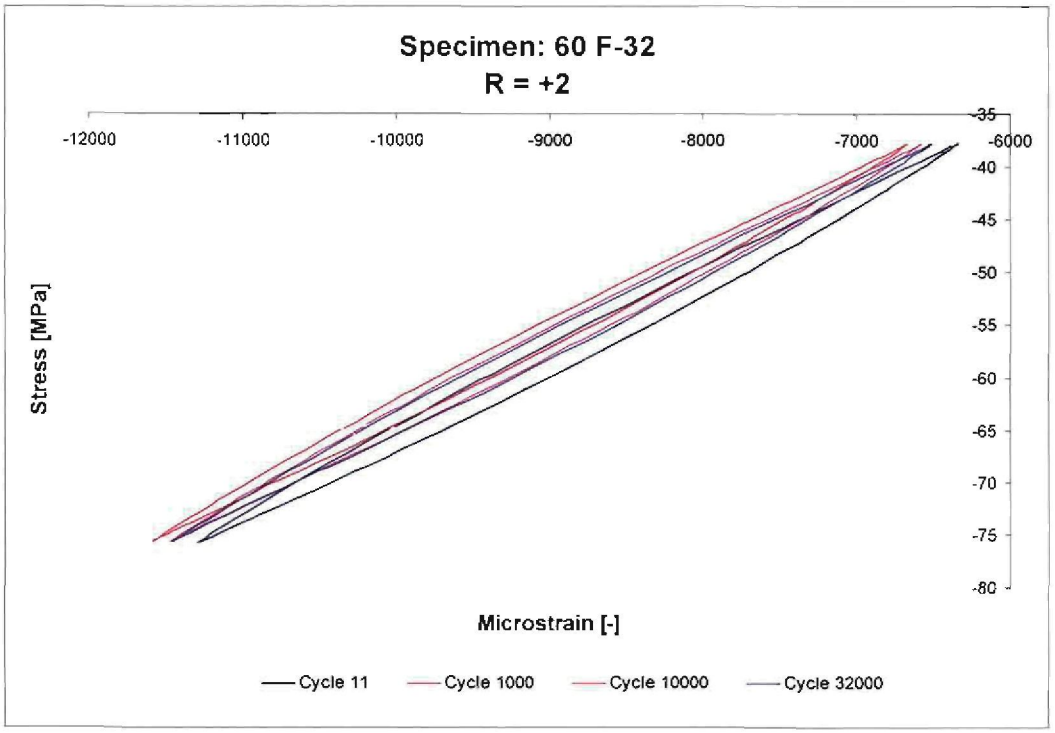


Figure 4-38: Stress Versus Strain (Hysteresis Loop) as Function of Life for R = +2

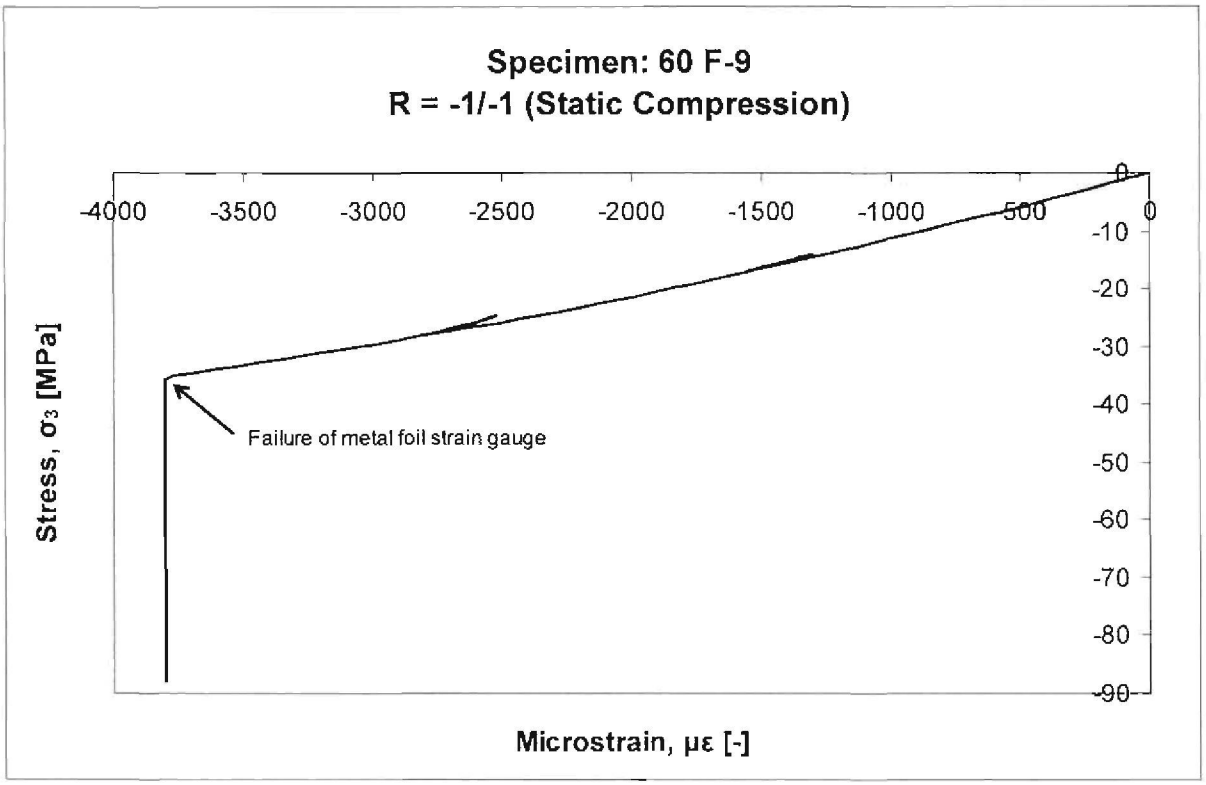


Figure 4-39: Stress Versus Strain for R = -1/-1 (Compression Test)

4.7.7 Modulus of Elasticity

Three techniques are used to estimate the modulus of elasticity of NBG18. The first is the determination of the nonlinear stress-strain curve of NBG18 by fitting a second order polynomial to the static stress-strain curves. The second is the calculation of the chord moduli for various strain levels using the nonlinear equations. The third is a linear estimate of the modulus for all stress ratios that are determined by connecting the extremities of the stress-strain hysteresis curves.

The static stress-strain loading curves with the fitted polynomial equations are shown in Figure 4-40 and Figure 4-41 for tension and compression respectively.

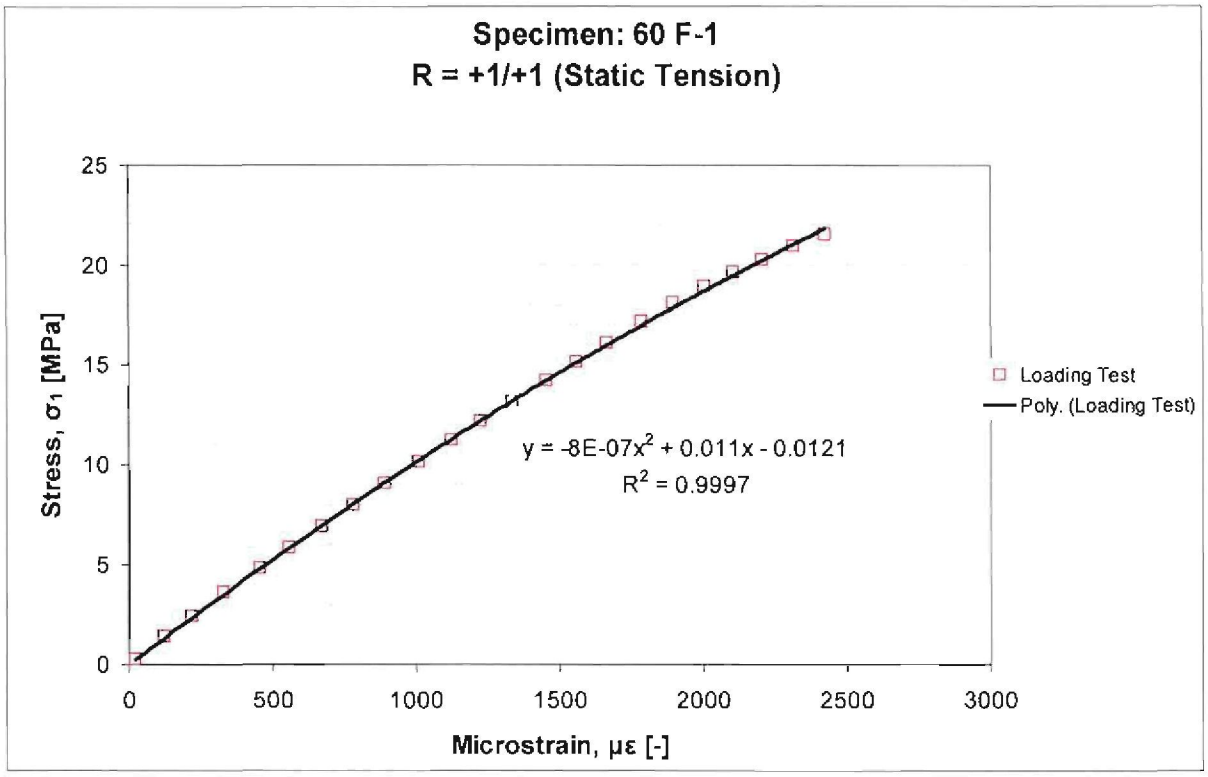


Figure 4-40: Best Fit Quadratic Equation of Tensile Loading - First Cycle

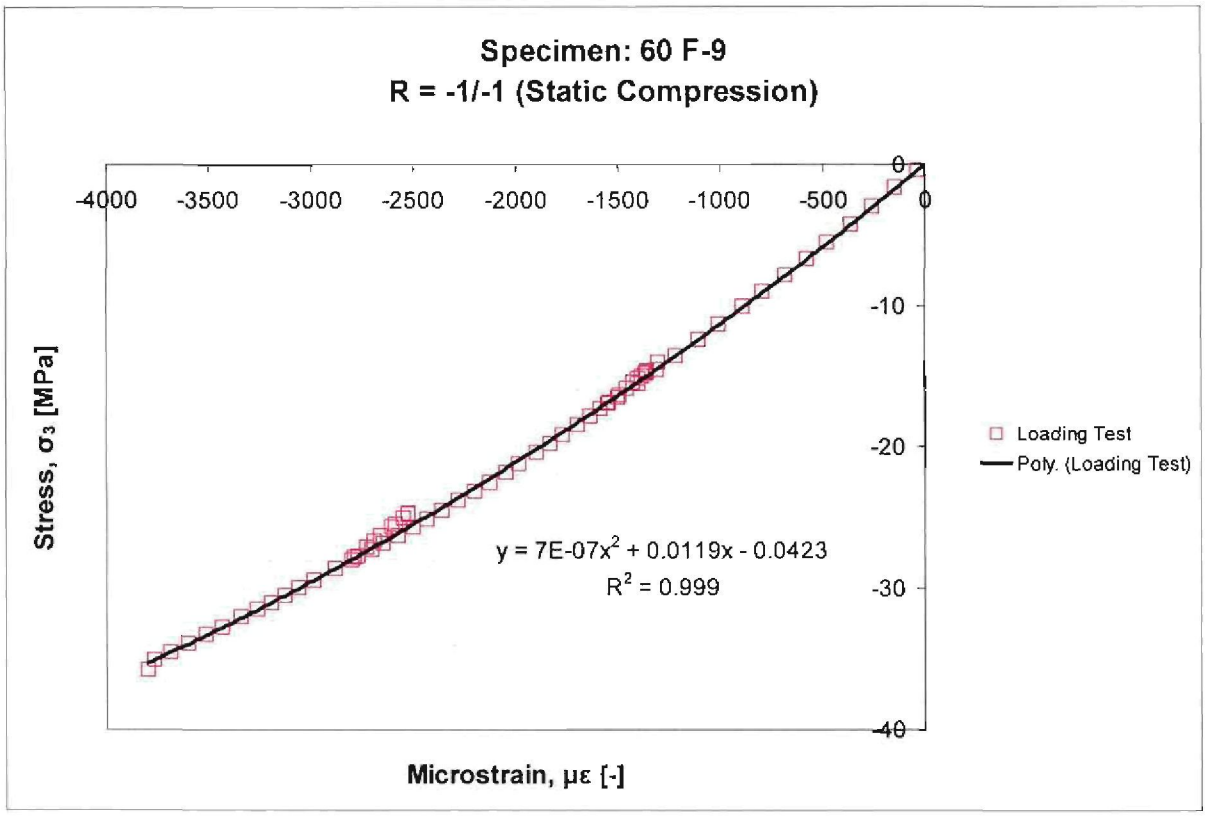


Figure 4-41: Best Fit Quadratic Equation of Compressive Loading - First Cycle

The nonlinear equations, that are only valid for first time loading of the graphite, are given by Eq. (4.9) to (4.12).

The resultant equations for tensile strains are:

$$\sigma = -8\times10^{-7}(\mu\varepsilon)^2 + 0.011(\mu\varepsilon) - 0.0121 \qquad ...(4.9)$$

and

$$E' = \frac{\partial\sigma}{\partial(\mu\varepsilon)} = -2\left(8\times10^{-7}\right)(\mu\varepsilon) + 0.011 \qquad ...(4.10)$$

Where:

$\sigma \equiv$ Maximum Principal Stress [MPa]

$\mu\varepsilon \equiv$ microstrain [μm/m]

$E' \equiv$ Tangent Modulus of Elasticity at any local strain [MPa]

The resultant equations for compressive strains are:

$$\sigma = 7\times10^{-7}(\mu\varepsilon)^2 + 0.0119(\mu\varepsilon) - 0.0423 \qquad ...(4.11)$$

and

$$E' = \frac{\partial\sigma}{\partial(\mu\varepsilon)} = -2(7\times10^{-7})(\mu\varepsilon) + 0.0119 \qquad ...(4.12)$$

Eq. (5.4) and (5.5) should be used only up to -4000 microstrain due to its limited strain range. The strain gauge failed early in this test, and that is causing the limitation.

The chord modulus of NBG18 is calculated from the static stress-strain curves for chord lines between the origin and a few stress fractions of the ultimate strength of the graphite. The results are summarized in Table 4-2

Table 4-2: Chord Moduli Based on Static Tensile and Compressive Loading Cycles.

% Ultimate Strength	Strain [μm/m]	Stress [MPa]	Modulus of Elasticity, E [MPa]
0	0	0.0	11000[1]
25	470	5.0	10598
50	975	10.0	10208
75	1530	14.9	9768
0	0	0.0	11900
25	-2015	-21.2	10510
50	-5060	-42.3	8366

A linear elastic modulus estimate is made by drawing a straight line through the extremities of the stress-strain hysteresis curves at the start of cycling and at 1000 cycles. The slope of this line is equal to the linearised modulus of elasticity for the relevant stress ratio. Two moduli are determined with this method, namely a tensile modulus and a compressive modulus. The graphical results are shown in **Appendix J**. The results are further analysed and summarized in Table 4-3.

[1] Derivative of quadratic equation at origin.

There is no significant change in modulus (change < 1%) as a function of number of hysteresis cycles for a low number of cycles (up to 1000 cycles). The direction of change (higher or lower) is also not consequent. The largest variations occur in compression or when the compressive excursions is more than double the tensile excursion (R = -2). The hysteretic losses are also largest for compression.

The overall average hysteretic modulus of elasticity can be taken as **10780 MPa** for tensile strength limiting load ratios and **7990 MPa** for compressive strength limiting load ratios.

Table 4-3: Stress-Strain Hysteresis Curve Based Moduli

Stress Ratio, R	Specimen	E_2 [MPa]	E_{1000} [MPa]	% Change
+0.5	60 F-8	10606	10618	0.11
0	60 F-23	11375	11367	-0.07
-0.5	60 G-16	10836	10841	0.05
-1	60 G-7	10462	10445	-0.16
-2	60 G-23	10581	10661	0.76
-∞	60 F-25	8297	8232	-0.78
+2	60 F-32	7681	7732	0.66
				Average
SUT Dominant Average		10772	10786	**10779**
SUC Dominant Average		7989	7982	**7986**

The specimens that are used for measuring the static stress-strain curves are both X-direction specimens which mean they are parallel to the grain direction. The median modulus of elasticity of specimens, parallel to the grain direction, is calculated from the test data contained in [2.17]. The value of the dynamic modulus of elasticity is 12150 MPa. This is compared with the average of the tangent moduli of the static tensile and compressive tests at zero strain (derivatives of nonlinear equations). The average tangent modulus is 11450 MPa.

The average tangent modulus is 5,8% lower than the measured dynamic modulus. It must be pointed out however that the static modulus was determined from 2 specimens only, while the tests of dynamic modulus comprised 104 specimens.

4.7.8 Run-Out Specimens

The samples that experienced run-out are tested in static tension or compression, depending on the type of loading of the fatigue test, to confirm that they are stronger than the average specimens. Table 4-4 shows the results of the post-fatigue static tests.

Table 4-4: Fracture Loads and Strengths of Specimens that Ran Out

Specimen	Testing method	Maximum Force, [kN]	Principal Stress, [MPa]
61 B-22	Tension	2.869	21.62
60 G-22	Tension	2.963	22.31
60 H-15	Tension	2.699	20.32
61 A-12	Tension	2.931	22.09
61 A-13	Tension	3.082	23.23
61 D-9	Tension	2.482	18.73
61 J-15	Compression	-11.449	-86.20
61 B-16	Compression	-11.261	-84.91
60 L-16	Compression	-10.744	-80.91

4.7.9 Fracture Position

The position of the fractures for the fatigue tested samples is shown in **Appendix E**. Unfortunately the test setup for the compressive loading conditions did not allow for accurate determination of the fracture position due to extensive shatter of the reduced section.

4.8 DISCUSSION

4.8.1 Fatigue Test Design

The uniaxial fatigue test design, using the S70 specimen, proves to be simple (and therefore cost effective) yet adequate to determine the uniaxial fatigue properties of medium to fine grain graphite (average grain size less than 1,3 mm or maximum grain size less than 2,6 mm).

Accurate alignment of the custom designed grips of the servo-hydraulic testing machine to the residual strain values, shown in **Appendix D**, is a time consuming task. The Instron AlignPRO software and jig proves to be a useful tool to attain acceptable alignment, which is essential for these tests.

The positions of the tensile fractures confirm that the specimen design is good. No specimen failed outside the gauge section allowance, according to ASTM C749-92 (2005).

4.8.2 Absolute Values of Static Strength

The measured static strength values are first compared with the overall strength of the NBG18 material, calculated from measurements of all acceptable blocks. The Weibull characteristic value of tensile strength and shape factor in all directions of all accepted blocks are 21,6124 MPa and 10,0477 respectively as reported by Fechter (2007). This equates to a median S_{ut} = 20,8 MPa.

The experimental absolute value of 19,9 MPa compares well with this overall value, with an error of -4,3%.

Similarly, Fechter (2007) reports a Weibull characteristic value of compressive strength and shape factor in all directions of all "acceptable" blocks of 81,6659 MPa and 9,9494 respectively. This equates to a median S_{uc} = 78,7 MPa.

The experimental absolute value of 84,7 MPa compares well with this overall value, with an error of +7,6%.

Next, the values measured in this research are compared with measurements of the specific blocks, that were done by the manufacturer. According to SGL Carbon Group (2006), Block A is billet numbers 25 and Block B is billet number 11. In the same report, the manufacturer's test results for 8 tensile and 4 compressive tests are given. These results are compared with results from this research in Table 4-5. The percentage error in this table is the deviation of the S70 values from the SGL Carbon values. Results of other non-destructive tests (electrical resistivity and dynamic modulus), also presented in the mentioned reference, suggest that Block B may be slightly stronger than Block A. The S70 static tests do not suggest that Block B may be the better block, while the manufacturer's tests do. Neither the SGL Carbon results nor the S70 results represent the absolute strength of the blocks, due to the variability of graphite tests and the low number of specimens per

block. However, the S70 tests yield absolute values with less variance and which are closer to the median values for NBG18.

Table 4-5: Comparison of Median Strengths of Blocks

	SGL Carbon Block A (60)	S70 Tests Block A (60)	% Error	SGL Carbon Block B (61)	S70 Tests Block B (61)	% Error
Sut [MPa]	21.0	20.4	-2.8	22.1	19.9	-9.9
Suc [MPa]	72.2	85.3	18.1	86.2	82.7	-4.0

4.8.3 S-N Diagrams

Fatigue data captured at R = 0 and R = +0,5 is not satisfactory due to the large scatter, aggravated by the small slopes of the S-N curves. The other S-N curves are acceptable, although more tests at R = -1 will improve the level of confidence in this critical load ratio.

In general, least damage occurs in graphite when the midrange stress is high but the stress amplitude is low and vice versa.

4.8.4 Relative Fatigue Strength

Although one expects the damage due to R = -2 to be more severe than that due to R = -1, the regression curves predict more damage for fully reversed fatigue at more than 300 cycles. This means that there must be some physical mechanism (which is not understood at present) that improves the strength of the graphite as the compressive stress excursion exceeds the tensile stress excursion. This unexpected behaviour of graphite was also observed by Schmidt (2001a) who found a regression equation from his tests that predicted more damage from R = -1 than from R = -2 in one of three sets of tests. The test campaign is too limited to deduce that this behaviour is typical for NBG18.

This may imply that the "worst" fatigue characteristics for design purposes can be determined from a single fully reversed (R = -1) fatigue test. All other load ratios will yield more conservative results. This observation may be tested by comparison of the R = -1 and R = -4 fatigue results for NBG-18 graphite.

4.8.5 Hysteresis Loops

There is always a large strain offset between the first cycle and successive cycles. This can either be attributed to creep or settling of the strain gauge or its adhesive or it can be actual damage of the graphite. Subsequent hysteresis loops remain in the same position or show slow "plastic strain" or damage accumulation over life. In contrast to this, when the stress level is successively increased, Yoda and Eto (1983) observed a significant continual offset or "plastic strain".

The plastic strain offset is not consistently in the direction of the design limiting strength of the material, as expected. This cannot be explained, since the Wheatstone bridge is fully temperature compensated which means that changes in environmental temperature cannot cause this phenomenon.

The inside area of the hysteresis loops (energy dissipation per cycle) varies significantly between the specimens. The larger the work done on the specimen, the larger is the loss in energy. Compressive hysteresis loops have therefore much more area than tensile loops.

Reduction in elastic modulus during these fatigue tests, at stress levels of the order of 70% ultimate strength, is negligible contrary to what is expected for a progressively damaged material (mostly insignificant).

The metal foil strain gauges are typically rated for approximately 4000 $\mu\varepsilon$ in fatigue loading up to 1×10^6 cycles. The R = +2 specimen's strain gauge survived more than 32000 cycles at strains up to -11500 $\mu\varepsilon$ without any obvious gauge damage.

The applicability of metal foil strain gauges to graphite testing needs more investigation because of the high strain values of graphite, the possible reinforcing effect of the epoxy adhesive and the observed strain offset during the first cycle.

4.8.6 Run-Out Specimens

Only one out of six tensile and one out of three compressive specimens failed at a stress level below the median static strength of the material, which confirms that these specimens are at the high end of the strength distribution. Assuming that the principle of Miner's rule (cumulative fatigue damage) also applies to graphite, the undamaged strength of these specimens is at even higher values.

4.8.7 Modulus of Elasticity

The nonlinear equations for elastic modulus of NBG18 are valid only for first cycle loading of the graphite. The chord moduli yield slightly lower values, but suffer from the same restrictions as the nonlinear equations because it is essentially calculated from the nonlinear equations.

The hysteretic moduli can be reduced to two values, that can be used for design purposes, namely a tensile and compressive elastic modulus. The latter moduli seem to best represent the actual stress-strain behaviour of the graphite for perturbations about a specific general stress state.

4.8.8 Constant-Life Diagram

In Figure 4-42, the 10^5 cycles, 50% probability uniaxial fatigue characteristics of NBG18 is compared with those of V483T and V483T2, which are fine-grain nuclear grade graphite types, as reported by Schmidt (2001a). It is evident that NBG18 has superior fatigue characteristics to V483T and V483T2.

Although the V483T measurements were not done for all load ratios, the two constant-life graphs are quite similar, which increases the confidence in these results.

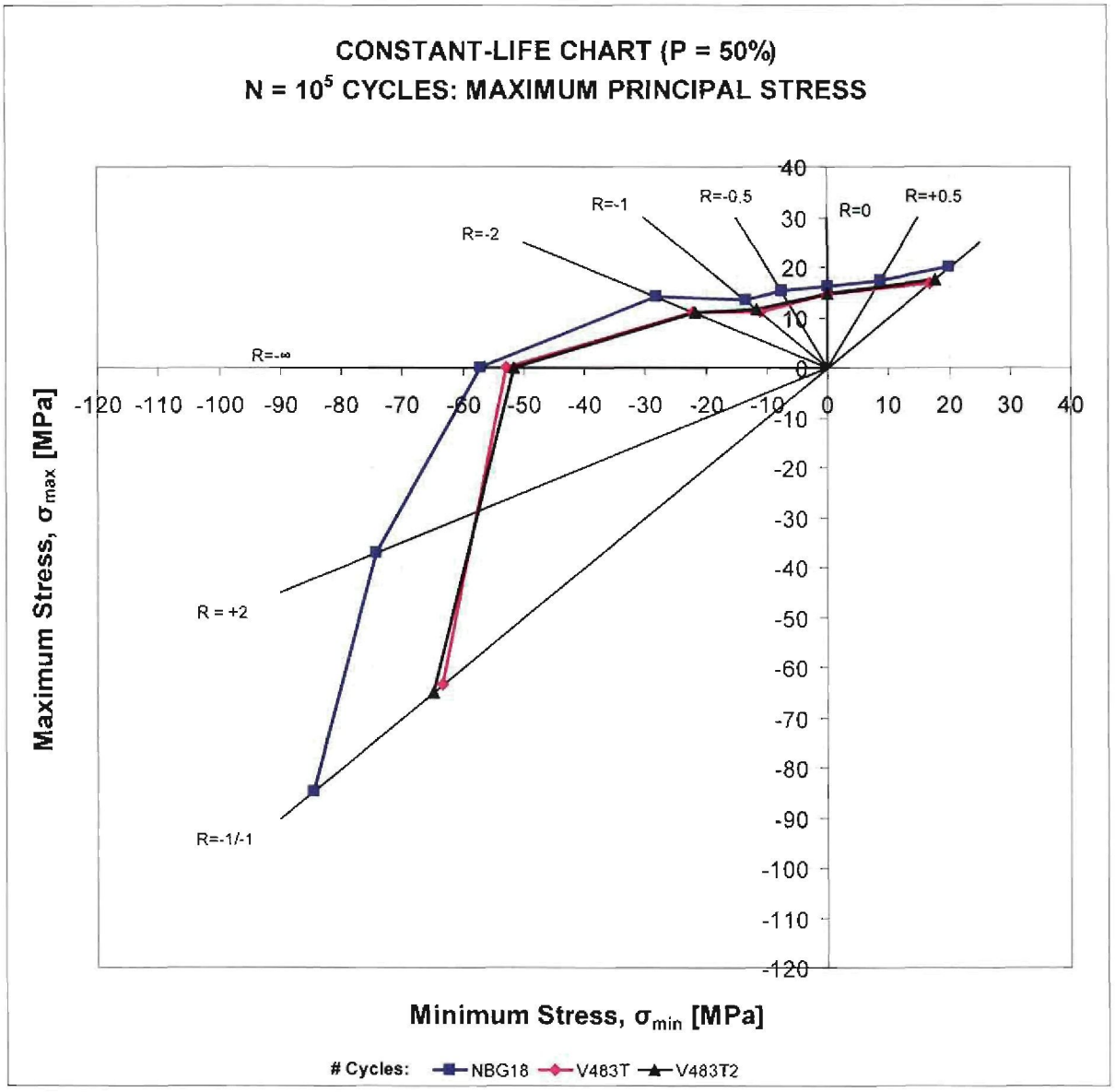


Figure 4-42: Constant-Life Diagram Comparison Based on Maximum Principal Stress

4.9 SUMMARY AND CONCLUSIONS

A proposal of a new low cost specimen, for the determination of the uniaxial fatigue characteristics of medium to fine grain graphite is justified.

The S70 specimens are machined to maximise cylindricity and to minimise pre-test damage due to induced clamping stresses.

The uniaxial fatigue characteristics of NBG18 are successfully determined through a comprehensive range of load ratios using the S70 specimen and a suitably modified servo-

hydraulic fatigue testing machine, incorporating an alignment fixture and collet grips. The test facility is located in the Automotive Components Testing Station (ACTS) at the Nelson Mandela Metropolitan University, Port Elizabeth.

The static strengths, as determined through material acceptance testing, are confirmed.

The measured S-N diagrams show that graphite has significantly more scatter than metallic materials (as is well known). The slopes of these curves are quite small, predicting large allowable stress conditions for low cycle fatigue applications. The predicted allowable peak stress at 10^6 cycles (for 50% failure probability) is more than 50% of the static strength of the graphite for all load ratios. Load ratios with high midrange stress and low stress amplitudes generally cause least damage to the graphite and vice versa. In these tests, R = -1 causes most damage (slightly more than R = -2).

NBG18 graphite is superior to V483T and V483T2 graphite with regard to static and fatigue strength, with an average increase of 18,5% and 18,1% respectively.

The multiaxial fatigue characteristics of NBG18 are presented in Chapter 5, after which a comparison between uniaxial and multiaxial characteristics is presented in Chapter 6.

Chapter 5

MULTIAXIAL FATIGUE TESTS

5.1 INTRODUCTION

In Chapter 4, the uniaxial fatigue characteristics of NBG18 are presented and discussed. The multiaxial fatigue characteristics of this material are presented in this chapter. The multiaxial loading state is obviously more complex than uniaxial loading, since the material is subject to at least two principal stresses in the former, whereas in the latter, the material is only subject to one principal stress.

A multiaxial fatigue test design, that suits the aim of this research, is proposed and justified in Section 5.2 and 5.3. The aim is to propose a "maximum damage" multiaxial specimen and to determine the fatigue characteristics of NBG18 with this specimen, across the same range of load ratios as for the uniaxial tests, in South Africa.

The multiaxial fatigue tests are further divided into two sets. The first is a reference set of data on virgin material i.e. material that is not damaged by mechanical loading or radiation before the test. The second is a set of data on material that is exposed to isostatic pressure loading equivalent to the PBMR system design pressure, prior to fatigue testing.

The fatigue characteristics of the graphite are determined for the same comprehensive range of loads, as for the uniaxial tests.

5.2 SPECIMEN DESIGN

5.2.1 Existing Geometries

First, the existing geometries are analysed to determine whether one suits the aim of this research.

The illustration of the geometries and a relative cost comparison are presented in Section 4.5.1 of Chapter 4. The following multiaxial specimens can comply with the load range requirement, illustrated in Figure 2-2, of Chapter 2: S2, S8 and S9. (Specimen S17 was published after the S60B specimen had been designed, but would not have altered the

decision, because it is similar to S9.) It is clear that the existing geometries are all expensive and all require expensive equipment. None complies with the general design requirements of low specimen cost and low equipment cost, stated in Section 4.3 of Chapter 4.

A new specimen design is required to conform to the general requirements as well as the requirement of "maximum damage". The obvious loading mechanism is hydrostatic, to conform to the low equipment cost requirement. With the selection of a hydrostatic loading mechanism, one of the following two basic geometries can be selected:

- Cylindrical with one free end
- Spherical

5.2.2 Specific Design Requirements

After the decision was made to design a new specimen based on hydrostatic loading, the following specific design requirements were added to the generic requirements mentioned before:

- Multiaxial specimen to be insensitive to grain orientation
- Maximum hydraulic system pressure: 35 MPa.

The requirement that the specimen be insensitive to the grain orientation of the material originates from the Burchell fracture model that the pores in a near-isotropic grade graphite material may be more randomly orientated than generally assumed (Burchell *et al.*, 2006). This is particularly true for near-isotropic grade graphite, like NBG18. The term "grain orientation" is used here to describe the preferential alignment of the coke filler particles (and therefore also pores) due to the forming process (Haag, 2004).

The ideal geometry to achieve the requirement to be insensitive to grain direction is a hollow sphere, as shown in Figure 5-1. The loci of grain orientation, shown in red, are all possible grain directions relative to the specimen's axis that will yield lowest strength, for any stress ratio. In other words, these directions will cause Mode I crack propagation in the specimen that will eventually lead to failure (ASTM E1823-96, 2002). However, the practicalities of machining such a specimen and loading thereof, significantly compromises this ideal geometry.

The requirement for the specimen to be insensitive to grain orientation immediately eliminates the cylindrical type specimens like S9, as illustrated in Figure 5-2. The loci of

alignment axes of specimen S9 to yield the lowest strength values are shown in this figure. It consists of the axis of the specimen (provided that the specimen is loaded significantly in the axial direction) and any radial direction, perpendicular to the specimen axis.

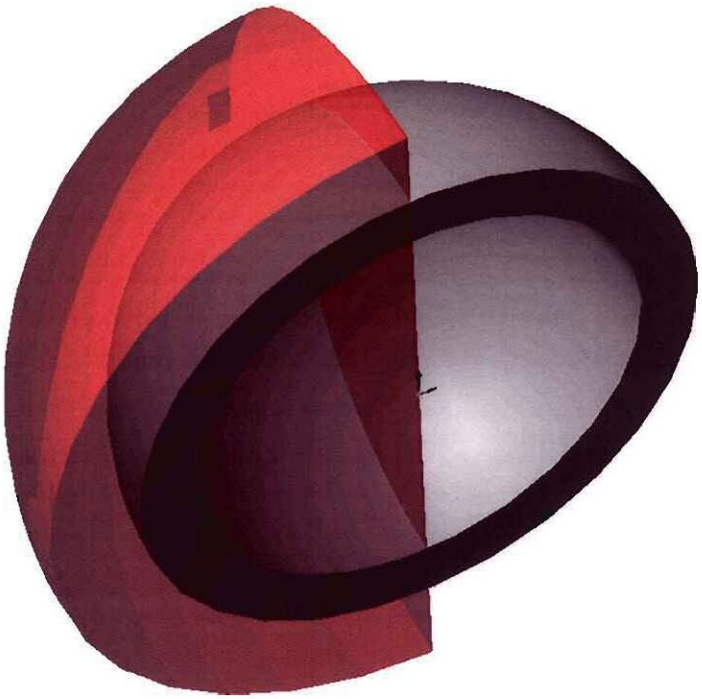


Figure 5-1: Full Section Showing Alignment Axes of Spherical Specimen with Grain Direction to Yield Lowest Strength

A hemisphere is the only geometry that complies fully with the stated requirements of "maximum damage" as well as insensitivity to grain orientation. The ideal of a hemispherical geometry is the starting point for the design of the S60B specimen.

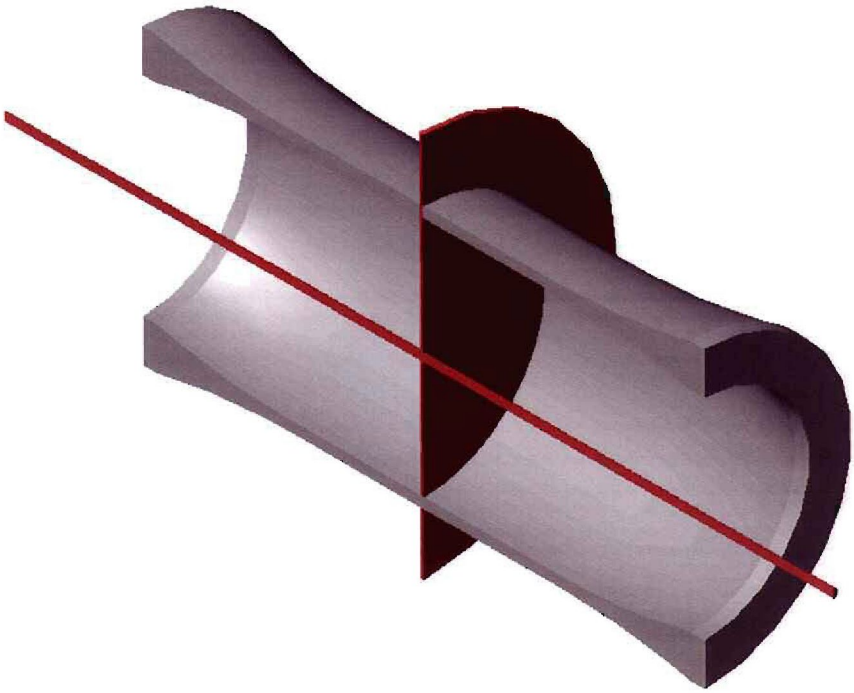


Figure 5-2: Full Section Showing Alignment Axes of Specimen S9 with Grain Direction to Yield Lowest Strength

5.2.3 Analysis Methodology

5.2.3.1 Description of Methodology

The fundamental analysis of the principal stresses in a loaded ideal specimen is done using Engineering Equation Solver (EES), version 7.450-3D. The Modified Maximum Deformation Energy (MDE) stress is calculated along with the Von Mises stress and the principal stresses on the inner wall of the sphere for both external as well as internal pressure loading of the specimen. The basic geometry of the sphere is determined for a maximum hydraulic pressure of 26,2 MPa and the constraint that the wall thickness of the specimen shall be equal to or greater than 10 x average grain size (or 5 x maximum grain size).

A quarter section model of each trial specimen is generated with Solidworks and subsequently analysed with Algor v.17 Finite Element Analysis (FEA) software. The MDE stress intensity is calculated for some key nodes in the model using an Excel Spreadsheet. The final analysis is done at PBMR with their Marc code that is modified to calculate the MDE stresses directly. The logic diagram that illustrates this design methodology is shown in Figure 5-3.

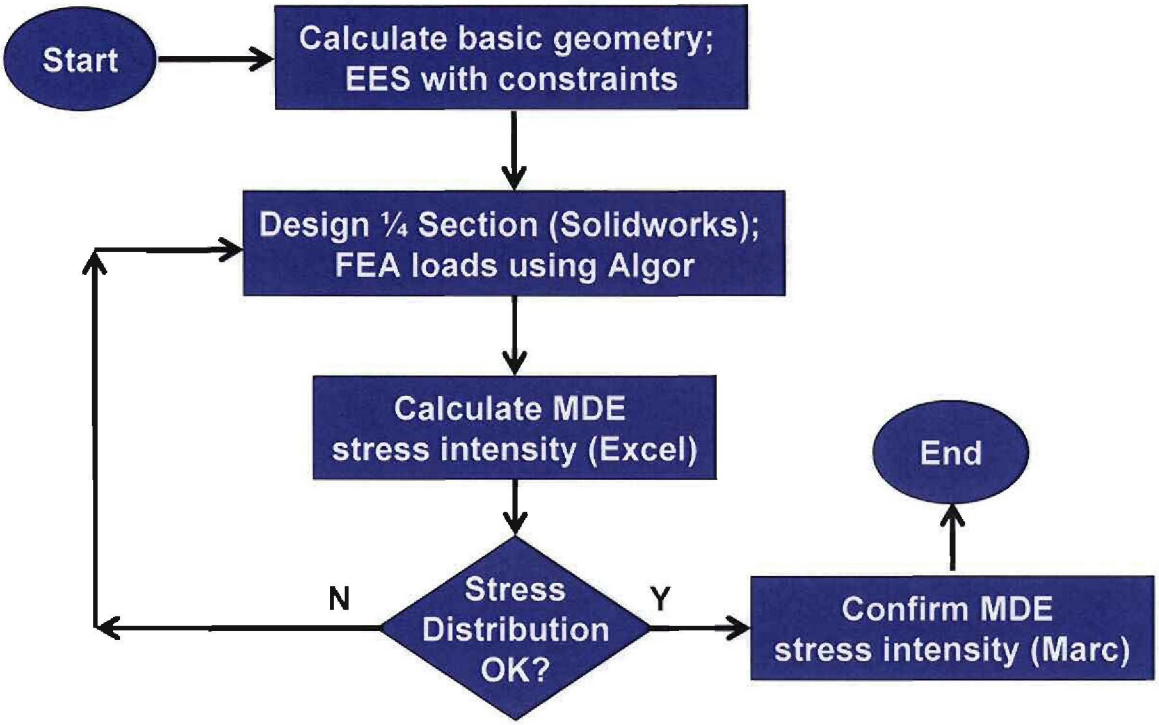
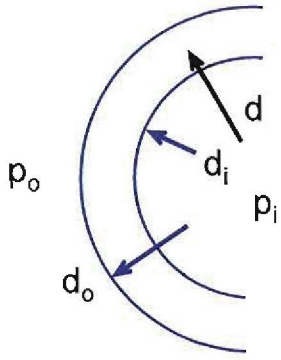


Figure 5-3: Logic Diagram Illustrating Design Methodology For Multiaxial Specimen

5.2.3.2 Governing Equations for Basic Geometry

The governing equations for the stresses in an unconstrained thick-walled cylinder (Shigley *et al.*, 2004) and sphere (Ryder, 1969), written in terms of diameters rather than radii, are shown in Figure 5-4 and Figure 5-5 respectively.

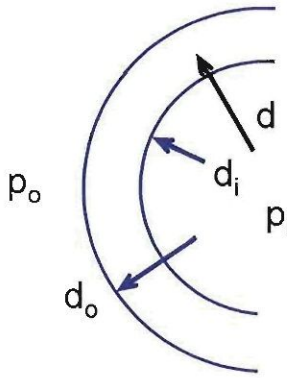


$$\sigma_t = \frac{p_i d_i^{\,2} - p_o d_o^{\,2} - d_i^{\,2}.d_o^{\,2}\left(p_o - p_i\right)/d^2}{d_o^{\,2} - d_i^{\,2}}$$

$$\sigma_r = \frac{p_i d_i^{\,2} - p_o d_o^{\,2} + d_i^{\,2}.d_o^{\,2}\left(p_o - p_i\right)/d^2}{d_o^{\,2} - d_i^{\,2}}$$

$$\sigma_l = \frac{p_i d_i^{\,2} - p_o d_o^{2}}{d_o^{\,2} - d_i^{\,2}}$$

Figure 5-4: General Equations for Stresses in a Thick-walled Cylinder



$$\sigma_t = \frac{p_i d_i^3 - p_o d_o^3 - d_i^3 . d_o^3 (p_o - p_i)/(2.d^3)}{d_o^3 - d_i^3}$$

$$\sigma_r = \frac{p_i d_i^3 - p_o d_o^3 + d_i^3 . d_o^3 (p_o - p_i)/d^3}{d_o^3 - d_i^3}$$

$$\sigma_l = \sigma_t$$

Figure 5-5: General Equations for Stresses in a Thick-walled Sphere

Where :

$\sigma_t \equiv$ Tangential Stress [MPa]
$\sigma_r \equiv$ Radial Stress [MPa]
$\sigma_l \equiv$ Longitudinal Stress [MPa]
$d_i \equiv$ Internal Diameter [mm]
$d_o \equiv$ External Diameter [mm]
$d \equiv$ Diameter at which stress is calculated [mm]
$p_i \equiv$ Internal Pressure [MPa]
$p_o \equiv$ External Pressure [MPa]

Shigley *et al.* (2004) propose a wall thickness-to-diameter ratio of less than 2,5% as the criterion for simplified calculations with thin-walled theory to yield satisfactory results.

For internal pressure only and
$d_o = 96$ mm
$d_i = 78$ mm
Thick - Walled Sphere equations yield the following maximum stress condition at inner wall :

$\sigma_1 = \sigma_2 = \sigma_t = (2.24)p_i$ .....(5.1)
$\sigma_3 = \sigma_r = p_i$

Thick - Walled Cylinder equations yield the following maximum stress condition at inner wall :

$\sigma_1 = \sigma_t = (4.89)p_i$ .....(5.2)
$\sigma_2 = \sigma_l = (1.94)p_i$
$\sigma_3 = \sigma_r = p_i$

Given the mean properties of NBG18 from Fechter (2007) and the selected dimensions as shown in Eq.(5.1), the theoretical stress states of a sphere are calculated as shown in Table 5-1. The tolerance added is for the plus and minus 50 micron geometric tolerance assumed for the geometry.

The nominal wall thickness of the sphere is 9 mm which complies with the design requirement of 10 x mean grain size. It is clear from the data in the table that the MDE stress of 31 MPa is approximately 50% more than the mean Ultimate Tensile Strength of the graphite, which is 21 MPa. The specified maximum hydraulic system pressure of 35 MPa, is sufficient to fracture a spherical specimen of these dimensions.

Table 5-1: Calculated Theoretical Stresses in a Sphere

Loading Mode	Inside Wall		Outside Wall	
	MDE Stress, σ_v [MPa]	Von Mises Stress, σ_{vm} [MPa]	MDE Stress, σ_v [MPa]	Von Mises Stress, σ_{vm} [MPa]
Internal Pressure of 10,6 MPa	30,95 ± 0,18	34,3 ± 0,14	23,12 ± 0,18	18,4 ± 0,14
External Pressure of 26,18 MPa	31,06 ± 0,13	84,71 ± 0,34	24,77 ± 0,12	45,44 ± 0,34

5.2.3.3 Stress Distribution in Gauge Section

The theoretical stress distribution through the gauge section, assuming an ideal spherical geometry is shown in Figure 5-6 and Figure 5-7 for internal and external pressurization respectively.

The proposed stress to be used as an indication of the equivalent stress state in this specimen is the Volume Weighted MDE stress. Any volume weighted stress is calculated for the gauge section using Eq.(5.3).

$$\text{Volume Weighted } \sigma = \frac{\sum_i A_i.\sigma_i}{\sum_i A_i} = \frac{\sum_{i=1}^{n-1}\left(r_{i+1}^{\ 3} - r_i^{\ 3}\right)\sigma_i}{\left(r_n^{\ 3} - r_1^{\ 3}\right)} \quad \ldots(5.3)$$

where:

$\sigma_i \equiv$ Local stress at radius r_i
$A_i \equiv$ Local gauge area between r_i and $(r_i + \partial r)$
$\partial r \equiv 0{,}020$ mm (determined by sensitivity analysis to yield error less than 0,2%)
$r_1 \equiv$ Inner radius of sphere
$r_n \equiv$ Outer radius of sphere
$r_{i+1} - r_i = \partial r$

It is found that the volume weighted stress is a constant factor of the maximum stress, for any pressure loading (assuming constant nominal geometry). This factor, called the volume weighting factor, is thus the ratio of volume weighted stress to maximum stress.

The following legend applies to these figures:

$f = \frac{S_{ut}}{S_{uc}} = \frac{19{,}91}{84{,}67} \equiv$ Ratio of median static strengths as determined through uniaxial tests
$\nu \equiv$ Poisson's Ratio = 0,21 for NBG18
P_A ≡ Internal pressure applied to R39 surface [MPa]
P_B ≡ External pressure applied to R48 surface [MPa]
h, g ≡ Load scaling or shape factors [-]
Lc MDE ≡ KTA 3232 Probability of survival of the graphite in the gauge section [-]
VMDE ≡ Volume weighted MDE stress [MPa]
VWMD = Ratio of Volume Weighted MDE stress to Maximum MDE stress [-]
Lc σ1 ≡ Probability of survival of the graphite in the gauge section using Maximum Principal stress in lieu of MDE stress in Eq.(4.5) [-]
Vσ1 ≡ Volume weighted Maximum Principal stress [MPa]
VWS = Ratio of Volume Weighted Maximum Principal stress to maximum Maximum Principal stress [-]
σ_r ≡ Radial normal stress (principal stress) [MPa]
σ_t ≡ Tangential normal stress (principal stress) [MPa]
σ_v ≡ MDE stress [MPa]
R39 ≡ Inner radius of gauge section [mm]
R48 ≡ Outer radius of gauge section [mm]

The success of the KTA 3232 failure criterion is discussed further in Section 5.10 of this chapter. The purpose of these figures is to give the reader insight into the theoretical variation in tangential, radial and MDE stress through the wall of the S60B specimen.

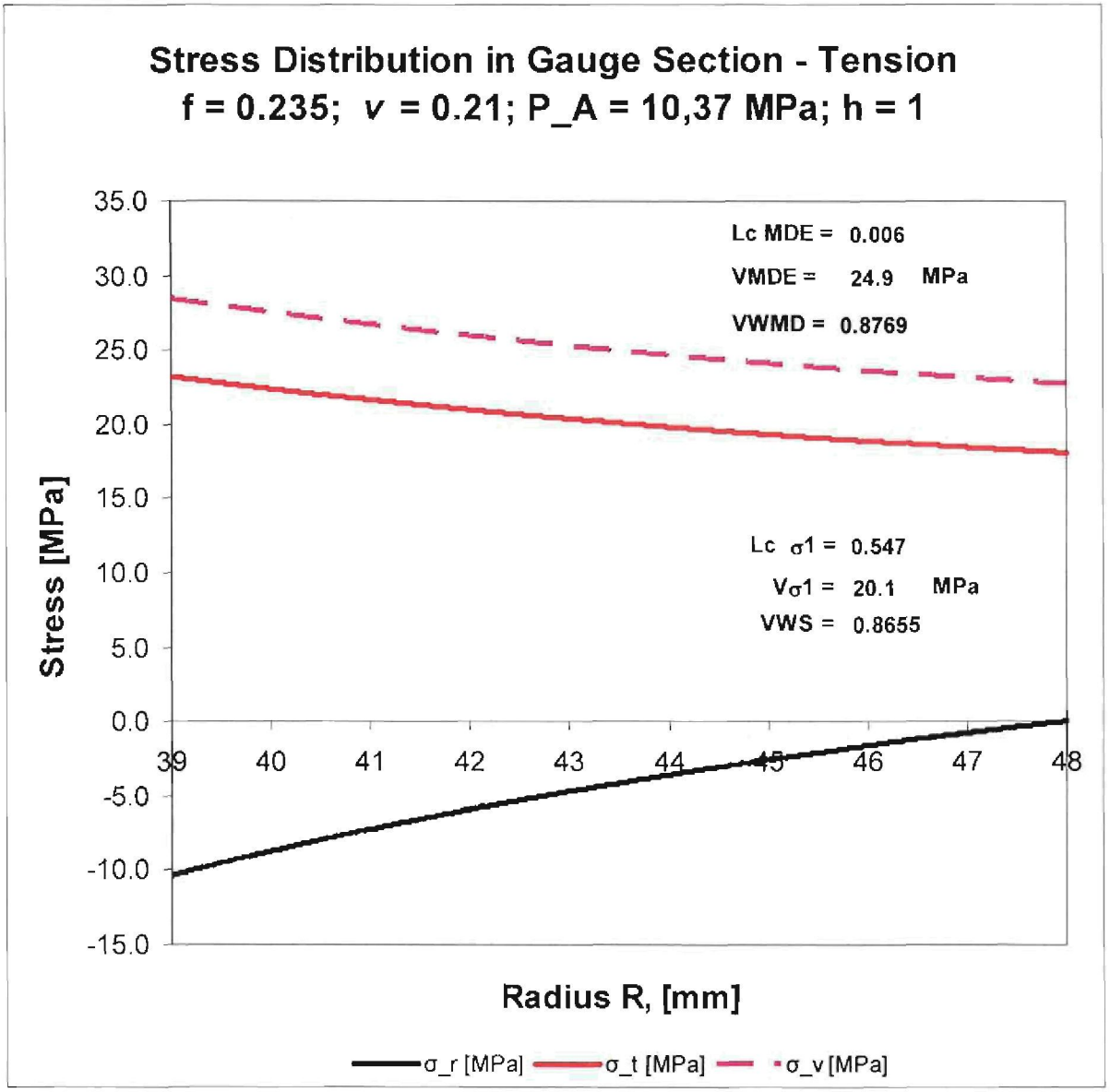


Figure 5-6: Ideal Theoretical Stress Distribution through Gauge Section Wall - Tension

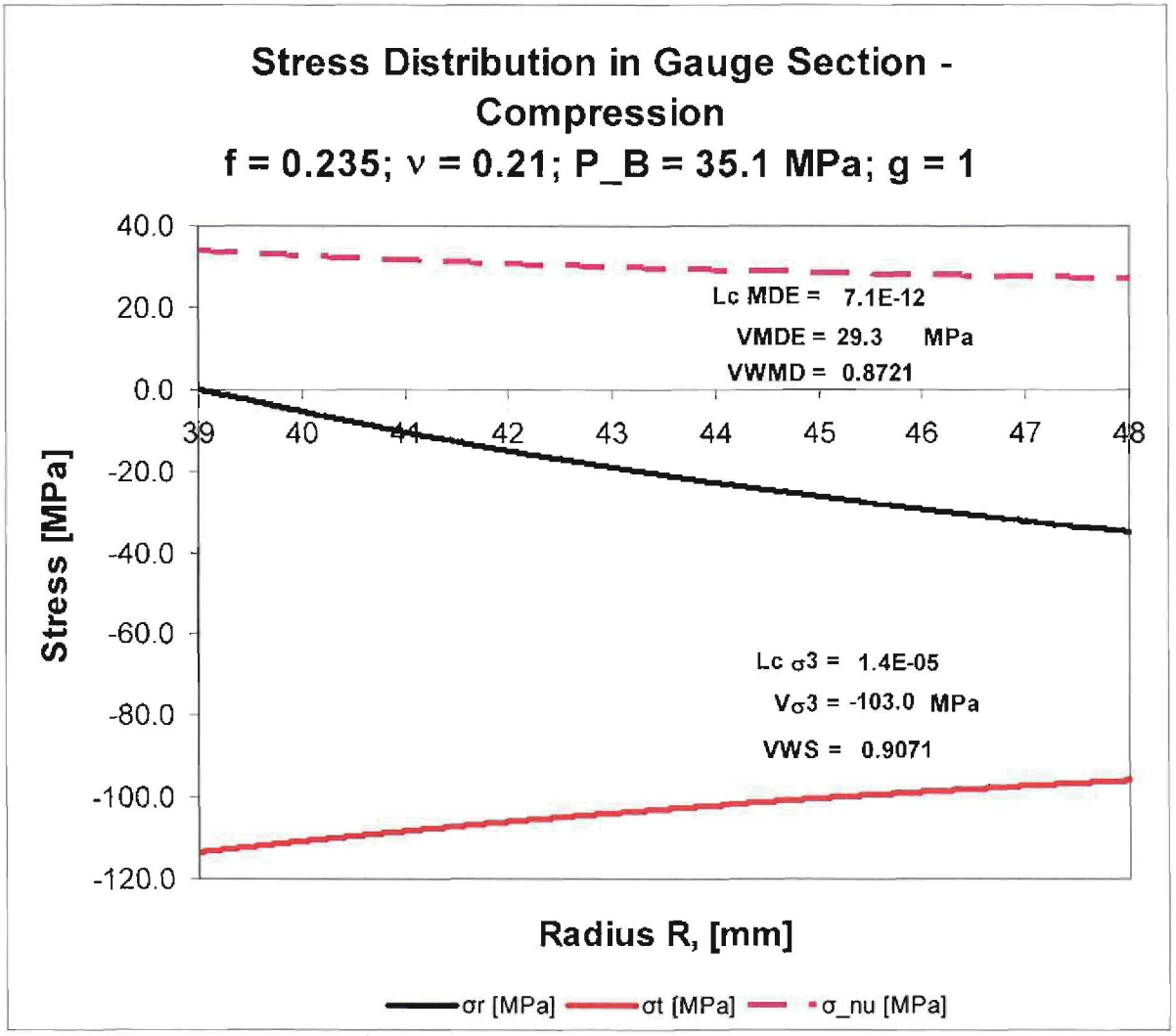


Figure 5-7: Ideal Theoretical Stress Distribution through Gauge Section Wall – Compression

5.2.4 Design for Stress Distribution

The stress distribution in the S9 specimen was determined through FEA for reference purposes. The stress distribution of this specimen is shown in the quarter section FEA model illustrated in Figure 5-8.

An acceptable stress distribution is one which conforms to the following two qualitative requirements:

- The stress distribution is equal in all parts of the gauge section (within a certain tolerance band for quantitative assessment)

- The stress reduces gradually in the transition from the gauge section to the attachment i.e. there is no stress concentration in the transition piece.

The number in square brackets is the node number, followed by the MDE stress and Von Mises stress (in curved brackets), both in MPa units. The geometry of the transition zone from cylinder to attachment flange is well designed, as is evident from the stress distribution plot in this figure.

The development of the S60B test specimen progressed sequentially through the configurations shown in Figure 5-9. Initially, a constraint to refrain from undercutting the bore was chosen for the development of the specimen, primarily for manufacturability. This initial self selected constraint was later abandoned when it became clear that a smooth reduction in stress from the gauge section to the flange was not possible without this feature (as from specimen S50N).

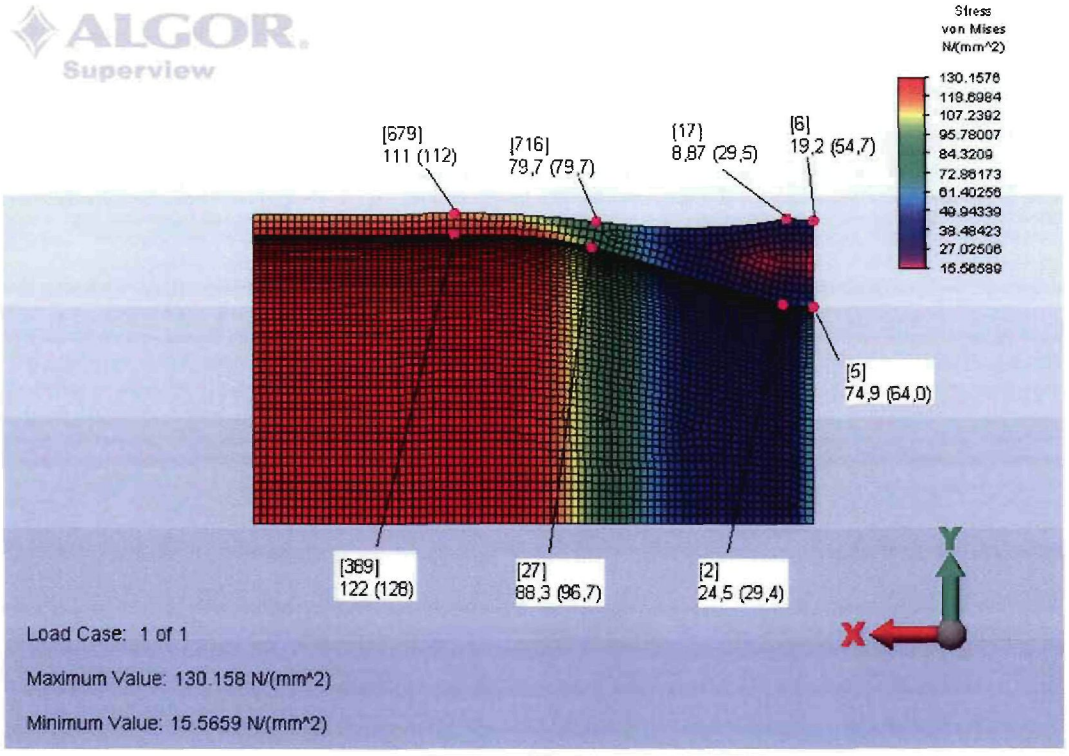


Figure 5-8: Stress Distribution in Specimen S9 Subject to Internal Pressurization Only

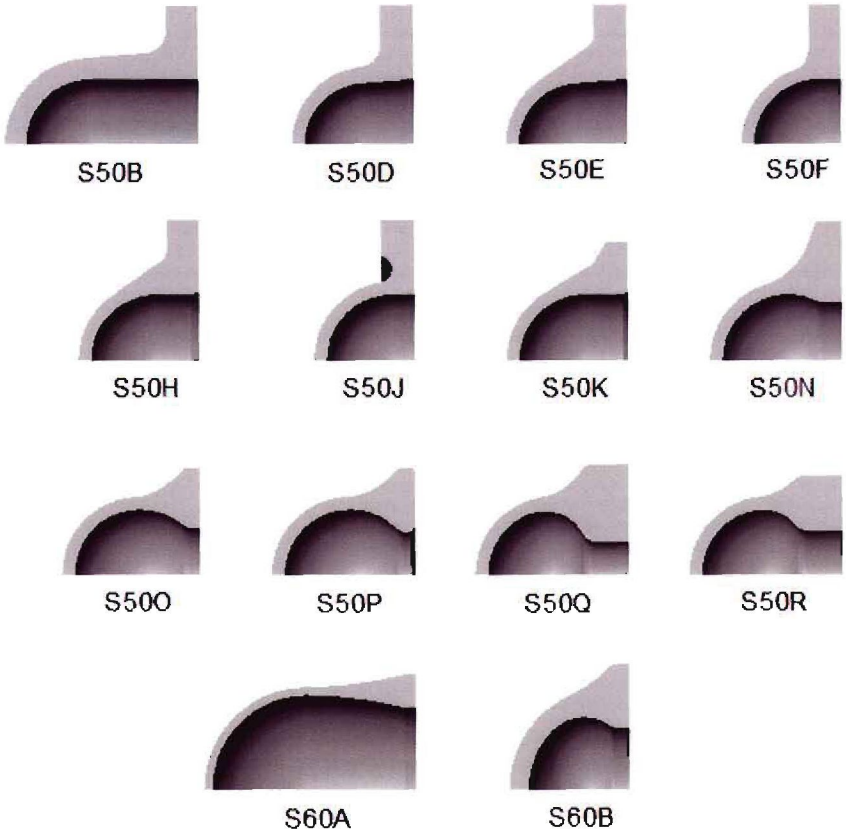


Figure 5-9: Sequential Development of the Multiaxial Fatigue Specimen Geometry

The initial designs (up to S50K) also attempted to eliminate the need for a bonded base plate for clamping the specimen. Sealing problems as well as unacceptable stress patterns forced the use of a base plate, which obviously makes the specimen more expensive. Specimen S60A had the same transition geometry as Specimen S9.

The main difficulty with the design is the transformation from the spherical section to the flange or base section. The reason for this difficulty lies with the stress characteristics of a pressurized sphere as compared with a pressurized cylinder. In a sphere, the transverse (hoop) and longitudinal (meridional) stresses are both tangential stresses and are equal while in a cylinder, the transverse (hoop) stress is approximately a factor 2 higher than the longitudinal stress, as shown in Eq.(5.1) and Eq.(5.2). This is illustrated in Figure 5-11, where the semi-sphere is attached directly to the transition geometry of specimen S9.

The more spherical the specimen is made, the more difficult it becomes to machine its inside, as is evident in specimen S50Q.

Von Mises and Maximum Principal stresses are used to evaluate the stress distributions in the specimen geometries during the geometry development phase. The MDE stresses are calculated in an Excel spreadsheet for geometries that looked promising.

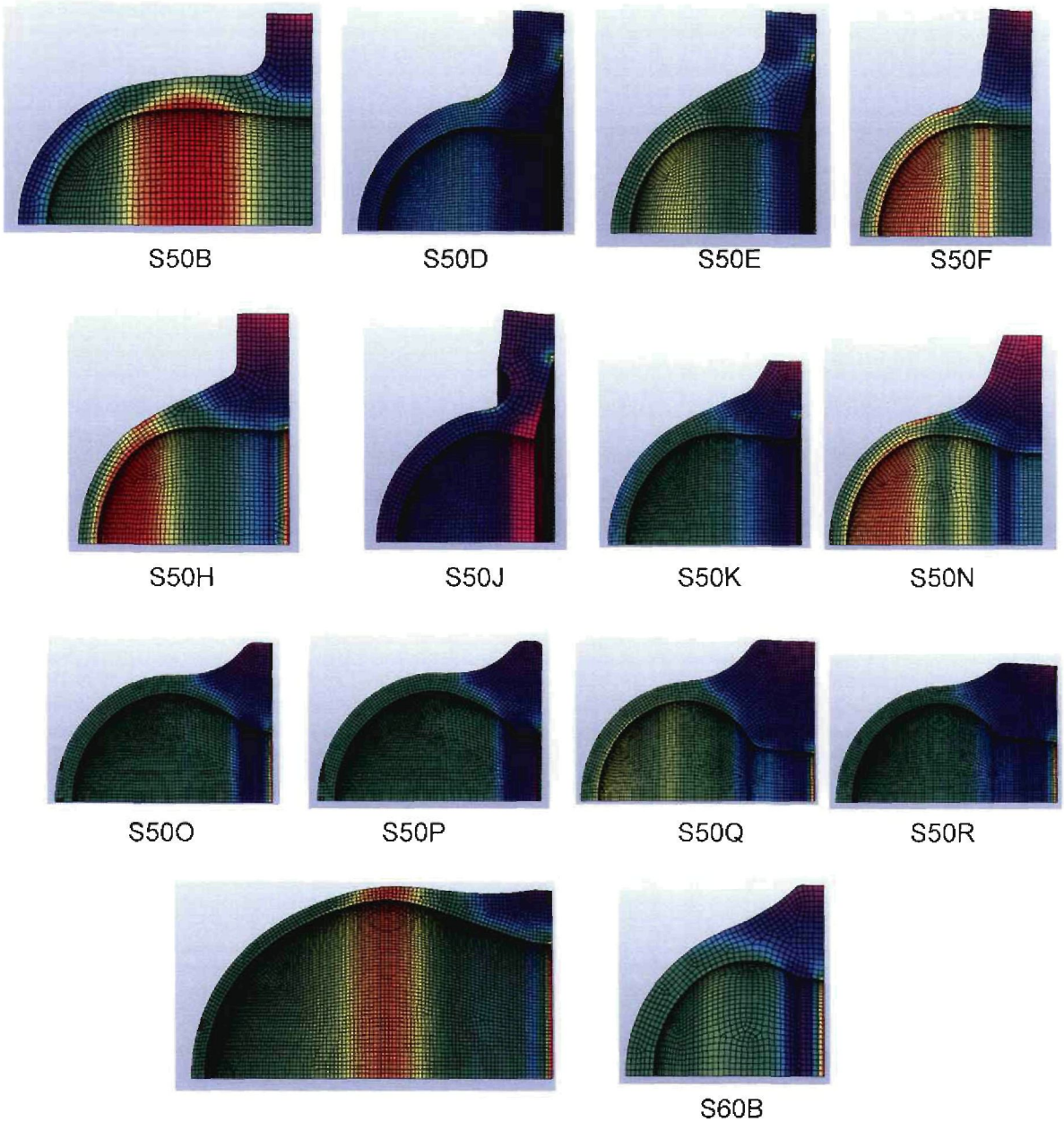


Figure 5-10: Maximum Principal Stress Contours during Sequential Development of the Specimen - Tensile Loading (Internal Pressurization).

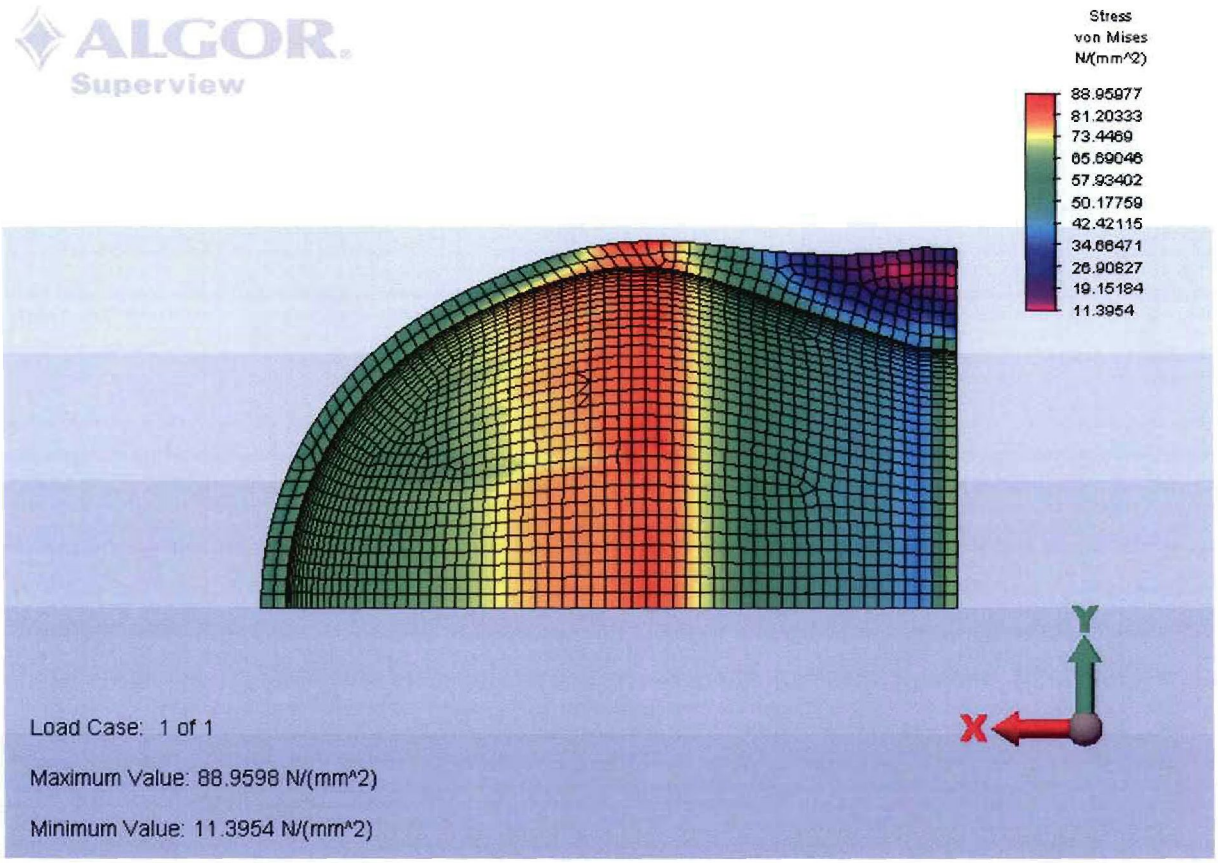


Figure 5-11: Von Mises Stress Distribution in Internally Pressurized Specimen S60A

Although the stress distribution patterns of the other specimens in Figure 5-9 are not shown, detailed analyses for both internal and external pressurization were done for all to arrive at the "best" geometry within the time and cost constraints of the project, namely that of specimen S60B. Roberts (2006) documented the complete development of the S60B specimen in a FEA design report. Algor software was used in the FEA with a mesh size of at least 4 elements through the gauge thickness of the specimen. The Maximum Principal stress contours of the specimens in tensile loading is shown in Figure 5-10, as one example of the relative stress distribution, during development of the geometry of the multiaxial test specimen.

Qualitatively, an acceptable stress distribution is one that has the maximum stress uniformly distributed in the gauge section of the specimen with a smooth reduction in stress towards the clamping or attachment zone. The achieved tolerance for maximum stress variation at a constant radius in the gauge section was 12,5%.

Although the initial intent was to design the specimen to be insensitive to grain orientation, this goal could not be achieved as explained above. The geometry that was finally selected

for the multiaxial fatigue specimen was that of S60B. The locus of alignment axes of specimen S60B to yield the lowest strength values is shown in Figure 5-12. It consists of a cone that is co-linear with the specimen axis with a 90° apex angle. *This means that only 3 orientations are required to determine the weakest strength of an anisotropic material of which the grain orientation cannot be predetermined.*

The sampling plan discussed in Chapter 3, requires samples to be orientated parallel and perpendicular to the grain flow direction in the vibration moulded graphite block. If one assumes equal properties in the plane of the grain direction, in other words no difference between the length and width direction of the brick, there is always a position in the gauge section of the S60B specimen that will lead to cracking in Mode I orientation.

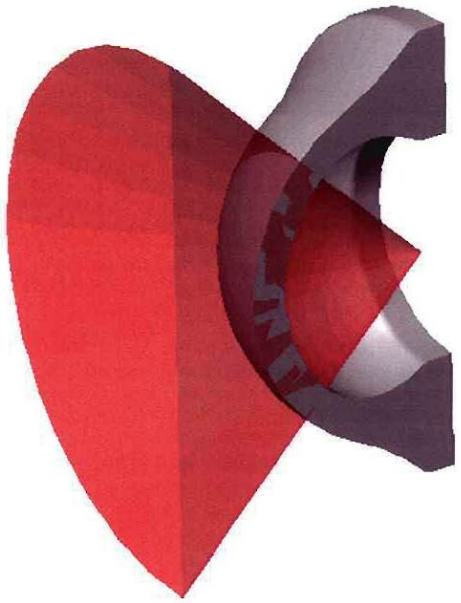


Figure 5-12: Full Section Showing 90° Alignment Cone of Specimen S60B with Grain Direction to Yield Lowest Strength

The maximum variation in MDE stress at the inner wall within the gauge section is 12,5%, which is large, compared to that of existing materials test specimens. However, the highest stresses in the gauge section are localised and therefore constitute a small volumetric percentage of the gauge volume. Its contribution to the probability of survival, as defined by Eq.(4.5) is therefore small.

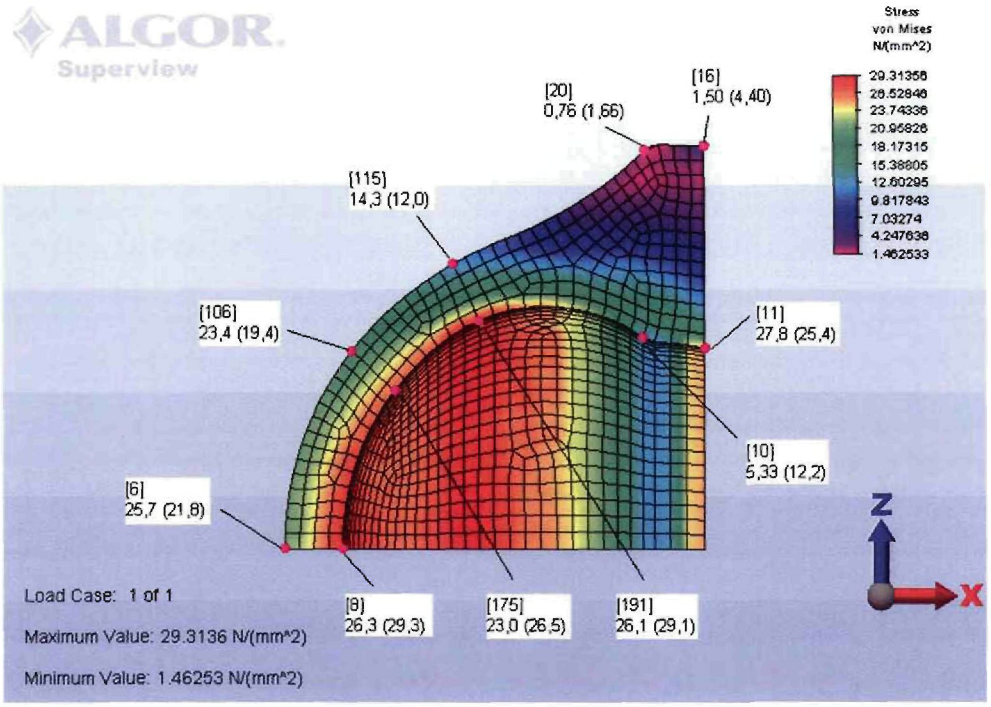


Figure 5-13: Von Mises Stress Distribution in Internally Pressurized Specimen S60B (MDE and Von Mises Stresses Shown For Specific Nodes)

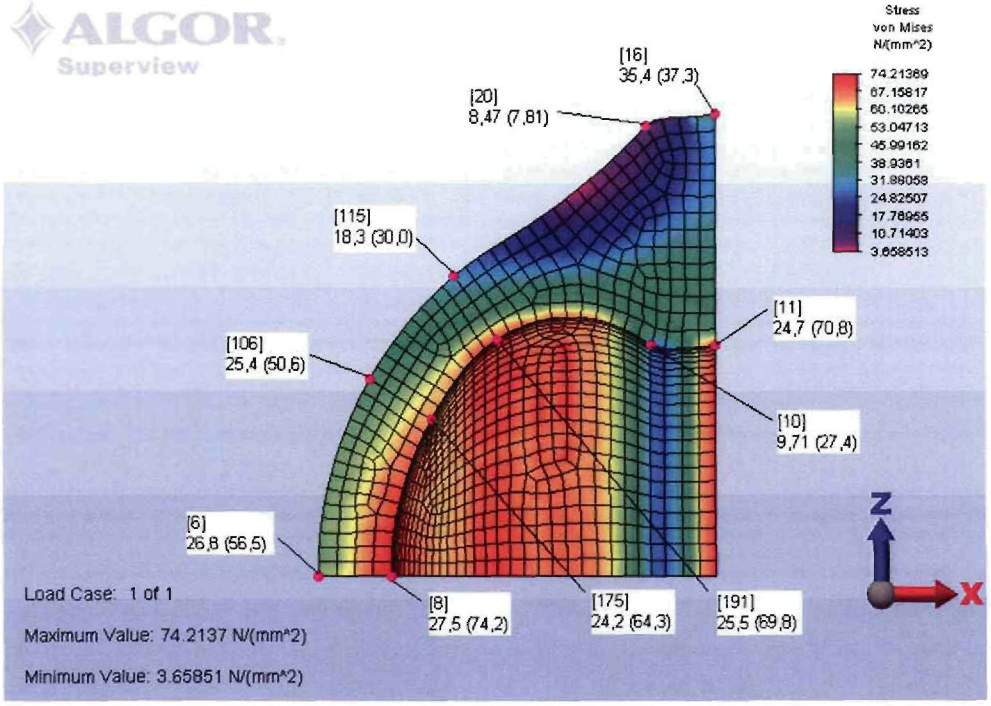


Figure 5-14: Von Mises Stress Distribution in Externally Pressurized Specimen S60B (MDE and Von Mises Stresses Shown For Specific Nodes)

The stress distribution of the maximum and minimum principal stress are shown in Figure 5-15 and Figure 5-16 for internal (tensile) and Figure 5-17 and Figure 5-18 for external (compressive) pressurization respectively.

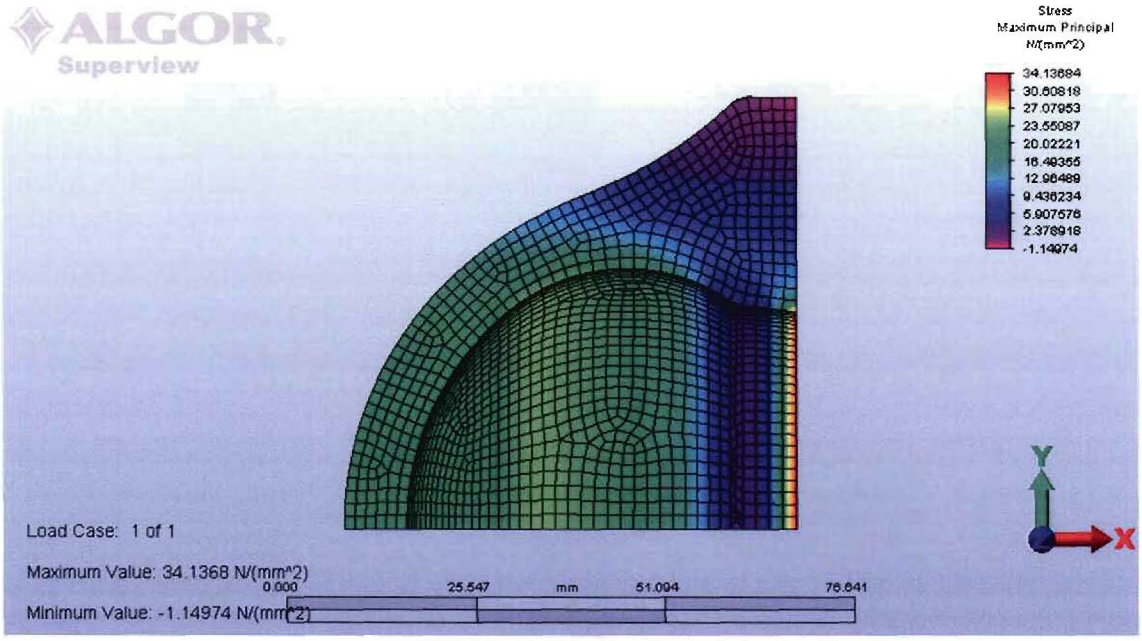


Figure 5-15: Maximum Principal Stress Distribution for 10 MPa Internal Pressure

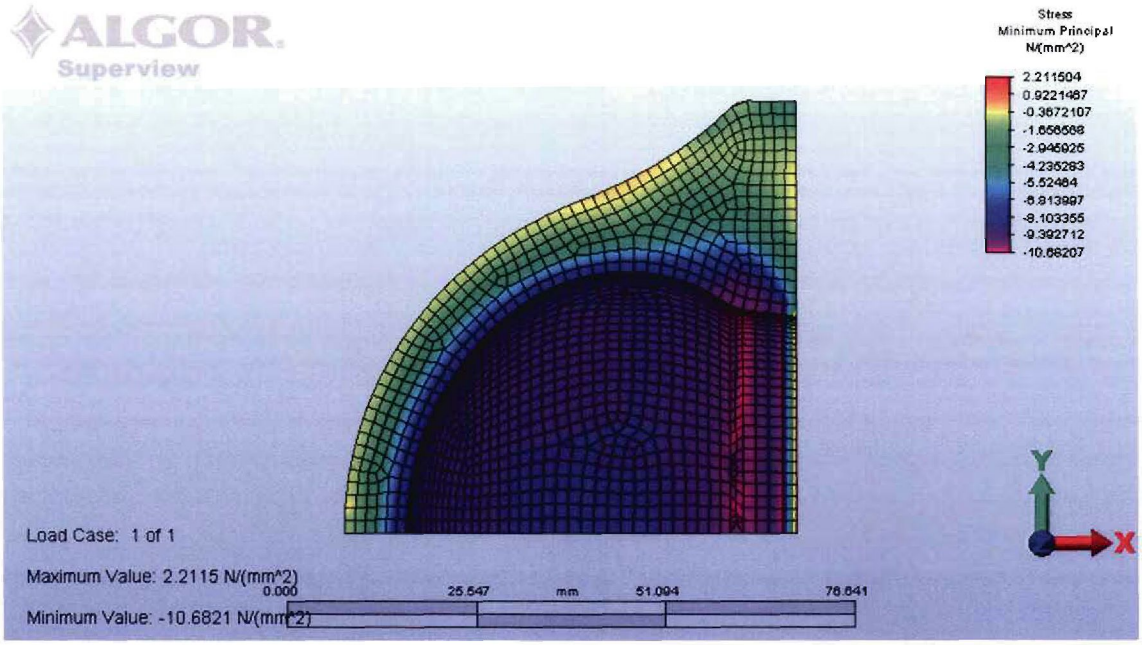


Figure 5-16: Minimum Principal Stress Distribution for 10 MPa Internal Pressure

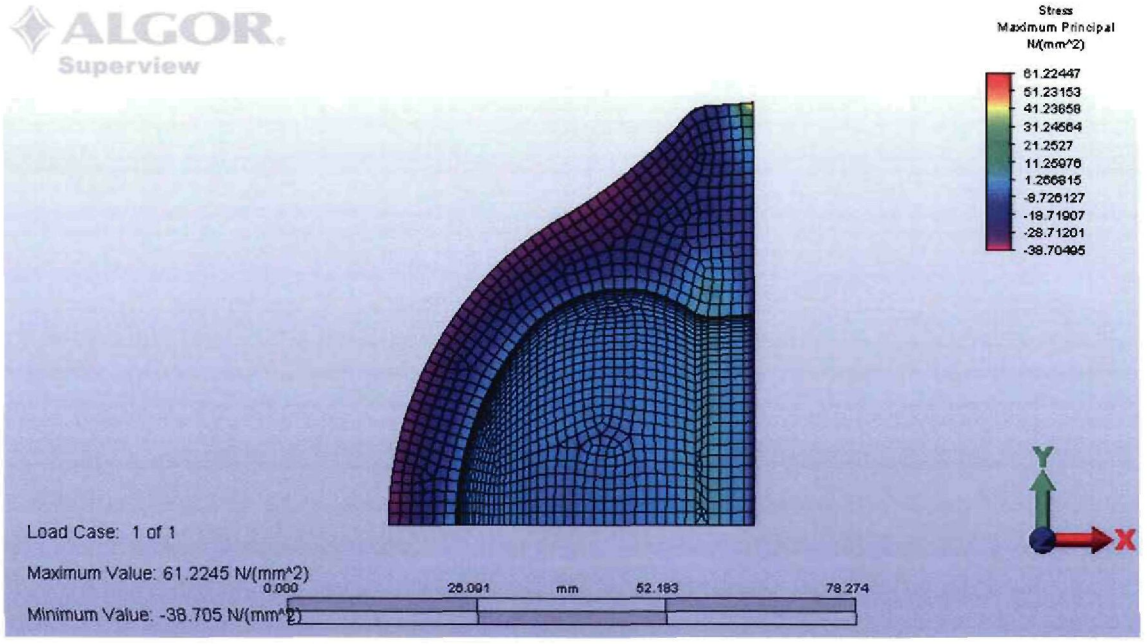


Figure 5-17: Maximum Principal Stress Distribution for 35 MPa External Pressure

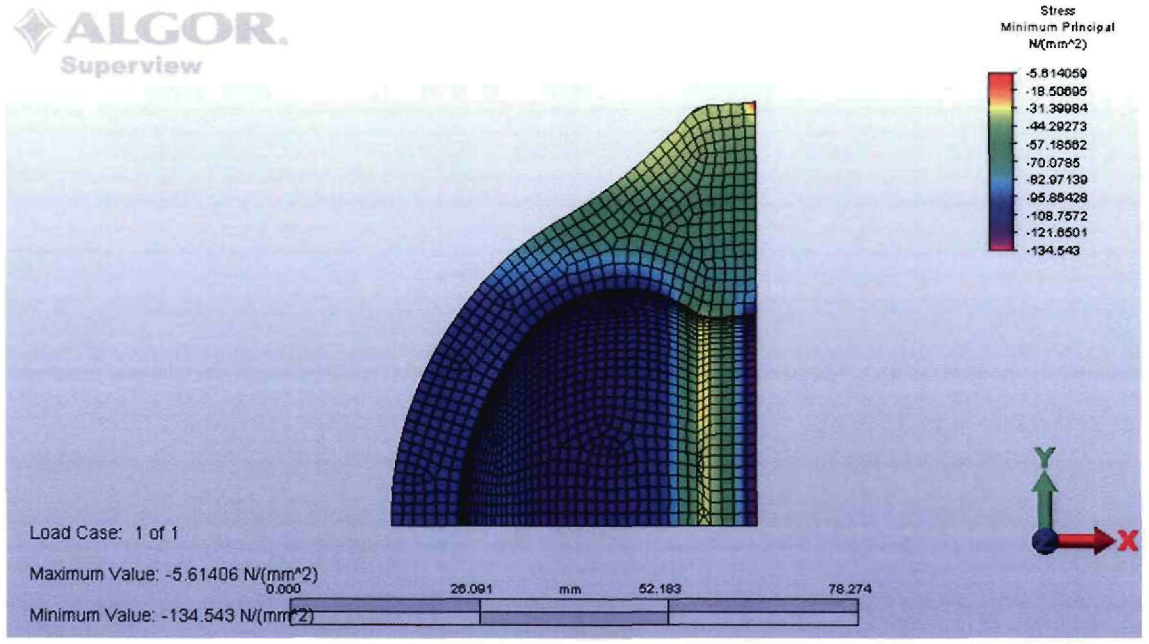


Figure 5-18: Minimum Principal Stress Distribution for 35 MPa External Pressure

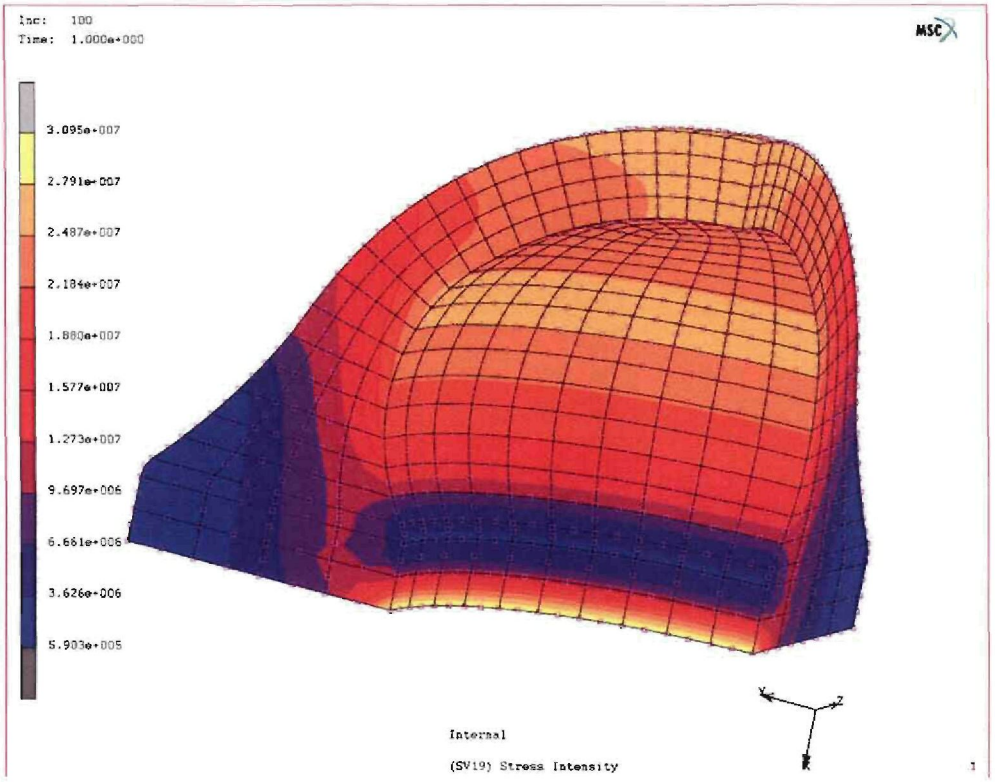


Figure 5-19: MDE Stress Distribution for Internal Pressurization (Tension)

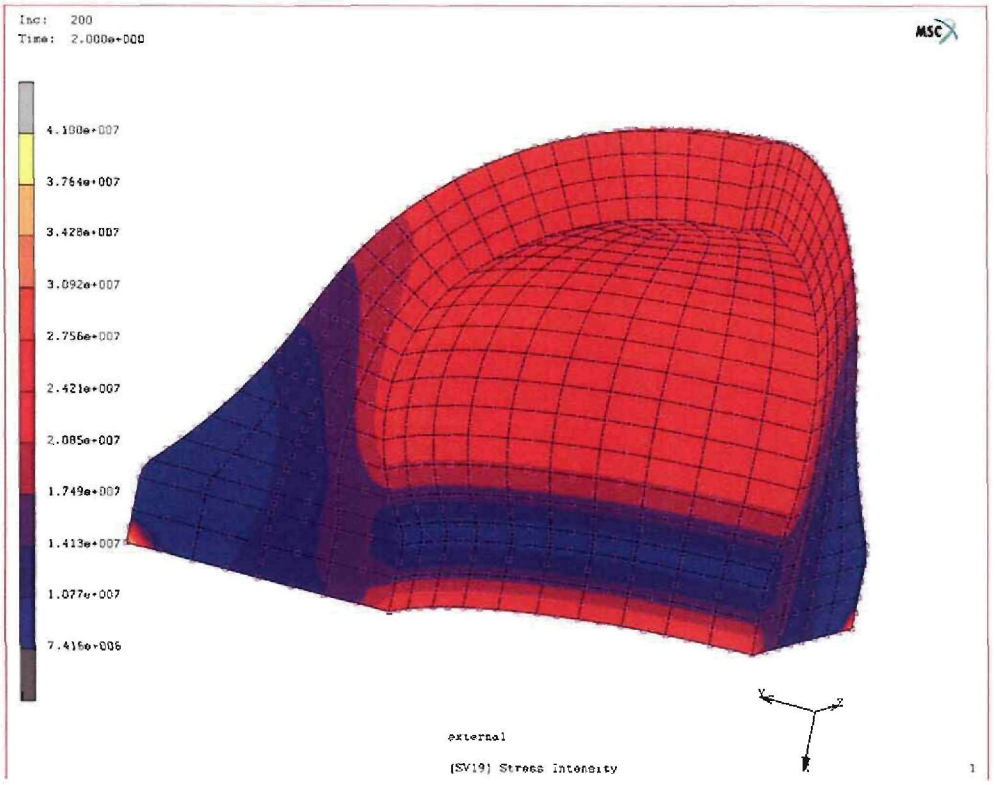


Figure 5-20: MDE Stress Distribution for External Pressurization (Compression)

The FEA design of the S60B specimen is confirmed by PBMR through analysis with their specially adapted software (Marc) with resultant stresses directly displayed as MDE stress. The MDE stress distributions are shown in Figure 5-19 and Figure 5-20 for internal (tensile) and external (compressive) pressurization respectively

The maximum tensile stress in the adhesive bonding the graphite specimen to its base plate depends on the bore diameter of the specimen. The maximum stress is calculated as 3,62 MPa for an internal hydraulic pressure of 10,6 MPa which is much lower than the 25 MPa Ultimate Tensile Strength of the epoxy adhesive, used in this application.

5.2.5 Failure Zone Verification

Six specimens are machined from RFS grade material according to the Specimen Cutting Plan. The machining trials confirm that (subject to some minor development) it is possible to machine the S60B specimen in one setup in conformance with its predefined no-clamping zones. Only the removal of the parting-off stub (typically ø8) requires a second setup, which affects only a small surface area (and thus volume) of the specimen.

Three of these specimens are subject to static external pressure loading and two to static internal pressure loading to failure, in a hydraulic test chamber, illustrated in Figure 5-21.

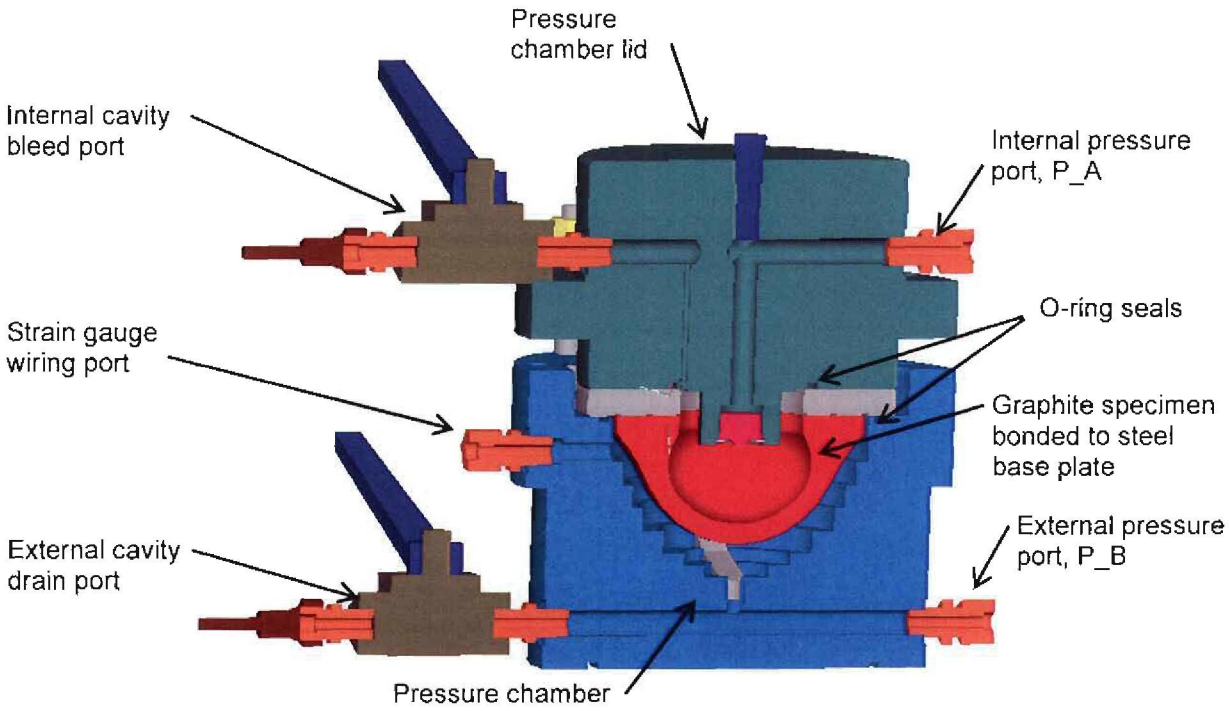


Figure 5-21: Full Section Model of S60B Specimen in Hydraulic Test Chamber

The purpose of these tests is to confirm that failure occurs in the gauge section of the specimen, as predicted by the Weibull analysis that is done by PBMR in accordance with the KTA 3232 design methodology. According to this analysis, the S60B specimen, manufactured from NBG18, has a 2,7% probability of failure in its remaining parts for an overall probability of failure of 59,6%, shown in Figure 5-22, at an internal pressure of 10 MPa.

Likewise, it has a 2,0% probability of failure in its remaining parts for an overall probability of failure of 78,0%, shown in Figure 5-23, at an external pressure of 25 MPa.

The reliability of the S60B specimen (R_3) can be modelled as the reliability of the gauge section (R_2) and the reliability of the remaining part (R_1). Refer to Eq.(5.4).

Reliability of two subsystems in series is given by Blanchard & Fabrycky (2006) :

$R_3 = R_1.R_2$ because 2 subsystems are in series (if one fails, system fails)

$$\therefore (1-P_{F3}) = (1-P_{F1})(1-P_{F2})$$

$$\therefore (1-P_{F2}) = \frac{(1-P_{F3})}{(1-P_{F1})}$$

$$\therefore P_{F2} = 1-\left[\frac{(1-P_{F3})}{(1-P_{F1})}\right] \qquad .....(5.4)$$

Where :

P_{F1} ≡ Probability of failure in remainder of specimen [-]

P_{F2} ≡ Probability of failure in gauge section of specimen [-]

P_{F3} ≡ Probability of failure of specimen [-]

The ratio of failure probability in the gauge section versus the remainder, using Eq.(5.4) to calculate P_{F2} is 21,6 : 1 and 38,8 : 1 for tensile and compressive loads respectively. This indicates a strong preference towards failure in the gauge section.

Figure 5-24 is a photograph of the failure zones of RFS grade graphite. The failure zones due to external pressurization of the specimens are relatively small single cavities in the spherical section. The debris from the compressive stress failure is graphite crumbs.

The failure zones due to internal pressurization of the specimens are larger cap-cracks, of which two extended beyond the spherical section of the specimen. Tensile failure does not produce any crumbs. Since it is not possible to determine the origin of the cracks, the extension of the cracks beyond the spherical section is attributed to post-failure bending stresses. As long as a tensile crack runs through the gauge section, it is assumed to cause the failure, and treated as an acceptable test.

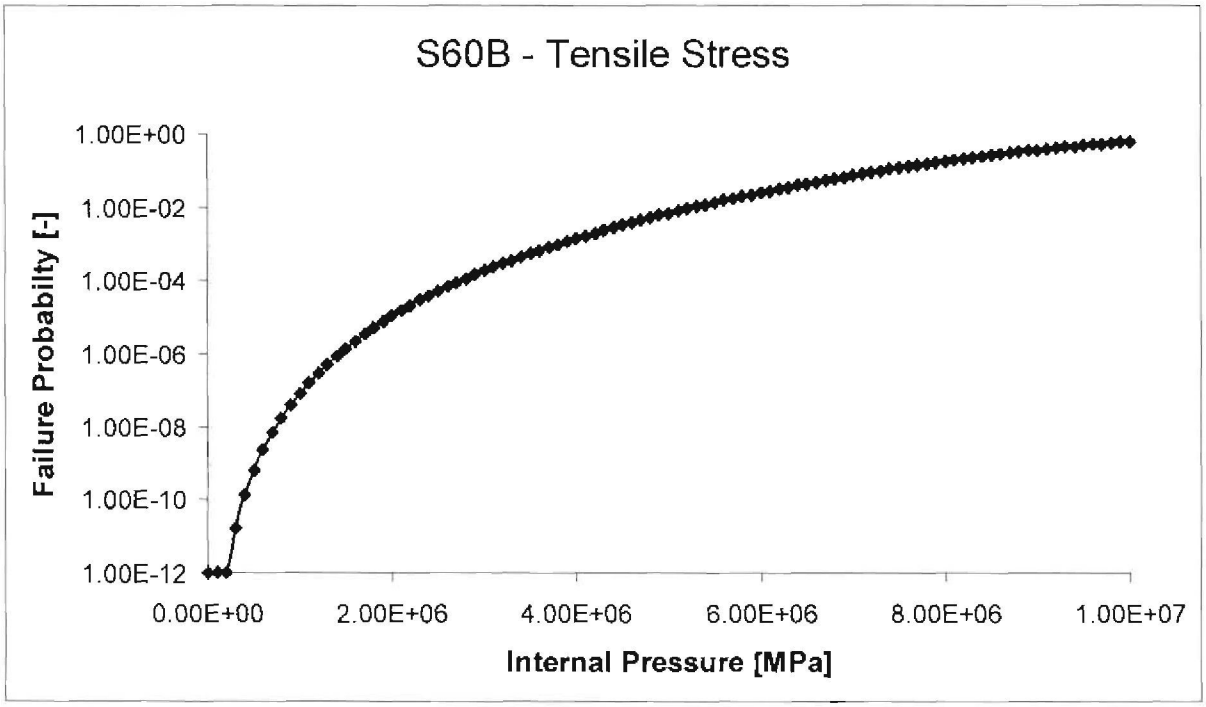


Figure 5-22: Failure Probability of S60B in Tension

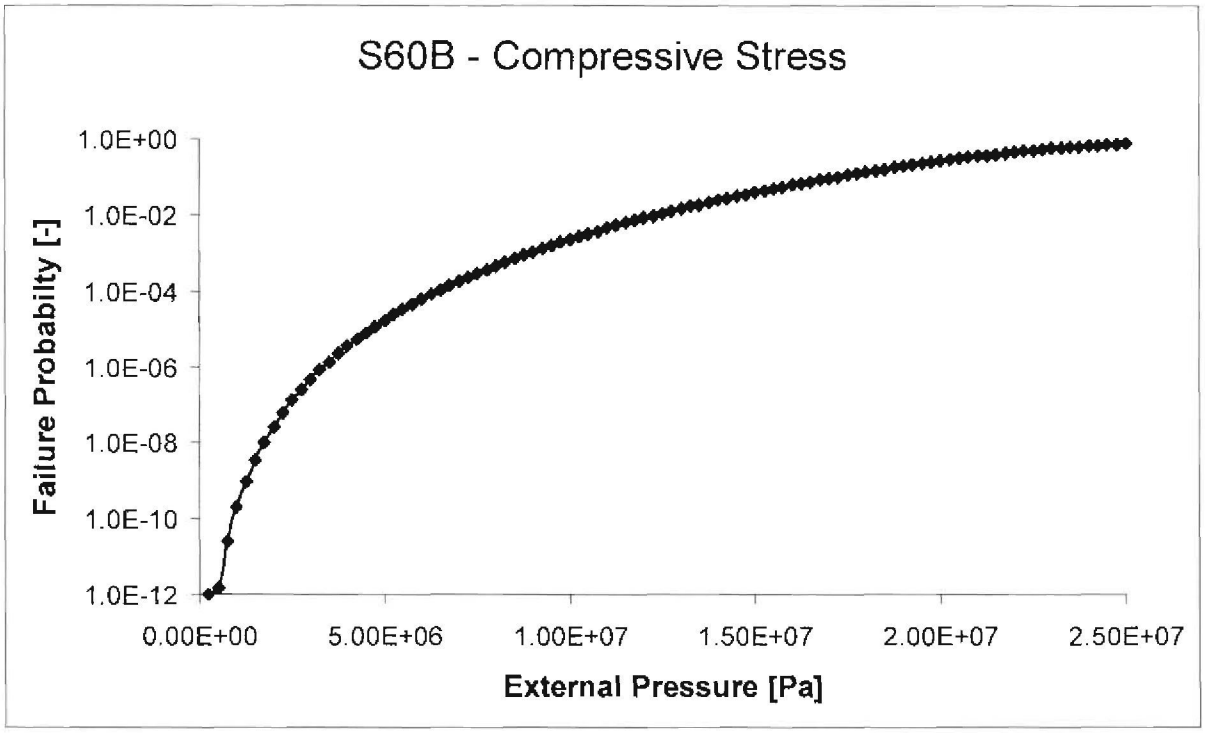


Figure 5-23: Failure Probability of S60B in Compression



Figure 5-24: Compression (Left) and Tensile (Right) Failure Zone of Specimen S60B in RFS Grade Graphite

It is safe to conclude that the risk of a failure originating at or near the base of the specimen, as may be suggested by Figure 5-13 and Figure 5-14, is small.

5.2.6 Summary

As hypothesised in the conclusions of Section 2.4 in Chapter 2, the "most damaging" multiaxial stress state may be one where the two Maximum Principal stresses are in phase, as in the case of a hollow hemisphere. The third principal stress is always negative or zero (compressive). This stress state is expected to yield the most conservative strength characteristics of the graphite in tension. In compression, there is no experience base on which an expectation regarding the severity of induced damage can be founded. As a first guess, it is one of the contenders for determining the most conservative strength characteristics of graphite, where the other candidates are:

- Two equal large compressive principals and a third small tensile principal stress
- One large compressive principal with two equal small tensile principal stresses

Because a cylindrical specimen does not comply with the requirement of insensitivity to grain direction, the basic shape of the proposed multiaxial specimen is hemispherical. The stress distribution in the transition from sphere to flange drives the geometric design.

After the S60B specimen geometry was finalised, it was subjected to the cost comparison, as discussed in Section 4.5.1 of Chapter 4. The results show that the S60B fatigue specimen is approximately 6 times cheaper to manufacture than specimen S9. Both from a specimen cost point of view, as well as from an equipment cost point of view, specimen S60B is the more cost effective specimen.

To summarise, the S60B specimen is superior to all the referred multiaxial specimen geometries from the following points of view:

- Simplicity of stress state
- Cost of specimen
- Cost of test equipment
- Insensitivity to grain orientation
- "Maximum damage" loading configuration

The S60B specimen is inferior to specimen S9 with regard to stress distribution in the gauge section.

The basic geometry of the S60B test specimen is shown in Figure 5-25 with the nominal dimensions as indicated. The other dimensions and tolerances are shown in the detailed drawings of the S60B specimen in **Appendix B**.

The specimen consists of two parts, bonded together with Pratley Quickset Steel (a high strength epoxy adhesive). The test section of the graphite part is essentially a thick-walled partial sphere, which transitions to a flange.

The nominal dimensions, as shown in Figure 5-25, are:

A = 9.0 mm B = 39.0 mm C = 90.0° D = 58.0 mm E = 116.0 mm

All pressure sealing is performed on the base plate. The graphite, which is exposed to the hydraulic oil, is sealed with a RTV silicone sealant.

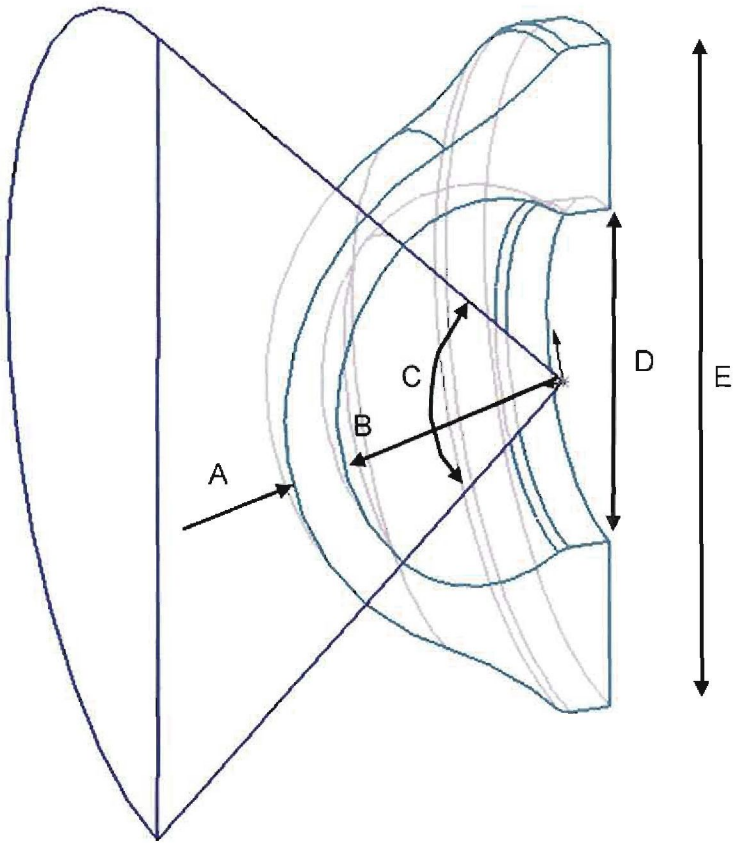


Figure 5-25: Full Section of Graphite Part of S60B Specimen, Showing Nominal Geometry

5.3 DEVELOPED MDE STRESS

The stress state in the multiaxial specimen is much more complicated, than in the uniaxial specimen. The stress states at the peaks and valleys of the fully reversed, principal stress based load ratio are shown at the inner and outer wall of the S60B multiaxial specimen in Figure 5-26 to Figure 5-29. The principal stress excursions, MDE stress excursion and developed MDE stress excursion are shown in Figure 5-30. The MDE stress can either be the maximum MDE stress (inner wall location) or the arithmetical linear average of the inner and outer wall MDE stresses or the volume weighted average MDE stress. A volume weighted average is proposed in this research (see Section 5.2.3.3).

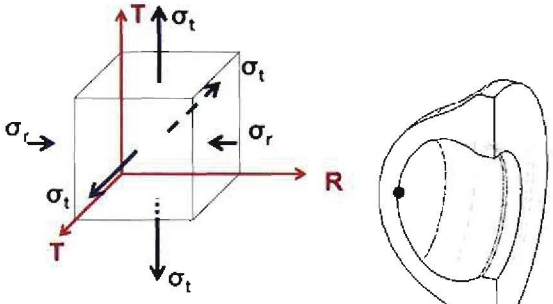


Figure 5-26: Tensile Stress State at Inner Wall of Multiaxial Specimen

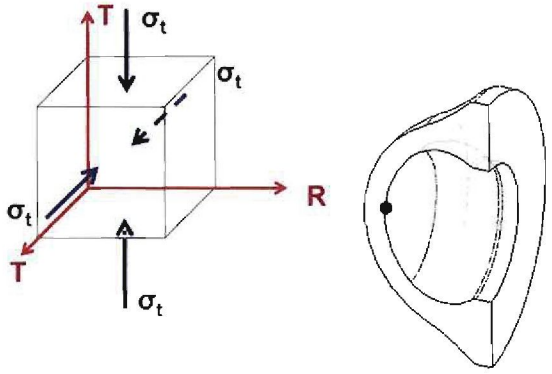


Figure 5-28: Compressive Stress State at Inner Wall of Multiaxial Specimen

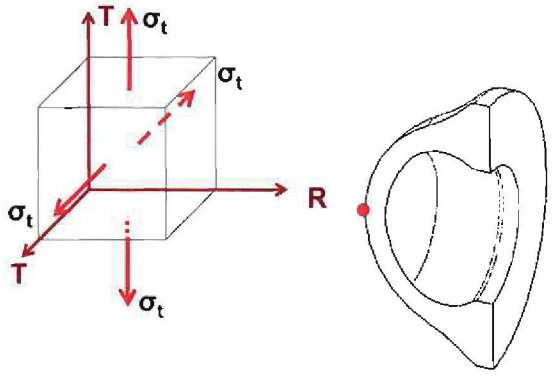


Figure 5-27: Tensile Stress State at Outer Wall of Multiaxial Specimen

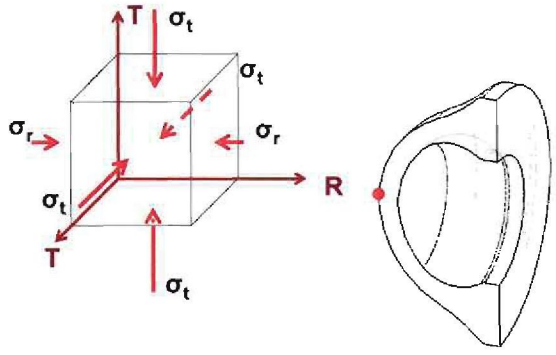


Figure 5-29: Compressive Stress State at Outer Wall of Multiaxial Specimen

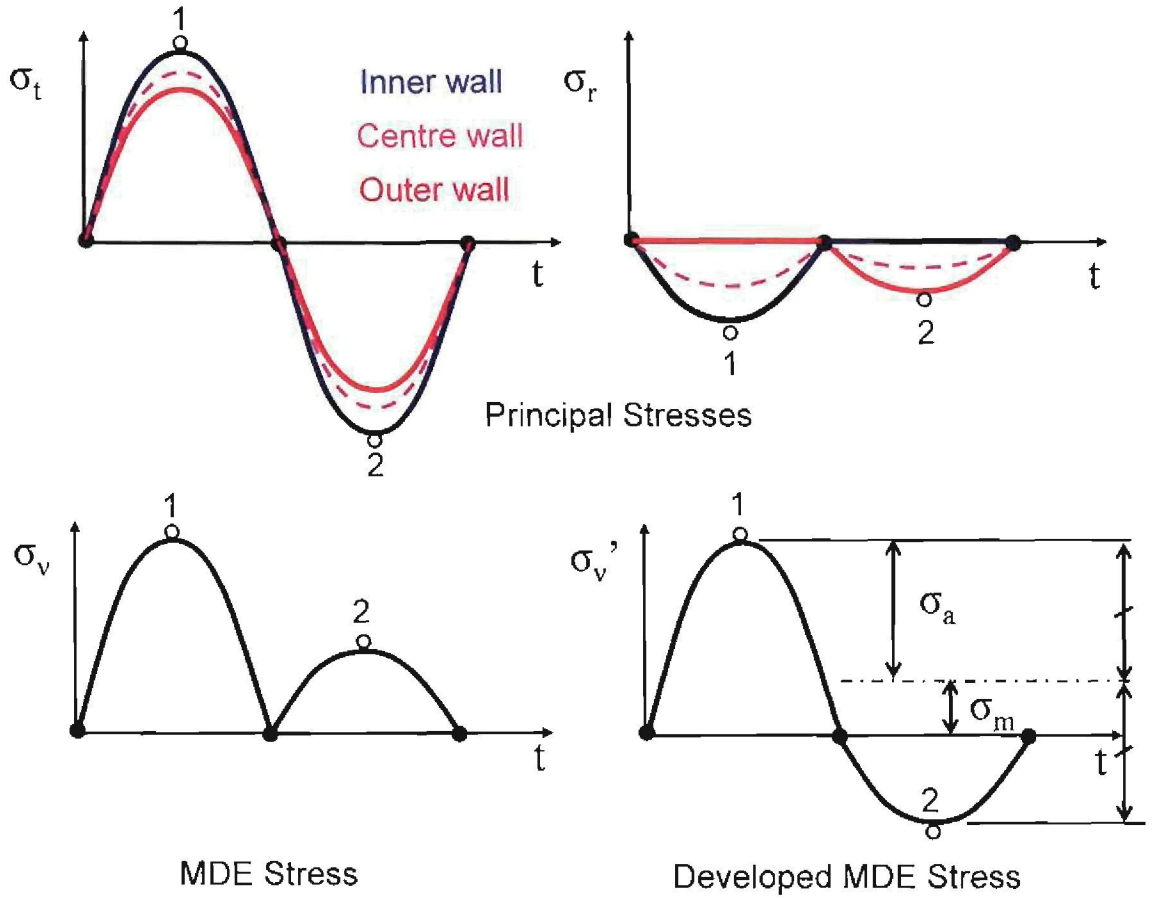


Figure 5-30: Maximum Principal Stress Excursion for R = -1, Related MDE Stress Excursion and Developed MDE Stress Excursion in Multiaxial Specimen

5.4 FATIGUE TESTING EQUIPMENT

The Multiaxial Fatigue Testing System comprises a custom built hydrostatic test chamber with maximum hydraulic pressure capability of 35 MPa and precision pressure transducers to sense the pressure loading (see Figure 5-32). The high level subsystems of the Multiaxial Fatigue Testing System and their inter-relations are shown in Figure 5-31.

The system is controlled via a Labview 7.1 control and data acquisition program and National Instruments (NI) PCI 4472 and PCI 6221 data acquisition cards.

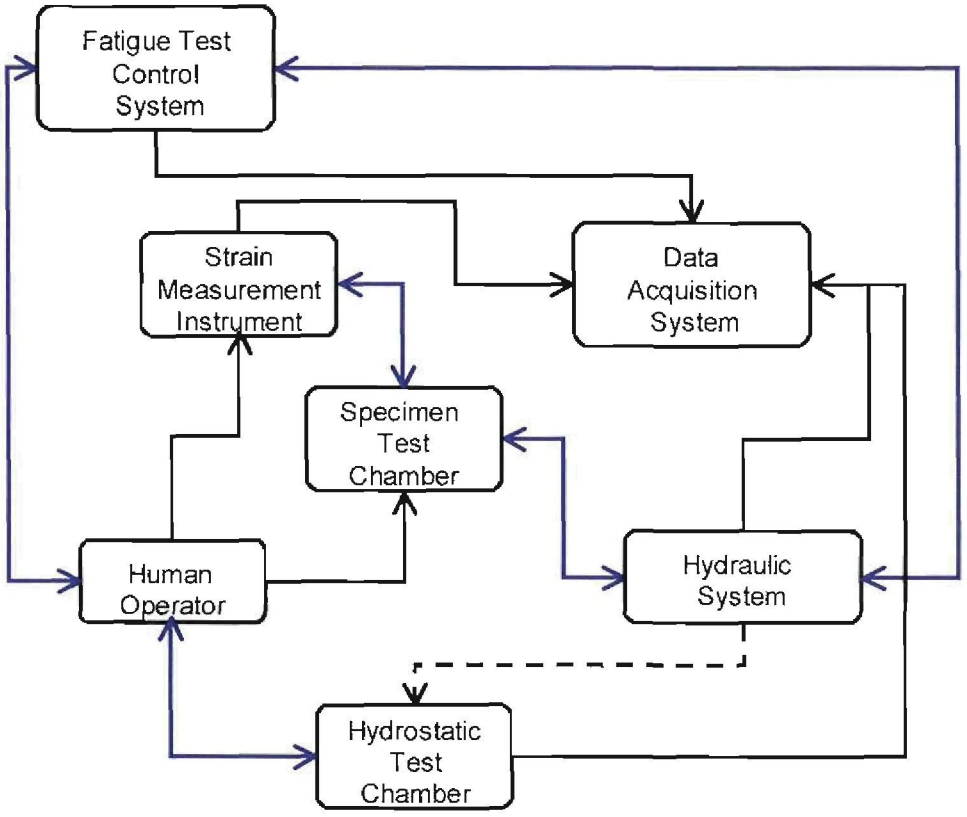


Figure 5-31: Subsystems and Relations of Multiaxial Fatigue Testing System

The Moog servovalve has an onboard controller to control the pressure independently. The Moog controller parameters can be adjusted online using a CAN-bus interface. Since the hydraulic system is prone to resonate at its natural frequency (especially if there is some entrapped air in the system), it is quite difficult to achieve the specified ± 1% control accuracy and repeatability. A high proportional gain is required for high accuracy control, but a high gain also causes control instability at the resonant frequency of the system.

The hydraulic test chamber went through a number of modifications as the tests progressed, to improve the effectiveness of bleeding of the hydraulic fluid, to remove entrapped air inside the specimen loading volume.

The "best" Moog valve pressure control parameter sets that are attained by trial-and-error are saved and used for all tests at that specific load ratio. All load ratios have different parameter sets for pressure control.

Hydraulic oil temperature control and back-up data acquisition is established via a second PC, running Labview 7.1 software, and a NI PCI 6024 data acquisition card.

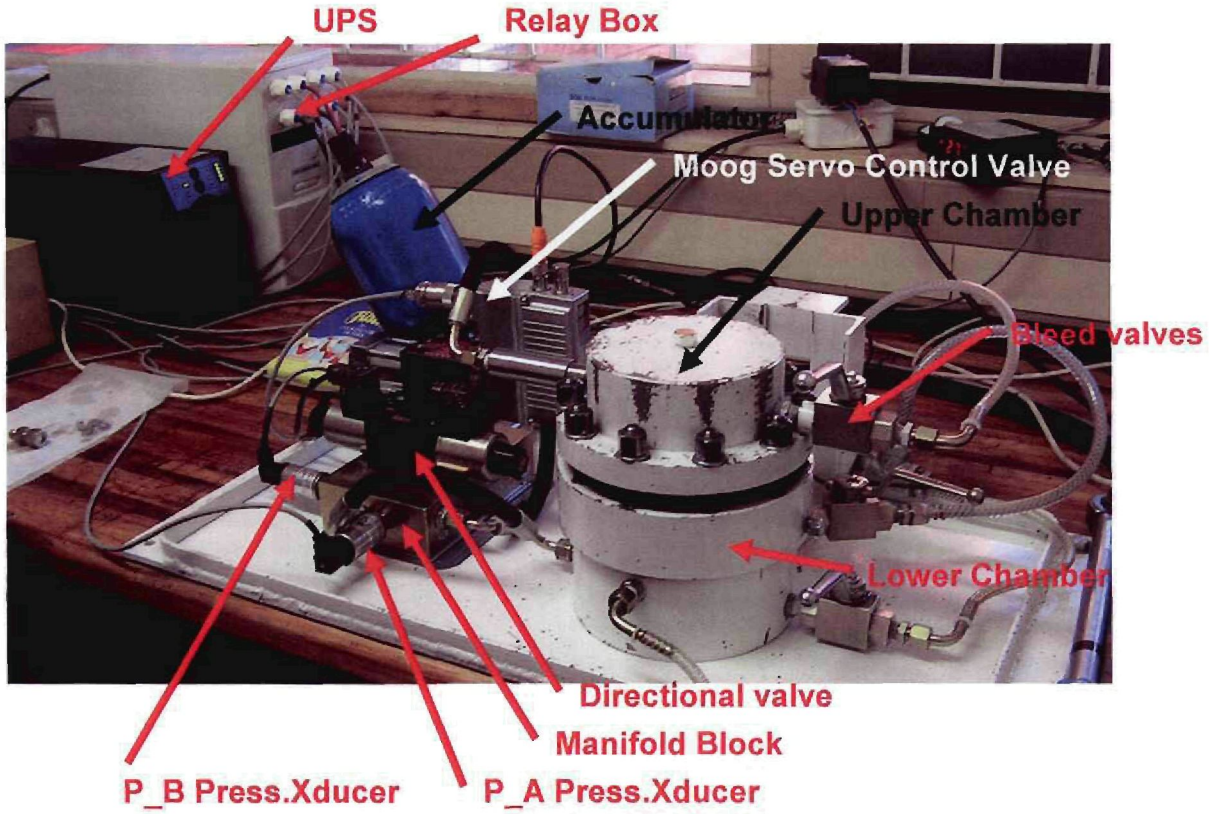


Figure 5-32: Multiaxial Fatigue Test System

The Isostatic Test Chamber that is used to load the PIE specimens is shown in Figure 5-33.



Figure 5-33: Isostatic Test Chamber Being Pressurized

5.5 MACHINING REQUIREMENTS

The same machining requirements that are specified for the uniaxial specimens are applicable to the multiaxial specimens (refer to Section 4.6.1).

Typical radial clamping and "no clamping" zones are shown in Figure 5-34.

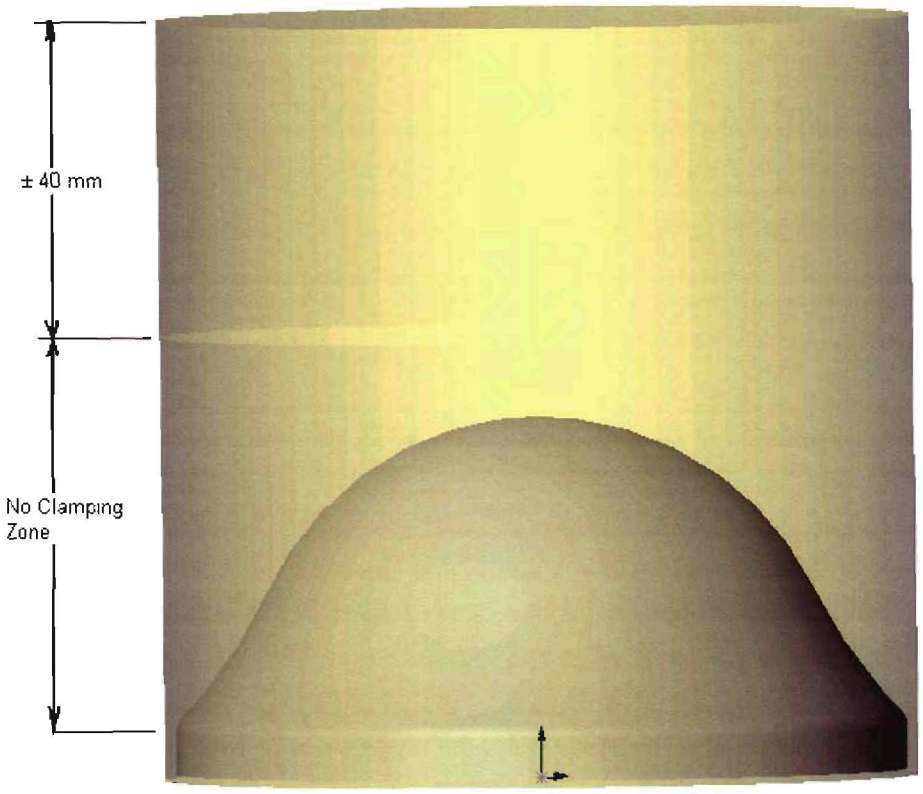


Figure 5-34: Typical No Clamping Zone of S60B Specimen

5.6 CONDITION OF SPECIMENS

The NBG18 multiaxial fatigue specimens are all machined by SGL Carbon and shipped to the North-West University. The samples are supplied in the as-machined condition. The wall thickness of the specimens is measured using a 5 micron resolution digital readout on a milling machine, a 2 micron resolution dial gauge and special arbors (See Figure 5-35). The wall thickness in the test section is in many cases found to be out of specification due to an incorrect machining operation to remove the stub after parting. The inside diameter of the test specimen is assumed to be the nominal diameter and the outside diameter is calculated using the mean of the wall thickness measurements.

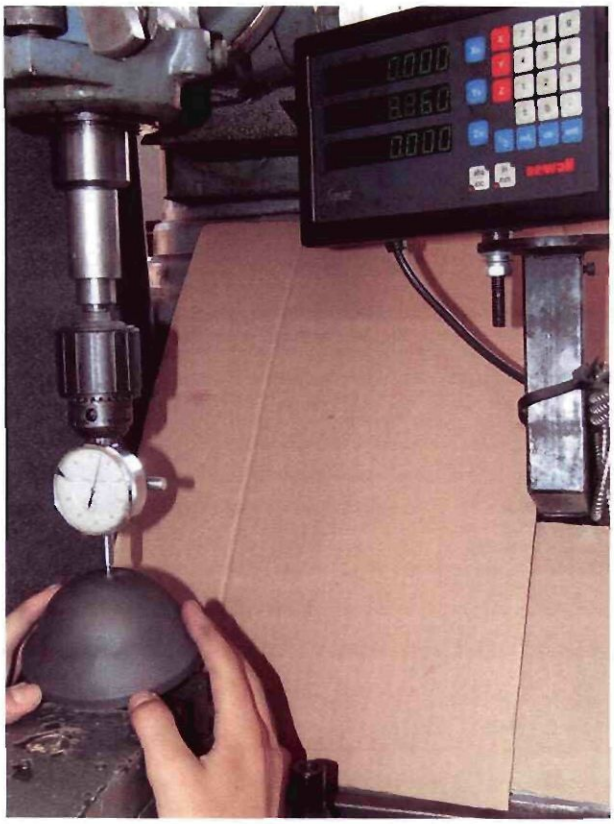


Figure 5-35: Wall Thickness Measurement of S60B Specimen

The severity of the observed wall thickness error is investigated by doing a sensitivity analysis of the theoretical stress distribution through the gauge section of the specimen.

The effect of geometry on the theoretical stress in the test section is evaluated by changing the wall thickness by up to 10 tolerance bands on each side. The results of this analysis are shown in Figure 5-36. Two tolerance band deviations (in the worst combination) to either side yield less than 2% deviation in stress condition, for both internal and external pressurization of the specimen. The specimen is slightly more sensitive to geometrical deviations under internal pressurization as compared with external pressurization. The Volume Weighted MDE (VMDE) stress is approximately double as sensitive to geometric deviations as the Maximum Principal stress. The following legend applies to the mentioned figure:

σ_W_Po	≡	Volume Weighted MDE stress under external pressurization
σ3	≡	Maximum Principal stress under external pressurization
σ_W_Pi	≡	Volume Weighted MDE stress under internal pressurization
σ1	≡	Maximum Principal stress under internal pressurization

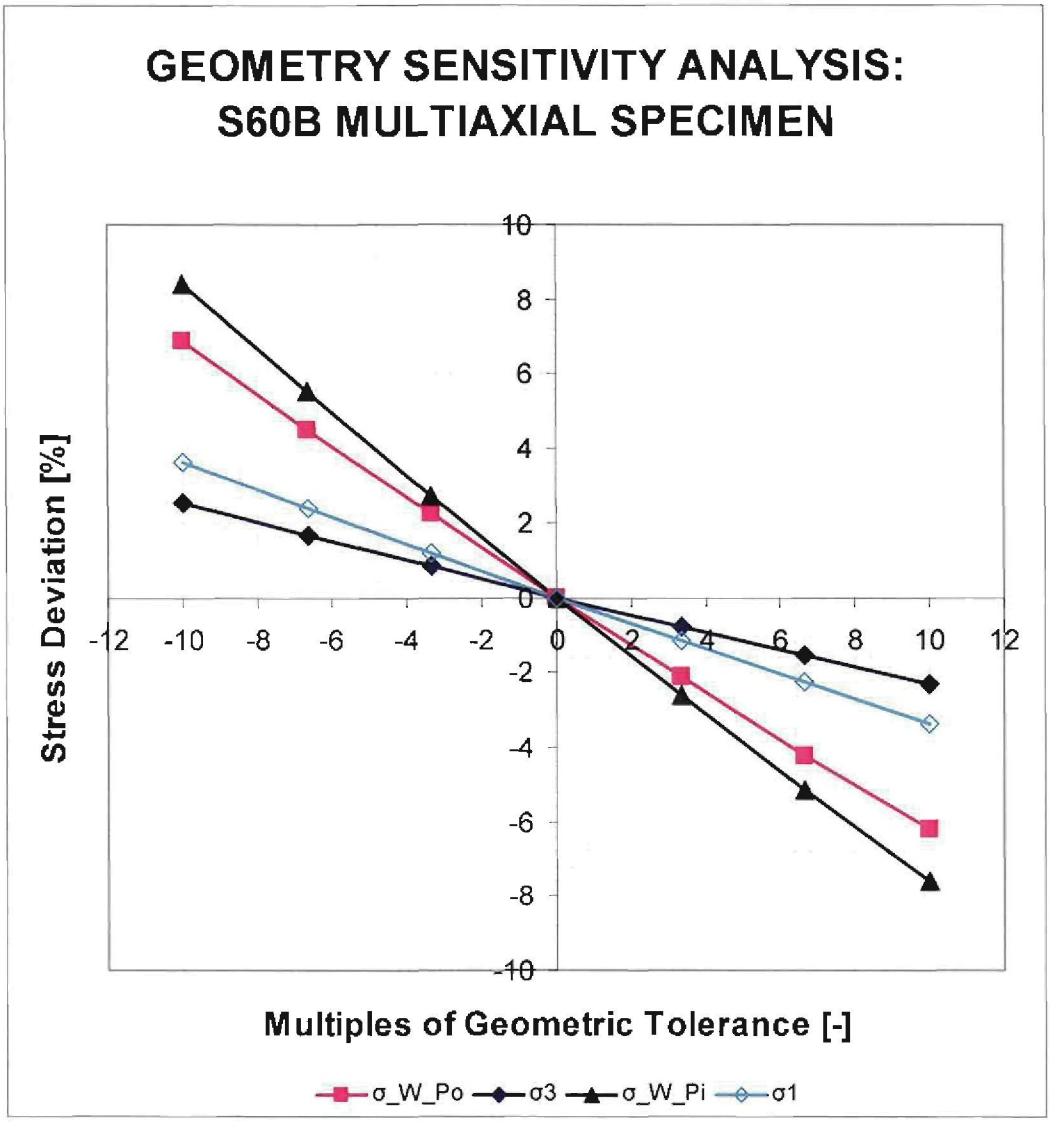


Figure 5-36: Sensitivity Analysis of Geometry of S60B Specimen

The mass of the specimens is measured on a Sartorius model L420P mass balance. (See **Appendix F** for calibration certificate.)

The Base plates are acquired by the NWU according to the design drawing. The graphite specimens are bonded to the base plates according to the specified procedure (refer to the detail drawing). This procedure involves washing with water and dishwashing soap, drying in an oven at 60 ± 5°C, cleaning with acetone, handling with latex gloves and volumetric dispensing of the two components of the epoxy using modified syringes. Some of the mentioned activities are illustrated in Figure 5-37 to Figure 5-39.

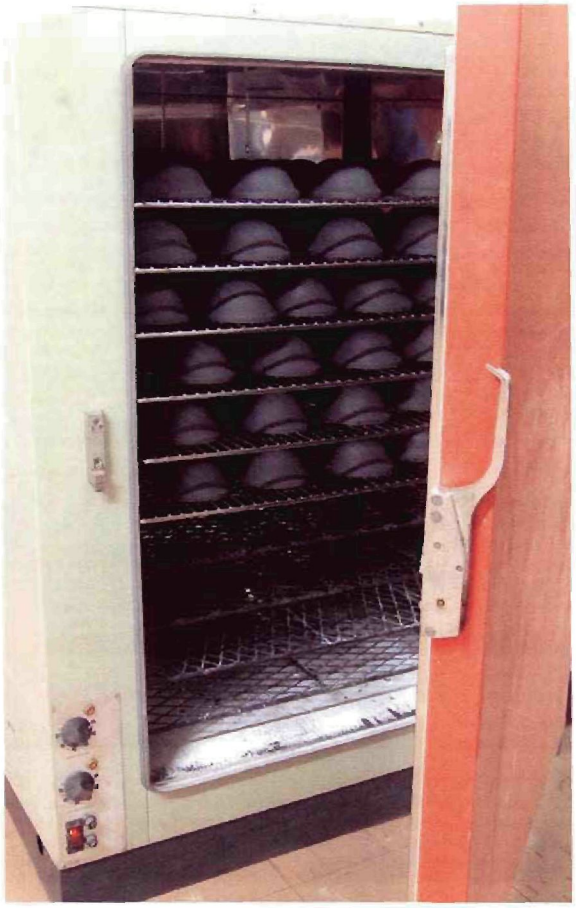


Figure 5-37: Drying of Graphite Specimens after Washing



Figure 5-38: Bonding of Graphite Specimen to Base Plate

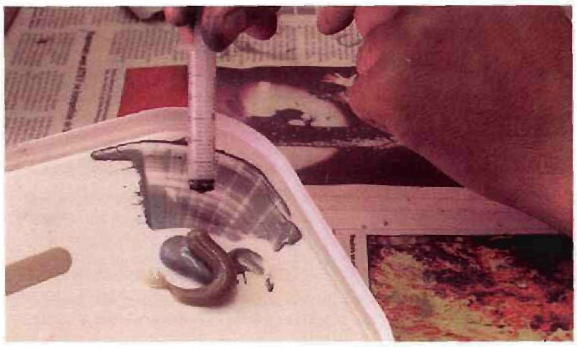


Figure 5-39: Volumetric Dispensing of Two Parts of Epoxy

5.7 CALIBRATION

5.7.1 Load Measurement System

The pressure measurement system consists of the following subsystems:

- Two pressure transducers, measuring the pressure in the upper (P_A) and lower (P_B) chambers of the pressure vessel
- The data acquisition cards

- Wiring
- Software conversion factors.

This system is calibrated as a whole using an Ashford dead weight tester. Refer to **Appendix F** for all the relevant calibration certificates.

5.7.2 Strain Measurement System

HBM 1-XY91-6/120 type gauges are applied to the graphite samples using HBM X280 epoxy glue. The gauges are connected into a full Wheatstone bridge in the manner shown in Figure 5-40 and Figure 5-41. Gauges R2 and R4 are dummy gauges, bonded onto the two opposite sides of a graphite strip and placed into the hydraulic oil in the sump in order to have approximately the same temperature as the specimen.

The gauge factor for the gauges is 2,03 and the bridge factor due to the Wheatstone bridge connection is 5,075 μV/(μm/m).

Calibration is done by means of a precision shunt resistor. The resistance value is 5 kΩ ± 0,01%. During the calibration process, the shunt resistor is connected across gauge 1 in order to simulate an output voltage. The simulated strain value is calculated using Eq.(5.5) as derived in **Appendix K**, analogous to the examples presented by Dally and Riley (1978).

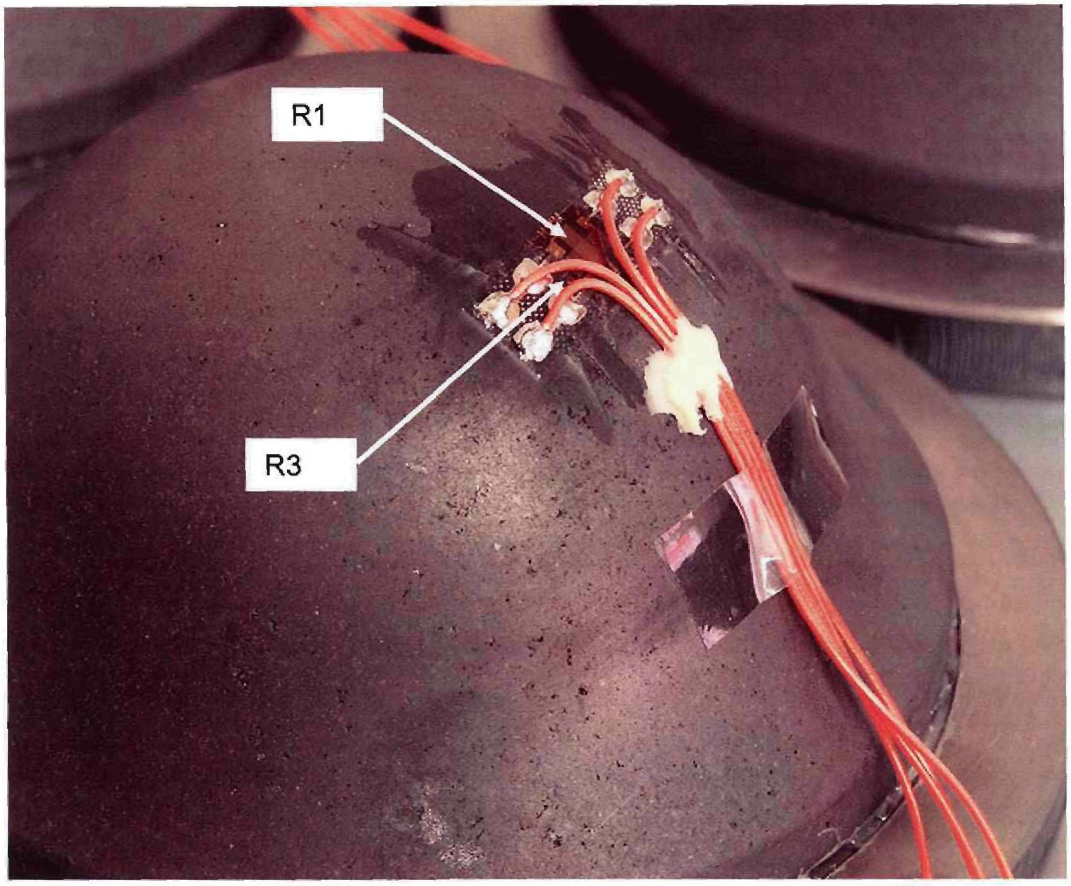


Figure 5-40: Example of Gauged Sample

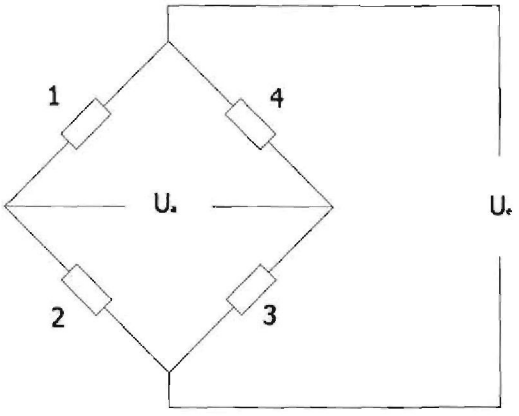


Figure 5-41: Wheatstone Bridge Configuration

$$\varepsilon_c \approx \frac{-R_1}{2(R_1 + R_c)G} \qquad \text{.....(5.5)}$$

Where:

ε_c = simulated strain

G = strain gauge factor

R_1 = 120Ω (gauge 1 resistance)

R_c = shunt resistor value

The ε_c calculated for the 5 kΩ shunt resistor is -5773 μm/m. Refer to **Appendix F** for all the relevant calibration certificates.

5.8 TEST PROCEDURE

Specimens are allocated to all tests according to the specimen allocation plan, shown in Appendix A. In the event of an unsuccessful test and the availability of spare specimens, the spare specimens are allocated according to a colour coding, which indicate the orientation and location of the specimen in the original graphite block.

5.8.1 Isostatic Loading

All specimens that are exposed to isostatic loading prior to fatigue testing (PIE specimens), are overall sealed, exposed to the pressure, unsealed, washed, dried, bonded to their base plates and resealed in preparation for fatigue testing.

All specimens allocated to fully reversed fatigue cycling, are loaded in one batch in the Isostatic Test Chamber. After the specimens are loaded into the chamber, the Isostatic Test Chamber is filled with water. An Enerpac hydraulic hand pump is used to pressurize the chamber. The pressure is maintained for 8 minutes (480 seconds). The pressure profile of the first isostatic loading batch is shown in Figure 5-42. The specimens, allocated to the static tests are treated in a second batch.

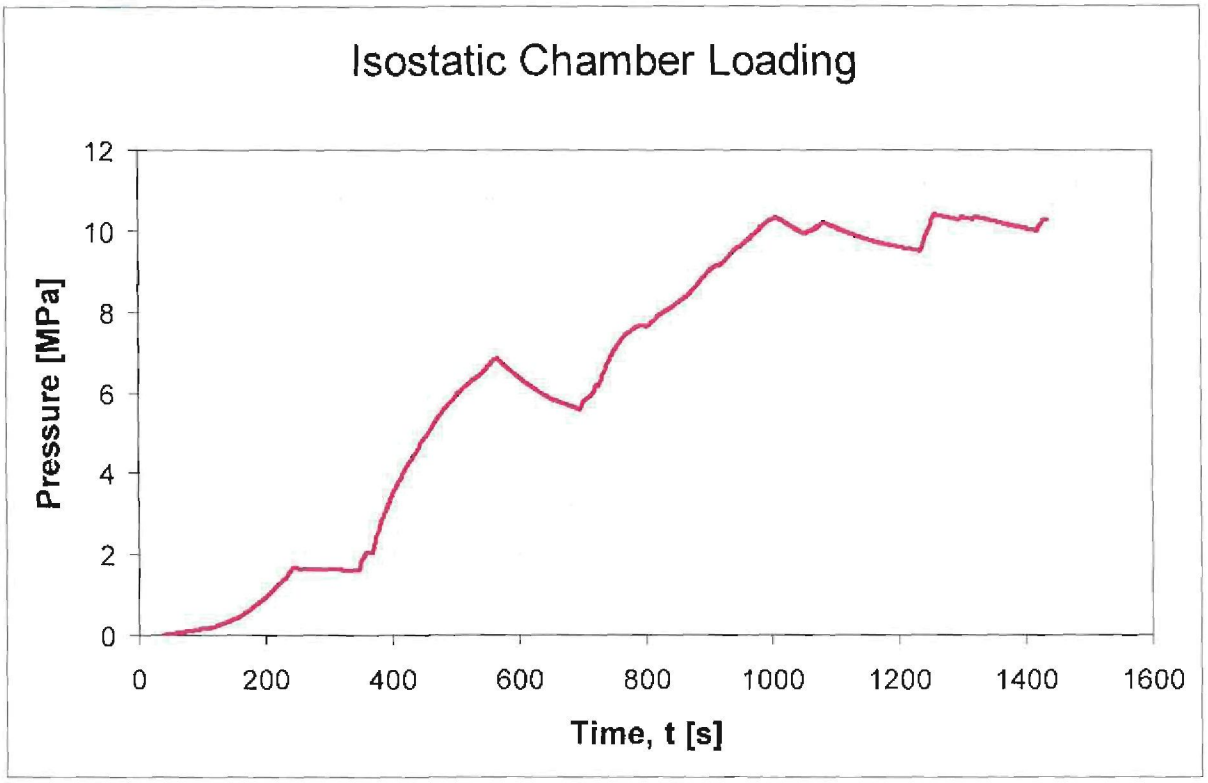


Figure 5-42: Pressure Profile of Isostatic Loading

5.8.2 Fatigue Testing

Eight specimens, from locations explained in Chapter 3, are tested for each load setting. One specimen per load ratio is strain gauged, to measure the stress-strain characteristic at that R-value. Four load settings are used for each dynamic load ratio, resulting in 32 specimens per R-value. Eight specimens are used for each of the two static R-values.

Static tests are conducted using an Enerpac hydraulic hand pump to pressurise the pressure chamber of the multiaxial fatigue test system, shown in Figure 5-32. The specimen is installed into the test chamber with disposable oil filters at either side of the gauge section to contain the graphite debris of the fracture. The relevant pressure cavities are bled to remove entrapped air. The data acquisition software is started and the hand pump is used to load the specimen until fracture. Upon fracture, the data acquisition software is stopped and the specimen is removed from the pressure chamber.

A procedure, similar to the one summarised above is used for the fatigue tests. The main difference is that the hydraulic power pack is used as the power source, in stead of the hand pump. The test operators perform the tests according to a work instruction sheet and a test log is completed to document all events.

As a starting point, the first load for all tests is guessed at approximately 85% of the average ultimate force (tensile or compression). The subsequent loads are then predicted assuming a straight line approximation on a log-log scale, using the results of the static data and the results obtained from the first load. Failure is defined as a detectable oil leak and run-out is defined as $6x10^4$ cycles.

For the PIE tests, eight specimens are tested in static tension and eight in static compression. As for the virgin graphite, four load setting with eight specimens per load are loaded in R = -1 mode.

5.9 MULTIAXIAL RESULTS

5.9.1 Mechanical Properties From Static Tests, R = 1

Of the virgin material, seven standard test pieces are successfully tested in tension and nine in compression.

Of the pre-test isostatic exposed material, seven standard test pieces are successfully tested in tension and compression. The average (50% probability) data is summarised in Table 5-2.

Table 5-2: Summary of Static Strength of Multiaxial Specimens

Parameter	Virgin Material	Pre-test Isostatic Exposed Material	% Difference
Median Ultimate Tensile Load [MPa]	10.14	10.25	1.08
Median Maximum Principal Stress – Tension [MPa]	23.18	23.26	0.35
	(1σ = 8,4%)	(1σ = 4,4%)	
Median VW Maximum Principal Stress – Tension [MPa]	20.1	20.1	0.00
Median Volume Weighted MDE Stress (tension) [MPa]	24.9	24.7	-0.80
Median Ultimate Compressive Load [MPa]	34.82	33.99	-2.38
Median Maximum Principal Stress – Compression [MPa]	-113.51	-111.70	-1.59
	(1σ = 1,8%)	(1σ = 2,9%)	
Median VW Maximum Principal Stress – Compression [MPa]	-103.0	-101.3	-1.65
Median Volume Weighted MDE Stress (compression) [MPa]	29.3	28.8	-1.71

Two strain gauged samples (1 tension and 1 compression) form part of above tests. The strain gauged samples are prepared according to the method as explained in Section 5.7.2.

5.9.2 Tabular Presentation

All results and test conditions are given in **Appendix H**.

5.9.3 Graphical Presentation – S-N Diagrams

The S-N diagrams of the multiaxial fatigue tests are shown in Figure 5-43 to Figure 5-50. Curves of Maximum Principal stress and Maximum MDE stress (with their regression formulae) are shown in these diagrams. The material supplier's Poisson ratio of 0,21 is used in the calculation of the maximum MDE stress. The S-N curves are fitted in the same way as for the uniaxial results. Refer to Section 4.7.3 of Chapter 4 for a description of the procedure.

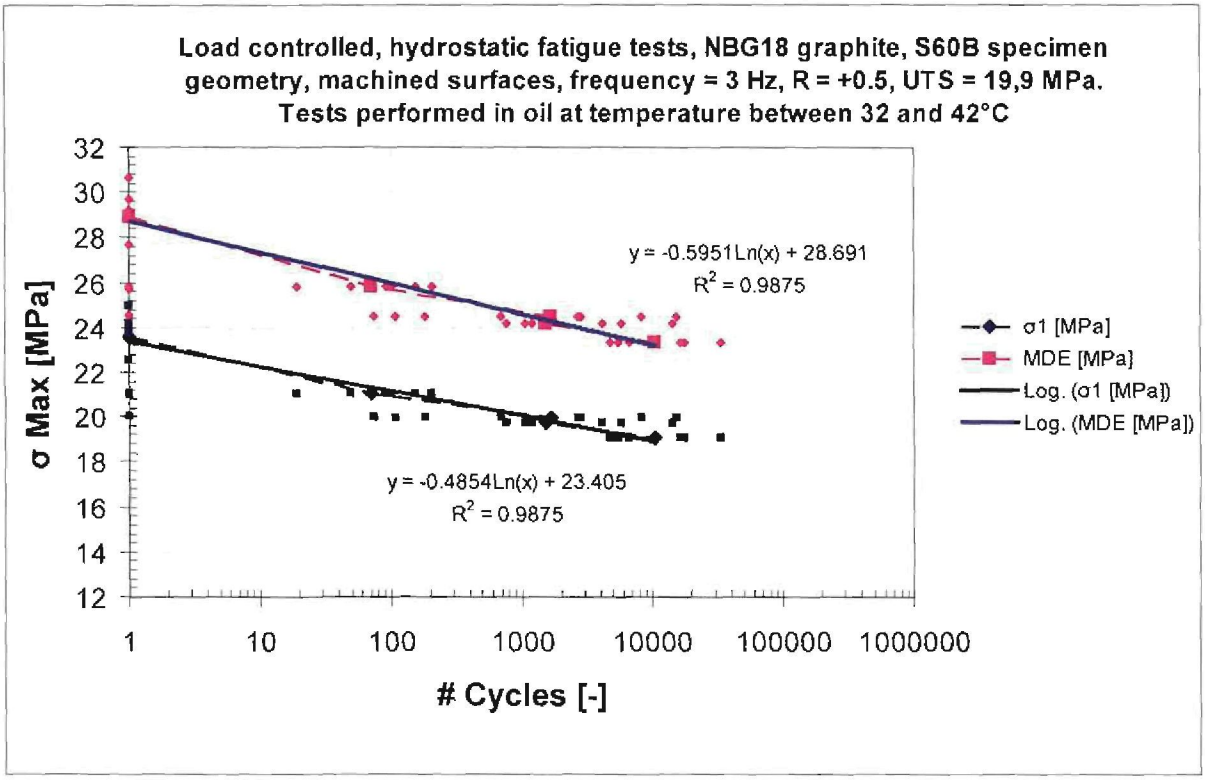


Figure 5-43: S-N Diagram for R = +0.5, Multiaxial Fatigue

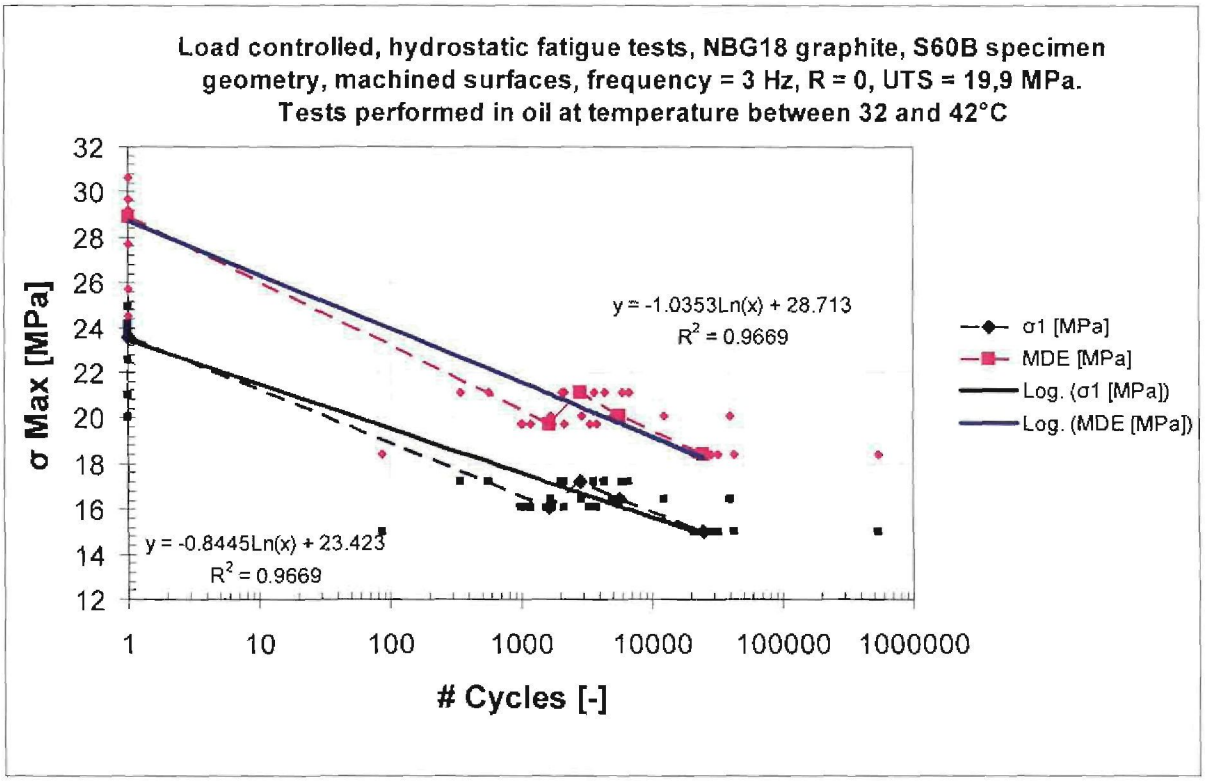


Figure 5-44: S-N Diagram for R = 0, Multiaxial Fatigue

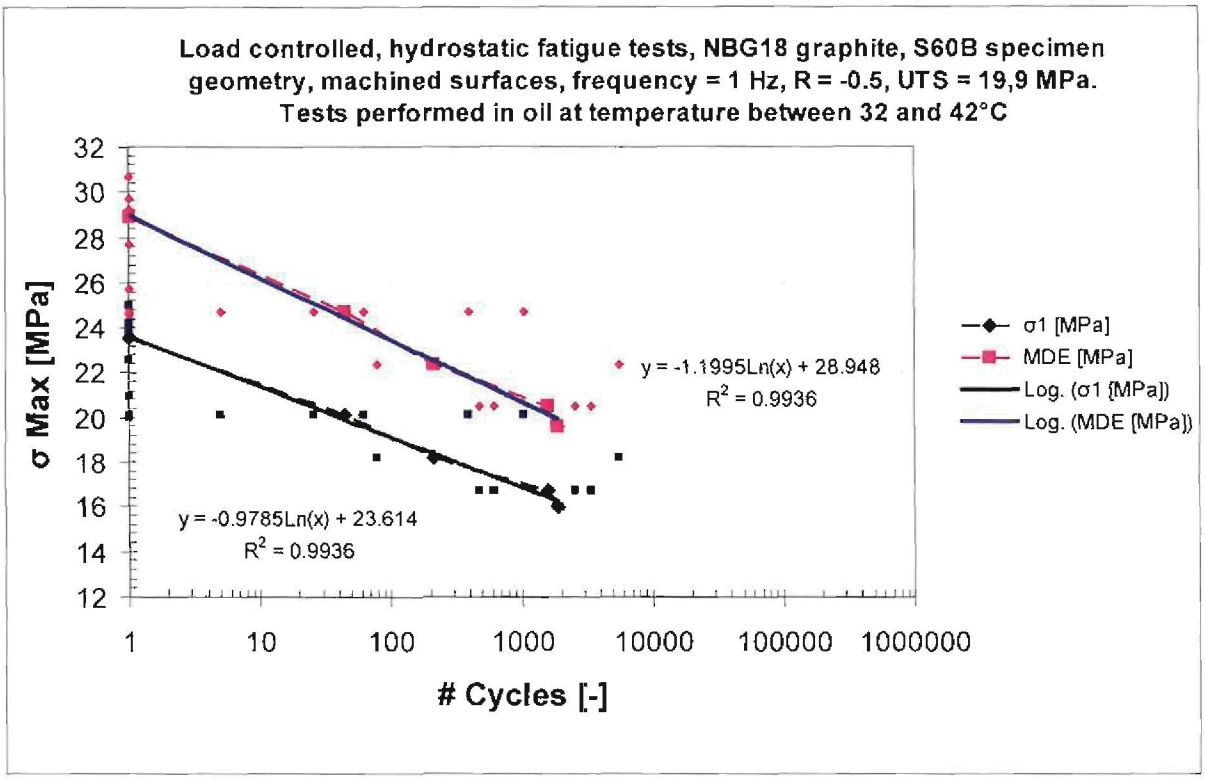


Figure 5-45: S-N Diagram for R = 0.5, Multiaxial Fatigue

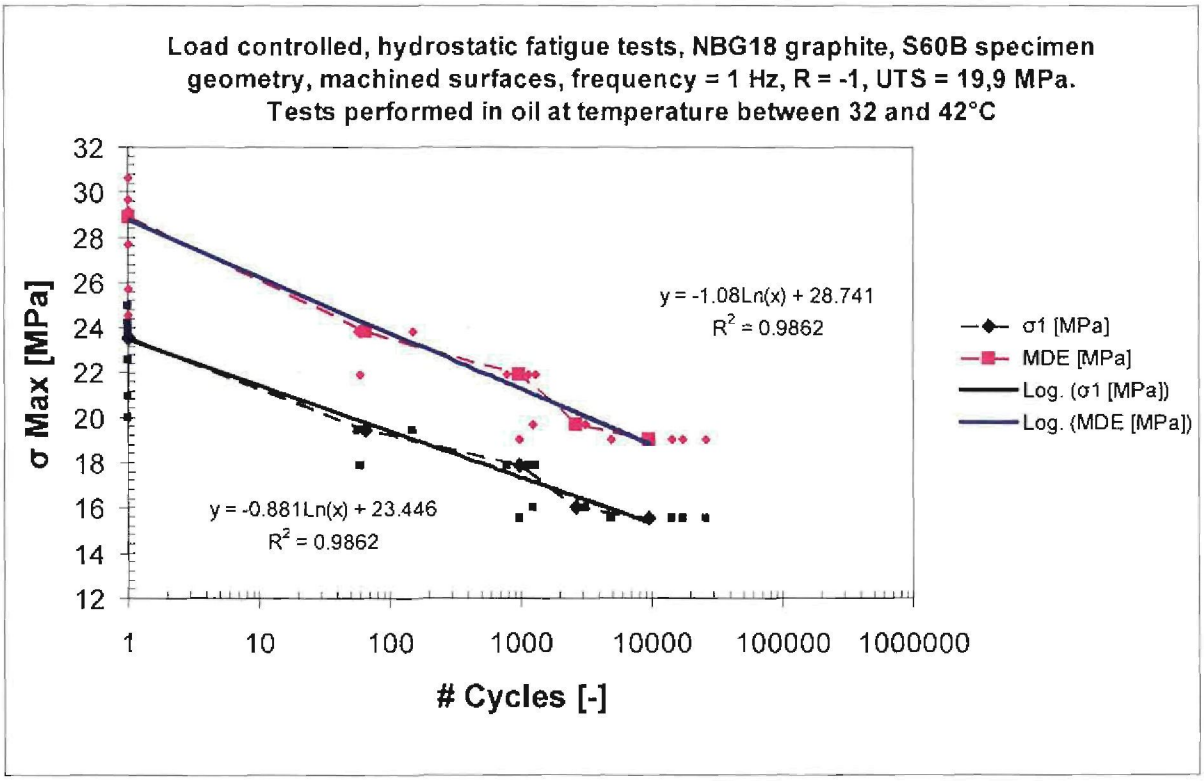


Figure 5-46: S-N Diagram for R = 1, Multiaxial Fatigue

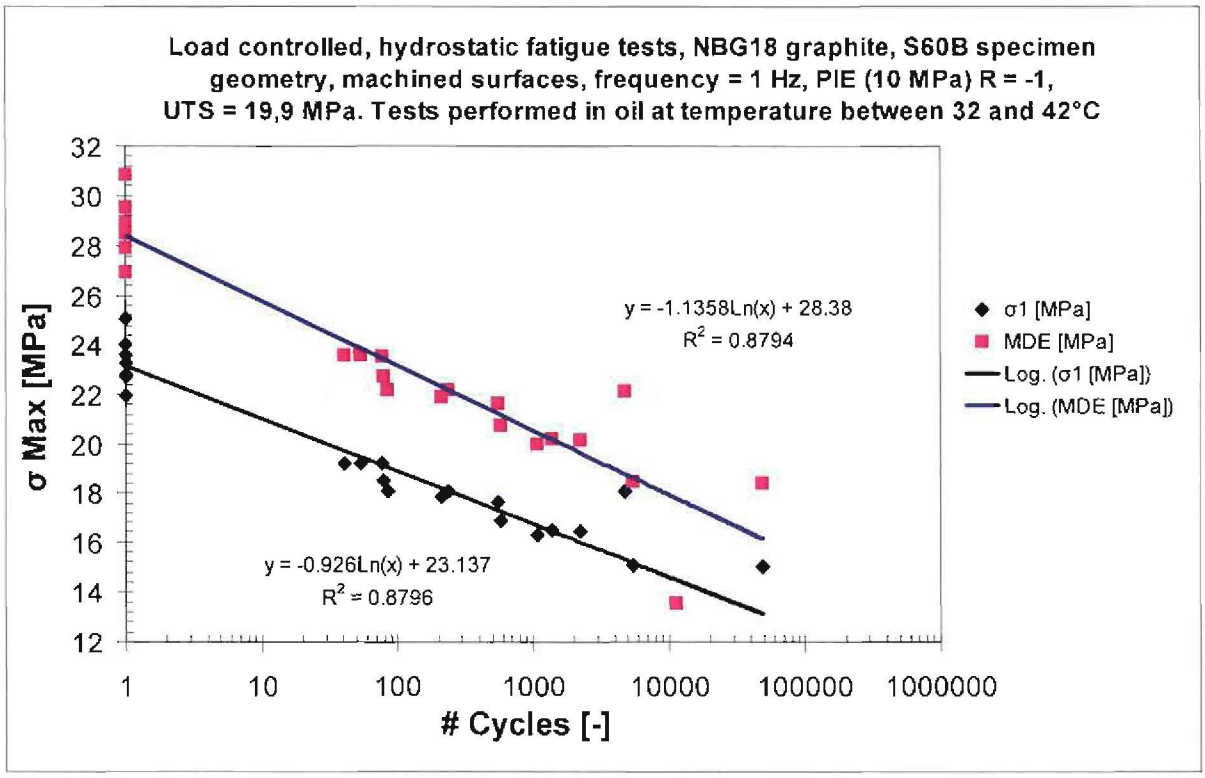


Figure 5-47: S-N Diagram for PIE R = 1, Multiaxial Fatigue

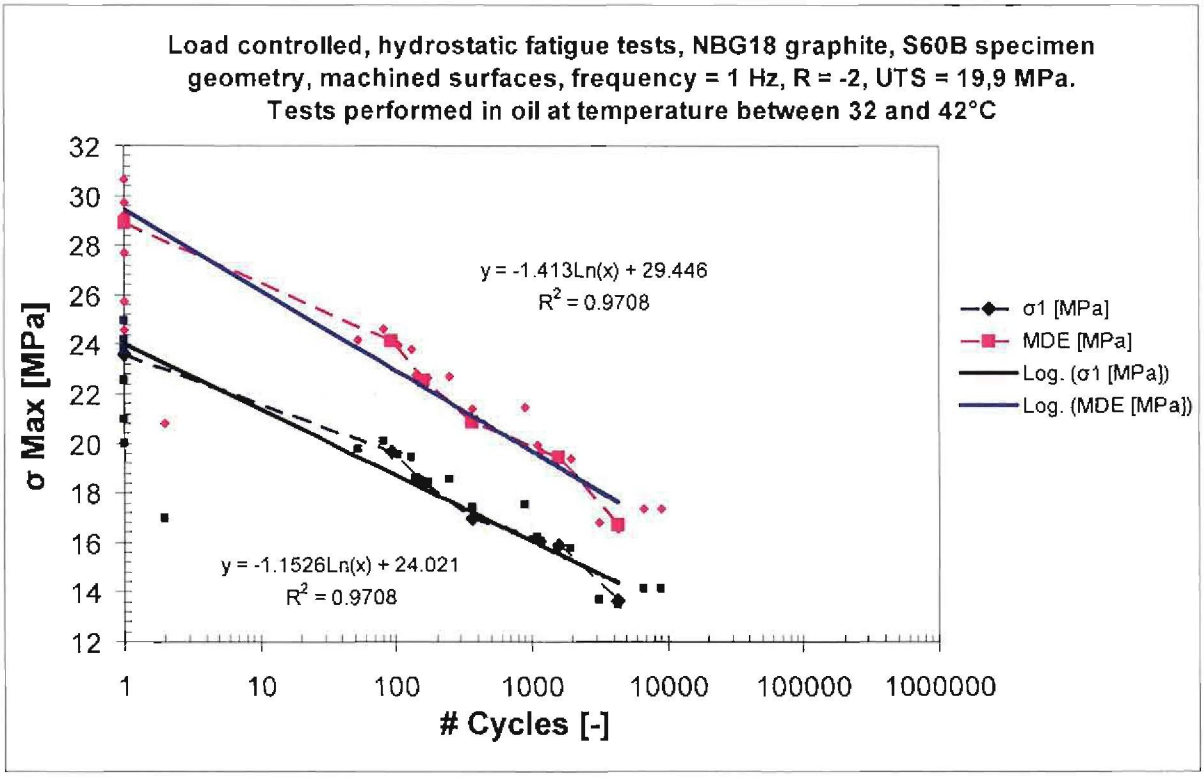


Figure 5-48: S-N Diagram for R = -2, Multiaxial Fatigue

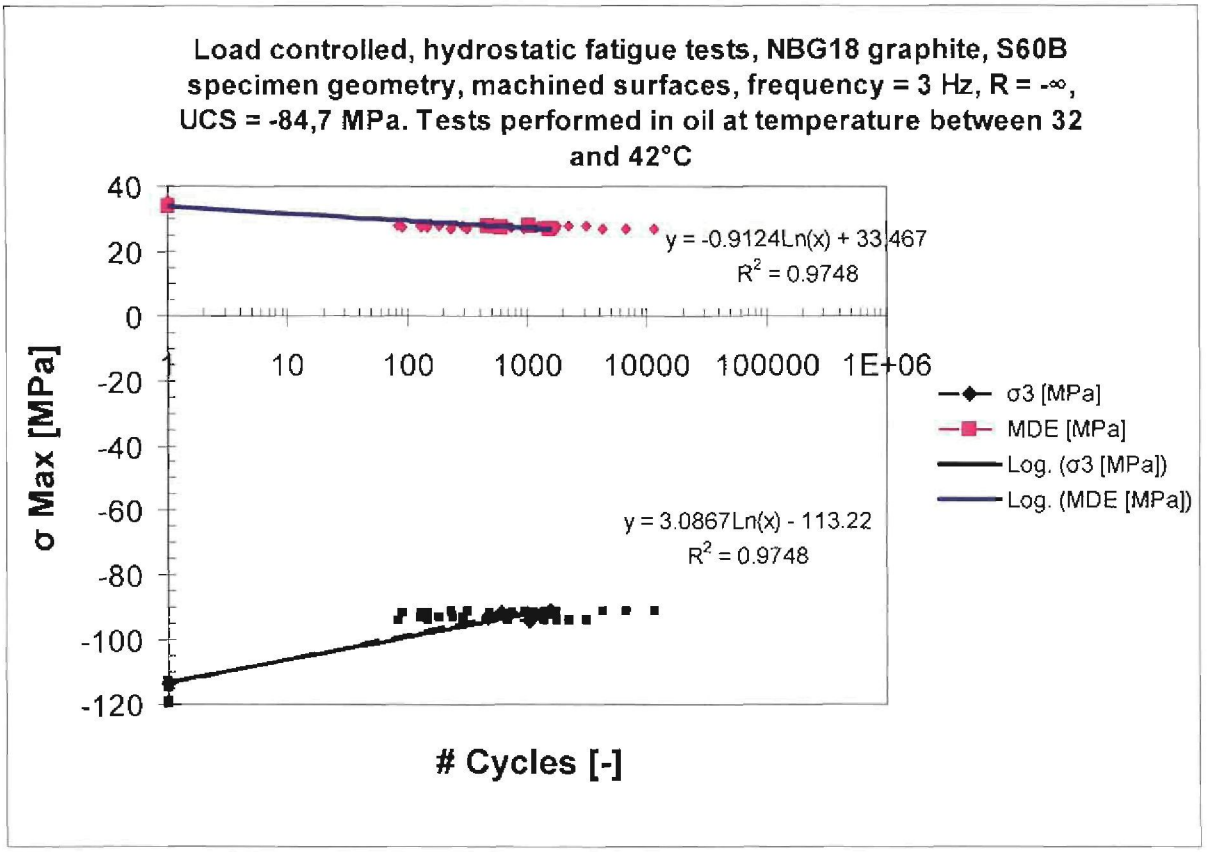


Figure 5-49: S-N Diagram for R = -∞, Multiaxial Fatigue

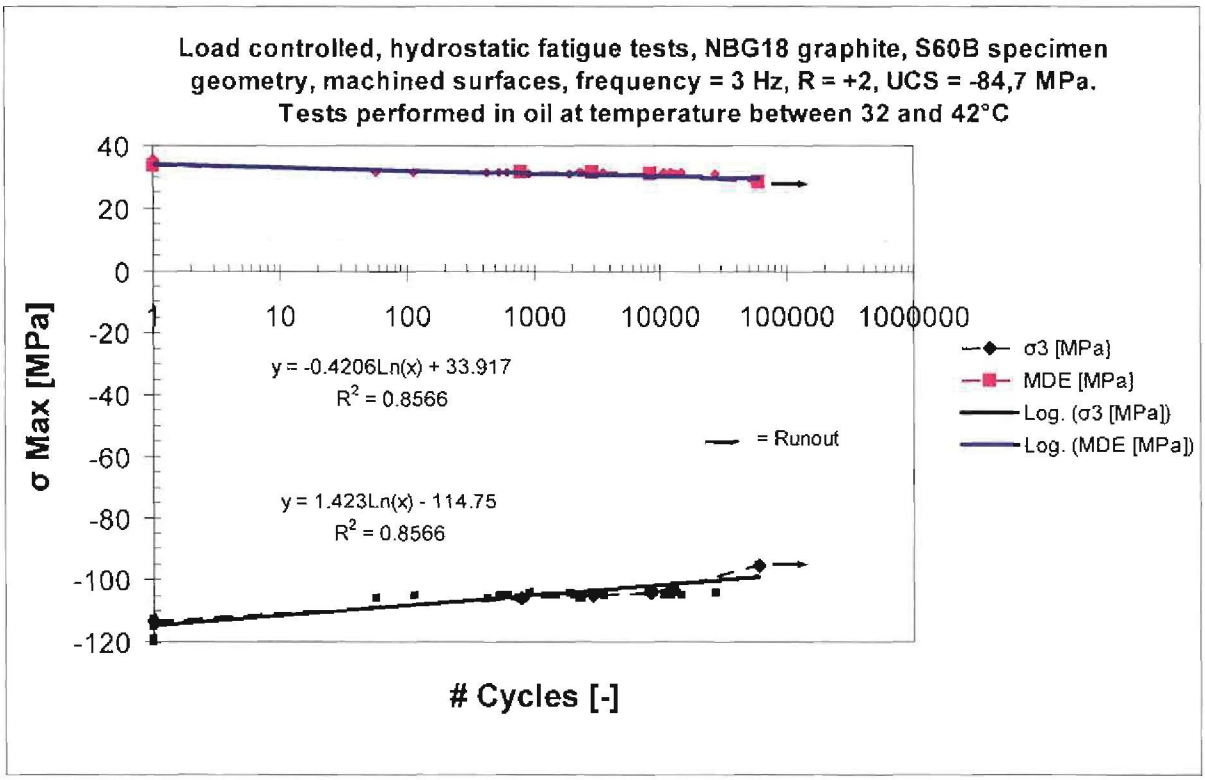


Figure 5-50: S-N Diagram for R = +2, Multiaxial Fatigue

5.9.4 Combined S-N Diagrams

The regression equations, determined from the S-N diagrams, are used to predict the allowable Maximum Principal stress as a function of life. These curves are combined in Figure 5-51 to Figure 5-53 to graphically show the effect of the load ratio on the slope of these lines.

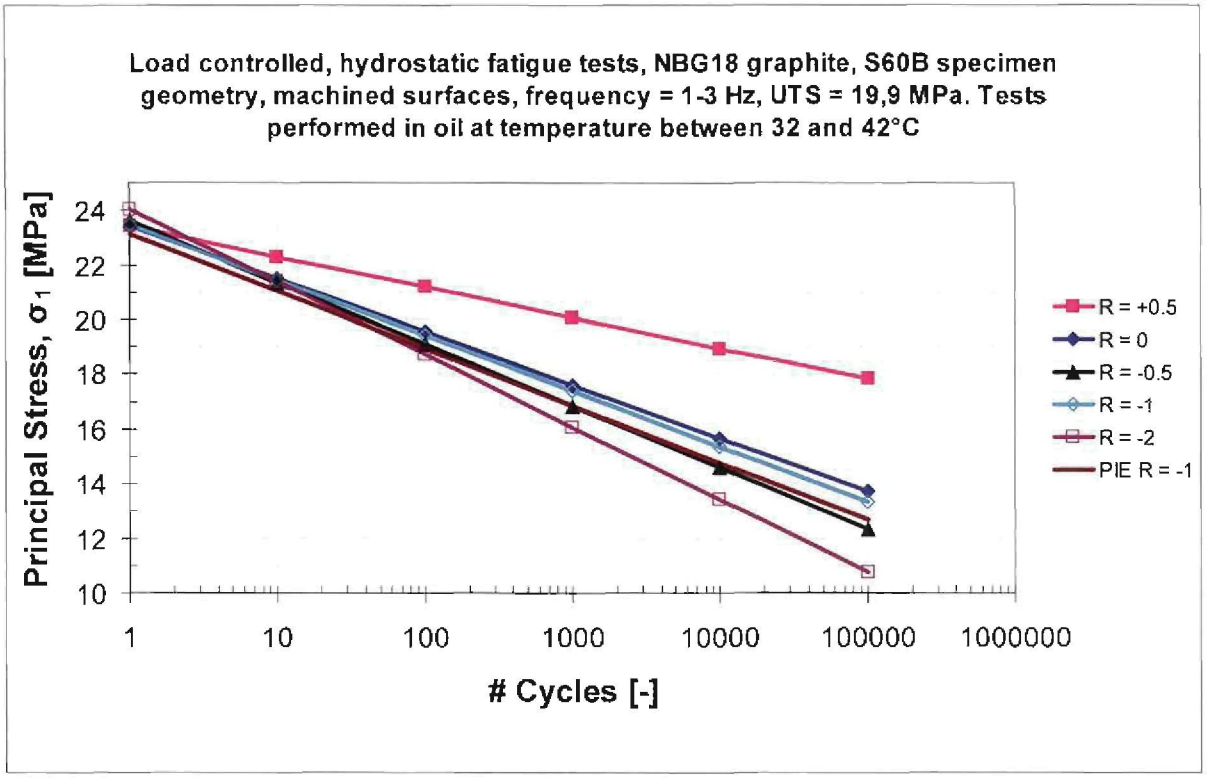


Figure 5-51: Combined S-N Diagram for Tension Dominant R-values, Multiaxial Fatigue

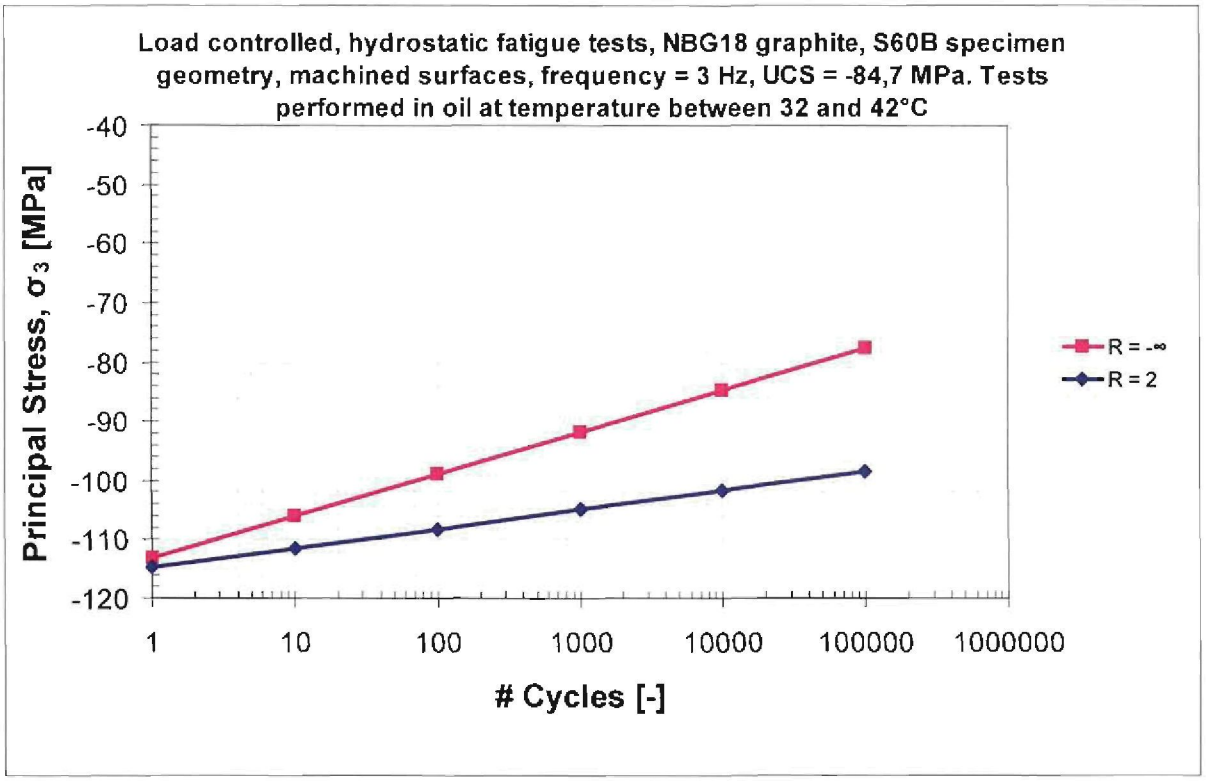


Figure 5-52: Combined S-N Diagram for Compression Dominant R-values, Multiaxial Fatigue

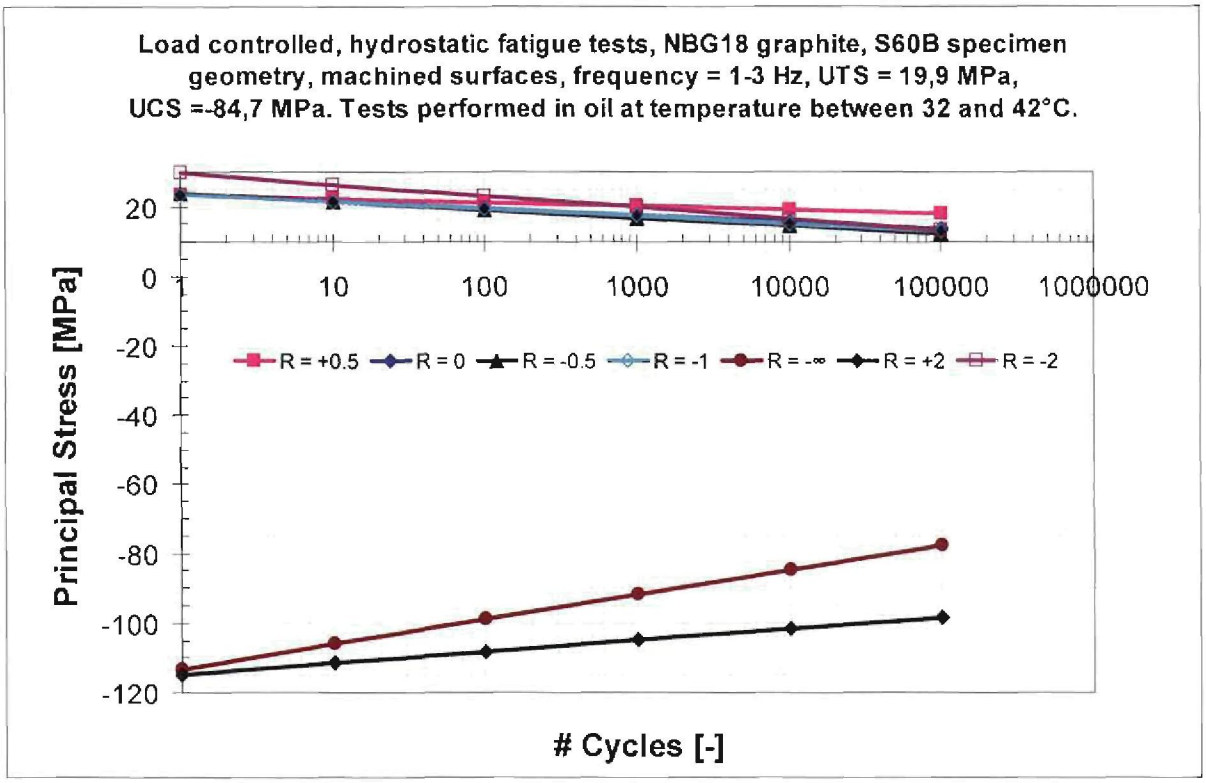


Figure 5-53: Combined S-N Diagram for All R-values, Multiaxial Fatigue

5.9.5 Constant-Life Diagrams

The constant-life chart for 50% failure probability based on Maximum Principal stress is shown in Figure 5-54, in terms of midrange stress and stress amplitude. The fatigue life is calculated using the regression equations of the S-N curves of Section 5.9.3.

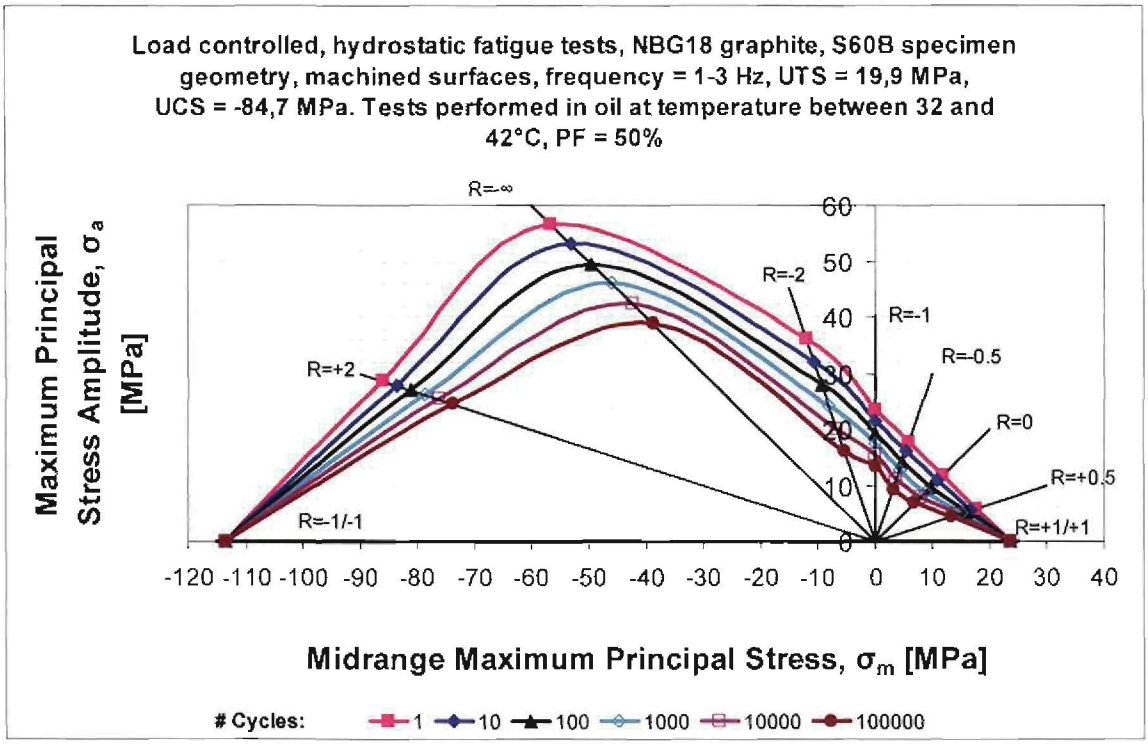


Figure 5-54: Constant-Life Chart for Maximum Principal Stress

Since the Maximum Principal stress varies slightly through the wall thickness of the gauge section, the Volume Weighted (VW) Maximum Principal stress is calculated as one possible measure of the effective stress condition in the gauge section. The constant-life chart using the VW Principal stress is shown in Figure 5-55.

Another possible measure of the effective stress condition in the gauge section is the maximum MDE stress. The constant-life chart using the maximum MDE stress is shown in Figure 5-56. As for the case of the Maximum Principal stress, only the inner skin of the gauge section is subject to the maximum MDE stress, with the remaining volume subjected to lower stress levels due to the stress variation through the wall thickness. Therefore, another possible measure of the effective stress condition in the gauge section is the Volume Weighted MDE stress. The constant-life chart using the VW MDE stress is shown in Figure 5-57.

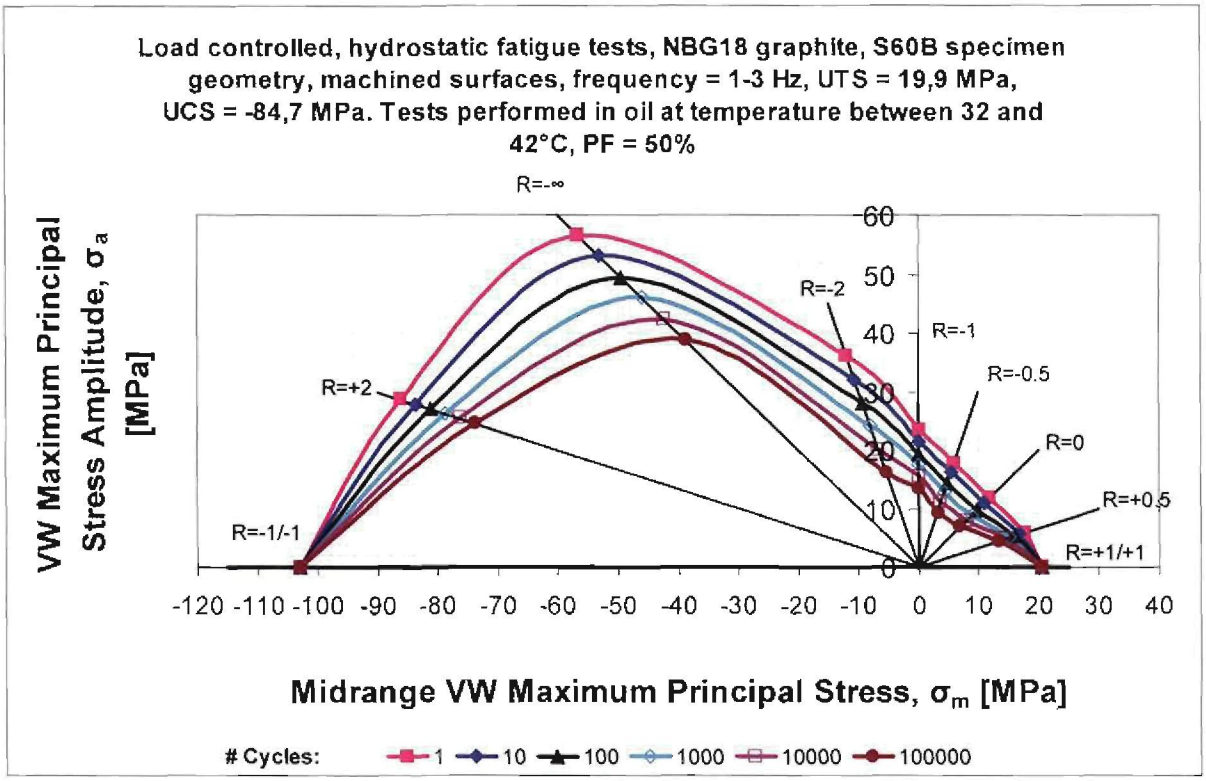


Figure 5-55: Constant-Life Chart for Volume Weighted Maximum Principal Stress

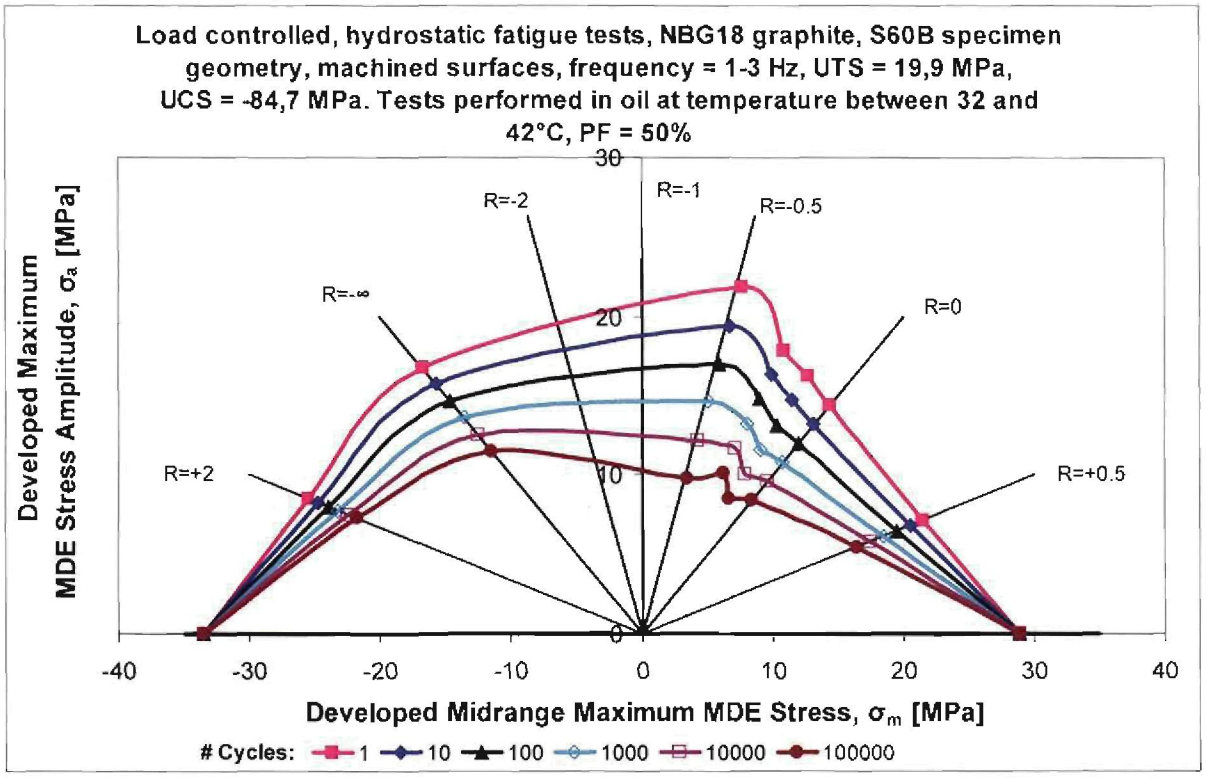


Figure 5-56: Constant-Life Chart for Maximum MDE Stress

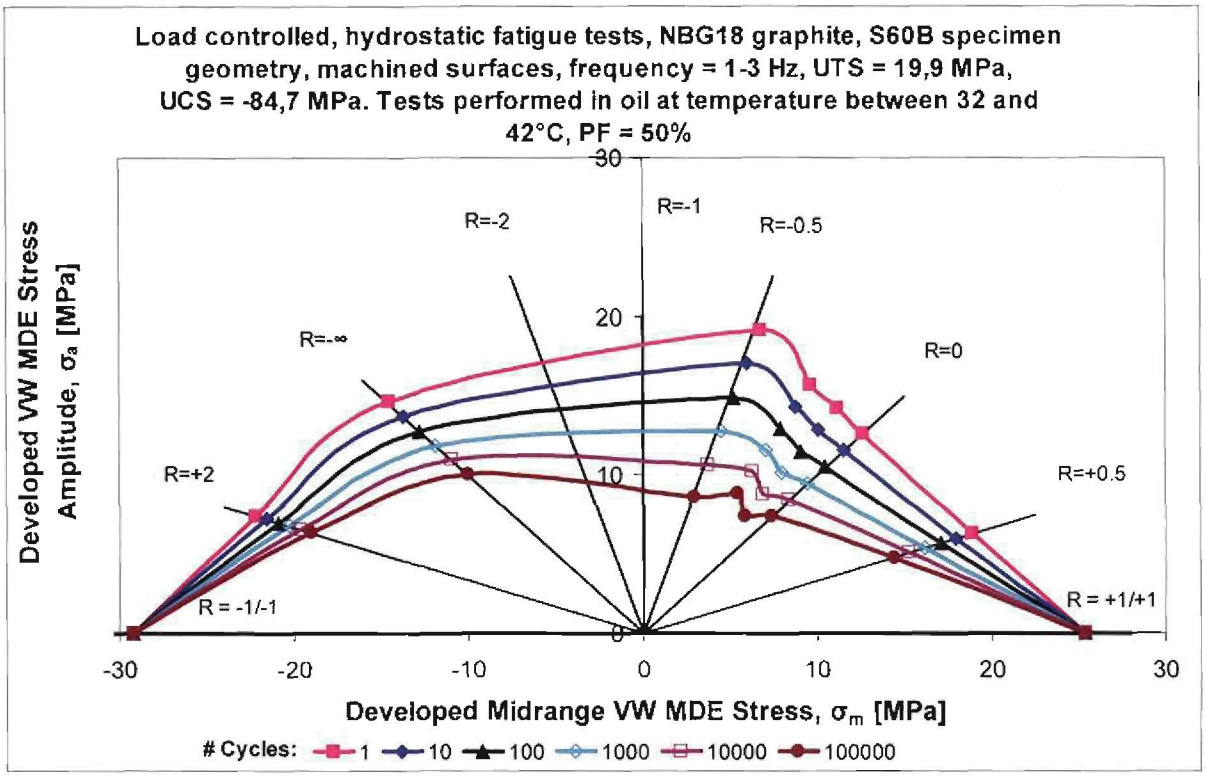


Figure 5-57: Constant-Life Chart for Volume Weighted MDE Stress

5.9.6 Verification of Equality of Tangential Strains

The assumption that the two tangential strains (latitudinal and longitudinal strain) are equal on the gauge section of the S60B specimen is verified by measuring the strains of these gauges independently using two quarter bridge configurations. The two channels are first calibrated using a precision shunt resistor as before. The two channels are calibrated to within 0,1% error relative to one another.

The result of this verification is shown in Figure 5-58 for two strain excursions up to approximately 800 microstrain. The coordinates of the maxima are shown on the graph. The maximum latitudinal strain is 2.7% and 2.4% more than the maximum longitudinal strain for cycle 6 and 7 respectively.

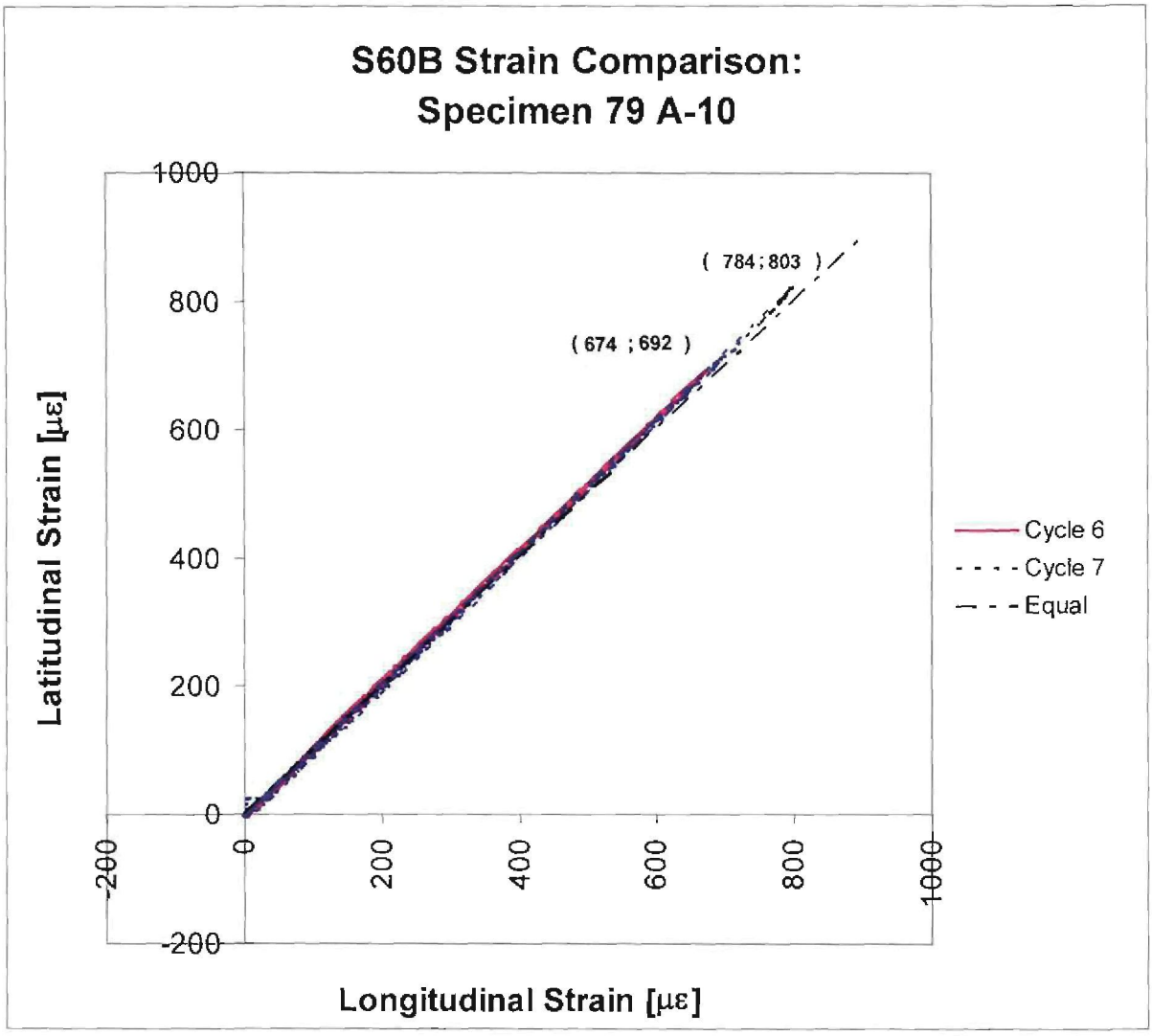


Figure 5-58: Verification of Equality of Tangential Strains

5.9.7 Stress versus Strain (Hysteresis Loops)

Graphical representations of the data for stress-strain cycles at different life cycles and for the various loading conditions are shown in Figure 5-59 to Figure 5-67.

The discontinuity in these traces around zero stress for load ratios that reverse direction (R = -0,5, R = -1) can be ascribed to bandwidth restrictions of the Analogue-to-Digital Card (ADC) and/or the Vishay strain gauge amplifier. The pressure drops abruptly as the valve direction is switched before the pressure reaches a value of zero, as is illustrated in Figure 5-73, Section 5.10.4.

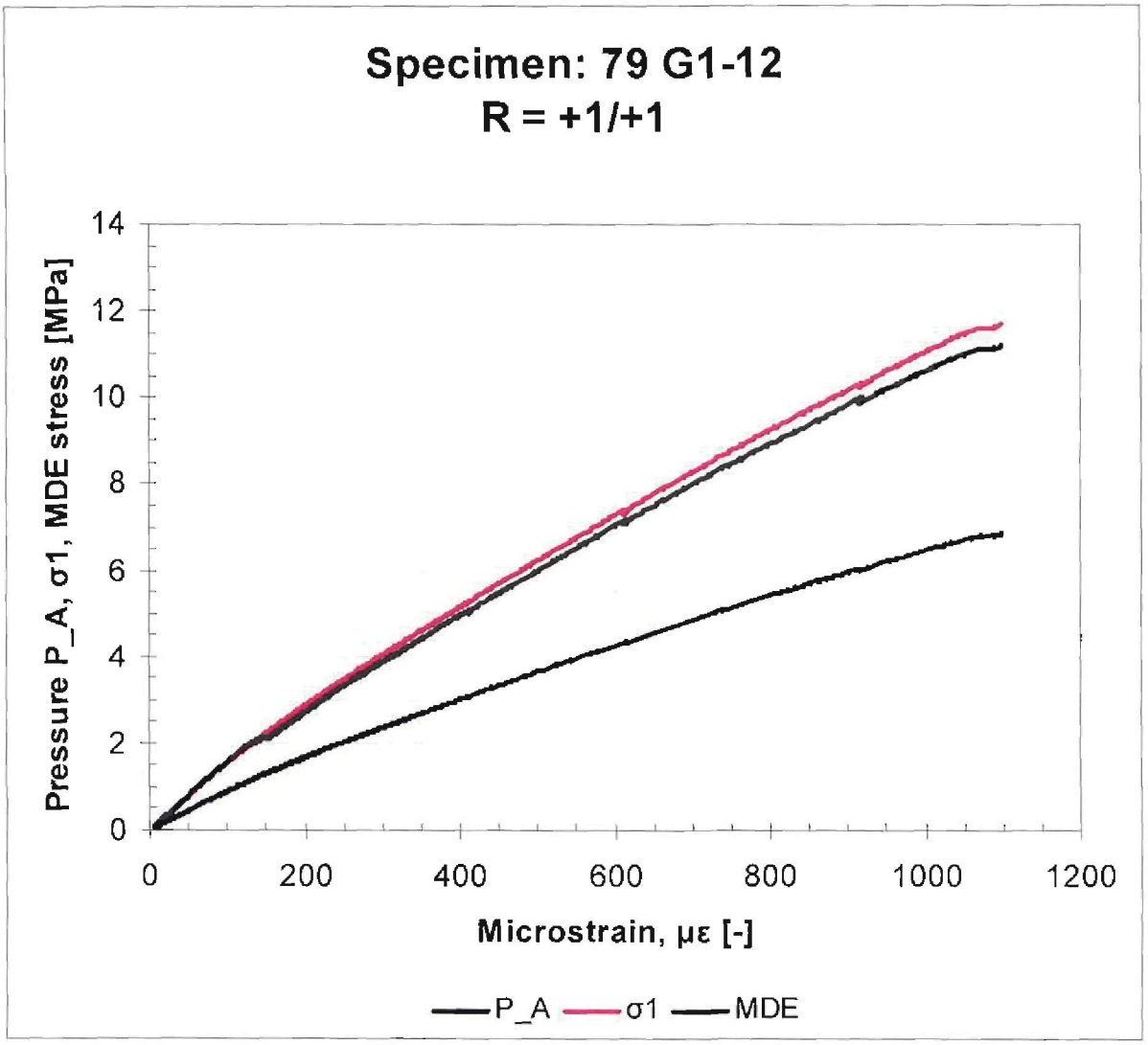


Figure 5-59: Stress Versus Strain for R = +1/+1 (Tensile Test)

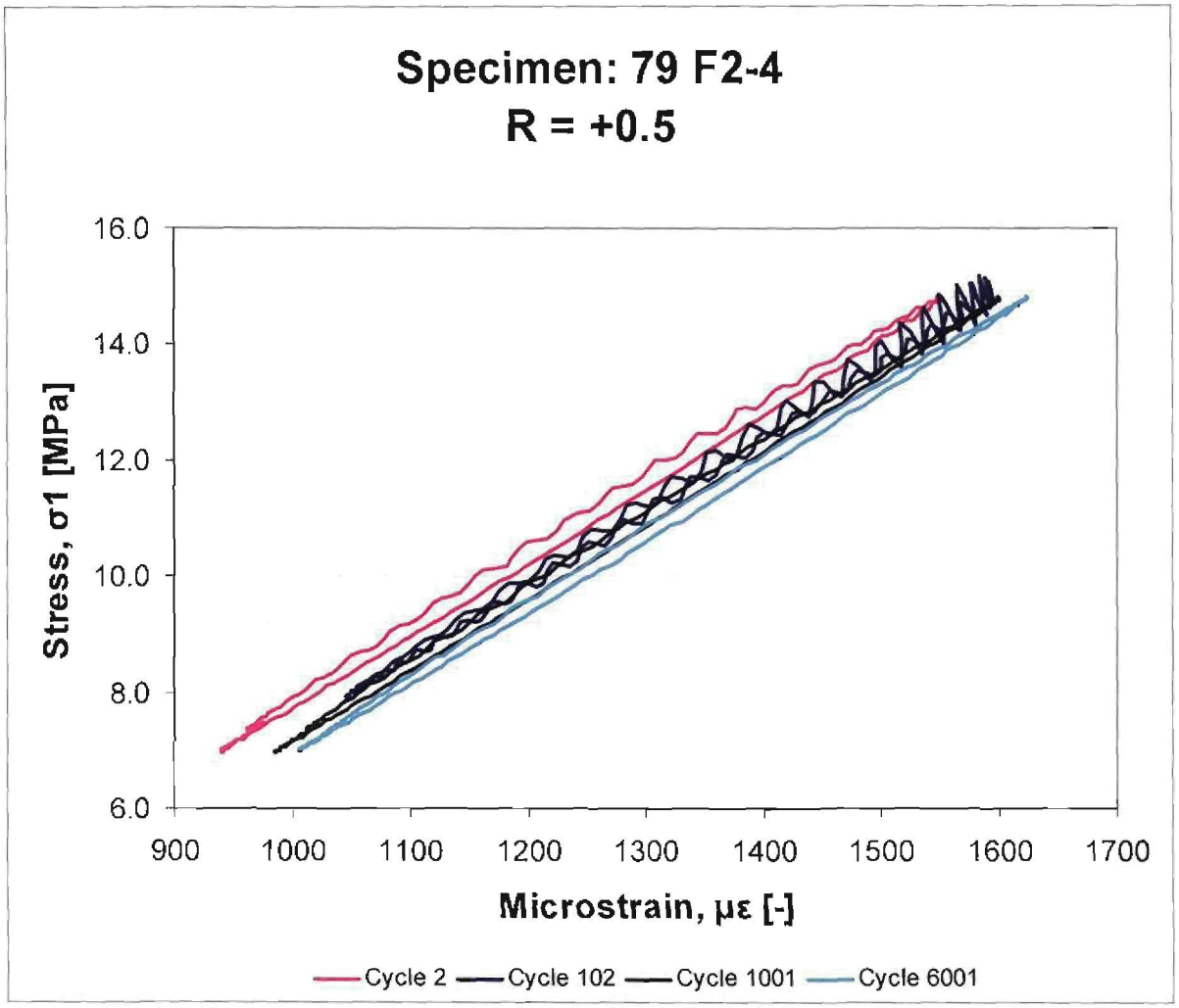


Figure 5-60: Stress Versus Strain (Hysteresis Loop) as Function of Life for R = +0.5

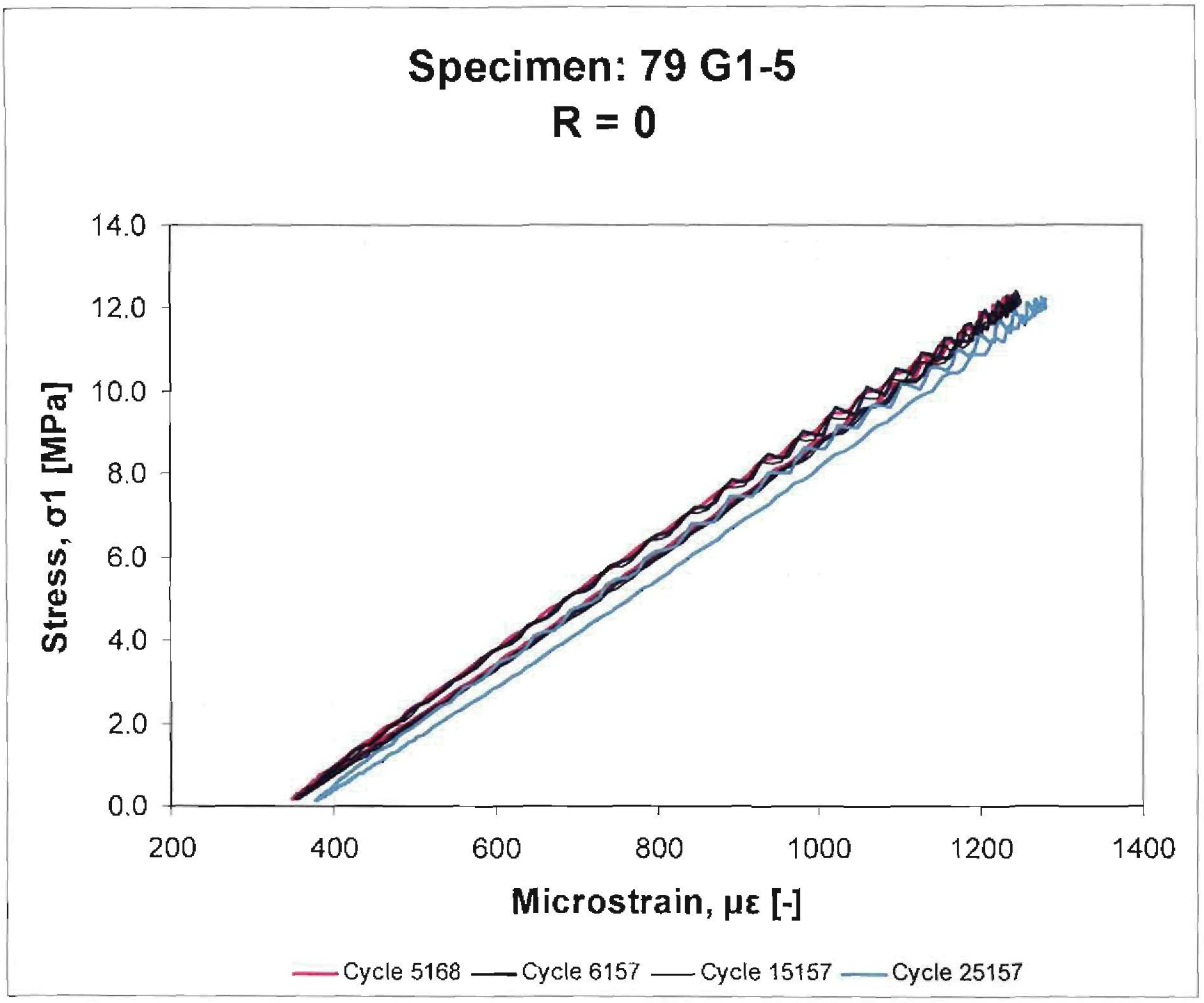


Figure 5-61: Stress Versus Strain (Hysteresis Loop) as Function of Life for R = 0

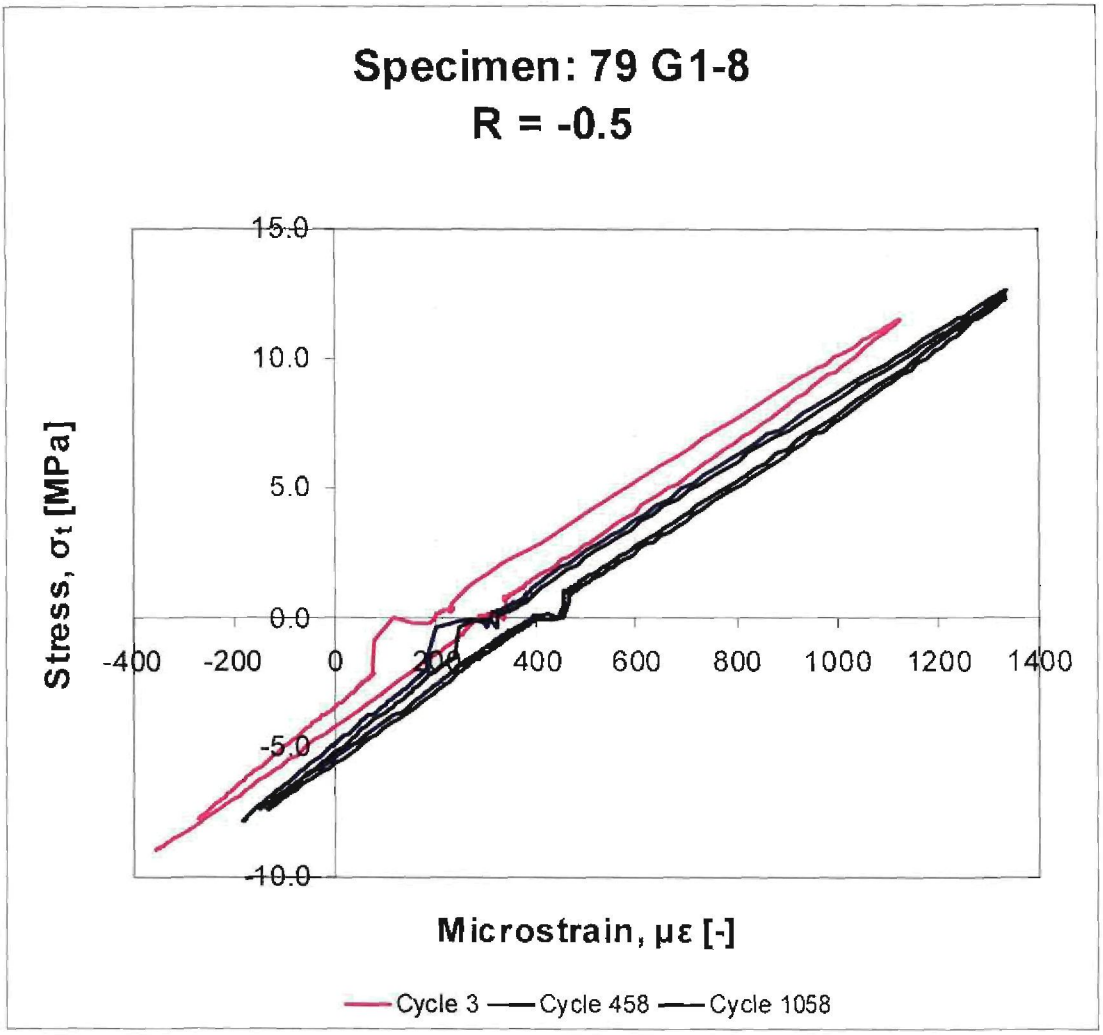


Figure 5-62: Stress Versus Strain (Hysteresis Loop) as Function of Life for R = -0.5

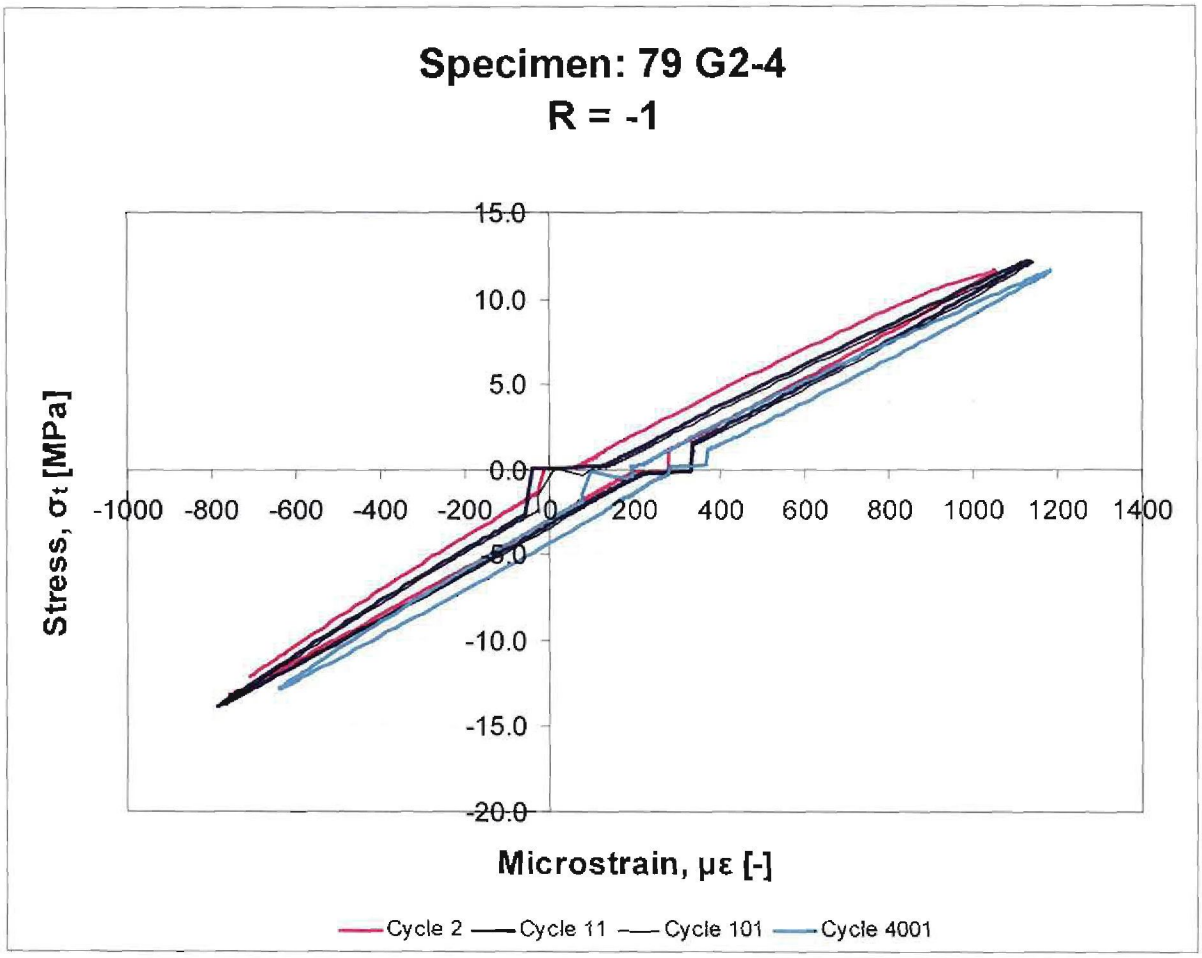


Figure 5-63: Stress Versus Strain (Hysteresis Loop) as Function of Life for R = -1

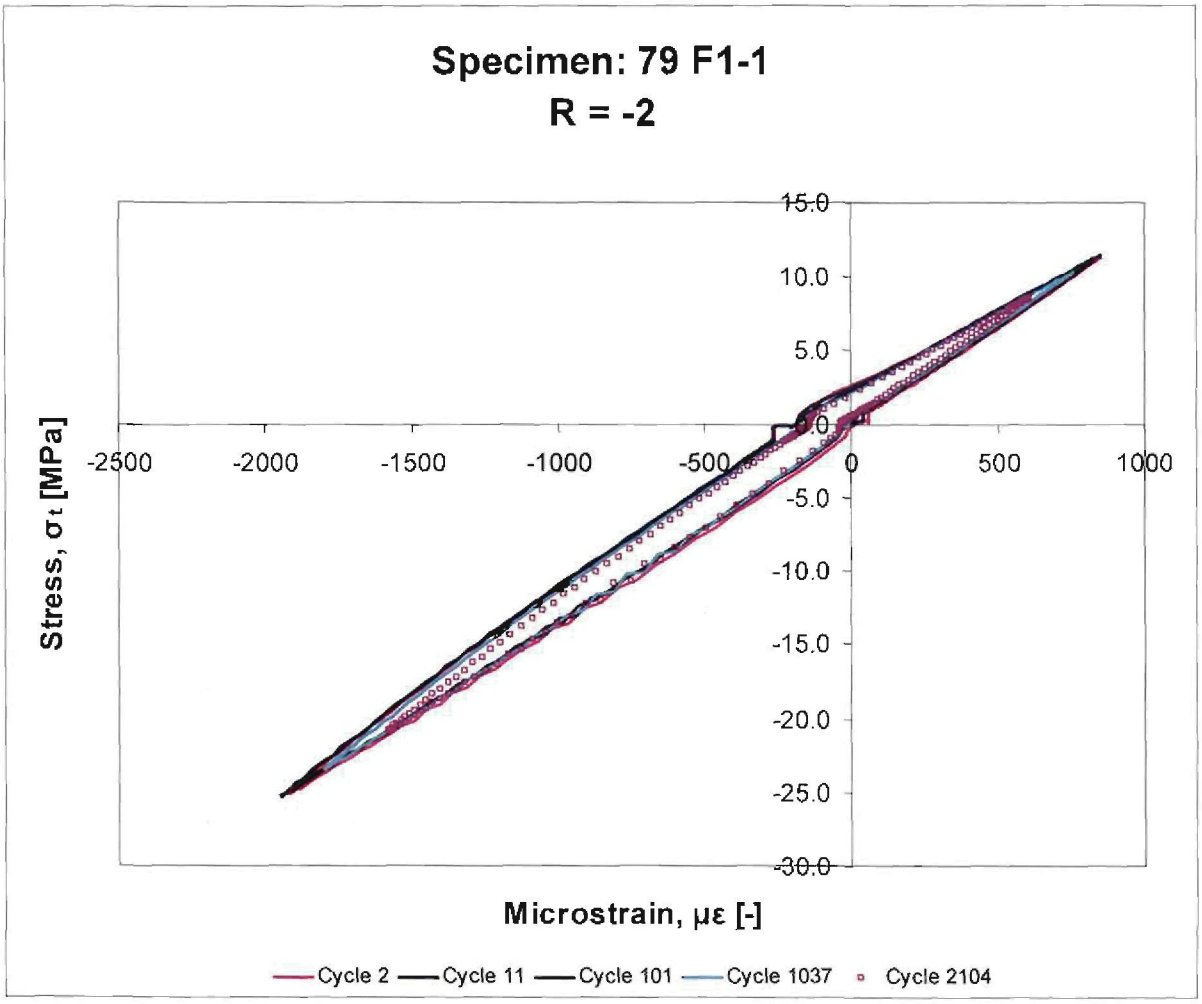


Figure 5-64: Stress Versus Strain (Hysteresis Loop) as Function of Life for R = -2

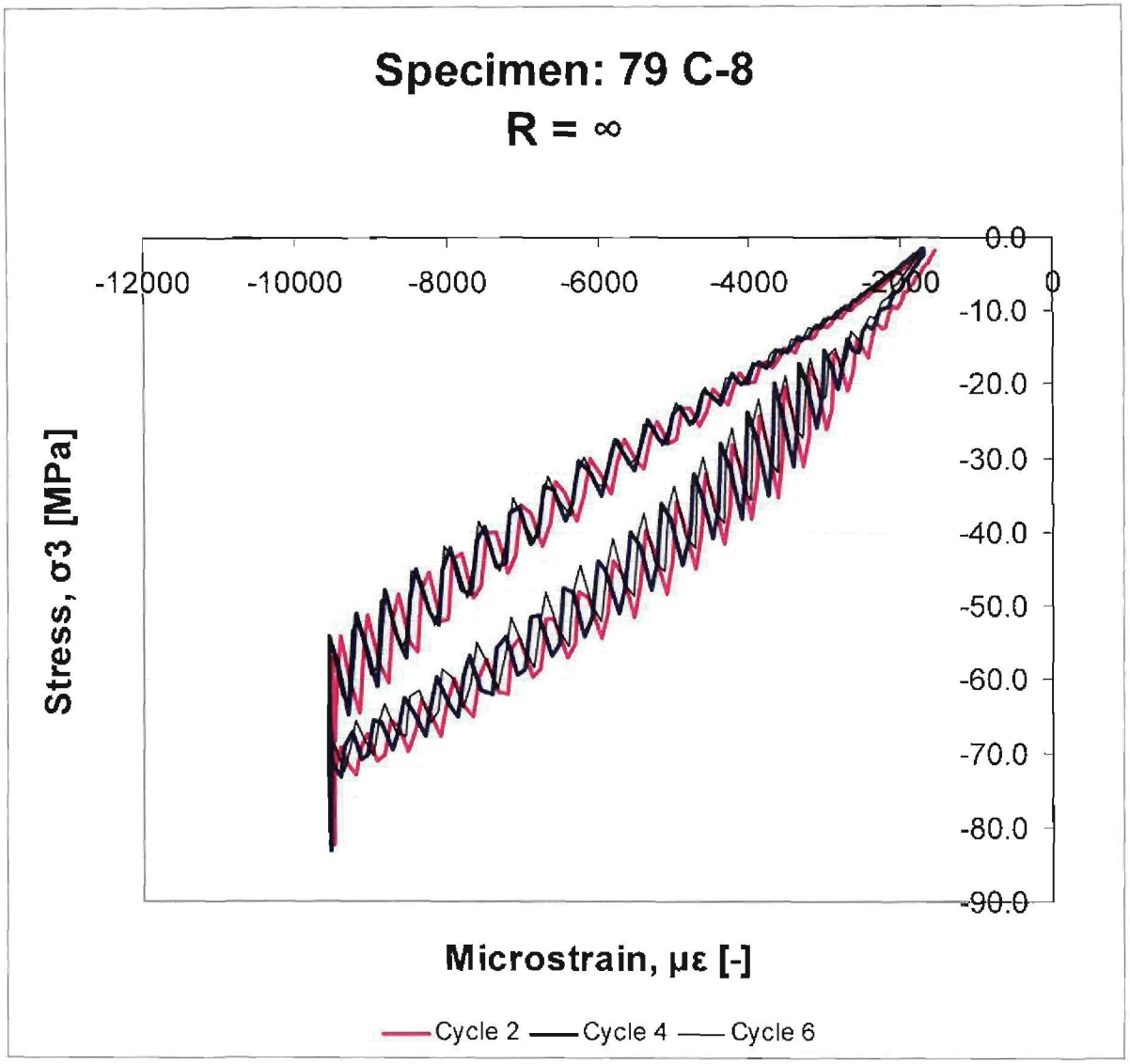


Figure 5-65: Stress Versus Strain (Hysteresis Loop) as Function of Life for R = -∞

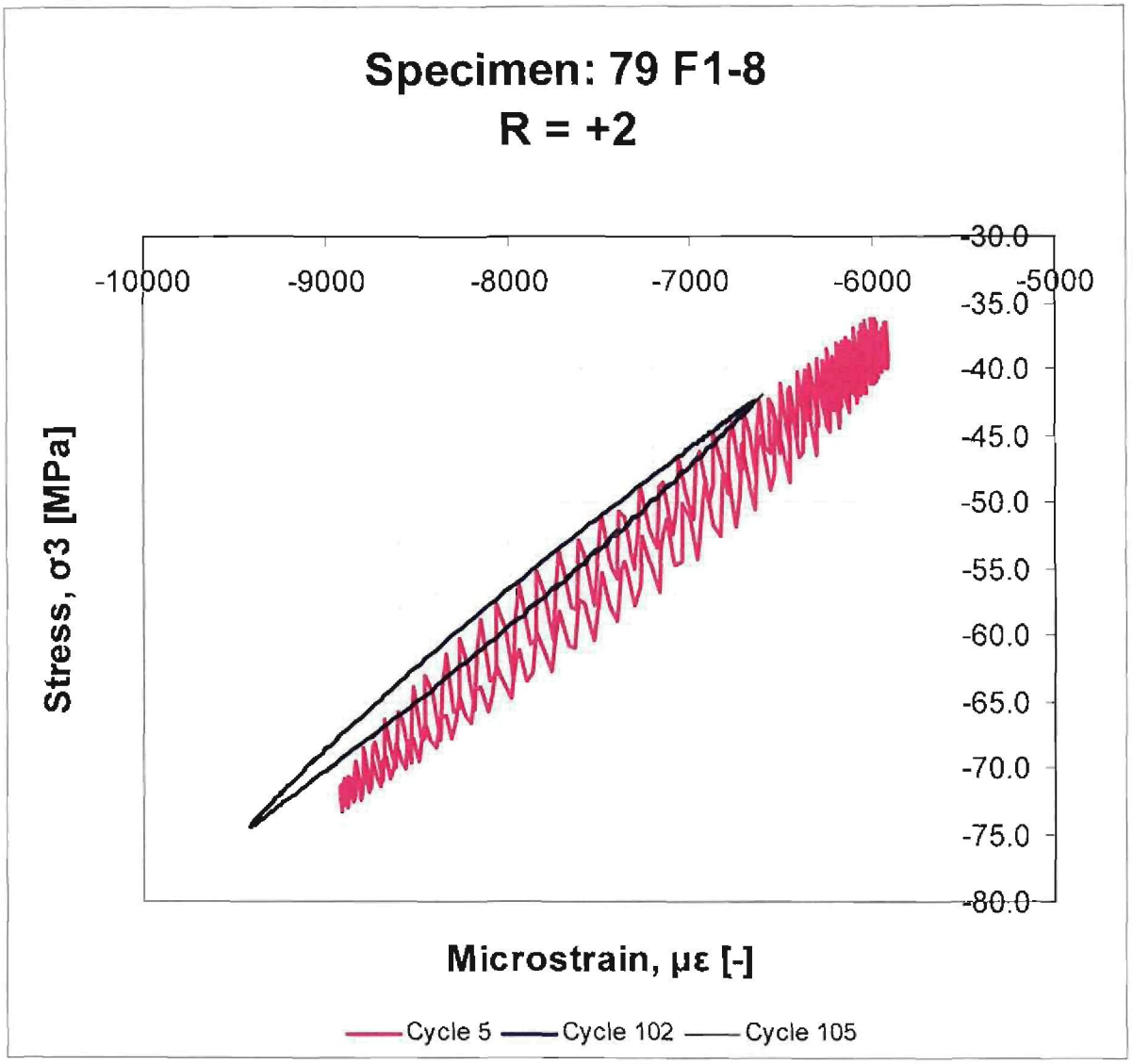


Figure 5-66: Stress Versus Strain (Hysteresis Loop) as Function of Life for R = +2

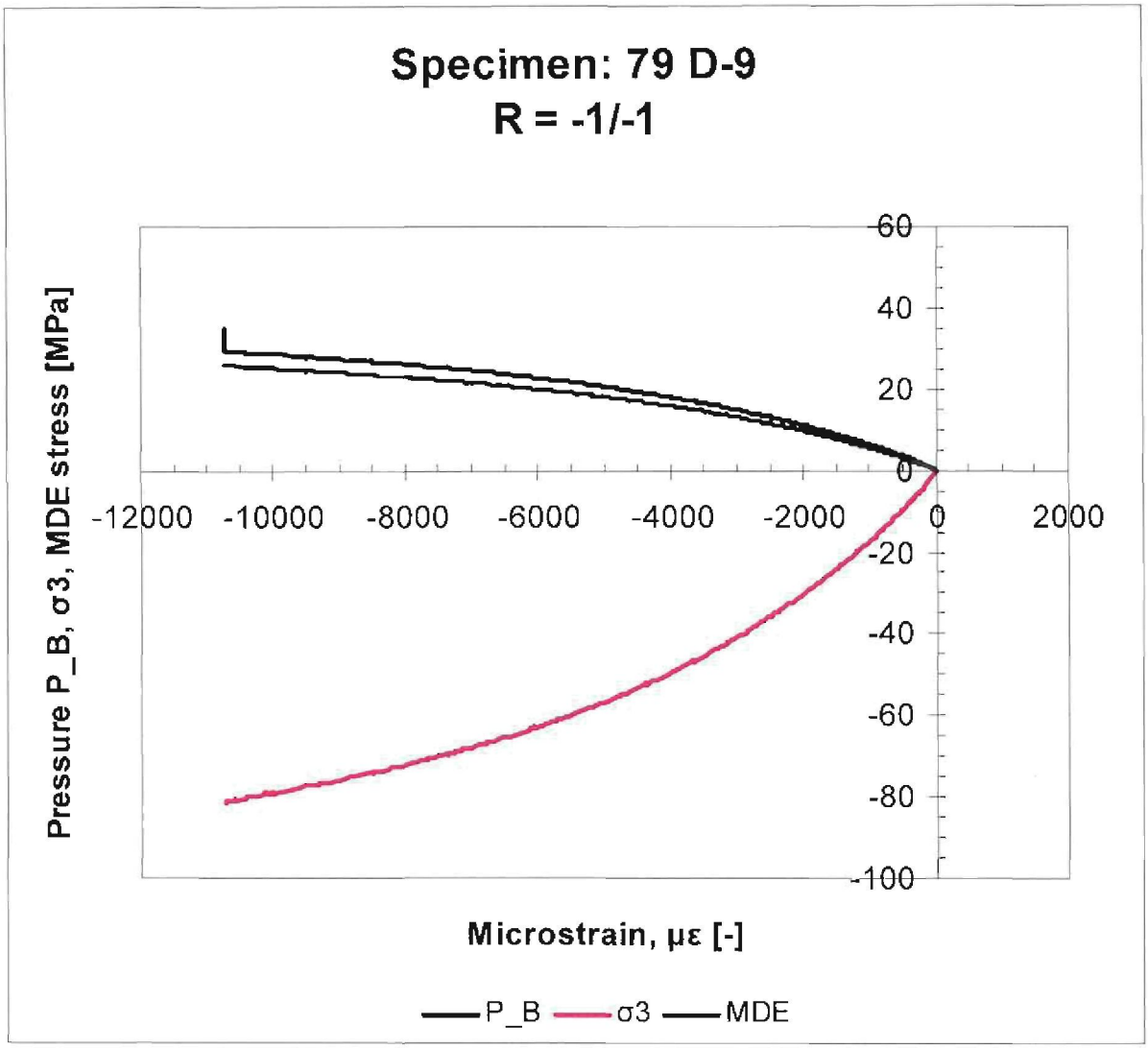


Figure 5-67: Stress Versus Strain for R = -1/-1 (Compression Test)

5.9.8 Fracture Position

The position of the fractures for the multiaxial samples is shown in **Appendix I**. Tensile fractures exhibit one of 4 fracture types: An O-type, H-type, D-type and E-type fracture, as shown in Figure 5-68, Figure 5-69, Figure 5-70 and Figure 5-71 respectively. Compressive fractures are all similar, O-type fractures. A typical compressive fracture is shown in Figure 5-72.

Some specimens fail due to excessive leakage through the epoxy layer. Such failures are identified as L-type failures in the tabulated results.



Figure 5-68: Typical O-Type Fracture of 37 A2-10



Figure 5-69: Typical H-Type Fracture of 79 I-1



Figure 5-70: Typical D-Type Fracture of 79 K-1



Figure 5-71: Typical E-Type Fracture of 79 I-9



Figure 5-72: Typical O-Type Fracture in Compression of 37 C-10

5.10 DISCUSSION

5.10.1 Multiaxial Fatigue Test Design

The S60B specimen design proved to be cheap from a manufacturing and test facility point of view. However, the individual sealing of each specimen offsets its low machining cost. Data processing for absolute comparison was quite cumbersome, although there are no comparable graphite specimens with uniform stresses in their gauge sections, so data processing was on par with comparable specimens.

Although the finite element analysis predicts an additional stress variation of 12,5% in the gauge section due to non-ideal deformation in the transition section to the flange of the specimen, the measured fatigue properties compares well with those of the uniaxial test specimens. This highly localised stress variation seems to have no significant influence on the test results.

The bonding of the graphite to the steel base plate is a problem especially in tests with a direction changing Maximum Principal stress (change of sign). Tests with a more flexible adhesive (SikaFast 5215) of lower strength, do not fail in the same mode as the high strength epoxy (complete separation of the specimen from the base plate). However, the failure mode of the more flexible adhesive is leakage through the adhesive layer, which renders the specimen unserviceable.

The S60B is adequate to determine the multiaxial fatigue properties of medium to fine grain graphite (average grain size less than 0,9 mm). In order to reduce the bond failures in the specimens, the flange surface area should be increased to reduce the nominal stress level in the adhesive.

5.10.2 Absolute Values of Static Strength

The measured static strength values are only compared with the overall strength of the NBG18 material, calculated from measurements of all acceptable blocks. The median Maximum Principal stress value of 23,2 MPa over-estimates the S_{ut} = 20,8 MPa of the material by +11,5%.

The Volume Weighted Maximum Principal stress, with a weighing factor of 0,8655 for tension, predicts the static tensile strength well, with an error of only -3,4%.

The Volume Weighted MDE stress, with a weighing factor of 0,877 (calculated using the results of the uniaxial tests), over-estimates the static tensile strength, with an error of 19,7%. This is unacceptable.

The median Maximum Principal stress value of 113,5 MPa over-estimates the S_{uc} = 78,7 MPa of the material by +44,2%, which is totally unacceptable. This extremely high compressive strength, exhibited by the S60B specimen, cannot be explained by any of the generally accepted failure hypotheses.

Even the Volume Weighted Maximum Principal stress, with a weighing factor of 0,90706, predicts the static compressive strength poorly, with an error of +30,9%.

The Volume Weighted MDE stress, with a weighing factor of 0,872 (calculated using the results of the uniaxial tests), over-estimates the static compressive strength with an error of +40,9%, which is also unacceptable.

Refer to Figure 5-6 and Figure 5-7, Section 5.2.3.3. These figures show the ideal stress distribution through the wall section at the static fracture point (static design condition). The hydraulic pressures were recalculated for nominal geometry (reference condition) to yield the same MDE stress as determined by the tests. The Volume Weighted MDE stress (VMDE in graph) as well as the probability of survival according to the KTA 3232 design rule (Lc MDE in graph) are shown on these graphs. For the reference tensile strength condition, the Volume Weighted MDE stress of 24,9 MPa exceeds the MDE failure criterion of 19,91 MPa by 25% for these specific blocks of graphite (UTS from uniaxial tests). The KTA probability of survival of 0,6% (50% confidence level) confirms this. Similarly, for the reference compressive condition, the Volume Weighted MDE stress of 29,3 MPa exceeds the MDE failure criterion of 19,91 MPa by 47%. The KTA probability of survival of $7,1 \times 10^{-10}$ % (50% confidence level) confirms this.

From an investigation of the mode of failure, it is evident that much more energy is required to fracture the S60B specimen in compression. The debris from a compressive failure consists of graphite crumbs, as mentioned before, while for a tensile failure, only a single circumferential crack or at most (as for the case of a H-type fracture), a few cracks are grown. Physically, it is easy to imagine that if the graphite is subject to equal sub-critical biaxial compressive stresses, it will reinforce the material, preventing slip along planes of maximum shear stress in its microstructure due to some internal material friction effect. This

intuitive explanation is supported by the Coulomb-Navier hypothesis that is referenced by Taylor *et al.* (1967). In the context of this discussion, sub-critical means: "below the uniaxial compressive strength of the material". In such a state, failure due to a third principal compressive stress is inhibited as compared with the same compressive stress acting on stress-free material.

Regarding the pre-isostatic load exposed specimens, the static compression (R = -1/-1) and tensile (R = +1/+1) tests are performed successfully. The static compressive strength of PIE specimens is 1,65% and 1,71% lower than that of unexposed material, based on Volume Weighted Maximum Principal and Volume Weighted MDE stress respectively.

Similarly, the static tensile strength of PIE specimens is 0,0% and 0,8% lower than that of unexposed material, based on Volume Weighted Maximum Principal and Volume Weighted MDE stress respectively.

5.10.3 S-N Diagrams

Quite a number of specimens of R = -0,5, R = -1 and R = -2 failed at the adhesive bond between graphite and steel. No cohesive bond failures occurred. These failures are attributed to the reversing nature of the principal stress in the bond at the mentioned load ratios combined with the deflection of the graphite. Such a mode of fatigue loading of the bond superimposes a bending moment onto the axial load of the bond. The superimposed bending moment changes sign between tensile and compressive loading of the specimen, which causes crack growth from the inner as well as the outer edges of the bond, resulting in rapid bond failure after only a few cycles.

Fatigue data captured at R = 0 and R = +0,5 is not satisfactory due to the large scatter, aggravated by the small slopes of the S-N curves. The other S-N curves are acceptable, although more tests at R = -1 and R = -2 will improve the level of confidence in these critical load ratios. The general observation for uniaxial fatigue that states that least damage occurs in graphite when the midrange stress is high but the stress amplitude is low, also holds true for multiaxial fatigue.

The distribution of test points for $R = -\infty$ is unsatisfactory. More load sets at high values and load sets at low values are required to improve the confidence level of these results.

The PIE R = -1 tests have many leakage failures, which causes a large variation in attained stress amplitudes. The S-N curve fit is done through the individual data points, rather than

the medians of the load cases. The slope of the S-N curve is steeper for the PIE specimens, suggesting that damage may be induced by pretest isostatic exposure of the graphite.

5.10.4 Relative Fatigue Strength

The physical comparison in Figure 5-73 gives some insight into the relative nature of the stresses of the stress ratios under investigation. The hydraulic system resonance in the R = -0,5, R = -∞ and R = +2 traces can be observed in this figure. For R = -0,5, the resonance occurs in the upper chamber, while for the other two, pressurisation is only of the lower chamber. The lower chamber was at that stage clearly more prone to instability than the upper chamber. A large effort to minimise this effect was made before continuing with the stress reversal load ratios. Modifications were made to obtain more equal volumes of oil in the two chambers. This enabled one set of control parameters to control both chamber pressures acceptably well. However, insufficient removal of entrapped air and varying thickness of the specimen sealant remain the biggest contributors to control resonance.

As expected, of all tensile strength limiting load ratios, the R = -2 load ratio causes most damage to the graphite. The fact that the predicted slope of the R = -0,5 S-N curve is steeper than that of R = -1 is attributed to inaccurate estimates of actual pressure loads due to hydraulic resonance.

The slope of the PIE R = -1 S-N curve is steeper than that of R = -1, suggesting that NBG18 graphite, that is exposed to 10 MPa isostatic loads prior to testing, may well be slightly weaker than virgin graphite. The predicted fatigue strength of PIE specimens subject to R = -1 loading for 100 cycles and 10000 cycles is respectively 2,7% and 4,7% lower than the fatigue strength of unexposed specimens. This observation is supported by the small reduction (< 4%) in the static tensile and compressive strength of the NBG18.

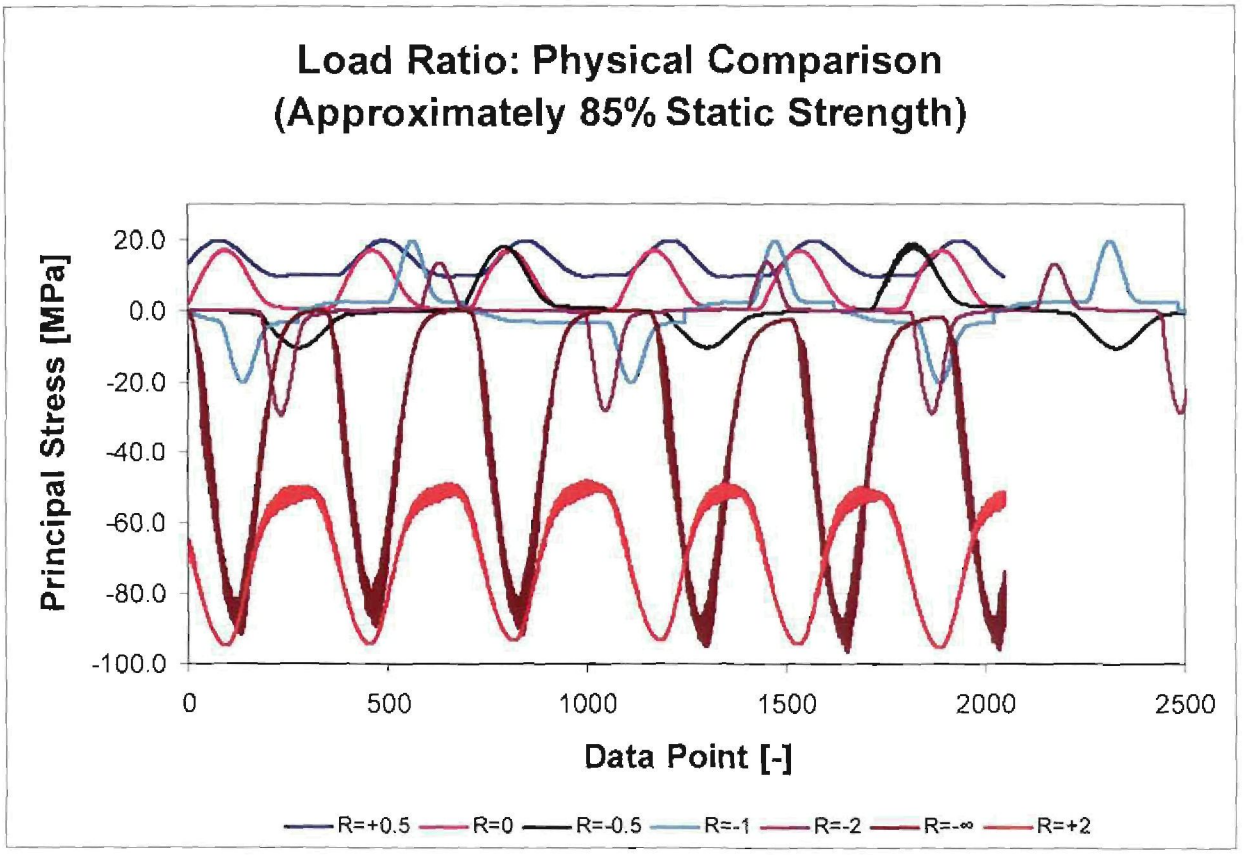


Figure 5-73: Comparison of Physical Stress Excursions of Load Ratios Near 85% Static Strength

5.10.5 Hysteresis Loops

The hydraulic system resonance is clearly seen in Figure 5-65 and Figure 5-66. In the latter figure, it disappears from 100 cycles onwards, as the air is worked out of the loading volume.

Similar to the uniaxial stress-strain results, the reduction in elastic modulus during the fatigue tests, at stress levels of the order of 70% ultimate strength, is negligible contrary to what is expected for a progressively damaged material (mostly insignificant).

In contrast with the uniaxial tests, the plastic strain offset in the multiaxial tests are consistently in the direction of the design limiting strength of the material, as expected. The initial plastic strain offset is large (similar to the uniaxial test results), after which the plastic strain gradually increases with life, in the direction of the life-limiting strain.

5.11 SUMMARY AND CONCLUSIONS

The multiaxial fatigue characteristics of NBG18 are successfully determined for the envisaged load ratios, using the S60B specimen and a low cost, custom designed servo-hydraulic fatigue testing machine.

Using the VW Maximum Principal stress as failure criterion, NBG18 graphite exhibits the same ultimate tensile strength in static multiaxial loading as in uniaxial loading.

The uniaxial static compressive strength cannot be related to the multiaxial static compressive strength, using the Maximum Principal stress -, VW Maximum Principal stress -, Maximum MDE stress – or VW MDE stress criterion. Either the definition of MDE stress in Eq.(4.3), as presented in Section 4.4 of Chapter 4, and/or its assumed constant Poisson ratio value, and/or the simplified linear relationship between stress and strain is so far from the truth, that our simple models are inadequate to explain the compressive strength results of NBG18, measured with the S60B specimen.

The latitudinal and longitudinal strains, measured on the gauge section are equal to within 3%, which implies that the bridge configuration yields accurate average strain results at strains within the design rating of the metal foil strain gauge.

Similar to the uniaxial results, the measured S-N diagrams in multiaxial loading show that graphite has significantly more scatter than metallic materials. The slopes of these curves are quite small, predicting large allowable stress conditions for low cycle fatigue applications. The predicted allowable peak stress at 10^6 cycles (for 50% failure probability) is more than 42% of the static strength of the graphite for all load ratios. The general trend observed from the uniaxial tests, that load ratios with high midrange stress and low stress amplitudes cause least damage to the graphite and vice versa, holds true for multiaxial tests. In these tests, R = -2 caused most damage, as expected.

Pretest Isostatic Exposure at 10 MPa may reduce the fatigue as well as the static strength of NBG18 graphite. The observed reduction is small (of the order of magnitude of the experimental error) and therefore inconclusive, although all 3 test ensembles yielded equal or lower strength values.

In Chapter 6, the uniaxial and multiaxial fatigue characteristics of NBG18 are compared.

Chapter 6

COMPARISON OF UNIAXIAL AND MULTIAXIAL FATIGUE CHARACTERISTICS

6.1 INTRODUCTION

The uniaxial fatigue tests on NBG18 graphite, conducted with the novel S70 specimen, are presented in Chapter 4. Chapter 5 presents the multiaxial fatigue tests on this material, conducted with the novel S60B specimen. In the present chapter, the fatigue characteristics of NBG18, based on uniaxial loading and multiaxial loading are compared and discussed.

The comparisons include static strength measurements, hysteresis loops, constant-life charts and fatigue reduction factors.

6.2 STATIC STRENGTH

A graphical comparison of the static strength of NBG18 as measured by uniaxial tests and multiaxial tests is shown in Figure 6-1. It is evident that the UTS of the material, expressed by the Maximum Principal stress is quite similar in both loading configurations. The uniaxial tests provided the UCS of NBG18 commensurate with the results measured by the supplier. The Maximum Principal stress measured under multiaxial compression loading is appreciably larger than under uniaxial loading.

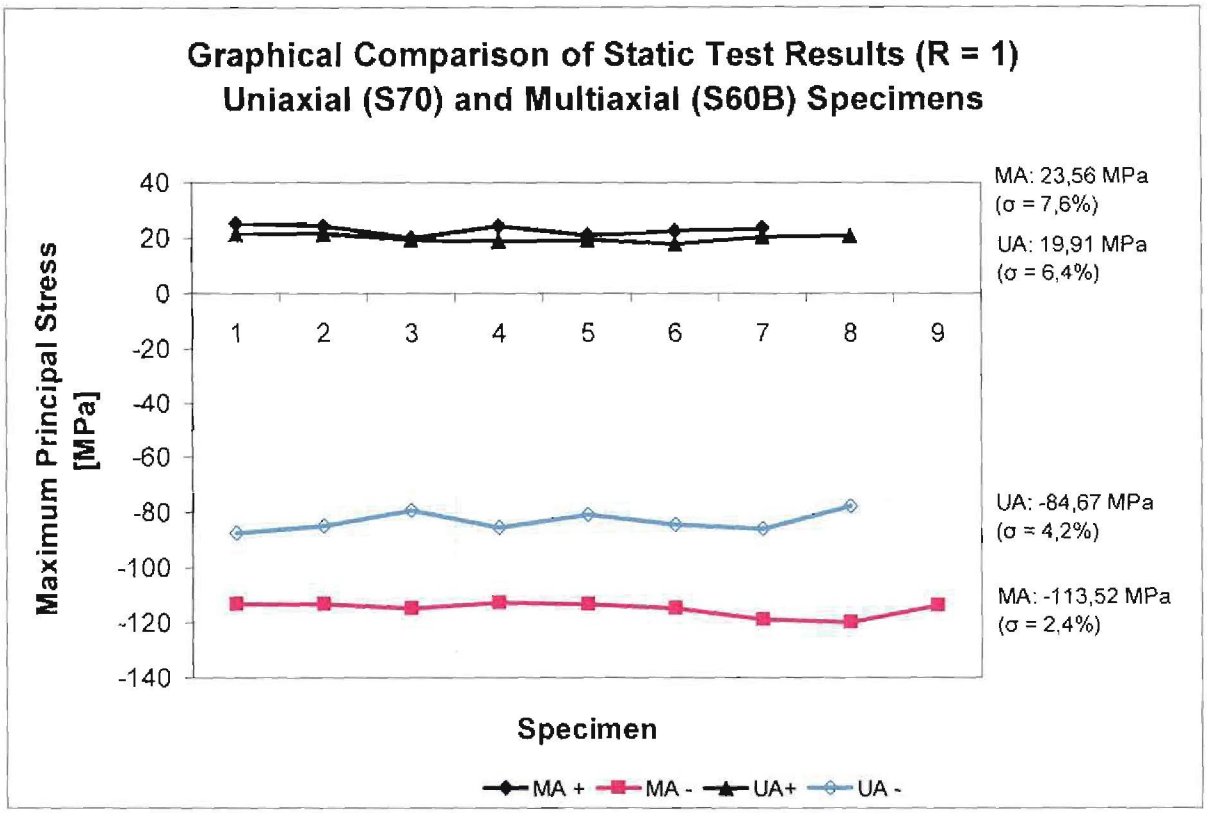


Figure 6-1: Graphical Comparison of Static Test Results (R = 1)

One explanation for the greater compressive strength in the MA case is the fact that this stress is restricted to the inner wall of the specimen, as explained in Chapter 5. In the uniaxial specimen, the whole volume of the gauge section is at the critical stress. It is concluded from an examination of the flexural versus bending strength results, that the higher the volume of graphite subject to a high stress, the higher the probability of failure. According to Schmidt (2003), this stress-volume effect is integrated into the KTA 3232 design rule. However, the Maximum Principal stress variation is only about ±14% in tension and ± 9% in compression.

This was compensated for by calculating a volume weighted equivalent stress as explained in Section 5.2.3.3 of Chapter 5. The volumetric stress distribution contributes about 10% of this 40% discrepancy, as shown in Section 6.4.2. The remaining 30% must be linked to the geometry of the specimen and its loading state. The concept of internal friction may be a clue in explaining this discrepancy, but it is not addressed in this research (Taylor *et al.*, 1967).

The standard deviation in tensile and compressive results obtained with uniaxial and multiaxial loading were of similar magnitude. The standard deviation in compressive results was about half the value obtained in tensile results.

6.3 STRESS-STRAIN CHARACTERISTICS

The combined stress-strain curves of the uniaxial and multiaxial static tensile and compressive tests are shown in Figure 6-2 and Figure 6-3 respectively. It can be seen from these figures that the multiaxial loading condition of the graphite causes it to appear more rigid (higher stiffness i.e. E-value) than when loaded uniaxially. This is particularly true for compressive loading where the multiaxial loading shows a 36% higher E-value over 2000 μm/m than the uniaxial loading. One reason for this is that the strains in these figures are not directly comparable because the other principal stresses alters the strain in the multiaxial specimen according to Eq.(6.1), taken from Shigley *et al.* (2004).

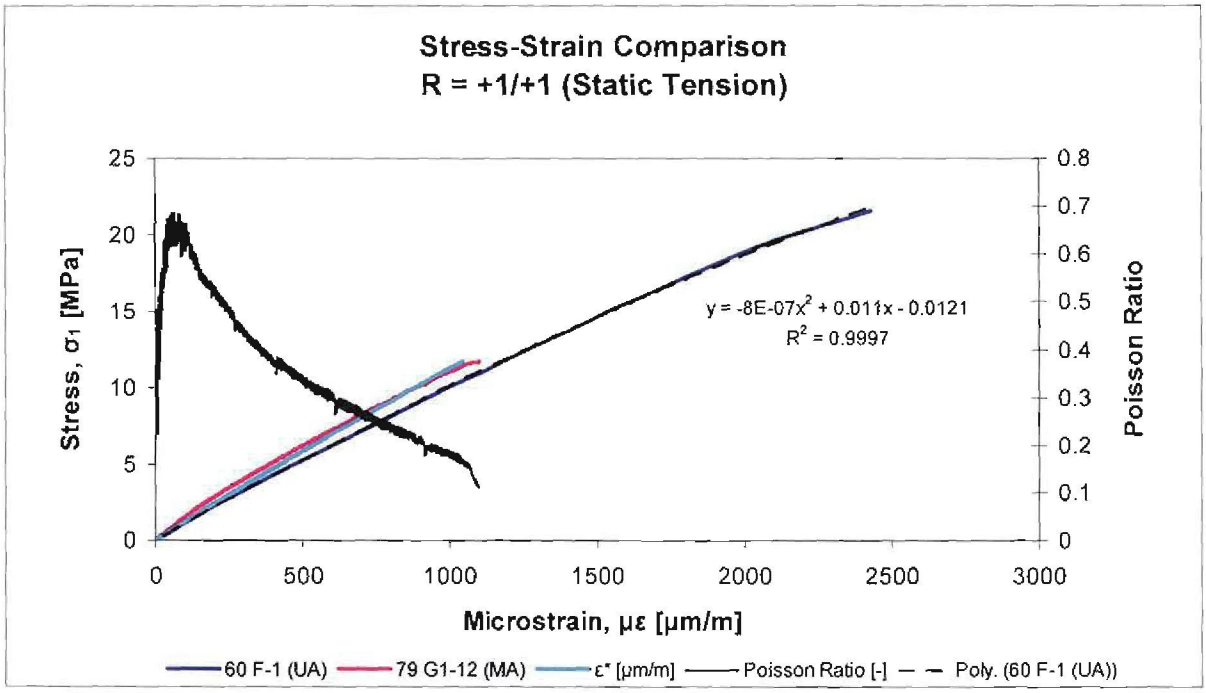


Figure 6-2: Stress-Strain Comparison in Tension

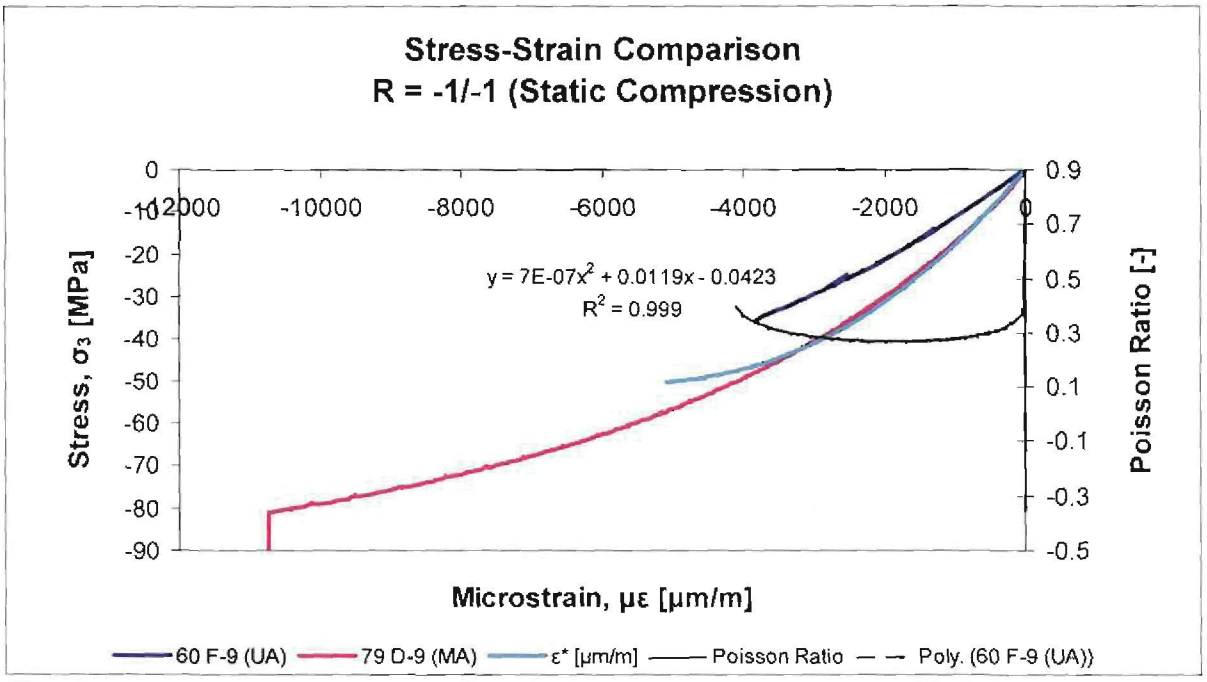


Figure 6-3: Stress-Strain Comparison in Compression

$$\varepsilon_1 = \frac{\sigma_1}{E} - \frac{\nu.\sigma_2}{E} - \frac{\nu.\sigma_3}{E} \qquad \text{.....(6.1)}$$

$$\varepsilon_2 = \frac{\sigma_2}{E} - \frac{\nu.\sigma_1}{E} - \frac{\nu.\sigma_3}{E}$$

$$\varepsilon_3 = \frac{\sigma_3}{E} - \frac{\nu.\sigma_1}{E} - \frac{\nu.\sigma_2}{E}$$

Two other uncertainties are:

- Whether the strain gauge measurement system measures strain accurately from the first loading or whether some strain cycling is needed to settle the measurement
- To what extent does the epoxy adhesive that bonds the metal foil strain gauge to the graphite, reinforces the graphite whereby the graphite's true stress-strain characteristic is altered

The non-linearity of the stress-strain curve is evident from the compressive loading condition where the strains are large.

The validity of these observations need to be confirmed by dedicated tests to compare the strain measurements of strain gauges to that of an extensometer in uniaxial tests, especially at large strains.

The data are analysed by calculating a momentary Poisson ratio. Second order polynomials are fit to the uniaxial stress-strain curves to obtain analytical expressions for both the tension and compression excursions. (It is assumed that the stress-strain relationship between tension and compression is different for graphite. Although it can be checked by examining the R = -1 hysteresis curve, it was not done in this research.)

UNIAXIAL :

$\sigma_j = E_j.\varepsilon_j$

$$\therefore \varepsilon_j = \frac{\sigma_j}{E_j} \qquad \text{.....(6.2)}$$

MULTIAXIAL :

Since the two tangential principal stresses are equal on a sphere, (6.1) reduces to :

$$\varepsilon_i = \sigma_{ti}.\frac{(1-\nu_i)}{E_i} - \sigma_{ri}.\left(\frac{\nu_i}{E_i}\right) \qquad \text{.....(6.3)}$$

Assume isotropic material properties and $E_{UA} = E_{MA}$

Substitute (6.2) in (6.3) for each of the two multiaxial stresses, using the uniaxial compressive and tensile relations between stress and strain :

$$\varepsilon_i = \varepsilon_j(\sigma_{ti}).(1-\nu_i) - \nu_i.\varepsilon_j(\sigma_{ri}) \qquad \text{.....(6.4)}$$

$$\therefore \nu_i = \frac{\varepsilon_j(\sigma_{ti}) - \varepsilon_i}{\left(\varepsilon_j(\sigma_{ti}) + \varepsilon_j(\sigma_{ri})\right)} \qquad \text{.....(6.5)}$$

Where :

$$\varepsilon_j(\sigma_{ti}) = \frac{-0.011 + \sqrt{0.011^2 - 4(-8\times10^{-7})(-0.0121-\sigma_{ti})}}{2.(-8\times10^{-7})} \quad \text{(for tension only)} \qquad \text{.....(6.6)}$$

and

$$\varepsilon_j(\sigma_{ri}) = \frac{-0.0119 + \sqrt{0.0119^2 - 4(7\times10^{-7})(-0.0423-\sigma_{ri})}}{2.(7\times10^{-7})} \quad \text{(for tension and compression)} \qquad \text{...(6.7)}$$

and

$$\varepsilon_j(\sigma_{ti}) = \frac{-0.0119 + \sqrt{0.0119^2 - 4(7\times10^{-7})(-0.0423-\sigma_{ti})}}{2.(7\times10^{-7})} \quad \text{(for compression only)} \qquad \text{.....(6.8)}$$

The momentary Poisson ratio is an indication of how well the uniaxial and multiaxial stress-strain curves correspond. The former is the value that is required for a fit of the multiaxial strain, using the measured uniaxial relationships. If the momentary Poisson ratio has a constant value, the assumptions for this analysis are true.

For the tensile excursion, the momentary Poisson ratio varies a lot. The predicted multiaxial stress-strain curve using the uniaxial characteristics and a constant Poisson ratio of 0.21 is shown by the curve designated ε^* in this figure.

For the compressive excursion, the momentary Poisson ratio is fairly constant. A Poisson ratio of 0.295 is used in the predicted multiaxial stress-strain curve, which yields a good fit up to 3800 μm/m, which is the limiting value of recorded uniaxial strain. The deviation after this strain value is attributed to extrapolation error.

6.4 CONSTANT-LIFE CHARTS

Constant-life charts are presented in Chapter 4 and 5 based on the S-N diagrams that are constructed from the fatigue test results. These charts show the predicted allowable ratio of stress amplitude versus midrange stress, for all possible combinations in fatigue loading that have a 50% probability of surviving the number of cycles drawn as constant-life contours in these charts.

In the following constant-life chart comparisons, the predicted fatigue life of NBG18 for 10 and 100000 cycles in uniaxial and multiaxial loading are given in terms of the various stress parameters. The stress parameter that makes the charts match at the two static strength data points, i.e. R = +1/+1 and R = -1/-1, is an appropriate failure criterion for these 50% failure probability results.

6.4.1 Maximum Principal Stress

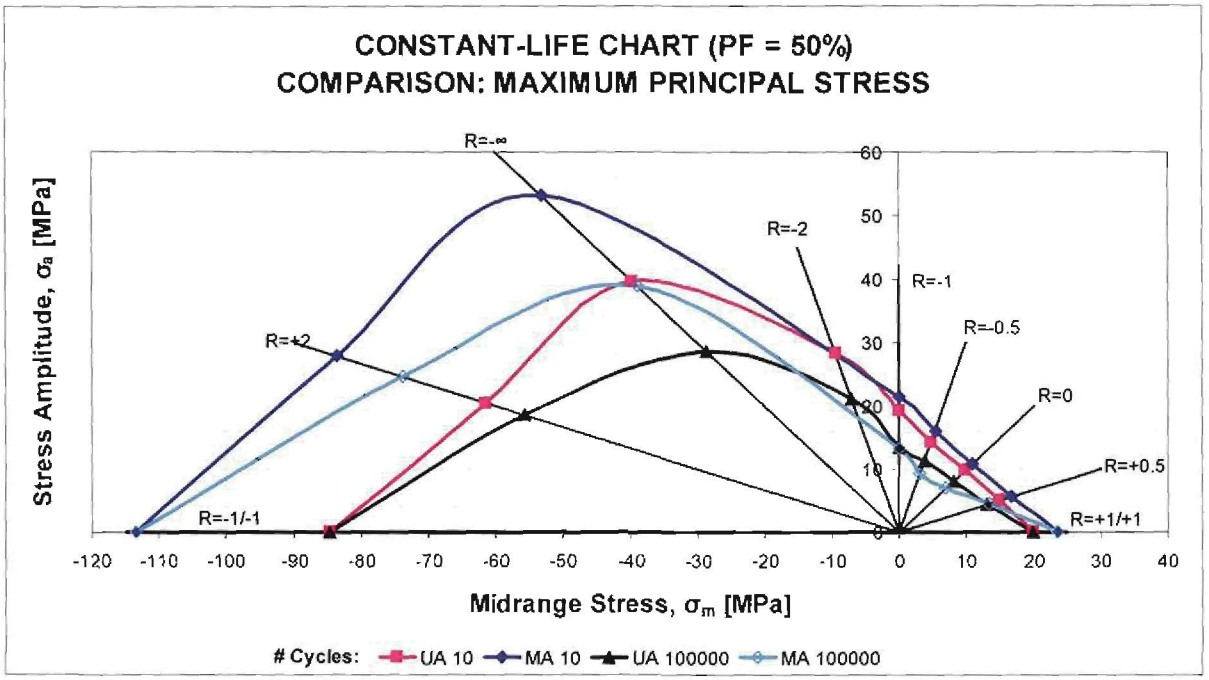


Figure 6-4: Comparison of Constant Life Charts - Uniaxial and Multiaxial Stress Based on Maximum Principal Stress

Refer to the matching of the static strengths of the uniaxial and multiaxial tests in Figure 6-4. Clearly, the Maximum Principal stress is not a good basis for comparison of the strength of the two graphite specimens. One expects the multiaxial specimen to definitely have a lower static tensile strength and perhaps a higher static compressive strength than the uniaxial specimen. Figure 6-4 shows a higher static tensile strength and a much higher static compressive strength for the multiaxial specimen, as discussed in Section 6.2.

6.4.2 Volume Weighted Maximum Principal Stress

The Volume Weighted Maximum Principal stress, shown in Figure 6-5, is definitely a better indication of the compressive stress condition in the multiaxial specimen than the Maximum Principal stress, although still not good enough.

In the tensile region, this stress parameter gives an excellent match of the UTS.

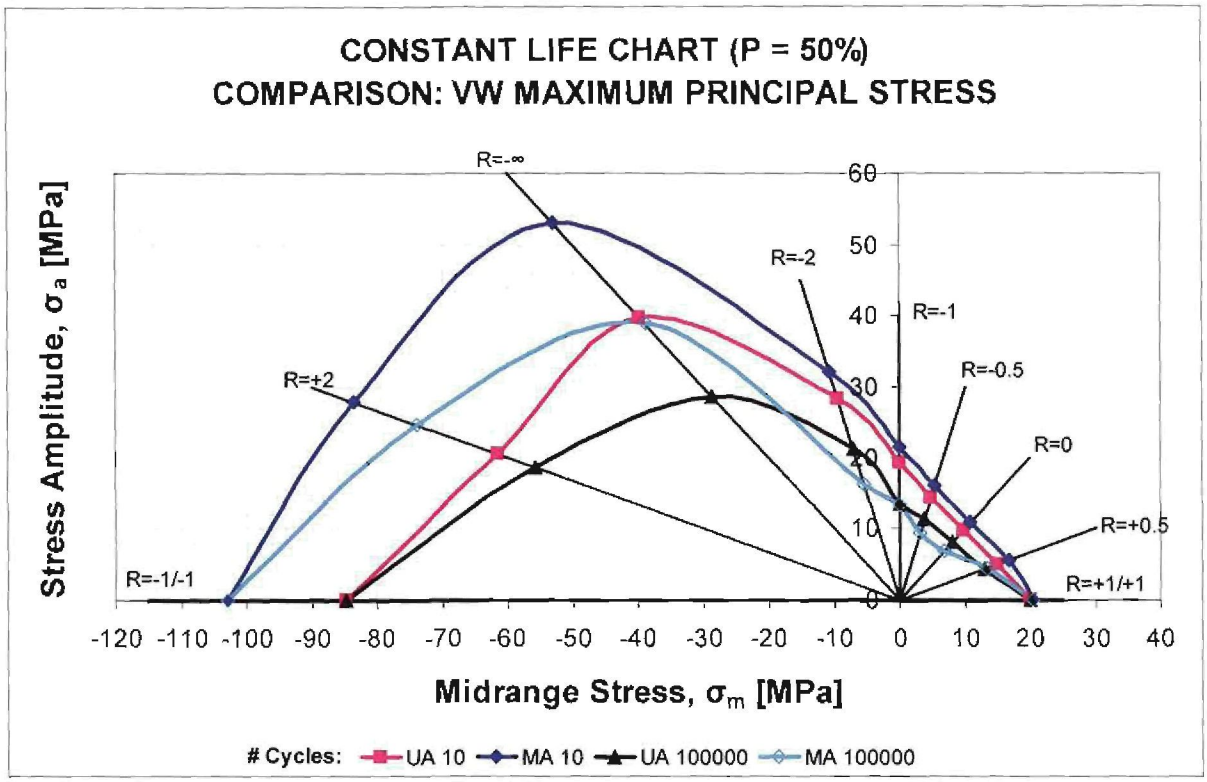


Figure 6-5: Comparison of Constant-Life Charts - Uniaxial and Multiaxial Stress Based on Volume Weighted Maximum Principal Stress

6.4.3 Maximum MDE Stress

The maximum MDE stress criterion, as proposed in its "developed" format, is much worse than the Maximum Principal stress criterion, as shown in Figure 6-6. At all R-values except R = -0.5 and R = -2, the multiaxial constant-life chart allows much higher maximum MDE stress values than the uniaxial constant-life chart.

Since the maximum MDE stress forms the basis of strength evaluation in graphite design, this is a major concern.

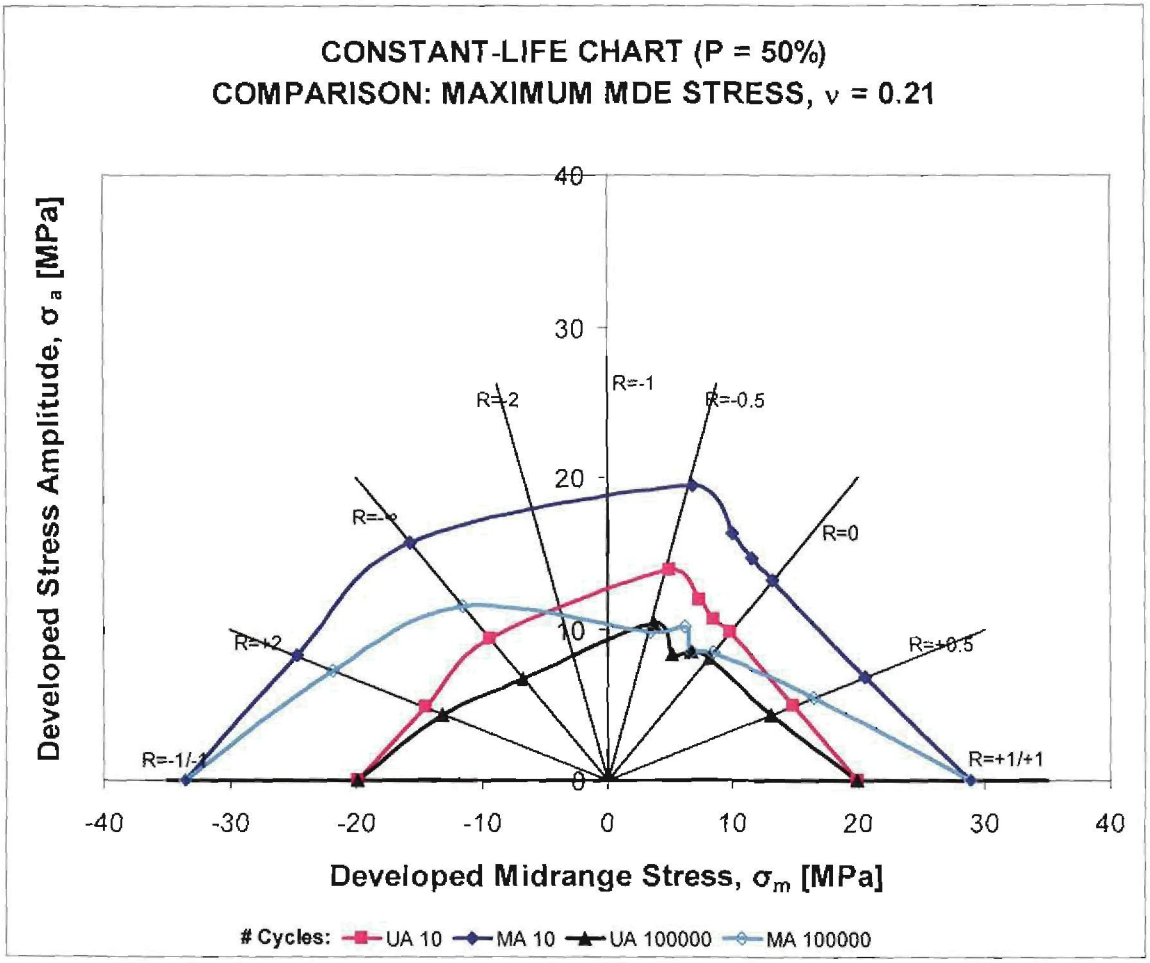


Figure 6-6: Comparison of Constant Life Charts - Uniaxial and Multiaxial Stress Based on Maximum MDE Stress

6.4.4 Volume Weighted MDE Stress

The Volume Weighted MDE stress criterion is a simple failure criterion, which shows much improvement over the maximum MDE stress prediction, as shown in Figure 6-7. The values of the volume weighting factors are 0,877 and 0,872 for tensile and compressive loading respectively, for a constant Poisson ratio of 0,21.

The Volume Weighted MDE stress in multiaxial loading produces an error of approximately 25% for UTS and 50% for UCS, as compared to the uniaxial loading state.

Comparing the errors of the Volume Weighted MDE and Volume Weighted Maximum Principal stress criteria, *the Volume Weighted Maximum Principal stress criterion provides the better prediction of the failure of the S60B multiaxial specimen in NBG18 graphite, but still not good enough.*

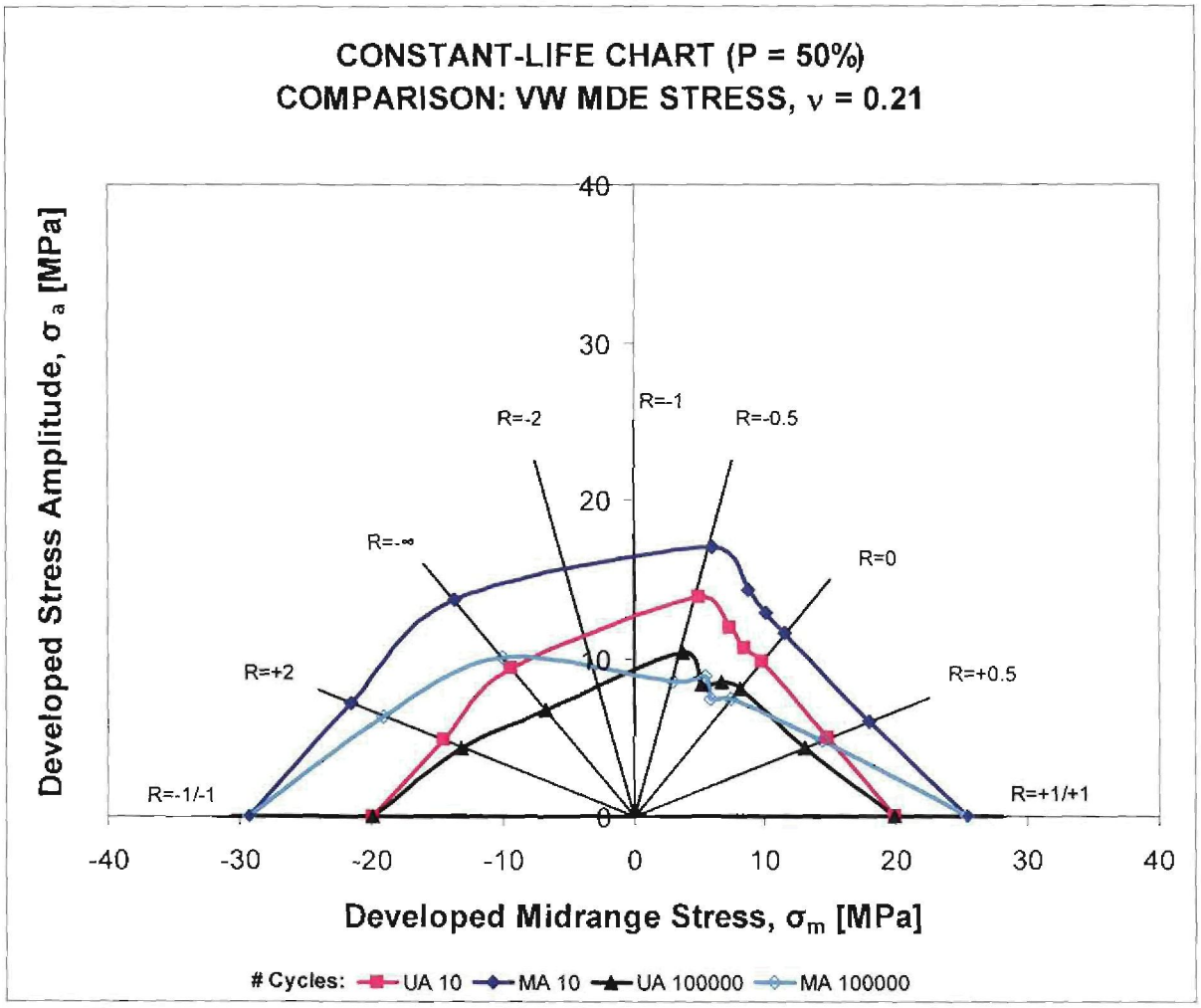


Figure 6-7: Comparison of Constant Life Charts - Uniaxial and Multiaxial Stress Based on Volume Weighted MDE Stress

Another attempt to match the probability of failure of the S60B specimen is made by varying the Poisson ratios in the calculation of the MDE stress. The static tensile and compressive failure conditions are matched by varying the Poisson ratio of the MDE stress calculation. This is permissible, because the variable ν in the MDE formula, does no longer represent the material property, according to Schmidt (2001b). The Poisson ratio is altered in a trial-and-error fashion until a 50% probability of survival is attained, using Eq.(4.5) with the experimentally determined Weibull characteristic and shape parameters from Fechter (2007). This iterative procedure yields Poisson ratios of 0,448 and 0,531 for tension and compression respectively. These values are much higher than the values estimated from the stress-strain characteristics in Section 6.3, but are presented here, because it gives some insight into the problem. The respective volume weighting factors for the mentioned Poisson

ratios are 0,908 and 0,689. Changing the Poisson ratio of the MDE calculation has major ramifications that start with the stress distribution through the wall of the specimen, updating the regression equations of the S-N diagrams and end with the constant-life diagram. The result of this attempt is shown in Figure 6-8. There seems to be a constant offset in static strength values of approximately 2 MPa in the tensile direction. Overall, this match is encouraging.

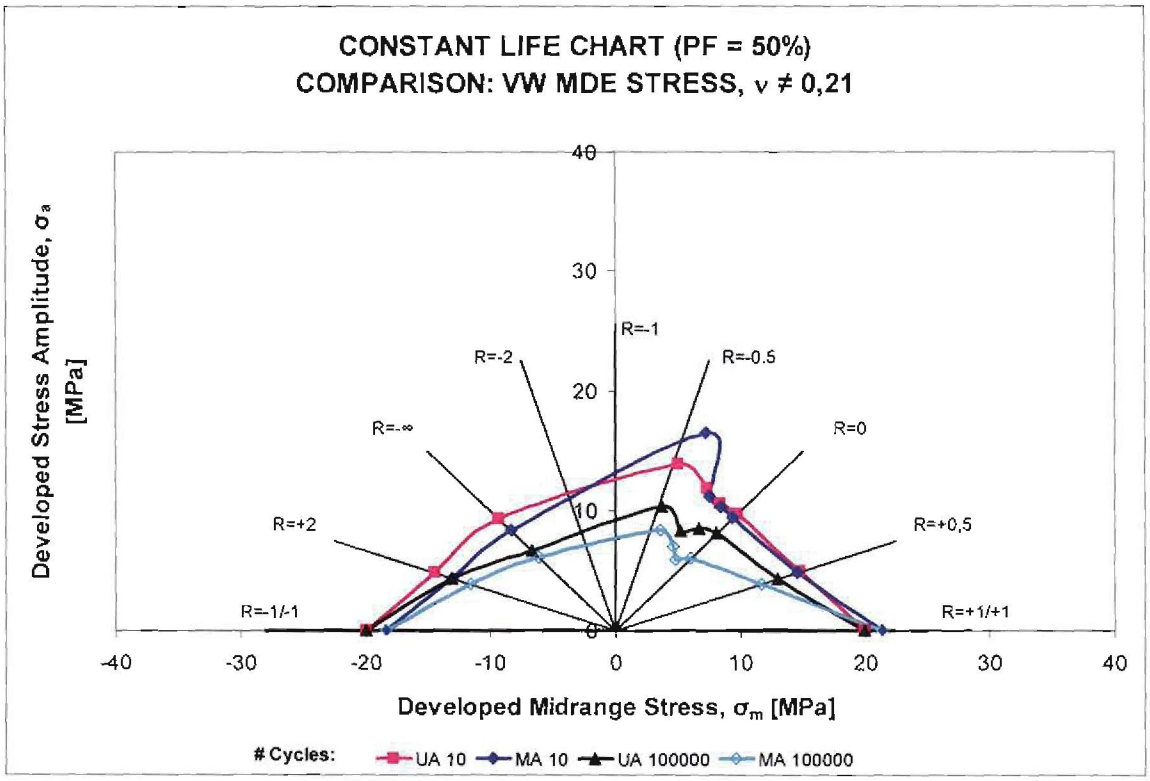


Figure 6-8: Comparison of Constant Life Charts - Uniaxial and Multiaxial Stress Based on Volume Weighted MDE Stress with Modified Poisson Ratios

Another attempt to match the probability of failure of the S60B specimen is made by varying the Poisson ratios in the calculation of the MDE stress. The static tensile and compressive failure conditions are matched by varying the Poisson ratio of the MDE stress calculation. This is permissible, because the variable ν in the MDE formula, does no longer represent the material property, according to Schmidt (2001b). The Poisson ratio is altered in a trial-and-error fashion until a 50% probability of survival is attained, using Eq.(4.5) with the experimentally determined Weibull characteristic and shape parameters from Fechter (2007). This iterative procedure yields Poisson ratios of 0,448 and 0,531 for tension and compression respectively. These values are much higher than the values estimated from the stress-strain characteristics in Section 6.3, but are presented here, because it gives some insight into the problem. The respective volume weighting factors for the mentioned Poisson

ratios are 0,908 and 0,689. Changing the Poisson ratio of the MDE calculation has major ramifications that start with the stress distribution through the wall of the specimen, updating the regression equations of the S-N diagrams and end with the constant-life diagram. The result of this attempt is shown in Figure 6-8. There seems to be a constant offset in static strength values of approximately 2 MPa in the tensile direction. Overall, this match is encouraging.

The last attempt presented here is one that is not based on any physical motivation. Arbitrary stress reduction factors are calculated to force coincidence of the uniaxial and multiaxial constant-life curves of Figure 6-7 at both static conditions. A factor of 0,805 and 0,698 was determined for tension and compression governed load ratios respectively. These factors, which are called *shape factors* for lack of a better description, are applied to the Volume Weighted MDE stresses to yield the surprising similarity between the uniaxial and multiaxial constant-life lines shown in Figure 6-9.

Although the purpose of this research is not to find an appropriate failure criterion, the following observation can be made:

> *There is some strength phenomenon in graphite, that is not accounted for in the formulation of the Volume Weighted MDE stress, that enables the S60B multiaxial fatigue specimen to survive 1,24 (1/0,805) larger tensile and 1,43 (1/0,698) larger compressive stresses than the S70 uniaxial specimen in the same material under static and low cycle fatigue conditions.*

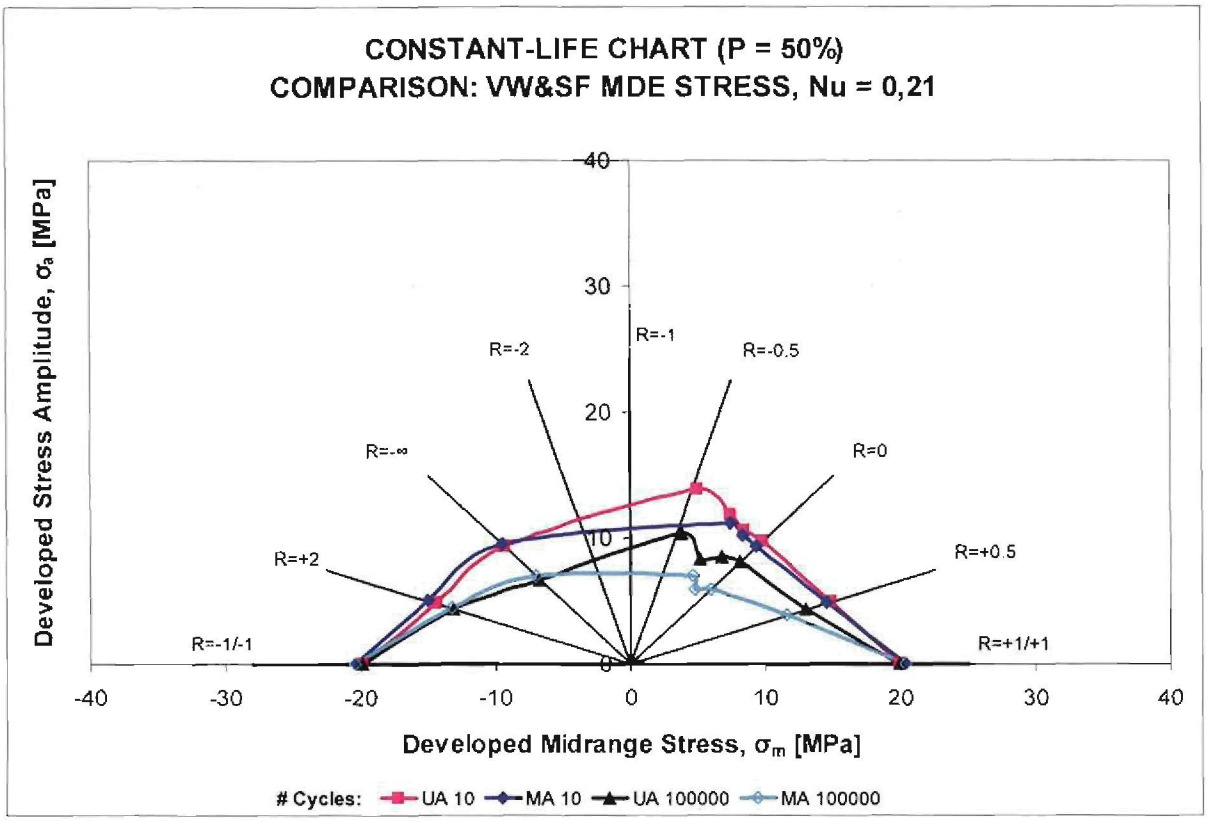


Figure 6-9: Comparison of Constant Life Charts - Uniaxial and Multiaxial Stress Based on Volume Weighted MDE Stress with Arbitrary Shape Factor

6.5 FATIGUE STRENGTH FACTORS

Fatigue strength factors are calculated by normalising the predicted fatigue strength by the governing static strength for each load ratio. The results are shown in Figure 6-10 and Figure 6-11 for the uniaxial and multiaxial tests respectively.

The Maximum Principal stress fatigue factors of the multiaxial loading scenario are more than that of the uniaxial loading scenario, as expected. The smallest fatigue strength factor for a life of 10^5 cycles is 45% for R = -2 in the multiaxial test and 65% for R = -1 in the uniaxial test.

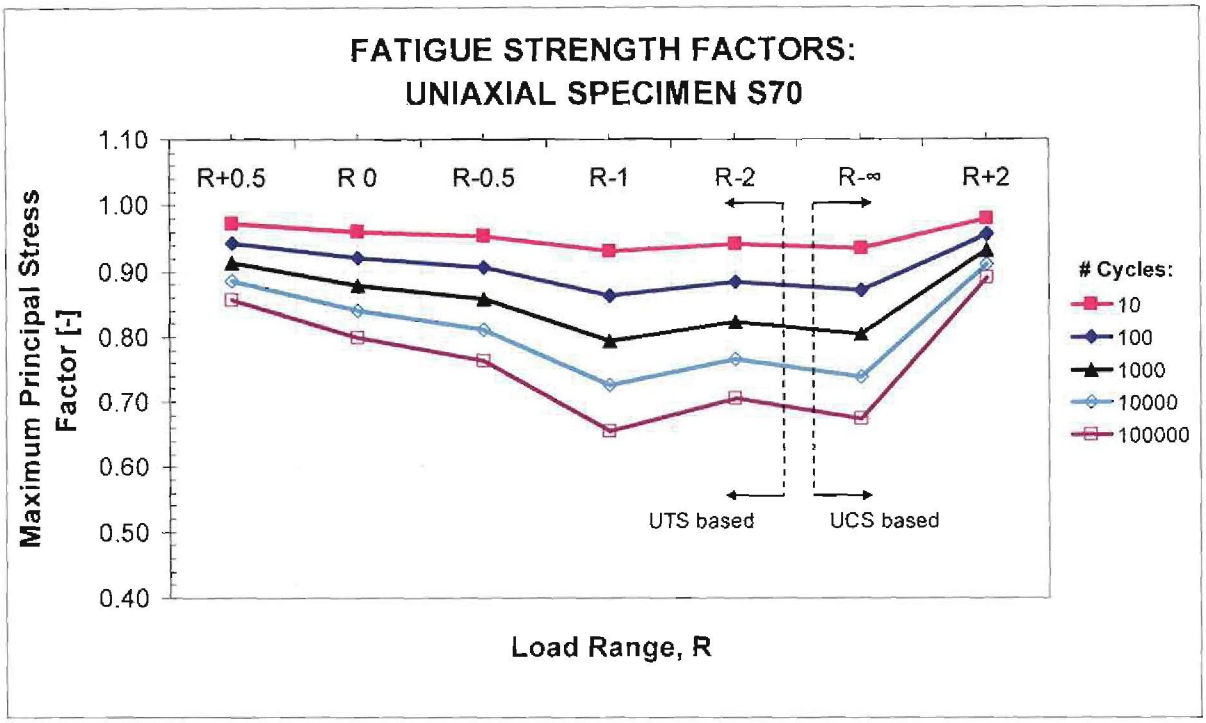


Figure 6-10: Uniaxial Fatigue Strength Factors

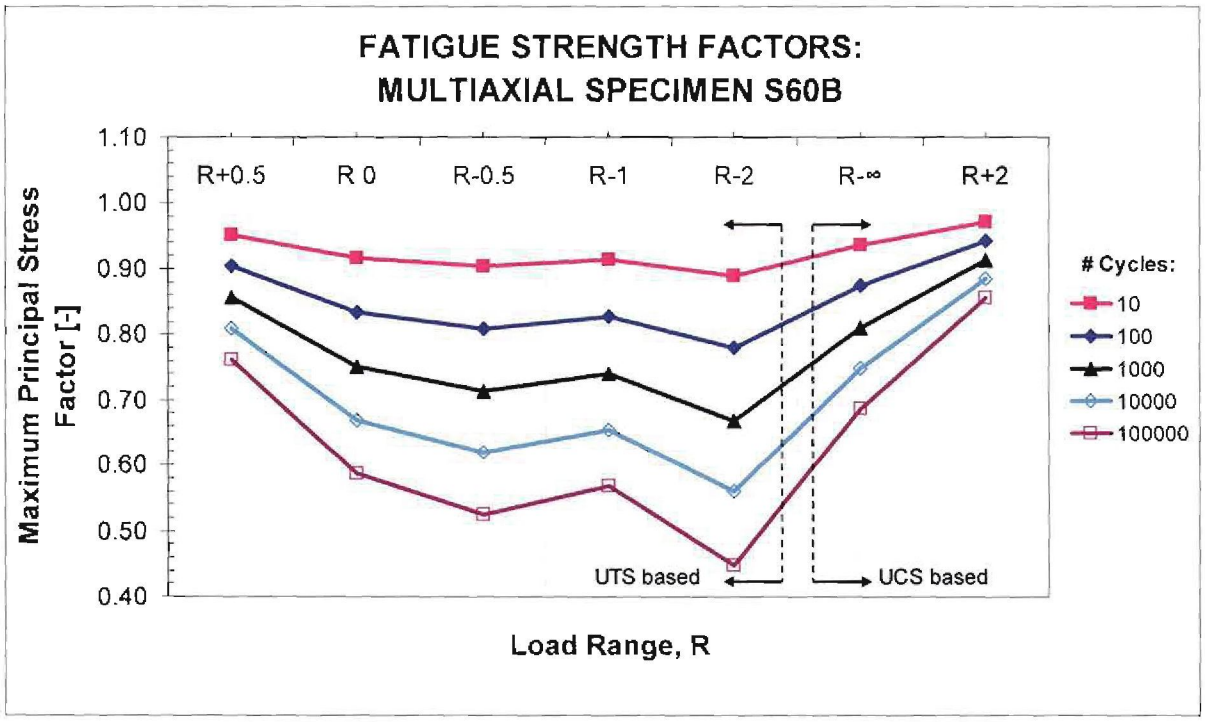


Figure 6-11: Multiaxial Fatigue Strength Factors

Comparing the fatigue strength factors for fully reversed (R = -1) Maximum Principal stress loading as shown in Figure 6-12, the multiaxial loading yields a fatigue strength factor that is

4,1 % lower than uniaxial loading at a low cycle number of 100, which is a typical high excursion fatigue cycle count in high temperature gas cooled reactors. For the R = -2 stress ratio at 100 cycles, multiaxial loading yields a fatigue strength factor that is 11,7% lower than for uniaxial loading.

However, the typical uniaxial fatigue strength factor for R = -2 is expected to be generally lower than for R = -1. Similarly, the typical multiaxial fatigue strength factor for R = -1 is expected to fall between R = -0,5 and R = -2. Therefore, the typical fatigue strength factor expected for the worst stress ratio is from the UA R = – 1 to the MA R = -2 line, which is less than 10% at 100 cycles.

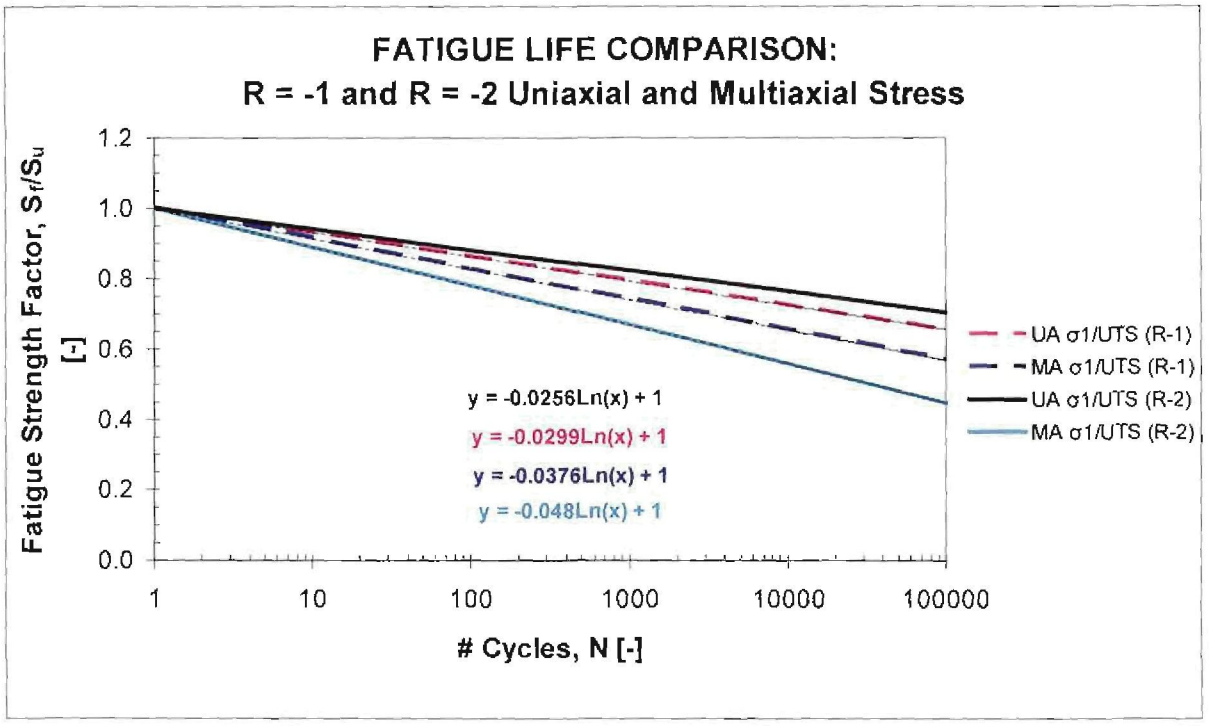


Figure 6-12: Fully Reversed Maximum Principal Stress Fatigue Life Comparison

6.6 CONCLUSIONS

6.6.1 Static Strength

The UTS and UCS of NBG18 graphite, measured with the S70 uniaxial specimen, compare well with the supplier's results.

The Volume Weighted Maximum Principal stress predicts the static tensile strength of the S60B multiaxial specimen well, but the compressive strength prediction is unacceptable. The S60B specimen fails at substantially higher stresses than predicted.

The KTA-3232 methodology fails to predict the static multiaxial failure of the S60B specimen to acceptable accuracies, without modifying the Poisson ratio in the MDE formula.

6.6.2 Stress-Strain Characteristics

A technique is proposed to use the uniaxial stress-strain relation to determine the high strain Poisson ratio from the multiaxial stress-strain characteristics. A large-strain Poisson ratio of 0.295 is determined from a single set of measurements for NBG18 graphite in compression. A representative Poisson value is not found by this technique for the tensile data, but the standard value of 0.21 yields a good multiaxial stress-strain relation in comparison with the measured data. Due to the statistical variation in graphite, a large number of tests are required to determine the median values of the large strain Poisson ratios.

Another important conclusion is that the Poisson ratio, like the modulus of elasticity, seems to be a function of the sense of the load (tensile or compressive) and the magnitude of the strain.

6.6.3 S-N Diagrams

The uniaxial specimen S-N curves establish a good baseline for the fatigue properties of NBG18 graphite. More testing is required in the R = -1, R = 0 and R = +0,5 load ranges to improve the level of confidence in these results.

The most critical of the explored load ranges is R = -2 in multiaxial loading and R = -1 in uniaxial loading. The physics of crack growth suggest that R = 1/f, where $f = S_{ut}/S_{uc}$ should be most critical. This should be investigated further.

The multiaxial specimen S-N curves have larger slopes than that of the uniaxial specimen, as expected.

The expected effect of multiaxial testing in lieu of uniaxial testing is less than 10% when low cycle numbers are of interest, as in the case of high temperature gas cooled reactors.

6.6.4 Constant-Life Charts

The best matching of the static strength properties in the constant-life charts of the uniaxial and multiaxial fatigue characteristics of NBG18, is found with the Volume Weighted Maximum Principal stress. This makes the Maximum Principal stress criterion the best for life prediction in fatigue loading under multiaxial loading conditions. The multiaxial fatigue charts predict larger allowable stresses for load ratios that are governed by the compressive strength of the graphite.

For the Volume Weighted MDE stress base, the multiaxial fatigue chart allows much larger stresses than the uniaxial fatigue chart, except at R = -0,5 and R = -2.

Surprising similar shapes for the uniaxial and multiaxial constant-life charts is synthesized by the application of arbitrary shape factors and KTA 3232 motivated Poisson ratios.

The mismatch between the static strength values of the uniaxial and multiaxial fatigue tests is an indication that the KTA 3232 failure criterion (applied to the gauge section only), based on MDE stresses is still not good enough to predict the fatigue life of a component under multiaxial loading conditions. *A better failure criterion will probably include variable Poisson ratios and/or moduli of elasticity.*

6.6.5 Fatigue Strength Factors

The tests show that the 50% probability low cycle fatigue strength of NBG18 is above 75% of its static strength. Low cycle in this context is 100 cycles, which is important for HTR design applications.

Chapter 7

CONCLUSIONS

7.1 UNIAXIAL FATIGUE TESTS

A comprehensive range of uniaxial fatigue tests was conducted in South Africa on NBG18 graphite. These results are representative of the average low end fatigue characteristics of NBG18 since the specimens are taken from both parallel and perpendicular to grain directions, near edge and centre locations from two graphite blocks of lower end acceptable strength. Although some additional tests are required at a few load ratios to improve the reliability of the data, future tests can now focus on critical load ratios. Critical load ratios are load ratios that produce most damage in the material. R = -0.5, R = -1, R = -2 and R = -1/f are all potentially critical load ratios.

The fatigue characteristics of this material are summarised on constant-life charts. NBG18 is superior to V483T2 for all combinations of stress amplitude and midrange stress, as shown in Figure 4-42 in Chapter 4.

A novel fatigue test specimen, the S70 specimen is designed for these tests. The S70 fatigue test specimen proves to be an acceptable design and the novel idea of friction gripping to simplify alignment of the apparatus is a success.

The uniaxial fatigue testing capability is established at the Automotive Components Test Station, Nelson Mandela Metropolitan University, Port Elizabeth.

7.2 MULTIAXIAL FATIGUE TESTS

A design of a novel multiaxial fatigue specimen, the S60B specimen is conducted. The main features of this design are the low cost of the specimens, the low cost of the test equipment, the relative simplicity of the stress state, the relative insensitivity of the specimen to grain orientation and the loading for "maximum damage" attained from the spherical geometry.

A test rig is designed and constructed in South Africa to conduct these tests. A comparable set of fatigue results for NBG18 graphite under multiaxial loading conditions is acquired on

this test rig, except for load ratio R = -2. Some minor modifications to this rig are required to improve these tests.

These modifications are:

- Improvement of specimen sealing by custom designed seals that remain part of the rig in stead of the specimen
- Better matching of chamber volumes to yield the same fundamental hydraulic resonance frequency for upper and lower chamber

The multiaxial static strength characteristics, determined through these tests, do not match the uniaxial fatigue characteristics satisfactorily, using the KTA 3232 design methodology. *However, the comprehensive set of data acquired through these tests can serve as an ideal test vehicle to do research on a more appropriate failure criterion for graphite.*

The multiaxial fatigue testing capability is established at the School of Mechanical Engineering, Potchefstroom Campus of the North-West University.

7.3 PRETEST ISOSTATIC EXPOSED SPECIMEN EXPLORATION

NBG18 graphite, that is exposed to 10 MPa isostatic loads prior to testing, may well be slightly weaker than virgin graphite, as is evident from consistently equal or lower static and R = -1 fatigue strengths. The measured reduction in strength is less than 3% for all static strengths and a fatigue life of 100 cycles.

This preliminary conclusion needs to be confirmed by further tests.

7.4 PROPOSALS FOR FURTHER RESEARCH

Following from the results and the limitations of this research, the following proposals are made for further investigation:

- *Use the large range of NBG18 test data, measured through this research, to find a more suitable criterion for prediction of the static and fatigue failure of graphite under multiaxial and uniaxial loads*
- Quantify the mechanical strength behaviour of irradiated NBG18

- Investigate the applicability of metal foil strain gauges for stress-strain measurements on graphite with regard to first cycle effects, effect of strain gauge cement on graphite properties, independent direct and Poisson strain measurements and accuracy of high strain data

- Confirm the observed possible damage at reactor operating pressure in pre-test isostatically exposed NBG18 graphite, through simpler uniaxial fatigue tests with the S70 specimen at R = -2, R = -1/-1 and R = +1/+1

- Do high quantity (at least 32 specimens) uniaxial fatigue test at R = $-S_{uc}/S_{ut}$ to verify the hypothesis that it should have the highest strength reduction factors of all load ranges

- Do additional uniaxial tests for R = +0,5, R = 0, R = -1 to increase the confidence level in the present results

REFERENCES

ASTM C565-93. 2005. Standard test methods for tension testing of carbon and graphite mechanical materials. (*In* Annual Book of ASTM Standards, Vol 05.05. West Conshohocken, PA: ASTM.)

ASTM C749-92. 2005. Standard test method for tensile stress-strain of carbon and graphite. (*In* Annual Book of ASTM Standards, Vol 05.05. West Conshohocken, PA: ASTM.)

ASTM E1012-99. 2002. Standard practice for verification of specimen alignment under tensile loading. (*In* Annual book of ASTM standards, Vol. 03.01. West Conshohocken, PA: ASTM.)

ASTM E1049-85. 2002. Standard practices for cycle counting in fatigue analysis. (*In* Annual book of ASTM standards, Vol. 03.01. West Conshohocken, PA: ASTM.)

ASTM E1823-96. 2002. Standard terminology relating to fatigue and fracture testing. (*In* Annual book of ASTM standards, Vol. 03.01. West Conshohocken, PA: ASTM.)

ASTM E1942-98. 2002. Standard guide for evaluating data acquisition systems used in cyclic fatigue and fracture mechanics testing. (*In* Annual book of ASTM standards, Vol. 03.01. West Conshohocken, PA: ASTM.)

ASTM E466-96. 2002. Standard practice for conducting force controlled constant amplitude axial fatigue tests of metallic materials. (*In* Annual book of ASTM standards, Vol. 03.01. West Conshohocken, PA: ASTM.)

ASTM E468-90. 2002. Standard practice for presentation of constant amplitude fatigue test results for metallic materials. (*In* Annual book of ASTM standards, Vol. 03.01. West Conshohocken, PA: ASTM.)

ASTM E74-02. 2002. Standard practice of calibration of force-measuring instruments for verifying the force indication of testing machines. (*In* Annual book of ASTM standards, Vol. 03.01. West Conshohocken, PA: ASTM.)

BAZAJ, D.K. & COX, E.E. 1969. Stress-concentration factors and notch-sensitivity of graphite. *Carbon*, 7:689-697.

BLANCHARD, B.S. & FABRYCKY, W.J. 2006. Systems engineering and analysis. 4th ed. Upper Saddle River, NJ: Prentice Hall.

BOEY, S.Y. & BACON, D.J. 1986a. Bend strength of graphite under pressure. *Carbon*, 24(5):571–574.

BOEY, S.Y. & BACON, D.J. 1986b. Deformation of polycrystalline graphite under pressure. *Carbon*, 24(5):557–564.

BROCKLEHURST, J.E. 1977. Fracture of Polycrystalline Graphite. (*In* Thrower, P.A. & Walker, P.L., *Eds.* Chemistry & Physics of Carbon, 13:145-280. Marcel Dekker, New York.)

BURCHELL, T., YAHR, T. & BATTISTE, R. 2006. Modelling the multiaxial strength of nuclear graphite. 3rd International Topical Meeting on High Temperature Reactor Technology, Johannesburg, SA, Oct 01 – 04, (2006)

DALLY, J.W. & RILEY, W.F. 1978. Experimental stress analysis. 2nd ed. Tokyo: McGraw-Hill.

DIN 51914 : 1985-04. 1985. Testing of carbonaceous materials: determination of tensile strength: solid materials. Translation from German by Gerd Haag (not checked). Berlin: Deutsches Institut fur Normung.

FASH, J.W., SOCIE, D.F. & MCDOWELL, D.L. 1985. Fatigue life estimates for a simple notched component under biaxial loading. (*In* Miller, K.J. & Brown, M.W., *Eds.* Multiaxial fatigue, ASTM STP 853. Philadelphia, PA: ASTM. pp. 497–513.)

FECHTER, M. 2007. Material Data Sheet: NBG-18 Graphite. (PBMR Doc. No. 027253, Rev 2A.) Centurion. (Unpublished.)

FOUND, M.S., FERNANDO, U.S. & MILLER, K.J. 1985. Requirements of a new multiaxial fatigue testing facility. (*In* Miller, K.J. & Brown, M.W., *Eds.* Multiaxial fatigue, ASTM STP 853. Philadelphia, PA: ASTM. pp. 463–481.)

HAAG, G. 2004. Manufacture of reactor graphite. (Presentation to PBMR by Forschungszentrum Jülich, Germany at PBMR Graphite workshop on 25-25 November 2004.) Centurion. (Unpublished.)

HO, F.H., VOLLMAN, R.E., YU, H. & ADSIT, N.R. 1983. Biaxial failure surfaces of 2020 and PGX graphites. (*In* 7th International Conference on Structural Mechanics in Reactor

Technology. Paper presented at SMiRT-7 held in Chicago on 22 - 26 Aug. Chicago, IL. pp. 127-134.)

LEE, S.B. 1985. A criterion for fully reversed out-of-phase torsion and bending. (*In* Miller, K.J. & Brown, M.W., *Eds.* Multiaxial fatigue, ASTM STP 853. Philadelphia, PA: ASTM. p. 553–568.)

LEESE, G.E. & MORROW, J. 1985. Low cycle fatigue properties of a 1045 steel in torsion. (*In* Miller, K.J. & Brown, M.W., Eds. Multiaxial fatigue, ASTM STP 853. Philadelphia, PA: ASTM. p. 482–496.)

LOSTY, H.H.W. 1962. Radiation effects on mechanical properties. (*In* Nightingale, R.E., *Ed.* Nuclear graphite, Academic press inc., New York. pp. 316-318.)

MARUYAMA, T., ETO, M. & OKU, T. 1987. Elastic modulus and bend strength of a nuclear graphite at high temperature. *Carbon*, 25(6):723-726.

MCDIARMID, D.L. 1985. Fatigue under out-of-phase biaxial stresses of different frequencies. (*In* Miller, K.J. & Brown, M.W., *Eds.* Multiaxial fatigue, ASTM STP 853. Philadelphia, PA: ASTM. pp. 606–621.)

MITCHELL, M.N. 2005. Identification of the key parameters defining the life of graphite core components. (*In* 18th International Conference on Structural Mechanics in Reactor Technology. Paper presented at SMiRT-18 held in Beijing, China on 7 - 12 Aug. Beijing, pp. 127-134.)

NIGHTINGALE, R.E., YOSHIKAWA, H.H & LOSTY, H.H.W. 1962. Physical properties. (*In* Nightingale, R.E., *Ed.* Nuclear graphite, Academic press inc., New York. p. 153.)

NOMURA, S., KUROSAWA, T., IMAI, H., ETO, M. & OKU, T. 1986. A graphite corrosion rate equation under high concentration water-vapor in helium and an estimation of the VHTR support post corrosion and strength. (*In* Specialists' meeting on graphite component structural design, JAERI Tokai (Japan), 8 – 11 September. International Atomic Energy Agency, Vienna (Austria). International working group on gas cooled reactors. IWGGCR—11, pp. 195–200).

PRICE, R.J. 1978. Cyclic fatigue of near-isotropic graphite: influence of stress cycle and neutron irradiation. *Carbon,* 16:367-372.

ROBERTS, J.G. 2006. Fatigue specimen design report: PBMR reactor graphite. (J Roberts M-Tech report no. phd03, rev.B.) Potchefstroom. (Unpublished.)

RYDER, G.H. 1969. Strength of materials. 3rd ed. London: Macmillan Press.

SCHMIDT, A. 2000. Multiaxial stress states in graphite. (Explanatory report no GBRA 050 310, Westinghouse Reaktor GmbH.) Mannheim, Germany. (Unpublished.)

SCHMIDT, A. 2001a. Low cycle fatigue of graphite. (Explanatory report no. GBRA 050309, Westinghouse Reaktor GmbH). Mannheim, Germany. (Unpublished.)

SCHMIDT, A. 2001b. Multiaxial stress states in graphite. (Explanatory report no. GBRA 050310, Westinghouse Reaktor GmbH.) Mannheim, Germany. (Unpublished.)

SCHMIDT, A. 2003. Regulation for the design of the internals of the high temperature reactor. (Explanatory report no. GBRA 065942, Westinghouse Reaktor GmbH, May version.) Mannheim, Germany. (Unpublished).

SGL Carbon Group. 2006. Grade development report for NBG-18. (Report No. SGL-GDR-001, Rev.02.) Bonn. (Unpublished.)

SHIGLEY, J.E., MISCHKE, C.R. & BUDYNAS, R.G. 2004. Mechanical engineering design. 7th ed. New York: McGraw-Hill.

SOCIE, D.F., WAILL, L.A. & DITTMER, D.F. 1985. Biaxial fatigue of Inconel 718 including mean stress effects. (*In* Miller, K.J. & Brown, M.W., *Eds.* Multiaxial fatigue, ASTM STP 853. Philadelphia, PA: ASTM. pp. 463–481.)

SOCIETY OF AUTOMOTIVE ENGINEERS. 1997. Fatigue Design Handbook, AE22. 3rd ed. Warrendale, PA:SAE.

SONSINO, C.M. & GRUBISIC, V. 1985. Fatigue behavior of cyclically softening and hardening steels under multiaxial elastic-plastic deformation. (*In* Miller, K.J. & Brown, M.W., *Eds.* Multiaxial fatigue, ASTM STP 853. Philadelphia, PA: ASTM. pp. 586–605.)

TAYLOR, R., BROWN, R.G., GILCHRIST, K., HALL, E., KELLY, B.T., MORRIS, F. & HODDS, A.T. 1967. The mechanical properties of reactor graphites. U.K.A.E.A. TRG Report 1319 (C), JNPC-MWP(GSG)/P(66)83. Culcheth, U.K.

TUCKER, M.O., ROSE, A.P.G. & BURCHELL, T.D. 1986. The fracture of polygranular graphites. *Carbon*, 24(5):581–602.

VENTER, P.J., MITCHELL, M.N. & FORTIER, F. 2005. PBMR reactor design and development. (*In* 18th International Conference on Structural Mechanics in Reactor Technology. Paper presented at SMiRT-18 held in Beijing on 7 - 12 August. Beijing.

pp. 4452-4466.)

YODA S. & ETO, M. 1983. The tensile deformation behavior of nuclear-grade isotropic graphite posterior to hydrostatic loading. *Journal of Nuclear Materials*, 118:214-219.

YODA, S., ETO, M. & IOKA, I. 1984. Effects of prehydrostatic loading on mechanical and physical properties of nuclear-grade graphites. *Journal of Nuclear Materials*, 125:104–110.

ZUKAS, E.G. & GREEN, W.V. 1971. Creep behaviour of hot isostatically pressed graphite. *Carbon*, 9:341–344.

APPENDIX A

Specimen Allocation Plan

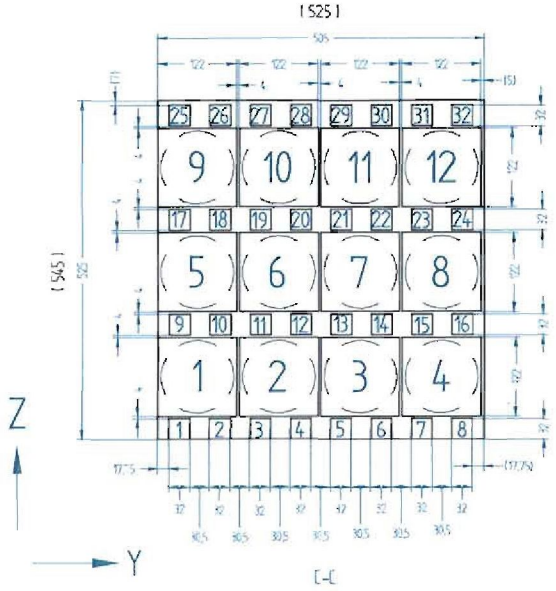
No.	Load Combination	Load Amplitudes	Align	Location	Block	Qty.	# R-values	Total Qty.	Specimen SN			Commissioning							
									R = +1/+1	R = -1/-1		Alignmnt	Strain	Commis	SPARE				
1	R = +1/+1 or -1/-1	1	X	Edge	A	1	2	2	60 F-1	60 F-9		60 F-25		60 F-26					
2	R = +1/+1 or -1/-1	1	X	Centre	A	1	2	2	60 F-3	60 F-11		60 N-16		60 G-6					
3	R = +1/+1 or -1/-1	1	Z	Edge	A	1	2	2	60 N-1	60 N-2		60 G-30		60 N-11					
4	R = +1/+1 or -1/-1	1	Z	Centre	A	1	2	2	60 N-3	60 N-5				61 D-8					
5	R = +1/+1 or -1/-1	1	X	Edge	B	1	2	2	61 A-1	61 A-9									
6	R = +1/+1 or -1/-1	1	X	Centre	B	1	2	2	61 A-3	61 A-11									
7	R = +1/+1 or -1/-1	1	Z	Edge	B	1	2	2	61 D-1	61 D-2									
8	R = +1/+1 or -1/-1	1	Z	Centre	B	1	2	2	61 D-3	61 D-4									
				Total Static Samples				14	R = +0.5				R = +0.0				R = -0.5		
									^2	^3	^4	^5	^2	^3	^4	^5	^2	^3	^4	^5
9	R = +0.5/0/-0.5/-1/-2/-∞/+2	4	X	Edge	A	4	7	28	60 F-17	60 F-24	60 F-2	60 F-8	60 F-10	60 F-16	60 F-18	60 F-23	60 G-1	60 G-8	60 G-17	60 G-16
10	R = +0.5/0/-0.5/-1/-2/-∞/+2	4	X	Centre	A	4	7	28	60 F-6	60 F-14	60 F-28	60 F-29	60 F-4	60 F-5	60 F-12	60 F-13	60 F-20	60 F-21	60 G-3	60 G-11
11	R = +0.5/0/-0.5/-1/-2/-∞/+2	4	Z	Edge	A	4	7	28	60 H-1	60 H-2	60 H-9	60 H-10	60 J-1	60 J-2	60 J-9	60 J-10	60 L-1	60 L-2	60 L-9	60 L-10
12	R = +0.5/0/-0.5/-1/-2/-∞/+2	4	Z	Centre	A	4	7	28	60 H-4	60 H-5	60 H-12	60 H-13	60 H-3	60 H-6	61 H-12	61 H-13	60 J-4	60 J-5	60 J-3	60 J-6
13	R = +0.5/0/-0.5/-1/-2/-∞/+2	4	X	Edge	B	4	7	28	61 A-2	61 A-10	61 A-17	61 B-1	61 A-25	61 B-9	61 B-17	61 B-2	61 B-10	61 B-18	61 B-25	61 A-26
14	R = +0.5/0/-0.5/-1/-2/-∞/+2	4	X	Centre	B	4	7	28	61 A-4	61 A-5	61 A-12	61 A-13	61 A-20	61 A-21	61 B-4	61 B-5	61 B-12	61 B-13	61 A-19	61 A-22
15	R = +0.5/0/-0.5/-1/-2/-∞/+2	4	Z	Edge	B	4	7	28	61 D-9	61 D-10	61 F-1	61 F-2	61 F-9	61 F-10	61 H-1	61 H-2	61 H-9	61 H-10	61 J-1	61 J-2
16	R = +0.5/0/-0.5/-1/-2/-∞/+2	4	Z	Centre	B	4	7	28	61 D-11	61 F-3	61 F-4	61 F-11	61 D-12	61 F-12	61 H-3	61 H-4	60 H-11	60 H-14	61 J-3	61 J-4
				Total Fatigue Samples (Virgin)				224	R = -1											
									^2	^3	^4	^5								
17	R = -1	4	X	Edge	A	4	1	4												
18	R = -1	4	X	Centre	A	4	1	4												
19	R = -1	4	Z	Edge	A	4	1	4												
20	R = -1	4	Z	Centre	A	4	1	4												
21	R = -1	4	X	Edge	A	4	1	4												
22	R = -1	4	X	Centre	A	4	1	4												
23	R = -1	4	Z	Edge	A	4	1	4												
24	R = -1	4	Z	Centre	A	4	1	4												
				Total Fatigue Samples (Isostati				32												

Location	Block	Qty.	# R-values	Total Qty.															
Edge	A	1	2	2															
Centre	A	1	2	2															
Edge	A	1	2	2															
Centre	A	1	2	2															
Edge	B	1	2	2															
Centre	B	1	2	2															
Edge	B	1	2	2															
Centre	B	1	2	2															
Total Static Samples				14	R = -1				R = -2				R = -∞				R = +2			
					^2	^3	^4	^5	^2	^3	^4	^5	^2	^3	^4	^5	^2	^3	^4	^5
Edge	A	4	7	28	60 G-2	60 G-9	60 G-18	60 G-7	60 G-15	60 G-24	60 G-10	60 G-23	60 G-25	60 G-26	60 F-7	60 F-15	60 G-31	60 G-32	60 F-31	60 F-32
Centre	A	4	7	28	60 G-14	60 G-19	60 G-22	60 G-4	60 G-5	60 G-12	60 G-13	60 G-20	60 G-21	60 G-28	60 G-29	60 F-19	60 F-22	60 F-27	60 F-30	60 G-27
Edge	A	4	7	28	60 H-7	60 H-8	60 H-15	60 H-16	60 N-8	60 J-7	60 J-8	60 J-15	60 J-16	60 L-7	60 L-8	60 L-15	60 L-16	60 N-9	60 N-10	60 N-7
Centre	A	4	7	28	60 J-12	60 J-13	60 J-11	60 J-14	60 L-4	60 L-5	60 L-3	60 L-6	60 L-12	60 L-13	60 L-11	60 L-14	60 N-4	60 N-6	60 N-12	60 N-13
Edge	B	4	7	28	61 A-18	61 B-26	61 A-8	61 A-16	61 A-24	61 A-31	61 A-23	61 A-32	61 A-7	61 A-15	61 B-32	61 B-7	61 B-15	61 B-23	61 B-8	61 B-16
Centre	B	4	7	28	61 B-20	61 B-21	61 B-3	61 B-6	61 B-11	61 B-14	61 B-19	61 B-22	61 A-6	61 A-14	61 A-28	61 A-29	61 B-27	61 B-28	61 B-29	61 B-30
Edge	B	4	7	28	61 J-9	61 J-10	61 D-15	61 D-16	61 F-7	61 F-8	61 F-15	61 F-16	61 H-7	61 H-8	61 H-15	61 H-16	61 J-7	61 J-8	61 J-15	61 J-16
Centre	B	4	7	28	61 J-11	61 J-12	61 D-5	61 D-13	61 D-14	61 F-5	61 F-6	61 F-13	61 F-14	61 H-5	61 H-6	61 H-11	61 H-14	61 J-5	61 J-6	61 J-13
Total Fatigue Samples (Virgin)				224																
Edge	A	4	1	4																
Centre	A	4	1	4																
Edge	A	4	1	4																
Centre	A	4	1	4																
Edge	A	4	1	4																
Centre	A	4	1	4																
Edge	A	4	1	4																
Centre	A	4	1	4																
Total Fatigue Samples (Isostati				32																

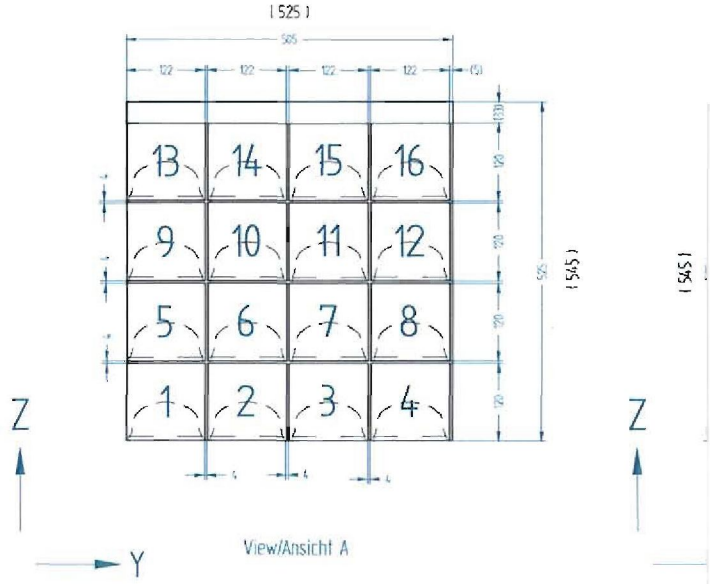
No.	Load Combination	Load Amplitudes	Align	Location	Block	Qty.	# R-values	Total Qty.	Specimen SN			Commissioning							
									R = +1/+1	R = -1/-1		SCRAP	Commiss	SPARE					
1	R = +1/+1 or -1/-1	1	X	Edge	A	1	2	2	79 F1-1	79 D-9			79 B-9	79 A-9					
2	R = +1/+1 or -1/-1	1	X	Centre	A	1	2	2	79 F1-2	79 F1-6		79 G1-12	79 B-10	37 E-3					
3	R = +1/+1 or -1/-1	1	Z	Edge	A	1	2	2	79 O-1	79 O-5		79 G1-3		37 C-16					
4	R = +1/+1 or -1/-1	1	Z	Centre	A	1	2	2	79 O-2	79 O-3		37 K-15	79 A-12	37 E-8					
5	R = +1/+1 or -1/-1	1	X	Edge	B	1	2	2	37 A1-1	37 A1-5			79 F1-5						
6	R = +1/+1 or -1/-1	1	X	Centre	B	1	2	2	37 A1-2	37 A1-6			79 A-16	79 I-11					
7	R = +1/+1 or -1/-1	1	Z	Edge	B	1	2	2	37 E-1	37 E-5			79 F2-3						
8	R = +1/+1 or -1/-1	1	Z	Centre	B	1	2	2	37 E-2	37 E-6				37 E-14					
									79 E-9	79 A-10									
									79 B-12										
					Total Static Samples			14	R = +0.5				R = +0.0				R = -0.5		
									^2	^5	^4	^3	^2	^3	^4	^5	^4	^3	^2	^5
9	R = +0.5/0/-0.5/-1/-2/-∞/+2	4	X	Edge	A	4	7	28	79 F1-9	79 F2-4	79 F2-1	79 F1-12	79 F2-5	79 F2-8	79 F2-9	79 F2-12	79 G1-1	79 G1-4	79 G1-9	79 G1-8
10	R = +0.5/0/-0.5/-1/-2/-∞/+2	4	X	Centre	A	4	7	28	79 F1-3	79 F1-7	79 F1-10	79 F1-11	79 F2-2	79 B-14	79 F2-6	79 F2-7	79 F2-10	79 F2-11	79 G1-2	79 G1-6
11	R = +0.5/0/-0.5/-1/-2/-∞/+2	4	Z	Edge	A	4	7	28	79 I-1	79 I-5	79 I-9	79 I-13	79 K-1	79 K-5	79 K-9	79 K-13	79 M-1	79 M-5	79 M-9	79 M-13
12	R = +0.5/0/-0.5/-1/-2/-∞/+2	4	Z	Centre	A	4	7	28	79 I-6	79 I-7	79 I-10	79 O-15	79 I-2	79 I-3	79 I-14	79 I-15	79 K-3	79 E-11	79 K-6	79 K-7
13	R = +0.5/0/-0.5/-1/-2/-∞/+2	4	X	Edge	B	4	7	28	37 A2-1	37 A2-5	37 A2-9	37 B1-1	37 A1-9	37 B1-5	37 B1-9	37 B2-1	37 B2-5	37 B2-9	37 C-1	37 C-5
14	R = +0.5/0/-0.5/-1/-2/-∞/+2	4	X	Centre	B	4	7	28	37 A2-2	37 A2-3	37 A2-6	37 A2-7	37 A2-10	37 A2-11	37 B1-2	37 B1-3	37 B1-6	37 B1-7	37 A1-10	37 A1-11
15	R = +0.5/0/-0.5/-1/-2/-∞/+2	4	Z	Edge	B	4	7	28	37 E-9	37 E-13	37 G-1	37 G-5	37 G-9	37 G-13	37 I-1	37 I-5	37 I-9	37 I-13	37 K-1	37 K-5
16	R = +0.5/0/-0.5/-1/-2/-∞/+2	4	Z	Centre	B	4	7	28	79 A-11	37 G-2	37 G-6	37 G-10	37 E-10	37 G-14	37 I-2	37 I-6	37 I-10	37 I-14	37 K-2	37 K-6
				Total Fatigue Samples (Virgin)				224								79 G1-5		37 E-4	79 D-12	
																	0.77	0.82	0.85	0.72
									R = -1											
									^2	^3	^4	^5			R = +1/+1	R = -1/-1				
17	R = -1	4	X	Edge	A	4	1	4	79 B-1	79 B-5	79 B-4	79 B-8			37 C-12	79 D-16				
18	R = -1	4	X	Centre	A	4	1	4	79 B-2	79 B-3	79 B-6	79 B-7			79 D-10	79 D-15				
19	R = -1	4	Z	Edge	A	4	1	4	79 A-1	79 A-5	79 A-4	79 A-8			79 O-16	79 E-13				
20	R = -1	4	Z	Centre	A	4	1	4	79 A-2	79 A-3	79 A-6	79 A-7			79 E-14	79 O-14				
21	R = -1	4	X	Edge	A	4	1	4	79 D-1	79 D-4	79 D-5	79 D-8			79 D-13	79 B-16				
22	R = -1	4	X	Centre	A	4	1	4	79 D-2	79 D-3	79 D-6	79 D-7			79 D-11	79 C-15				
23	R = -1	4	Z	Edge	A	4	1	4	79 E-1	79 E-5	79 E-4	79 E-8			79 E-16	79 A-13				
24	R = -1	4	Z	Centre	A	4	1	4	79 E-2	79 E-3	79 E-6	79 E-7			79 E-15	79 A-15				
				Total Fatigue Samples (Isostati				32				79 E-12			79 B-11	79 A-14				

Location	Block	Qty.	# R-values	Total Qty.																	
Edge	A	1	2	2																	
Centre	A	1	2	2																	
Edge	A	1	2	2																	
Centre	A	1	2	2																	
Edge	B	1	2	2																	
Centre	B	1	2	2																	
Edge	B	1	2	2																	
Centre	B	1	2	2																	
	Total Static Samples			14	R = -1				R = -2				R = -∞			0.9	R = +2				
					^2	^4	^3	^5	^2	^3	^4	^5	^5	^2	^3	^4	^3	^2	^5	^4	
Edge	A	4	7	28	79 G2-1	79 G2-5	79 G2-9	79 G2-4	79 G2-8	79 G2-12	79 C-1	79 C-5	79 C-9	79 C-13	79 C-4	79 C-8	79 C-12	79 C-16	79 F1-8	79 F1-4	
Centre	A	4	7	28	79 G1-7	79 G1-10	79 G1-11	79 G2-2	79 G2-3	79 G2-6	79 G2-7	79 G2-10	79 G2-11	79 C-2	79 C-3	79 C-6	79 C-7	79 C-10	79 C-14	79 C-11	
Edge	A	4	7	28	79 I-4	79 I-8	79 I-12	79 I-16	79 O-4	79 K-4	79 K-8	79 K-12	79 K-16	79 M-4	79 M-8	79 M-12	79 M-16	79 O-12	79 O-13	79 O-8	
Centre	A	4	7	28	79 K-10	79 K-11	79 K-14	79 K-15	79 M-2	79 M-3	79 M-6	79 M-7	79 M-10	79 M-11	79 M-14	37 G-15	79 O-6	79 O-7	79 O-10	79 O-11	
Edge	B	4	7	28	37 C-9	37 C-13	37 A1-4	37 A1-8	37 A1-12	37 A2-4	37 A2-8	37 A2-12	37 B1-4	37 B1-8	37 B1-12	37 B2-4		37 B2-12	37 C-8	37 C-4	37 B2-8
Centre	B	4	7	28	37 B1-10	37 B1-11	37 B2-2	37 B2-3	37 B2-6	37 B2-7	37 B2-10	37 B2-11	37 C-2	37 C-3	37 C-6	37 C-7	37 C-10	37 C-11	37 C-14	37 C-15	
Edge	B	4	7	28	37 K-9	37 K-13	37 E-12	37 E-16	37 G-4	37 G-8	37 G-12	37 G-16	37 I-4	37 I-8	37 I-12	37 I-16	37 K-4	37 K-8	37 K-12	79 O-9	
Centre	B	4	7	28	37 K-10	37 K-14	37 E-7	37 E-11	37 E-15	37 G-3	37 G-7	37 G-11	79 K-2	37 I-3	37 I-7	37 I-11		37 K-3	37 K-11	37 K-7	37 I-15
Total Fatigue Samples (Virgin)				224										79 M-15			1		0.8		0.92
					0.85	0.73	0.8	0.67								0.9					
											37 A1-7										
Edge	A	4	1	4																	
Centre	A	4	1	4																	
Edge	A	4	1	4																	
Centre	A	4	1	4									37 K-16								
Edge	A	4	1	4																	
Centre	A	4	1	4																	
Edge	A	4	1	4																	
Centre	A	4	1	4																	
Total Fatigue Samples (Isostati				32																	

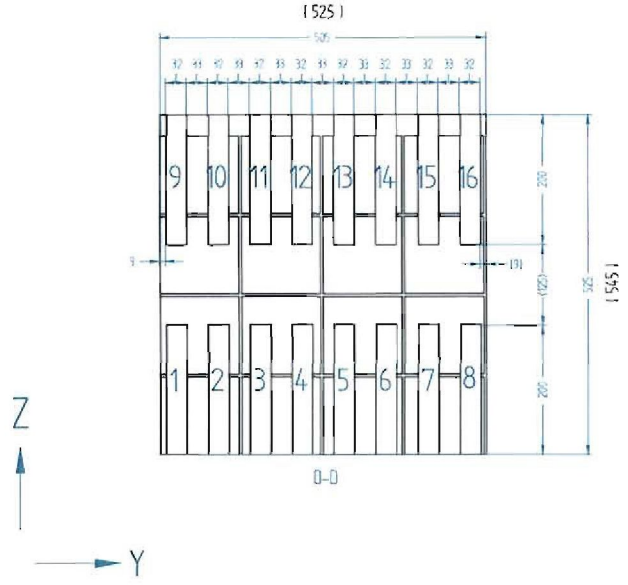
Section F; G;
(F1; F2) (G1; G2)



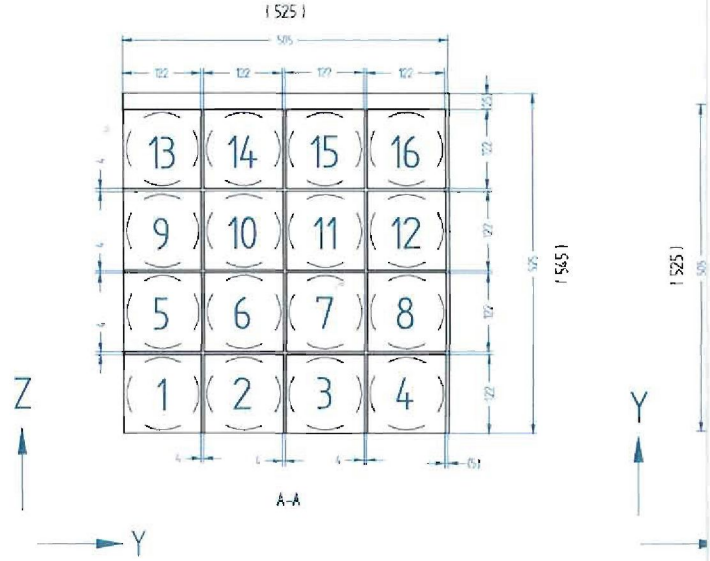
Section A; E;
and I; K; M; O.



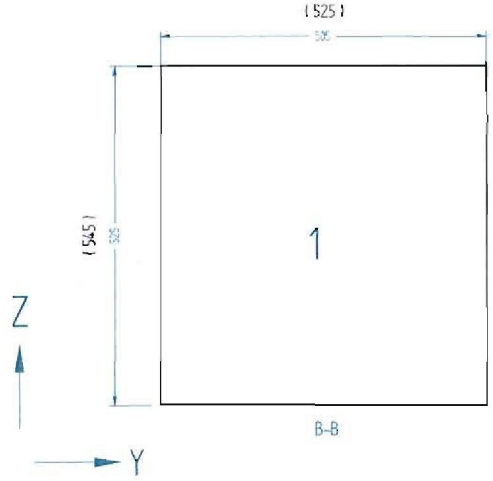
Section H; J; L; N;



Section B, C; D;

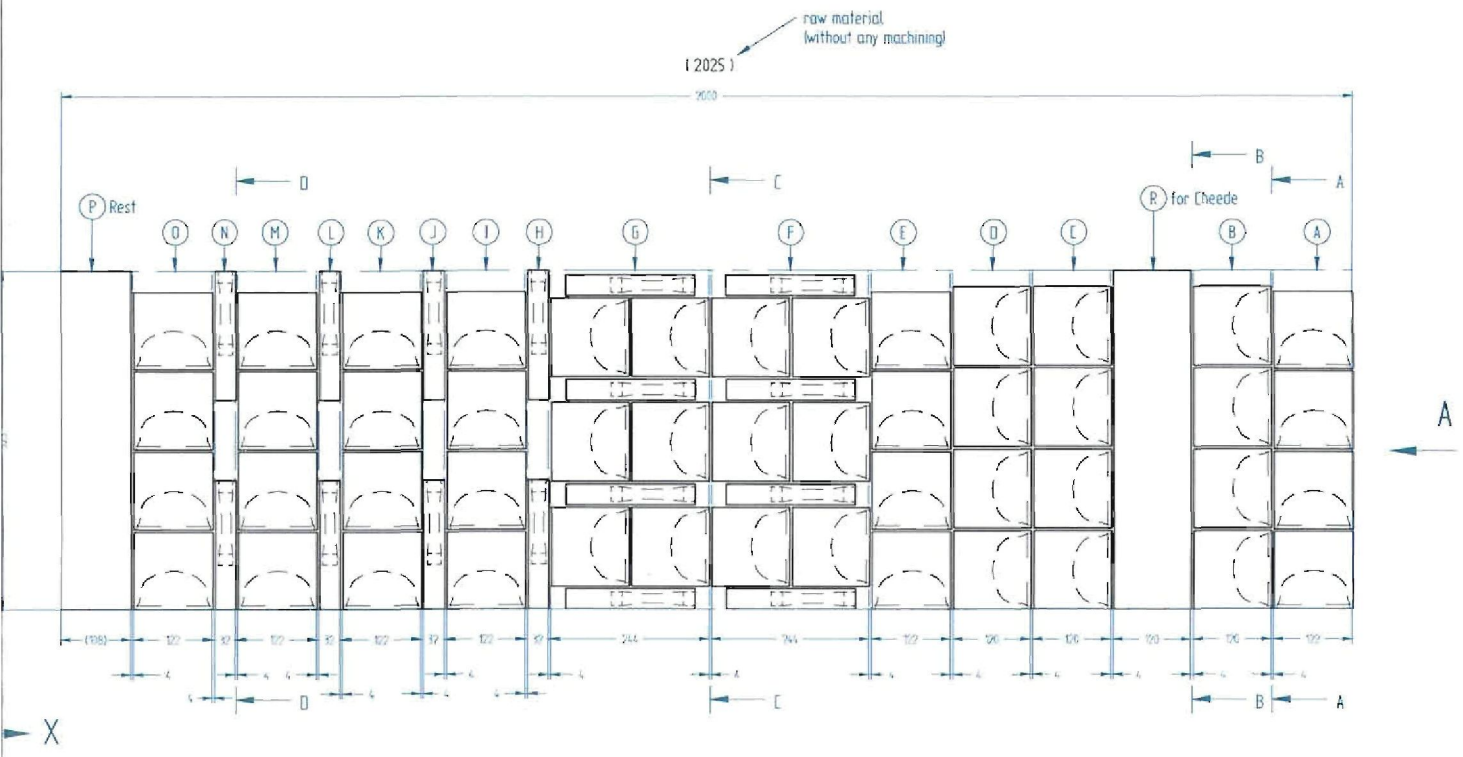


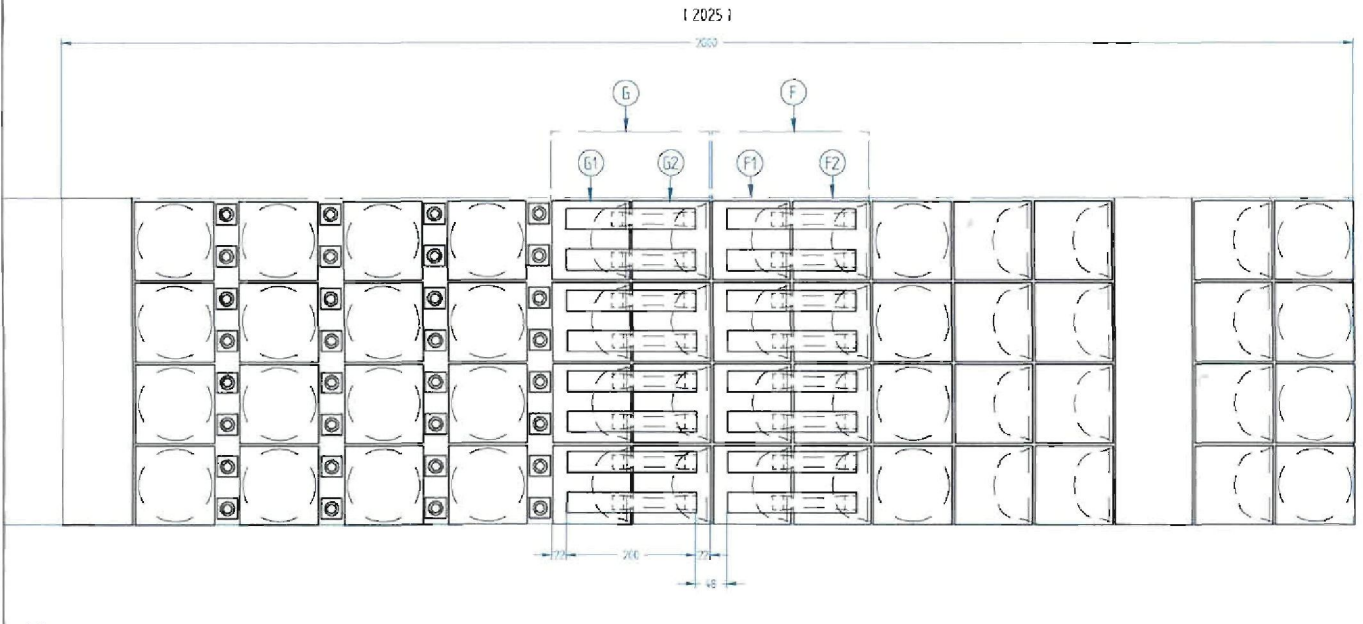
Section R for Chedde

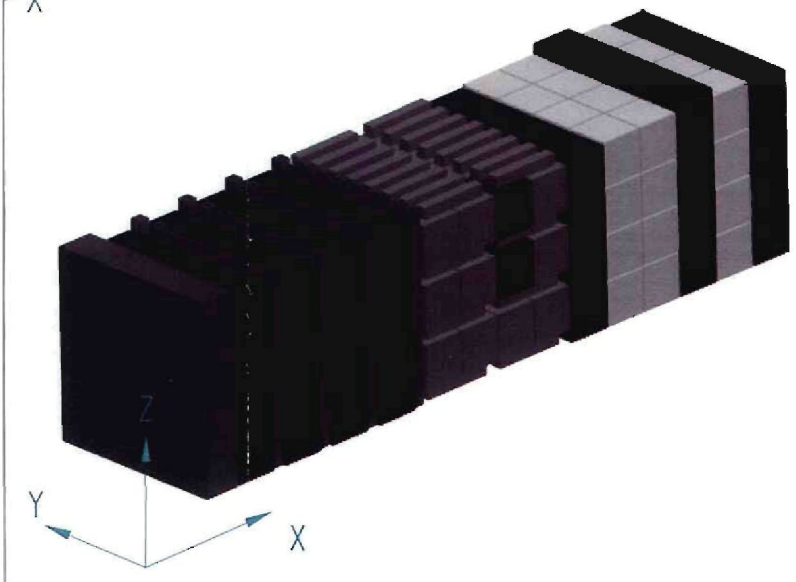


TEILE-GRAVUR IMMER IN X-RICHTUNG

PART ENGRAVING ALWAYS IN X-DIRECTION





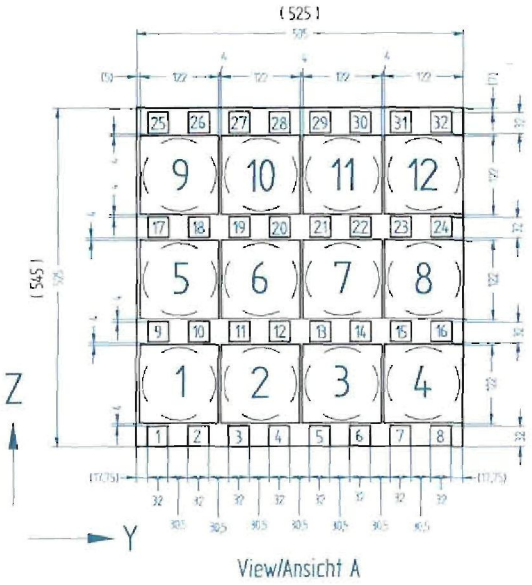


50

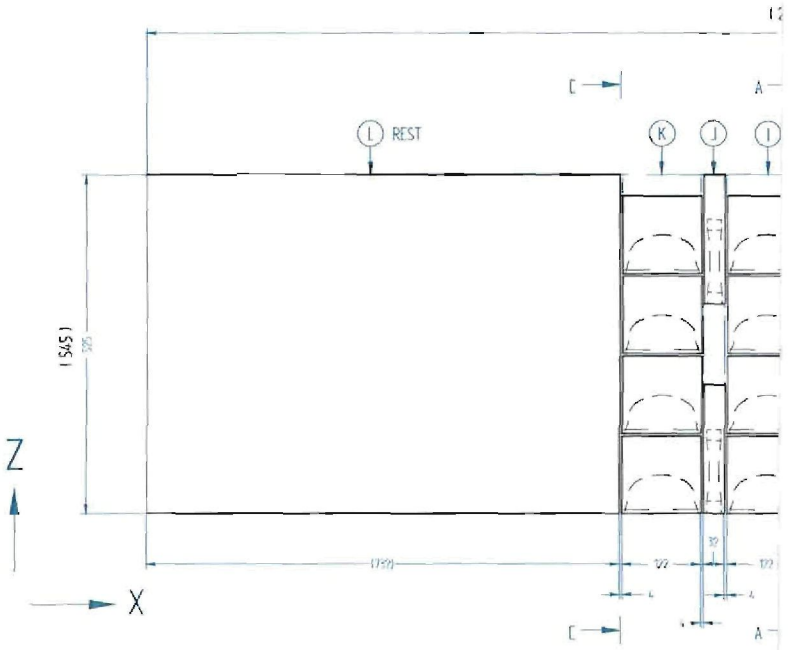
freigegeben/released

Material

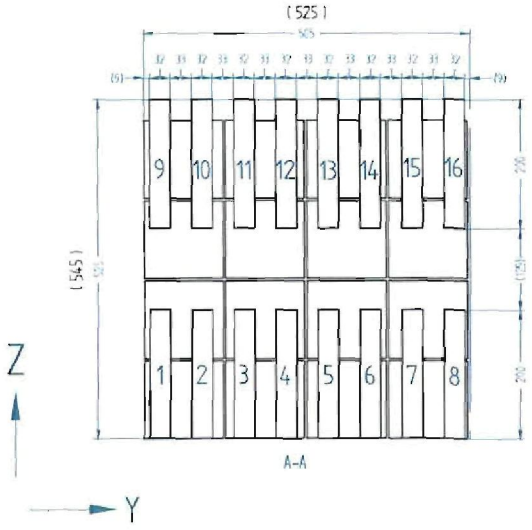
Section A; B;
(A1; A2) (B1; B2)

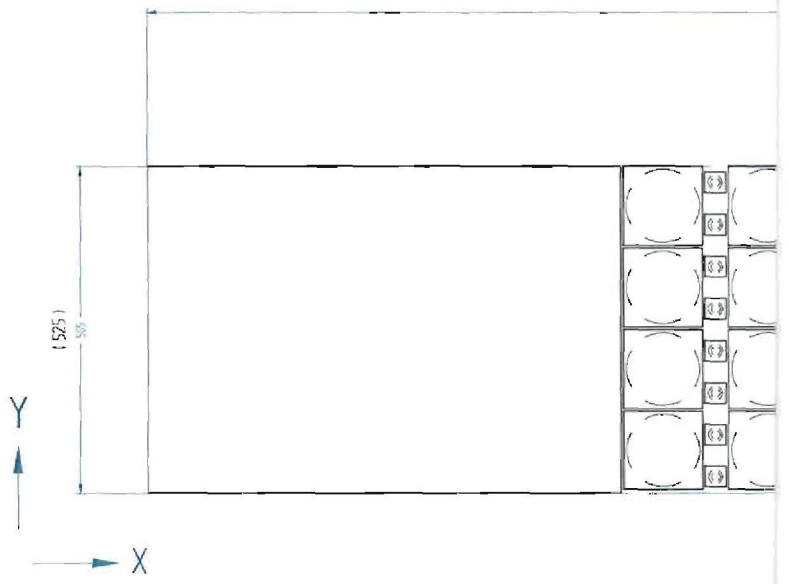


View/Ansicht A



Section D; F; H; J



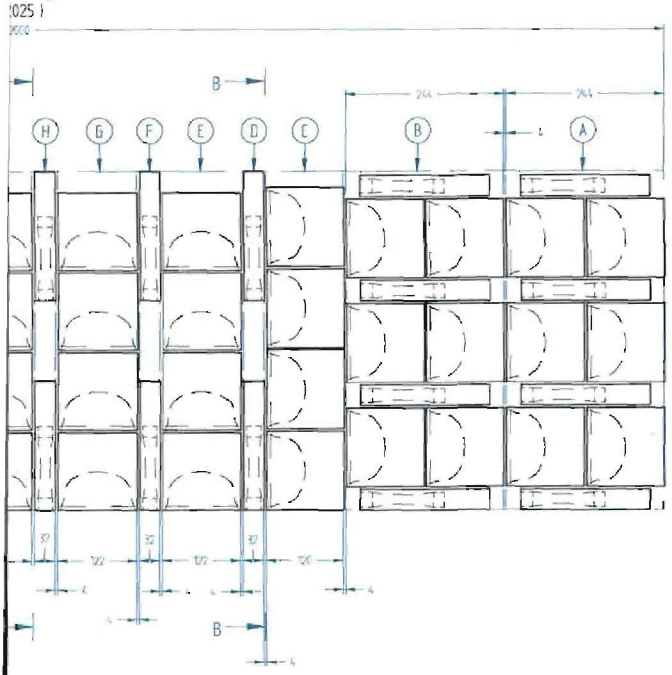


TEILE-GRAVUR IMMER IN X-RICHTUNG

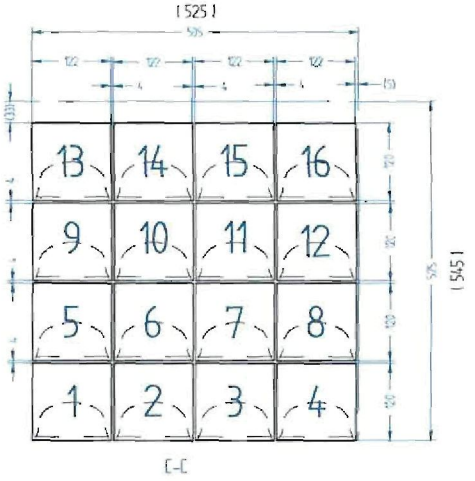
PART ENGRAVING ALWAYS IN X-DIRECTION



raw material
(without any machining)



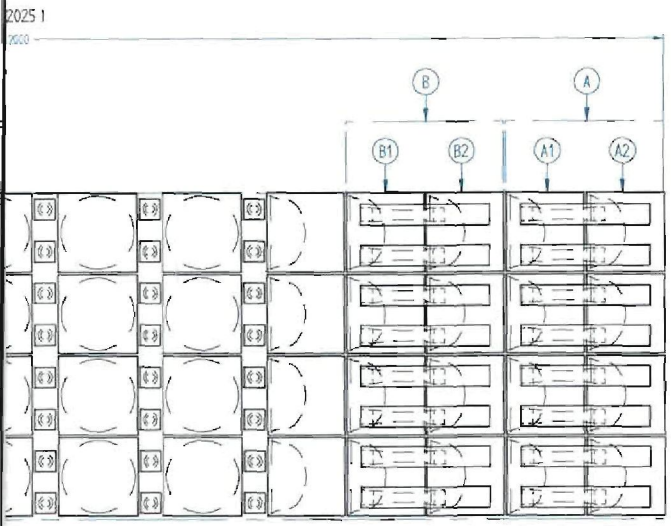
Section E; G; I; K



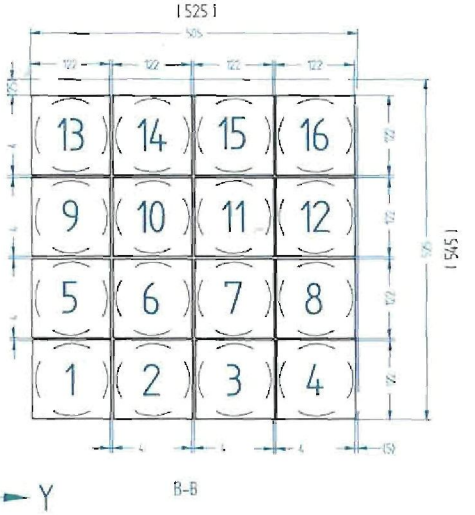
A

Z

Y

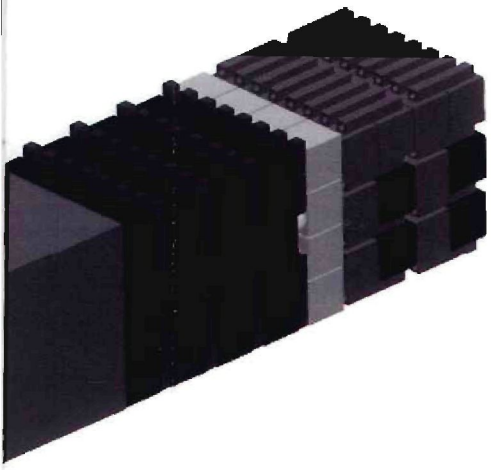


Section C



Z

Y



X

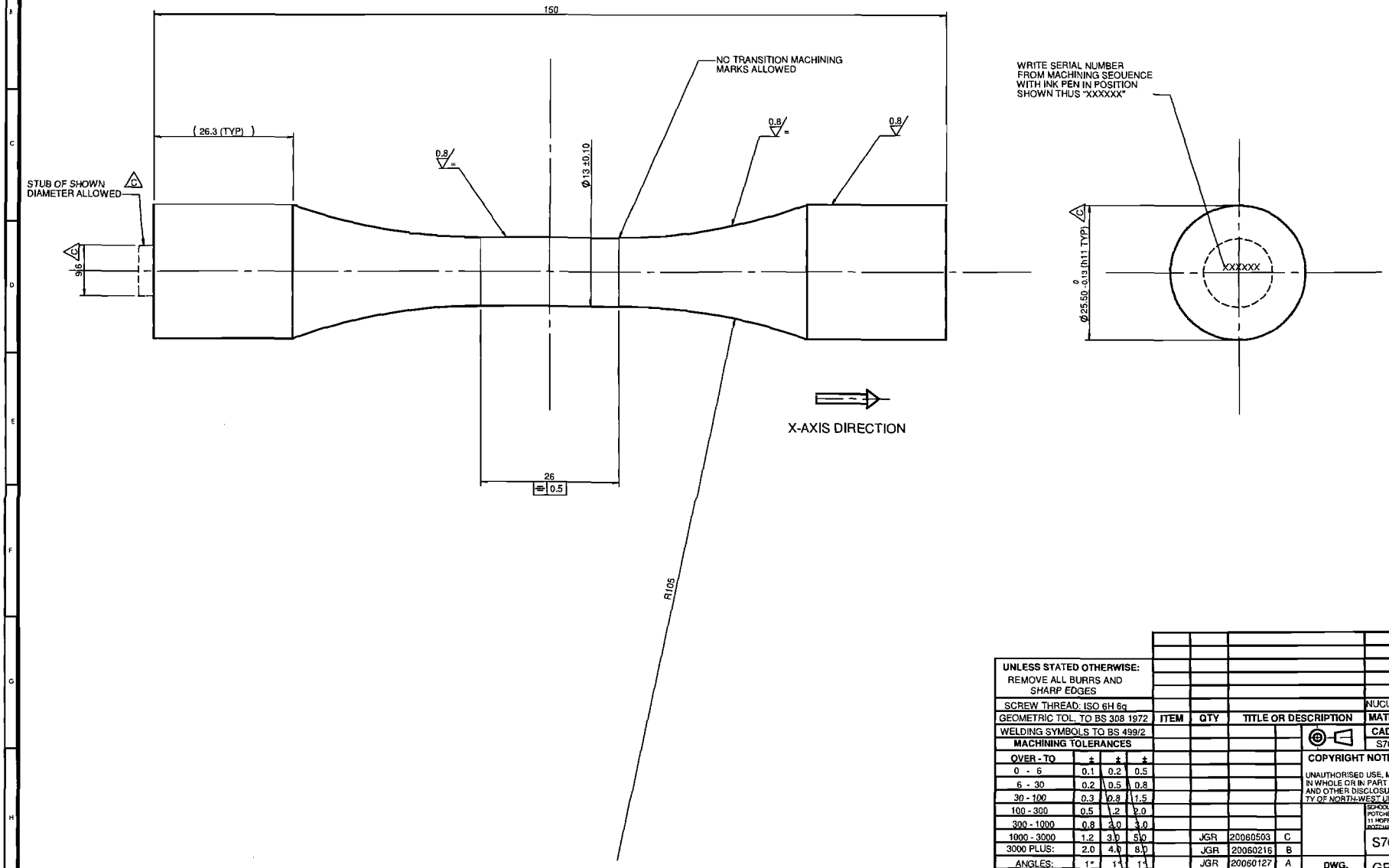
50

freigegeben/released

Material				
		Datum / Date	Name	Name
		07.06.2006	Pesic	Pesic
		Bearbeitet / Drawn	Pesic	06.06.2006
		Geprüft / Approved	Pesic	06.06.2006
		Benennung / Title: CUT LAYOUT B		
		Schutzvermerk / Copyright DIN 34-1		
		SGL CARBON GROUP		
		Sach-Zeichn.-Nr. / SGL-Drawing-No.: 108506		
		Blatt / Sheet: 1	von / of: 1	Rev.: 01

APPENDIX B

Drawings



UNLESS STATED OTHERWISE: REMOVE ALL BURRS AND SHARP EDGES			
SCREW THREAD: ISO 6H 6g			
GEOMETRIC TOL. TO BS 308 1972			
WELDING SYMBOLS TO BS 499/2			
MACHINING TOLERANCES			
OVER - TO	±	±	±
0 - 6	0.1	0.2	0.5
6 - 30	0.2	0.5	0.8
30 - 100	0.3	0.8	1.5
100 - 300	0.5	1.2	2.0
300 - 1000	0.8	2.0	3.0
1000 - 3000	1.2	3.0	5.0
3000 PLUS:	2.0	4.0	8.0
ANGLES:	1°	1°	1°
SURFACE FIN:	1.6	6.3	12.5

ITEM	QTY	TITLE OR DESCRIPTION	APPR.	DRAWN	DATE	REV.
				JGR	20060503	C
				JGR	20060216	B
				JGR	20060127	A

NUCLEAR GRAPHITE, NBG18 [SGL]

MATERIAL/DRAWING -/PART No

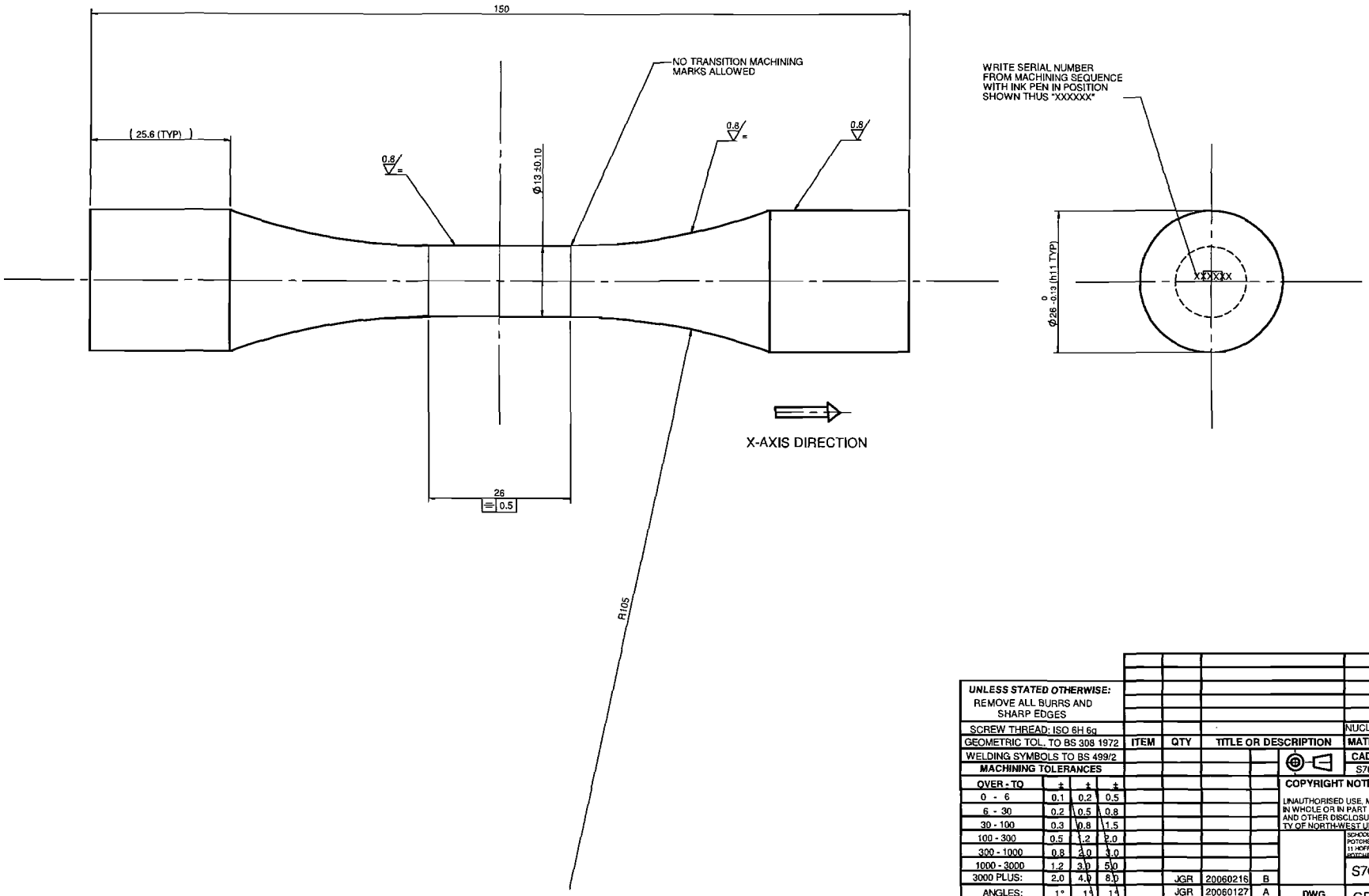
CAD FILENAME: S70 | SCALE: 2 : 1

COPYRIGHT NOTICE:
UNAUTHORISED USE, MANUFACTURE OR REPRODUCTION IN WHOLE OR IN PART IS PROHIBITED. DRAWING, DESIGN AND OTHER DISCLOSURES IS THE INTELLECTUAL PROPERTY OF NORTH-WEST UNIVERSITY. ALL RIGHTS RESERVED.

SCHOOL FOR MECHANICAL AND MATERIALS ENGINEERING
POTCHEFSTROOM CAMPUS OF NW-U
11 HOFFMAN STREET
POTCHEFSTROOM 2520

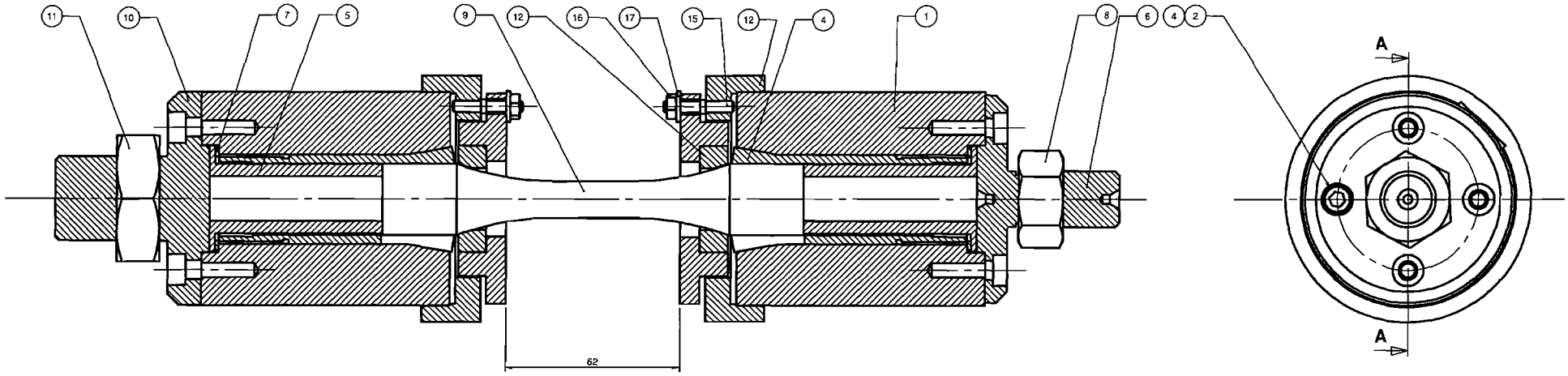
S70 ASTM E 466

DWG. No. GRA-S70-02 | C



UNLESS STATED OTHERWISE: REMOVE ALL BURRS AND SHARP EDGES									NUCLEAR GRAPHITE, NBG18 [SGL]	
SCREW THREAD: ISO 6H 6g									**MATERIAL/DRAWING -/PART No**	
GEOMETRIC TOL. TO BS 308 1972				ITEM	QTY	TITLE OR DESCRIPTION				
WELDING SYMBOLS TO BS 499/2									**CAD FILENAME:**	**SCALE:**
MACHINING TOLERANCES									S70	2 : 1
OVER - TO	±	±	±						**COPYRIGHT NOTICE:**	
0 - 6	0.1	0.2	0.5						UNAUTHORISED USE, MANUFACTURE OR REPRODUCTION IN WHOLE OR IN PART IS PROHIBITED. DRAWING, DESIGN AND OTHER DISCLOSURES IS THE INTELLECTUAL PROPERTY OF NORTH-WEST UNIVERSITY. ALL RIGHTS RESERVED.	
6 - 30	0.2	0.5	0.8							
30 - 100	0.3	0.8	1.5							
100 - 300	0.5	1.2	2.0						SCHOOL FOR MECHANICAL AND MATERIALS ENGINEERING, POTCHEFSTROOM CAMPUS OF NW-U, 11 HOFFMAN STREET, POTCHEFSTROOM 2520	
300 - 1000	0.8	2.0	3.0							
1000 - 3000	1.2	3.0	5.0						S70 ASTM E 466	
3000 PLUS:	2.0	4.0	8.0		JGR	20060216	B			
ANGLES:	1°	1°	1°		JGR	20060127	A	**DWG. No.**	GRA-S70-02	B
SURFACE FIN:	1.6	6.3	12.5	APPR.	DRAWN	DATE	REV.			

B-2



SECTION A-A

ITEM	QTY	TITLE OR DESCRIPTION	MATERIAL/DRAWING -/PART No
17	6	WASHER, SPRING, M5	
16	6	NUT, M5	GR. 8
15	6	GRUB SCREW, M5 x 25	GR. 8.8
14	2	TENSION CLAMP 2	GRA-S70-22-02
13	2	THRUST CAP 2	GRA-S70-24-02
12	2	THRUST RING	GRA-S70-26-02
11	1	NUT, HALF, M30 x 2	GR. 8
10	1	2CC TO CYL.ROD	GRA-S70-14-02
9	1	S70 ASTM E 466	GRA-S70-02
8	1	NUT, M20 x 1.5	GR. 8
7	2	WAVED WASHER, EPL 31	36.5 x 30 x 0.38 (3 WAVE)
6	1	2CC TO LOADCELL	GRA-S70-12-02
5	2	SPECIMEN STOP	GRA-S70-10-02
4	AR	SCREW LOCK COMPOUND	LOCTITE 243
3	2	COLLET, 5C, 26 DIA	L385E/385E-R26-5C-COLLET
2	8	SHC SCREW, 1/4 x 1	HIGH TENSILE
1	2	2CC COLLET CHUCK	KALAMAZOO INDUSTRIES

UNLESS STATED OTHERWISE:
REMOVE ALL BURRS AND SHARP EDGES

SCREW THREAD: ISO 6H 6g

GEOMETRIC TOL. TO BS 308 1972

WELDING SYMBOLS TO BS 499/2

MACHINING TOLERANCES

OVER - TO	±	±	±
0 - 6	0.1	0.2	0.5
6 - 30	0.2	0.5	0.8
30 - 100	0.3	0.8	1.5
100 - 300	0.5	1.2	2.0
300 - 1000	0.8	2.0	3.0
1000 - 3000	1.2	3.0	5.0
3000 PLUS:	2.0	4.0	8.0
ANGLES:	1°	1°	1°
SURFACE FIN:	1.6	6.3	12.5

CAD FILENAME: UNIAXIAL_GRIP'A

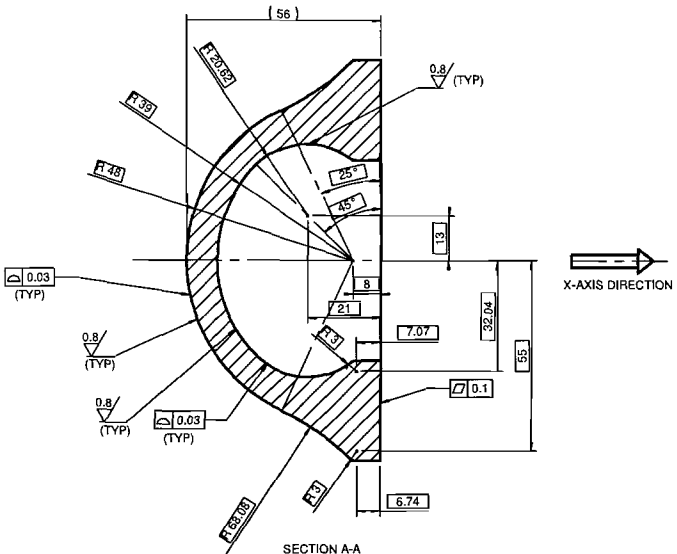
SCALE: 1 : 1

COPYRIGHT NOTICE:
UNAUTHORISED USE, MANUFACTURE OR REPRODUCTION IN WHOLE OR IN PART IS PROHIBITED. DRAWING, DESIGN AND OTHER DISCLOSURES IS THE INTELLECTUAL PROPERTY OF NORTHWEST UNIVERSITY. ALL RIGHTS RESERVED.

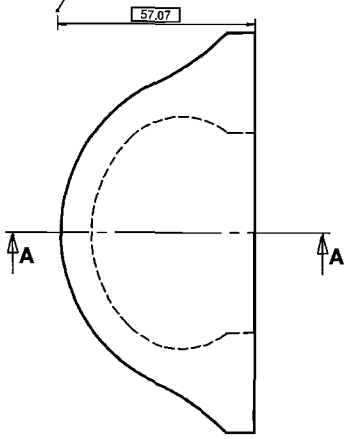
SCHOOL OF MECHANICAL ENGINEERING
POTCHEFSTROOM CAMPUS OF NW-U
11 HOFFMAN STREET
POTCHEFSTROOM 2520

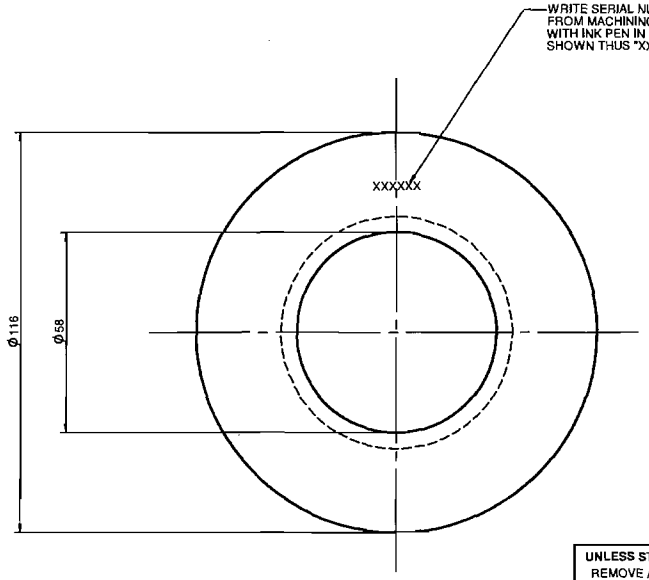
UNIAXIAL GRIP ASSY

APPR.	DRAWN	DATE	REV.	DWG. No.
	JGR	20070129	A	GRA-S70-28-03 A



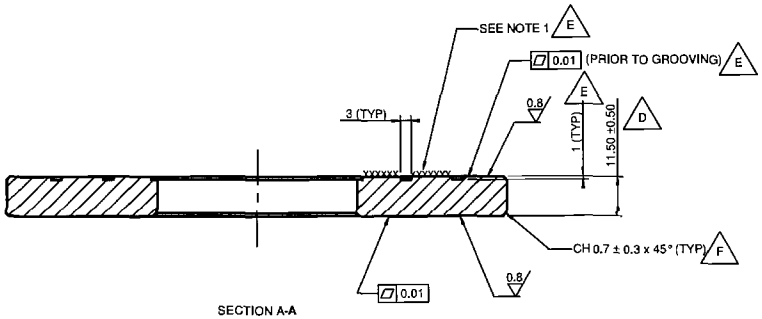
SECTION A-A



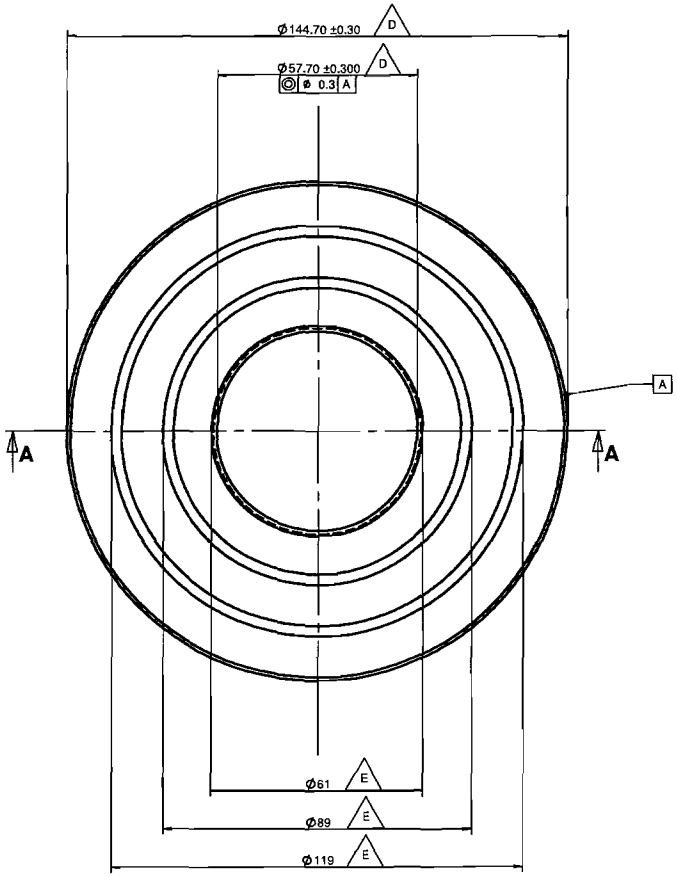


UNLESS STATED OTHERWISE: REMOVE ALL BURRS AND SHARP EDGES								GRAPHITE, NBG-18 (SGL)	
SCREW THREAD: ISO 6H 6g									
GEOMETRIC TOL. TO BS 308 1972				*ITEM*	*QTY*	*TITLE OR DESCRIPTION*		*MATERIAL/DRAWING -/PART No*	
WELDING SYMBOLS TO BS 499/2								*CAD FILENAME:*	*SCALE:*
MACHINING TOLERANCES								S60B	1 : 1
OVER - TO	±	±	±					**COPYRIGHT NOTICE:**	
0 - 6	0.1	0.2	0.5					UNAUTHORISED USE, MANUFACTURE OR REPRODUCTION IN WHOLE OR IN PART IS PROHIBITED. DRAWING, DESIGN AND OTHER DISCLOSURES IS THE INTELLECTUAL PROPERTY OF NORTH-WEST UNIVERSITY. ALL RIGHTS RESERVED.	
6 - 30	0.2	0.5	0.8						
30 - 100	0.3	0.8	1.5						
100 - 300	0.5	1.2	2.0						
300 - 1000	0.8	2.0	3.0						
1000 - 3000	1.2	3.0	5.0					SCHOOL FOR MECHANICAL AND MATERIALS ENGINEERING POTCHEFSTROOM CAMPUS OF NW-U 11 HOFFMAN STREET POTCHEFSTROOM 2531	
3000 PLUS:	2.0	4.0	8.0		JGR	20060216	B	S60B	
ANGLES:	1°	1°	1°		JGR	20050916	A	DWG. No. GRA-S60B-08-02	B
SURFACE FIN:	1.6	6.3	12.5	APPR.	DRAWN	DATE	REV.		

8-4



SECTION A-A



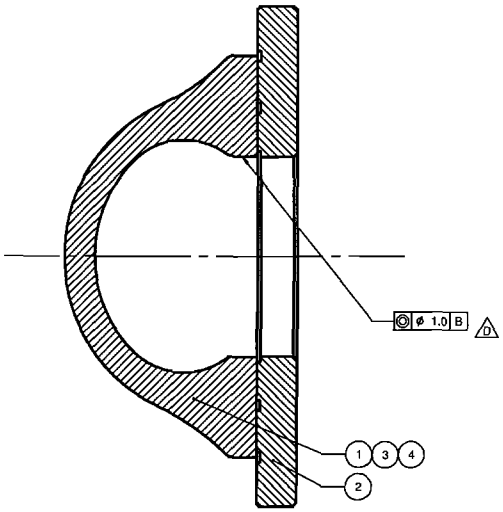
NOTES: E

1. ROUGHEN BY SANDING WITH P40 GRIT SANDING PAPER
2. DEGREASE AND PAINT WITH DEOXIDINE TO INHIBIT CORROSION

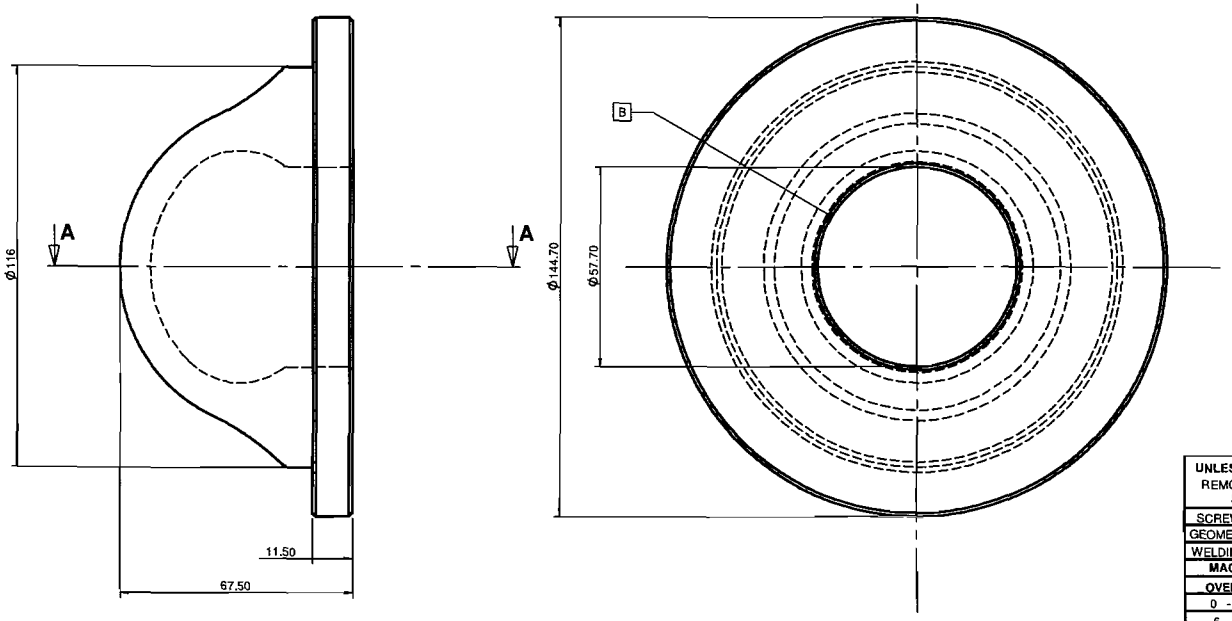
UNLESS STATED OTHERWISE: REMOVE ALL BURRS AND *SHARP EDGES*									
SCREW THREAD: ISO 6H 6g								SABS 300WA LC PLATE, 12 THK	
GEOMETRIC TOL. TO BS 308 1972	ITEM	QTY	TITLE OR DESCRIPTION					MATERIAL/DRAWING -/PART No	
WELDING SYMBOLS TO BS 499/2								CAD FILENAME:	SCALE:
MACHINING TOLERANCES								S60B_BASE'F	1 : 1
OVER - TO	±	±	±					COPYRIGHT NOTICE:	
0 - 6	0.1	0.2	0.5					UNAUTHORISED USE, MANUFACTURE OR REPRODUCTION IN WHOLE OR IN PART IS PROHIBITED. DRAWING, DESIGN AND OTHER DISCLOSURES IS THE INTELLECTUAL PROPERTY OF NORTH-WEST UNIVERSITY. ALL RIGHTS RESERVED.	
6 - 30	0.2	0.5	0.8						
30 - 100	0.3	0.8	1.5		JGR	20060615	F		
100 - 300	0.5	1.2	2.0		JGR	20060424	E		
300 - 1000	0.8	2.0	3.0		JGR	20060224	D		
1000 - 3000	1.2	3.0	5.0		JGR	20060119	C		
3000 PLUS:	2.0	4.0	8.0		JGR	20060118	B		
ANGLES:	1°	1°	1°		JGR	20051005	A		
SURFACE FIN:	1.6	6.3	12.5	APPR.	DRAWN	DATE	REV.	DWG. No.	GRA-S60B-10-02 F

SCHOOL FOR MECHANICAL AND MATERIALS ENGINEERING
POTCHEFSTROOM CAMPUS OF NW-U
11 HOFFMAN STREET
POTCHEFSTROOM 2520

S60B BASE



SECTION A-A



NOTES: C

1. WASH ITEM 1 IN DISHWASHING SOAP AND DRY FOR 4 HOURS @ 60°C.
2. CLEAN BONDING SURFACE OF ITEM 2 WITH ACETONE.
3. APPLY MIXED EPOXY EVENLY ONTO BONDING SURFACE OF ITEM 1 WITH MIXING SPATULA.
4. DISTRIBUTE EPOXY IN BOND EVENLY BY PERFORMING SMALL ORBITAL MOTIONS WITH ITEM 1 RELATIVE TO ITEM 2, WHILE PRESSING.
5. ALIGN ITEMS 1 AND 2 AS SPECIFIED AND LEAVE 15 MIN.TO SET.
6. CURE FOR 24 HOURS @ ROOM TEMPERATURE BEFORE SEALING.
7. SEAL INNER SURFACE OF ITEM 1 FIRST BY ROTATING IN LATHE AT 30 r/min.
8. SEAL OUTER SURFACE OF ITEM 2 AND CLEAN SEALING SURFACE 11mm WIDE FROM OUTER DIAMETER.

D

ITEM	QTY	TITLE OR DESCRIPTION	MATERIAL/DRAWING -/PART No
4	45 ml	SEALANT RTV	SPIREX RED GASKET MAKER
3	5 ml	EPOXY	PRATLEY STEEL, QUICKSET
2	1	S60B BASE	GRA-S60B-10-02
1	1	S60B	GRA-S60B-08-02

UNLESS STATED OTHERWISE: REMOVE ALL BURRS AND SHARP EDGES
SCREW THREAD: ISO 6H 6g
GEOMETRIC TOL. TO BS 308 1972
WELDING SYMBOLS TO BS 499/2
MACHINING TOLERANCES

OVER - TO	±	±	±
0 - 6	0.1	0.2	0.5
6 - 30	0.2	0.5	0.8
30 - 100	0.3	0.8	1.5
100 - 300	0.5	1.2	2.0
300 - 1000	0.8	2.0	3.0
1000 - 3000	1.2	3.0	5.0
3000 PLUS:	2.0	4.0	8.0
ANGLES:	1°	1°	1°
SURFACE FIN:	1.6	6.3	12.5

APPR.	DRAWN	DATE	REV.
	JGR	20060907	D
	JGR	20060703	C
	JGR	20060522	B
	JGR	20051005	A

CAD FILENAME: S60B SPECIMEN.D | SCALE: 1 : 1

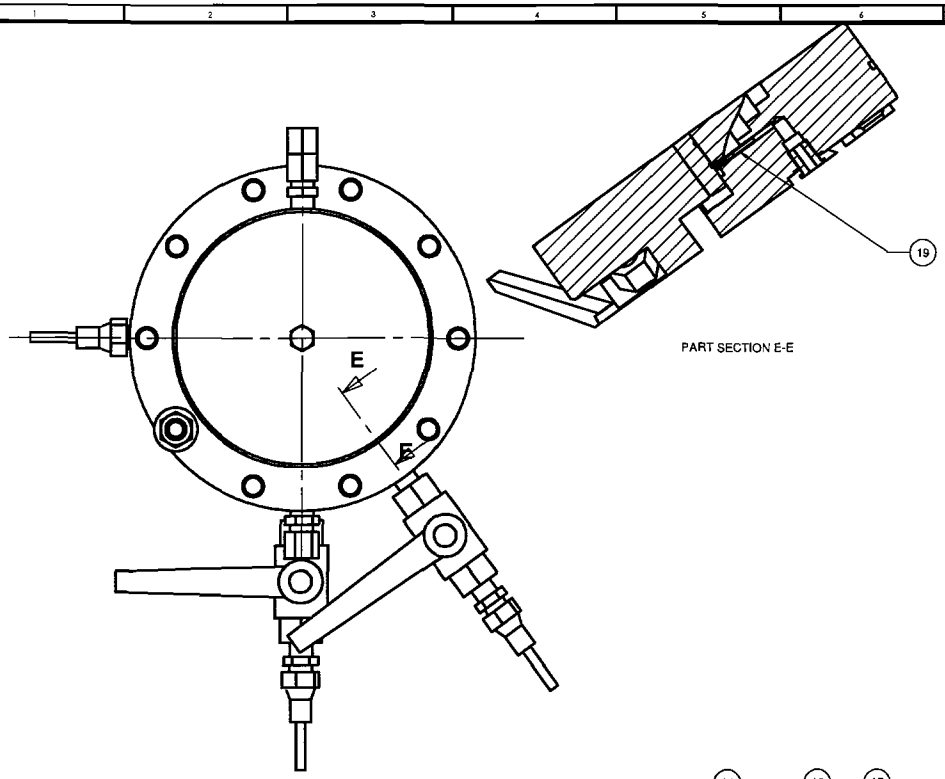
COPYRIGHT NOTICE:
UNAUTHORISED USE, MANUFACTURE OR REPRODUCTION IN WHOLE OR IN PART IS PROHIBITED. DRAWING, DESIGN AND OTHER DISCLOSURES IS THE INTELLECTUAL PROPERTY OF NORTH-WEST UNIVERSITY. ALL RIGHTS RESERVED.

SCHOOL FOR MECHANICAL AND MATERIALS ENGINEERING
POTCHEFSTROOM CAMPUS OF NW-U
11 HOFFMAN STREET
POTCHEFSTROOM 2520

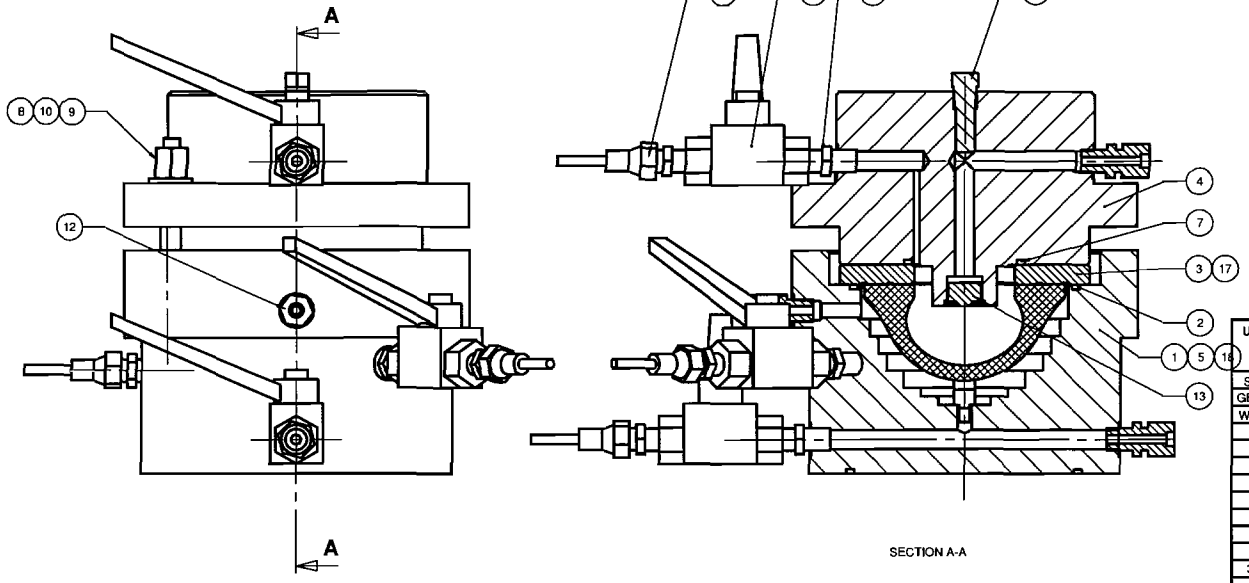
S60B SPECIMEN

DWG. No. GRA-S60B-06-03 D

9-8



PART SECTION E-E



SECTION A-A

20			
19	1	BLEED TUBE	GRA-S60B-70-02
18	1	FILLER	GRA-S60B-72-02
17	2	COOKING OIL FILTER	FILTERA [PICK N PAY]
16	3	500 BAR 1/4" BALL VALVE	
15	3	1/4-NPT NIPPLE	1N-04
14	3	METRIC 90 SWEPT ELBOW	21191-1404
13	1	1/2" TAP AERATOR	
12	1	1/4" TUBE - 1/4" NPT FITTING	SWAGELOK, B-400-1-4-BT
11	1	PLUG	GRA-S60B-12-02
10	10	NUT, M12	FNM12
9	10	WASHER, NARROW, M12	HARD
8	10	STUD, M12 x 80	SM12 x 80
7	1	O-RING	PARKER 2-230 VITON SH90A
6			
5	3	DOWEL, M5 x 35	
4	1	FIXTURE, TOP	GRA-S60B-04-02
3	1	S60B SPECIMEN	GRA-S60B-06-03
2	1	O-RING	PARKER 2-250 VITON SH90A
1	1	FIXTURE, BOTTOM	GRA-S60B-02-02

ITEM	QTY	TITLE OR DESCRIPTION	MATERIAL/DRAWING -/PART No

UNLESS STATED OTHERWISE:
REMOVE ALL BURRS AND SHARP EDGES

SCREW THREAD: ISO 6H 6g
GEOMETRIC TOL. TO BS 308 1972
WELDING SYMBOLS TO BS 499/2

MACHINING TOLERANCES

OVER - TO	±	±	±
0 - 6	0.1	0.2	0.5
6 - 30	0.2	0.5	0.8
30 - 100	0.3	0.8	1.5
100 - 300	0.5	1.2	2.0
300 - 1000	0.8	2.0	3.0
1000 - 3000	1.2	3.0	5.0
3000 PLUS:	2.0	4.0	8.0
ANGLES:	1°	1°	1°
SURFACE FIN:	1.6	6.3	12.5

APPR.	DRAWN	DATE	REV.
	JGR	20070719	E
	JGR	20070712	D
	JGR	20060113	C
	JGR	20051103	B
	JGR	20051005	A

CAD FILENAME: S60B_FIXTURE'E
SCALE: 1 : 1

COPYRIGHT NOTICE:
UNAUTHORISED USE, MANUFACTURE OR REPRODUCTION IN WHOLE OR IN PART IS PROHIBITED. DRAWING, DESIGN AND OTHER DISCLOSURES IS THE INTELLECTUAL PROPERTY OF NORTH-WEST UNIVERSITY. ALL RIGHTS RESERVED.

SCHOOL FOR MECHANICAL AND MATERIALS ENGINEERING
POTCHEFSTROOM CAMPUS OF NW-U
11 HOFFMAN STREET
POTCHEFSTROOM 2520

S60B TEST JIG

DWG. No. GRA-S60B-00-03 E

APPENDIX C

Uniaxial Fatigue Tests Table

UNIAXIAL FATIGUE RESULTS TABLE

Appendix C

DATE	TIME	ID	THEORETICAL		ACTUAL LOADS		NO OF CYCLES	COMMENTS				MASS OF S70 [g]	DIAMETER(MEAN) OF TEST SECTION [mm]	NATURAL FREQUENCY [Hz] MODE 1:	NATURAL FREQUENCY [Hz] MODE 2:	DIR	BLOCK POS.	CLOCK POS.
			MAX LOAD	MIN LOAD	MAX LOAD	MIN LOAD		TEMP	% HUM	R-RATIO	FREQ							
06 March 2007	13:30	60J14	2.047	-2.047	2.06	-2.08	1279	27.9	75.1	-1	8	90.62	13	925	3130	Z	A	12
07 March 2007	12:10	60J11	1.67	-1.67	1.67	-1.69	3546	28.6	56.5	-1	8	90.61	13.003	920	3125	Z	A	12
08 March 2007	08:10	60J12	0.88	-0.88	0.9	-0.9	201423	23.9	55.1	-1	8	90.45	13.002	914.99	3085	Z	A	12
09 March 2007	10:40	60J13	2.4	-2.4	2.4	-2.41	52	26	69	-1	1	90.61	13.001	920	3085	Z	A	12
12 March 2007	10:40	61D5	1.5	-2.1	1.504	-1.503	200000	26	63	-1	8	90.37	12.992	930	3150	Z	B	6
13 March 2007		61J11	2.27	-2.27			815			-1	8	91.12	13.004	930	3180	Z	B	12
13 March 2007	10:40	61J12	2.1	-1.67	2.1	-2.1	802	26	58	-1	8	90.91	13.004	925	3145	Z	B	12
13 March 2007	11:40	61A8	1.67	-1.67	1.672	-1.67	41331	26	58	-1	8	89.58	12.996	930	3160	X	AA	5
14 March 2007	07:00	61B3	1.67	-1.67	1.67	-1.67	2476	24	60	-1	8	89.39	12.997	910	3190	X	A	6
14 March 2007	07:20	61D15	1.67	-1.67	1.67	-1.67	200000	24	59	-1	8	90.81	12.997	930	3175	Z	B	1
14 March 2007	15:00	60G18	1.67	-1.67	1.67	-1.67	200000	25.9	57.7	-1	8	91.06	13	935	3190	X	B	9
15 March 2007	07:50	60G22	1.67	-1.67	1.67	-1.67	200000	24	62	-1	8	91.43	13.005	939.99	3160	X	B	0
15 March 2007	15:00	60H15	1.67	-1.67	1.67	-1.67	200000	24	60	-1	8	91.18	13.006	925	3145	Z	B	1
16 March 2007	12:30	60G2	2.4	-2.4	2.4	-2.4	161	27	59	-1	8	90.61	12.998	930	3150	X	B	7
16 March 2007		60G14	2.4	-2.4	2.4	-2.4	231	27	59	-1	8	91.19	13.003	935	3200	X	B	0
16 March 2007		60H7	2.4	-2.4	2.4	-2.4	112	27	59	-1	8	90.78	13.003	920	3115	Z	B	5
16 March 2007	13:13	61A18	2.4	-2.4	2.4	-2.4	677	27	59	-1	8	90.44	12.992	945	3240	X	AA	9
16 March 2007		61B20	2.4	-2.4	2.4	-2.4	53	27	59	-1	8	90.75	12.993	945	3210	X	A	0
16 March 2007		61J9	2.4	-2.4	2.4	-2.4	149	27	59	-1	8	90.93	13.004	920	3120	Z	B	11
16 March 2007		60G9	2.27	-2.27	2.27	-2.27	266	27	59	-1	8	90.39	13.003	925	3140	X	B	9
16 March 2007		60G19	2.27	-2.27	2.27	-2.27	790	27	59	-1	8	91.22	13.004	939.99	3170	X	B	0
19 March 2007		61B21	2.27	-2.27	2.27	-2.27	458	21	51	-1	8	90.78	12.995	950	3190	X	A	0
19 March 2007		61B26	2.27	-2.27	2.27	-2.27	1747	21	51	-1	8	90.79	12.995	950	3210	X	A	11
19 March 2007		60H8	2.27	-2.27	2.27	-2.27	292	21	51	-1	8	90.42	13.004	914.99	3120	Z	B	5
19 March 2007		61J10	2.27	-2.27	2.27	-2.27	4516	21	51	-1	8	91.28	13.003	930	3170	Z	B	11
21 March 2007	08:15	60G4	2.53	-2.53	2.53	-2.53	35	22	58	-1	1	90.29	12.999	920	3125	X	B	6
21 March 2007	08:30	60H16	2.53	-2.53	2.53	-2.53	21	22	58	-1	1	91.28	13.007	925	3130	Z	B	1
21 March 2007	08:40	61A16	2.53	-2.53	2.53	-2.53	9	22	58	-1	1	90.15	12.993	950	3205	X	AA	5
21 March 2007	08:50	61D13	2.53	-2.53	2.53	-2.53	17	22	58	-1	1	90.73	12.994	930	3170	Z	B	12
21 March 2007	09:00	61B6	2.53	-2.53	2.53	-2.53	10	22	58	-1	1	89.03	12.998	905	3095	X	A	6
21 March 2007		61J11	2.53	-2.53	2.53	-2.53	815	20	58	-1	1	91.12	13.004	930	3180	Z	B	12
22 March 2007	12:00	61D16	2.53	-2.53	2.53	-2.53	77	23	55	-1	1	90.65	12.995	930	3185	Z	B	1
26 March 2007	14:15	60F13	2.238	0	2.238	0	31042	25.5	47.2	0	8	91.02	12.998	939.99	3180	X	B	0
27 March 2007		60J10	2.238	0	2.238	0	860	25.6	46.7	0	8	90.68	13	925	3120	Z	A	11
27 March 2007		61B2	2.238	0	2.238	0	296	25.5	46.7	0	8	89.91	12.998	920	3110	X	A	7
27 March 2007		61B5	2.238	0	2.238	0	804	25.7	46.7	0	8	89.76	13	920	3100	X	A	6
27 March 2007		61H13	2.238	0	2.238	0	761	25.6	46.7	0	8	90.95	12.995	930	3165	Z	B	12
27 March 2007		61H2	2.238	0	2.238	0	265	25.7	46.7	0	8	90.78	12.994	925	3145	Z	B	7
27 March 2007		61H4	2.238	0	2.238	0	71237	25.6	46.7	0	8	90.52	12.993	920	3130	Z	B	6
27 March 2007	14:30	60F10	2.37	0	2.238	0	225	25	47.5	0	2	90.63	12.997	930	3160	X	B	9
27 March 2007	14:45	61F9	2.37	0	2.238	0	155	26	48	0	2	90.92	12.994	920	3130	Z	B	11
27 March 2007	15:00	60J1	2.37	0	2.238	0	377	26	47.5	0	2	90.25	13.001	910	3085	Z	A	7
27 March 2007	15:15	60H3	2.37	0	2.238	0	710	26	47	0	2	90.78	13.002	925	3135	Z	B	6
27 March 2007	15:30	61A20	2.37	0	2.238	0	94	26	47	0	2	90.33	12.99	939.99	3235	X	AA	0
27 March 2007	15:40	61D12	2.37	0	2.238	0	496	26	48	0	2	90.74	12.996	930	3155	Z	B	12
27 March 2007	15:50	60F4	2.37	0	2.238	0	316	26	47.5	0	2	90.04	12.989	920	3095	X	B	6
27 March 2007	16:00	61A25	2.37	0	2.238	0	1233	26	48	0	2	90.32	12.992	939.99	3190	X	AA	11
28 March 2007	10:30	60F5	2.53	0	2.53	0	137	25.2	58.6	0	1	89.99	12.99	925	3130	X	B	6
28 March 2007		60F16	2.53	0	2.53	0	37	25.2	58.6	0	1	90.57	13	925	3120	X	B	3
28 March 2007		60H6	2.53	0	2.566	-0.559	1	25.2	58.6	0	1	90.73	13.004	920	3100	Z	B	6

UNIAXIAL FATIGUE RESULTS TABLE

Appendix C

DATE	TIME	ID	THEORETICAL		ACTUAL LOADS		NO OF CYCLES	COMMENTS				MASS OF S70 [g]	DIAMETER(MEAN) OF TEST SECTION [mm]	NATURAL FREQUENCY [Hz] MODE 1:	NATURAL FREQUENCY [Hz] MODE 2:	DIR	BLOCK POS.	CLOCK POS.
			MAX LOAD	MIN LOAD	MAX LOAD	MIN LOAD		TEMP	% HUM	R-RATIO	FREQ							
28 March 2007		60J2	2.53	0	2.566	-0.559	112	25.2	58.6	0	1	90.72	13.002	920	3125	Z	A	7
28 March 2007		61A21	2.53	0	2.566	-0.559	169	25.2	58.6	0	1	90.29	12.992	945	3200	X	AA	0
28 March 2007		61B9	2.53	0	2.566	-0.559	83	25.2	58.6	0	1	90.63	12.997	935	3170	X	A	9
28 March 2007		61F10	2.53	0	2.566	-0.556	1	25.2	58.6	0	1	91.15	12.998	930	3150	Z	B	11
28 March 2007	12:00	61F12	2.53	0	2.566	-0.556	369	25.2	58.6	0	1	90.86	12.998	930	3135	Z	B	12
29 March 2007	08:45	60F12	2.651	0	2.56	0	181	28	73	0	2	90.9	12.998	939.99	3215	X	B	0
29 March 2007	09:00	60F18	2.651	0	2.56	0	178	28	73	0	2	90.72	12,987	935	3165	X	B	9
29 March 2007	09:10	60J9	2.651	0	2.596	0	4	28	73	0	2	90.58	13.001	914.99	3065	Z	A	11
29 March 2007	09:20	61H12	2.651	0	2.56	0	231	28	73.5	0	2	90.94	12.995	935	3175	Z	B	12
29 March 2007	09:30	61B17	2.651	0	2.56	0	565	28	73.5	0	2	90.57	12.994	939.99	3190	X	A	9
29 March 2007	09:40	6184	2.651	0	2.595	-0.764	1	28	73.5	0	2	89.29	12.995	905	3080	X	A	6
29 March 2007	09:47	61H1	2.651	0	2.5	0	9	28	73.5	0	2	90.37	12.995	910	3070	Z	B	7
29 March 2007	09:50	61H3	2.651	0	2.56	0	283	29	73.5	0	2	90.68	12.993	925	3165	Z	B	6
31 March 2007	08:30	60F17	2.238	1.119	2.238	1.119	24583	24.2	71.2	0.5	8	90.02	12.991	920	3135	X	B	9
31 March 2007	08:30	60F6	2.238	1.119	2.238	1.119	432	24.8	71.2	0.5	8	89.94	12.986	914.99	3110	X	B	6
31 March 2007	08:30	60H1	2.238	1.119	2.238	1.119	200000	25	71.2	0.5	8	90.13	12.999	910	3105	Z	B	7
31 March 2007	08:30	60H4	2.238	1.119	2.238	1.119	27114	24.2	71.2	0.5	8	90.79	13.002	920	3125	Z	B	6
31 March 2007	08:30	61A2	2.238	1.119	2.238	1.119	200000	24.2	74.6	0.5	8	89.69	12.995	930	3160	X	AA	7
31 March 2007	08:30	61A4	2.238	1.119	2.238	1.119	336	24.2	75.2	0.5	8	89.36	13.001	925	3140	X	AA	6
31 March 2007	08:30	61D9	2.238	1.119	2.238	1.119	200000	26.5	72	0.5	8	90.82	12.99	920	3095	Z	B	11
31 March 2007	08:30	61D11	2.238	1.119	2.238	1.119	200000	27	70	0.5	8	90.88	12.997	925	3150	Z	B	12
05 April 2007	08:30	60F24	2.494	1.247	2.495	1.25	1916	24.1	69.3	0.5	8	90.75	12.99	930	3150	X	B	3
05 April 2007	10:00	60F14	2.494	1.247	2.495	1.25	10118	24.1	69.3	0.5	8	90.94	13.005	939.99	3200	X	B	0
05 April 2007	10:30	60H2	2.494	1.247	2.495	1.25	227	24.1	69.3	0.5	8	90.64	12.998	920	3140	Z	B	7
05 April 2007	11:00	60H5	2.494	1.247	2.495	1.25	152151	24.1	69.3	0.5	8	90.88	13	914.99	3095	Z	B	6
07 April 2007	10:00	61A10	2.494	1.247	2.495	1.25	200000	26	59.3	0.5	8	90.66	12.994	945	3230	X	AA	9
09 April 2007	09:00	61A5	2.494	1.247	2.495	1.25	755	24	65	0.5	8	89.15	12.998	920	3085	X	AA	6
09 April 2007	09:15	61D10	2.494	1.247	2.495	1.25	26	26	66.8	0.5	8	91.09	12.999	930	3150	Z	B	11
09 April 2007	09:20	61F3	2.494	1.247	2.495	1.25	66 49	26	68	0.5	8	90.55	12.993	930	3155	Z	B	6
11 April 2007	08:30	60F24	2.574	1.287	2.574	1.287	1066	25	68	0.5	8	90.75	12.99	930	3150	X	B	3
11 April 2007	09:00	60F28	2.574	1.287	2.574	1.287	19	26	68	0.5	8	90.05	12.993	920	3120	X	B	12
11 April 2007	09:05	60H9	2.574	1.287	2.574	1.287	1	25	68	0.5	8	90.99	13.004	920	3120	Z	B	11
11 April 2007	09:20	60H12	2.574	1.287	2.574	1.287	242	26	68	0.5	8	90.58	13.003	914.99	3115	Z	B	12
12 April 2007	09:00	61A17	2.574	1.287	2.574	1.287	227	24	71	0.5	8	90.37	12.992	945	3185	X	AA	9
12 April 2007	09:20	61A12	2.574	1.287	2.574	1.287	200000	24	71	0.5	8	90.71	12.999	955	3230	X	AA	0
13 April 2007	09:00	61F1	2.574	1.287	2.574	1.287	16	24	69	0.5	8	90.47	12.997	920	3105	Z	B	7
13 April 2007	09:15	61F4	2.574	1.287	2.574	1.287	649	25	70	0.5	8	90.46	12.994	925	3115	Z	B	6
16 April 2007	12:08	60F29	2.363	1.182	2.363	1.182	5113	23.3	53.5	0.5	8	90.05	12.992	925	3115	X	B	12
16 April 2007	12:41	60H10	2.363	1.182	2.363	1.182	120948	23	53	0.5	8	90.91	13.003	925	3120	Z	B	11
16 April 2007	15:45	60H13	2.363	1.182	2.363	1.182	8435	25	54	0.5	8	90.79	13.002	920	3105	Z	B	12
17 April 2007	08:10	61B17	2.363	1.182	2.363	1.182	2615	21	61	0.5	8	90.57	12.994	939.99	3190	X	A	9
17 April 2007	08:20	61F2	2.363	1.182	2.363	1.182	200000	23	54	0.5	8	90.67	12.996	925	3115	Z	B	7
17 April 2007	14:00	61A13	2.363	1.182	2.363	1.182	200000	25	56	0.5	8	90.7	12.996	955	3210	X	AA	0
18 April 2007	08:00	61F11	2.363	1.182	2.363	1.182	38	21.4	54	0.5	8	90.92	12.996	930	3165	Z	B	12
18 April 2007	09:15	60H11	2.231	-1.115	2.231	-1.115	527	21.4	55	-0.5	8	90.76	13.004	930	3150	Z	B	12
18 April 2007	10:35	60F20	2.231	-1.115	2.231	-1.115	2462	22	56	-0.5	8	90.99	12.992	939.99	3190	X	B	0
18 April 2007	11:15	60G1	2.231	-1.115	2.231	-1.115	343	22	56	-0.5	8	90 48	12.998	935	3160	X	B	7
18 April 2007	12:00	60J4	2.231	-1.115	2.231	-1.115	2664	23	56	-0.5	8	90.85	13.001	920	3130	Z	A	6
18 April 2007	12:10	60L1	2.231	-1.115	2.231	-1.115	606	23	56	-0.5	8	90.05	12.997	914.99	3105	Z	A	7
18 April 2007	12:15	61B10	2.231	-1.115	2.231	-1.115	7417	24	56	-0.5	8	90.9	12.997	945	3190	X	A	9

UNIAXIAL FATIGUE RESULTS TABLE

DATE	TIME	ID	THEORETICAL		ACTUAL LOADS		NO OF CYCLES	COMMENTS				MASS OF S70 [g]	DIAMETER(MEAN) OF TEST SECTION [mm]	NATURAL FREQUENCY [Hz] MODE 1:	NATURAL FREQUENCY [Hz] MODE 2:	DIR	BLOCK POS.	CLOCK POS.
			MAX LOAD	MIN LOAD	MAX LOAD	MIN LOAD		TEMP	% HUM	R-RATIO	FREQ							
18 April 2007	12:30	61B12	2.231	-1.115	2.231	-1.115	27996	24	56	-0.5	8	90.81	12.995	950	3200	X	A	0
18 April 2007	13:50	61H9	2.231	-1.115	2.231	-1.115	2506	24	56	-0.5	8	90.94	12.997	920	3100	Z	B	11
19 April 2007	09:10	60G8	2.363	-1.182	2.363	-1.182	113	22.6	68.3	-0.5	8	90.1	13.002	910	3070	X	B	5
19 April 2007	09:20	60F21	2.363	-1.182	2.363	-1.182	2027	22.5	68	-0.5	8	91.01	12.991	935	3160	X	B	0
19 April 2007	10:40	60L2	2.363	-1.182	2.363	-1.182	324	22.7	68.5	-0.5	8	90.51	12.996	920	3115	Z	A	7
19 April 2007	10:45	60J5	2.363	-1.182	2.363	-1.182	326	22.9	69	-0.5	8	90.83	13.001	914.99	3115	Z	A	6
19 April 2007	10:50	61B18	2.363	-1.182	2.363	-1.182	426	22.5	68.3	-0.5	8	90.69	12.994	939.99	3175	X	A	9
19 April 2007	10:55	61B13	2.363	-1.182	2.363	-1.182	1000	22.5	68.6	-0.5	8	90.81	12.996	950	3215	X	A	0
19 April 2007	11:00	61H10	2.363	-1.182	2.363	-1.182	540	22.5	68.9	-0.5	8	91.24	12.995	925	3165	Z	B	11
19 April 2007	11:10	60H14	2.363	-1.182	2.363	-1.182	302	22.6	68.2	-0.5	8	91.02	13.001	925	3135	Z	B	12
21 April 2007		60G3	2.441	-1.22	2.475	1.231	6	24	60	-0.5	8	90.43	12.997	920	3135	X	B	6
21 April 2007		60G17	2.441	-1.22	2.445	1.221	126	24	60	-0.5	8	90.52	12.999	930	3160	X	B	9
21 April 2007		60J3	2.441	-1.22	2.445	1.221	247	24	60	-0.5	8	90.84	13.001	920	3110	Z	A	6
21 April 2007		60L9	2.441	-1.22	2.445	1.221	26	24	60	-0.5	8	90.62	13.002	920	3130	Z	A	11
21 April 2007		61A19	2.441	-1.22	2.45	1.23	16	24	60	-0.5	8	90.38	12.993	939.99	3195	X	AA	0
21 April 2007		61B25	2.441	-1.22	2.444	1.22	51	24	60	-0.5	8	90.72	12.994	939.99	3160	X	A	11
21 April 2007		61J1	2.441	-1.22	2.444	1.22	108	24	60	-0.5	8	90.57	12.999	914.99	3105	Z	B	7
21 April 2007		61J3	2.441	-1.22	2.444	1.238	11	24	60	-0.5	8	90.74	12.999	925	3165	Z	B	6
21 April 2007		60G11	2.153	-1.076	2.153	-1.076	5311	24	60	-0.5	8	91.18	13.003	935	3155	X	B	0
21 April 2007		60J6	2.153	-1.076	2.153	-1.076	4719	24	60	-0.5	8	90.88	13.003	920	3110	Z	A	6
21 April 2007		60L10	2.153	-1.076	2.153	-1.076	2669	24	60	-0.5	8	90.76	13.004	930	3150	Z	A	11
21 April 2007		61A22	2.153	-1.076	2.153	-1.076	169104	24	60	-0.5	8	90.35	12.991	950	3215	X	AA	0
21 April 2007		61A26	2.153	-1.076	2.153	-1.076	1712	24	60	-0.5	8	90.18	12.991	939.99	3190	X	AA	11
21 April 2007		61J2	2.153	-1.076	2.153	-1.076	11885	24	60	-0.5	8	90.87	12.999	925	3160	Z	B	7
21 April 2007		61J4	2.153	-1.076	2.153	-1.076	5118	24	60	-0.5	8	90.6	13	925	3145	Z	B	6
24 April 2007	14:36	60G21	0	-9.329	0	-9.329	588	24	62	-∞	8	91.34	13.001	935	3175	X	B	0
24 April 2007		60G25	0	-9.329	0	-9.329	4453	24	63	-∞	8	91.56	12.996	955	3230	X	B	11
25 April 2007	07:25	60J16	0	-9.329	0	-9.329	376	22.3	69.5	-∞	8	91.21	13.002	925	3115	Z	A	1
25 April 2007		60L12	0	-9.329	0	-9.329	76	22.3	69.5	-∞	8	90.44	13.006	920	3115	Z	A	12
25 April 2007		61A6	0	-9.329	0	-9.329	26	22.3	69.5	-∞	8	88.91	12.998	920	3100	X	AA	6
25 April 2007		61A7	0	-9.329	0	-9.329	20	22.3	69.5	-∞	8	88.52	12.996	914.99	3115	X	AA	5
25 April 2007		61F14	0	-9.329	0	-9.329	3039	22.3	69.5	-∞	8	91.02	13.003	935	3160	Z	B	12
25 April 2007		61H7	0	-9.329	0	-9.329	501	22.3	69.5	-∞	8	90.65	12.998	930	3140	Z	B	5
26 April 2007	09:15	60G26	0	-8.78	0	-8.78	130	23	70	-∞	8	90.77	12.996	935	3180	X	B	11
26 April 2007	11:00	60G28	0	-8.78	0	-8.78	157	23	70	-∞	8	90.15	12.998	920	3115	X	B	12
26 April 2007		60L7	0	-8.78	0	-8.78	3466	23	70	-∞	8	90.75	13.007	925	3110	Z	A	5
26 April 2007	12:00	60L13	0	-8.78	0	-8.78	307	23	70	-∞	8	90.55	13.003	925	3130	Z	A	12
26 April 2007	12:15	61A14	0	-8.78	0	-8.78	100000	23	70	-∞	8	90.57	12.995	955	3240	X	AA	0
26 April 2007		61H5	0	-8.78	0	-8.78	5016	23.5	68.1	-∞	8	90.54	13.002	925	3145	Z	B	6
26 April 2007		61A15	0	-8.78	0	-8.78	100000	24.2	65	-∞	8	90.55	12.992	955	3245	X	AA	3
06 May 2007		61H8	0	-8.78	0	-8.78	940	27	42.6	-∞	8	90.08	12.998	920	3125	Z	B	5
04 May 2007		60F7	0	-9.878	0	-9.619	20	23	72	-∞	2	90.16	13	920	3120	X	B	5
04 May 2007		60G29	0	-9.878	0	-9.26	9	23	72	-∞	2	90.08	13.001	914.99	3105	X	B	12
04 May 2007		60L8	0	-9.878	0	-9.859	51	23	72	-∞	2	90.38	13.004	914.99	3125	Z	A	5
04 May 2007		60L11	0	-9.878	0	-9.869	78	23	72	-∞	2	90.52	13.007	925	3135	Z	A	12
04 May 2007		61A28	0	-9.878	0	-9.828	23	23	72	-∞	2	89.74	12.991	930	3150	X	AA	12
04 May 2007		61B32	0	-9.878	0	-9.88	329	23	72	-∞	2	90.83	12.996	980	3265	X	A	1
04 May 2007		61H6	0	-9.878	0	-9.808	72	23	72	-∞	2	90.55	13.001	925	3140	Z	B	5
04 May 2007		61H15	0	-9.878	0	-9.868	205	23	72	-∞	2	91.01	12.998	939.99	3160	Z	B	1
06 May 2007		60F19	0	-10.426	0	-10.427	76	26.5	40.3	-∞	2	90.93	12.983	939.99	3175	X	B	0

UNIAXIAL FATIGUE RESULTS TABLE

Appendix C

DATE	TIME	ID	THEORETICAL		ACTUAL LOADS		NO OF CYCLES	COMMENTS				MASS OF S70 [g]	DIAMETER(MEAN) OF TEST SECTION [mm]	NATURAL FREQUENCY [Hz] MODE 1:	NATURAL FREQUENCY [Hz] MODE 2:	DIR	BLOCK POS.	CLOCK POS.
			MAX LOAD	MIN LOAD	MAX LOAD	MIN LOAD		TEMP	% HUM	R-RATIO	FREQ							
06 May 2007		60L14	0	-10.426	0	-10.444	26	26.5	41	-∞	2	90.71	13.003	930	3120	Z	A	12
06 May 2007		60L15	0	-10.426	0	-10.435	26	26.5	41.2	-∞	2	90.97	13.003	930	3140	Z	A	1
06 May 2007		61A29	0	-10.426	0	-10.457	6	26.5	40	-∞	2	89.69	12.993	935	3180	X	AA	12
06 May 2007		61B7	0	-10.426	0	-9.851	4	26.5	42.1	-∞	2	88.77	12.996	905	3090	X	A	5
06 May 2007		61H11	0	-10.426	0	-10.428	51	26.5	41.5	-∞	2	91.1	12.996	935	3165	Z	B	12
06 May 2007		61H16	0	-10.426	0	-10.394	21	26.5	39.2	-∞	2	90.69	12.998	930	3155	Z	B	1
08 May 2007	11:45	60F22	-4.939	-9.878	-4.939	-9.878	200000	24.3	60.2	2	10	91.09	12.995	939.99	3200	X	B	0
09 May 2007	08:00	60G31	-4.939	-9.878	-4.939	-9.878	200000	22.8	58.7	2	10	91.08	12.999	935	3165	X	B	1
09 May 2007	14:00	60L16	-4.939	-9.878	-4.939	-9.878	200000	23	60	2	10	91.05	13.003	925	3120	Z	A	1
28 June 2007	11:00	61J7	-4.939	-9.878	-4.939	-9.878	200000	23	60	2	20	90.46	13.002	930	3160	Z	B	5
28 June 2007	14:00	61H14	-4.939	-9.878	-4.939	-9.878	200000	20	55	2	20	91.01	12.998	935	3180	Z	B	12
28 June 2007	17:00	61B27	-4.939	-9.878	-4.939	-9.878	200000	20	50	2	20	90.36	12.995	939.99	3175	X	A	12
28 June 2007	20:00	61B15	-4.939	-9.878	-4.939	-9.878	200000	20	50	2	30	90.8	12.994	955	3230	X	A	5
28 June 2007	23:00	60N4	-4.939	-9.878	-4.939	-9.878	200000	18	50	2	30	90.72	12.999	925	3155	Z	A	6
09 May 2007	08:45	60F30	-5.213	-10.426	-5.256	-10.336	21	24	50	2	10	90.21	12.996	925	3135	X	B	12
09 May 2007	08:59	60F31	-5.213	-10.426	-5.213	-10.424	51	24	50	2	5	90.83	12.996	935	3180	X	B	1
09 May 2007	10:10	61J6	-5.213	-10.426	-5.215	-10.43	126	24	50	2	5	90.39	13.001	930	3155	Z	B	6
09 May 2007	10:23	60N10	-5.213	-10.426	-5.228	-10.428	301	24	50	2	5	90.53	13	930	3140	Z	A	11
09 May 2007	10:43	61B8	-5.213	-10.426	-5.165	-9.841	1	24	50	2	5	88.67	12.995	910	3060	X	A	5
09 May 2007	10:55	61B29	-5.213	-10.426	-5.217	-10.4	21	24	50	2	5	89.9	12.996	930	3165	X	A	12
09 May 2007	10:59	60N12	-5.213	-10.426	-5.213	-10.429	126	24	50	2	5	90.24	12.998	914.99	3150	Z	A	12
10 May 2007		61J15	-5.213	-10.426	-5.213	-10.42	200000	24	50	2	10	90.99	13.004	935	3170	Z	B	1
11 May 2007	13:00	60F27	-5.378	-10.756	-5.301	-10.782	4	25	60	2	1	90.36	12.993	925	3120	X	B	12
11 May 2007	13:18	60G32	-5.378	-10.756			1100	25	60	2	1	91.59	12.999	950	3215	X	B	1
11 May 2007	13:25	60N6	-5.378	-10.751	-5.395	-10.592	59	25	60	2	5	90.69	12.999	920	3135	Z	A	6
11 May 2007	13:30	60N9	-5.378	-10.751	-5.429	-10.676	17	25	60	2	5	90.31	13.002	910	3120	Z	A	11
11 May 2007	13:44	61B23	-5.378	-10.751	-5.38	-10.754	465	25	60	2	5	90.65	12.995	955	3245	X	A	3
11 May 2007	13:55	61B28	-5.378	-10.751	-5.549	-10.504	4	25	60	2	5	90.07	12.996	930	3150	X	A	12
11 May 2007	14:00	61J5	-5.378	-10.751	-5.396	-10.703	477	25	60	2	5	90.59	12.998	930	3125	Z	B	6
11 May 2007	14:10	61J8	-5.378	-10.751	-5.391	-10.696	58	25	60	2	5	90.02	13.002	920	3110	Z	B	5
11 May 2007	14:20	60G27	-5.103	-10.207	-5.127	-10.134	28	25	60	2	10	90.45	12.999	925	3130	X	B	12
15 May 2007	08:10	60N7	-5.103	-10.207	-5.103	-10.207	200000	25	60	2	10	90.58	12.998	925	3145	Z	A	5
15 May 2007	14:18	60N13	-5.103	-10.207	-5.103	-10.207	80	20	80	2	10	90.41	13	914.99	3095	Z	A	12
15 May 2007	14:25	61B16	-5.103	-10.207	-5.103	-10.207	200000	20	80	2	10	90.48	12.995	950	3205	X	A	5
15 May 2007	20:00	61B30	-5.103	-10.207	-5.163	-10.007	180	20	80	2	10	90.07	12.999	939.99	3185	X	A	12
15 May 2007	20:11	61J13	-5.103	-10.207	-5.103	-10.207	200000	20	80	2	10	91.01	13.005	930	3160	Z	B	12
16 May 2007	08:00	61J16	-5.103	-10.207	-5.103	-10.207	2420	18	75	2	10	90.45	13.003	925	3155	Z	B	1
21 May 2007	09:58	61A24	2.363	-4.725	2.355	-4.724	51	16	48.3	-2	8	90.02	13	950	3240	X	AA	3
21 May 2007	10:15	61F7	2.363	-4.725	2.36	-4.72	251	16	48.3	-2	8	90.44	12.994	930	3140	Z	B	5
21 May 2007	10:53	60G15	2.363	-4.725	2.36	-4.72	140	16	48.3	-2	8	91.04	12.999	930	3150	X	B	5
21 May 2007	11"00	60G5	2.363	-4.725	2.36	-4.72	101	16	48.3	-2	8	90.3	12.998	920	3120	X	B	6
21 May 2007	11:05	61B11	2.363	-4.725	2.36	-4.72	838	16	48.3	-2	8	91.02	12.997	945	3210	X	A	0
21 May 2007	11:10	60L4	2.363	-4.725	2.36	-4.72	26	16	48.3	-2	8	90.66	13.002	925	3150	Z	A	6
21 May 2007	11:33	60N8	2.363	-4.725	2.36	-4.72	16	16	48.3	-2	8	90.32	13.001	920	3135	Z	A	5
21 May 2007	11:40	61D14	2.363	-4.725	2.36	-4.72	51	16	48.3	-2	8	90.79	12.994	930	3175	Z	B	12
24 May 2007	08:00	60G12	2.44	-4.88	2.437	-4.88	76	16	53	-2	8	91.31	13.002	939.99	3185	X	B	0
24 May 2007	08:21	60G24	2.44	-4.88	2.448	-4.88	26	16	53	-2	8	91.1	13.004	935	3175	X	B	3
24 May 2007	08:25	60J7	2.44	-4.88	2.461	-4.906	26	16	51	-2	8	90.78	13.002	914.99	3125	Z	A	5
24 May 2007	08:37	60L5	2.44	-4.88	2.441	-4.96	25	16	51	-2	8	90.81	13.003	920	3125	Z	A	6
24 May 2007	08:43	61A31	2.44	-4.88	2.44	-4.876	101	16	51	-2	8	90	12.992	950	3220	X	AA	1

UNIAXIAL FATIGUE RESULTS TABLE

Appendix C

DATE	TIME	ID	THEORETICAL		ACTUAL LOADS		NO OF CYCLES	COMMENTS				MASS OF S70 [g]	DIAMETER(MEAN) OF TEST SECTION [mm]	NATURAL FREQUENCY [Hz] MODE 1:	NATURAL FREQUENCY [Hz] MODE 2:	DIR	BLOCK POS.	CLOCK POS.
			MAX LOAD	MIN LOAD	MAX LOAD	MIN LOAD		TEMP	% HUM	R-RATIO	FREQ							
24 May 2007	08:50	61B14	2.44	-4.88	2.44	-4.876	247	16	51	-2	8	90.77	12.994	950	3210	X	A	0
24 May 2007	08:54	61F5	2.44	-4.88	2.44	-4.88	203	16	51	-2	8	90.44	12.992	925	3135	Z	B	6
24 May 2007	09:00	61F8	2.44	-4.88	2.439	-4.88	26	16	51	-2	8	89.93	12.993	920	3115	Z	B	5
24 May 2007	09:42	60G10	2.27	-4.54	2.274	-4.538	51	17	53	-2	8	90.84	13.002	930	3170	X	B	9
24 May 2007	09:52	61F6	2.27	-4.54	2.271	-4.541	51	17	53	-2	8	90.42	12.992	930	3150	Z	B	6
24 May 2007	09:55	60G13	2.27	-4.54	2.27	-4.54	379	17	53	-2	8	91.27	13.002	939.99	3180	X	B	0
24 May 2007	10:00	60L3	2.27	-4.54	2.27	-4.542	51	17	53	-2	8	90.57	12.997	920	3110	Z	A	6
24 May 2007	10:15	60J8	2.27	-4.54	2.229	-4.621	16	17	53	-2	8	90.45	13.002	910	3085	Z	A	5
24 May 2007	10:20	61F15	2.27	-4.54	2.27	-4.54	444	17	53	-2	8	90.96	12.991	939.99	3170	Z	B	1
24 May 2007	10:25	61A23	2.27	-4.54	2.27	-4.54	842	17	53	-2	8	90.27	12.989	955	3220	X	AA	3
24 May 2007	10:30	61B19	2.27	-4.54	2.27	-4.54	399	17	53	-2	8	90.75	12.994	939.99	3190	X	A	0
24 May 2007	10:35	60J15	1.89	-3.78	1.89	-3.78	106985	17	53	-2	8	91.12	13	925	3155	Z	A	1
24 May 2007	16:00	60L5	1.89	-3.78	1.89	-3.78	89695	21.6	41.6	-2	8	90.84	13.002	925	3135	Z	A	6
25 May 2007	08:08	61F16	1.89	-3.78	1.89	-3.78	678	18.5	54	-2	8	90.64	12.992	930	3165	Z	B	1
25 May 2007	08:38	61B22	1.89	-3.78	1.89	-3.78	200000	18.5	54	-2	8	90.68	12.998	950	3205	X	A	0
25 May 2007	14:30	61F13	1.89	-3.78	1.89	-3.78	14424	21	53.5	-2	8	90.88	12.991	935	3175	Z	B	12
26 May 2007	09:20	61A32	1.89	-3.78	1.89	-3.78	1284	19	49.5	-2	8	90.33	12.999	955	3245	X	AA	1
26 May 2007	10:00	60G20	1.89	-3.78	1.89	-3.78	82018	20.8	53.2	-2	8	91.22	13	939.99	3175	X	B	0
31 May 2007	13:00	60F23	2.238	0	2.238	0	100000	21	58	0	8	91.11	12.993	935	3195	X	B	3
01 June 2007	13:26	60G7	1.67	-1.67	1.67	-1.67	100000	23	59	-1	8	90.42	13.002	920	3125	X	B	5
04 June 2007	14:20	60G16	2.153	-1.076	2.153	-1.076	102026	23.1	55.6	-0.5	8	90.85	12.999	930	3165	X	B	3
04 June 2007	10:00	60G23	1.89	-3.78	1.89	-3.78	69738	23.1	55.6	-2	8	91.45	13.006	939.99	3180	X	B	3
05 June 2007	08:00	60F15	0	-8.78			*no test**	22.8	53	∞	8	90.83	13.002	935	3170	X	B	3
05 June 2007	12:00	60F8	2.238	1.119	2.238	1.119	5965	22	52	0.5	8	90	12.996	914.99	3100	X	B	5
07 June 2007	09:00	60F32	-5.02	-10.04	-5.02	-10.04	100000	22.2	52	2	8	91.61	12.998	950	3210	X	B	1
07 June 2007	14:30	60F25	0	-8.78	0	-8.78	*±7000**	22.5	52	∞	8	91.39	12.99	950	3245	X	B	11
31 May 2007	13:00	60F9	-11.65	compressive strain one cycle only								90.16	12.998	930	3135	X	B	9
31 May 2007	14:00	60F1	2.858	tensile strain one cycle only								89.94	12.989	925	3120	X	B	7

** strain gauge failed*

APPENDIX D

Uniaxial Fatigue Test Alignment Reports

Report 1: AlignPro device - Date: 2007/02/22

Operator:	G Gouws and DG Hattingh
Reference N°:	Initial Alignment Test Set-Up
Temperature:	21°C
Frame ID:	Instron Fatigue Machine 25kN Load Cell
Time & Date:	07:31AM & 2007/02/22
Project No:	NO001
Specification:	ASTM E1012 : 1999
Unit System:	S.I.
Hardware ID:	AP-USB-350-01 [A]
Description:=	16 ch - 16 bit device with USB interface
Alignment Cell Type:	Standard
Alignment Cell:	Instron 8000-171 Cylindrical 8 Gauges – ALIGN
Cell Description:	Cylindrical - 8 Gauges
Material:	Alloy Steel 817M40
Total Length (lt):	185 mm
Length (l):	50 mm
Diameter (Ø):	8 mm
No Gauges:	8
Type Gauges:	350 ohms
Gauge Factor:	2.05
Separation (lg):	37.5 mm
Alignment Load:	4.2 kN
Test Comments:	Customised load train.

Alignment Data Summary:

Field Designation	e1 (με)	e2 (με)	e3 (με)	e4 (με)	Ave.	b1 (με)	b2 (με)	b3 (με)	b4 (με)	Max bending (με)	% Bending
Top Gauges (1 to 4)	377.930	372.903	377.650	374.704	**375.797**	2.133	-2.894	1.853	-1.092	0.912	**0.243**
Bottom Gauges (5 to 8)	374.303	370.855	373.045	372.672	**372.719**	1.585	-1.864	0.326	-0.047	1.105	**0.297**

Report 2: AlignPro device - Date: 2007/03/07

Operator:	G Gouws
Reference N°:	Alignment Test Set-Up before commencement of Fatigue tests.
Temperature:	26°C
Frame ID:	Instron Fatigue Machine 25kN Load Cell
Time & Date:	12:08:44 PM 2007/03/07
Project No:	NO 001
Specification:	ASTM E1012 : 1999
Unit System:	S.I.
Hardware ID:	AP-USB-350-01 [A]
Description:=	16 ch - 16 bit device with USB interface
Alignment Cell Type:	Standard
Alignment Cell:	Instron 8000-171 Cylindrical 8 Gauges – ALIGN
Cell Description:	Cylindrical - 8 Gauges
Material:	Alloy Steel 817M40
Total Length (lt):	185 mm
Length (l):	50 mm
Diameter (Ø):	8 mm
No Gauges:	8
Type Gauges:	350 ohms
Gauge Factor:	2.05
Separation (lg):	37.5 mm
Alignment Load:	3 kN
Test Comments:	Customised load train. Test Loads are estimated to be around 2kN

Alignment Data Summary:

Field Designation	e1 (µE)	e2 (µE)	e3 (µE)	e4 (µE)	Ave.	b1 (µE)	b2 (µE)	b3 (µE)	b4 (µE)	Max Bending (µE)	% Bending
Top Gauges (1 to 4)	216.323	215.572	211.139	215.543	**214.644**	1.679	0.928	-3.505	0.899	2.592	**1.208**
Bottom Gauges (5 to 8)	214.819	209.682	211.065	217.439	**213.251**	1.567	-3.569	-2.186	4.188	4.309	**2.020**

Report 3: AlignPro device - Date: 2007/03/23

Operator:	G Gouws
Reference N°:	First Alignment Test during Fatigue tests.
Temperature:	23
Frame ID:	Instron Fatigue Machine 25kN Load Cell
Time & Date:	23 March 2007 at 12:00
Project No:	NO 001
Specification:	ASTM E1012 : 1999
Unit System:	S.I.
Hardware ID:	AP-USB-350-01 [A]
Description:=	16 ch - 16 bit device with USB interface
Alignment Cell Type:	Standard
Alignment Cell:	Instron 8000-171 Cylindrical 8 Gauges – ALIGN
Cell Description:	Cylindrical - 8 Gauges
Material:	Alloy Steel 817M40
Total Length (lt):	185 mm
Length (l):	50 mm
Diameter (Ø):	8 mm
No Gauges:	8
Type Gauges:	350 ohms
Gauge Factor:	2.05
Separation (lg):	37.5 mm
Alignment Load:	2.4kN
Test Comments:	Test done after completion R = -1

Alignment Data Summary:

Field Designation	e1 (µE)	e2 (µE)	e3 (µE)	e4 (µE)	Ave.	b1 (µE)	b2 (µE)	b3 (µE)	b4 (µE)	Max Bending (µE)	% Bending
Top Gauges (1 to 4)	237	241	239	238	**239**	-1.93	2.49	0.26	-0.82	**1.99**	**0.83**
Bottom Gauges (5 to 8)	236	237	242	237	**238**	-1.45	-1.37	4.11	-1.29	**2.78**	**1.17**

Report 4: Align Pro device - Date: 2007/04/24

Operator:	G Gouws
Reference N°:	Second Alignment Test during Fatigue tests.
Temperature:	26
Frame ID:	Instron Fatigue Machine 25kN Load Cell
Time & Date:	24 April 2007 at 12:30
Project No:	NO 001
Specification:	ASTM E1012 : 1999
Unit System:	S.I.
Hardware ID:	AP-USB-350-01 [A]
Description:=	16 ch - 16 bit device with USB interface
Alignment Cell Type:	Standard
Alignment Cell:	Instron 8000-171 Cylindrical 8 Gauges – ALIGN
Cell Description:	Cylindrical - 8 Gauges
Material:	Alloy Steel 817M40
Total Length (lt):	185 mm
Length (l):	50 mm
Diameter (Ø):	8 mm
No Gauges:	8
Type Gauges:	350 ohms
Gauge Factor:	2.05
Separation (lg):	37.5 mm
Alignment Load:	3kN
Test Comments:	Test done before R = ∞

Alignment Data Summary:

Field Designation	e1 (µE)	e2 (µE)	e3 (µE)	e4 (µE)	Ave.	b1 (µE)	b2 (µE)	b3 (µE)	b4 (µE)	Max Bending (µE)	% Bending
Top Gauges (1 to 4)	308.5	307.9	309.7	307.4	**308.4**	0.12	-0.46	1.33	-0.99	**0.66**	**0.21**
Bottom Gauges (5 to 8)	303.6	304.3	305.3	309.9	**305.8**	-2.16	-1.49	-0.45	4.11	**2.92**	**0.96**

Report 5: Align Pro device - Date: 2007/05/06

Operator:	G Gouws
Reference Nº:	Third Alignment Test during Fatigue tests.
Temperature:	23
Frame ID:	Instron Fatigue Machine 25kN Load Cell
Time & Date:	06 May 2007 at 15:00
Project No:	NO 001
Specification:	ASTM E1012 : 1999
Unit System:	S.I.
Hardware ID:	AP-USB-350-01 [A]
Description:=	16 ch - 16 bit device with USB interface
Alignment Cell Type:	Standard
Alignment Cell:	Instron 8000-171 Cylindrical 8 Gauges – ALIGN
Cell Description:	Cylindrical - 8 Gauges
Material:	Alloy Steel 817M40
Total Length (lt):	185 mm
Length (l):	50 mm
Diameter (Ø):	8 mm
No Gauges:	8
Type Gauges:	350 ohms
Gauge Factor:	2.05
Separation (lg):	37.5 mm
Alignment Load:	3kN
Test Comments:	Test done before R =+2;-2

Alignment Data Summary:

Field Designation	e1 (µE)	e2 (µE)	e3 (µE)	e4 (µE)	Ave.	b1 (µE)	b2 (µE)	b3 (µE)	b4 (µE)	Max Bending (µE)	% Bending
Top Gauges (1 to 4)	316.8	311.7	310.8	316.8	**314**	2.783	-2.337	-3.228	2.782	**3.947**	**1.257**
Bottom Gauges (5 to 8)	312.1	312.7	313.2	314.7	**313.2**	-1.052	-0.472	0.02	1.504	**1.124**	**0.359**

Report 6: Align Pro device - Date:2007/05/28

Operator:	G Gouws
Reference Nº:	Third Alignment Test during Fatigue tests.
Temperature:	20°C
Frame ID:	Instron Fatigue Machine 25kN Load Cell
Time & Date:	28 May 2007 at 12:30
Project No:	NO 001
Specification:	ASTM E1012 : 1999
Unit System:	S.I.
Hardware ID:	AP-USB-350-01 [A]
Description:=	16 ch - 16 bit device with USB interface
Alignment Cell Type:	Standard
Alignment Cell:	Instron 8000-171 Cylindrical 8 Gauges – ALIGN
Cell Description:	Cylindrical - 8 Gauges
Material:	Alloy Steel 817M40
Total Length (lt):	185 mm
Length (l):	50 mm
Diameter (Ø):	8 mm
No Gauges:	8
Type Gauges:	350 ohms
Gauge Factor:	2.05
Separation (lg):	37.5 mm
Alignment Load:	3kN
Test Comments:	Test done before testing strain gauged samples

Alignment Data Summary:

Field Designation	e1 (µE)	e2 (µE)	e3 (µE)	e4 (µE)	Ave.	b1 (µE)	b2 (µE)	b3 (µE)	b4 (µE)	Max Bending (µE)	% Bending
Top Gauges (1 to 4)	300.06	301.53	303.62	297.19	**300.60**	-0.54	0.93	3.02	-3.41	**2.81**	**0.93**
Bottom Gauges (5 to 8)	300.33	301.24	296.77	299.25	**299.40**	0.93	1.84	-2.62	-0.15	**2.04**	**0.68**

Report 1: Graphite sample
Date: 22 February 2007

Operator:	W. Rall, G. Gouws and D. Hattingh
Reference Nº:	Initial Test tests.
Temperature:	25C
Frame ID:	Instron Fatigue Machine 25kN Load Cell
Time & Date:	13:00 & 22/02/2007
Project No:	NO 001
Specification:	ASTM E1012 : 1999
Unit System:	S.I.
Hardware ID:	DM 20 Strain Amplifier
Description:	4 channel
Alignment Cell:	Strain Gauged Graphite Sample
Material:	Graphite
Total Length (lt):	Mm
// Length :	50 mm
Diameter (Ø):	Mm
No Gauges:	4
Type Gauges:	120 ohms
Gauge Factor:	2.06
Alignment Load:	See Results table.
Test Comments:	None

Results:

LOAD	**N**	**895**	**912**	**796**	**915**	**879**
Strain gauge position	**Degrees**	**0**	**90**	**180**	**270**	**0**
Strain Measurement	e_1	630	603	535	606	613
	e_2	630	583	543	580	612
	e_3	610	592	570	589	580
	e_4	616	606	564	612	585
Average Strain	e_{ave}	**621.5**	**596**	**553**	**596.75**	**597.5**
$e_1 - e_{ave}$	**b1**	8.5	7	-18	9.25	15.5
$e_2 - e_{ave}$	**b2**	8.5	-13	-10	-16.75	14.5
$e_3 - e_{ave}$	**b3**	-11.5	-4	17	-7.75	-17.5
$e_4 - e_{ave}$	**b4**	-5.5	10	11	15.25	-12.5
$0.5\ (x + y)^{0.5}$	**B**	12.2066	12.748	20.40833	18.11767	21.31901
$(b1 - b3)^2$	**x**	400	121	1225	289	1089
$(b2 - b4)^2$	**y**	196	529	441	1024	729
$(B/e_{ave})x100$	**$\%B_{Max}$**	**2.0**	**2.1**	**3.7**	**3.0**	**3.6**

Report 2 : Graphite sample
Date : 07 March 2007

Operator:	W. Rall, G. Gouws
Reference N°:	Initial Test tests.
Temperature:	24C
Frame ID:	Instron Fatigue Machine 25kN Load Cell
Time & Date:	16:00 & 07/03/2007
Project No:	NO 001
Specification:	ASTM E1012 : 1999
Unit System:	S.I.
Hardware ID:	DM 20 Strain Amplifier
Description:	4 channel
Alignment Cell:	Strain Gauged Graphite Sample
Material:	Graphite
Total Length (lt):	Mm
// Length :	50 mm
Diameter (Ø):	--mm
No Gauges:	4
Type Gauges:	120 ohms
Gauge Factor:	2.06
Alignment Load:	875N
Test Comments:	None

Results:

LOAD	**N**	**875**	**875**	**875**	**875**	**875**
Strain gauge position	**Degrees**	90	180	270	0	90
Strain Measurement	e_1	583	563	599	592	574
	e_2	616	573	570	594	608
	e_3	608	601	578	562	602
	e_4	573	594	600	561	570
Average Strain	e_{ave}	**595**	**582.75**	**586.75**	**577.25**	**588.5**
$E_1 - e_{ave}$	**b1**	-12	-19.75	12.25	14.75	-14.5
$e_2 - e_{ave}$	**b2**	21	-9.75	-16.75	16.75	19.5
$e_3 - e_{ave}$	**b3**	13	18.25	-8.75	-15.25	13.5
$e_4 - e_{ave}$	**b4**	-22	11.25	13.25	-16.25	-18.5
$0.5\,(x + y)^{0.5}$	**B**	24.86966	21.70829	18.30983	22.2991	23.60085
$(b1 - b3)^2$	**x**	625	1444	441	900	784
$(b2 - b4)^2$	**y**	1849	441	900	1089	1444
$(B/e_{ave})x100$	**$\%B_{Max}$**	**4.2**	**3.7**	**3.1**	**3.9**	**4.0**

Report 3 : Graphite sample
Date : 23 March 2007

Operator:	G. Gouws
Reference Nº:	Initial Test tests.
Temperature:	23C
Frame ID:	Instron Fatigue Machine 25kN Load Cell
Time & Date:	23 March 2007 at 13:45
Project No:	NO 001
Specification:	ASTM E1012 : 1999
Unit System:	S.I.
Hardware ID:	DM 20 Strain Amplifier
Description:	4 channel
Alignment Cell:	Strain Gauged Graphite Sample
Material:	Graphite
Total Length (lt):	Mm
// Length :	50 mm
Diameter (Ø):	--mm
No Gauges:	4
Type Gauges:	120 ohms
Gauge Factor:	2.06
Alignment Load:	875N
Test Comments:	None

Results:

LOAD	**N**	**875**	**875**	**875**	**875**	**875**
Strain gauge position	**Degrees**	90	180	270	0	90
Strain Measurement	e_1	566	565	590	586	573
	e_2	571	560	566	558	587
	e_3	581	595	563	562	569
	e_4	584	581	573	588	580
Average Strain	e_{ave}	**575.5**	**575.25**	**573**	**573.5**	**577.25**
$E_1 - e_{ave}$	**b1**	-9.5	-10.25	17	12.5	-4.25
$e_2 - e_{ave}$	**b2**	-4.5	-15.25	-7	-15.5	9.75
$e_3 - e_{ave}$	**b3**	5.5	19.75	-10	-11.5	-8.25
$e_4 - e_{ave}$	**b4**	8.5	5.75	0	14.5	2.75
$0.5 (x + y)^{0.5}$	**B**	9.92	18.31	13.95	19.21	4.03
$(b1 - b3)^2$	**x**	225	900	729	576	16
$(b2 - b4)^2$	**y**	169	441	49	900	49
$(B/e_{ave})x100$	**$\%B_{Max}$**	**1.7**	**3.2**	**2.4**	**3.3**	**0.7**

APPENDIX E

Uniaxial Specimen Fracture Locations

R = +0,5



Figure 1: 60 F-2



Figure 2: 60 F-6



Figure 3: 60 F-14



Figure 4: 60 F-17



Figure 5: 60 F-24



Figure 6: 60 F-24



Figure 7: 60 F-28



Figure 8: 60 F-29



Figure 9: 60 H-1



Figure 10: 60 H-2



Figure 11: 60 H-4



Figure 12: 60 H-5



Figure 13: 60 H-9



Figure 14: 60 H-10



Figure 15: 60 H-13



Figure 16: 61 A-2



Figure 17: 61 A-4



Figure 18: 61 A-5



Figure 19: 61 A-10



Figure 20: 61 A-17



Figure 21: 61 B-1



Figure 22: 61 D-10



Figure 23: 61 D-11



Figure 24: 61 F-1



Figure 25: 61 F-2



Figure 26: 61 F-3



Figure 27: 61 F-4



Figure 28: 61 F-11



Figure 29: 61 H-12

R = 0



Figure 30: 60 F-4



Figure 31: 60 F-5



Figure 32: 60 F-10



Figure 33: 60 F-10



Figure 34: 60 F-12



Figure 35: 60 F-13



Figure 36: 60 F-16



Figure 37: 60 F-18



Figure 38: 60 H-3



Figure 39: 60 H-6



Figure 40: 60 J-1



Figure 41: 60 J-2



Figure 42: 60 J-9



Figure 43: 60 J-10



Figure 44: 61 A-20



Figure 45: 61 A-21



Figure 46: 61 A-25



Figure 47: 61 B-2



Figure 48: 61 B-4



Figure 49: 61 B-5



Figure 50: 61 B-9



Figure 51: 61 B-17



Figure 52: 61 D-12



Figure 53: 61 F-9



Figure 54: 61 F-10



Figure 55: 61 F-12



Figure 56: 61 H-1



Figure 57: 61 H-2



Figure 58: 61 H-3



Figure 59: 61 H-4



Figure 60: 61 H-12



Figure 61: 61 H-13

R = -0,5



Figure 62: 60 F-20



Figure 63: 60 F-21



Figure 64: 60 G-1



Figure 65: 60 G-3



Figure 66: 60 G-8



Figure 67: 60 G-11



Figure 68: 60 G-17



Figure 69: 60 H-10



Figure 70: 60 H-11



Figure 71: 60 H-14



Figure 72: 60 J-3



Figure 73: 60 J-4



Figure 74: 60 J-5



Figure 75: 60 J-6



Figure 76: 60 L-1



Figure 77: 60 L-2



Figure 78: 60 L-9



Figure 79: 60 L-10



Figure 80: 61 A-19



Figure 81: 61 A-22



Figure 82: 61 A-26



Figure 83: 61 B-10



Figure 84: 61 B-12



Figure 85: 61 B-13



Figure 86: 61 B-18



Figure 87: 61 B-25



Figure 88: 61 H-9



Figure 89: 61 J-1



Figure 90: 61 J-2



Figure 91: 61 J-3



Figure 92: 61 J-4

R = -1



Figure 93: 60 G-2



Figure 94: 60 G-4



Figure 95: 60 G-9



Figure 96: 60 G-14



Figure 97: 60 G-18



Figure 98: 60 G-19



Figure 99: 60 H-7



Figure 100: 60 H-8



Figure 101: 60 H-16



Figure 102: 60 J-11



Figure 103: 60 J-12



Figure 104: 60 J-13



Figure 105: 60 J-14



Figure 106: 61 A-8



Figure 107: 61 A-16



Figure 108: 61 A-18



Figure 109: 61 B-3



Figure 110: 61 B-6



Figure 111: 61 B-20



Figure 112; 61 B-21



Figure 113: 61 B-26



Figure 114: 61 D-5



Figure 115: 61 D-13



Figure 116: 61 D-15



Figure 117: 61 D-16



Figure 118: 61 J-9



Figure 119: 61 J-10



Figure 120: 61 J-11



Figure 121: 61 J-12

R = -2



Figure 122: 60 B-5



Figure 123: 60 G-10



Figure 124: 60 G-12



Figure 125: 60 G-13



Figure 126: 60 G-15



Figure 127: 60 G-20



Figure 128: 60 G-24



Figure 129: 60 J-7



Figure 130: 60 J-8



Figure 131: 60 J-15



Figure 132: 60 L-3



Figure 133: 60 L-4



Figure 134: 60 L-5



Figure 135: 60 L-6



Figure 136: 60 N-8



Figure 137: 61 A-23



Figure 138: 61 A-24



Figure 139: 61 A-31



Figure 140: 61 A-32



Figure 141: 61 B-11



Figure 142: 61 B-14



Figure 143: 61 B-19



Figure 144: 61 D-14



Figure 145: 61 F-5



Figure 146: 61 F-6



Figure 147: 61 F-7



Figure 148: 61 F-8



Figure 149: 61 F-13



Figure 150: 61 F-15



Figure 151: 61 F-16

APPENDIX F

Calibration Certificates

INSTRON

Instron Limited
Coronation Road ■ High Wycombe, Bucks HP12 3SY ■ UK
Tel: +44 1494 464646 ■ Fax: +44 1494 456123 ■ www.instron.com

Test Certificate

Cat. No.: 8000-171 **Serial No.:** 0038 **Tested By:** 1646

Readout Device No.: P34320 **Date:** 25-01-2007

Temperature: 22 °C **Proving Device No.:** P32300

Catalogue No.:	Static Rating at 1000 με
8000-171	10.4kN
8000-172	16.3kN
8000-173	14.9kN
8000-174	6.2kN

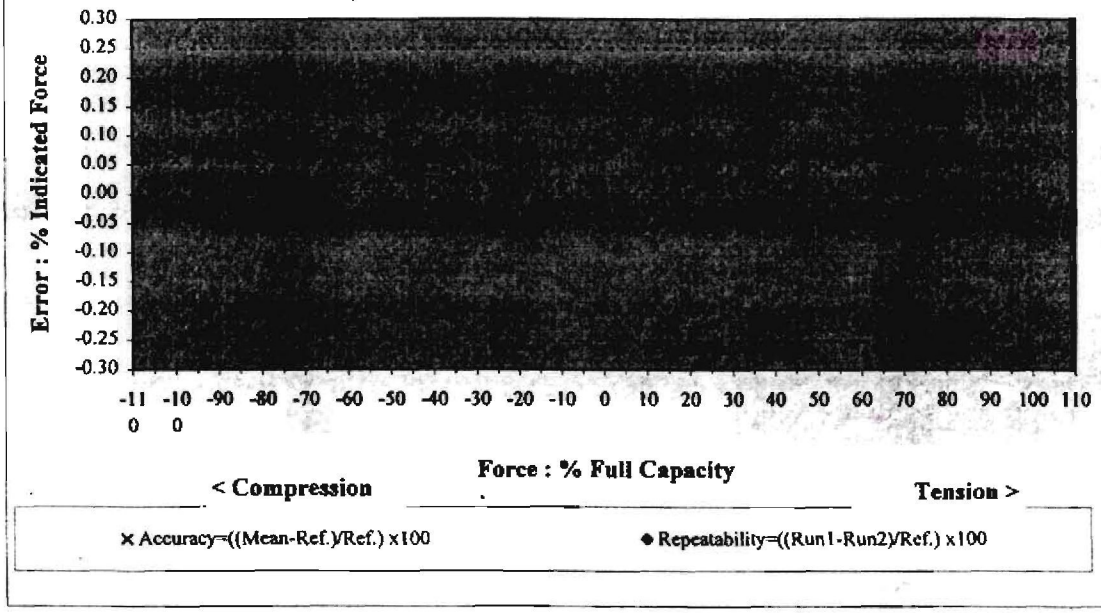
Instron certifies that this Alignment Cell has been tested using force calibration apparatus traceable to the National Physical Laboratory of the United Kingdom and when used with Instron Align Pro Software and electronics (8000-170) & alignment fixtures will meet with the requirements of ASTM E1012 i.e. calculations of bending strain.

Instron Limited
Coronation Road ■ High Wycombe, Bucks HP12 3SY ■ UK
Tel: +44 1494 464646 ■ Fax: +44 1494 456123 ■ www.instron.com

Loadcell Test Certificate

Catalogue No. : 2527-101	Proving System: Ring: 3280 Nobel: P34067
Serial No. : 55556	Readout Device No. P34068
Capacity : 25kN	Tested by : RGH
Temp. : 21°C	Date : 22 Dec 2006

Test Results



Notes :

1] Loadcell accuracy has been found to be equal to or better than ±0.25% of the indicated force.

2] Additional system calibration is required to ensure compliance with BS EN ISO 7500-1 class 0.5 and ASTM E4.

3] Instron calibration apparatus is traceable to the National Physical Laboratory of the United Kingdom.

INSTRON
Instron Limited
Coronation Road ■ High Wycombe, Bucks HP12 3SY ■ UK
Tel: +44 1494 464646 ■ Fax: +44 1494 456123 ■ www.instron.com

Accelerometer Test Report

Catalogue No.
2527-101
Transducer Full-scale [KN]
25
Serial No.
55556
Tested By
19
Tested Date
21 December 2006
Tested Time
3:43 pm
IAC Serial No.
W006510
IAC Version No.
07.89.00
Phantom Stiffness - Compensation OFF
6.5341
Phantom Stiffness - Compensation ON : RUN 1
0.0749
Phantom Stiffness - Compensation ON : RUN 2
0.0179
Phantom Stiffness Average (Run1, Run2)
0.0464
Phantom Stiffness Reduction Factor
140.821
Load Compensation Coefficient - Compensation ON : RUN 1
0.0647
Load Compensation Coefficient - Compensation ON : RUN 2
0.0655
Load Compensation Coefficient Repeatability (Abs)
0.0008
Load Compensation Coefficient Repeatability (%)
1.24
Test Software - DYN_LOAD32.EXE
Version 1.56 27-Nov-2006
Phantom Stiffness Status
PASSED
Load Compensation Status
PASSED
Overall Result
PASSED

CALIBRATION SHEET: STRAIN CHANNEL

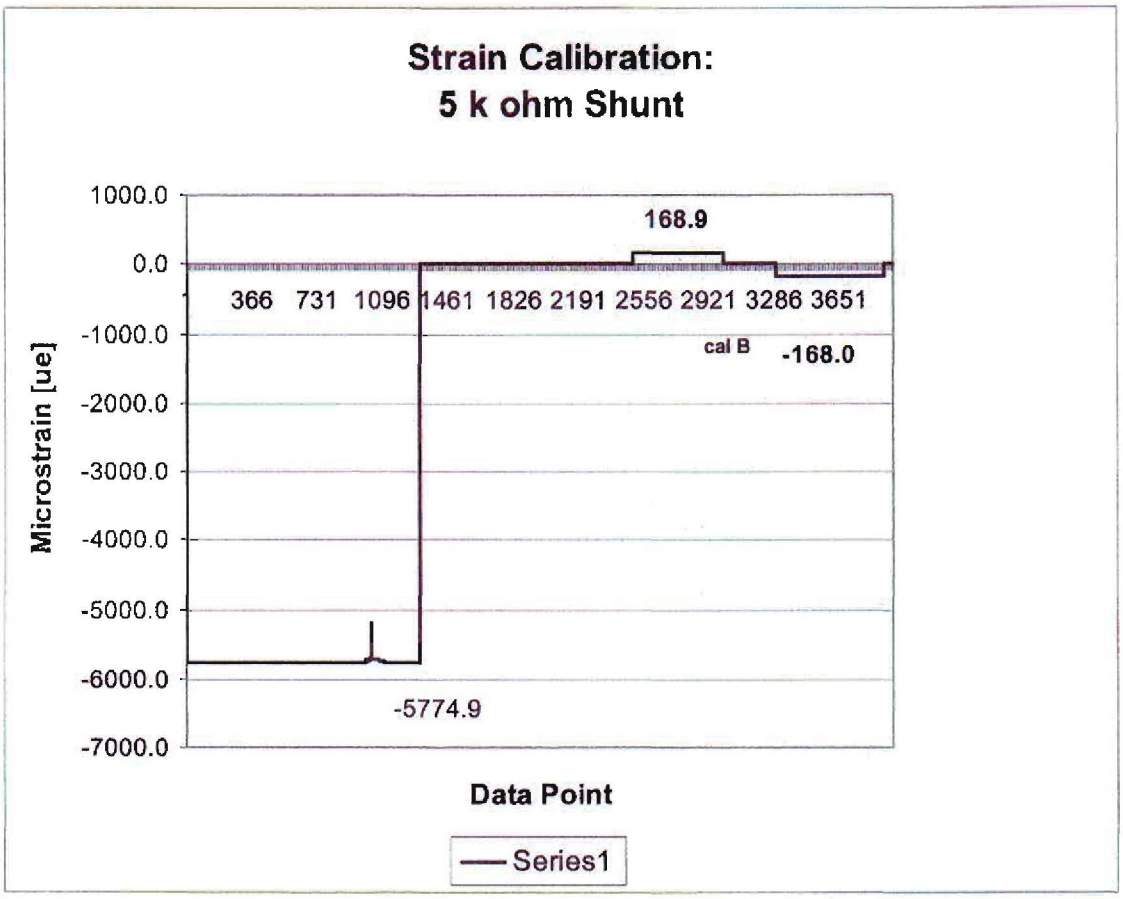
Reference Document: GRA-S60B-52-02	**Issue: A**	**Circuit: AI0 Dev1**
Description: LOOP DIA: STRAIN		**CH No: 0**
Inspector's Name: J G Roberts	**Page 1 of 2**	**Date: 30-05-07**

No.	COMPONENT DESCRIPTION	SERIAL NUMBER
1	HBM 1-XY91-6/120, k=2,03	Lot A383/27, 812026313
2	Strain Gauge Amplifier, Vishay 2120, Ch 1	022822
3	PCI-4472 DAQ card, National Instruments, "Dev1"	0X10FF7FA
4	Digital Multimeter, Fluke 75	3358352
5	Labview Program: "Calibration_Strain_R2.vi"	S60B_79_A-10.lvm
6	Precision Resistor	5 kΩ, ± 0,01%
7	Software Scale: (1V/1000 ue)	Strain
8	Inactive Gauges: HBM 1-LY11-6/120, k=2,05	Lot A383/27, 812024165

No.	MEASUREMENTS, ADJUSTMENTS AND/OR SETTINGS	MEAN VALUE
1	Warm-up time:	> 2 h
2	Excitation voltage:	5,00 V dc
3	Gain:	97,3 x 2
4	Cal A [ue]:	168,9 ue
5	Cal B [ue]:	-168,0 ue
6	Theoretical Calibration Strain Value for Shunt Resistor:	-5773 ue
7	Bridge Factor [V/e]:	5,075
8		
9		
10		

REMARKS:

TEL: 083 308 0418
FAX: 018 293 3915



CONCESSION REFERENCE:	INSPECTOR'S SIGNATURE:

CALIBRATION SHEET: PRESSURE CHANNEL

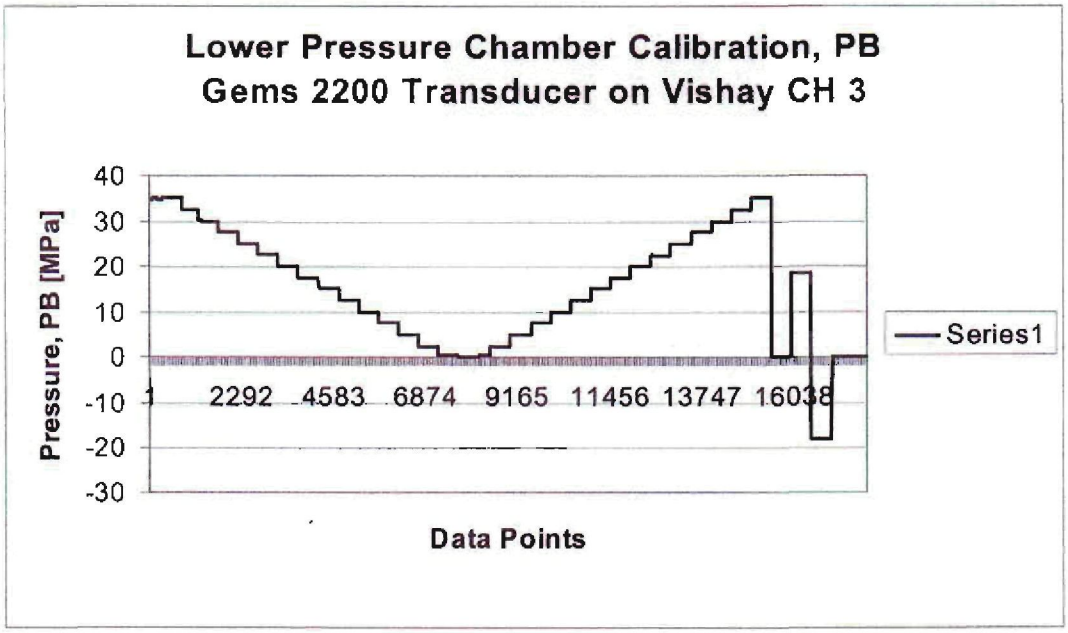
Reference Document: GRA-S60B-58-02	Issue: A	Circuit; AI2 Dev1
Description: LOOP DIA: P_B		CH No: 2
Inspector's Name: J G Roberts	Page 1 of 2	Date: 04-06-07

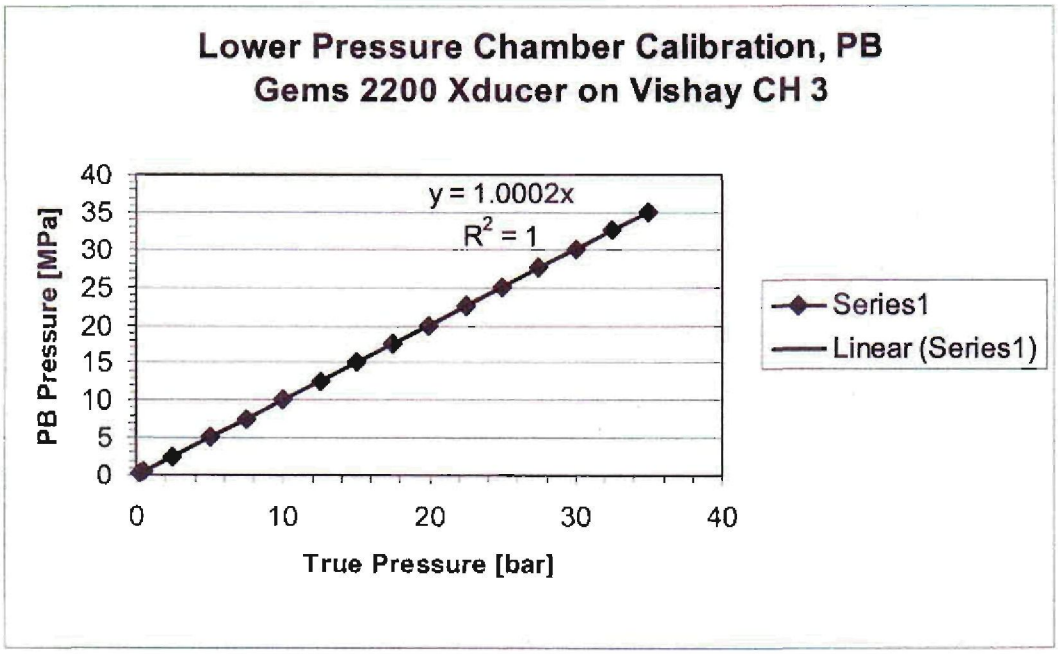
No.	COMPONENT DESCRIPTION	SERIAL NUMBER
1	Pressure Transducer, GEMS 2200 Series, 400 bar	Y051765
2	Strain Gauge Amplifier, Vishay 2120, Ch 3	022900
3	PCI-4472 DAQ card, National Instruments, "Dev1"	0X10FF7FA
4	Digital Multimeter, Fluke 75	3358352
5	Labview Program: "Calibration_PB_R4.vi"	gems400_a.lvm
6	Budenberg 1305BB portable gauge tester, Certified P3392	INA-80691
7	Software Scale: (1V / 3,6MPa)	GEMS400

No.	MEASUREMENTS, ADJUSTMENTS AND/OR SETTINGS	MEAN VALUE
1	Warm-up time:	> 2 h
2	Excitation voltage:	5,00 V dc
3	Gain:	113,5 x 2
4	Cal A [MPa]:	18,411
5	Cal B [MPa]:	-18,048
6	Value of gravitational acceleration, G:	9,80665
7	Mass Loading Sequence: EE, AA, A, B, C, D, E, I, G, J, K, F, H, L, M	
8	Mass Unloading Sequence: M, L, H, F, K, J, G, I, E, D, C, B, A, AA, EE	
9		
10		
11		

REMARKS: Run 2 s time delay; record Dev1 at 1000 Hz (2 values) with compression ratio of 2.

TEL: 083 308 0418
FAX: 018 293 3915





CONCESSION REFERENCE:	INSPECTOR'S SIGNATURE:

TEL: 083 308 0418
FAX: 018 293 3915

CALIBRATION SHEET: PRESSURE CHANNEL

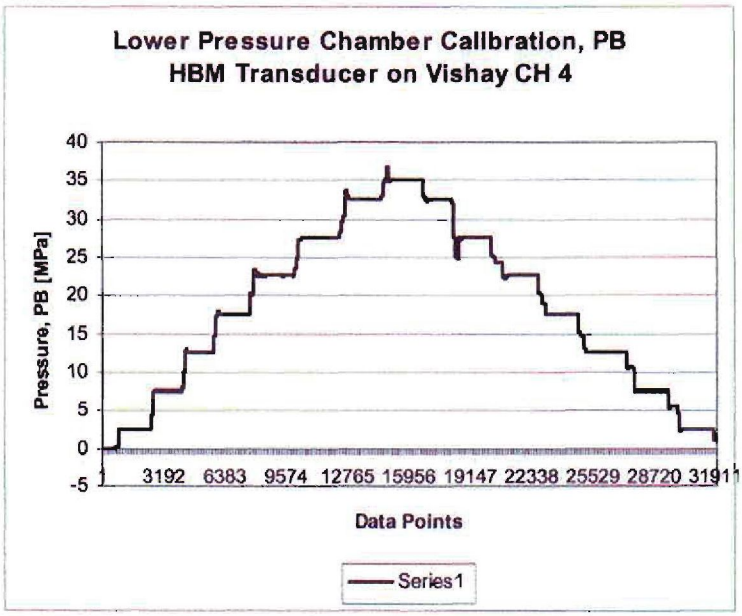
Reference Document: GRA-S60B-58-02	**Issue: A**	**Circuit: AI2 Dev1**
Description: LOOP DIA: P_B (Temp)		**CH No: 3**
Inspector's Name: J G Roberts	**Page 1 of 2**	**Date: 29-03-07**

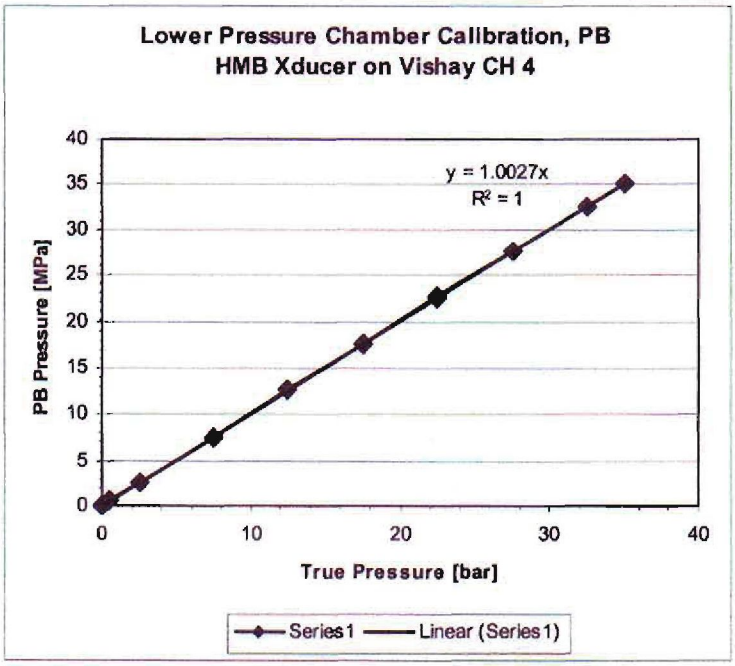
No.	COMPONENT DESCRIPTION	SERIAL NUMBER
1	Pressure Transducer, HBM P3MA, 500 bar, 2mV/V	B38689
2	Strain Gauge Amplifier, Vishay 2120, Ch 4	022900
3	PCI-4472 DAQ card, National Instruments, "Dev1"	0X10FF7FA
4	Digital Multimeter, Fluke 75	3358352
5	Labview Program: "Calibration_PBH_R1.vi"	PB_kal_070329_4
6	Budenberg 1305BB portable gauge tester, Certified P3392	INA-80691
7	Software Scale: (1V / 5MPa)	HBM500

No.	MEASUREMENTS, ADJUSTMENTS AND/OR SETTINGS	MEAN VALUE
1	Warm-up time:	> 2 h
2	Excitation voltage:	5,00 V dc
3	Gain:	497,0 x 2
4	Cal A [bar]:	12,53
5	Cal B [bar]:	-12,51
6	Value of gravitational acceleration, G:	9,80665
7	Mass Loading Sequence: EE, AA+A, B+C, D+E, I+G, J+K, F+H, L+M	
8	Mass Unloading Sequence: M+L, H+F, K+J, G+I, E+D, C+B, A+AA	
9		
10		
11		

REMARKS: Run 2 s time delay; record Dev1 at 1000 Hz (2 values) with compression ratio of 2.

TEL: 083 308 0418
FAX: 018 293 3915





CONCESSION REFERENCE:	INSPECTOR'S SIGNATURE:
	J Roberts

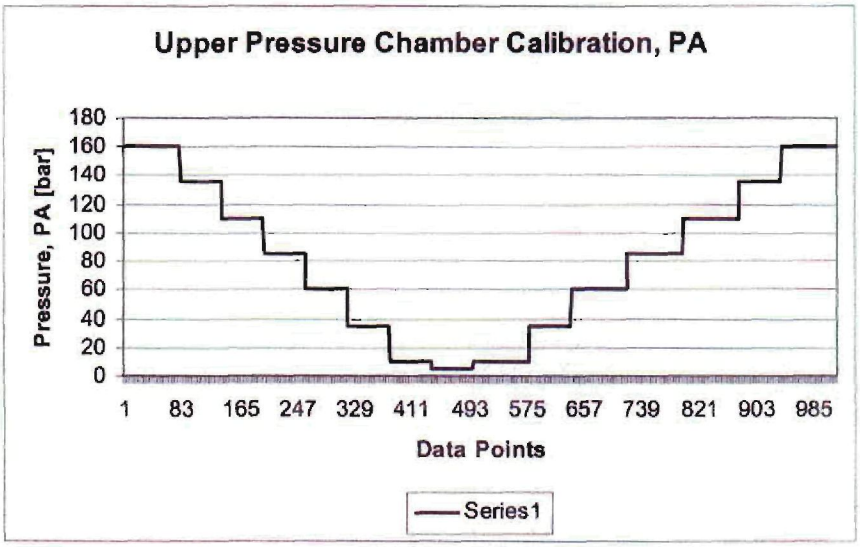
CALIBRATION SHEET: PRESSURE CHANNEL

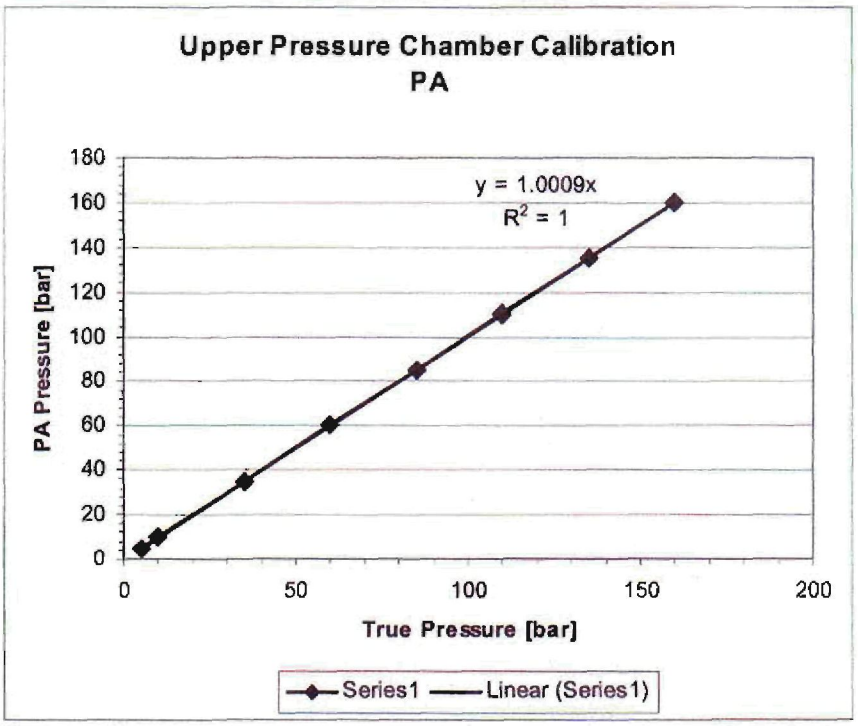
Reference Document: GRA-S60B-56-02	**Issue: A**	**Circuit: AI1 Dev1**
Description: LOOP DIA: P_A		**CH No: 1**
Inspector's Name: J G Roberts	**Page 1 of 2**	**Date: 18-12-06**

No.	COMPONENT DESCRIPTION	SERIAL NUMBER
1	Pressure Transducer, GEMS 2200 Series, 160 bar	W061409
2	Strain Gauge Amplifier, Vishay 2120, Ch 2	022822
3	PCI-4472 DAQ card, National Instruments, "Dev1"	0X10FF7FA
4	Digital Multimeter, Fluke 75	3358352
5	Labview Program: "Calibration_PA_R1.vi"	PA_kal.lvm
6	Budenberg 1305BB portable gauge tester, Certified P3392	INA-80691
7	Software Scale: (1V / 2MPa)	GEMS160

No.	MEASUREMENTS, ADJUSTMENTS AND/OR SETTINGS	MEAN VALUE
1	Warm-up time:	> 2 h
2	Excitation voltage:	5,00 V dc
3	Gain:	81,0 x 2
4	Cal A [bar]:	53,56
5	Cal B [bar]:	-53,63
6	Value of gravitational acceleration, G:	9,80665
7	Mass Loading Sequence: EE, DD, A, B, C, D, E, I	
8	Mass Unloading Sequence: I, E, D, C, B, A, DD	
9		
10		
11		
12		

REMARKS:





CONCESSION REFERENCE:	INSPECTOR'S SIGNATURE:

Sarto Mass Services CC
Reg No. CK 2001/049589/23
363 Oak Avenue, Ferndale, Randburg
PO Box 15, Randburg 2125
Tel: (011) 787-9179
Fax: (011) 787-9180

SANAS ACCREDITED LABORATORY No : 1415

Customer: North West University Environment: Clean

Location: Room 210 Next Due: March 2007

CALIBRATION CERTIFICATE

№ 013409

JOB CARD No.:

(This on-site calibration certificate is issued under the authority and conditions granted by SANAS. It may not be reproduced except in full without the written approval of the laboratory)

DETAILS OF INSTRUMENT : Make: SARTORIUS Model: 44207

Serial No.: 11800187 Capacity: 620g

Graduations: 0,0001g

CALIBRATION PROCEDURE : The instrument has been calibrated with standard weights of known value, traceable to the national standard, in accordance with Procedure No. ~~ZSM/CP~~ SMS001/CP

TRACEABILITY : Certificate No.: MVM 4484 Dated: Oct 2006

CALIBRATION RESULTS :

REPEATABILITY	ACCURACY AND LINEARITY		
	LOAD APPLIED g	BEFORE g	AFTER g
1. 200,0000g	0	0	0
2. 200,0000g	1,00005	1,0000g	1,0000g
3. 200,0000g	10,00001	10,0001g	10,0000g
4. 200,0000g	100,0000	100,0025g	100,0000g
5. 200,0000g	200,0004	200,0045g	200,0000g
6. 200,0000g	300,0004	300,0049g	300,0000g
Standard Deviation:			

ECCENTRIC ERROR			DISCRIMINATION		
Load Applied:	Maximum Error:		Weight Added	At load of	Response
100,0015g		100,0015g			
	100,0000g				
100,0000g		100,0000g			

REMARKS:

EXPANDED UNCERTAINTY : The reported uncertainties of measurement are based on a standard uncertainty multiplied by a coverage factor of k=2, which, unless specifically stated otherwise, provides a level of confidence of app. 95%.

± 0001g

VALIDITY OF CALIBRATION : This calibration was done on-site. The values in this certificate are correct at the time of calibration. Subsequently the accuracy will depend on such factors as the care exercised in handling and use of the instrument as well as the frequency of use. Re-calibration should be performed after such a period which is chosen to ensure that the instrument's accuracy remains within the desired limits.

CALIBRATED BY : R. MYNHARDT (PRINT NAME) (SIGNATURE)

DATE CALIBRATED AND ISSUED : 10/11/06 AUTHORISED SIGNATORY

Certificate of Calibration

SANAS ACCREDITED LABORATORY

SANAS accredited laboratory no's 139/239/339/539/1439

The South African National Accreditation Service (SANAS) is a signatory to the multilateral agreement of the European co-operation for Accreditation of Laboratories (EA) and the bilateral agreement with the Chinese National Laboratory Accreditation (CNLA) organisations for the recognition of calibration certificates.

Certificate No	: P3392		
Manufacturer	: Budenberg		
Description	: Portable gauge tester		
Model No	: 1305BB		
Serial No	: INA-80691		
Plant No	: None		
Calibrated for	: North-West University, Potchefstroom		
Temperature	: 24 °C		
Relative humidity	: 53 %RH		
Date of calibration	: 24 to 31 October 2006		
Expiry date	: 31 October 2008	Issue date	: 31 October 2006
Calibrated by	: J.W.H. Prinsloo/ F.J.C. Martins	Checked by	:

This certificate is issued without alteration, and in accordance with the conditions of accreditation granted by the SANAS. It is a correct record of the measurements made at the time of calibration. Copyright of this certificate is owned jointly by the SANAS and InterCal and may not be reproduced other than in full, except with the prior written approval of the SANAS and InterCal. The values given in this certificate were correct at the time of calibration. Subsequently the accuracy will depend on factors such as care exercised in handling the instrument and frequency of use. Recalibration should be performed after a period which has been chosen to ensure that, under normal circumstances, the instruments accuracy remains within the desired limits. The accuracies of all measurements were traceable to the national measuring standards as maintained in South Africa, unless otherwise noted. The uncertainties of measurement were estimated for a coverage factor of k=2 which approximates a 95% confidence level.

SANAS Authorised Signatory

F.J.C. Martins Pressure

G.Snelling Mass

Accredited Calibration Services CC Reg: CK1992/28397/23 T/A "InterCal"
Labotec Park, 21 Bavaria Road, Midrand
PO Box 10907 Vorna Valley 1686
Tel: (011) 315 4321 Fax: (011) 312 1322 e-mail: intercal@intercal.co.za www.intercal.co.za

Members: PS Haarhoff GC Snelling

Certificate of Calibration

Certificate No: P3392

1. Standards and equipment

Fixed Asset ID	Make	Model	Description	Serial Number	Certificate No	Cal Due Date
2-03	Fluke	700P07	Pressure Transducer	6250711	P3257	Aug-2008
2-05	Fluke	700P30	Pressure Transducer	69553007	PS/P-2729	Jul-2008
2-10	SI Pressure	PC6 Pro	Pressure Calibrator	5801	P3255	Aug-2008

2. Procedure

2.1 The UUT (Unit Under Test) was calibrated by measuring the pressure as generated by the UUT in terms of EAL G26.

2.2 A pressure transducer was used to measure the UUT output.

2.3 The UUT was loaded with mass pieces, starting with the piston and then measuring the pressure as generated by the UUT. The first mass piece was loaded and the pressure measured. This next mass piece was added and the pressure measured. This was continued until all the mass pieces were loaded. The data reported is the average value of three readings.

2.4 Pressures for the individual mass pieces were determined by calculation using the ΔP method.

2.5 The calibration medium was oil.

2.6 The UUT piston temperature was taken to be at the ambient temperature of 24 °C and corrected to 20 °C by a factor of 0.00243 %/ °C for stainless steel pistons.

2.7 All values reported are for a standard gravity of Gs=9.80665 m/s^2. Care should be taken to apply local gravity corrections during use.

2.8 The mass of the UUT mass pieces and piston assemblies were determined in accordance with procedure 14/P/001.

2.9 The mass pieces were marked A through FF prior to calibration.

SANAS Authorised Signatory

Certificate of Calibration

Certificate No: P3392

3. **Results**

3.1 **High Pressue Piston "D"**

UUT Mass No.		Measured UUT output Pressure with reference to standard gravity of 9.80665 m/s^2 (kPa)					
	A	B	C	D	E	F	G
	Mass (g)	Nominal Pressure per mass piece	Determined Pressure per mass	Nominal cumalative pressure (Mass No. + piston/ loading table)	Cumalative pressure (Mass No. + piston/ loading table)	Difference pressure of the cumalative pressure	% Relative error of the cumalative pressure
A	2014.78	2500	2499	2750	2749	-1.0	-0.03
B	2015.72	2500	2500	5250	5249	-0.6	-0.01
C	2015.37	2500	2498	7750	7748	-2.2	-0.03
D	2015.26	2500	2500	10250	10248	-1.8	-0.02
E	2014.48	2500	2497	12750	12746	-4.4	-0.03
F	2014.40	2500	2498	15250	15244	-6.0	-0.04
G	2015.33	2500	2500	17750	17744	-5.6	-0.03
H	2015.17	2500	2497	20250	20242	-8.2	-0.04
I	2015.57	2500	2504	22750	22746	-3.8	-0.02
J	2015.40	2500	2495	25250	25242	-8.4	-0.03
K	2015.28	2500	2499	27750	27741	-9.0	-0.03
L	2015.34	2500	2495	30250	30236	-13.6	-0.04
M	2015.03	2500	2502	32750	32739	-11.2	-0.03
N	2014.54	2500	2497	35250	35236	-13.8	-0.04
O	2014.12	2500	2496	37750	37733	-17.4	-0.05
P	2015.23	2500	2499	40250	40232	-18.0	-0.04
Q	2014.87	2500	2494	42750	42726	-23.6	-0.06
R	2014.89	2500	2500	45250	45227	-23.2	-0.05
S	2015.34	2500	2499	47750	47726	-23.8	-0.05
T	2015.33	2500	2496	50250	50223	-27.4	-0.05
U	2015.03	2500	2496	52750	52719	-31.0	-0.06
V	2014.94	2500	2498	55250	55217	-32.6	-0.06
W	2015.42	2500	2498	57750	57716	-34.2	-0.06
X	2015.42	2500	2495	60250	60211	-38.8	-0.06
Y	2015.58	2500	2496	62750	62708	-42.4	-0.07
Z	2015.24	2500	2500	65250	65208	-42.0	-0.06
AA	1613.55	2000	1999	67250	67207	-42.7	-0.06
BB	806.62	1000	998	68250	68205	-44.6	-0.07
CC	806.57	1000	999	69250	69205	-45.4	-0.07
DD	403.25	500	501	69750	69706	-44.3	-0.06
EE	201.6367	250	250	70000	69955	-44.8	-0.06
FF	201.6889	250	247	70250	70202	-48.3	-0.07
Piston	201.6811	250	250	Incl. in above	Incl. in above	Incl. in above	Incl. in above
The effective area (A_0) of the pison was determined to be 7.9069 mm^2 ± 0.0063 mm^2							

Uncertainty of measurement: Pressure: ± 0.06 %
Mass: ± 0.015 %

SANAS Authorised Signatory

Certificate of Calibration

Certificate No: P3392

3.2 Low Pressue Piston "C"

UUT Mass No.		Measured UUT output Pressure with reference to standard gravity of 9.80665 m/s^2 (kPa)					
	A	B	C	D	E	F	G
	Mass (g)	Nominal Pressure per mass piece	Determined Pressure per mass	Nominal cumalative pressure (Mass No. + piston/ loading table)	Cumalative pressure (Mass No. + piston/ loading table)	Difference pressure of the cumalative pressure	% Relative error of the cumalative pressure
A	2014.78	500	501	550	550	0.5	0.09
B	2015.72	500	500	1050	1051	0.6	0.05
C	2015.37	500	500	1550	1551	0.6	0.04
D	2015.26	500	498	2050	2048	-1.6	-0.08
E	2014.48	500	501	2550	2550	-0.2	-0.01
F	2014.40	500	499	3050	3049	-1.1	-0.04
G	2015.33	500	500	3550	3549	-1.0	-0.03
H	2015.17	500	499	4050	4048	-2.0	-0.05
I	2015.57	500	500	4550	4548	-1.9	-0.04
J	2015.40	500	500	5050	5048	-2.3	-0.05
K	2015.28	500	500	5550	5547	-2.7	-0.05
L	2015.34	500	499	6050	6046	-3.6	-0.06
M	2015.03	500	499	6550	6545	-4.6	-0.07
N	2014.54	500	499	7050	7045	-5.5	-0.08
O	2014.12	500	500	7550	7545	-5.4	-0.07
P	2015.23	500	501	8050	8046	-4.3	-0.05
Q	2014.87	500	497	8550	8543	-7.2	-0.08
R	2014.89	500	499	9050	9042	-8.2	-0.09
S	2015.34	500	500	9550	9542	-8.1	-0.08
T	2015.33	500	501	10050	10043	-7.0	-0.07
U	2015.03	500	500	10550	10543	-6.9	-0.07
V	2014.94	500	499	11050	11042	-7.8	-0.07
W	2015.42	500	498	11550	11540	-9.8	-0.08
X	2015.42	500	500	12050	12040	-9.7	-0.08
Y	2015.58	500	500	12550	12540	-9.6	-0.08
Z	2015.24	500	499	13050	13039	-10.5	-0.08
AA	1613.55	400	400	13450	13439	-10.7	-0.08
BB	806.62	200	199	13650	13639	-11.2	-0.08
CC	806.57	200	200	13850	13839	-10.8	-0.08
DD	403.25	100	98	13950	13937	-12.6	-0.09
EE	201.6367	50	51	14000	13989	-11.5	-0.08
FF	201.6889	50	49	14050	14038	-12.4	-0.09
Piston	201.4491	50	49	Incl. in above	Incl. in above	Incl. in above	Incl. in above
The effective area (A_0) of the pison was determined to be 39.594 mm^2 ± 0.032 mm^2							

Uncertainty of measurement: Pressure: ± 0.06 %
Mass: ± 0.015 %

SANAS Authorised Signatory

Certificate of Calibration

Certificate No: P3392

4. Comments

4.1 Care should be taken by the user to correct the pressure at his location, by a factor of k which is determined by $Gl_{of\ user}$ / Gs. The true pressure generated is thus the pressure at Gs from the above table multiplied by k.

4.2 The results reflected in this certificate were entered directly on PC.

----- End of document -----

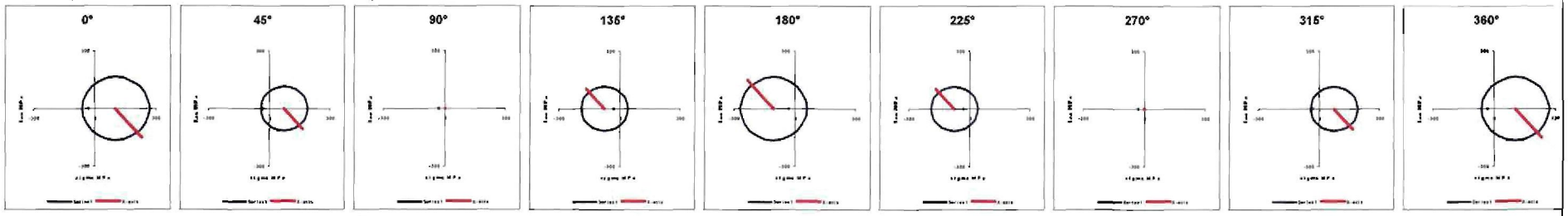
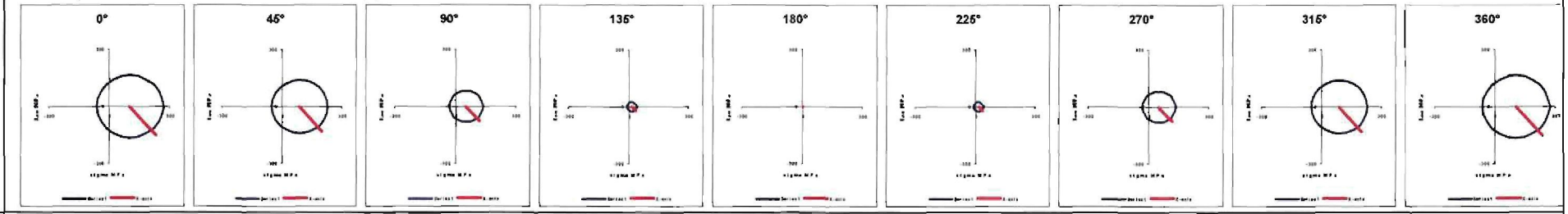
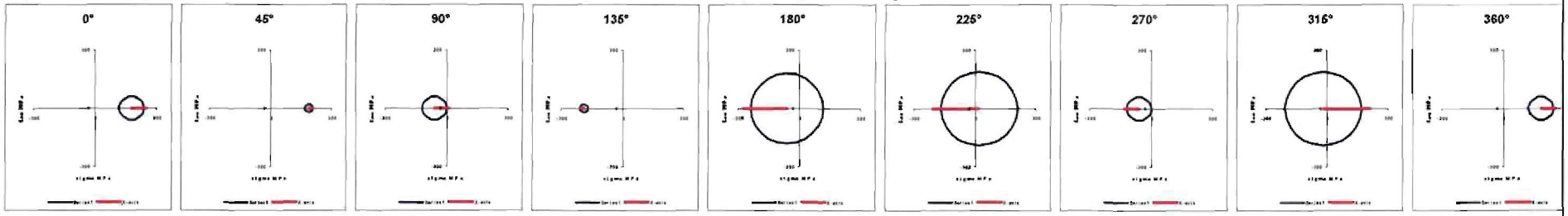
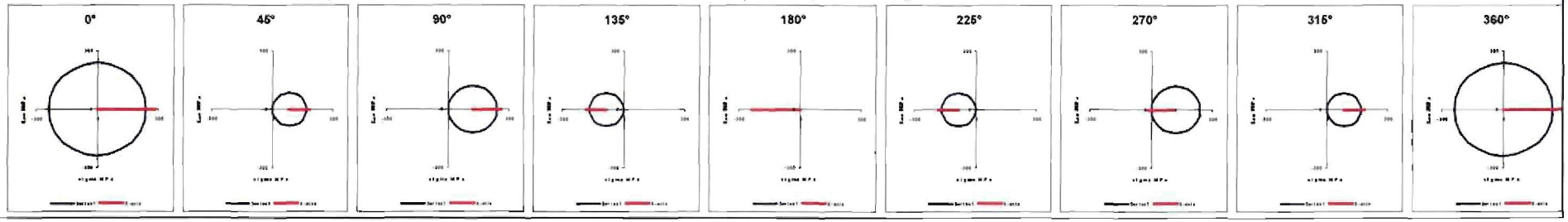
SANAS Authorised Signatory

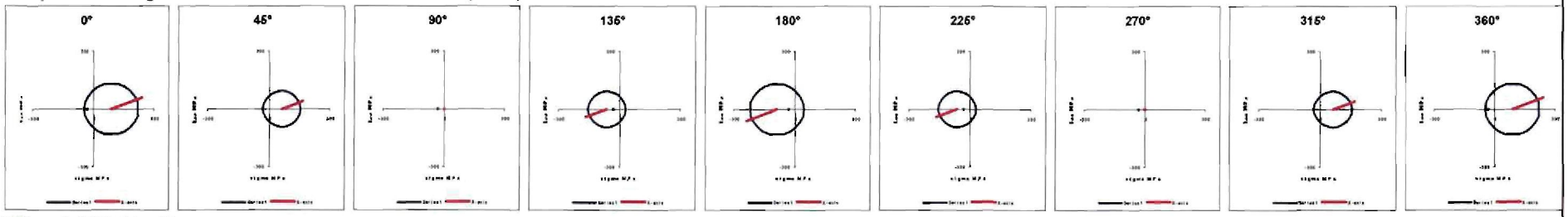
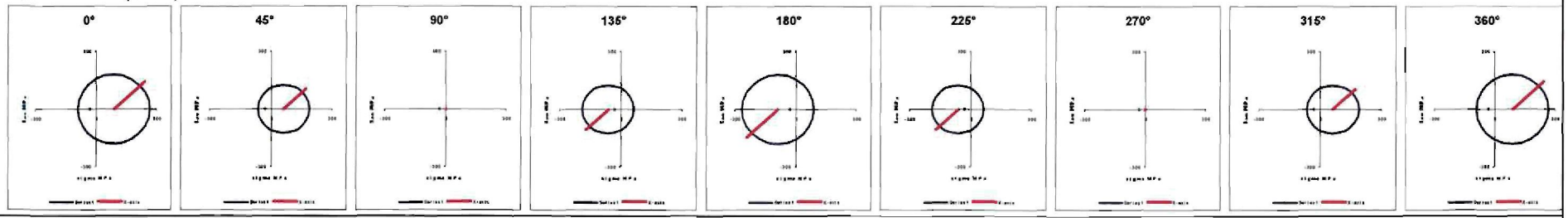
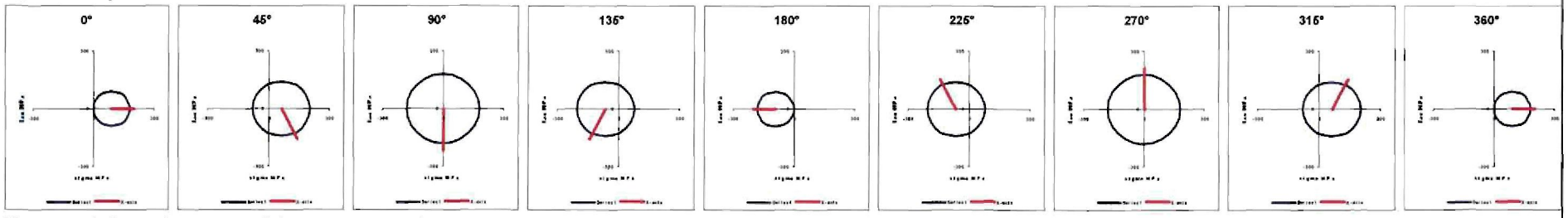
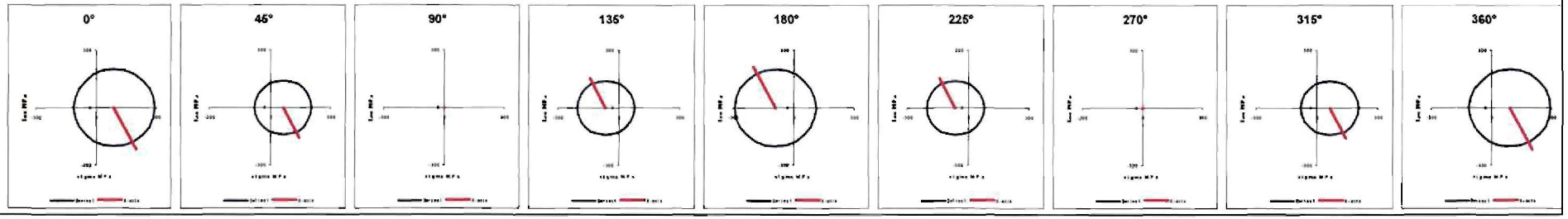
APPENDIX G

Mohr Circle Excursions

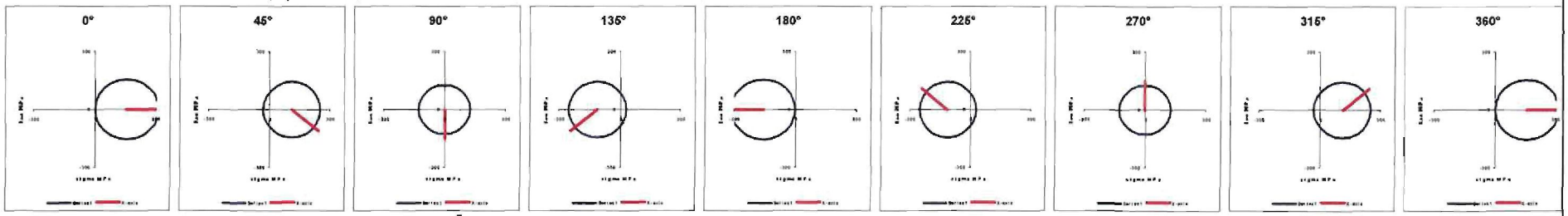
The numbers in the following table refer to the specimen number in Figure 2-1 of Chapter 2 and in Figure 4-4 of Chapter 4.

The radial line from the centre of the circle indicates the axis of loading of the specimen (usually the longitudinal axis). The axis which is perpendicular to the loading axis in the physical domain (opposite direction to the shown axis on the Mohr circle) is not shown.

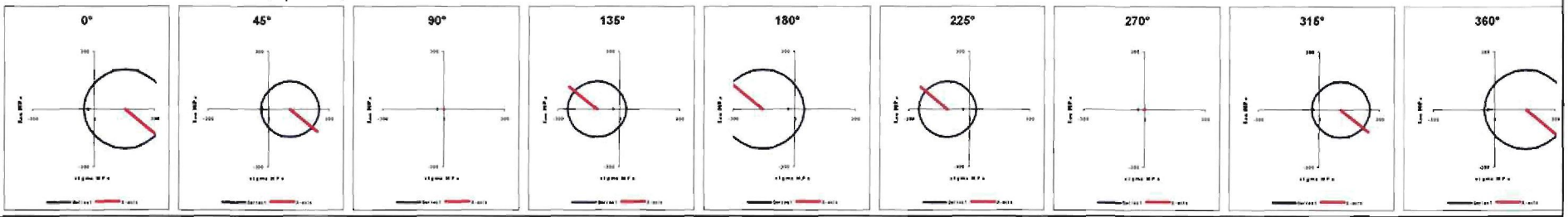
No	Mohr-Circle Stress Excursions
S1	R = -1 (Combined Axial and Torsional)  R = 0 (Combined Axial and Torsional) 
S2	Equal amplitude, hoop stress frequency 2x axial stress, hoop stress leads by 60° phase angle  Equal amplitude, hoop stress frequency 2x axial stress, hoop stress leads by 180° phase angle 

No	Mohr-Circle Stress Excursions
S3	Torque/Bending moment in root radius = 0.581 (0.7?)  T/B = 1.378 (1.4?) 
S4	90° Out-of-phase axial load and torsion  0° or 180° Out-of-phase axial load and torsion 

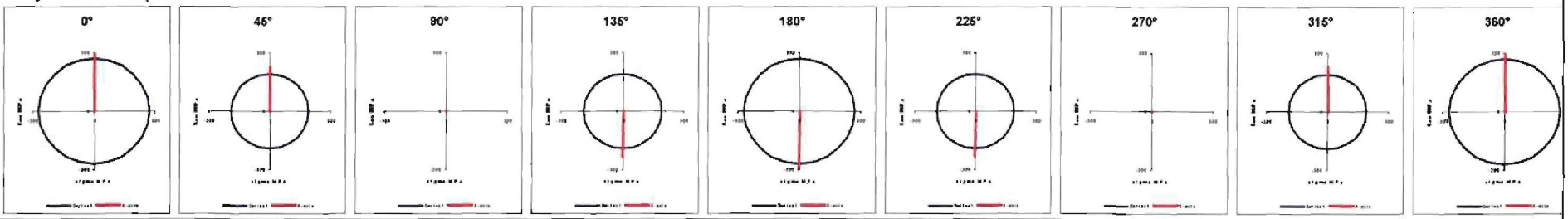
No	Mohr-Circle Stress Excursions
S10	B : T = 314 : 127 MPa/MPa, φ = 90°, N = 1 x 10^5

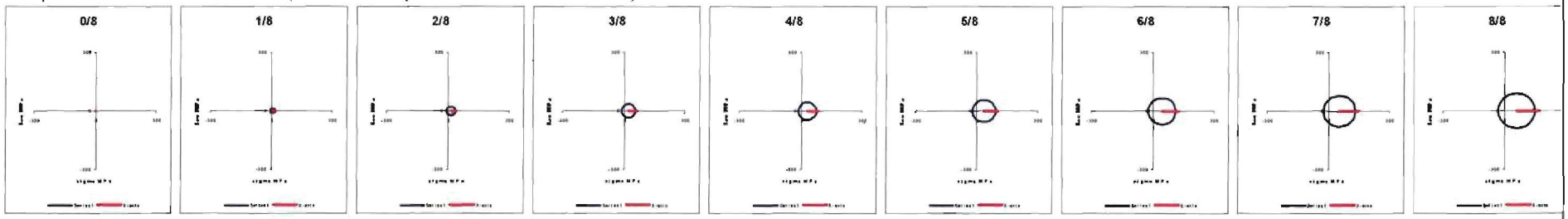
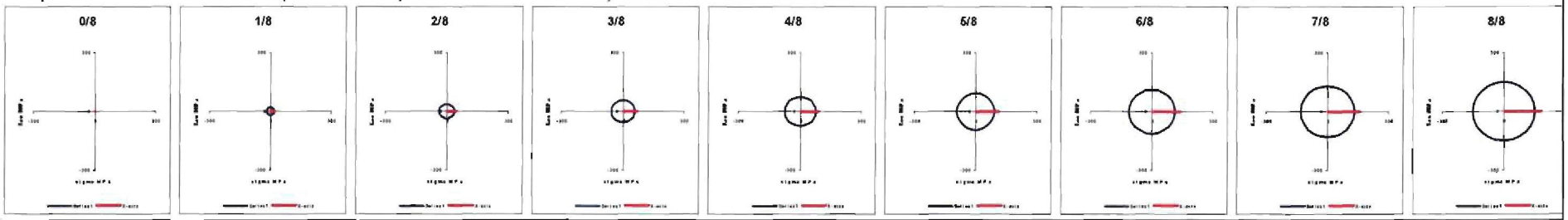
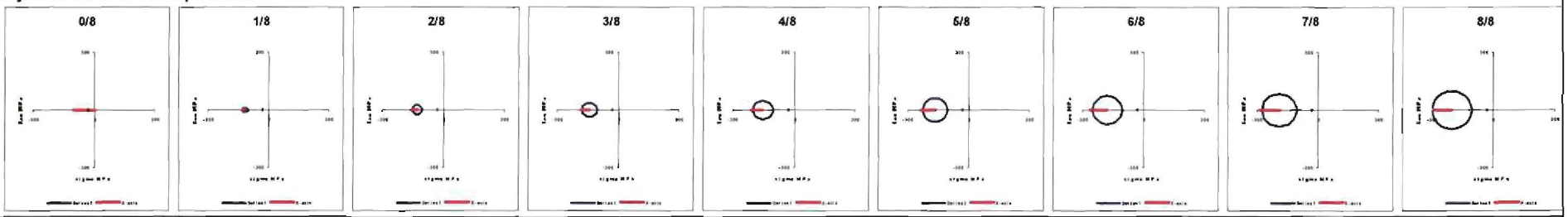


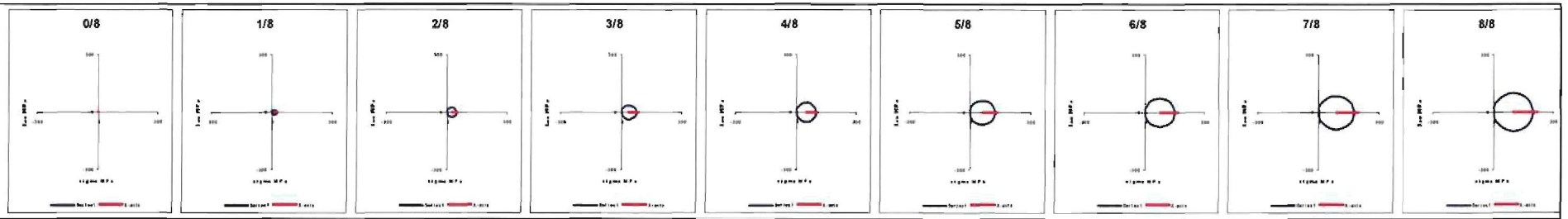
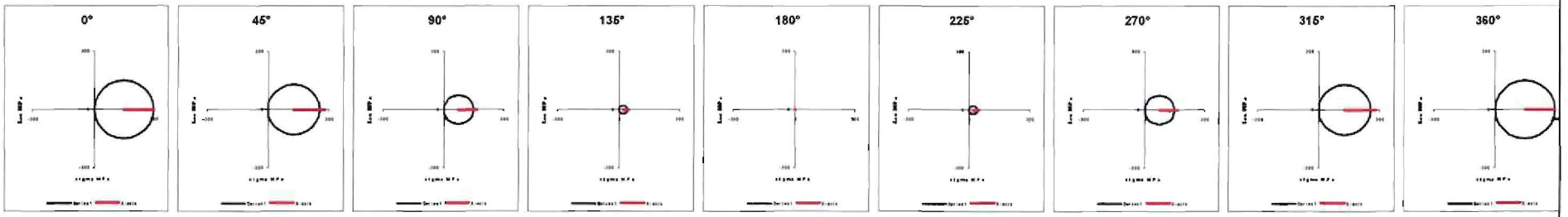
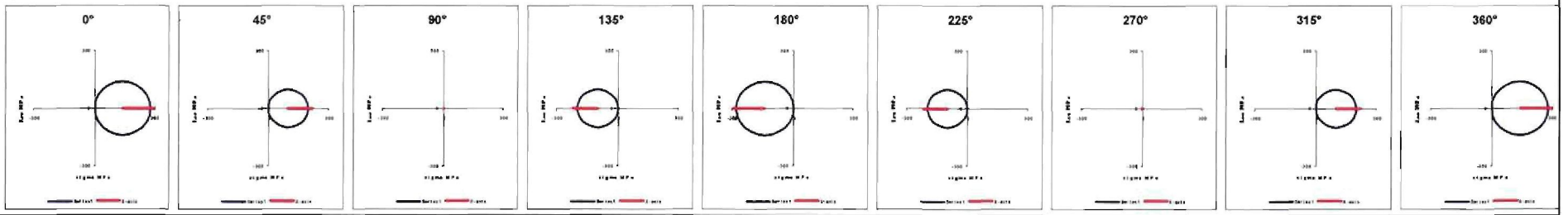
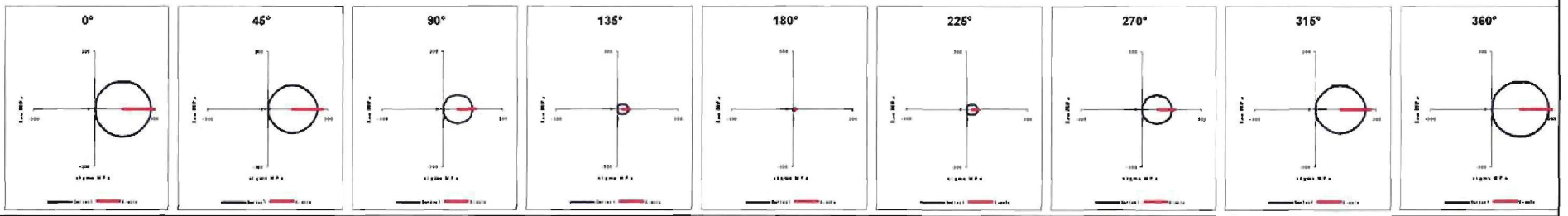
B : T = 309 : 134 MPa/MPa, φ = 0°, N = 1 x 10^5

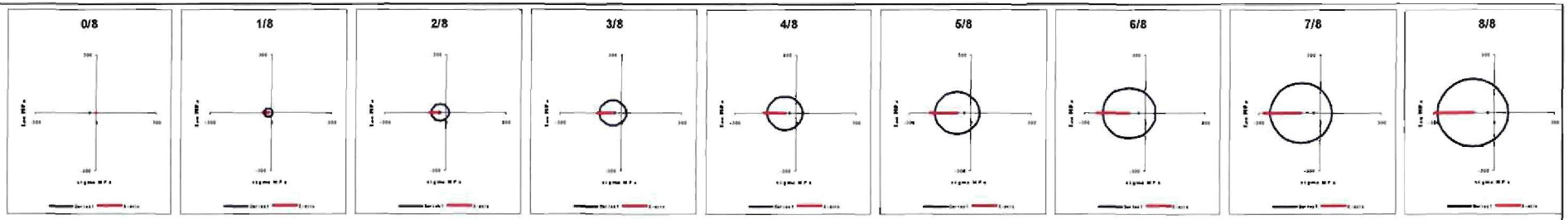
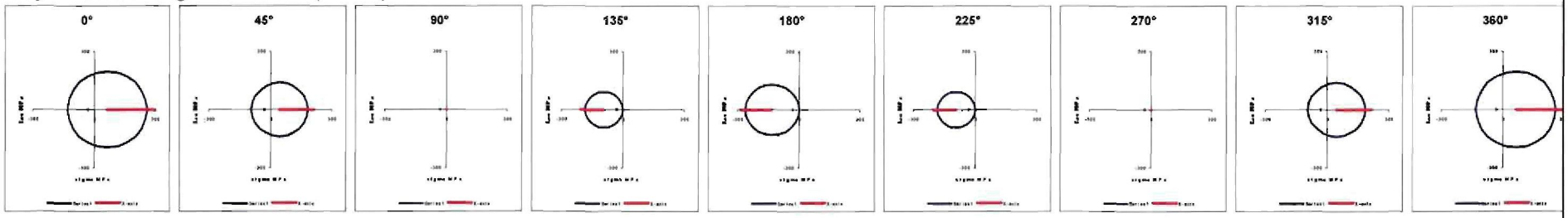
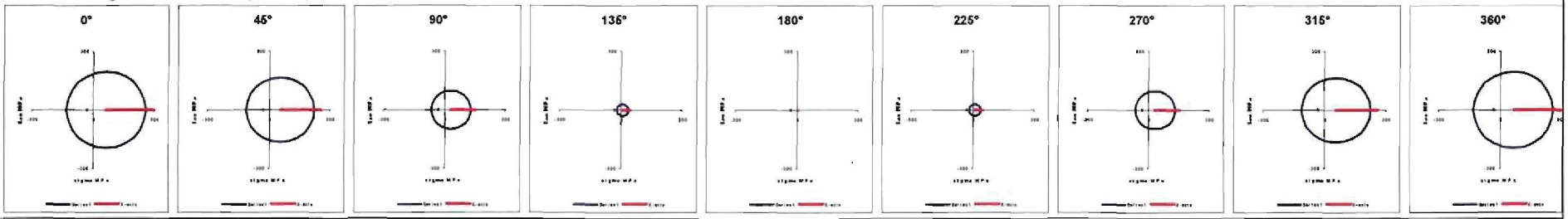
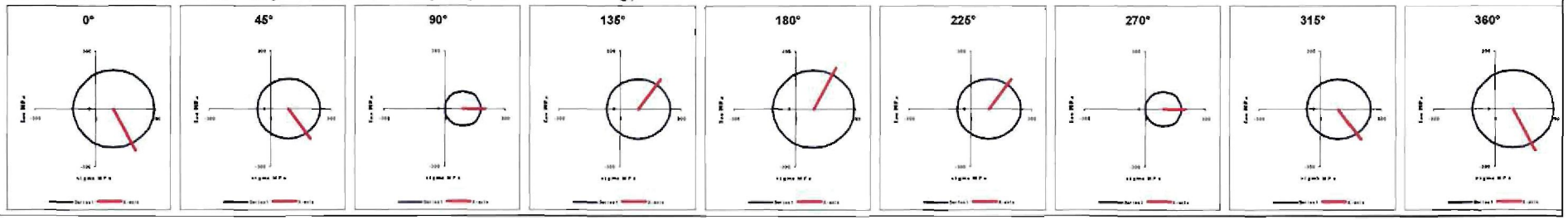


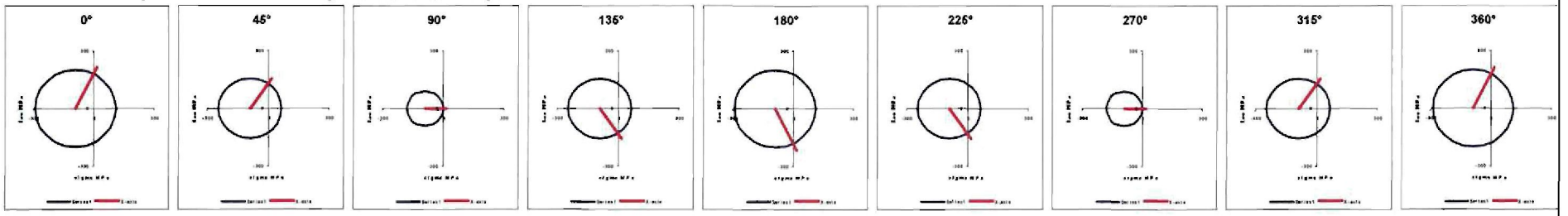
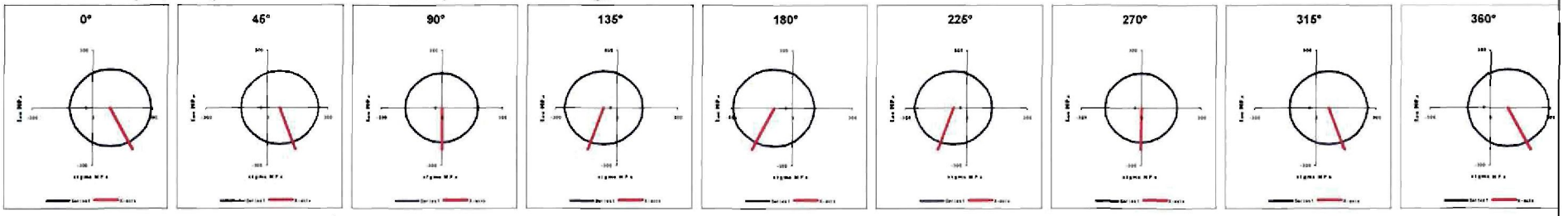
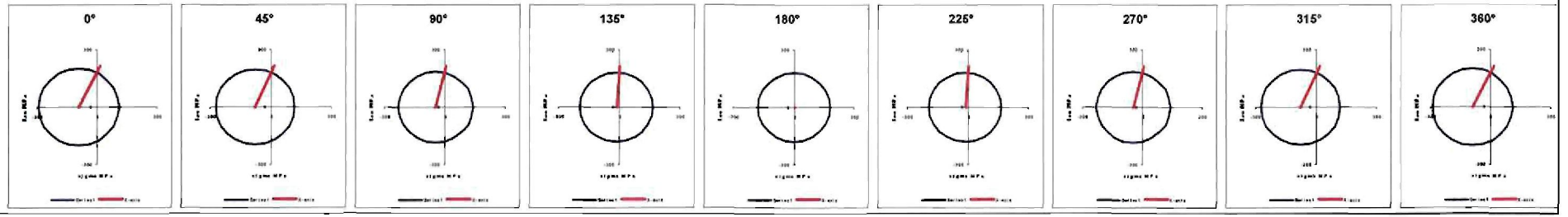
S11	Fully reversed pure torsion



No	Mohr-Circle Stress Excursions
S17	Hoop : Axial stress = +1 : +1 (Max is Hoop & Radial stress circle)  Hoop : Axial stress = +1 : -1 (Max is Hoop & axial stress circle) 
S5	Hydrostatic & Compressive Test 
S6	Tensile Test

	
No	Mohr-Circle Stress Excursions
S12	R = 0  R = -1 
S7	R = 0.05/0.95 = 0.0523 
S9	σθ : σz = +1 : -4 (z-axis shown)

	
No	Mohr-Circle Stress Excursions
S60	Fully reversed tangential stress (R = -1)  Tensile tangential stress (R = 0) 
80	Constant Tensile Load; Fully Reversed Torque (Bi-axial Loading) 

	Constant Compressive Load; Fully Reversed Torque 
No	Mohr-Circle Stress Excursions
80	Constant Torque; Fully Reversed Axial Load (Bi-axial Loading)  Constant Torque; R = 0 Axial Load 

APPENDIX H

Multiaxial Fatigue Tabular Results

MULTIAXIAL FATIGUE RESULTS TABLE

Appendix H

Spec.#	Date	Time	Temp [°C]	N [cycles]	R_t	Ampl [%]	PA max	PA min	PB max	PB min	σ max	σ min	R_a	F-Type	Dir	Block Pos	Clock Pos	M [g]	tc [mm]	dt1 [µm]	dt2 [µm]	dt3 [µm]	dt4 [µm]	t [mm]	f1 [Hz]	g [-]	h [-]	D [mm]
79 I-1	2007-06-16	17:06	27.5	1	0.5	92			0.0	0.00	0.0	0.0	#DIV/0!	H	X	B	7	396.6	8.855	50	50	50	50	8.905	3400	2.257855	-3.25785	95.810
37 E-9	2007-06-16	17:56	26.7	19	0.5	92	9.45	4.64	0.0	0.00	22.2	10.9	0.49	H	X	B	9	399.79	8.515	40	40	40	40	8.555	3400	2.345048	-3.34505	95.110
79 F1-3	2007-06-16	16:48	27.8	49	0.5	92	9.42	4.62	0.0	0.00	21.1	10.3	0.49	H	Z	B	6	400.31	8.95	40	40	40	40	8.99	3387.5	2.237729	-3.23773	95.980
79 A-11	2007-06-18	11:17	30.4	50	0.5	92	9.42	4.61	0.0	0.00	22.1	10.8	0.49	H	Z	AA	0	396.4	8.52	40	40	40	30	8.5575	3437.5	2.344399	-3.3444	95.115
37 A2-1	2007-06-16	16:09	27.3	91	0.5	92	9.42	4.62	0.0	0.00	21.3	10.4	0.49	O	X	AA	7	393.48	8.865	40	40	30	40	8.9025	3350	2.258453	-3.25845	95.805
79 I-6	2007-06-16	17:21	27.3	101	0.5	92	9.42	4.62	0.0	0.00	21.3	10.4	0.49	O	X	B	0	399.31	8.845	60	60	60	60	8.905	3418.8	2.257855	-3.25785	95.810
37 A2-2	2007-06-16	16:35	27.8	155	0.5	92	9.42	4.62	0.0	0.00	21.3	10.4	0.49	O	X	AA	6	399.44	8.835	70	50	60	50	8.8925	3443.8	2.260848	-3.26085	95.785
79 F1-9	2007-06-16	16:22	27.5	206	0.5	92	9.42	4.62	0.0	0.00	21.1	10.3	0.49	O	X	B	11	401.24	8.935	60	60	50	50	8.99	3418.8	2.237729	-3.23773	95.980
37 G-5	2007-06-16	11:52	30.9	74	0.5	87	8.92	4.36	0.0	0.00	20.1	9.8	0.49	H	Z	B	9	399.77	8.84	90	90	90	90	8.93	3387.5	2.251895	-3.25189	95.860
37 B1-1	2007-06-16	11:03	29.4	108	0.5	87	8.92	4.32	0.0	0.00	20.1	9.7	0.48	H	Z	A	7	398.83	8.87	40	50	50	40	8.915	3400	2.255467	-3.25547	95.830
79 F1-11	2007-06-16	10:42	29.1	184	0.5	87	8.91	4.33	0.0	0.00	19.9	9.7	0.49	O	X	B	12	400.79	8.93	60	60	60	60	8.99	3381.3	2.237729	-3.23773	95.980
79 I-13	2007-06-15	21:14	30.9	698	0.5	87	8.92	4.39	0.0	0.00	20.2	9.9	0.49	H	X	B	11	398.67	8.845	60	50	50	50	8.8975	3412.5	2.25965	-3.25965	95.795
37 A2-7	2007-06-16	11:20	29.7	2664	0.5	87	8.92	4.26	0.0	0.00	20.1	9.6	0.48	O	X	AA	0	396.38	8.855	60	50	50	50	8.9075	3412.5	2.257257	-3.25726	95.815
37 G-10	2007-06-16	12:09	31.1	2807	0.5	87	8.92	4.24	0.0	0.00	20.3	9.7	0.48	O	X	B	0	402.39	8.775	60	60	40	50	8.8275	3437.5	2.276551	-3.27655	95.655
79 O-15	2007-06-15	19:33	31.9	8237	0.5	87	8.92	4.98	0.0	0.00	20.0	11.2	0.56	H	Z	A	12	400.17	8.945	30	40	30	40	8.98	3437.5	2.240077	-3.24008	95.960
79 F1-12	2007-06-16	13:50	29.7	15278	0.5	87	8.96	4.35	0.0	0.00	20.0	9.7	0.49	O	Z	B	1	402.31	8.935	60	60	50	55	8.9913	3412.5	2.237436	-3.23744	95.983
79 I-9	2007-06-18	16:40	32.3	E	0.5	86			0.0	0.00	0.0	0.0	#DIV/0!	E	X	B	9	398.1	8.85	50	50	50	50	8.9	3406.3	2.259051	-3.25905	95.800
79 F2-1	2007-06-18	12:16	29.7	762	0.5	86	8.83	4.22	0.0	0.00	19.8	9.5	0.48	O	X	B	7	399.22	8.95	30	30	40	20	8.98	3368.7	2.240077	-3.24008	95.960
37 A2-9	2007-06-18	13:04	29.9	1065	0.5	86	8.84	4.28	0.0	0.00	19.9	9.6	0.48	H	X	AA	11	397.23	8.865	60	60	60	60	8.925	3418.8	2.253084	-3.25308	95.850
37 G-1	2007-06-18	13:25	30.2	1209	0.5	86	8.86	4.24	0.0	0.00	20.0	9.6	0.48	O	X	B	7	397	8.935	-20	-20	-20	-30	8.9125	3281.3	2.258063	-3.25606	95.825
37 A2-6	2007-06-18	11:38	29.8	1508	0.5	86	8.82	4.22	0.0	0.00	19.9	9.5	0.48	H	Z	AA	0	396.41	8.865	50	50	40	40	8.91	3393.8	2.25666	-3.25666	95.820
79 F1-10	2007-06-18	15:41	35.7	4101	0.5	86	8.82	4.32	0.0	0.00	19.7	9.7	0.49	O	Z	B	0	400.48	8.935	60	60	60	60	8.995	3393.8	2.236557	-3.23656	95.990
79 I-10	2007-06-18	16:54	32.5	5678	0.5	86	8.82	4.28	0.0	0.00	19.9	9.7	0.49	H	X	B	0	399.76	8.835	60	60	60	60	8.895	3431.2	2.260249	-3.26025	95.790
37 G-6	2007-06-18	13:47	30.5	14121	0.5	86	8.82	4.28	0.0	0.00	19.9	9.6	0.49	O	X	B	0	401.1	8.865	70	70	60	60	8.93	3431.2	2.251895	-3.25189	95.860
37 A2-5	2007-06-19	09:30		E	0.5	83			0.0	0.00	0.0	0.0	#DIV/0!	H	X	AA	9	396.09	8.845	60	50	50	50	8.8975	3400	2.25965	-3.25965	95.795
37 A2-3	2007-06-19	10:10	32.0	33745	0.5	83	8.52	4.10	0.0	0.00	19.2	9.3	0.48	H	X	AA	6	394.56	8.85	70	60	50	60	8.91	3356.3	2.25666	-3.25666	95.820
79 F2-4	2007-06-22	13:07	31.9	6555	0.5	83	8.52	4.00	0.0	0.00	19.1	8.9	0.47	O	Z	B	5	399.6	8.93	80	70	50	50	8.9925	3375	2.237143	-3.23714	95.985
79 F1-7	2007-06-18	21:50	31.3	4772	0.5	83	8.53	4.04	0.0	0.00	19.1	9.0	0.47	O	Z	B	0	402.28	8.945	50	50	50	50	8.995	3418.8	2.236557	-3.23656	95.990
79 I-5	2007-06-18	20:25	30.0	5500	0.5	83	8.53	4.02	0.0	0.00	19.3	9.1	0.47	O	X	B	9	397.85	8.865	30	30	30	30	8.895	3406.3	2.260249	-3.26025	95.790
79 I-7	2007-06-18	22:37	34.0	16405	0.5	83	8.54	4.14	0.0	0.00	19.3	9.4	0.48	H	X	B	0	399.69	8.85	50	50	50	50	8.9	3425	2.259051	-3.25905	95.800
37 E-13	2007-06-19	14:02	35.2	17545	0.5	83	8.52	4.02	0.0	0.00	20.0	9.4	0.47	O	X	B	11	400.25	8.48	60	60	50	60	8.5375	3412.5	2.349599	-3.3496	95.075
37 G-2	2007-06-19	17:36	30.7	10282	0.5	83	8.51	4.04	0.0	0.00	19.2	9.1	0.47	O	X	B	6	394.53	8.825	70	70	70	70	8.895	3218.8	2.260249	-3.26025	95.790
79 F2-5	2007-06-23	15:15	32.8	1723	0	89	6.94	0.07	0.0	0.00	15.5	0.2	0.01	O	Z	B	9	399.72	8.94	80	80	80	40	9.01	3343.8	2.23305	-3.23305	96.020
79 F2-2	2007-06-23	14:38	37.3	1024	0	89	7.30	0.06	0.0	0.00	16.3	0.1	0.01	O	X	B	6	400.35	8.935	60	70	60	70	9	3375	2.235387	-3.23539	96.000
79 K-1	2007-06-23	13:51	36.5	1587	0	89	7.02	0.07	0.0	0.00	15.9	0.2	0.01	O	X	A	7	398.34	8.855	50	50	50	50	8.905	3381.3	2.257855	-3.25785	95.810
79 I-2	2007-06-23	14:12	36.9	2120	0	89	7.10	0.07	0.0	0.00	16.0	0.2	0.01	O	X	A	6	396.59	8.85	50	50	50	50	8.9	3356.3	2.259051	-3.25905	95.800
37 A1-9	2007-06-23	12:57	34.6	3775	0	89	7.50	0.07	0.0	0.00	17.0	0.2	0.01	OH	X	A	5	398.07	8.82	40	20	20	20	8.845	3400	2.2723	-3.2723	95.690
37 A2-10	2007-06-23	13:31	36.4	1172	0	89	7.04	0.06	0.0	0.00	15.9	0.1	0.01	O	Z	AA	12	396.77	8.845	50	50	50	50	8.895	3412.5	2.260249	-3.26025	95.790
37 G-9	2007-06-23	12:39	34.4	1011	0	89	8.20	0.08	0.0	0.00	18.5	0.2	0.01	O	Z	B	9	399.8	8.87	50	50	50	50	8.92	3387.5	2.254275	-3.25427	95.840
37 E-10	2007-06-23	12:06	31.0	3327	0	89	7.38	0.07	0.0	0.00	17.4	0.2	0.01	O	X	B	0	401.44	8.48	50	50	50	50	8.53	3437.5	2.351556	-3.35156	95.060
79 F2-12	2007-06-25	04:16		E	0	76			0.0	0.00	0.0	0.0	#DIV/0!	E	X	B	1	401.91	8.945	50	30	30	50	8.985	3393.8	2.238902	-3.2389	95.970
79 F2-7	2007-06-25	03:58	30.6	E	0	76			0.0	0.00	0.0	0.0	#DIV/0!	E	X	B	0	401.96	8.94	50	40	60	30	8.985	3400	2.238902	-3.2389	95.970
79 K-13	2007-06-23	15:52	33.7	24578	0	76	6.30	0.06	0.0	0.00	14.2	0.1	0.01	O	X	A	11	398.56	8.855	60	60	60	60	8.915	3418.8	2.255467	-3.25547	95.830
79 I-15	2007-06-23	20:31	30.4	42970	0	76	7.22	0.10	0.0	0.00	16.3	0.2	0.01	O	Z	A	12	398.81	8.885	20	20	20	10	8.9025	3412.5	2.258453	-3.25845	95.805
37 B2-1	2007-06-23	15:37		E	0	76			0.0	0.00	0.0	0.0	#DIV/0!	E	Z	A	7	398.94	8.9	20	20	20	20	8.92	3381.3	2.254275	-3.25427	95.840
37 B1-3	2007-06-23	19:48	28.5	E	0	76			0.0	0.00	0.0	0.0	#DIV/0!	E	X	A	6	399.01	8.88	40	40	30	30	8.915	3393.8	2.255467	-3.25547	95.830
37 I-5	2007-06-25	01:42	36.9	20790	0	76	6.10	0.08	0.0	0.00	13.8	0.2	0.01	O	X	B	9	399.93	8.87	50	50	40	40	8.915	3418.8	2.255467	-3.25547	95.830
79 G1-5	2007-06-25	11:12	29.6	32163	0	76	6.72	0.08	0.0	0.00	15.0	0.2	0.01	O	X	B	9	400.5	9.016					9.016	3381.3	2.231651	-3.23165	96.032
37 I-6	2007-06-25	01:27	39.0	528	0	76	8.20	0.84	0.0	0.00	18.5	1.9	0.10	O	X	B	0	400.2	8.85	80	80	80	80	8.93	3431.2	2.251895	-3.25189	95.860
79 F2-9	2007-06-20	14:42	37.8	39835	0	80	5.80	0.06	0.0	0.00	13.0	0.1	0.01	O	Z	B	11	400.69	8.93	40	50	60	60	8.9825	3387.5	2.239489	-3.23949	95.965
79 F2-6	2007-06-20	11:14	36.6	12412	0	80	7.46	0.10	0.0	0.00	16.7	0.2	0.01	O	Z	B	0	401.52	8.94	40	40	40	30	8.9775	3387.5	2.240664	-3.24066	95.955
79 K-9	2007-06-20	13:34	35.3	5663	0	80	6.68	0.08	0.0	0.00	15.1	0.2	0.01	H	X	A	9	398.02	8.87	40	40	40	40	8.91	3406.3	2.25666	-3.25666	95.820
79 I-14	2007-06-19	21:44		E	0	80			0.0	0.00	#DIV/0!	#DIV/0!	#DIV/0!	E	X	A	12							#DIV/0!		#DIV/0!	#DIV/0!	#DIV/0!
37 B1-9	2007-06-20	10:12	32.5	5806	0	80	7.55	0.15	0.0	0.00	17.0	0.3	0.02	O	X	A	11	399.05	8.875	40	40	40	40	8.915	3493.7	2.255467	-3.25547	95.830
37 B1-2	2007-06-20	12:59	35.0	2876	0	80	7.34	0.10	0.0	0.00	16.6	0.2	0.01	O	X	A	6	399.35	8.88	40	40	30	30	8.915	3418.8	2.255467	-3.25547	95.830
37 I-1	2007-06-22	23:49	29.7	1684	0	80	7.50	0.13	0.0	0.00	16.9	0.3	0.02	O	Z	B	7	396.54	8.905	40	40	40	30	8.9425	3293.8	2.248928	-3.24893	95.885
37 I-2	2007-06-19	20:49	35.8	4995	0	80	7.10	0.11	0.0	0.00	16.0	0.2	0.02	O	Z	B	6	394.26	8.91	0	0	0	0	8.91	3268.8	2.25666	-3.25666	95.620

MULTIAXIAL FATIGUE RESULTS TABLE

Spec.#	Date	Time	Temp [°C]	N [cycles]	R_t	Ampl [%]	PA max	PA min	PB max	PB min	σ max	σ min	R_a	F-Type	Dir	Block Pos	Clock Pos	M [g]	tc [mm]	dt1 [µm]	dt2 [µm]	dt3 [µm]	dt4 [µm]	t [mm]	f1 [Hz]	q [-]	h [-]	D [mm]
79 F2-8	2007-06-23	02:33	30.5	2033	0	84	7.70	0.12	0.0	0.00	17.2	0.3	0.02	O	X	B	3	401.46	8.94	80	80	50	50	9.005	3387.5	2.234218	-3.23422	96.010
79 B-14	2007-06-23	00:46	29.6	340	0	84	8.22	0.13	0.0	0.00	18.6	0.3	0.02	O	X	A	12	394.5	8.84	60	60	60	60	8.9	3356.3	2.259051	-3.25905	95.800
79 K-5	2007-06-23	01:11	29.3	4388	0	84	7.48	0.10	0.0	0.00	16.9	0.2	0.01	H	X	A	9	397.84	8.835	70	70	70	70	8.905	3412.5	2.257855	-3.25785	95.810
79 I-3	2007-06-23	02:14	30.2	563	0	84	8.18	0.14	0.0	0.00	18.5	0.3	0.02	O	X	A	6	396.61	8.86	40	40	50	40	8.9025	3368.7	2.258453	-3.25845	95.805
37 B1-5	2007-06-23	09:44	29.6	3613	0	84	8.10	0.10	0.0	0.00	18.3	0.2	0.01	O	Z	A	9	398.91	8.875	40	40	40	40	8.915	3418.8	2.255467	-3.25547	95.830
37 A2-11	2007-06-23	02:59	31.9	2127	0	84	7.70	0.12	0.0	0.00	17.4	0.3	0.02	H	Z	AA	12	395.18	8.85	60	60	60	50	8.9075	3412.5	2.257257	-3.25728	95.815
37 G-13	2007-06-23	10:21	32.0	6749	0	84	7.25	0.07	0.0	0.00	16.4	0.2	0.01	O	X	B	11	401.35	8.83	60	60	50	60	8.8875	3431.2	2.262047	-3.26205	95.775
37 G-14	2007-06-23	11:14	36.8	5998	0	84	6.40	0.08	0.0	0.00	14.5	0.2	0.01	HO	X	B	12	401.67	8.925	-20	-20	-30	-20	8.9025	3443.8	2.258453	-3.25845	95.805
79 G1-1	2007-07-16	11:07	36.6	2572	-0.5	77	6.8	0	3.0	0.00	15.2	-9.5	-0.63	D	X	B	7	398.68	8.935	60	50	60	60	8.9925	3375	2.237143	-3.23714	95.985
79 F2-10	2007-07-20	18:27	38.3	472	-0.5	77	7.60	0	2.9	0.00	17.5	-9.3	-0.53	O	X	B	12	400.41	8.93	30	50	50	30	8.97	3393.8	2.242429	-3.24243	95.940
79 M-1	2007-07-16	08:41	40.1	3441	-0.5	77	7.14	0	3.5	0.00	16.1	-11.2	-0.70	O	Z	A	7	395.68	8.885	30	20	20	30	8.91	3393.8	2.25666	-3.25666	95.820
79 K-3	2007-12-06	13:12		E	-0.5	77		0		0.00	#DIV/0!	#DIV/0!	#DIV/0!	E	Z	A	6	396.75						#DIV/0!	3356.3	#DIV/0!	#DIV/0!	#DIV/0!
37 B2-5	2007-07-16	15:19	42.9	610	-0.5	77	7.86	0	3.4	0.00	17.7	-11.1	-0.62	D	X	A	9	399.54	8.875	40	30	30	30	8.9075	3425	2.257257	-3.25726	95.815
37 B1-6	2007-07-16	20:27		E	-0.5	77		0		0.00	0.0	0.0	#DIV/0!	E	X	A	0	399.59	8.86	50	50	50	50	8.91	3425	2.25666	-3.25666	95.820
37 I-9	2007-06-12	15:07	40.6	898	-0.5	77		0		0.00	0.0	0.0	#DIV/0!	L	Z	B	9	399.49	8.875	10	10	20	10	8.8875	3418.8	2.262047	-3.26205	95.775
37 I-10	2007-07-16	13:47		E	-0.5	77		0		0.00	0.0	0.0	#DIV/0!	E	Z	B	0	401.89	8.905	20	20	30	20	8.9275	3443.8	2.252489	-3.25249	95.855
79 G1-4	2007-07-20	16:44	40.1	79	-0.5	62	6.12	0	3.0	0.00	18.4	-9.9	-0.54	D	X	B	5	398.47	8.795	70	70	60	70	8.8625	3362.5	2.268066	-3.26807	95.725
79 F2-11	2007-07-20	12:55	39.4	E	-0.5	82		0		0.00	0.0	0.0	#DIV/0!	E	X	B	12	400.4	8.92	80	90	100	60	9.0025	3375	2.234802	-3.2348	96.005
79 M-5	2007-07-20	12:03		E	-0.5	82		0		0.00	0.0	0.0	#DIV/0!	E	Z	A	9	397.3	8.885	30	30	30	30	8.915	3431.2	2.255467	-3.25547	95.830
79 E-11	2007-07-20	11:35	39.1	211	-0.5	82	8.5	0	2.9	0.00	19.9	-9.8	-0.49	D	Z	B	0	399.5	8.5	60	60	50	50	8.555	3412.5	2.345048	-3.34505	95.110
37 B2-9	2007-07-20	15:53		E	-0.5	82		0		0.00	0.0	0.0	#DIV/0!	E	X	A	11	399.15	8.845	60	60	60	60	8.905	3387.5	2.257855	-3.25785	95.810
37 B1-7	2007-07-16	17:08	37.8	5575	-0.5	82	7.45	0	2.5	0.00	16.8	-8.3	-0.49	O	X	A	0	398.83	8.86	60	60	60	60	8.92	3418.8	2.254275	-3.25427	95.840
37 I-13	2007-07-20	15:13		E	-0.5	82		0		0.00	0.0	0.0	#DIV/0!	E	Z	B	11	400.84	8.875	40	50	20	30	8.91	3431.2	2.25666	-3.25666	95.820
37 I-14	2007-07-16	16:32		E	-0.5	82		0		0.00	0.0	0.0	#DIV/0!	E	Z	B	12	400.31	8.915	20	20	20	20	8.935	3450	2.250707	-3.25071	95.870
37 E-4	2007-07-20	17:09	41.3	201	-0.5	82	8.16	0	3.1	0.00	19.2	-10.3	-0.53	D	Z	B	5	393.41	8.49	50	40	50	40	8.535	3243.7	2.350251	-3.35025	95.070
79 G1-9	2007-06-26	17:15		E	-0.5	75		0		0.00	0.0	0.0	#DIV/0!	E	X	B	11	399.63	8.91	40	40	40	40	8.95	3406.3	2.247151	-3.24715	95.900
79 G1-2	2007-07-13	22:07	38.6	1	-0.5	85		0		0.00	0.0	0.0	#DIV/0!	O	X	B	6	398.74	8.91	10	10	10	10	8.92	3356.3	2.254275	-3.25427	95.840
79 M-9	2007-07-05	11:19		E	-0.5	85		0		0.00	0.0	0.0	#DIV/0!	E	Z	A	9	397.46	8.9	10	10	10	10	8.91	3437.5	2.25666	-3.25666	95.820
79 K-6	2007-07-13	23:02		E	-0.5	85		0		0.00	#DIV/0!	#DIV/0!	#DIV/0!	E	Z	A	0	399.31						#DIV/0!	3412.5	#DIV/0!	#DIV/0!	#DIV/0!
37 C-1	2007-07-13	22:43	38.7	5	-0.5	85	10.4	0	6.1	0.00	24.4	-20.4	-0.84	O	X	B	7	398.29	8.515	20	20	30	30	8.54	3387.5	2.348948	-3.34895	95.080
37 A1-10	2007-07-13	23:41	37.6	26	-0.5	85	10.5	0	5.8	0.00	23.8	-18.9	-0.80	H	X	A	12	397.58	8.82	80	50	50	70	8.8825	3431.2	2.263248	-3.26325	95.765
37 K-1	2007-07-13	23:20	37.4	62	-0.5	85	9	0	3.0	0.00	20.3	-9.8	-0.48	H	Z	B	7	397	8.9	20	20	20	10	8.9175	3268.8	2.254871	-3.25487	95.835
37 K-2	2007-07-13	19:38	31.1	391	-0.5	85	8.1	0	3.2	0.00	18.3	-10.4	-0.57	D	Z	B	6	394.65	8.87	50	50	50	50	8.92	3268.8	2.254275	-3.25427	95.840
79 D-12	2007-06-26	18:11	29.6	1039	-0.5	85	8.01	0	3.2	0.00	18.1	-10.6	-0.58	O	X	A	3	398.57	8.855	40	40	30	30	8.89	3393.8	2.261447	-3.26145	95.780
79 G1-8	2007-07-21	15:48	38.7	1856	-0.5	72	7.2	0	3.0	0.00	16.2	-9.7	-0.60	D	X	B	3	400.22	8.9	50	50	50	50	8.95	3400	2.247151	-3.24715	95.900
79 G1-6	2007-07-20	19:14		E	-0.5	72		0		0.00	0.0	0.0	#DIV/0!	E	X	B	0	402.47	8.95	40	50	40	40	8.9925	3381.3	2.237143	-3.23714	95.985
79 M-13	2007-07-21	12:57		E	-0.5	72		0		0.00	0.0	0.0	#DIV/0!	E	Z	A	11	397.44	8.88	30	30	30	30	8.91	3425	2.25666	-3.25666	95.820
79 K-7	2007-07-21	13:35		E	-0.5	72		0		0.00	#DIV/0!	#DIV/0!	#DIV/0!	E	Z	A	0	399.26						#DIV/0!	3412.5	#DIV/0!	#DIV/0!	#DIV/0!
37 C-5	2007-07-20	20:56		E	-0.5	72		0		0.00	0.0	0.0	#DIV/0!		X	B	9	399.13	8.52	20	40	50	40	8.5575	3400	2.344399	-3.3444	95.115
37 A1-11	2007-07-21	10:47		E	-0.5	72		0		0.00	0.0	0.0	#DIV/0!	E	X	A	12	397.36	8.83	40	50	40	40	8.8725	3425	2.265655	-3.26565	95.745
37 K-5	2007-07-20	19:33	39.4	1975	-0.5	72	7.11	0	2.7	0.00	16.0	-8.7	-0.54	O	Z	B	9	400.26	8.86	60	60	60	50	8.9175	3412.5	2.254871	-3.25487	95.835
37 K-6	2007-07-21	11:46	41.0	1828	-0.5	72	7.15	0	2.7	0.00	16.1	-8.7	-0.54	D	Z	B	0	400.88	8.87	60	50	60	50	8.925	3425	2.253084	-3.25308	95.850
79 G2-1	2007-07-25	08:40		E	-1	85		0		0.00	0.0	0.0	#DIV/0!	E	X	B	7	397.6	8.865	60	60	60	60	8.925	3381.3	2.253084	-3.25308	95.850
79 G1-7	2007-12-06	09:58	40.0	149	-1	85	8	0	5.5	0.00	18.0	-17.7	-0.99	O	X	B	0	400.62	8.91	30	30	30	30	8.94	3350	2.24952	-3.24952	95.880
79 I-4	2007-07-25	11:05	35.0	57	-1	85	8.7	0	6.3	0.00	19.6	-20.4	-1.04	O	Z	A	5	396.37	8.855	60	50	50	50	8.9075	3381.3	2.257257	-3.25726	95.815
79 K-10	2007-12-06	12:01	41.4		-1	85		0		0.00	0.0	0.0	#DIV/0!	L	Z	A	0	399.5		16.046	16.043	16.036	16.039	8.902	3425	2.258572	-3.25857	95.804
37 C-9	2007-07-25	11:32		E	-1	85		0		0.00	0.0	0.0	#DIV/0!	E	X	B	9	399.81	8.495	60	60	50	50	8.55	3400	2.346346	-3.34635	95.100
37 B1-10	2007-07-25	13:04	37.4	66	-1	85	8.69	0	6.2	0.00	19.6	-20.3	-1.03	O	X	A	12	398.59	8.855	50	50	50	50	8.905	3406.3	2.257855	-3.25785	95.810
37 K-9	2007-07-25	12:29	36.6	148	-1	85	8.75	0	6.3	0.00	19.8	-20.5	-1.04	H	Z	B	9	400.09	8.84	70	70	60	60	8.905	3393.8	2.257855	-3.25785	95.810
37 K-10	2007-12-06	11:33	42.3	135	-1	85	8.5	0	6.0	0.00	19.2	-19.5	-1.02	O	Z	B	0	401.38	8.935	-20	-20	-20	-20	8.915	3450	2.255467	-3.25547	95.830
79 G2-5	2007-12-04	14:17	38.4	8762	-1	73	6.33	0	4.4	0.00	14.2	-14.1	-0.99	O	X	B	9	398.45	8.905	40	30	20	30	8.935	3387.5	2.250707	-3.25071	95.870
79 G1-10	2007-12-05	16:00		E	-1	73		0		0.00	0.0	0.0	#DIV/0!	E	X	B	12	401.12	8.93	70	70	60	60	8.995	3381.3	2.236557	-3.23656	95.990
79 I-8	2007-07-24	09:24	38.3	1251	-1	73	7.28	0	5.2	0.00	16.5	-17.0	-1.04	O	Z	A	3	398.9	8.85	50	50	50	40	8.8975	3406.3	2.25965	-3.25965	95.795
79 K-11	2007-12-05	08:00	34.5	19105	-1	73	6.11	0	4.0	0.00	13.8	-13.1	-0.95	D	Z	A	0	399.69		16.016	16.039	16.043		8.894	3406.3	2.260568	-3.26057	95.787
37 C-13	2007-07-24	16:41	39.4	2634	-1	73	7.08	0	5.0	0.00	16.6	-16.7	-1.01	O	X	B	11	400.26	8.525	50	50	50	50	8.575	3418.8	2.339869	-3.33987	95.150
37 B1-11	2007-07-24	19:05		E	-1	73		0		0.00	0.0	0.0	#DIV/0!	E	X	A	12	398.54	8.85	60	60	60	60	8.91	3418.8	2.25668	-3.25668	95.820
37 K-13	2007-07-24	11:06	39.7	2638	-1	73	7.38	0	5.3	0.00	16.7	-17.3	-1.04	O	Z	B	11	401.61	8.845	60	70	60	50	8.905	3431.2	2.257855	-3.25785	95.810

MULTIAXIAL FATIGUE RESULTS TABLE

Appendix H

Spec.#	Date	Time	Temp [°C]	N [cycles]	R_t	Ampl [%]	PA max	PA min	PB max	PB min	σ max	σ min	R_a	F-Type	Dir	Block Pos	Clock Pos	M [g]	tc [mm]	dt1 [µm]	dt2 [µm]	dt3 [µm]	dt4 [µm]	t [mm]	f1 [Hz]	g [-]	h [-]	D [mm]
37 K-14	2007-07-24	13:29	40.0	3160	-1	73	7.04	0	4.9	0.00	15.9	-16.0	-1.01	E	Z	B	12	400.75	8.875	60	50	40	50	8.925	3437.5	2.253084	-3.25308	95.850
79 G2-9	2007-12-06	09:09	36.0	871	-1	80	6.98	0	4.8	0.00	15.7	-15.5	-0.99	O	X	B	11	399.44	8.87	70	70	70	60	8.9375	3406.3	2.250113	-3.25011	95.875
79 G1-11	2007-07-21	18:26	36.2	59	-1	80	8.12	0	5.9	0.00	18.3	-19.3	-1.06	O	X	B	12	398.96	8.905	40	40	40	40	8.945	3368.7	2.248335	-3.24834	95.890
79 I-12	2007-07-21	19:20	39.7	1164	-1	80	8.02	0	5.7	0.00	18.1	-18.5	-1.02	H	Z	A	3	399.67	8.92	-10	-10	-10	-10	8.91	3425	2.25666	-3.25666	95.820
79 K-14	2007-07-21	21:24		E	-1	80		0		0.00	#DIV/0!	#DIV/0!	#DIV/0!	E	Z	A	12	398.24						#DIV/0!	3387.5	#DIV/0!	#DIV/0!	#DIV/0!
37 A1-4	2007-07-21	21:52	39.2	787	-1	80	7.96	0	5.9	0.00	18.1	-19.2	-1.06	H	X	A	5	397.78	8.765	80	80	70	60	8.8375	3456.3	2.27412	-3.27412	95.675
37 B2-2	2007-07-23	17:10	40.4	1300	-1	80	7.49	0	5.4	0.00	16.9	-17.6	-1.04	D	X	A	6	399.61	8.885	30	30	30	30	8.915	3418.8	2.255467	-3.25547	95.830
37 E-12	2007-07-23	16:20		E	-1	80		0		0.00	0.0	0.0	#DIV/0!	E	Z	B	3	400.17	8.495	50	50	40	40	8.54	3556.2	2.348948	-3.34895	95.080
37 E-7	2007-12-05	23:00	33.7	1917	-1	80	6.55	0	4.6	0.00	15.4	-15.3	-0,99	O	Z	B	0	400.46	8.515	40	40	40	40	8.555	3450	2.345046	-3.34505	95.110
79 G2-4	2007-07-25	18:32	35.3	4884	-1	67	6.93	0	5.0	0.00	15.6	-16.2	-1.04	D	X	B	5	398.32	8.86	70	70	70	70	8.93	3368.7	2.251895	-3.25189	95.860
79 G2-2	2007-07-23	10:11		E	-1	67		0		0.00	0.0	0.0	#DIV/0!	E	X	B	6	398.71	8.885	50	60	50	50	8.9375	3387.5	2.250113	-3.25011	95.875
79 I-16	2007-07-21	22:42	39.6	14416	-1	67	7.04	0	5.1	0.00	15.9	-16.7	-1.05	D	Z	A	1	400.03	8.85	60	60	50	60	8.9075	3425	2.257257	-3.25726	95.815
79 K-15	2007-07-23	07:17		E	-1	67		0		0.00	#DIV/0!	#DIV/0!	#DIV/0!	E	Z	A	12	398.86						#DIV/0!	3412.5	#DIV/0!	#DIV/0!	#DIV/0!
37 A1-8	2007-07-23	18:31	38.7	25965	-1	67	6.14	0	4.3	0.00	13.9	-14.0	-1.01	E	X	A	3	398.74	8.83	60	60	50	40	8.8825	3462.5	2.263248	-3.26325	95.765
37 B2-3	2007-07-25	14:46	36.5	979	-1	67	6.97	0	5.0	0.00	15.7	-16.4	-1.04	D	X	A	6	399.3	8.935	-20	-20	-20	-20	8.915	3418.8	2.255467	-3.25547	95.830
37 E-16	2007-07-23	07:39	40.3	4877	-1	67	6.89	0	5.0	0.00	16.2	-16.6	-1.03	DH	Z	B	1	399.63	8.485	70	70	70	70	8.555	3437.5	2.345048	-3.34505	95.110
37 E-11	2007-07-22	12:28	38.0	17201	-1	67	7.01	0	5.2	0.00	16.4	-17.2	-1.05	O	Z	B	0	400.24	8.54	10	10	10	10	8.55	3456.3	2.346346	-3.34635	95.100
79 B-15	2008-01-31	13:57	31.1		-1	85		0		0.00	0.0	0.0	#DIV/0!	E	X	A	12	394.9	8.855	50	40	40	50	8.9	3362.5	2.259051	-3.25905	95.800
79 C-5	2008-01-29	15:41	29.1		-1	67	5.59	0	3.9	0.00	12.6	-12.6	-0.99	L	X	A	9	397.17	8.82	80	70	70	80	8.895	3362.5	2.260249	-3.26025	95.790
79 G2-8	2007-12-10	10:50	36.8	103	-2	85	8.66	0	11.9	0.00	19.6	-38.7	-1.98	D	X	B	3	399.53	8.865	40	40	40	40	8.905	3406.3	2.257855	-3.25785	95.810
79 G2-3	2007-12-12	08:28	31.7	131	-2	85	8.61	0	11.9	0.00	19.4	-38.8	-2.00	H	X	B	6	397.84	8.915	0	0	0	0	8.915	3381.3	2.255467	-3.25547	95.830
79 O-4	2007-12-12	08:55	35.4	52	-2	85	8.8	0	12.0	0.00	19.7	-38.8	-1.96	D	Z	AA	5	398.53	8.925	50	40	40	40	8.9675	3412.5	2.243018	-3.24302	95.935
79 M-2	2007-12-07	16:30	44.6	>134	-2	85	6.46	0	9.6	0.00	14.6	-31.2	-2.15	H	Z	A	6	396.93	8.875	50	50	50	50	8.925	3400	2.253084	-3.25308	95.850
37 A1-12	2008-01-15	17:44	37.1	891	-2	85	7.74	0	11.2	0.00	17.5	-36.5	-2.08	O	X	A	1	397.29	8.83	50	60	50	50	8.8825	3425	2.263248	-3.26325	95.765
37 B2-6	2007-12-15	10:13	29.8	81	-2	85	8.88	0	12.2	0.00	20.1	-39.6	-1.97	H	X	A	0	399.5	8.845	60	60	50	50	8.9	3431.2	2.259051	-3.25905	95.800
37 G-4	2007-12-07	17:10	41.5	1090	-2	85	7.2	0	10.2	0.00	16.2	-33.3	-2.05	O	Z	B	5	393.13	8.88	40	40	40	40	8.92	3250	2.254275	-3.25427	95.840
37 E-15	2008-01-15	11:49	33.1	366	-2	85	7.4	0	10.8	0.00	17.4	-36.2	-2.08	D	Z	B	12	400.69	8.52	0	0	0	0	8.52	3462.5	2.35417	-3.35417	95.040
79 G2-12	2007-12-10	12:00	43.8	248	-2	80	8.21	0	10.9	0.00	16.5	-35.6	-1.92	O	X	B	1	399.74	8.905	0	0	0	0	8.905	3406.3	2.257855	-3.25785	95.810
79 G2-6	2007-12-10	11:20	34.9	148	-2	80	8.25	0	10.9	0.00	16.6	-35.4	-1.91	O	X	B	0	400.47	8.86	70	80	80	70	8.935	3418.8	2.250707	-3.25071	95.870
79 K-4	2008-01-16	09:51	30.3	1944	-2	80	6.99	0	10.2	0.00	15.8	-33.1	-2.10	O	Z	A	5	397.09		16.043	16.038	16.04		8.901	3368.7	2.258732	-3.25873	95.803
79 M-3	2007-12-11	08:33	40.2	1185	-2	80	7.1	0	10.1	0.00	16.0	-33.0	-2.06	O	Z	A	6	397.41	8.845	50	50	50	50	8.895	3393.8	2.260249	-3.26025	95.790
37 A2-4	2008-01-16	09:23	35.8	391	-2	80	7.38	0	10.5	0.00	16.7	-34.3	-2.06	E	X	AA	5	391.44	8.89	30	0	20	10	8.905	3356.3	2.257855	-3.25785	95.810
37 B2-7	2007-12-11	18:58	33.2	7438	-2	70	6.13	0	8.9	0.00	13.8	-29.0	-2.10	E	X	A	0	398.64	8.86	60	60	60	60	8.92	3418.8	2.254275	-3.25427	95.840
37 G-8	2007-12-15	10:34	33.4	173	-2	80	8.19	0	11.3	0.00	18.5	-36.6	-1.98	D	Z	B	3	399.97	8.85	70	70	60	70	8.9175	3450	2.254871	-3.25487	95.835
37 G-3	2007-12-12	09:12	36.1	140	-2	80	8.24	0	11.3	0.00	18.6	-36.9	-1.98	O	Z	B	6	393.23	8.855	60	60	60	60	8.915	3237.5	2.255467	-3.25547	95.830
79 C-1	2007-08-29	11:32	42.4	>600	-2	70	6.75	0	9.3	0.00	15.3	-30.2	-1.98	L	X	A	7	396.46	8.82	70	80	60	75	8.8913	3381.3	2.261148	-3.26115	95.783
79 G2-7	2007-08-29	10:54	40.5	<300, >200	-2	70	7.21	0	9.7	0.00	16.3	-31.4	-1.93	E	X	B	0	400.04	8.88	30	40	30	30	8.9125	3406.3	2.256063	-3.25606	95.825
79 K-8	2007-07-30	09:58	38.6	29	-2	70	7.53	0	10.1	0.00	17.0	-33.0	-1.94	E	Z	A	3	398.8		16.045	16.041	16.042	16.042	8.904	3418.8	2.258214	-3.25821	95.807
79 M-6	2007-07-28	15:59	36.9	11	-2	70		0		0.00	0.0	0.0	#DIV/0!	E	Z	A	0	398.77	8.87	50	50	50	50	8.92	3437.5	2.254275	-3.25427	95.840
37 A2-8	2008-01-16	12:43	30.5	80	-2	75	6.7	0	9.6	0.00	15.1	-31.3	-2.07	E	X	AA	3	397.23	8.86	60	50	50	40	8.91	3431.2	2.25666	-3.25666	95.820
37 B2-10	2007-08-29	12:41	38.2	<10	-2	70	6.35	0	9.1	0.00	14.4	-29.7	-2.07	E	X	A	12	398.52	8.825	70	70	60	60	8.89	3406.3	2.261447	-3.26145	95.780
37 G-12	2007-08-29	12:15	40.3	40	-2	70	7.07	0	10.1	0.00	16.0	-32.8	-2.05	E	Z	B	3	400.5	8.86	30	20	20	10	8.88	3462.5	2.263849	-3.26385	95.760
37 G-7	2007-08-29	13:12	39.5	>9000	-2	70	6.27	0	9.1	0.00	14.1	-29.6	-2.10	D	Z	B	0	400.62	8.86	60	60	60	60	8.92	3431.2	2.254275	-3.25427	95.840
79 G2-10	2007-12-11	10:45	35.5	3143	-2	70	6.07	0	8.7	0.00	13.7	-28.5	-2.08	D	X	B	12	398.09	8.88	20	20	20	20	8.9	3381.3	2.259051	-3.25905	95.800
79 K-12	2007-12-12	18:42	36.6	4333	-2	70	5.97	0	8.7	0.00	13.5	-28.4	-2.11	O	Z	A	3	399.07		16.043	16.041	16.05	16.075	8.913	3425	2.255884	-3.25588	95.827
79 M-7	2007-12-11	15:10	37.0	7826	-2	70	6.2	0	8.9	0.00	14.0	-29.2	-2.08	E	Z	A	0	399.31	8.84	60	50	50	50	8.8925	3443.8	2.260848	-3.26085	95.785
37 A2-12	2007-12-12	09:39	34.4	6731	-2	70	6.26	0	9.0	0.00	14.1	-29.3	-2.07	O	X	AA	1	396.59	8.84	60	60	60	40	8.895	3450	2.260249	-3.26025	95.790
37 B2-11	2007-12-12	16:22	33.5	5137	-2	70	6.22	0	8.8	0.00	14.1	-28.7	-2.04	E	X	A	12	398.14	8.83	60	70	60	70	8.895	3400	2.260249	-3.26025	95.790
37 G-16	2008-01-16	15:19	32.9	2	-2	70	7.5	0	9.9	0.00	17.0	-32.4	-1.91	D	Z	B	1	400.56	8.835	60	60	60	60	8.895	3437.5	2.260249	-3.26025	95.790
37 G-11	2008-01-14	11:45	34.0	7035	-2	70	6.22	0	9.0	0.00	14.0	-29.1	-2.08	E	Z	B	0	400.88	8.86	70	70	60	60	8.925	3462.5	2.253084	-3.25308	95.850
79 F1-1	2008-02-02	14:59	28.1	>2079	-2	70	5.39	0	8.1	0.00	12.1	-26.2	-2.17	L	X	B	7	399.53	8.955	40	40	40	40	8.995	3387.5	2.236557	-3.23656	95.990
37 A1-7	2008-01-31	14:36	33.3		-2	85		0		0.00	0.0	0.0	#DIV/0!	E	X	A	0	398.79	8.825	60	60	60	60	8.885	3456.3	2.262648	-3.26265	95.770
79 B-13	2008-01-31	15:16	36.4		-2	85		0		0.00	0.0	0.0	#DIV/0!	E	X	B	0	395.53	8.85	50	50	50	50	8.9	3393.8	2.259051	-3.25905	95.800
37 A1-3	2008-01-31	15:00	32.7		-2	85		0		0.00	0.0	0.0	#DIV/0!	L	X	A	6	399.14	8.83	60	60	40	40	8.88	3437.5	2.263849	-3.26385	95.760
79 B-10	2008-02-01	15:30	30.8		-2	85		0		0.00	0.0	0.0	#DIV/0!	E	X	A	0	396.43	8.855	30	30	40	50	8.8925	3387.5	2.260848	-3.26085	95.785
79 B-9	2008-02-02	14:05	24.8		-2	80		0		0.00	0.0	0.0	#DIV/0!	E	X	A	9	396.04	8.855	50	50	50	50	8.905	3400	2.257855	-3.25785	95.810
79 A-12	2008-02-02	14:19	27.8		-2	80		0		0.00	0.0	0.0	#DIV/0!	E	Z	AA	3	396.4	8.51	50	40	50	50	8.5575	3437.5	2.344399	-3.3444	95.115

MULTIAXIAL FATIGUE RESULTS TABLE

Spec.#	Date	Time	Temp [°C]	N [cycles]	R_t	Ampl [%]	PA max	PA min	PB max	PB min	σ max	σ min	R_a	F-Type	Dir	Block Pos	Clock Pos	M [g]	tc [ms]	dt1 [µm]	dt2 [µm]	dt3 [µm]	dt4 [µm]	t [ms]	f1 [Hz]	g [-]	h [-]	D [mm]
79 C-13	2007-07-03	21:20	22.1	1116	-∞	94	0	0	29.0	0.28	-0.9	-94.5	103.57	O	X	A	11	397.25	8.84	60	60	50	50	8.895	3400	2.260249	-3.26025	95.790
79 C-2	2007-07-03	22:15	24.2	472	-∞	94	0	0	29.0	0.26	-0.8	-94.6	111.54	O	X	A	6	397.42	8.815	60	80	70	70	8.885	3381.3	2.262648	-3.26265	95.770
79 M-4	2007-07-03	23:37	22.9	233	-∞	94	0	0	30.2	1.20	-3.9	-98.3	25.17	O	Z	A	5	397.04	8.865	50	50	40	50	8.9125	3400	2.256063	-3.25606	95.825
79 M-11	2007-07-03	21:59	23.4	582	-∞	94	0	0	29.9	0.94	-3.1	-97.2	31.81	O	Z	A	0	398.78	8.87	60	60	60	60	8.93	3431.2	2.251895	-3.25189	95.860
37 B1-8	2007-07-03	20:46	24.1	1244	-∞	94	0	0	28.8	0.25	-0.8	-93.7	115.20	O	X	A	3	399.16	8.865	60	50	50	50	8.9175	3450	2.254871	-3.25487	95.835
37 C-3	2007-07-03	20:30	28.1	291	-∞	94	0	0	28.7	0.50	-1.7	-96.0	57.40	O	X	B	6	398.06	8.525	30	40	30	30	8.5575	3387.5	2.344399	-3.3444	95.115
37 I-8	2007-07-03	22:44	23.1	593	-∞	94	0	0	28.6	0.23	-0.7	-93.0	124.35	O	Z	B	3	398.78	8.925	0	0	0	0	8.925	3443.8	2.253084	-3.25308	95.850
37 I-3	2007-07-03	21:44	22.9	183	-∞	94	0	0	27.7	0.24	-0.8	-90.5	115.42	O	Z	B	3	391.65	8.88	-10	-10	-10	-10	8.87	3250	2.266257	-3.26626	95.740
79 M-15	2007-07-04	00:46	25.5	128	-∞	94	0	0	27.0	0.17	-0.6	-87.8	158.82	O	Z	A	12	398.49	8.895	40	30	40	35	8.9313	3425	2.251598	-3.2516	95.863
79 C-4	2007-07-04	20:02	21.0	672	-∞	92	0	0	28.6	0.09	-0.3	-93.2	317.78	O	X	A	5	396.58	8.885	20	20	10	10	8.9	3375	2.259051	-3.25905	95.800
79 C-3	2007-07-04	21:43	23.6	83	-∞	92	0	0	31.3	2.00	-6.5	-102.1	15.65	O	X	A	6	397.28	8.815	80	80	70	80	8.8925	3381.3	2.260848	-3.26085	95.785
79 M-8	2007-07-04	19:42	21.6	1357	-∞	92	0	0	28.7	0.10	-0.3	-93.4	287.00	O	Z	A	3	398.67	8.87	60	50	60	50	8.925	3425	2.253084	-3.25308	95.850
79 M-14	2007-07-04	21:28	23.0	290	-∞	92	0	0	29.9	0.60	-2.0	-97.3	49.83	O	Z	A	12	397.58	8.895	30	30	30	30	8.925	3412.5	2.253084	-3.25308	95.850
37 B1-12	2007-07-04	19:12	22.0	3130	-∞	92	0	0	29.2	0.09	-0.3	-94.9	323.89	O	X	A	1	398.76	8.88	60	30	40	30	8.92	3443.8	2.254275	-3.25427	95.840
37 C-6	2007-07-04	18:43	22.9	2180	-∞	92	0	0	28.4	0.08	-0.3	-95.0	355.00	O	X	B	0	400.66	8.49	70	70	60	60	8.56	3425	2.34375	-3.34375	95.120
37 I-12	2007-07-04	21:12	21.0	144	-∞	92	0	0	29.8	0.45	-1.5	-97.7	66.22	O	Z	B	3	399.52	8.815	10	10	20	0	8.825	3437.5	2.27716	-3.27716	95.650
37 I-7	2007-07-04	20:19	21.4	1775	-∞	92	0	0	28.8	0.10	-0.3	-93.9	288.00	O	Z	B	0	400.38	8.85	40	40	40	40	8.89	3418.8	2.261447	-3.26145	95.780
79 C-8	2007-07-05	07:32	23.3	230	-∞	90	0	0	28.0	0.15	-0.5	-91.3	186.67	O	X	A	3	398.09	8.875	10	20	10	10	8.8875	3400	2.262047	-3.26205	95.775
79 C-6	2007-07-04	00:11	23.2	1387	-∞	90	0	0	29.2	0.30	-1.0	-95.2	97.33	O	X	A	0	398.35	8.815	80	80	80	80	8.895	3400	2.260249	-3.26025	95.790
79 M-12	2007-07-04	17:31	22.8	938	-∞	90	0	0	28.8	0.17	-0.6	-93.6	169.41	O	Z	A	3	398.86	8.885	50	50	50	50	8.935	3437.5	2.250707	-3.25071	95.870
37 G-15	2007-07-04	13:00	25.3	6737	-∞	90	0	0	27.8	0.10	-0.3	-90.5	278.00	O	Z	B	12	401.43	8.81	110	110	110	110	8.92	3456.3	2.254275	-3.25427	95.840
37 B2-4	2007-07-04	18:00	24.3	4206	-∞	90	0	0	28.6	0.08	-0.3	-93.1	357.50	O	X	A	5	398.31	8.865	50	50	50	50	8.915	3412.5	2.255467	-3.25547	95.830
37 C-7	2007-07-04	16:22	21.5	312	-∞	90	0	0	25.3	0.10	-0.3	-84.7	253.00	O	X	B	0	400.26	8.495	40	60	40	50	8.5425	3418.8	2.348297	-3.3483	95.085
37 I-16	2007-07-04	16:38	22.2	1694	-∞	90	0	0	27.5	0.07	-0.2	-89.4	392.86	O	Z	B	1	399.24	8.91	20	20	20	20	8.93	3462.5	2.251895	-3.25189	95.860
37 I-11	2007-07-04	14:53	22.5	11551	-∞	90	0	0	28.4	0.02	-0.1	-92.3	1420.00	O	Z	B	0	400.93	8.91	30	30	30	30	8.94	3462.5	2.24952	-3.24952	95.880
79 C-9	2007-07-04	23:25	25.7	1090	-∞	87	0	0	27.1	0.08	-0.3	-88.3	338.75	O	X	A	9	396.98	8.83	70	70	70	60	8.8975	3393.8	2.25965	-3.25965	95.795
79 G2-11	2007-07-04	22:27	24.3	131	-∞	87	0	0	28.5	0.31	-1.0	-92.7	91.94	O	X	B	12	399.28	8.895	30	40	40	30	8.93	3381.3	2.251895	-3.25189	95.860
79 K-16	2007-07-05	00:06	23.4	1115	-∞	87	0	0	28.0	0.19	-0.6	-91.1	147.37	O	Z	A	1	399.87	8.917	0	0	0	0	8.917	3406.3	2.25499	-3.25499	95.834
79 M-10	2007-07-04	23:46	26.4	147	-∞	87	0	0	32.3	3.90	-12.7	-105.2	8.28	O	Z	A	0	398.68	8.875	40	40	40	40	8.915	3431.2	2.255467	-3.25547	95.830
37 B1-4	2007-07-04	22:44	24.0	478	-∞	87	0	0	27.5	0.10	-0.3	-89.5	275.00	O	X	A	5	398.33	8.86	60	60	50	50	8.915	3443.8	2.255467	-3.25547	95.830
37 C-2	2007-07-04	23:03	24.3	90	-∞	87	0	0	31.0	2.25	-7.5	-103.7	13.78	O	X	B	6	398.69	8.52	30	40	20	30	8.55	3362.5	2.346346	-3.34635	95.100
37 I-4	2007-07-04	22:06	23.2	1201	-∞	87	0	0	28.9	0.48	-1.6	-93.9	60.21	O	Z	B	5	392.2	8.925	10	10	10	10	8.935	3243.7	2.250707	-3.25071	95.870
79 K-2	2007-07-05	08:16	23.7	731	-∞	87	0	0	27.9	0.08	-0.3	-90.8	348.75	O	Z	A	6	396.81	8.885	30	30	30	30	8.915	3375	2.255467	-3.25547	95.830
79 C-12	2007-07-02	11:18	26.4	1020	2	1	0	0	32.4	17.30	-56.4	-105.6	1.87	O	X	A	3	398.1	8.82	80	80	70	70	8.895	3400	2.260249	-3.26025	95.790
79 C-7	2007-06-30	18:50	22.6	832	2	1	0	0	32.0	15.60	-50.8	-104.3	2.05	O	X	A	0	398.16	8.83	70	70	70	70	8.9	3400	2.259051	-3.25905	95.800
79 M-16	2007-06-30	19:48	23.9	746	2	1	0	0	32.2	15.90	-51.8	-104.9	2.03	O	Z	A	1	399.28	8.84	70	70	70	65	8.9088	3443.8	2.256959	-3.25896	95.818
79 O-6	2007-07-02	12:39	25.0	353	2	1	0	0	33.2	18.90	-61.3	-107.6	1.76	O	Z	AA	0	400.63	8.935	40	40	30	50	8.975	3450	2.241252	-3.24125	95.950
37 C-10	2007-07-02	13:16	25.1	429	2	1	0	0	34.0	17.90	-58.4	-110.7	1.90	O	X	B	0	397.78	8.86	40	40	30	30	8.895	3406.3	2.260249	-3.26025	95.790
37 K-4	2007-06-30	19:23	23.0	57	2	1	0	0	34.3	19.50	-63.5	-111.7	1.76	O	Z	B	5	392.51	8.895	20	20	20	20	8.915	3250	2.255467	-3.25547	95.830
79 C-16	2007-07-02	23:29	27.5	910	2	94	0	0	31.4	16.20	-52.8	-102.4	1.94	O	X	A	1	397.66	8.84	50	50	60	60	8.895	3406.3	2.260249	-3.26025	95.790
79 C-10	2007-07-02	23:51	27.5	13234	2	94	0	0	32.0	17.20	-57.5	-107.0	1.86	O	X	A	0	400.5	8.485	60	80	60	80	8.555	3425	2.345048	-3.34505	95.110
79 O-12	2007-07-03	10:49	21.5	7872	2	94	0	0	32.4	18.00	-58.3	-105.0	1.80	O	Z	AA	3	400.66	8.93	60	50	50	50	8.9825	3450	2.239489	-3.23949	95.965
79 O-7	2007-07-03	08:16	25.2	1911	2	94	0	0	30.9	14.10	-45.8	-100.3	2.19	O	Z	AA	0	400.86	8.925	30	40	30	40	8.96	3456.3	2.244788	-3.24479	95.920
37 B2-12	2007-07-03	06:35	27.7	12891	2	94	0	0	32.3	18.30	-59.8	-105.2	1.77	O	X	A	1	398.45	8.845	70	70	70	60	8.9125	3450	2.256063	-3.25606	95.825
37 C-11	2007-07-03	01:32	29.4	8752	2	94	0	0	32.3	18.70	-62.7	-108.3	1.73	O	X	B	0	400.48	8.485	60	40	40	30	8.5275	3437.5	2.352209	-3.35221	95.055
37 K-8	2007-07-03	03:03	30.8	27409	2	94	0	0	32.4	18.70	-60.8	-105.4	1.73	O	Z	B	3	401	8.875	50	60	50	40	8.925	3456.3	2.253084	-3.25308	95.850
37 K-3	2007-07-03	05:58	28.6	3116	2	94	0	0	31.3	17.50	-57.0	-101.9	1.79	O	Z	B	6	393.83	8.86	60	50	50	50	8.9125	3193.8	2.256063	-3.25606	95.825
37 K-16	2007-06-28				2	80	0	0							Z	B	1	401.32	8.86	60	60	50	40	8.9125	3456.3	2.256063	-3.25606	95.825
79 F1-8	2007-07-03	13:52	30.5	60000	2	80	0	0	29.9	18.10	-58.6	-96.8	1.65	-	X	B	3	401.93	8.925	70	70	60	70	8.9925	3400	2.237143	-3.23714	95.985
79 C-14	2007-06-28	09:33	20.2	60000	2	80	0	0	25.8	14.00	-46.8	-86.2	1.84	-	X	A	12	399.26	8.51	60	70	60	60	8.5725	3400	2.340515	-3.34051	95.145
79 O-13	2007-06-29	23:15	28.1	60000	2	80	0	0	26.1	13.00	-42.2	-84.7	2.01	-	Z	AA	11	399.26	8.93	40	40	30	30	8.965	3443.8	2.243608	-3.24361	95.930
79 O-10	2007-06-29	17:22	25.6	60000	2	80	0	0	25.9	12.90	-41.8	-83.9	2.01	-	Z	AA	0	400.2	8.94	40	40	50	40	8.9825	3450	2.239489	-3.23949	95.965
37 C-8	2007-06-28	02:54	27.2	60000	2	80	0	0	26.3	14.20	-47.5	-88.0	1.85	-	X	B	3	400.2	8.485	60	80	60	60	8.55	3418.8	2.346346	-3.34635	95.100
37 C-14	2007-06-27	19:20	25.7	60000	2	80	0	0	17.4	9.60	-31.3	-56.7	1.81	-	X	B	12	395.72	8.825	80	80	80	70	8.9025	3343.8	2.258453	-3.25845	95.805
37 K-12	2007-06-29	10:49	30.7	60000	2	80	0	0	27.3	15.40	-50.1	-88.8	1.77	-	Z	B	3	399.96	8.865	60	60	50	50	8.92	3468.8	2.254275	-3.25427	95.840
37 K-11	2007-06-28	15:40	23.1	60000	2	80	0	0	26.5	13.90	-45.2	-86.2	1.91	-	Z	B	0	401.12	8.87	60	60	60	40	8.925	3450	2.253084	-3.25308	95.850
79 F1-4	2007-07-02	17:40	28.5	613	2	97	0	0	30.9	13.40	-43.4	-100.1	2.31	O	X	B	5	399.79	8.925	60	60	60	60	8.985	3362.5	2.238902	-3.2389	95.970

MULTIAXIAL FATIGUE RESULTS TABLE

Spec.#	Date	Time	Temp [°C]	N [cycles]	R_t	Ampl [%]	PA max	PA min	PB max	PB min	σ max	σ min	R_a	F-Type	Dir	Block Pos	Clock Pos	M [g]	tc [mm]	dt1 [µm]	dt2 [µm]	dt3 [µm]	dt4 [µm]	t [mm]	f1 [Hz]	g [-]	h [-]	D [mm]
79 C-11	2007-07-02	14:22	29.4	14553	2	97	0	0	33.1	18.90	-61.7	-108.1	1.75	O	X	A	0	398.03	8.815	60	60	60	50	8.8725	3400	2.265655	-3.26565	95.745
79 O-8	2007-07-02	22:37	34.0	2261	2	97	0	0	32.2	18.60	-60.2	-104.3	1.73	O	Z	AA	3	400.13	8.945	50	40	40	40	8.9875	3431.2	2.238316	-3.23832	95.975
79 O-11	2007-07-02	19:07	30.3	12095	2	97	0	0	33.5	19.90	-64.5	-108.6	1.68	O	Z	AA	0	400.92	8.935	40	50	40	40	8.9775	3450	2.240664	-3.24066	95.955
37 C-4	2007-07-02	17:02	23.9	115	2	97	0	0	31.0	13.60	-45.5	-103.8	2.28	O	X	B	5	397.56	8.5	50	50	40	40	8.545	3393.8	2.347646	-3.34765	95.090
37 C-15	2007-07-02	18:35	26.9	531	2	97	0	0	31.4	14.20	-47.4	-104.8	2.21	O	X	B	12	398.27	8.545	40	30	40	30	8.58	3418.8	2.338578	-3.33858	95.160
79 O-9	2007-07-02	20:42	30.2	3532	2	97	0	0	32.7	18.70	-60.6	-106.0	1.75	O	Z	AA	9	399.56	8.925	50	50	50	60	8.9775	3425	2.240664	-3.24066	95.955
37 K-7	2007-07-02	21:16	25.2	10755	2	97	0	0	33.2	19.40	-63.0	-107.9	1.71	O	Z	B	0	399.12	8.9	50	40	40	40	8.9425	3412.5	2.248928	-3.24893	95.885
37 B2-8	2007-06-30	00:34	30.0	60000	2	92	0	0	29.5	15.50	-50.5	-96.1	1.90	-	X	A	3	398.94	8.845	60	60	60	50	8.9025	3425	2.258453	-3.25845	95.805
37 I-15	2007-06-30	05:18	25.2	60000	2	92	0	0	29.5	15.60	-50.7	-95.9	1.89	-	Z	B	12	399.87	8.855	80	80	80	70	8.9325	3456.3	2.251301	-3.2513	95.865
79 B-1	2008-01-22	11:25	29.7	557	PIE -1	85	7.8	0	5.4	0.00	17.6	-17.6	-1.00	D	X	A	7	395.05	8.85	50	50	50	50	8.9	3366.7	2.259051	-3.25905	95.800
79 B-2	2008-01-17	17:16	35.8	4705	PIE -1	85	8	0	5.6	0.00	18.1	-18.2	-1.01	D	X	A	6	396.65	8.855	60	50	60	50	8.91	3393.8	2.25666	-3.25666	95.820
79 A-1	2008-01-22	09:34	27.4	41	PIE -1	85	8.2	0	5.7	0.00	19.2	-19.0	-0.99	O	Z	AA	7	392.37	8.505	50	50	50	50	8.555	3381.3	2.345048	-3.34505	95.110
79 A-2	2008-01-22	10:20	31.3	53	PIE -1	85	8.2	0	5.7	0.00	19.2	-19.1	-1.00	O	Z	AA	6	393.75	8.51	40	50	40	50	8.555	3351.3	2.345048	-3.34505	95.110
79 D-1	2008-01-22	09:13	27.5	78	PIE -1	85	8.5	0	5.9	0.00	19.2	-19.1	-0.99	D	X	A	7	396.49	8.83	80	60	70	60	8.8975	3362.5	2.25965	-3.25965	95.795
79 D-2	2008-01-17	16:38	33.2	84	PIE -1	85	8	0	5.5	0.00	18.1	-17.9	-0.99	O	X	A	6	397.13	8.835	60	60	50	50	8.89	3368.7	2.261447	-3.26145	95.780
79 E-1	2008-01-22	10:42	30.5	210	PIE -1	85	7.8	0	5.3	0.00	17.9	-17.6	-0.99	O	Z	B	7	396.23	8.485	60	60	50	50	8.54	3368.7	2.348948	-3.34895	95.080
79 E-2	2008-01-22	09:57	33.9	79	PIE -1	85	7.9	0	5.4	0.00	18.5	-18.0	-0.97	H	Z	B	6	396.83	8.505	60	60	50	50	8.56	3443.8	2.34375	-3.34375	95.120
79 B-5	2008-01-22	13:05	28.8	1366	PIE -1	80	7.3	0	5.0	0.00	16.5	-16.2	-0.98	O	X	A	9	395.99	8.855	50	50	40	40	8.9	3387.5	2.259051	-3.25905	95.800
79 B-3	2008-01-17	10:05	32.5	237	PIE -1	80	8	0	5.6	0.00	18.1	-18.2	-1.00	D	X	A	6	396.44	8.84	60	60	50	50	8.895	3387.5	2.260249	-3.26025	95.790
79 A-5	2008-01-17	10:30	32.6	1954	PIE -1	80	6.81	0	4.2	0.00	15.8	-14.0	-0.89	O	Z	AA	9	394.41	8.595	50	50	40	50	8.6425	3418.8	2.322571	-3.32257	95.285
79 A-3	2008-01-22	13:53	28.4	2249	PIE -1	80	7	0	4.7	0.00	16.4	-15.7	-0.95	D	Z	AA	6	394.38	8.51	50	40	50	50	8.5575	3393.8	2.344399	-3.3444	95.115
79 D-4	2008-01-22	12:25	29.1	1072	PIE -1	80	7.2	0	4.9	0.00	16.3	-16.0	-0.98	D	X	A	5	396.9	8.86	30	30	30	30	8.89	3362.5	2.261447	-3.26145	95.780
79 D-3	2008-01-17	12:10	28.3	514	PIE -1	80	7.17	0	5.3	0.00	16.2	-17.3	-1.07	D	X	A	6	397.28	8.835	50	60	50	50	8.8875	3356.3	2.262047	-3.26205	95.775
79 E-5	2008-01-17	12:57	27.5	5374	PIE -1	80	6.68	0	4.4	0.00	15.1	-14.2	-0.94	O	Z	B	9	396.85	8.865	50	50	50	50	8.915	3393.8	2.255467	-3.25547	95.830
79 E-3	2008-01-22	11:55	29.0	584	PIE -1	80	7.2	0	4.9	0.00	16.9	-16.4	-0.97	O	Z	B	6	396.41	8.5	60	50	50	60	8.555	3350	2.345048	-3.34505	95.110
79 B-4	2008-01-24	07:13	36.0	11854	PIE -1	73	6.2	0	4.2	0.00	14.0	-13.6	-0.97	D	X	A	5	395.51	8.855	50	50	40	40	8.9	3362.5	2.259051	-3.25905	95.800
79 B-6	2008-01-24	15:43	28.3	14710	PIE -1	73		0		0.00	0.0	0.0	#DIV/0!	L	X	A	0	397.13	8.85	40	50	50	50	8.8975	3412.5	2.25965	-3.25965	95.795
79 A-4	2008-01-23	17:46	29.4	9621	PIE -1	73		0		0.00	0.0	0.0	#DIV/0!	L	Z	AA	5	393.14	8.515	40	40	40	50	8.5575	3375	2.344399	-3.3444	95.115
79 A-6					PIE -1			0		0.00	0.0	0.0	#DIV/0!		Z	AA	0	395.93	8.5	60	60	50	60	8.5575	3431.2	2.344399	-3.3444	95.115
79 D-5	2008-01-23	12:35	29.5	>6500	PIE -1	73	6.3	0	4.3	0.00	14.2	-14.0	-0.98	O	X	A	9	397	8.84	70	70	60	60	8.905	3381.3	2.257855	-3.25785	95.810
79 D-6	2008-01-21	17:35	27.5	>10000	PIE -1	73	5.9	0	3.8	0.00	13.4	-12.4	-0.93	E	X	A	0	398.55	8.825	40	60	60	60	8.88	3393.8	2.263849	-3.26385	95.760
79 E-4	2008-01-23	07:19	32.7		PIE -1	73		0		0.00	0.0	0.0	#DIV/0!	O	Z	B	5	396.32	8.5	60	60	60	60	8.56	3325	2.34375	-3.34375	95.120
79 E-6	2008-01-18	08:44	34.6	48406	PIE -1	73	6.4	0	4.2	0.00	15.0	-14.0	-0.94	O	Z	B	0	398.74	8.49	70	70	60	60	8.555	3418.8	2.345048	-3.34505	95.110
79 B-8	2008-01-29				PIE -1	67		0		0.00	0.0	0.0	#DIV/0!	E	X	A	3	396.71	8.86	0	0	0	0	8.86	3406.3	2.26867	-3.26867	95.720
79 B-7	2008-01-24	12:52	29.3	>3000	PIE -1	67	5.56	0	3.6	0.00	12.6	-11.7	-0.93	L	X	A	0	397.03	8.85	50	50	60	50	8.9025	3393.8	2.258453	-3.25845	95.805
79 A-8					PIE -1			0		0.00	0.0	0.0	#DIV/0!		Z	AA	3	395.35	8.51	50	50	50	50	8.56	3418.8	2.34375	-3.34375	95.120
79 A-7	2008-01-22	15:27	27.7	>8000	PIE -1	67	5.38	0	3.5	0.00	12.6	-11.7	-0.93	O	Z	AA	0	396.27	8.505	50	50	50	50	8.555	3418.8	2.345048	-3.34505	95.110
79 D-8	2008-01-25	07:34	27.8	>9823	PIE -1	67	5.66	0	3.8	0.00	12.8	-12.4	-0.97	L	X	A	3	398.46	8.835	60	60	60	50	8.8925	3387.5	2.260848	-3.26085	95.785
79 D-7	2008-01-25	13:04	34.7	11321	PIE -1	67	4.88	0	3.0	0.00	11.0	-9.8	-0.89	D	X	A	0	398.67	8.83	70	70	60	50	8.8925	3387.5	2.260848	-3.26085	95.785
79 E-8	2008-01-25	11:43	40.6		PIE -1	67		0		0.00	0.0	0.0	#DIV/0!	E	Z	B	3	398.67	8.49	60	50	50	60	8.545	3400	2.347646	-3.34765	95.090
79 E-7	2008-01-28	13:20	32.8	9187	PIE -1	67		0		0.00	0.0	0.0	#DIV/0!	L	Z	B	0	399.11	8.535	20	20	20	20	8.555	3406.3	2.345048	-3.34505	95.110
79 E-12	2008-01-31	13:18	31.0		PIE -1	85		0		0.00	0.0	0.0	#DIV/0!	E	Z	B	3	399.05	8.505	50	50	40	40	8.55	3412.5	2.346346	-3.34635	95.100
79 B-11	2008-01-31	12:53			PIE -1	85		0		0.00	0.0	0.0	#DIV/0!	E	X	A	0	396.56	8.85	50	50	50	50	8.9	3381.3	2.259051	-3.25905	95.800
79 A-14	2008-01-31	13:33			PIE -1			0		0.00	0.0	0.0	#DIV/0!	E	Z	AA	12	395.96	8.5	60	50	50	50	8.5525	3443.8	2.345697	-3.3457	95.105
79 D-14											0.0	0.0	#DIV/0!		X	B	12	396.36	8.855	50	50	40	40	8.9	3362.5	2.259051	-3.25905	95.800
79 F1-5											0.0	0.0	#DIV/0!		X	B	9	400.12	8.93	60	60	50	60	8.9875	3400	2.238316	-3.23832	95.975
79 A-16											0.0	0.0	#DIV/0!		Z	AA	1	396.13	8.515	40	40	40	40	8.555	3431.2	2.345048	-3.34505	95.110
79 G1-3											#DIV/0!	#DIV/0!			X	B	6	401.44						#DIV/0!	3381.3	#DIV/0!	#DIV/0!	#DIV/0!
37 E-8											0.0	0.0			Z	B	3	400.03	8.46	60	60	80	60	8.525	3450	2.352862	-3.35286	95.050
37 E-3											0.0	0.0			Z	B	6	393.36	8.505	60	60	60	50	8.5625	3250	2.343103	-3.3431	95.125
79 F2-3											0.0	0.0			X	B	6	400.18	8.925	50	40	60	60	8.9775	3375	2.240664	-3.24066	95.955
79 I-11											0.0	0.0			Z	A	0	400.17	8.835	60	60	60	60	8.895	3412.5	2.260249	-3.26025	95.790
79 E-9					+1/+1		10.653	0	0	0	25.0	0.0			Z	B	11	397.16	8.53	40	30	30	30	8.5625	3375	2.343103	-3.3431	95.125
37 E-1					+1/+1		10.302	0	0	0	24.2	0.0			Z	B	7	396.11	8.48	70	70	60	60	8.545	3287.5	2.347646	-3.34765	95.090
37 E-2					+1/+1		8.483	0	0	0	20.0	0.0			Z	B	6	394.67	8.465	40	50	40	40	8.5075	3256.3	2.357447	-3.35745	95.015
79 O-1					+1/+1		10.583	0	0	0	23.8	0.0			Z	AA	7	397.33	8.94	0	0	0	0	8.94	3387.5	2.24952	-3.24952	95.880
79 O-2					+1/+1		9.351	0	0	0	21.0	0.0			Z	AA	6	399.25	8.935	20	50	40	40	8.9725	3423	2.241841	-3.24184	95.945

MULTIAXIAL FATIGUE RESULTS TABLE

Spec.#	Date	Time	Temp [°C]	N [cycles]	R_t	Ampl [%]	PA max	PA min	PB max	PB min	σ max	σ min	R_a	F-Type	Dir	Block Pos	Clock Pos	M [g]	tc [mm]	dt1 [µm]	dt2 [µm]	dt3 [µm]	dt4 [µm]	t [mm]	f1 [Hz]	g [-]	h [-]	D [mm]
37 A1-1					+1/+1		9.975	0	0	0	22.6	0.0			X	A	7	397.87	8.825	80	80	50	50	8.89	3400	2.261447	-3.26145	95.780
79 G1-12					+1/+1						0.0	0.0		E	X	B	1	403.61	9.111	0	0	0	0	9.111	3412.5	2.209744	-3.20974	96.222
37 A1-6					-1/-1		0	0	34.7	0	0.0	-113.1			X	A	0	399.09	8.830	80	70	60	60	8.8975	3450	2.25965	-3.25965	95.795
37 A1-5					-1/-1		0	0	34.76	0	0.0	-113.5			X	A	9	398.77	8.820	60	50	50	60	8.875	3425	2.265053	-3.26505	95.750
79 F1-6					-1/-1		0	0	35.41	0	0.0	-114.6			X	B	0	401.98	8.925	70	70	60	60	8.99	3406.3	2.237729	-3.23773	95.980
79 O-3					-1/-1		0	0	34.78	0	0.0	-112.7			Z	AA	6	399.36	8.930	50	40	40	50	8.975	3393.8	2.241252	-3.24125	95.950
79 O-5					-1/-1		0	0	34.9	0	0.0	-113.1			Z	AA	9	399.54	8.930	60	60	40	40	8.98	3425	2.240077	-3.24008	95.960
37 E-5					-1/-1		0	0	34.34	0	0.0	-115.0			Z	B	9	399.60	8.485	50	50	50	50	8.535	3418.8	2.350251	-3.35025	95.070
37 E-6					-1/-1		0	0	35.36	0	0.0	-119.0			Z	B	0	400.89	8.440	50	50	30	30	8.48	3425	2.364691	-3.36469	94.960
79 D-9					-1/-1		0	0	34.82	0	0.0	-113.5			X	A	9	397.04	8.835	70	50	50	70	8.895	3387.5	2.260249	-3.26025	95.790
79 D-10					PIE +1/+1		10.06	0	0	0	22.7	0.0			X	A	0	398.37	8.83	80	70	60	50	8.895	3400	2.260249	-3.26025	95.790
37 C-12					PIE +1/+1		10.66	0	0	0	25.1	0.0			X	B	3	400.09	8.47	60	60	50	50	8.525	3443.8	2.352862	-3.35286	95.050
79 O-16					PIE +1/+1		10.53	0	0	0	23.6	0.0			Z	AA	1	401.12	8.935	60	50	60	50	8.99	3456.3	2.237729	-3.23773	95.980
79 E-14					PIE +1/+1		9.69	0	0	0	22.7	0.0			Z	B	12	398.39	8.5	60	60	50	50	8.555	3393.8	2.345048	-3.34505	95.110
79 D-11					PIE +1/+1		10.29	0	0	0	23.3	0.0			X	A	0	398.67	8.835	60	60	50	60	8.8925	3400	2.260848	-3.26085	95.785
79 E-16					PIE +1/+1		10.25	0	0	0	24.0	0.0			Z	B	1	399.29	8.53	30	40	30	30	8.5625	3418.8	2.343103	-3.3431	95.125
79 E-15					PIE +1/+1		9.73	0	0	0	21.9	0.0			Z	B	12	397.92	8.905	30	30	0	0	8.92	3375	2.254275	-3.25427	95.840
79 D-13					PIE +1/+1		10.01	0	0	0	22.6	0.0		E	X	A	11	398.09	8.825	70	70	60	50	8.8875	3406.3	2.262047	-3.26205	95.775
79 B-16					PIE -1/-1		0	0	34.31	0	0.0	-111.8			X	A	1	399.09	8.830	80	70	60	60	8.8975	3450	2.25965	-3.25965	95.795
79 O-14					PIE -1/-1		0	0	34.93	0	0.0	-114.0			Z	AA	12	398.77	8.820	60	50	50	60	8.875	3425	2.265053	-3.26505	95.750
79 A-15					PIE -1/-1		0	0	33.76	0	0.0	-109.3			Z	AA	12	401.98	8.925	70	70	60	60	8.99	3406.3	2.237729	-3.23773	95.980
79 A-13					PIE -1/-1		0	0	33.57	0	0.0	-108.8			Z	AA	11	399.36	8.930	50	40	40	50	8.975	3393.8	2.241252	-3.24125	95.950
79 D-15					PIE -1/-1		0	0	32.37	0	0.0	-104.9			X	A	12	399.54	8.930	60	60	40	40	8.98	3425	2.240077	-3.24008	95.960
79 D-16					PIE -1/-1		0	0	34.21	0	0.0	-114.6			X	A	1	399.6	8.485	50	50	50	50	8.535	3418.8	2.350251	-3.35025	95.070
79 C-15					PIE -1/-1		0	0	32.22	0	0.0	-108.4			X	A	12	400.89	8.440	50	50	30	30	8.48	3425	2.364691	-3.36469	94.960
79 E-13					PIE -1/-1		0	0	34.23	0	0.0	-111.6			Z	B	11	397.87	8.825	80	80	50	50	8.89	3400	2.261447	-3.26145	95.780

APPENDIX I

Multiaxial Specimen Fracture Locations

1 R = +1/+1



Figure 1: 79 F1-2

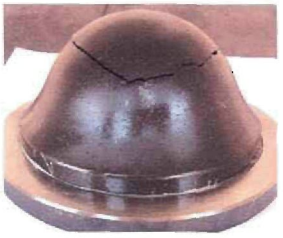


Figure 2: 79 O-1



Figure 3: 79 O-2



Figure 4: 37 A1-1



Figure 5: 79 A1-2

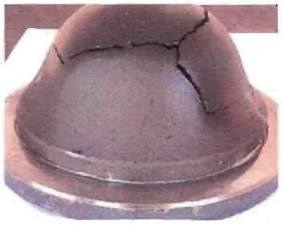


Figure 6: 37 E-1



Figure 7: 37 E-2



Figure 8: 79 E-9

2 R = +1/2



Figure 9: 79 F1-9



Figure 10: 79 F1-3



Figure 11: 79 I-1



Figure 12: 79 I-6



Figure 13: 37 A2-1



Figure 14: 37 A2-2



Figure 15: 37 E-9



Figure 16: 79 A-11



Figure 17: 79 F1-12



Figure 18: 79 F1-11



Figure 19: 79 I-13



Figure 20: 79 O-15



Figure 21: 37 B1-1



Figure 22: 37 A2-7



Figure 27: 79 I-9



Figure 32: 37 G-6



Figure 37: 37 A2-5

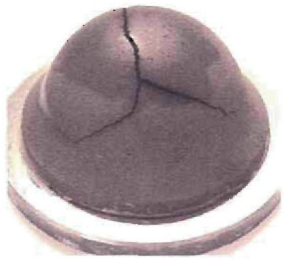


Figure 23: 37 G-5



Figure 28: 79 I-10



Figure 33: 79 F2-4



Figure 38: 37 A2-3



Figure 24: 37 G-10



Figure 29: 37 A2-9



Figure 34: 79 F1-7



Figure 39: 37 E-13



Figure 25: 79 F2-1



Figure 30: 37 A2-6



Figure 35: 79 I-5



Figure 40: 37 G-2



Figure 26: 79 F1-10



Figure 31: 37 G-1



Figure 36: 79 I-7

R = 0



Figure 41: 79 F2-5



Figure 42: 79 F2-2



Figure 43: 79 K-1



Figure 44: 79 I-2



Figure 45: 37 A1-9



Figure 46: 37 A2-10



Figure 47: 37 G-9



Figure 48: 37 E-10



Figure 49: 79 F2-8



Figure 50: 79 B-14



Figure 51: 79 K-5



Figure 52: 79 I-3



Figure 53: 37 B1-5



Figure 54: 37 A2-11



Figure 55: 37 G-13



Figure 56: 37 G-14



Figure 57: 79 F2-6



Figure 58: 79 K-9



Figure 59: 79 I-14



Figure 60: 37 B1-9



Figure 61: 37 B1-2



Figure 62: 37 I-1



Figure 63: 37 I-2



Figure 64: 79 F2-12



Figure 65: 79 F2-7



Figure 66: 79 K-13



Figure 67: 79 I-15



Figure 68: 37 B2-1



Figure 69: 37 B1-3



Figure 70: 37 I-5



Figure 71: 37 I-6



Figure 72: 79 G1-5

3 R = -1/2

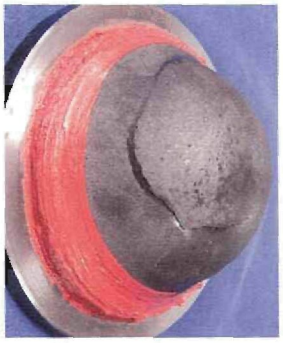


Figure 73: 79 G1-1

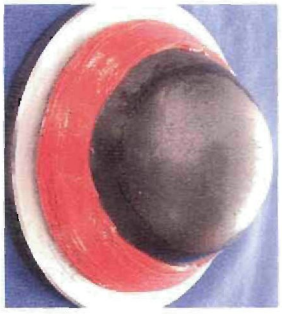


Figure 74: 79 F2-10

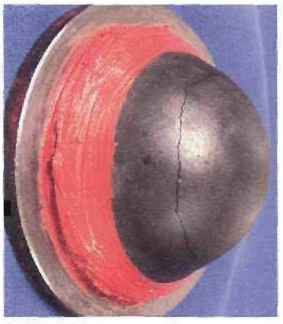


Figure 75: 79 M-1

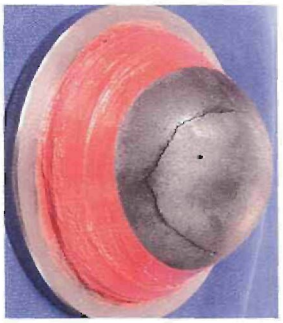


Figure 76: 37 B2-5



Figure 77: 37 B1-6



Figure 78: 79 G1-4



Figure 79: 79 E-11



Figure 80: 37 B2-9



Figure 81: 37 B1-7



Figure 82:37 E-4



Figure 83: 79 G1-2



Figure 84: 37 A1-10

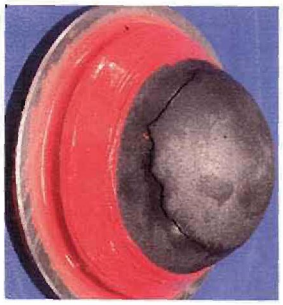


Figure 85: 79 D-12



Figure 86:79 G1-8



Figure 87:37 A1-11



Figure 88: 37 K-5



Figure 89:37 K-6

4 R = -1



Figure 90: 79 G1-7



Figure 91: 79 I-4



Figure 92: 37 C-9

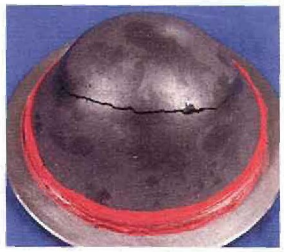


Figure 93: 37 B1-10

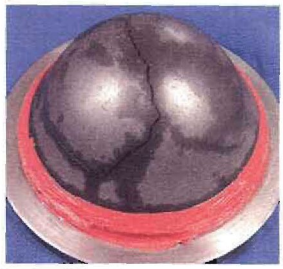


Figure 94: 37 K-9



Figure 95: 37 K-10



Figure 96: 79 G2-5



Figure 97: 79 I-8



Figure 98: 79 K-11

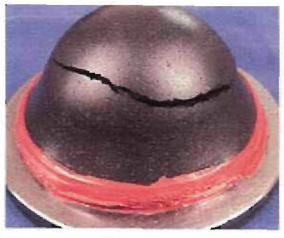


Figure 99: 37 C-13

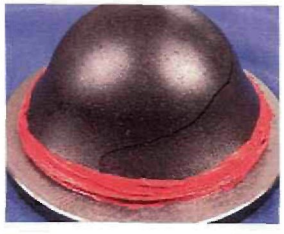


Figure 100: 37 B1-11



Figure 101: 37 K-13



Figure 102: 37 K-14



Figure 103: 79 G2-9

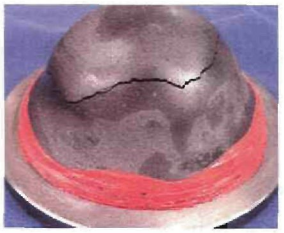


Figure 104: 79 G1-11



Figure 105: 79 I-12



Figure 106: 37 A1-4



Figure 107: 37 B2-2

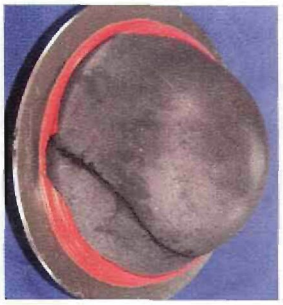


Figure 108: 37 E-12



Figure 109: 37 E-7

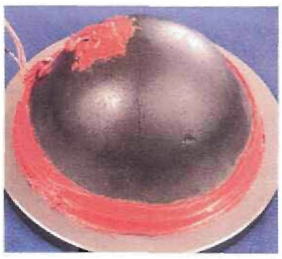


Figure 110: 79 G2-4



Figure 111: 79 G2-2

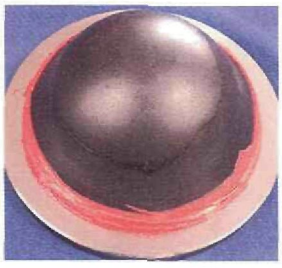


Figure 112: 79 I-16



Figure 113: 37 A1-8



Figure 114: 37 B2-3



Figure 115: 37 E-16

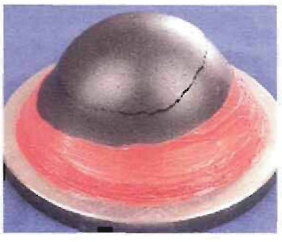


Figure 116: 37 E-11

5 R = -2



Figure 117: 79 G2-8



Figure 118: 79 G2-3



Figure 119: 79 O-4



Figure 120: 79 M-2



Figure 121: 37 A1-12



Figure 122: 37 B2-6



Figure 123: 37 G-4



Figure 124: 37 E-15



Figure 125: 79 G2-12



Figure 126: 79 G2-6



Figure 127: 79 K-4



Figure 128: 79 M-3



Figure 129: 37 A2-4



Figure 130: 37 B2-7



Figure 131: 37 G-8



Figure 132: 37 G-3



Figure 133: 79 G2-10



Figure 134: 79 K-12



Figure 135: 79 M-7



Figure 136: 37 A2-12



Figure 137: 37 B2-11



Figure 138: 37 G-16



Figure 139: 37 G-7

6 $R = -\infty$



Figure 140: 79 C-13



Figure 141: 79 G2-11



Figure 142: 79 K-16



Figure 143: 37 B1-4



Figure 144: 37 C-2



Figure 145: 37 I-4



Figure 146: 79 K-2



Figure 147: 79 C-4



Figure 148: 79 C-3



Figure 149: 79 M-8



Figure 150: 79 M-14



Figure 151: 37 B1-12



Figure 152: 37 C-6



Figure 153: 37 I-12



Figure 154: 37 I-7



Figure 155: 79 C-8



Figure 156: 79 C-6



Figure 157: 79 M-12



Figure 158: 37 B2-4



Figure 159: 37 C-7



Figure 160: 37 I-16



Figure 161: 37 I-11

7 R = +2



Figure 162: 79 C-12



Figure 163: 79 C-7



Figure 164: 79 M-16



Figure 165: 79 O-6



Figure 166: 37 C-10



Figure 167: 37 K-4



Figure 168: 79 C-16



Figure 169: 79 C-10



Figure 170: 79 O-12



Figure 171: 79 O-7



Figure 172: 37 B2-12



Figure 173: 37 C-11



Figure 174: 37 K-8



Figure 175: 37 K-3



Figure 176: 79 F1-4



Figure 177: 79 C-11



Figure 178: 79 O-8



Figure 179: 79 O-11



Figure 180: 37 C-4



Figure 181: 37 C-15



Figure 182: 79 O-9



Figure 183: 37 K-7

8 R = -1/-1



Figure 184: 79 D-9



Figure 185: 79 F1-6



Figure 186: 79 O-5



Figure 187: 79 O-3



Figure 188: 37 A1-5



Figure 189: 37 A1-6



Figure 190: 37 E-5



Figure 191: 37 E-6

PIE R = -1/-1



Figure 192: 79 D-16



Figure 193: 79 D-15



Figure 194: 79 E-13



Figure 195: 79 O-14

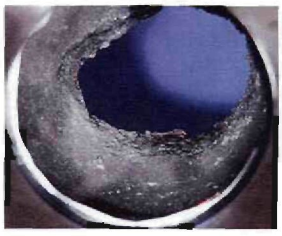


Figure 196: 79 B-16



Figure 197: 79 C-15



Figure 198: 79 A-13



Figure 199: 79 A-15

9 PIE R = +1/+1

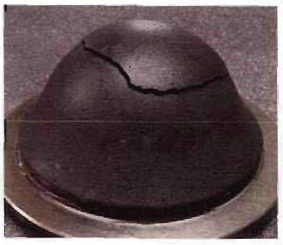


Figure 200: 79 E-14



Figure 201: 79 E-15



Figure 202: 79 E-16

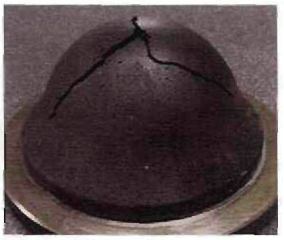


Figure 203: 37 C-12



Figure 204: 79 O-16



Figure 205: 79 D-10



Figure 206: 79 D-11

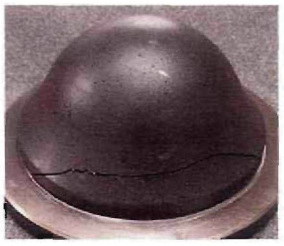


Figure 207: 79 D-13

10 PIE R = -1



Figure 208: 79 B-1



Figure 209: 79 B-2



Figure 210: 79 A-1



Figure 211: 79 A-2



Figure 212: 79 D-1



Figure 213: 79 D-2



Figure 214: 79 E-1



Figure 215: 79 E-2



Figure 216: 79 B-5



Figure 217: 79 B-3



Figure 218: 79 A-5



Figure 219: 79 A-3



Figure 220: 79 D-4



Figure 221: 79 D-3



Figure 222: 79 E-5

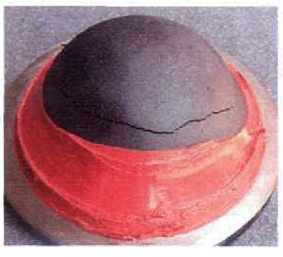


Figure 223: 79 E-3



Figure 224: 79 B-4



Figure 225: 79 B-6



Figure 226: 79 A-4



Figure 227: 79 A-6



Figure 228: 79 D-5



Figure 229: 79 D-6



Figure 230: 79 E-4



Figure 231: 79 E-6



Figure 232: 79 A-7



Figure 233: 79 D-7



Figure 234: 79 E-8

APPENDIX J

Modulus of Elasticity of NBG-18, Determined from S70 Uniaxial Tests

1 INTRODUCTION

The stress-strain curves of the uniaxial tests using the S70 specimen are measured assuming a constant Poisson ratio of 0,21. The strain measurements are made using metal foil strain gauges in a full bridge configuration with two longitudinal strains and two transverse strains. This assumption is probably incorrect, as suggested by the analysis of the relation between the uniaxial and multiaxial stress-strain relationships.

The results are presented as a first estimate of the large strain moduli of elasticity of NBG-18. It is evident from these results that a single modulus is inadequate to describe the relation between stress and strain for this nuclear grade graphite, since there is a marked difference between compressive and tensile behaviour of the graphite at large strains.

The tests show that the modulus of elasticity in compression is lower than the modulus of elasticity in tension. The higher the strain range, the larger the reduction in slope of the stress-strain curve.

For design purposes, the designer shall use the modulus that best simulates the loading state of his design.

2 FIRST CYCLE LOADING STRESS-STRAIN EQUATIONS

The stress-strain curve during static tensile and compressive loading of the NBG-18 is shown in Figure 1 and Figure 2 respectively.

The resultant equations for tensile strains are:

$$\sigma = -8\times10^{-7}(\mu\varepsilon)^2 + 0.011(\mu\varepsilon) - 0.0121 \qquad ...(1)$$

and

$$E' = \frac{\partial\sigma}{\partial(\mu\varepsilon)} = -2\left(8\times10^{-7}\right)(\mu\varepsilon) + 0.011 \qquad ...(2)$$

Where:

$\sigma \equiv$ Maximum Principal Stress [MPa]
$\mu\varepsilon \equiv$ microstrain [μm/m]
$E' \equiv$ Tangent Modulus of Elasticity at any local strain [MPa]

The resultant equations for compressive strains are:

$$\sigma = 7\times10^{-7}(\mu\varepsilon)^2 + 0.0119(\mu\varepsilon) - 0.0423 \qquad ...(3)$$

and

$$E' = \frac{\partial\sigma}{\partial(\mu\varepsilon)} = -2\left(7\times10^{-7}\right)(\mu\varepsilon) + 0.0119 \qquad ...(4)$$

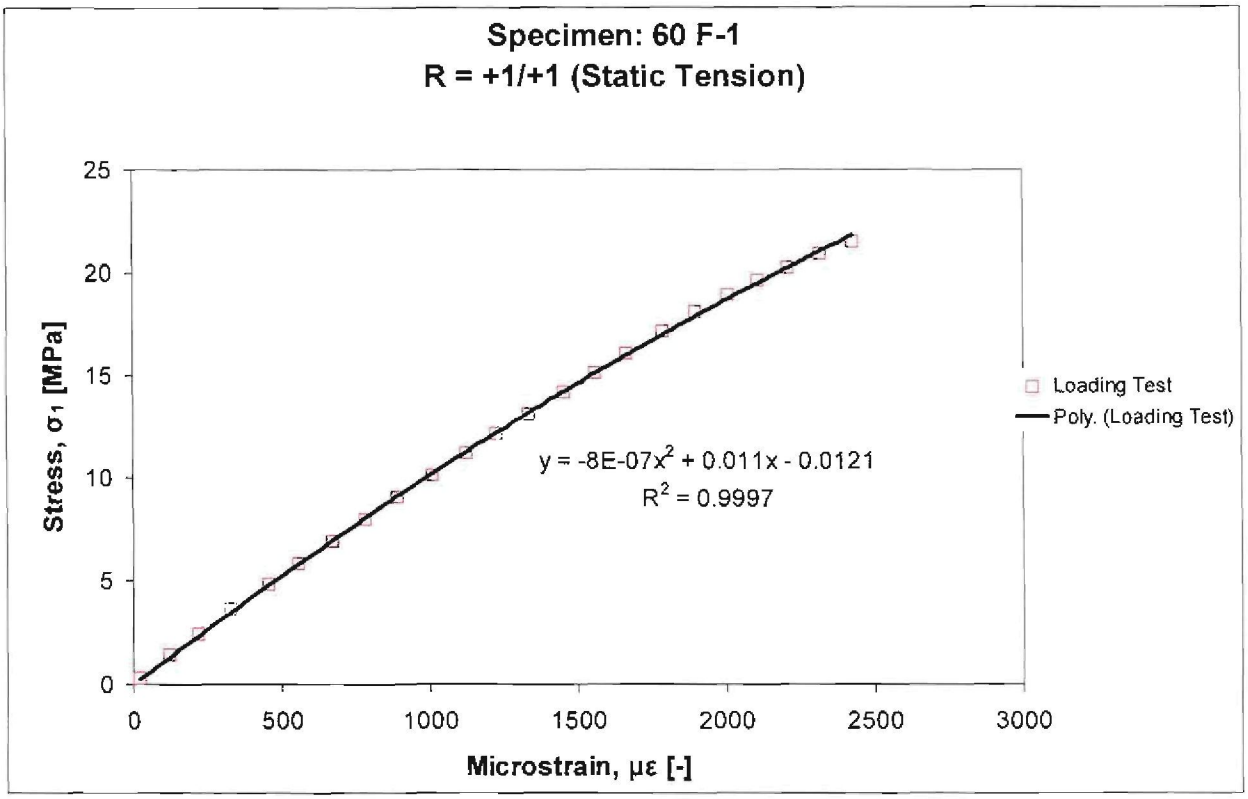


Figure 1: Best Fit Quadratic Equation of Tensile Loading - First Cycle

Eq. 3 and 4 should be used only up to -4000 microstrain due to its limited strain range. The strain gauge failed in this test, and that is causing the limitation.

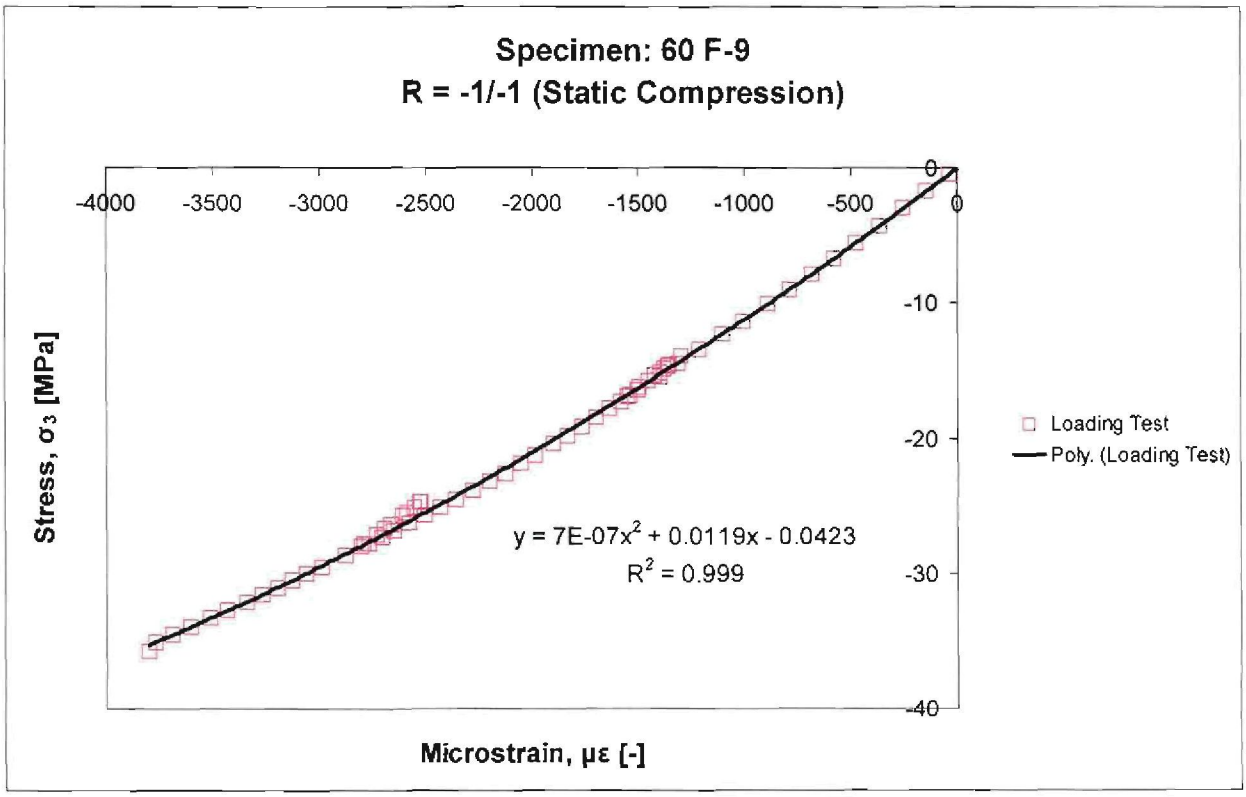


Figure 2: Best Fit Quadratic Equation of Compressive Loading - First Cycle

3 ESTIMATES OF LINEAR MODULI OF ELASTICITY OF NBG18 USING CHORD LINES

The chord line between the origin and the stress-strain curve at a specific strain is calculated for 0%, 25%, 50% and 75% stress relative to the median ultimate strengths of NBG18 as determined in the S70 uniaxial tests. These values are 19,91 MPa and 84,67 MPa for tension and compression respectively.

No value is given for 75% of compressive strength due to possible inaccuracies of the extrapolation, using the best fit equation.

The results are shown in Table 1.

Although the derivative of the quadratic equation at the origin should be equal to the measured dynamic modulus of elasticity, the values from these tests are lower, as discussed in paragraph 5.

Table 1: Chord Moduli Based on Static Tensile and Compressive Loading Cycles in Figure 1 and Figure 2 Respectively.

% Ultimate Strength	Strain [μm/m]	Stress [MPa]	Modulus of Elasticity, E [MPa]
0	0	0.0	11000[1]
25	470	5.0	10598
50	975	10.0	10208
75	1530	14.9	9768
0	0	0.0	11900
25	-2015	-21.2	10510
50	-5060	-42.3	8366

4 ESTIMATES OF LINEAR MODULI OF ELASTICITY OF NBG-18 FROM STRESS-STRAIN HYSTERESIS CURVES

A linear elastic modulus estimate is made by drawing a straight line through the extremities

[1] Derivative of quadratic equation at origin.

of the stress-strain hysteresis curves at the start of cycling and at 1000 cycles. The slope of this line is equal to the linearised modulus of elasticity for the relevant stress ratio. Two moduli are determined with this method, namely a tensile modulus and a compressive modulus. The graphical results are shown in Figure 3 to Figure 16. The results are further analysed and summarized in

Table 2.

There is no significant change in modulus (change < 1%) as a function of number of hysteresis cycles for a low number of cycles (up to 1000 cycles). The direction of change (higher or lower) is also not consequent. The largest variations occur in compression or when the compressive excursions is more than double the tensile excursion (R = -2). The hysteretic losses are also largest for compression.

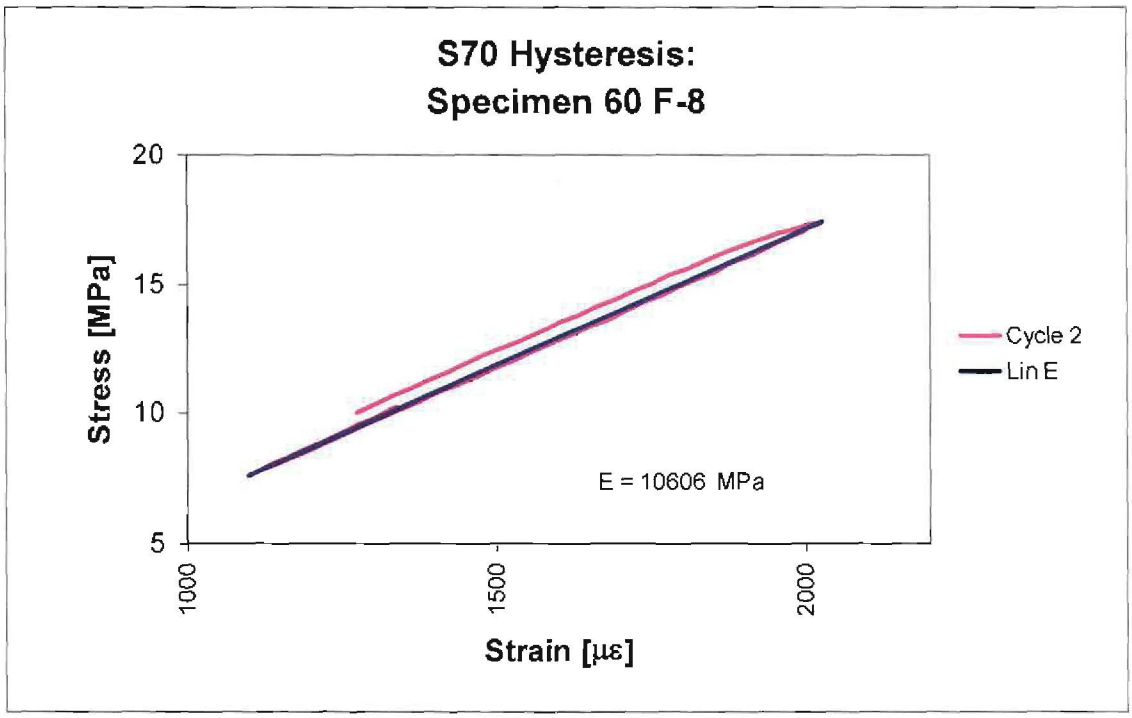


Figure 3: Modulus of Elasticity for R = +0.5 at Start of Cycling

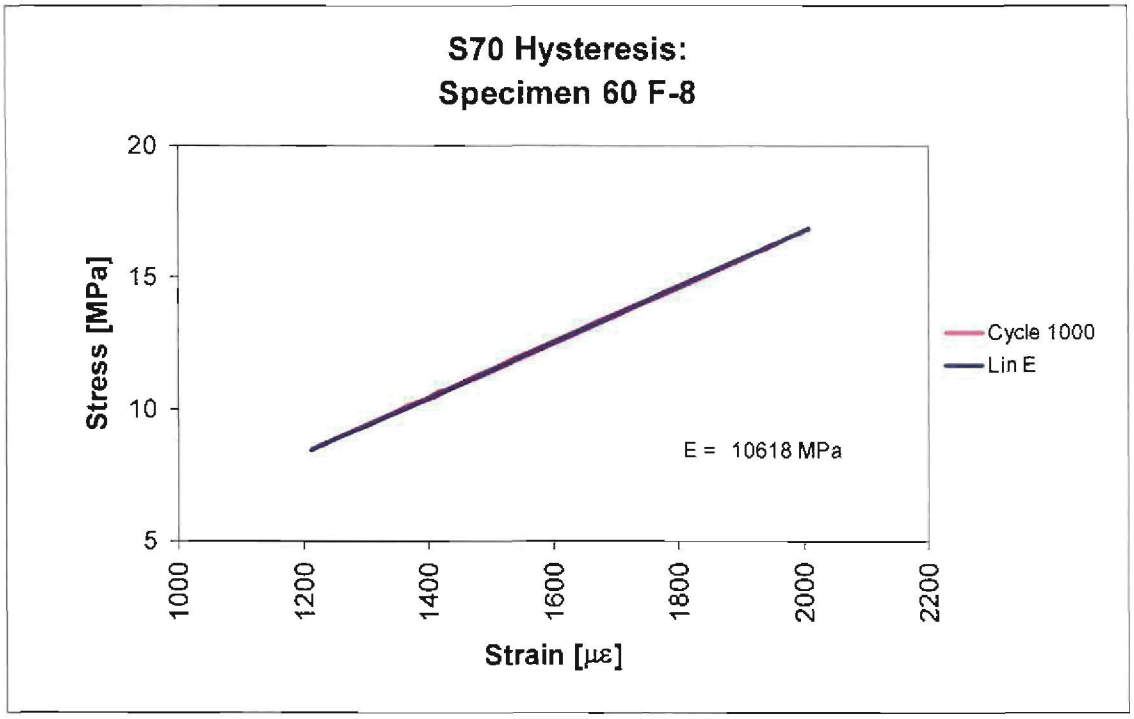


Figure 4: Modulus of Elasticity for R = +0.5 at 1000 Cycles

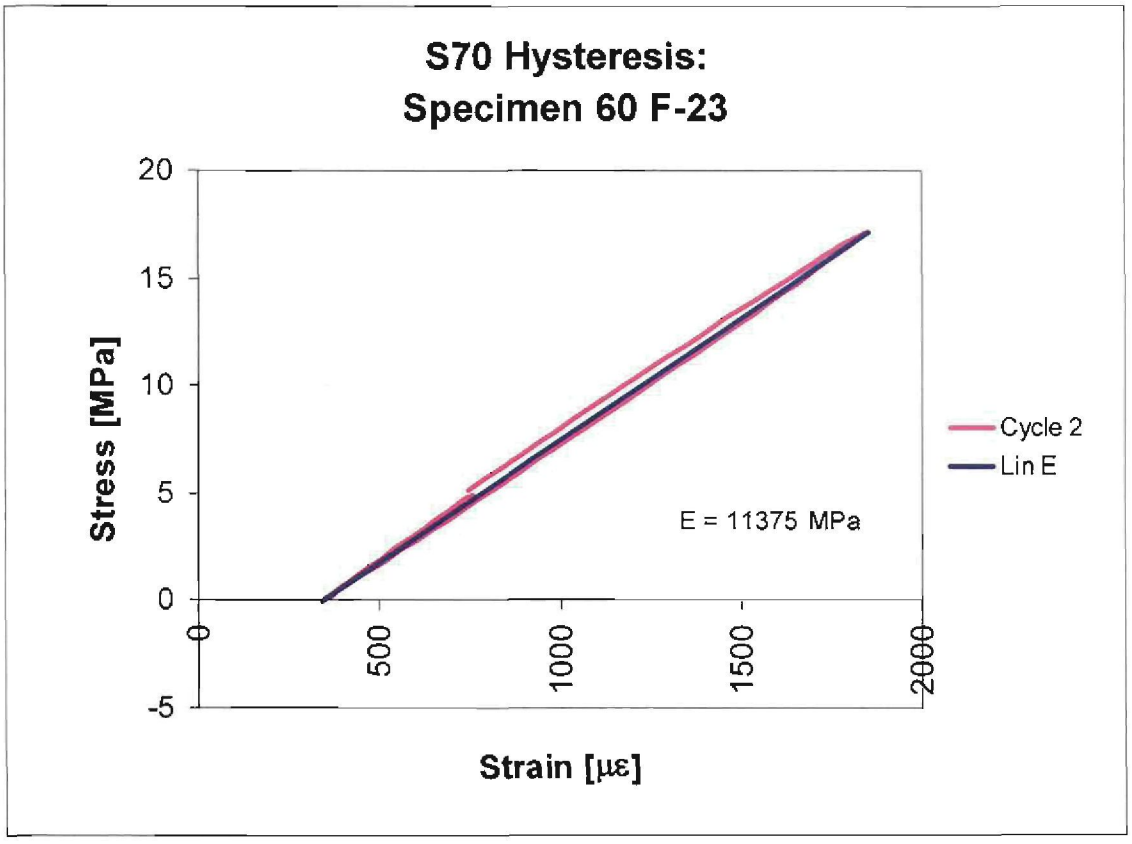


Figure 5: Modulus of Elasticity for R = 0 at Start of Cycling

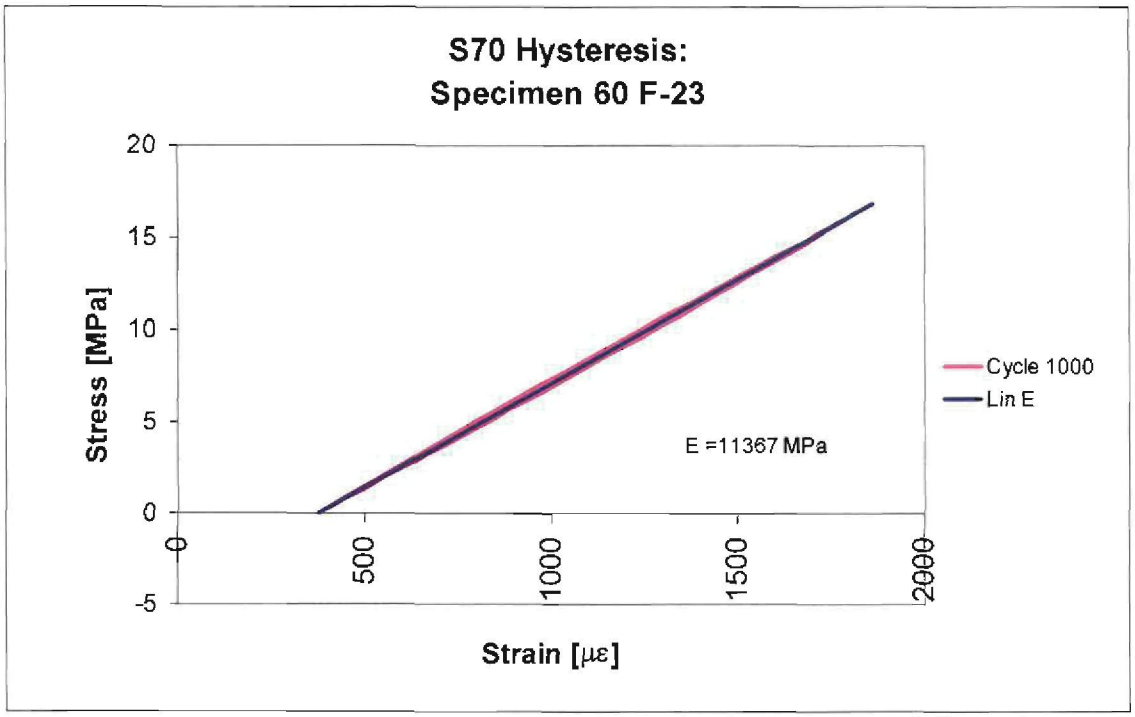


Figure 6: Modulus of Elasticity for R = 0 at 1000 Cycles

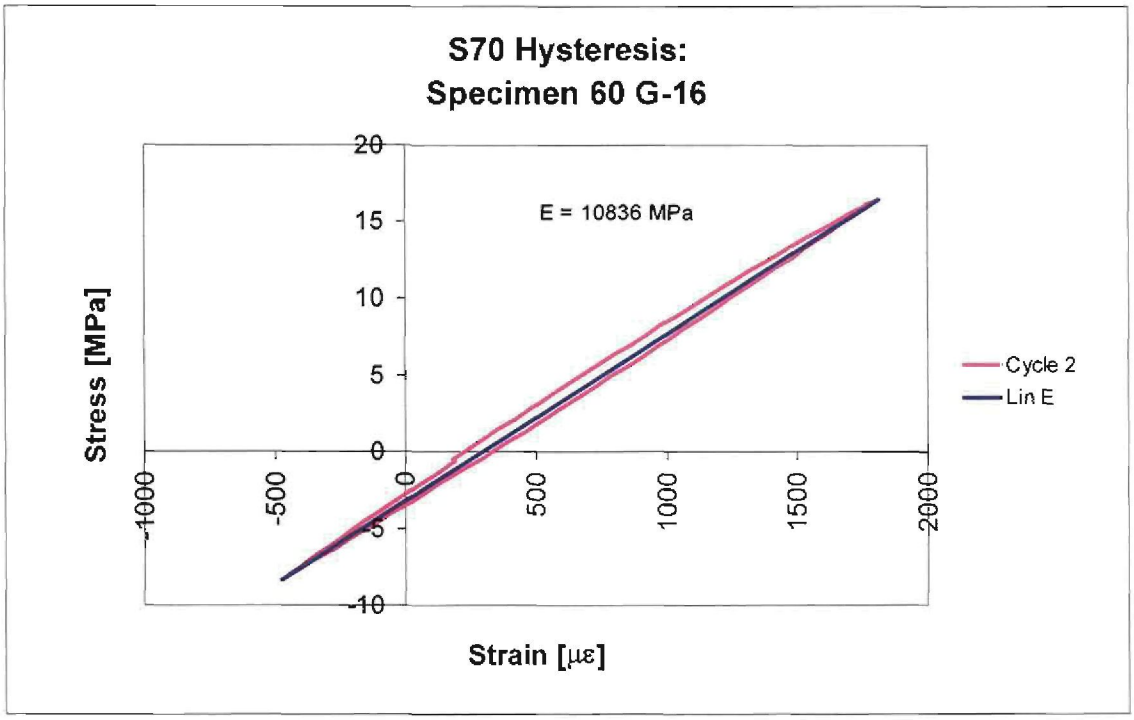


Figure 7: Modulus of Elasticity for R = -0,5 at Start of Cycling

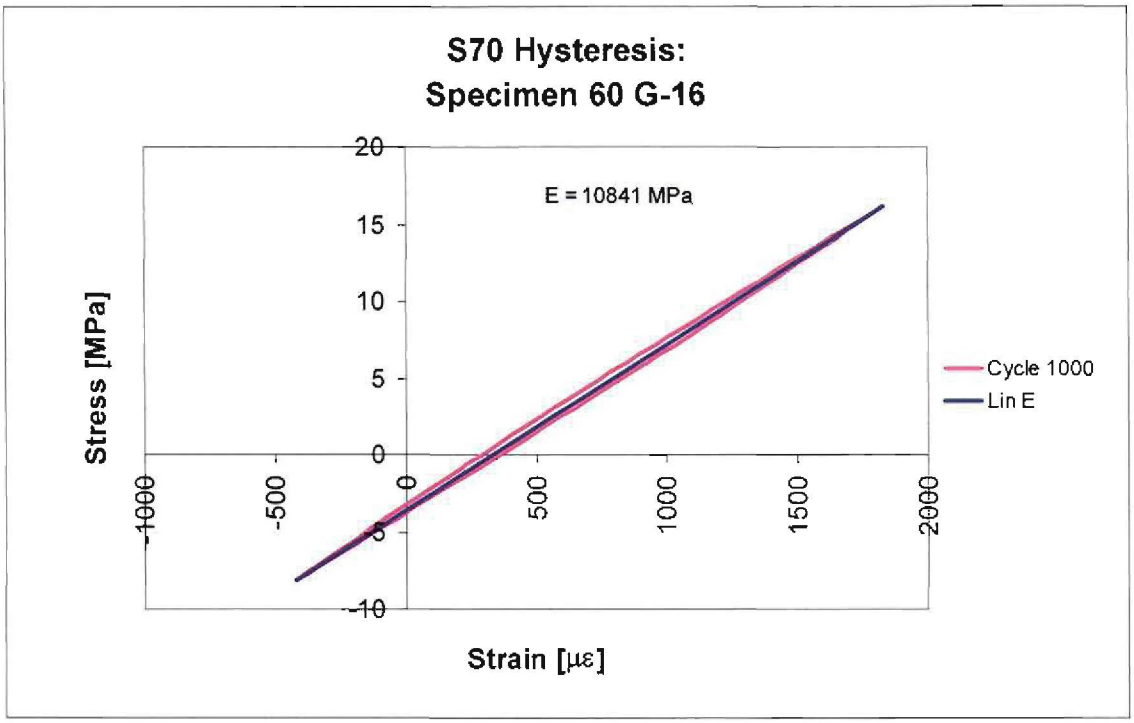


Figure 8: Modulus of Elasticity for R = -0.5 at 1000 Cycles

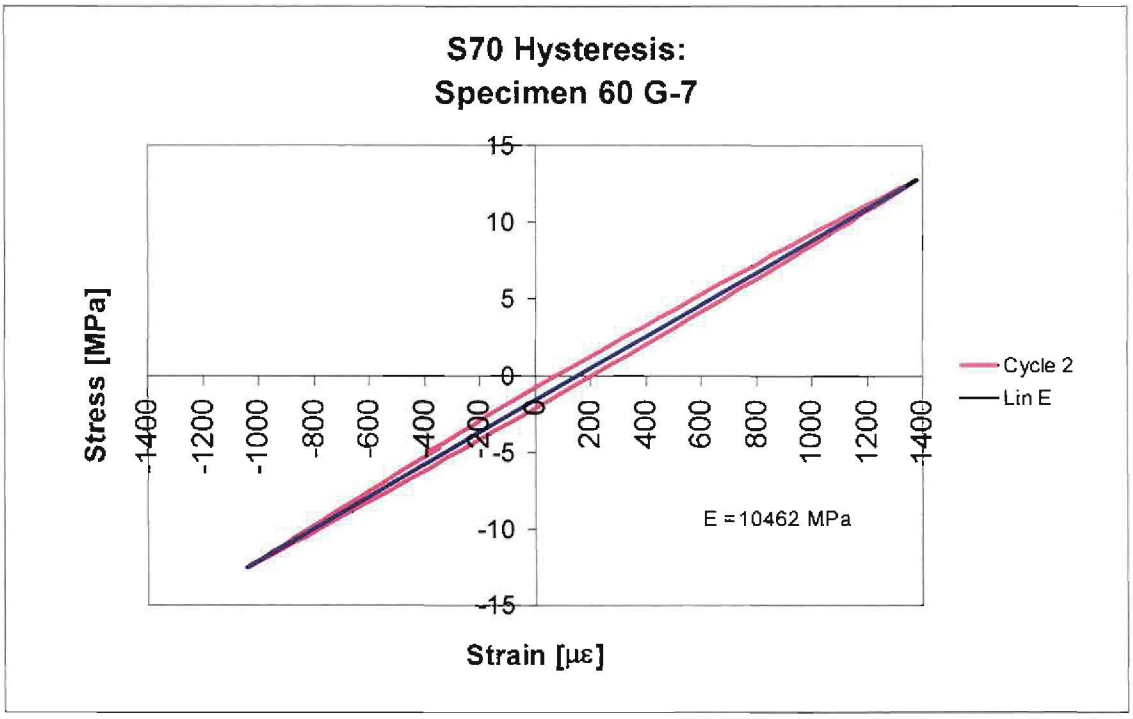


Figure 9: Modulus of Elasticity for R = -1 at Start of Cycling

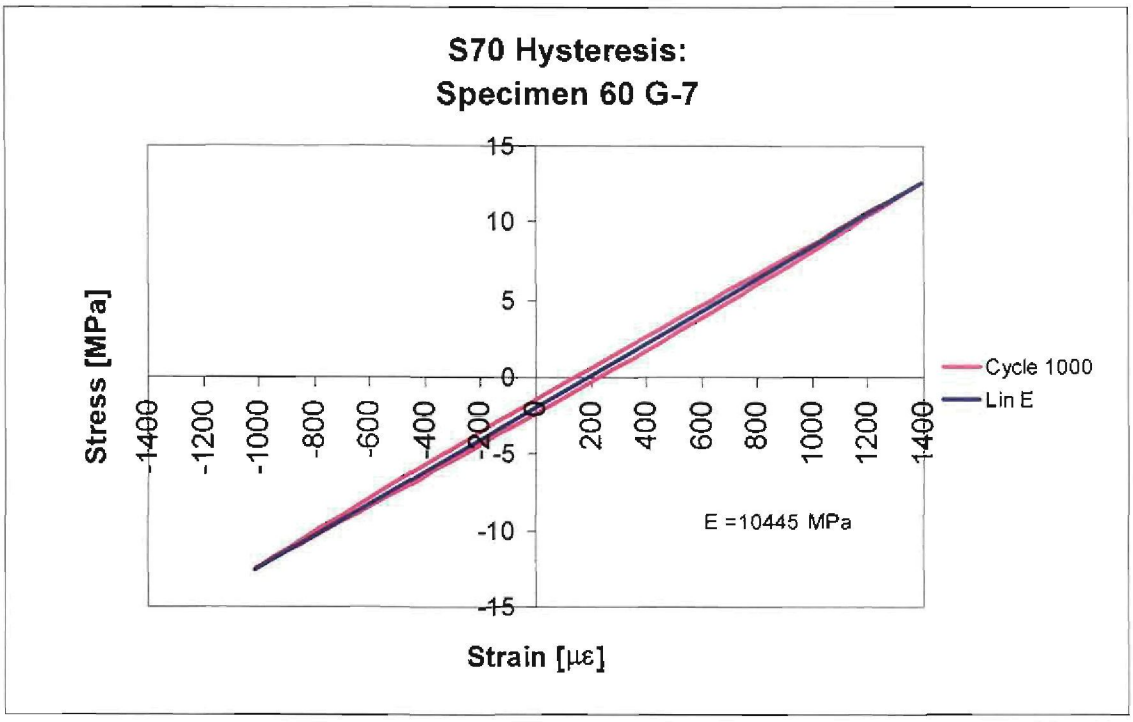


Figure 10: Modulus of Elasticity for R = -1 at 1000 Cycles

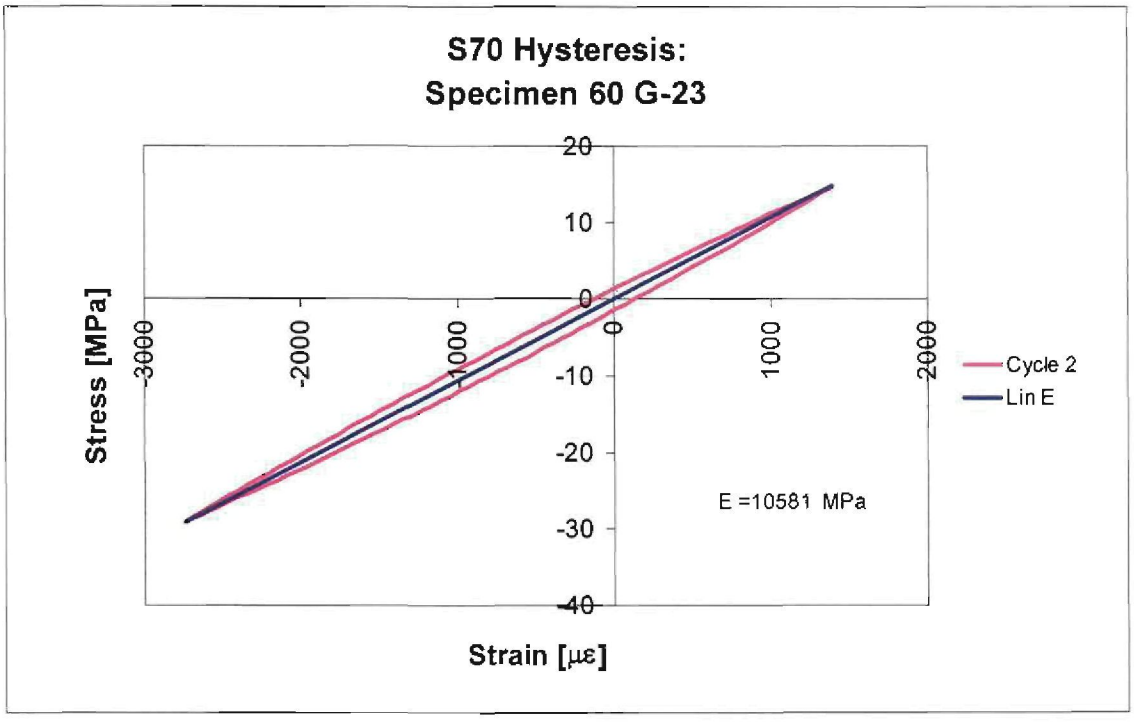


Figure 11: Modulus of Elasticity for R = -2 at Start of Cycling

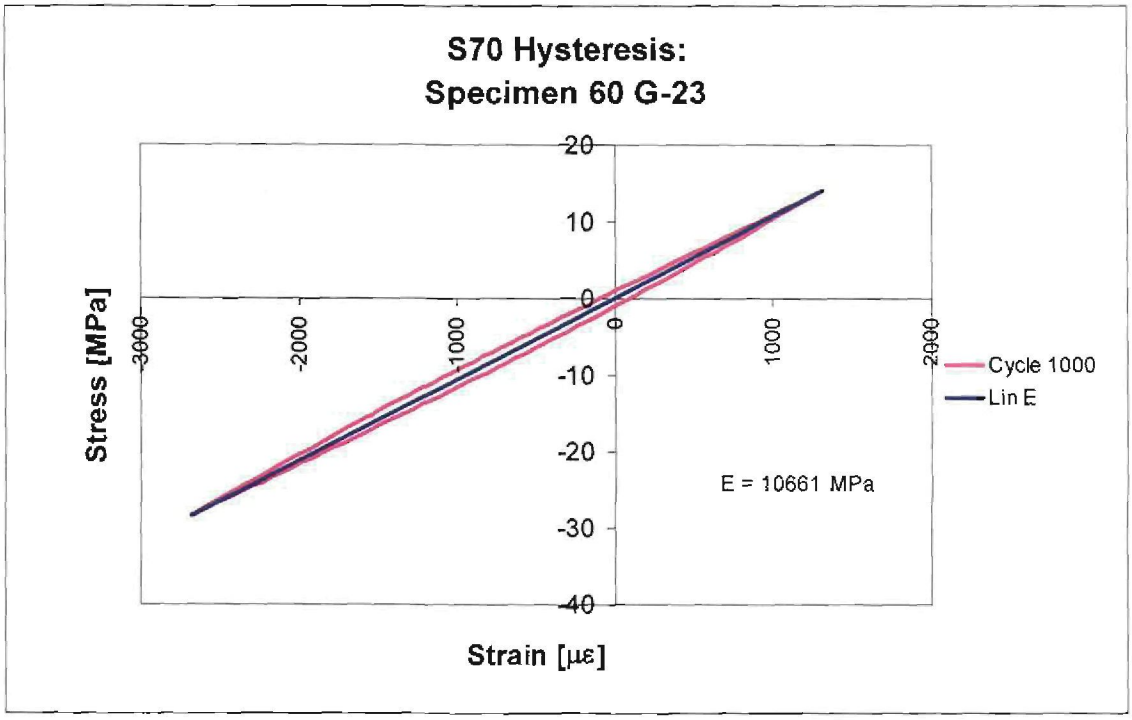


Figure 12: Modulus of Elasticity for R = -2 at 1000 Cycles

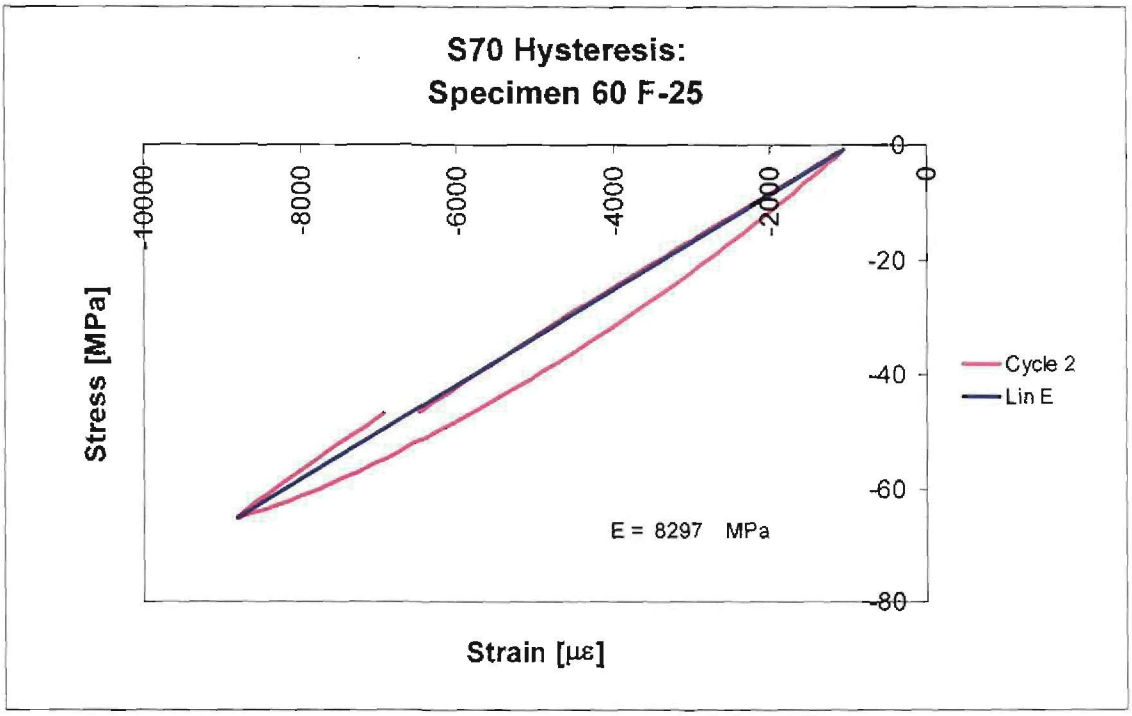


Figure 13: Modulus of Elasticity for R = - ∞ at Start of Cycling

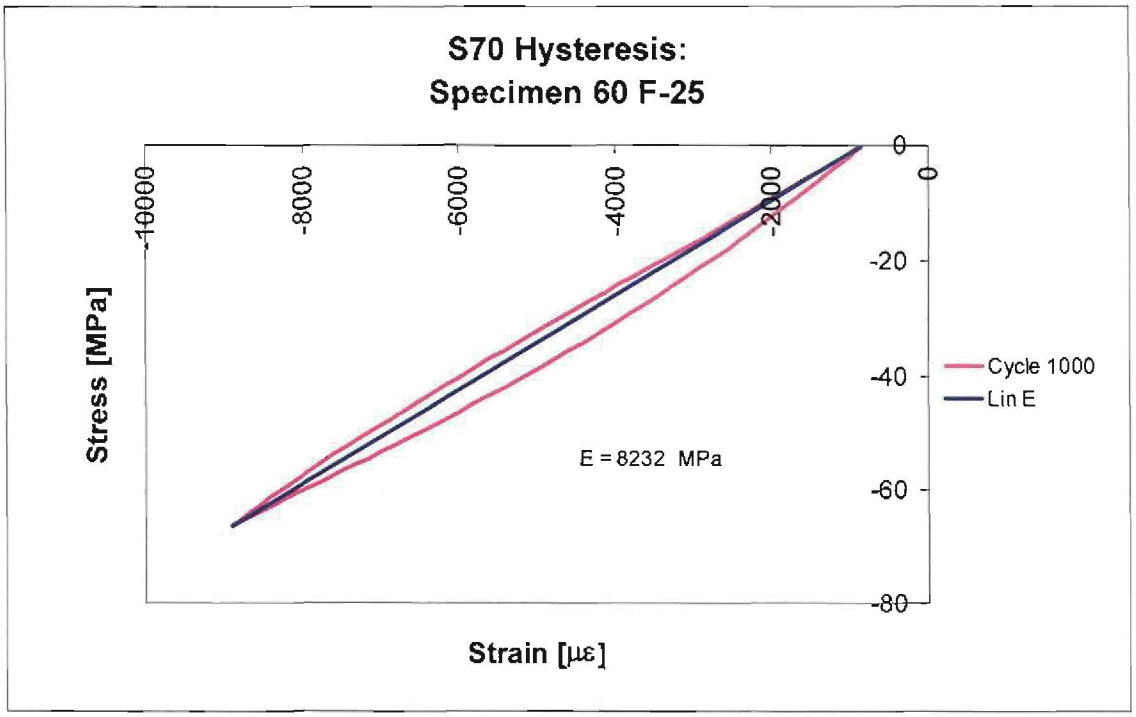


Figure 14: Modulus of Elasticity for R = - ∞ at 1000 Cycles

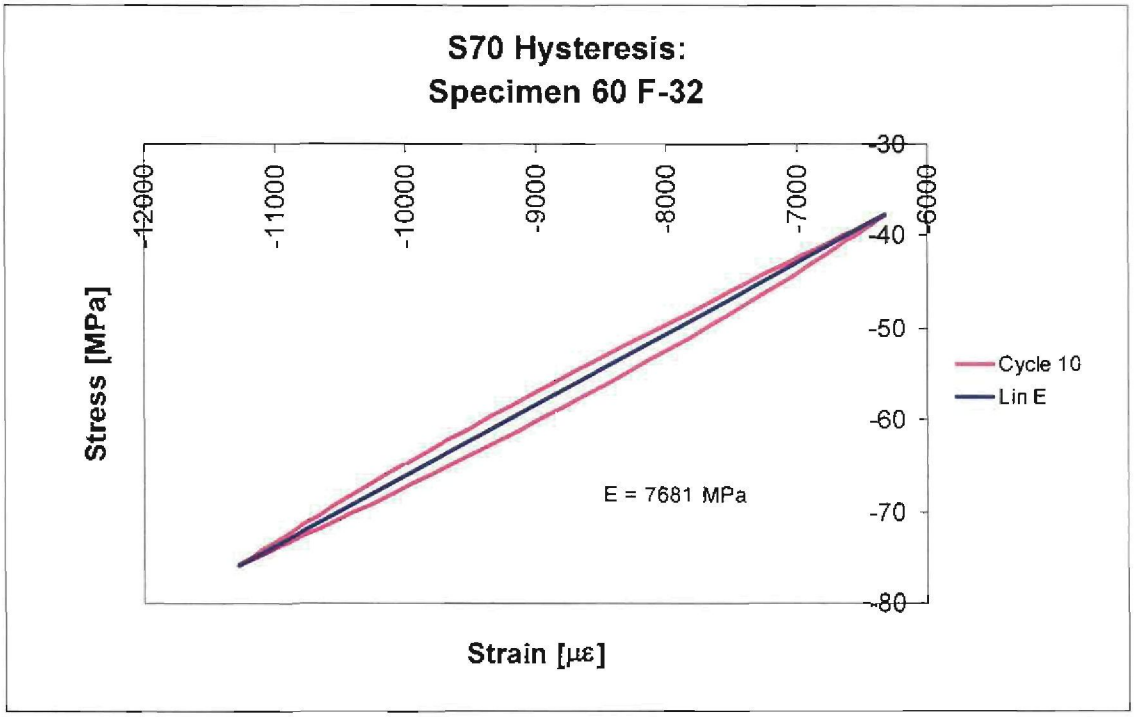


Figure 15: Modulus of Elasticity for R = +2 at Start of Cycling

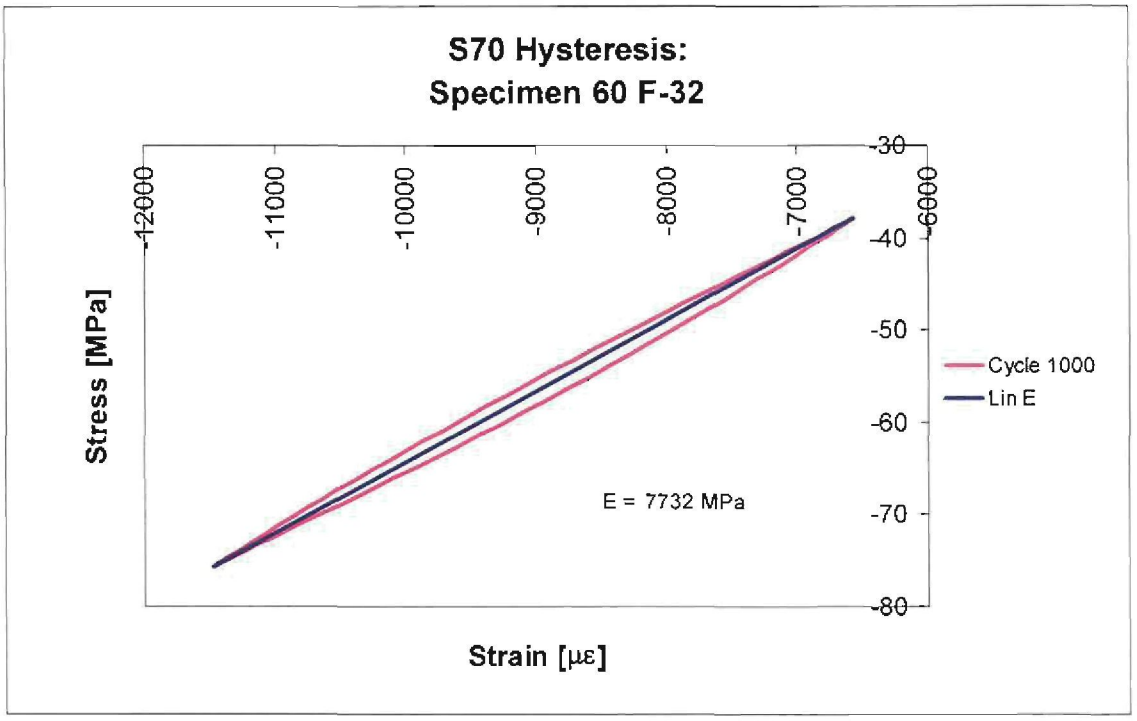


Figure 16: Modulus of Elasticity for R = +2 at 1000 Cycles

The moduli of elasticity are lower than those determined by the chord method or by the best fit polynomial of the static loading cases (quadratic equations), because the linearised hysteresis curve connects the two extremities of two curves with reducing slopes. However, for practical applications, these curves should model the true state of the material best, since all momentary effects like whether the graphite is loaded or unloaded, are averaged out.

In contrast, the tangent modulus, obtained from the derivative of the stress-strain equation, is a strong function of the sense of stress variation, i.e. loading or unloading.

Table 2: Stress-Strain Hysteresis Curve Based Moduli

Stress Ratio, R	Specimen	E_2 [MPa]	E_{1000} [MPa]	% Change
+0.5	60 F-8	10606	10618	0.11
0	60 F-23	11375	11367	-0.07
-0.5	60 G-16	10836	10841	0.05
-1	60 G-7	10462	10445	-0.16
-2	60 G-23	10581	10661	0.76
-∞	60 F-25	8297	8232	-0.78
+2	60 F-32	7681	7732	0.66
				Average
Tension Dominant Average		10772	10786	**10779**
Compression Dominant Average		7989	7982	**7986**

5 COMPARISON WITH DYNAMIC MODULUS BY SGL CARBON (TO DIN 51915)

The specimens that are used for measuring the static stress-strain curves are both X-direction specimens which mean they are parallel to the grain direction. The median modulus of elasticity of specimens, parallel to the grain direction, is calculated from the test data contained in "NBG 18 Database (10_05_2006).doc.xls". The value of the dynamic modulus of elasticity is 12150 MPa. This is compared with the average of the tangent moduli of the static tensile and compressive tests at zero strain (derivatives of nonlinear equations). The average tangent modulus is 11450 MPa.

The average tangent modulus is 5,8% lower than the measured dynamic modulus. It must be pointed out however that the static modulus was determined from 2 specimens only, while the tests of dynamic modulus comprised 104 specimens.

APPENDIX K

Shunt Calibration of Strain Measuring System

1 INTRODUCTION

The derivation in this appendix is done according to the method for a quarter bridge, that is presented in [30].

2 UNIAXIAL SPECIMEN

The S70 Specimen was equipped with two active gauges (R_1 and R_3 bonded in the longitudinal direction on the gauge section) and two Poisson gauges (R_2 and R_4 bonded in the transverse direction on the gauge section).

The following equations apply to metal foil strain gauges, arranged in a full Wheatstone bridge configuration as shown in Figure 1, and assuming equal strain due to uniform stress state in uniaxial gauge section:

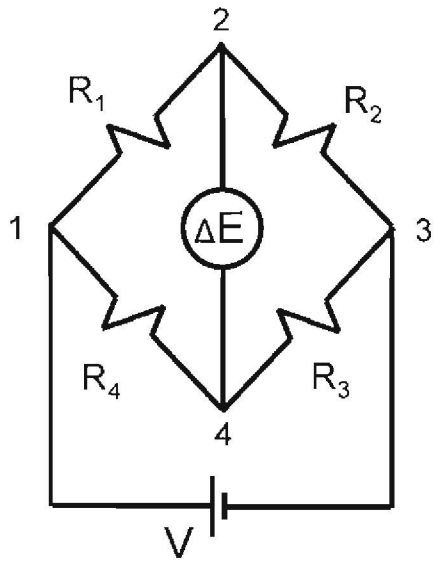


Figure 1: Wheatstone Bridge

For active gauges (R_1 and R_3):

$$\frac{\Delta R}{R} = G.\varepsilon \qquad \text{.....(K.1)}$$

For Poisson gauges (R_2 and R_4):

$$\frac{\Delta R}{R} = -\nu.G.\varepsilon \qquad \text{.....(K.2)}$$

Where :

$R \equiv$ Resistance value of gauge [Ω]

$G \equiv$ Gauge factor [-]

$\varepsilon \equiv$ Strain in gauge [-]

$\nu \equiv$ Poisson Ratio of test material [-]

The characteristic equation for the Wheatstone bridge is:

$$\frac{\Delta E}{V} = \frac{r}{(1+r)^2}\left[\frac{\Delta R_1}{R_1} + \frac{\Delta R_3}{R_3} - \frac{\Delta R_2}{R_2} - \frac{\Delta R_4}{R_4}\right] \qquad \text{.....(K.3)}$$

With :

$$r = \frac{R_2}{R_1} = 1 \qquad \text{.....(K.4)}$$

Substitute (K.4), (K.1) and (K.2) into (K.3):

$$\therefore \frac{\Delta E}{V} = \frac{1}{4}\left[2.G.\varepsilon + 2.\nu.G.\varepsilon\right]$$

$$\therefore \frac{\Delta E}{V} = \frac{G.\varepsilon(1+\nu)}{4} \qquad \text{.....(K.5)}$$

When R_1 is shunted with the calibration resistor R_c, the two resistors in parallel between 1 and 2 can be replaced by one equivalent resistor R_{1e} as shown in Figure 2.

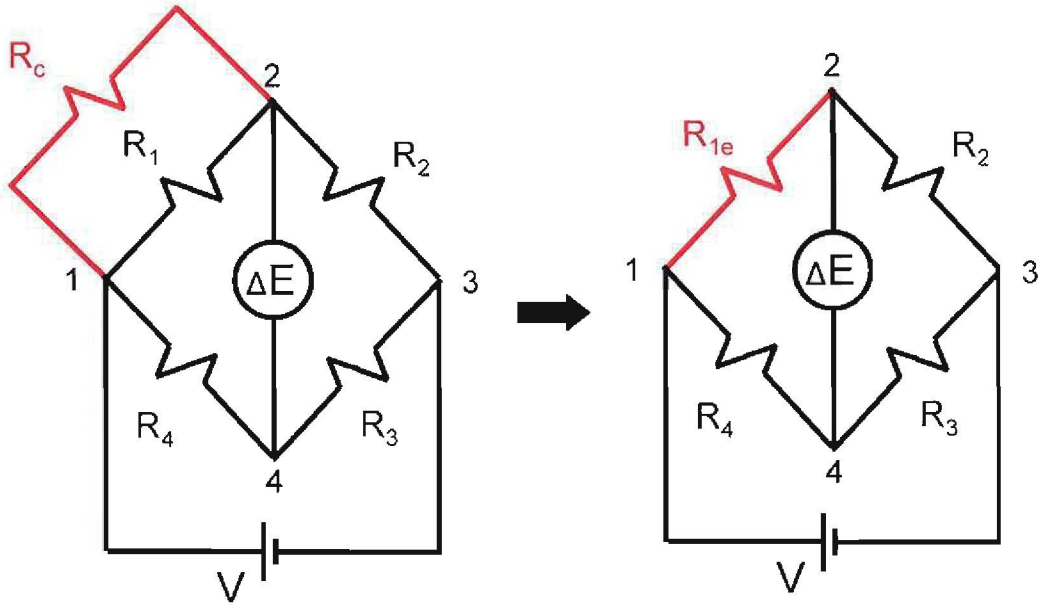


Figure 2: Equivalent Circuit with Calibration Shunt Resistor

$$R_{1e} = \frac{R_1 R_c}{(R_1 + R_c)} \qquad \text{.....(K.6)}$$

$$\therefore \frac{\Delta R_1}{R_1} = \frac{R_{1e} - R_1}{R_1} \qquad \text{.....(K.7)}$$

Substitute (K.6) into (K.7):

$$\therefore \frac{\Delta R_1}{R_1} = \frac{\frac{R_1 R_c}{(R_1 + R_c)} - R_1}{R_1}$$

$$= \frac{R_c}{(R_1 + R_c)} - 1$$

$$= \frac{R_c - R_1 - R_c}{(R_1 + R_c)}$$

$$= \frac{-R_1}{(R_1 + R_c)} \qquad \text{.....(K.8)}$$

Substitute (K.8) into (K.3) to get bridge output:

$$\therefore \frac{\Delta E}{V} = \frac{1}{4}\left[\frac{-R_1}{(R_1 + R_c)} + \frac{\Delta R_3}{R_3} - \frac{\Delta R_2}{R_2} - \frac{\Delta R_4}{R_4}\right]$$

$$= \frac{1}{4}\left[\frac{-R_1}{(R_1 + R_c)} + 0 - 0 - 0\right]$$

$$= \frac{-R_1}{4.(R_1 + R_c)} \qquad \text{.....(K.9)}$$

But the equivalent strain associated with this output can then be found by equating (K.9) and (K.5):

$$\therefore \frac{\Delta E}{V} = \frac{G.\varepsilon_c(1+\nu)}{4} = \frac{-R_1}{4.(R_1 + R_c)}$$

$$\therefore \varepsilon_c = \frac{-R_1}{2.G.(1+\nu)(R_1 + R_c)} \qquad \text{.....(K.10)}$$

3 MULTIAXIAL SPECIMEN

The S60B Specimen was equipped with two active gauges (R_1 and R_3 bonded in the tangential directions on the gauge section) and two dummy gauges (R_2 and R_4) that are not strained at all.

The following equations apply to metal foil strain gauges, arranged in a full Wheatstone bridge configuration as shown in Figure 1, and assuming equal strain due to uniform tangential stress state in multiaxial gauge section:

For active gauges (R_1 and R_3) :

$$\frac{\Delta R}{R} = G.\varepsilon \qquad \text{.....(K.1)}$$

For dummy gauges (R_2 and R_4) :

$$\frac{\Delta R}{R} = 0 \qquad \text{.....(K.11)}$$

Where :

$R \equiv$ Resistance value of gauge [Ω]

$G \equiv$ Gauge factor [-]

$\varepsilon \equiv$ Strain in gauge [-]

Substitute (K.4), (K.1) and (K.11) into (K.3):

$$\therefore \frac{\Delta E}{V} = \frac{1}{4}\left[2.G.\varepsilon + 0\right]$$

$$\therefore \frac{\Delta E}{V} = \frac{G.\varepsilon}{2} \qquad \text{.....(K.12)}$$

As for uniaxial specimen, the bridge output with shunt resistor is given by (K.9).

The equivalent strain associated with this output can then be found by equating (K.9) and (K.12):

$$\therefore \frac{\Delta E}{V} = \frac{G.\varepsilon_c}{2} = \frac{-R_1}{4.(R_1 + R_c)}$$

$$\therefore \varepsilon_c = \frac{-R_1}{2.G.(R_1 + R_c)} \qquad \text{.....(K.13)}$$

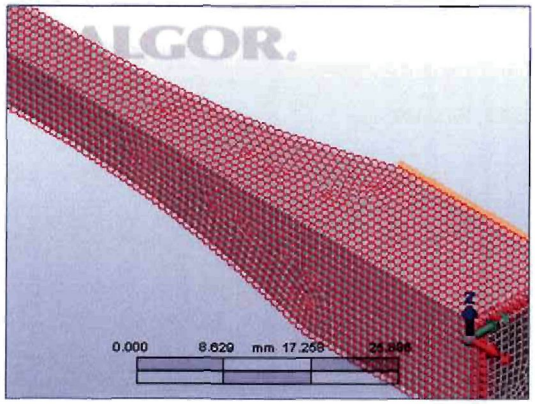
APPENDIX L

Finite Element Analysis Report

ALGOR®

Design Analysis

S70 Uniaxial Fatigue Test



Created By

J G Roberts
NW-University
Project created on 27/03/08.
Last updated on 28/03/08.

Checked By

J G Roberts
Project checked on 28/03/08.

Summary

Description

Ultimate Tensile Load

Model Information

Analysis Type - Static Stress with Linear Material Models
Units - Custom - (N, mm, s, deg C, K, V, ohm, A, J)
Model location - C:\DATA\Dok\Teken\Uniaxial\S78A

Analysis Parameters Information

Load Case Multipliers

Static Stress with Linear Material Models may have multiple load cases. This allows a model to be analyzed with multiple loads while solving the equations a single time. The following is a list of load case multipliers that were analyzed with this model.

Load Case	Pressure/Surface Forces	Acceleration/Gravity	Displaced Boundary	Thermal	Voltage
1	1	0	0	0	0

Multiphysics Information

Default Nodal Temperature	0 °C
Source of Nodal Temperature	None
Time step from Heat Transfer Analysis	Last

Processor Information

Type of Solver	Automatic
Disable Calculation and Output of Strains	No
Calculate Reaction Forces	Yes
Invoke Banded Solver	Yes
Avoid Bandwidth Minimization	No
Stop After Stiffness Calculations	No
Displacement Data in Output File	No
Stress Data in Output File	No
Equation Numbers Data in Output File	No
Element Input Data in Output File	No
Nodal Input Data in Output File	No
Centrifugal Load Data in Output File	No

Part Information

Part ID	Part Name	Element Type	Material Name
1	S78A	Brick	NBG18_nom

Element Properties used for:

- S78A

Element Type	Brick
Compatibility	Not Enforced
Integration Order	2nd Order
Stress Free Reference Temperature	0 °C

Material Information

NBG18_nom -Brick

Material Model	Standard
Material Source	Graphite_nuclear
Material Source File	C:\Program Files\ALGOR\matlibs\Graphite.mlb
Date Last Updated	2007/09/07-15:49:59
Material Description	Vibration Moulded, Nuclear Grade Reactor Graphite.
Mass Density	0.000000001873 N*s^2/mm/mm³
Modulus of Elasticity	11900 N/mm²
Poisson's Ratio	0.21
Shear Modulus of Elasticity	4917.4 N/mm²
Thermal Coefficient of Expansion	4.54e-6 1/°C

Load and Constraint Information

Loads

Load Set 1: Trek

Surface Forces

ID	Description	Part ID	Surface ID	Magnitude	Vx	Vy	Vz
2	Quarter tensile force	1	6	660	1	0	0

Surface Loads

Part ID	Surface ID	Element Type	Type	Parameters
1	3	Brick	Uniform Pressure	12 N/mm²

Constraints

Constraint Set 1: RW

Surface Boundary Conditions

ID	Description	Part ID	Surface ID	Tx	Ty	Tz	Rx	Ry	Rz
1	Z-Symmetry	1	5	No	No	Yes	Yes	Yes	No
2	Y-Symmetry	1	7	No	Yes	No	Yes	No	Yes
3	X-Symmetry	1	4	Yes	No	No	No	Yes	Yes

Processor Output

Processor Summary

```
 ALGOR (R) Static Stress with Linear Material Models
 Version 19.02-WIN 29-MAR-2006
 Copyright (c) 1984-2006 ALGOR, Inc. All rights reserved.

 **** Memory Dynamically Allocated = 519862 KB
-------------------------------------------------
                     DATE: MARCH 27, 2008
                     TIME: 08:10 AM
               INPUT MODEL: C:\DATA\Dok\Teken\Uniaxial\S78A

            PROGRAM VERSION: 19020002
            alg.dll VERSION: 19000002
       agsdb_ar.dll VERSION: 18000000
      algconfig.dll VERSION: 19020000
       algsolve.exe VERSION: 19020000
       amgsolve.exe VERSION: 03300000

-------------------------------------------------

1**** CONTROL INFORMATION

      number of node points          (NUMNP)   =         11336
      number of element types        (NELTYP)  =             1
      number of load cases           (LL)      =             1
      number of frequencies          (NF)      =             0
      analysis type code             (NDYN)    =             0
      equations per block            (KEQB)    =             0
      bandwidth minimization flag    (MINBND)  =             0
      gravitational constant         (GRAV)    =     9.8146E+03
      number of equations            (NEQ)     =         32006

 **** PRINT OF NODAL DATA SUPPRESSED
 **** PRINT OF EQUATION NUMBERS SUPPRESSED
 **** Hard disk file size information for processor:

      Available hard disk space on current drive =  76919.703 megabytes

      Gravity direction vector =  0.0000E+00  0.0000E+00 -1.0000E+00

1**** ELEMENT LOAD MULTIPLIERS

      load case      case A     case B     case C     case D     case E
      ---------    ---------- ---------- ---------- ---------- ----------

          1        1.000E+00  0.000E+00  0.000E+00  0.000E+00  0.000E+00

 **** Invoking Parallel Sparse Solver ...

 **** Symbolic Assembling Using the Row-Hits Matrix Profile ...
 **** Assembled in One Block.
 **** Real Sparse Matrix Assembly ...

1**** STIFFNESS MATRIX PARAMETERS

      minimum non-zero diagonal element =          2.1084E+03
      maximum diagonal element          =          3.7669E+05
      maximum/minimum                   =          1.7866E+02
      average diagonal element          =          1.5783E+04

      the minimum is found at equation 2: node=2 Ty
      the maximum is found at equation 32001: node=11335 Tx

      in the upper off-diagonal matrix:
      number of entries in the profile  = 2997821
      number of symbolic nonzero entries= 1124555
      number of real nonzero entries    = 1124555
 **** Sparse Matrix Assembled in One Block
 **** Load case 1
 **** Sparse Matrix Factorization ...
      Completing in-core solution (0)
 **** Sparse Matrix Solving ...
 **** End Sparse Solver Solution
```



```
            Reaction Sums and Maxima for Load Case       1

      Sum of applied forces
         X-Force      Y-Force      Z-Force     X-Moment     Y-Moment     Z-Moment
      6.6000E+02 -3.9983E+03  3.9983E+03  0.0000E+00  0.0000E+00  0.0000E+00

      Sum of reactions
         X-Force      Y-Force      Z-Force     X-Moment     Y-Moment     Z-Moment
     -3.5418E-11 -5.7459E-12  9.5343E-12  0.0000E+00  0.0000E+00  0.0000E+00

      Sum of residuals
         X-Force      Y-Force      Z-Force     X-Moment     Y-Moment     Z-Moment
      6.6000E+02 -3.9983E+03  3.9983E+03  0.0000E+00  0.0000E+00  0.0000E+00

      Sum of unfixed direction residuals
         X-Force      Y-Force      Z-Force     X-Moment     Y-Moment     Z-Moment
      3.5990E-11  1.6857E-11  2.8009E-12  0.0000E+00  0.0000E+00  0.0000E+00

      Largest applied forces and moments
            Node         Node         Node         Node         Node         Node
         X-Force      Y-Force      Z-Force     X-Moment     Y-Moment     Z-Moment
            2575         1104         1083            0            0            0
      5.3356E+00 -1.0161E+01  1.0161E+01  0.0000E+00  0.0000E+00  0.0000E+00

      Largest nodal reactions
            Node         Node         Node         Node         Node         Node
         X-Force      Y-Force      Z-Force     X-Moment     Y-Moment     Z-Moment
            1652         2659         2440            0            0            0
      2.0129E+01 -1.0615E+01  1.0871E+01  0.0000E+00  0.0000E+00  0.0000E+00

      Largest nodal residuals
            Node         Node         Node         Node         Node         Node
         X-Force      Y-Force      Z-Force     X-Moment     Y-Moment     Z-Moment
            1652         2659         2440            0            0            0
      2.0129E+01 -1.0615E+01  1.0871E+01  0.0000E+00  0.0000E+00  0.0000E+00

      Largest unfixed direction residuals
            Node         Node         Node         Node         Node         Node
         X-Force      Y-Force      Z-Force     X-Moment     Y-Moment     Z-Moment
            8180        11335        11335            0            0            0
     -6.8973E-12  4.6890E-12  2.8735E-12  0.0000E+00  0.0000E+00  0.0000E+00


1**** TEMPORARY FILE STORAGE (MEGABYTES)
     ------------------------------------
      UNIT NO.  7 :       0.244
      UNIT NO.  8 :       0.389
      UNIT NO.  9 :       0.000
      UNIT NO. 10 :       0.000
      UNIT NO. 11 :       0.000
      UNIT NO. 12 :       0.244
      UNIT NO. 13 :       0.244
      UNIT NO. 14 :       0.000
      UNIT NO. 15 :       0.000
      UNIT NO. 17 :       0.000
      UNIT NO. 51 :       1.417
      UNIT NO. 52 :      39.397
      UNIT NO. 54 :       0.122
      UNIT NO. 55 :       4.168
      UNIT NO. 56 :       8.335
      UNIT NO. 58 :       0.244
      UNIT NO. 59 :      12.870

      TOTAL       :      67.674 Megabytes
```

Meshing Results

Part 1 <S78A>

Status: the part successfully meshed.

Surface Mesh Statistics

Mesh operation	Solid mesh
Final mesh size	0.91546 mm
Elements created	3383

Solid Mesh Statistics

Mesh type	Mix of bricks, wedges, pyramids and tetrahedra
Watertight	Yes
Mesh has microholes	No
Total nodes	14576
Volume	6063.313355 mm^3
Total elements	11604

	Tetrahedra	Pyramids	Wedges	Bricks
Elements	1460	1088	215	8841
Volume %	0.93	1.46	0.74	96.87
Max. length ratio	169	28.3	5	4
Avg. length ratio	5.3	3.3	2	1.2
Avg. aspect ratio	1.3	1.3	1.1	1
Unconstrained aspect ratio	3.9	2.8	1.5	1.1

Log File

```
    SOLID MESH GENERATION BEFORE ANALYSIS
```

```
PROGRAM WILL USE THE FOLLOWING FILES:
    Input:  C:\DATA\Dok\Teken\Uniaxial\S78A.xgn
    Output: C:\DATA\Dok\Teken\Uniaxial\S78A.esd

COMMAND LINE:
    C:\Program Files\ALGOR\SolidX.exe -b=0 -zw=2 C:\DATA\Dok\Teken\Uniaxial\S78A -d=0 -u=13 -c=2 -t=1

TYPE OF OPERATION:
    Meshing only surface defined by part 1
    Generating bricks, wedges, pyramids and tetrahedra elements
```



```
    Automatically minimizing aspect ratio of solid elements


FINAL STATISTICS:
    Elements built (4,5,6,8 noded): 11604  ( 1460, 1088, 215, 8841 )
    Volume (4,5,6,8 noded %): 6063.313355 (   0.93,   1.46,   0.74,  96.87 )
    Number of nodes: 14576
    Length ratios (avg)     5.3,     3.3,     2.0,     1.2
    Length ratios (max)   169.0,    28.3,     5.0,     4.0
    Aspect ratio: unconstrained (   3.9,   2.8,   1.5,   1.1 )
    Average aspect ratios:      (   1.3,   1.3,   1.1,   1.0 )
    Used direct transfer of global surface data as input.
    Total used memory:   15.07 MB
    Number of restarts:   0
    Elapsed time: 0 minutes 6 seconds
```